ELECTRICAL CONDUCTIVITY IMAGING OF AQUIFERS CONNECTED TO WATERCOURSES.

A THESIS FOCUSED ON THE MURRAY DARLING BASIN, AUSTRALIA

by

David Andrew Allen, BScHons

This thesis has been submitted for the degree of

PhD in Groundwater Management,

Faculty of Science

University of Technology, Sydney

July 2007

CERTIFICATE OF AUTHORSHIP/ORIGINALITY

I certify that the work in this thesis has not previously been submitted for a degree nor has it been submitted as part of requirements for a degree except as fully acknowledged within the text.

I also certify that the thesis has been written by me. Any help that I have received in my research work and the preparation of the thesis itself has been acknowledged. In addition, I certify that all information sources and literature used are indicated in the thesis.

Signature of Candidate

_____

ABSTRACT

ELECTRICAL CONDUCTIVITY IMAGING OF AQUIFERS CONNECTED TO WATERCOURSES.

A thesis focused on the Murray Darling Basin, Australia.

by David Andrew Allen

Electrical imaging of groundwater that interacts with surface watercourses provides detail on the extent of intervention needed to accurately manage both resources. It is particularly important where one resource is saline or otherwise polluted, where spatial quantification of the interacting resources is critical to water use planning and where losses from surface waterways need to be minimized in order to transport water long distances. Geo-electric arrays or transient electromagnetic devices can be towed along watercourses to image electrical conductivity (EC) at multiple depths within and beneath those watercourses. It has been found that in such environments, EC is typically related primarily to groundwater salinity and secondarily to clay content. Submerged geo-electric arrays can detect detailed canal-bottom variations if correctly designed. Floating arrays pass obstacles easily and are good for surveying constricted rivers and canals. Transient electromagnetic devices detect saline features clearly but have inferior ability to detect fine changes just below beds of watercourses. All require that water depth be measured by sonar or pressure sensors for successful elimination of effects of the water layer on the data. The meandering paths of rivers and canals, combined with the sheer volume of data typically acquired in waterborne surveys, results in a geo-referencing dilemma that cannot be accommodated using either 2D imaging or 3D voxel imaging. Because of this, software was developed by the author which allows users to view vertical section images wrapped along meandering paths in 3D space so that they resemble ribbons.

Geo-electric arrays suitable for simultaneous imaging of both shallow and deep strata need exponentially spread receiver electrodes and elongated transmitter electrodes. In order to design and facilitate such arrays, signed monopole notation for arrays with

segmented elongated electrodes was developed. The new notation greatly simplified generalized geo-electric array equations and led to processing efficiency. It was used in the development of new array design software and automated inversion software including a new technique for stable inversion of datasets including data with values below noise level. The Allen Exponential Bipole (AXB) array configuration was defined as a collinear arrangement of 2 elongated transmitter electrodes followed by receiver electrodes spaced exponentially from the end of the second transmitter electrode. A method for constructing such geo-electric arrays for use in rivers and canals was developed and the resulting equipment was refined during the creation of an extensive set of EC imaging case studies distributed across canals and rivers of the Australian Murray-Darling Basin. Man made and natural variations in aquifers connected to those canals and rivers have been clearly and precisely identified in more than 1000 kilometres of EC imagery.

TABLE OF CONTENTS

LIST OF FIGURES

ACKNOWLEDGEMENTS

The author wishes to thank the following groups for their contributions to the project:

My Supervisor, N.P. Merrick, and co-supervisor, B. Kelly, of the National Centre for Groundwater Management, University of Technology, Sydney who provided advise, proof reading, funding negotiation and computer code, used as a basis for some code written for this thesis.

The Australian Co-operative Research Centre for Sustainable Rice Production who provided A$105 000 towards this thesis.

The NSW Department of Land and Water Conservation /Infrastructure Planning and Natural Resources / Natural Resources (perpetual name changers) who provided funding for surveys in the vicinity of Mildura. Michael Williams, principle hydrogeologist is thanked for his efforts in securing funding.

The Australian Federal Bureau of Rural Sciences who funded river surveys of the Border Rivers and the Tuckean Swamp – Richmond River

Zonge Engineering and Research Organization who provided equipment on a research rate rather than commercial rate.

Geoforce- who provided the Syscal Pro (1 month) and an assistant (8 days) on research rates.

Barry Porter - South Australian Department of Water, Land and Biodiversity Conservation and Brian Barrett – University of Adelaide, who assisted with organising and facilitating fieldwork at Waikerie.

Richard, Peter and Lorraine Stott – Whitton farmers - who provided access to their rice based farms and assisted with fieldwork in various ways.

Coleambally Irrrigation Cooperative Limited funded survey and reporting on the Argoon Channel and provided personnel and logistical assistance for much of the RiceCRC funded fieldwork.

Murray Irrigation who funded seepage measurement follow-up work on their canals.

Scott McInnes – Zonge Engineering and Research Organization who completed and conveyed to the author a similar geo-electric array appraisal for roll along imaging systems.

Saud Akbar of NSW Agriculture provided Idaho seepage measurements on farm canals.

Niels Christensen of EMmodel and Esben Auken of the Hydrogeophysics Group inverted some of the data so that comparison of inversion techniques could be made.

Andrea Viezolli and James Cull of Monash University who processed and studied some of the induced polarization data.

Dalcrom agricultural consultants who helped with siting of ploughed array tests.

Geoff Beecher and Brian Dunn of NSW Agriculture who provided advice and differential GPS equipment.

Greenspan who provided a pressure sensor and logger at research rates.

Most importantly I thank my wife and family who willingly coped with 3 and a half years of life on low, and at times no, income while I completed this thesis.

GLOSSARY

AXB geo-electric array. Allen Exponential Bipole geo-electric array is a collinear array with two elongated transmitter electrodes followed by receiver electrodes spaced at 2^n from the far end of the second transmitter electrode where *n* increments by any constant value (typically 1 or 0.5).

dBase. A dBase file is a relational database file, with the extension *.DBF following the dBase (now xBase) conventions. It is a very old and well supported format that allows indexing using separate *.MDX files.

EC. Electrical Conductivity (measured normally in µS/cm) is the inverse of resistivity.

EC Ribbon. An EC ribbon is a type of graphical presentation of multi-depth electrical conductivity data, where soundings are stitched together in a vertical image. The vertical image is wrapped along the track of that image presented in a 3D interface such as OpenGL. It is designed for use with towed multi-depth EC surveys.

Forward Modelling. Forward modelling is the process of determining the set of voltages that an instrument would measure over a particular theoretical model.

Geo-electric array. A geo-electric array is a collection of electrodes connected to the earth or water in such an arrangement that they can be used to image the substrate. The array is made up of quadrupoles (see definition) used individually to focus on various depths and/or parts of the substrate.

Inversion. Inversion is the process of iteratively simulating forward models and determining how well they fit field data and then proposing new models until a model that fits the field data well is found.

Quadrupole. A quadrupole is a set of two transmitter electrodes and two receiver electrodes. A geo-electric array contains a whole set of quadrupoles which may, or may not, contain electrodes common with other quadrupoles in the array. Each quadrupole is designed to focus at a particular depth when used to image the substrate.

Resistivity. Resistivity (measured in ohm.m) is the inverse of electrical conductivity

ShapeFile. A geographic format that adds a geo-indexing file (*.SHP) to a dBase file. The *.SHP file may contain points, lines, polygons or more complex features referenced in 2D or 3D. Additional index files and a projection file may supplement the *.SHP file. The format is detailed in a White Paper by ESRI (www.ESRI.com).

SPOT. Seepage penetrating observation tube – A vertical pipe infiltrometer for spot measurement of seepage in locally observed seepage spots (LOSSes). This is a simple reliable device for low accuracy spot measurement of absolute seepage rate at low EC anomalies in canals.

CHAPTER 1 - INTRODUCTION

1.1 Aim

Aim - This thesis aims to develop and demonstrate electrical conductivity (EC) imaging technology for application to investigation of surface water/groundwater interaction, principally in the Murray Darling Basin, Australia.

1.2 Introductory example

The approach of this thesis is much easier to grasp after viewing a sample of the end product. For this reason, some EC imagery is presented in Figures 1-1 and 1-2. Detailed explanation of these images will be provided in later chapters. The imagery, superimposed on a canal and river has been used to identify potential underground water storage sites as well as a localized site seeping more than 900 megalitres per year.

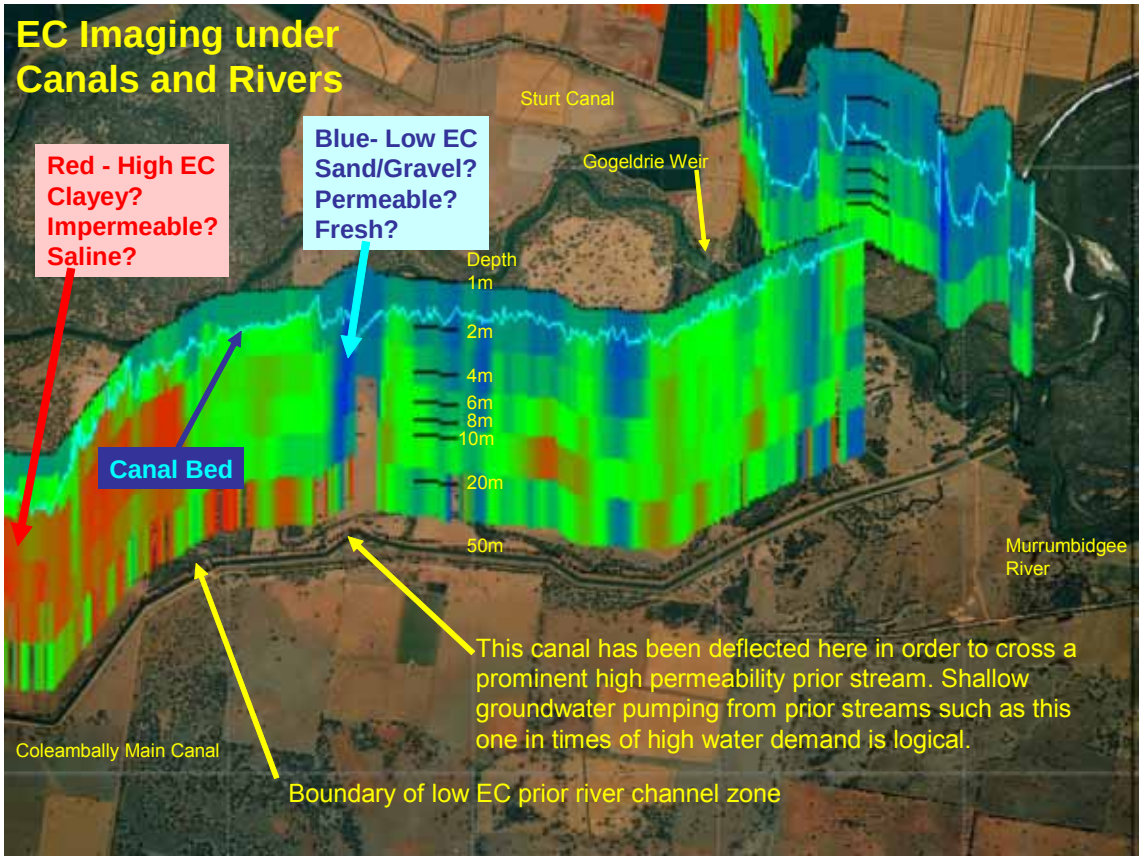

Figure 1.1 An example of EC imagery superimposed north of a canal and the Murrumbidgee River. Annotation explains the significance of the colour scale. Depth is projected downwards from the surface of the watercourses as shown.

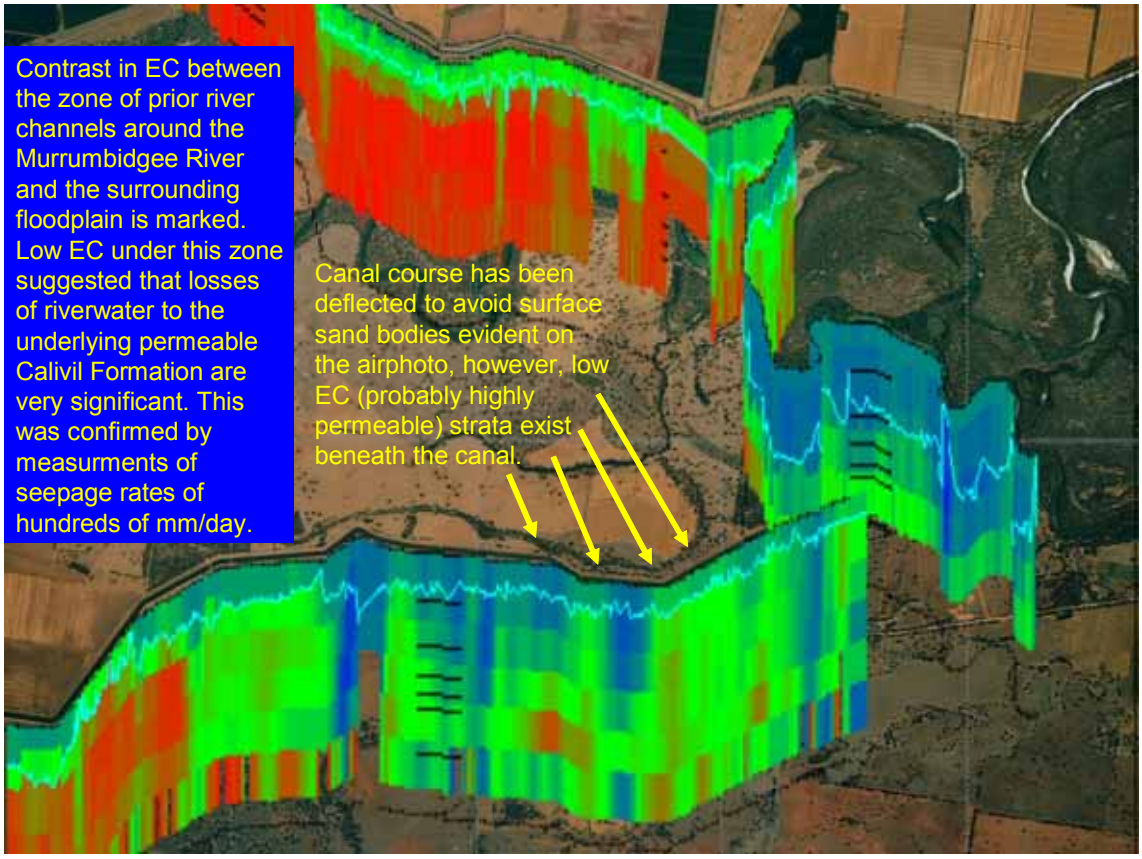

Figure 1.2 The EC ribbon of Figure 1-1 is projected south of a canal and the Murrumbidgee River here so that it can be compared with features on the north sides of the watercourses.

1.3 The need for EC imaging of groundwater beneath surface water bodies

The increase in demand for water and the increasing salinity that poses threats to water supplies and irrigated land have led to a growing demand for technology that conserves fresh water and protects land used for irrigation. An understanding of the interaction between surface water and groundwater is important for effective transportation of water in open channels and rivers. The identification of properties of aquifers directly beneath watercourses is particularly important. As such aquifers typically are heterogeneous, multiple depth spatial detail of those aquifers is also useful. Borehole data is prohibitively expensive. EC is the most useful property of such aquifers that can be imaged because it

relates to groundwater salinity and sediment texture and because it can be imaged quickly and non-invasively.

1.4 The approach to EC imaging used in this thesis

EC imaging can be conducted by direct sampling by suitably equipped augers or penetrometers although this is usually cost prohibitive except as a means of independent verification of data collected using other techniques. EC imaging can be conducted economically using geo-electric arrays, transient electromagnetic devices or frequency domain electromagnetic devices. Natural signals such as magnetotellurics can also be used to measure EC, however, in this thesis such techniques have been rejected due to the long measurement times and lack of vertical resolution of the depths required.

This thesis focuses on use of geo-electric arrays because, when towed along watercourses, they quickly produce clear unambiguous EC data of sub-watercourse aquifers. Induced polarization (IP) data also is produced as an added benefit. A little examination and utilization of electromagnetic techniques also has been conducted in this thesis.

Electronic and computational technology can be used to facilitate these new approaches to sub-watercourse aquifer investigation. This thesis shows how to combine and configure that technology into viable survey solutions. Case studies of surveys across the Australian Murray Darling Basin are presented. These case studies have been stored in a new database format designed to pave the way for formation of a national archive system for collection, storage and utilization of such surveys by others.

A combination of challenges, spread across multiple disciplines has been tackled, in order to demonstrate a new viable solution to investigating surface water/groundwater interaction. Although small scale geo-electric arrays have previously been tested experimentally from watercourses for various reasons in the past the techniques used were impractical at larger scales. An attempt is made here to facilitate cost-effective, production scale application to study the interaction of vast lengths of surface watercourses and groundwater. In addition, an attempt is made to enhance the quality of water-borne geo-electric surveys in every way that is economically viable.

On water, or underwater, geo-electric surveying is made easier by the fact that electrode contact resistance problems and problems with near surface inhomogeneities are reduced.

Surveys can be conducted continuously at a small fraction of the cost of traditional land surveys where electrodes conventionally are manually inserted in the ground.

Investigations of the interaction of groundwater with surface watercourses typically require the identification of fine scale variations in layered substrata just under the beds of the surface water courses. Therefore, a system which is more sensitive to near-surface variations is needed. This is achieved in systems that have sensitivity varying logarithmically with respect to depth. When designed optimally, geo-electric arrays on the surface of water or land naturally exhibit such a variation in sensitivity.

Table 1-1 presents a summary of the problems that have impeded sub-watercourse aquifer investigation in the past and the solutions used in this research study.

Table 1-1 – Problems and solutions in EC imaging of sub-watercourse aquifers.

Problem	Solution
Geo-electric surveys were being conducted using electrodes that needed to be hammered into the ground. High productivity was not possible in such a mode. Waterborne survey is impossible in such a mode, and surface water – groundwater interaction investigation mostly needs to be conducted under surface water bodies.	Continuous mode operation of floating and submersible geo-electric arrays linked with GPS (following Allen, 1991).

Problem	Solution
Large volumes of 3D data generated by the continuous survey technique could not be visualized in a manageable way using other than high end petroleum exploration software. Such software is not tailored to efficient use of EC data. The task of comparing the data with ground surface features that intersected the survey path was particularly troublesome.	3D ribbon presentation technique was refined and software developed.
No software was available for efficient continuous mode survey processing.	A software system for on the job processing and presentation was written.
Conventional electrode configurations were not suited to efficient shallow investigation in continuous mode.	New electrode array configurations were invented and evaluated.
Point source electrodes could not facilitate both shallow and deep investigation at the same time efficiently during towing.	Provision for elongated transmitter electrodes was added to processing algorithms by generalizing and extending existing geo-electrical array theory.
Inversion software suitable for fast robust inversion of continuously acquired data was not available.	Effective depth based inversion software was written.
Important details at the bottoms of water bodies were not being well resolved by floating arrays.	Submerged array equipment, theory and software was invented and tested.

Problem	Solution
Canal and upland river surveying involves numerous navigation obstacles such as weed which fouls propellers, bridges, fences, shallow water, overhanging trees, weirs etc.	An outboard motor propelled canoe or boat mounted system, truck with boom mounted system, and a lightweight airboat system light enough to lift easily over obstacles were developed for towing geo-electric arrays. Coupled with a 4wd mounted long reach crane, these craft could efficiently pass obstacles. Prototyping of radio-controlled miniature craft suitable for survey of extremely obstructed fenced canals was commenced.
Array designs that are robust, compact, easy to handle, cheap and easy to build and maintain and that could slide past obstacles were not available.	Robust geo-electric arrays, both floating and submerged, that would not catch on obstacles were designed and assembled.
Continuous mode geo-electric array systems suitable for surveying across irrigated land rather than water in Australia's dry conditions were not available.	Trials of a plowed, irrigated array were made in preparation for implementation of Danish technology for continuous surveying across ground. However, at the same time, Geometrics developed the superior Ohm-mapper multi-dipole capacitative geo-electric array.

Problem	Solution
Hypersaline groundwater often is an investigation target however it consumes almost all available signal leaving noisy data that implies the groundwater is hypersaline but restricts penetrations depth. Available inversion theory behaves erratically and erroneously with such data.	'Sub–noise data aware' inversion technique was invented. This recognizes what data is below noise level only due to the weakening of signal by conductive features. It proceeds by restricting inversion to models that would create such 'sub-noise' data.

1.5 A clarification of terminology - EC and resistivity

Traditionally, geo-electric survey data has been presented in units of resistivity (ohm metres or Ω.m) but water managers traditionally present resistivity data in units of the inverse of resistivity which is called electrical conductivity or EC, not to be confused with hydraulic conductivity. Values of EC in common use include micro-siemens per centimeter (μS/cm), deci-siemens per meter (dS/m), milli-siemens per meter and siemens per metre. Furthermore, these units are frequently abbreviated ambiguously in water management literature to 'EC units' or to μS which normally both mean μS/cm. In order to convey geo-electric imagery to water managers (the market for this type of geophysics) the author has decided to communicate in terms of electrical conductivity and to put dual scales of resistivity and electrical conductivity on graphs. Because μS/cm are most commonly used EC units, they have been chosen for scales even though they are not a preferred System International (SI) unit. All data files and computations, however, are completed in this work using ohm.metres, the system international units widely used in geo-electric literature. In software created in this PhD work, a conversion utility was developed to help deal with all this terminology. It is displayed in Figure 1-3.

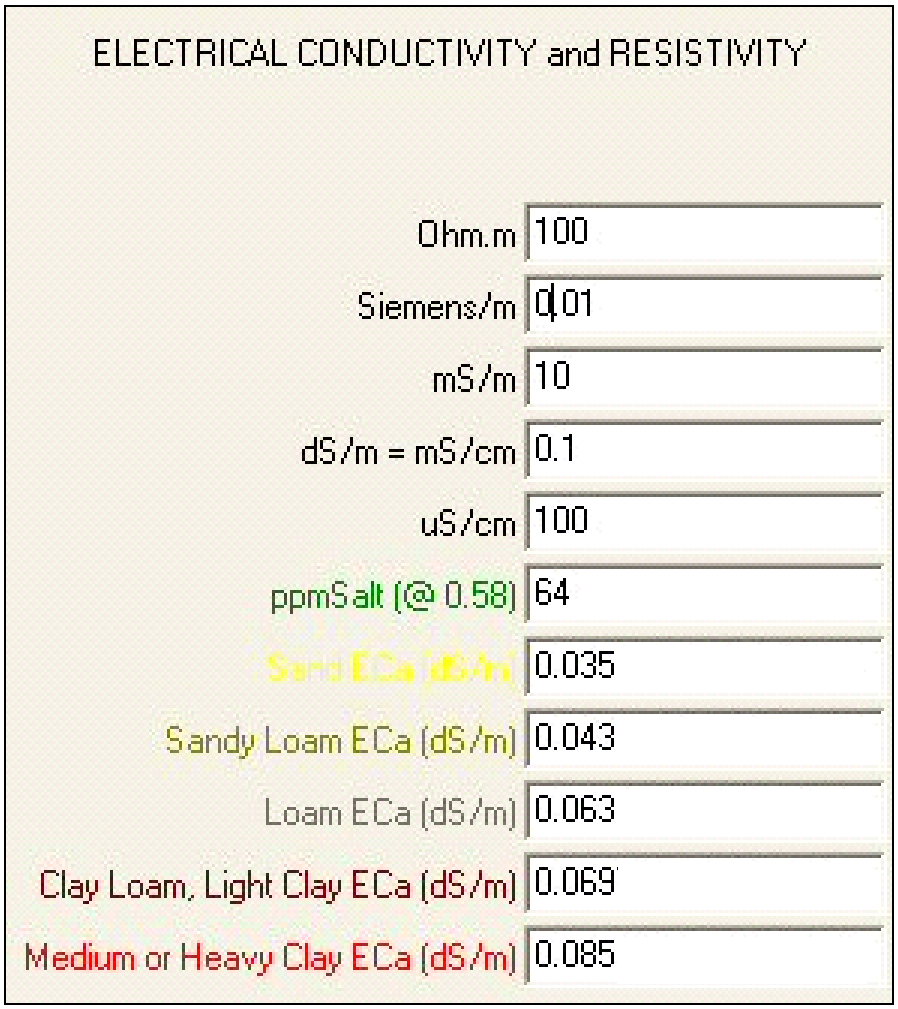

Figure 1.3 The relationship between various EC units (empirical soil texture based conversion factors, discussed in the text , are from Slavich and Petterson, 1993).

Conversion from EC units to salinity concentration (ppm) in water is given by a conversion factor of about 0.64 ppm per µS/cm (Gibbs, 2001). The exact value of the conversion factor depends on water chemistry and temperature and can easily vary by 20%. According to Emerson and Webster (1970), quoted in Merrick (1977), the average factor for natural Australian waters is about 0.68. Fetter (1988) gives the value of 0.58. Conversion from pore space water EC to bulk EC of saturated, unconsolidated sediment of various textures can be conducted empirically using factors obtained by Slavich and Petterson (1993).

1.6 Elementary correlation of seepage and saline inflow with EC

Electrical conductivity of solutions depend on concentration and composition of dissolved salts and suspended clays as well as temperature. Electrical conductivity of sediments

depends on sediment texture (clay, sand, and rock of various degrees of induration), salinity, cation exchange capacity and moisture content.

The following hypothesis is presented as an explanation of the significance of EC anomalies observed under canals:

> *'Low electrical conductivity anomalies under canals represent sites of anomalous freshwater flushing, by seeped canal water, of permeable sediment. Even before the flushing occurred, such sediment generally had low clay content, low salinity and, thus, low electrical conductivity due to leaching from rainfall, while surrounding sediment that retained more water suffered salinity concentration as a result of evapo-transpiration. An exception to this hypothesis exists in the case of canals passing over dry sediment capped by relatively impermeable sediment (eg. silt). The dry sediment can be identified by extremely low electrical conductivity.'*

Canals almost always recharge aquifers because they are elevated above the water table and so it is expected that the above hypothesis is robust beneath canals. Drains and rivers, on the other hand, are subject to discharge from aquifers at certain times and locations and so a robust simple interpretation of EC data collected from them is not possible. Fortunately, in highly saline environments where saline inflow is problematic, groundwater salinities are so high that salinity dominates EC imagery.

When probing the subsurface, both EM and geo-electric technique signals pass through both river or canal water and the ground beneath without distinction. The river or canal water EC does not typically vary significantly but the EC of the sediment beneath may vary considerably. Induced polarization data, also collected using geo-electric arrays, responds non-linearly to clay content – 2-20% clay giving a peak positive response (Brandes and Acworth, 2003).

Further discussion of EC correlation with various factors is included in Chapter 11 – 'Interpretation'.

1.7 A history of waterborne geo-electric surveying.

Geo-electric surveying has been used as early as the 1920's (Merrick, 1977) but was not applied from water until much later. Wantland (Smith & Turner, 1982), of the USA, was reported as using the technique to isolate canal seepage hot spots in 1962. He correlated low EC with high seepage, probably because, at the site he surveyed, seepage was saturating otherwise unsaturated ground. Smith and Turner (1982) attempted a similar survey in the Goulburn-Murray irrigation canals in 1982 and discovered an opposite correlation to that of Wantland, no doubt because they surveyed over clayey soils that retained soil moisture. They concluded that they were identifying sand lenses within a clayey host. These early surveys were done with just four electrodes and one measurement was taken per station and were impractical for large scale deployment.

In 1991, geo-electric surveys on water were conducted using an ABEM Terrameter SAS300B and a dipole dipole array suspended using air-filled plastic bottles (Allen, 1991 & 2001). Data were located by referencing to curves in the river picked off maps. Data was simply plotted as apparent resistivity versus effective depth in contour plots with connecting lines linking stations to their location on maps. Co-incidence of anomalies with increases in river salt load and mapped geologic features suggested that the array was able to detect saline inflow related to geological features below the Darling River in NSW, Australia. Figures 1-4 and 1-5 show a sample of the data obtained and the field operation.

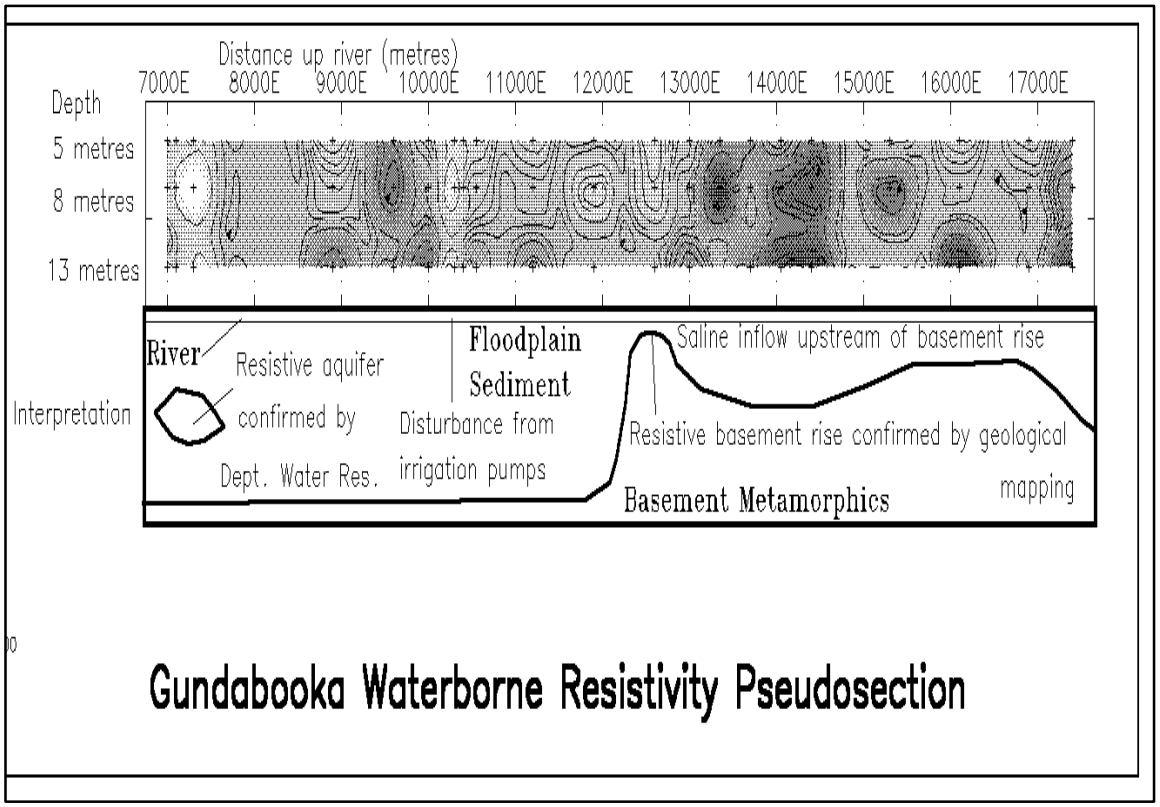

Figure 1.4 A resistivity survey of part of the Darling River SW of Bourke conducted by Allen (1991).

Figure 1.5 Rudimentary equipment used by Allen (1991) for investigating saline inflow to the Darling River.

In 1997, Zonge Engineering and Research Organization commenced similar surveys for identifying permeable aquifers beneath the Ohio River from which water for Louisville, Kentucky could be pumped (Snyder & Wightman, 1997) using their GDP32 receiver. Navigation was conducted using a GPS receiver. The survey successfully differentiated permeable aquifers from clays beneath the River. They could record data continuously on several channels simultaneously. Zonge also completed other similar surveys at about that time. They refined array construction using multicore cable and moulded takeouts incorporating tinned copper braid electrodes and applied 2D inversion to the data to create smoothed vertical sections. The sheer volume of data they could create with such a system proved to be impressive yet without a refined processing and 3D presentation system, use of the data proved to be laborious and interest in the technique again appeared to diminish.

Around 1997 Advanced Geoscience Incorporated began to experiment with similar surveys (AGI,1997) in seawater. Their approach seemed to be very similar to that of Zonge except they utilized an AGI Sting-Swift receiver.

Hotchkiss (2001) utilized geo-electric arrays for determining irrigation canal seepage in Nebraska, USA from 1991 to 2001. He used an Iris Instruments Syscal-R2 single channel receiver and collection was very slow. Although Hotchkiss's work was a significant advance in application of geo-electric surveying to seepage detection, it did not incorporate the continuous multi-channel data acquisition advances of Zonge and AGI. Hotchkiss created an array in a multi-pronged handheld probe which he pressed into the canal bottom. He also used a floating Schlumberger array with electrodes suspended from rods hanging from a rigid floating pipe. The electrodes were suspended because, with the length of floating pipe used, floating electrodes would have given a focus of depth of investigation that was within the canal, not the sediment beneath. One dimensional inversion was used to process data into layered models and Idaho seepage meters were used to relate the layered models statistically to seepage rates. Hotchkiss found that he could easily pinpoint seepage zones. The floating array was found to be superior to canal bottom sediment EC sampling for identifying seepage because it could image deeper below canals.

Around 2002, James Cull of Monash University, Victoria, Australia proposed to the Australian National Committee on Irrigation and Drainage (ANCID) that a towed flexible

floating array be used for detecting seepage. At about the same time, independently, this PhD was commenced proposing to image EC of aquifers, primarily beneath rivers, suffering salinity problems. A flexible floating electrode array was developed by the author. Zonge, who had been contracted by Sinclair Knight Mertz (acting for ANCID) to conduct surveys of canals in various irrigation areas as part of seepage investigation trials contracted the author to join in the fieldwork and supply the geo-electric array. It was stipulated that a 5m dipole-dipole array configuration be used so that 2D smooth model inversion could be done using Zonge software. Inversion of the 6 days of field data took about a week. Numerous 2D vertical sections were created and a geo-referencing dilemma became evident as cross-referencing between the sections and maps was attempted. It became clear that a better processing system had to be developed. That system is detailed in this thesis along with array design and other improvements that permit practical watercourse surveying.

Brian Barrett of Adelaide University conducted a Masters Thesis in 2002 in which he had to investigate saline inflow into the Murray River at Waikerie, South Australia. The author co-operatively surveyed at Waikerie with him and the assistance of Zonge, CRCLEME and the SA DLWBC. Barrett decided to additionally try waterborne transient electromagnetics at the site using the Zonge NanoTEM system and floating loops that he developed. Both systems functioned surprisingly well revealing the effect of saline groundwater interception bores on groundwater beneath the river. (See Barrett (2003) and the Waikerie case study included in chapter 15 of this thesis).

Also in 2003, NSW DIPNR funded the author to conduct six surveys of the Murray River in the vicinity of Mildura at 2-monthly intervals and the Cooperative Research Centre for Sustainable Rice Based Systems funded the author to conduct salinity investigation beneath irrigation canals and drains. In 2004, funding was received from the Bureau of Rural Sciences to survey on the Border Rivers and the Tuckean Swamp resulting in the library of surveys incorporated in this thesis. Some other minor surveys were funded by the author, a farmer (Richard Stott), Murray Irrigation Limited and Coleambally Irrigation Co-operative Limited.

CHAPTER 2 - AN INTRODUCTION TO TOWED GEO-ELECTRIC ARRAYS AND ELECTROMAGNETIC DEVICES.

2.1 Instrumentation summary

Data published in this thesis was collected using either geo-electric arrays or transient electromagnetic loops. GPS was used to position the surveys and Sonar or pressure sensors were used to profile water depth. Some data was collected by independent surveyors using frequency domain electromagnetic devices.

2.2 Theory of operation – geo-electric arrays

A full explanation of the electrode array resistivity measurement method is documented in Telford (1990) and Dobrin (1988). In brief, the resistivity method injects electrical current into the ground, or water using two electrodes and records the voltage generated between two other electrodes. Field data are converted to apparent resistivity or its reciprocal, apparent conductivity. The continuous floating and submerged imaging modes of data acquisition applied in this thesis use a string of exponentially spaced electrodes. Voltages between adjacent electrodes are read simultaneously at a frequency of 4 Hz and stored every 4 seconds. Wider spacings between transmitting and receiving electrodes give information at greater depths.

The arrays used in these surveys are optimised to sample at approximately logarithmically increasing depths and over as short as practical horizontal distance. The basic principles of operation are included in Figure 2-1 and equipment used is schematized in Figure 2-2 and displayed in Figure 2-3.

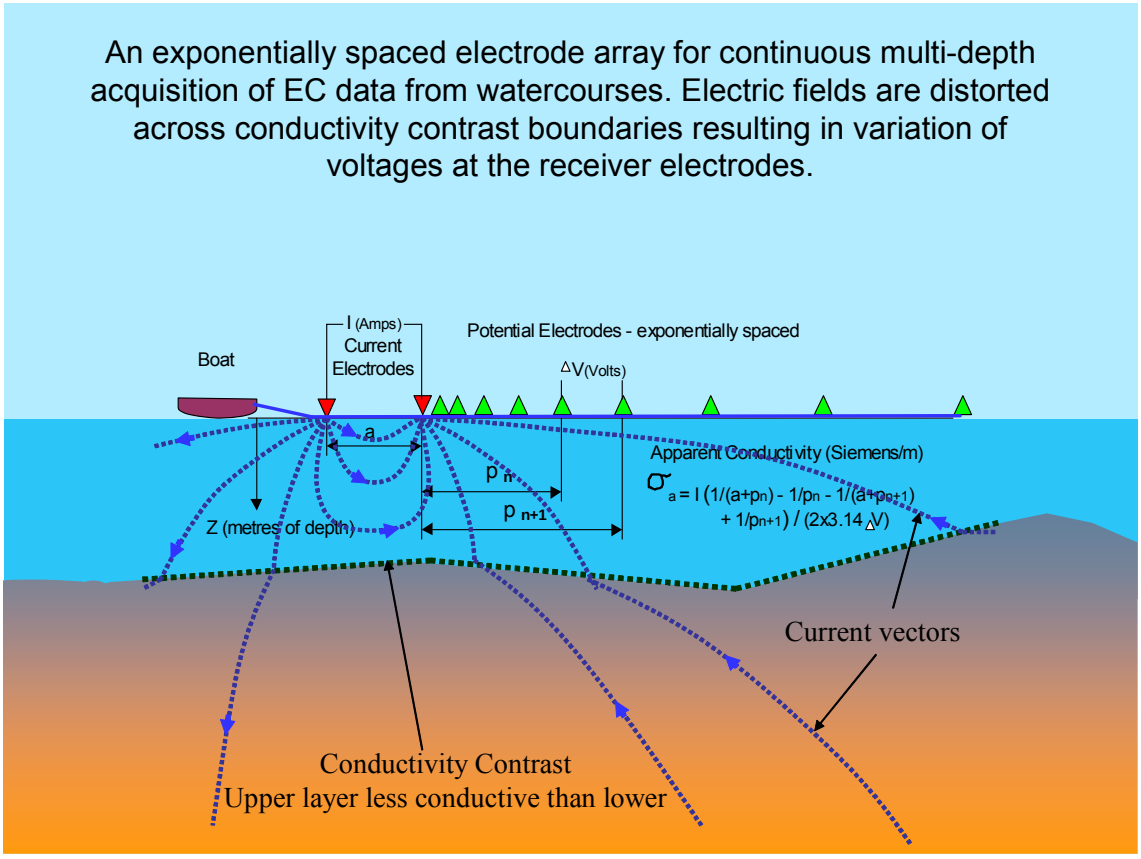

Figure 2.1 Principles of operation of geo-electric arrays

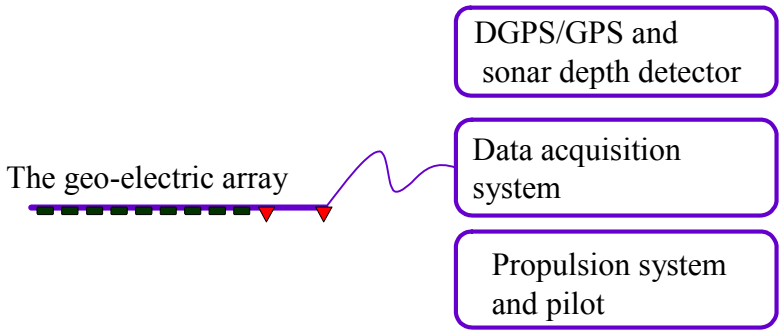

Figure 2.2 Components of a towed geo-electric surveying system

Figure 2.3 A geo-electric array and the Zonge geophysical data processor 32.

2.3 Theory of operation – transient electromagnetics

Transient electromagnetic (TEM) devices induce current in the ground by generating a changing magnetic field around a large wire loop as demonstrated in Figure 2-4. First current is transmitted through the loop, then the transmitter is shut off rapidly. Maxwell's equations show that a magnetic field (approximating a vertical dipole) is maintained when current is flowing through the loop. When current is shut off, the magnetic field cannot immediately extinguish itself. Instead, it induces eddy currents in local conductors such as the river water and ground. The eddy currents diffuse outwards and downwards like a horizontal smoke ring. The rate at which it diffuses is controlled by the conductivity of the ground through which it passes. As the current dissipates, its magnetic field also dissipates and this change can be detected by another coil at the surface, recorded with respect to time and then converted into an approximate conductivity/depth sounding. Because this research work focuses principally on geo-electric techniques, readers requiring further explanation of this fundamental theory are referred to Telford (1990), Parasnis (1986) and, for more depth, in Nabighian (1987).

In practice, it is difficult to measure and interpret the very early sample times needed to resolve the near-surface, so shallow features cannot be resolved using this technique. Before signal gets to a depth approximately equal to the distance between transmitter and receiver loop sides, it can be used to calculate EC but the depth sensitivity is invariant. Also, induction within the diameter of the cabling, time resolution of early time gates of commercial equipment and ambiguity of the transmitted waveform and time shifts between it and the receiver waveform cause errors that are most significant at early times. Additionally, TEM systems have bandwidth and inductive and capacitive effects that cause errors such as 'ringing' (Kamenetsky & Oelsner, 2000) that are most significant at early times.

The signal strength of TEM is maintained by conductive targets (eg. saline hot spots) so that detection of additional targets beneath is made difficult. In resistive ground/water, the TEM signal decays quickly resulting in deep penetration with poor resolution. Hence, TEM is good at finding saline hot spots and clay horizons, even if they are relatively deep, but it will not resolve much else. Due to problems with shallow features it has limited, but often adequate, ability to resolve what is happening right at the riverbed.

Barrett (2003), gives further details on the design and operation of the prototype floating transient electromagnetic loop system. Michael Hatch of Zonge refined the field deployment infrastructure of Barrett resulting in the device displayed in Figure 2-5.

TEM surveys may also be conducted from the ground in towed mode or from the air. These modes of propulsion and operation will be investigated in a Chapter 8 – 'Terrestrial EC imaging'.

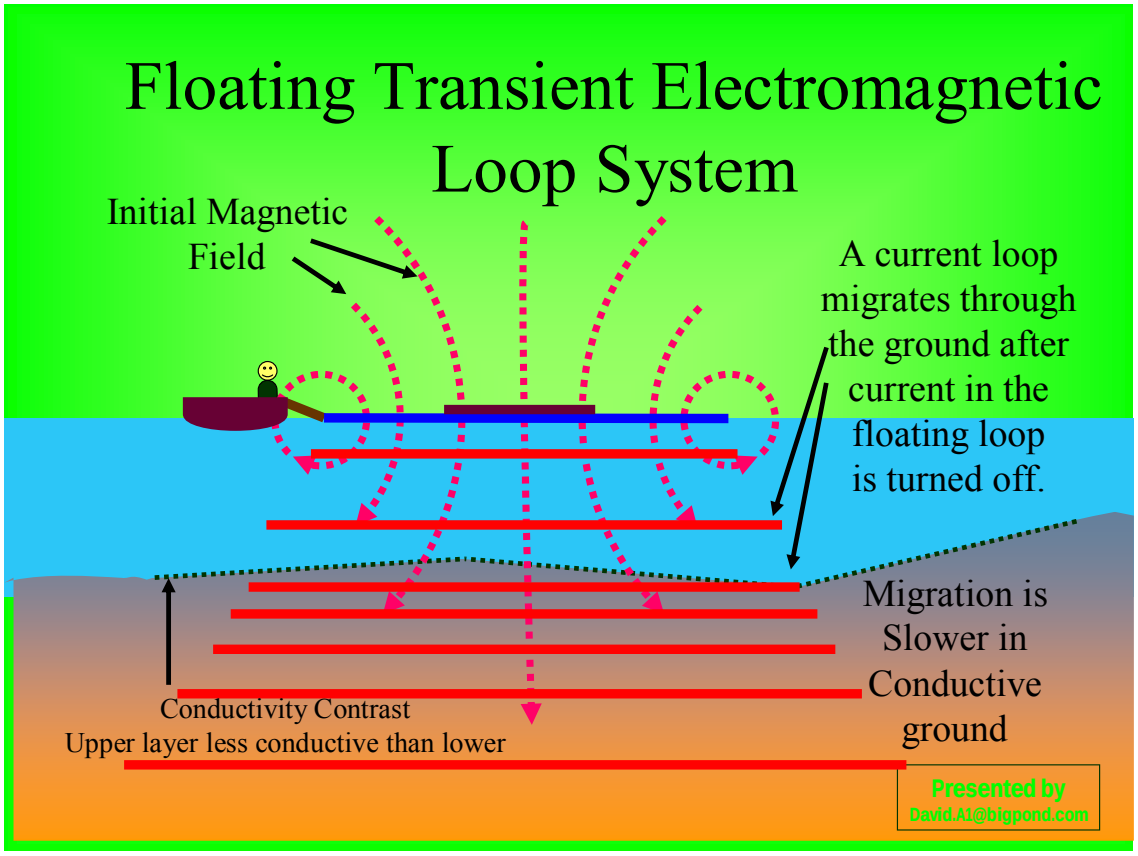

Figure 2.4 Principles of operation of transient electromagnetic devices

Figure 2.5 A floating transient electromagnetic device (Zonge NanoTEM) on the Darling Anabranch

2.4 Theory of operation – Frequency domain electromagnetic devices

Frequency domain electromagnetic (FDEM or FEM) devices transmit a sinusoidal waveform through a small coil, typically at kilohertz frequencies. Currents and resulting secondary magnetic fields are induced in the ground and a small receiver detects the field as with TEM. In FEM however, the primary field generated by the transmitting coil also is received and must be compensated for. Various depths of penetration are achieved by changing the coil spacings, raising the coils, varying coil orientations and changing operating frequency. Popular FEM equipment, the Geonics EM31 and EM38 (www.Geonics.com), may be used to survey canals and rivers (Harding 2002). They detect moderate to high conductivity features best. They can give dual depth information by varying coil orientation but most of the instruments cannot operate dual orientations in a single pass. In contrast, some DualEM (www.DualEM.com) FEM instruments can detect multiple orientation and, optionally, spacing data in one pass. The 'low induction number' approximation is used to generate a millisiemen/m readout from Geonics and DualEM instruments and correction curves are available from Geonics to correct these values at high conductivites. The EM31 and EM38, being single depth devices, are disadvantaged when surveying from water. They cannot separate water depth variation and responses from various layers in the ground. Possibly the biggest problem is that they do not see deep enough. Dighem (www.Fugro.com) is a multidepth airborne FDEM instrument that may be used for deeper studies under waterways; however it is the opinion of the author that variation in coupling due to topography would inhibit its viable use for detecting features just beneath watercourses. Additionally, at seepage hot spots along canals, seepage often dispels salt from beneath the canal and concentrates it in soil adjacent to the canal. Since the 'footprint' of an airborne instrument will include both the banks and the canal, interpretation of anomaly significance could be difficult.

CHAPTER 3 - MATHEMATICS FOR TOWED GEO-ELECTRIC ARRAYS

3.1 Abstract

Traditionally, geo-electric problems have been solved using equations containing a series of monopole terms. Each term gives the effect of one transmitter electrode on one receiver electrode. Except in simple geo-electric equations, such as apparent resistivity equations, elongated or plate electrodes have been treated as equivalent point sources. A new notation for geo-electric array parameters is presented here that facilitates the summing of monopole terms rather than dealing with each term in series. It is computationally simple and efficient for use with any electrode array with point, elongated or even plate electrodes distributed in a horizontal plane. For every combination of transmitter and receiver electrodes utilized in an array, elongated or plate electrodes are segmented into a series of equivalent point sources. Practically, combinations of widely separated electrodes require no segmentation. All the combinations of point sources, are then utilized in various equations and algorithms using sum notation. One dimensional forward modelling and inversion algorithms based on the notation are greatly simplified and do not require any *a priori* knowledge of array configuration. Additionally, the new notation facilitates detailed analysis of the performance of arrays. Demonstration of use of the notation for towed geo-electric array surveying is presented here. Towed arrays may be floating on water, resting on land, or submerged. In order to sample a large range of effective depths in a single pass, towed array transmitter electrodes need to be elongated so that they are several times longer than the distance between them and the closest receiver electrodes. This permits transmission of signal sufficient to be received by the most distant receiver electrodes. A new Exponential Bipole (XB) Array, designed for towed continuous survey, is discussed in the context of the new notation. It can be used with elongated transmitter electrodes in such a way that 1D inversion can be performed only marginally slower than for an equivalent array with only point electrodes.

3.2 Introduction

Geo-electric array notation has traditionally been specialized to particular array types. Individual terms for each quadrupole in an array were included in equations (even partially generalized equations) without any successful attempt at identifying behaviour of the terms that allowed them to be generalized. Most surveys were restricted to use of specific fixed configurations so that efficient fixed geometry processing could be conducted. A need for generalized arrays and thus generalized array notation was not of highest priority. Because modern computers have improved computational powers, continuous towed survey is now practical and array configurations need to be designed, not to fit geometrically simple arrangements that permit processing efficiency, but to function effectively at speed while simultaneously surveying a large range of exploration depths. Presented here is a notation that both simplifies and extends flexibility of design and use of geo-electric arrays.

Geo-electric surveying commenced with use of the Schlumberger, Wenner and Dipole-Dipole Arrays, all of which assume that all electrodes are point sources. This assumption is not valid with modern towed arrays and capacitive electrode towed arrays that both use elongated and plate electrodes to increase system performance. Therefore, there is a need for a notation that facilitates such electrodes and separates array complexity issues from actual forward modelling and inversion algorithms. In addition, should a notation be completely general and suitable for breaking down array complexity into the simplest possible of case, the monopole, then comprehensive array performance analysis is made possible.

The new notation – fractional signed monopole notation – considers the effect of individual pairs of electrodes or, in the case of linear electrodes, optimally sized electrode portions, and sums them using the principle of superposition. The pairs can be summed due to inclusion of a sign variable with the term for each pair. Previous partially generalized notation for geo-electric arrays (eg. Barker, 1989) did not include this sign variable and therefore had to list the terms individually. Four pairs of electrodes were typically considered so, in addition to being more flexible, equations and computer code using the new notation can be four times simpler than equivalent point electrode equations and code using the old notation.

Being particularly suited to towed arrays, the notation efficiently facilitates linear transmitter electrodes, which can transmit more efficiently than point source transmitter electrodes.

3.3 Why use elongated electrodes?

An elongated electrode may be defined as a cylindrical electrode of length, compared to its separation from adjacent electrodes, that precludes use of the assumption that it is a point electrode. Typically, it may be several times longer than its separation from adjacent electrodes.

In order to inject sufficient current for measurement of voltages between distant electrodes without use of high power transmitters or long stacking times, current electrodes in arrays designed for continuous acquisition need to be elongated and the spacing between current electrodes needs to be large. High power transmitters result in the added problem that electrodes sampling shallow effective depths receive signal that will overflow ADCs if not attenuated. An added benefit of elongated transmitter electrodes is that receiver electrodes that are only a fraction of the current electrode length away from the current electrode receive less voltage than if the current electrodes were point electrodes. This means that when attempting to simultaneously sample a very large range of effective depths, the signal level with respect to effective depth curve is flattened out so that need for attenuation of the shallow-sampling quadrupole signals is reduced.

In towed arrays, receiver electrodes are more likely to have manageable contact resistance if they are elongated. If the contact resistance approaches the ADC input impedance then measurement errors will occur. The errors will be particularly significant on the more distant electrodes where signal to noise levels are low. The problem is even more pronounced when capacitively coupled electrodes are used.

3.4 Pragmatic mathematics for use of elongated electrodes

Use of elongated electrodes complicates the processes of calculating apparent resistivities and effective depths. Data collected from receiver electrodes separated from the elongated current electrode by only a fraction of its length cannot be inverted rationally using conventional inversion software. Use of signed monopole voltages and resistivities for

elongated electrode segments, as introduced below, takes care of the introduced complications very efficiently for all practical purposes. The new mathematical notation also greatly simplifies many equations used for point source electrodes in the process and therefore can be used to create simpler and more generalized software code for use with any geo-electric arrays. With the optimization introduced below for discretizing the effect of the elongated electrodes, only a little additional time is required for processing data collected using practical geo-electrical arrays containing elongated transmitter electrodes than for geo-electric arrays with just point source electrodes.

Rather than discretizing the effects of elongated electrodes finitely, Day-Lewis, *et.al.* (2006) give an analytical solution, derived by Timofeev, for the geometric factor of a dipole-dipole array containing linear electrodes. Unfortunately, the work of Timofeev is not sufficient for derivation of geo-electric inversion algorithms. Day-Lewis, *et.al.* (2006) also present a way of conducting geo-electric inversion using an approximation of elongated electrodes by point electrodes. They go on to quantify, and warn of, the significant errors that can be created by such inversion.

Definition of the new mathematics for dealing with linear electrodes is as follows.

3.5 Monopole Voltages

Each configuration in a geo-electric array contains source and sink transmitter electrodes and a pair of receiver electrodes between which voltage difference is measured. By considering just one current and one potential electrode at once, all formulae and calculations relevant to geo-electric arrays are simplified. Only one inter-electrode distance needs to be considered at once. The monopole voltage, defined by Davis, Greenhalgh and Merrick (1980), for electrodes on the surface of a homogeneous half space is given, in units of volts, by:

Monopole voltage for electrodes on the surface of a half space :

$$V = \frac{\rho I}{2\pi} \cdot \frac{1}{r} \qquad (1)$$

where:

ρ = resistivity in Ohm.m which is the inverse of σ which is electrical conductivity in Siemens/metre,

I = electrical current in amps, and

r = the distance between the transmitter and receiver electrodes.

Results for all current-potential electrode pairs are then combined using the principle of superposition (Merrick and O'Neill, 1984).

3.6 Signed monopole voltages

In order to sum monopole voltages together, they need to be signed as positive or negative. The sign of each monopole is either plus or minus unity depending on the product of the signs of the polarity of the electrodes included in each monopole. When signs of the electrodes are not known, arbitrary allocation is sufficient for determination of absolute value of the voltage difference between the receiver electrodes of a geo-electric array configuration. One transmitter electrode must, however, be allocated as positive and the other negative. The same is true for the receiver electrodes. The sign assigned to the receiver electrode may be determined by whether it is connected to the positive or negative terminal of its receiver. Normally this is chosen so as to measure positive voltages between electrodes.

3.7 Signed monopole voltages for elongated electrode segments

Included in the sign of each monopole voltage can be a fraction between 0 and 1. This permits the effects of elongated electrodes to be discretized into representative point electrode effects. This procedure creates notation that is independent of transmitted current. Assuming that current flux is constant over the whole equipotential surface of elongated electrodes, the size of the fraction attributed to each monopole equals the length

of the relevant transmitter electrode segment divided by the length of the entire elongated electrode. The sum of all the signed fractions for a quadrupole will equal zero. Only the effect of elongation of transmitter electrodes will be dealt with in this paper but the possibility of the use of this notation for combinations of elongated and even plate electrodes is readily apparent. Figure 3.1 is a schematic of the process of segmenting an elongated transmitter electrode.

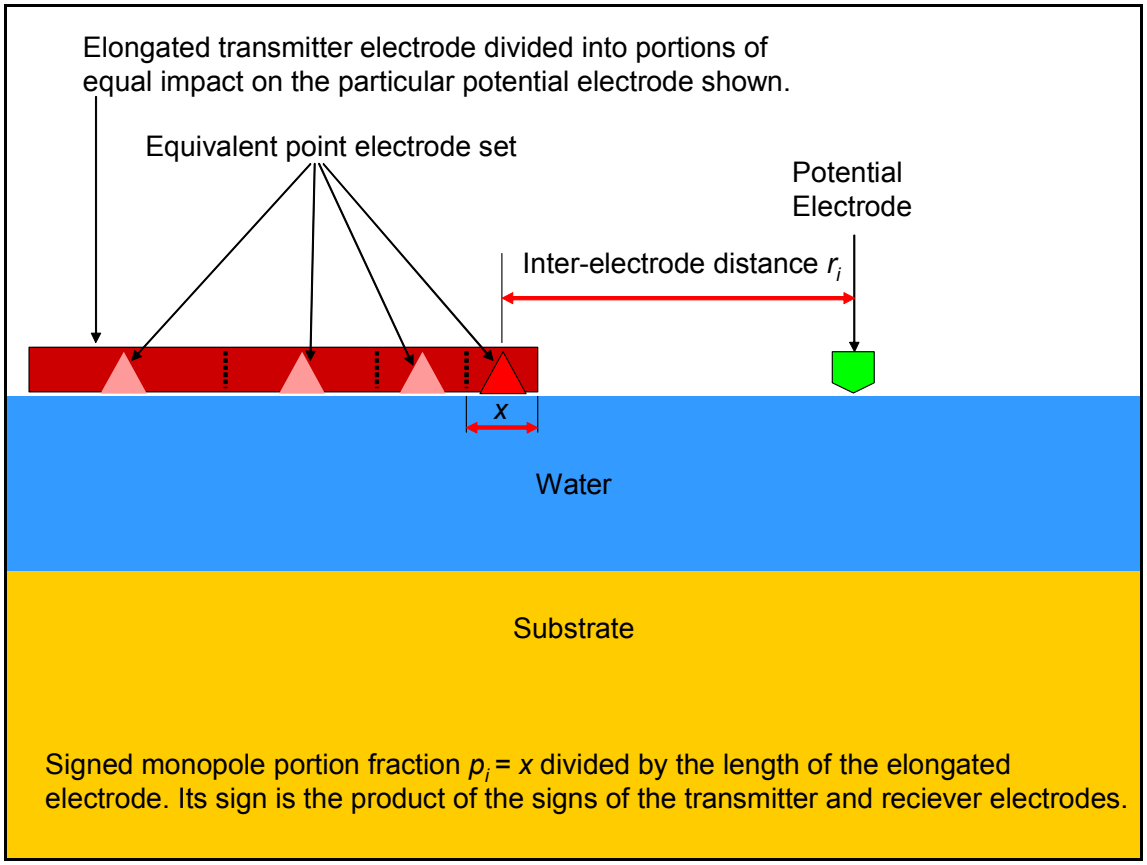

Figure 3.1 Transmitter electrode segmentation.

The voltage due to an individual signed monopole segment *i* in a geo-electric array on the surface of a homogeneous half space can be represented in units of volts by:

$$V_i = \frac{p_i}{r_i} \cdot \frac{I\rho}{2\pi} \tag{2}$$

where:

p_i = signed monopole portion (ie. fractional length) for monopole *i*, and
r_i = inter-electrode separation, in metres, between a transmitter electrode segment and a receiver electrode.

3.8 Geometric factors

Formulas for array configuration voltages and apparent resistivities group geometric effects together into a geometric factor which can be given for surface arrays in the new notation as:

$$\mathrm{K} = abs\left(\frac{2\pi}{\sum_{i=1}^{n} \frac{p_i}{r_i}} \right) \tag{4}$$

where:

K = geometric factor, and
n = number of monopoles (ie. the number of receiver electrode – transmitter electrode combinations).

Voltage difference and apparent resistivity of a surface array configuration is then given conventionally (Telford, 1990) by:

$$\Delta V = \frac{I\rho_a}{\mathrm{K}} \quad \text{and} \quad \rho_a = \frac{\mathrm{K}\Delta V}{I} \tag{4}$$

3.8.1 Comparison of the new and conventional ways of defining apparent resistivity

The logic and simplicity of the new notation may be easier to understand through observation of an example. The example of an α-Wenner array with an inter-electrode spacing of *a* is given. Using conventional notation, apparent resistivity would be defined as:

$$\rho_a = \frac{\Delta V}{I} abs\left(\frac{2\pi}{\frac{1}{r_{11}} + \frac{1}{r_{22}} - \frac{1}{r_{12}} - \frac{1}{r_{21}}} \right)$$

where:

$r_{11} = a$, $r_{22} = a$, $r_{12} = 2a$, and $r_{21} = 2a$

Using the new notation, apparent resistivity would be defined as:

$$\rho_a = \frac{\Delta V}{I} abs\left(\frac{2\pi}{\sum_{i=1}^{n} \frac{p_i}{r_i}} \right)$$

where:

n=4

$r_1 = a$, $r_2 = a$, $r_3 = 2a$, and $r_4 = 2a$

$p_1 = 1$, $p_2 = 1$, $p_3 = -1$, and $p_4 = -1$

When only dealing with α-Wenner array data, the new notation would not be of significant advantage, however, this example is given to show how the advantage of the new notation can become very significant when generalization is necessary and the complications of elaborate arrays need to be kept independent of inversion code.

3.9 Submerged arrays

Geometric factors for submerged arrays can be calculated similarly, after Daniels (1978), assuming a whole space but with images of two current sources above the surface. The

inter-electrode distances for those pseudo-sources then depend on the depth of the submerged array. The scenario can be observed in Figure 3-2.

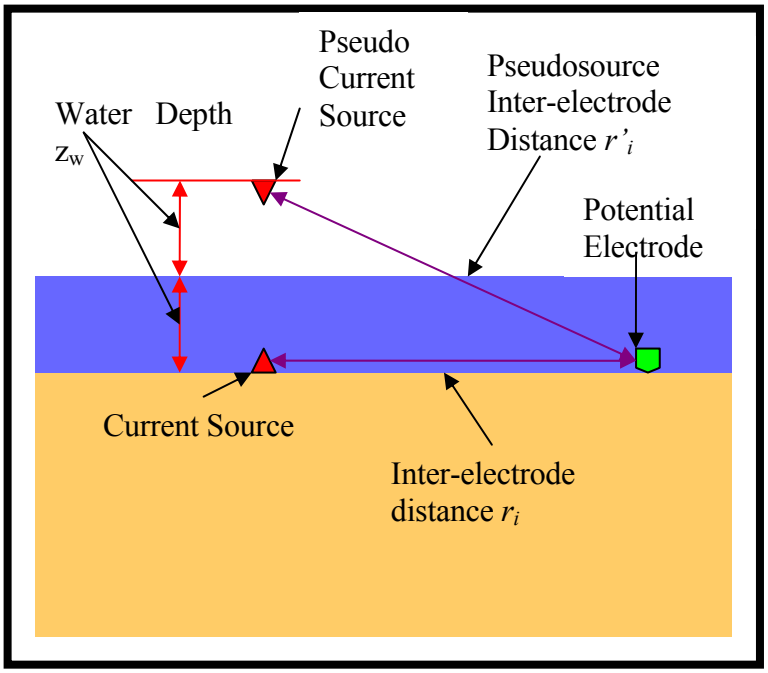

Figure 3.2 The concept of a pseudo-current source for mathematics for submerged arrays.

The inter-electrode distance to the pseudo-source is given by:

$$r'_i = \sqrt{r_i^2 + 4z_w^2} \tag{5}$$

where:

r'_i = *the inter-electrode distance to the pseudo-source, and*

z_w = *the water depth.*

The geometric factor for a submerged array then becomes:

$$K_{submerged} = \frac{4\pi}{\left(\sum_{i=1}^{n}\frac{p_i}{r_i} + \sum_{i=1}^{n}\frac{p_i}{r'_i}\right)} \tag{6}$$

In practice, apparent conductivities calculated using this geometric factor equation are of limited usefulness due to the prevalence of large contrasts between river/canal water and ground conductivities.

3.10 Signal Contribution Distributions

A homogeneous half space (or full space), can be divided up into a finite element grid of volume elements (or voxels) each with its own signal contribution to a geo-electric array. Roy and Apparao (1971) laid out the theory and it has been generalized (with resulting simplification) here using fractional signed monopole notation. For each voxel, the potential due to each current source is given by:

$$V(x,y,z) = \frac{\rho}{2\pi} \frac{I_C}{\sqrt{(x - x_C)^2 + y^2 + z^2}} \tag{7}$$

where:

x,y,z = rectangular co-ords of the half space (*z* positive downwards). For simplicity, the current electrodes are assumed to be on the line (*y=0, z=0*). One current electrode is normally used as the origin of the co-ordinate system,

V(x,y,z) = the voltage at the voxel situated at *x,y,z,*

Xc = the *x*-coordinate of the transmitter electrode, and

Ic = the signed current for each transmitter electrode portion (note that the sum of all *Ic* will sum to zero).

Roy and Apparao (1971) point out that the electric dipole moments of each voxel will be proportional to the electric field at each voxel times the voxel volume – ie.:

$$\overline{\mu} = \frac{1}{2\pi} \nabla V \cdot dxdydz \tag{8}$$

where:

$\mu(x,y,z)$ = the electric dipole moment of each voxel.

From there, they derive the voltage at each potential electrode resulting from the electric dipole moment of each voxel. The equation has been modified to a monopole equation here – ie.:

$$dV_P = (\vec{\mu} \cdot \nabla)\left(\frac{1}{\sqrt{(x - x_P)^2 + (y - y_P)^2 + z^2}}\right) \quad (9)$$

where:

x_P = the x – coordinate of the relevant receiver electrode and
y_P = the y – coordinate of the relevant receiver electrode.

Using the principle of superposition, the effect of all the current electrode/ receiver electrode portions can be combined. Because fractional signed monopole proportions combine signs of both the transmitter and receiver electrodes, the superposition can only be done at this stage, not earlier. The resulting formula for the signal coming from each signal contribution element, rewritten in the new notation is:

$$dV_{Surface} = \frac{\rho I}{4\pi^2} \cdot dz \left[\sum_{i=1}^{n} \frac{p_i \left\{ (x - x_{c_i})(x - x_{p_i}) + y(y - y_{p_i}) + z^2 \right\}}{\left\{ \left((x - x_{c_i})^2 + y^2 + z^2 \right) \left((x - x_{p_i})^2 + (y - y_{p_i})^2 + z^2 \right) \right\}^{3/2}} \right] \cdot dx \cdot dy \quad (10)$$

where:

x_{Ci}, y_{Ci} *(fixed as 0)*, x_{Pi} and y_{Pi} are the coordinates of the current and potential electrodes contributing to each fractional signed monopole voltage.

This equation can be extended to the case of a submerged array in a homogeneous half space by adding the variable h to represent the array depth (waterdepth) and using image theory as was done to calculate a geometric factor for a submerged array above. The constant of proportionality is halved as for the geometric factor equation. The resulting equation is:

$$dV_{Submerged} = \frac{\rho I}{8\pi^2} \cdot dz \left[\begin{array}{c} \sum_{i=1}^{n} \frac{p_i \left\{ \left(x - x_{c_i}\right)\left(x - x_{p_i}\right) + y\left(y - y_{p_i}\right) + \left(z - h\right)^2 \right\}}{\left\{ \left(\left(x - x_{c_i}\right)^2 + y^2 + \left(z - h\right)^2\right)\left(\left(x - x_{p_i}\right)^2 + \left(y - y_{p_i}\right)^2 + \left(z - h\right)^2\right) \right\}^{3/2}} + \\ \sum_{i=1}^{n} \frac{p_i \left\{ \left(x - x_{c_i}\right)\left(x - x_{p_i}\right) + y\left(y - y_{p_i}\right) + \left(z + h\right)\left(z - h\right) \right\}}{\left\{ \left(\left(x - x_{c_i}\right)^2 + y^2 + \left(z + h\right)^2\right)\left(\left(x - x_{p_i}\right)^2 + \left(y - y_{p_i}\right)^2 + \left(z - h\right)^2\right) \right\}^{3/2}} \end{array} \right] \cdot dx \cdot dy \tag{11}$$

where:

h = the waterdepth in metres.

3.11 Depth of Investigation Characteristic

Depth of investigation characteristic (DIC) gives geo-electric array sensitivity with respect to depth. It has been obtained by Roy and Apparao (1971) by integrating the last equation over the entire *xy* plane. It is normalized to create a Normalized DIC (NDIC) by dividing it by the total response of the halfspace (ie. DIC integrated with respect to z from zero to infinity). As with the geometric factor, the NDIC can be calculated using inter-electrode distances and signed proportions assigned to each inter-electrode distance.

3.11.1 Derivation of generalized normalized depth of investigation

Note: Comprehension of this derivation is not necessary for understanding the rest of this thesis and readers may skip to 3.11.2 if they wish.

The DIC definition of Roy and Apparao (1971) is as follows (Note that it is equally applicable to both submerged and surface arrays even though they did not consider submerged arrays):

$$DIC = \int_{x=y=-\infty}^{x=y=+\infty} dV_{P_1P_2} \tag{12}$$

Converting to fractional signed monopole notation we get:

$$DIC(z) = \sum_{i=1}^{n} \int_{x=y=-\infty}^{x=y=+\infty} dV_{p_i} \tag{13}$$

Note that the P_1P_2 subscript in the equation of Roy and Apparao (1971) represents the summed result between two potential electrodes while the p_i in the new equation represents the result just for each fractional signed monopole *i*.

Roy and Apparao (1971) give a general derivation and solution of a useful integral in an appendix using Fourier transform pairs. The integral and its solution is:

$$I(a,b,c,z)=\int_{x=y=-\infty}^{x=y=+\infty}\frac{x(x-a)+y(y-b)+z(z-c)}{\left(x^2+y^2+z^2\right)^{3/2}\left\{(x-a)^2+(y-b)^2+(z-c)^2\right\}^{3/2}}.dxdy$$

$$=\frac{4\pi(2z-c)}{\left\{a^2+b^2+(2z-c)^2\right\}^{3/2}}\ for(z-c)>0 \qquad (14)$$

$$and=0\ for(z-c)<0$$

By substituting x-x_{ci} for x, x_{pi} - x_{ci} for a, and y_{pi} for b in this standard integral, it can be seen that the DIC for surface based geo-electric arrays can be found:

$$DIC(z)_{Surface}=\frac{\rho I}{4\pi^2}\cdot dz\cdot\sum_{i=1}^{n}\frac{p_i\cdot 8\pi z}{\left((x_{P_i}-x_{C_i})^2+4z^2\right)^{3/2}} \qquad (15)$$

By substituting:

$$r_i=x_{P_i}-x_{C_i}$$

and moving constant terms out of the summed part of the equation and multiplying by the sign of the geometric factor, in order to get the sign of the DIC correct, we get a final formula for DIC:

$$DIC(z)_{Surface}=\mathrm{sgn}(\sum_{i=1}^{n}\frac{p_i}{r_i})\cdot\frac{2\rho Iz}{\pi}\cdot dz\cdot\sum_{i=1}^{n}\frac{p_i}{\left(r_i^2+4z^2\right)^{3/2}} \qquad (16)$$

DIC is converted to NDIC by integrating from the surface to infinite depth – the equivalent of this is division by the half space voltage calculated previously. When DIC is

normalized to create NDIC, the sign correction can be removed because signs of the DIC and the half space response cancel out.

3.11.2 Normalized depth of investigation characteristic

The formula for NDIC of any array lying on the surface of a half space is:

$$NDIC(z)_{Surface} = dz.4z \frac{\sum_{i=1}^{n} \frac{p_i}{\left(r_i^2 + 4z^2\right)^{3/2}}}{\sum_{i=1}^{n} \frac{p_i}{r_i}} \qquad (17)$$

where:

- z = depth in metres (a range of 10^{-2} to 10^{3} can be sampled as this effectively covers the depth of investigation of most arrays),
- dz = a small increment in z (increments of 10^{n} have been used where n=0.001),
- $\sum_{i=1}^{n}$ = the set of interelectrode distances and proportions. It simplifies to i=1 to 4 for standard 4 point electrode arrays,
- r_i = inter-electrode distance *i,* and
- p_i = signed proportion for inter-electrode distance *i.*

Even though this generalized equation facilitates a great variety of much more complicated array configurations than those presented by Roy and Apparao (1971), it can be seen that it is simpler and more regularly structured for computational application.

3.12 Cumulative normalized depth of investigation characteristic

Merrick (1997) gives a cumulative NDIC function for linear arrays which can be extended to a generalized array in the same way as the NDIC function to give the following result:

$$CumNDIC(z)_{Surface} = dz.4z\frac{\sum_{i=1}^{n}\frac{p_i}{\sqrt{r_i^2+4z^2}}}{\sum_{i=1}^{n}\frac{p_i}{r_i}} \quad (18)$$

3.13 Effective Depths

Effective depth is the depth above which 50% of signal contribution effect is derived (Edwards, 1977). Effective depths over homogeneous earth are calculated by accumulating normalized depth of investigation characteristic curves up to (or down to) the depth where the area under the curve equals 0.5. Effective depths are estimated by iterating *dz* in the following formula until it is solved for $Z_{effective}$ or by picking the ordinate off the point on a CumNDIC graph with a CumNDIC of 0.5:

$$0.5 = \int_{z=0}^{z_{effective}} NDIC(z).dz \quad (19)$$

Similarly, **10% resolution** can be calculated by subtracting z for 0.5 from z for 0.6 and **extended effective depth** can be calculated by summing to 0.9 (see Merrick 1997). '10% resolution' is proportional to the minimum thickness of layer of a particular conductivity contrast that can be detected right at the effective depth of a particular quadrupole. 'Extended effective depth' is a good indication of the maximum depth at which a particular quadrupole can detect conductivity contrast. Detection limits also depend, however on noise levels, other sources of heterogeneity and conductivity contrast.

3.14 Calculation of DIC and NDIC curves for cases of a 2 layered halfspace.

Geo-electric array NDIC varies according to layering in the ground. Put another way, if conductivity contrast between various layers in the ground varies more than an infinitesimal amount, then geo-electric NDIC curves will also change. It is interesting to note here, for comparison, that frequency domain electromagnetic NDIC, assuming the low induction number approximation, does not vary when conductivity of layers in the ground vary. Using reflection coefficients and image theory, geo-electric NDIC for the two layer halfspace case can be calculated.

Roy and Apparao (1971) show how to calculate NDIC for two layer cases. Recapitulating - A layer of thickness h and resistivity ρ_1 rests over a halfspace of resistivity ρ_2. For a current electrode +I at (0,0,0), the potentials V_1 and V_2 at any point (x,y,z) for $0 \le z \le h$ and $z \ge h$ are:

$$V_1 = \frac{\rho_1 I}{2\pi}\left[\frac{1}{\sqrt{x^2+y^2+z^2}} + \sum_{m=1}^{\infty}\left\{\frac{k^m}{\sqrt{x^2+y^2+(z+2mh)^2}} + \frac{k^m}{\sqrt{x^2+y^2+(z-2mh)^2}}\right\}\right] \tag{20}$$

$$0 \le z \le h,$$

and

$$V_2 = \frac{\rho_1 I}{2\pi}\cdot(1+k)\cdot\left[\frac{1}{\sqrt{x^2+y^2+z^2}} + \sum_{m=1}^{\infty}\left\{\frac{k^m}{\sqrt{x^2+y^2+(z+2mh)^2}}\right\}\right] \tag{21}$$

$$z \ge h,$$

where the reflection coefficient k is given by:

$$k = \frac{\rho_2 - \rho_1}{\rho_2 + \rho_1} \tag{22}$$

Proceeding in the way shown by Roy and Apparao (1971) using the standard integral given before, but with the new simple generalized notation, we can show that, for $z \le h$:

$$DIC(z)_{2\,Layer,\,z\le h} = \frac{\rho_1 I}{2\pi}\cdot dz \cdot \sum_{i=1}^{n} p_i\left[\frac{4z}{\left(r_i^2+4z^2\right)^{3/2}} + \sum_{m=1}^{\infty}\frac{k^m(2z+2mh)}{\left(r_i^2+(2z+2mh)^2\right)^{3/2}}\right] \tag{23}$$

and for $z \ge h$:

$$DIC(z)_{2\,Layer,\,z\ge h} = \frac{\rho_1 I}{2\pi}\cdot dz \cdot (1+k)\cdot \sum_{i=1}^{n} p_i\left[\frac{4z}{\left(r_i^2+4z^2\right)^{3/2}} + \sum_{m=1}^{\infty}\frac{k^m(2z+2mh)}{\left(r_i^2+(2z+2mh)^2\right)^{3/2}}\right] \tag{24}$$

If DIC is not normalized, it should have its sign corrected by multiplication with the sign of the homogeneous half space geometric factor – i.e.: $DICSignCorrection = \mathrm{sgn}(\sum_{i=1}^{n}\frac{p_i}{r_i})$

Normalization of two layer DIC can be achieved by integrating the DIC from depths of zero to infinity.

The two layer DIC formula includes an infinite series that may be approximated by a finite series. In order to determine the effect of truncating the series, various truncations were conducted on a model and the differences in the normalization factor noted. The model was of 100:1 contrast with a configuration with an effective depth equal to the 1st layer depth. With two terms, a 3% error in area under the curve was noted; with four terms, 0.5%; with six terms, 0.1%; compared to a reference of 10 terms, assumed to be in error by 0.0%.

3.15 Multiple horizontal layer models

Signed segmented monopole notation can be used also in multiple layer model calculations. For multiple layer modelling, image theory presented for the two-layer case above becomes excessively complicated and slow. As a result, modelling of multiple layers is done using Bessel and transform functions as explained here.

The fundamental relation for a point source of current on the surface of a half-space is given by O'Neill and Merrick (1984) as:

$$V(r) = \frac{I}{2\pi}\int_0^\infty T(\lambda) J_0(\lambda r) d\lambda \qquad (25)$$

where:

T = resistivity transform in the horizontal plane containing the electrode array,
J_0 = Bessel function of order zero,
λ = an integration constant, and
r = the distance from the point source.
The integral is solved using convolution and digital filters (O'Neill and Merrick, 1984).

Recall that apparent resistivity is the resistivity a homogeneous earth that would give the same response. Apparent resistivity for the layered model can then be calculated by summing signed fractional monopole voltages as follows:

$$\rho_{apparent} = K \cdot \frac{\sum_{i=1}^{n} p_i \cdot V(r_i)}{I} \tag{26}$$

Where $V(r_i)$ is the voltage at the surface of a layered earth due to monopole i (see equation 25).

Multiple layer forward modelling using transform functions will be further explained in Chapter 5.

3.16 Optimal segmentation of elongated transmitter electrodes of finite length

The effect of elongated electrodes can be discretized by replacing inter-electrode distances of monopoles in all equations with fractionally weighted sets of inter-electrode distances that split the long current electrode up into appropriately sized segments that can be treated as point sources. Each is weighted by its fraction of the total length of the electrode. Potential electrodes that are a long distance away from the linear current electrodes will be able to treat the linear electrode as a point source. For closer receiver electrodes, the elongated transmitter electrode needs to be divided into just enough parts to give the required level of accuracy in calculations. Closer parts of the linear electrode will have greater effect on the receiver electrode and will therefore need to be divided into smaller parts. An algorithm for choosing appropriate portion sizes in linear or moderately curved electrode arrays is as follows:

- Calculate the length of each successive portion of the electrode using:

$$p_i = \left(r + \sum_{j=0}^{i-1} p_j \right) c(1+c)^2 \tag{27}$$

where:

pi = portion length of electrode portion i,

p_0 = zero (initial condition),

r = inter-electrode distance for the closest parts of the electrodes, and

c = a constant determining how finely the linear electrode should be discretized. A value of about 0.25 is recommended (smaller for more

precise results). Determination of acceptable values of c is conducted in the Chapter Four.

- Add the portion to the sum of portions (initially zero),
- Determine if the sum of portions is longer than the electrode,
- Repeat last two steps until the length of the electrode < sum of portions,
- Equally compress portions to fit electrode length exactly,
- Make an array of inter-electrode distances for each of the portions,
- Normalize the portions by the total electrode length, and
- Multiply the portions by the sign (1 or -1) attributed to the equivalent non-discretized inter-electrode separation.

This algorithm assumes that current flux is constant across the entire equipotential surface of the elongated electrode. Linear receiver electrodes are probably only useful at great distances from transmitter electrodes where they can be considered as point sources. In this scenario, segmentation of them is not necessary. If they are used near a transmitter electrode they will also distort the electric field they are trying to measure thus making theory presented here invalid. The segmentation equation has a second purpose in that it can be used to determine what length of receiver electrode will be acceptable at each position in an array if it must be assumed to be a point source.

3.17 Conclusion

Traditional geo-electric notation utilizes series of monopole or more complex terms in unnessesarily complex, and often restrictive, algorithms and formulae. A notation is possible that permits summing of signed monopole voltages to give quadrupole voltages and apparent resistivities. Should the signed monopole voltages contain a fraction term, then they can readily accommodate quadrupoles containing elongated or even plate electrodes. With such a notation, it is possible to completely separate geo-electric array complexity from apparent resistivity formulae, forward modelling and inversion algorithms, normalized depth of investigation formulae, effective depth formulae and signal contribution element formulae. Such separation readily accommodates object oriented programming of geo-electric software.

CHAPTER 4 - EXPONENTIAL BIPOLE ARRAYS.

4.1 Introduction

The last chapter presented mathematics suitable for evaluating and designing geo-electric arrays. In this chapter, the design of a new type of array and evaluation and comparison of numerous geo-electric arrays will be presented using graphs generated using the mathematics laid out in the last chapter.

Waterborne geo-electric imaging has typically been conducted using many of the same parameters and innovations as used for ground based surveys. This chapter aims to demonstrate new parameters and innovations suited to waterborne imaging. Towed geo-electric array design must optimize a balance of signal strength maximization, exploration depth resolution, weight and drag minimization, crosstalk and current leakage minimization and simple, minimal response to three dimensional heterogeneity. Various Exponential Bipole Array Configurations were developed in order to facilitate this optimization.

4.2 Definitions of Exponential Bipole Arrays

A bipole is set of two electrodes of opposite polarity and may be compared to a dipole which is a set of two electrodes of opposite polarity separated infinitesimally. An exponential bipole (XB) array may be defined as a collinear array of two transmitter electrodes followed by receiver electrodes spaced exponentially from the end of the second transmitter electrode. Consecutive receiver electrodes are used in pairs along with the transmitter electrodes in order to measure electrical conductivity at approximately exponentially spaced depths. A more specific geo-electric array configuration ideally suited to towed surveying may be called, for want of a simple descriptive name, the Allen Exponential Bipole (AXB) Array. It is an exponential bipole array which may have elongated, rather than point, transmitter electrodes. Receiver electrode spacing is in reference to the end of the elongated electrode, not its midpoint. An example is presented in Figure 4-1. These arrays are a refinement of the pole-multidipole array of Merrick (1974).

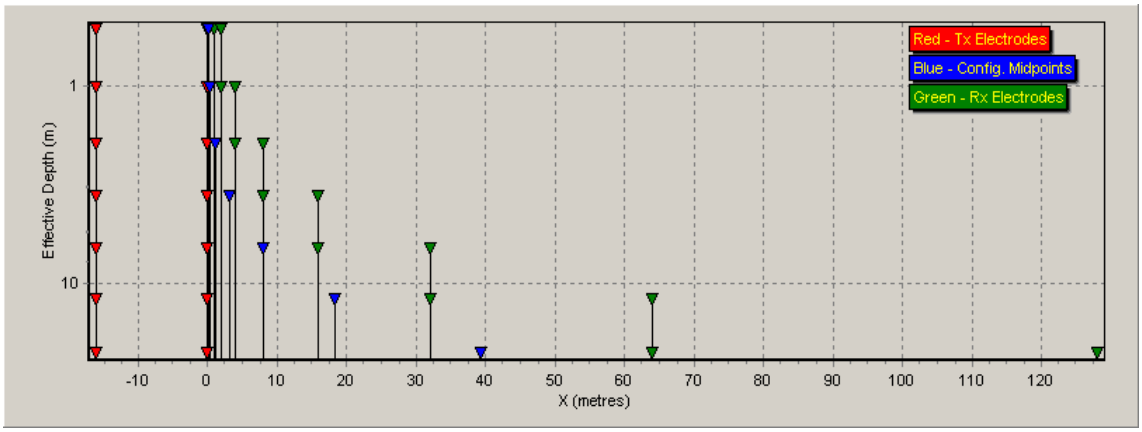

Figure 4.1 Sample 144m Exponential Bipole array electrode configurations plotted at their respective effective depths (calculated using equation 19).

XB arrays differ from Inverse Schlumberger arrays, which also have exponentially spaced receiver electrodes in that all the receiver electrode pairs are on one side of the transmitter electrodes, rather than straddling them. This difference results in XB arrays being much more focussed laterally, shorter for the same depth of investigation, and easier to tow due to most of the electrodes being near the towing device rather than the centre of the array.

A balance of several parameters can be optimized when designing arrays for surface water / groundwater interaction investigation. Discussion of the new array configuration and the most important of those parameters follows.

4.3 Depth Resolution

The nature of potential field geophysics results in an logarithmic change of resolution with respect to depth. In order to make best use of available resolution for a given noise level, geo-electric arrays need to sample depth in approximately exponential increments. Traditional arrays such as the Schlumberger and Wenner arrays do this as do AXB Arrays (see Figure 4-1). In contrast, dipole-dipole arrays sample depth in an almost linear manner. This contrast is evident from comparison of Figures 4-2 and 4-3. Usually, most depth resolution is required just under the base of surface water bodies rather than at the surface of them. Submersible geo-electric arrays facilitate this type of depth resolution distribution better than floating arrays.

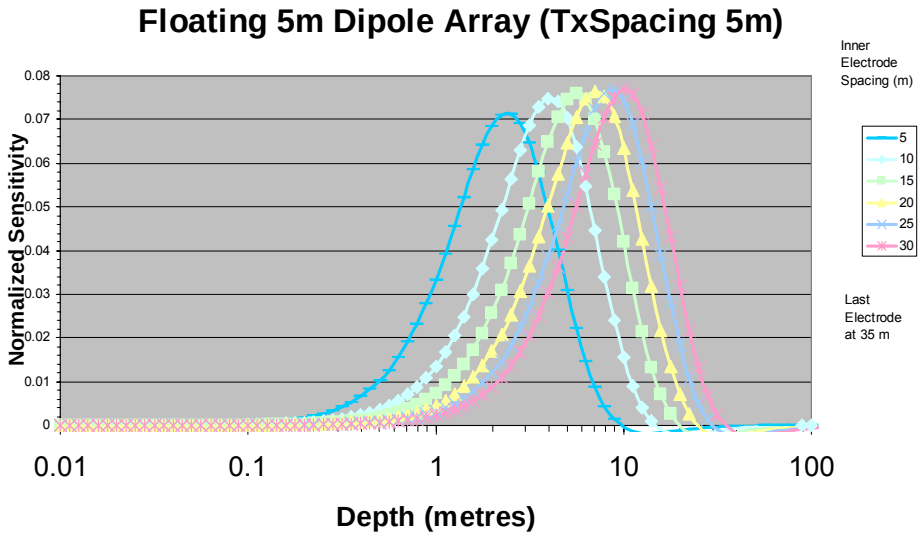

Figure 4.2 Distribution of signal with respect to depth (calculated using equation 17) for a Dipole-Dipole Array. Note that a small range of depths is sampled very well. In practice, the deeper sampling configurations rarely receive enough signal to be of much use.

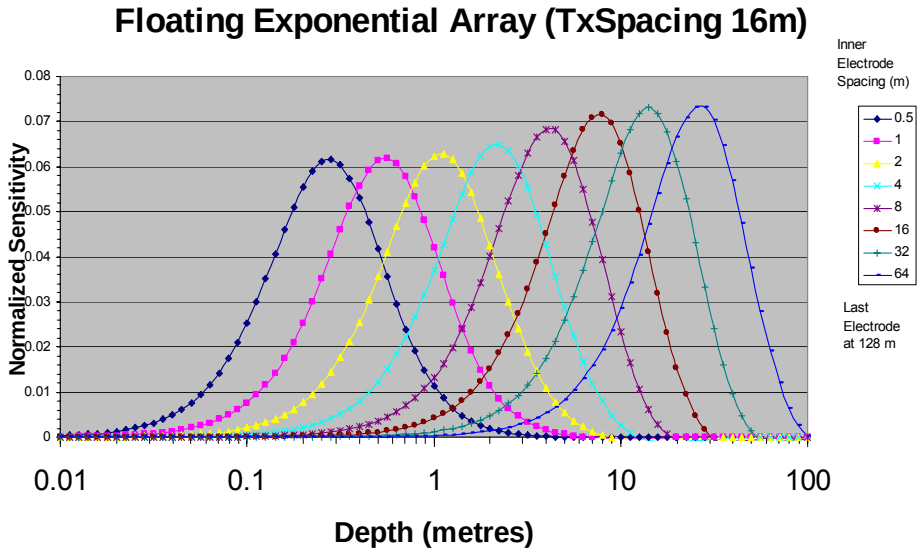

Figure 4.3 Distribution of signal with respect to depth (calculated using equation 17) for an Allen Exponential Bipole Array. In contrast to the Dipole Dipole array, distribution of sampled depths is very even.

4.4 Signal Strength

As a result of towed arrays transmitting from two electrodes while receiving simultaneously from many electrode pairs, stacking duration must be the same for all pairs regardless of signal strength. An optimal array for towing would therefore deliver good signal and minimal decay of signal strength with respect to sampled depth. A graph of signal strength versus effective depth for various arrays is presented in Figure 4-4. Wenner and some Schlumberger arrays produce the strongest signal while the Dipole Dipole array produces the weakest and fastest decaying signal strength of all commonly used arrays. Should linear transmitter electrodes be used in an Allen Exponential Bipole array, then contact resistance can be reduced, greatly increasing signal strength particularly at more distant electrodes.

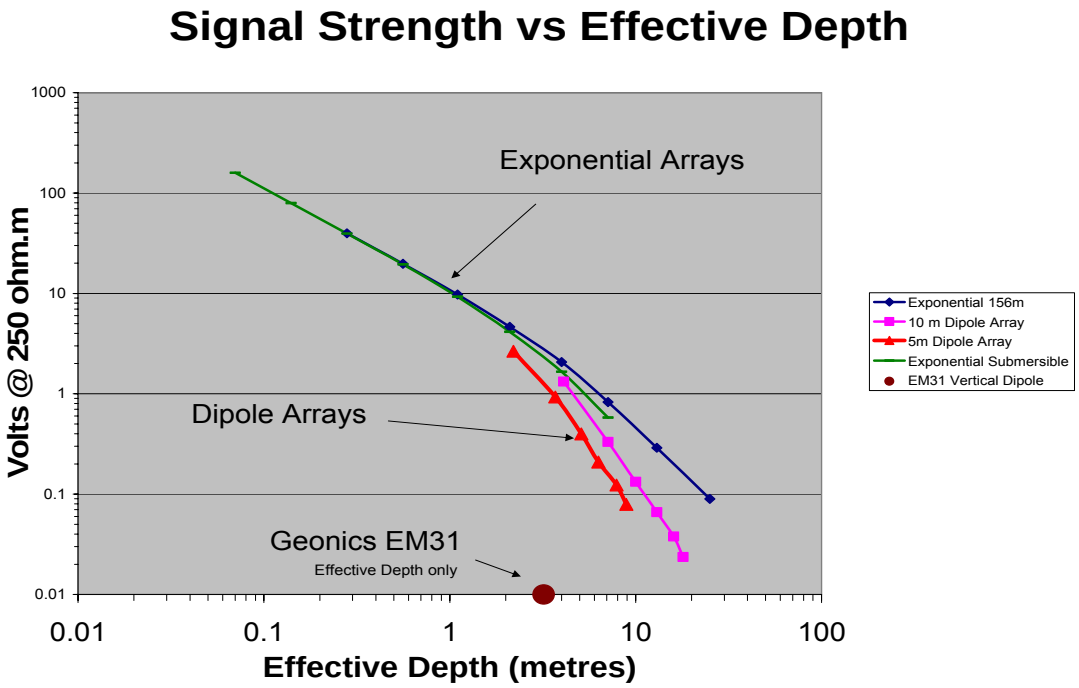

Figure 4.4 Signal strength (eqn. 4) versus effective depth (eqn. 19) for various arrays over a halfspace with resistivity of 250 ohm.m. The 156m exponential bipole array has a transmitter electrode separation of 16 metres and receiver electrodes spaced at 2^n where n ranges from -1 to 7. The exponential submersible array has a transmitter electrode separation of 8 metres and receiver electrodes spaced at 2^n where n ranges from -3 to 5. Geonics EM31 vertical dipole effective depth has been included simply for convenient comparison.

4.5 Weight, drag, crosstalk and current leakage

The reason that the Allen Exponential Bipole Array has been utilized in preference to Wenner and Inverse Schlumberger configurations, which have higher signal strengths, is that the heavy transmitter electrodes can be placed close to the towing device and that the number of wires needed in the cable decreases rapidly with distance from the second transmitter electrode. This means that the cross section area of the cable (and float if installed) may quickly diminish as it passes away from the towing device. A much more manageable cable weight results. Streamlining of the cable also becomes possible as a result. This reduces cable drag which in turn makes the cable more navigable because a cable with high drag, particularly at a great distance from the towing device, will tend to slew sideways rather than follow its course when towed along meandering watercourses. Crosstalk and current leakage problems are very difficult to manage in cables designed for use in water. In the Allen Exponential Bipole array, the lengths of high voltage wires are minimized resulting in less potential for current leakage and crosstalk problems.

4.6 Simple minimal response to three dimensional heterogeneity

The effect of three dimensional heterogeneity on various arrays can be studied using signal contribution element images. Such images show that most signal is contributed from parts of the substrate near closely spaced transmitter - receiver electrode pairs. Therefore the ideal array for simplifying and minimizing the effect of three dimensional heterogeneity is the theoretical Pole - Pole array configuration which has two electrodes at infinity. The Exponential Bipole Array has only one closely spaced pair in each of the shallower quadrupoles and approximates the Pole–Pole configuration. Midpoint of response of each quadrupole can be calculated using signal contribution element analysis. Software called HydroGeoImager (Allen 2006) has a facility which allows users to generate signal contribution sections for any array configuration in any plane parallel to the xz plane (non-curving arrays are entirely within this plane by default). Figure 4-5 presents a signal contribution element image for just one quadrupole in a submerged AXB array. Observing that the electrodes have been posted at the effective depth of the quadrupole (not the actual vertical position of the electrodes), one can see how the sensitivity of this configuration is focused only around the substrate around the central two electrodes. The footprint (ie. the horizontal extent of high sensitivity) of the

quadrupole can be considered to be closely focused around the inner transmitter and receiver electrodes. In comparison, the footprints of Schlumberger and Wenner configurations are distributed around the entirety of each quadrupole. Figure 4-6 presents a signal contribution element image of a Wenner array, this time on the surface. In Figure 4-1 the midpoints of response of all the quadrupoles of an AXB array are displayed, as blue triangles, at their respective effective depths. The midpoints stack almost underneath each other near the surface but skew away from the transmitter electrodes as effective depth is increased. This conformant response of all quadrupoles in the array is critical for 1D inversion in the presence of 3D near surface heterogeneities. It greatly reduces the severity of horizontal smoothing that must be conducted prior to inversion.

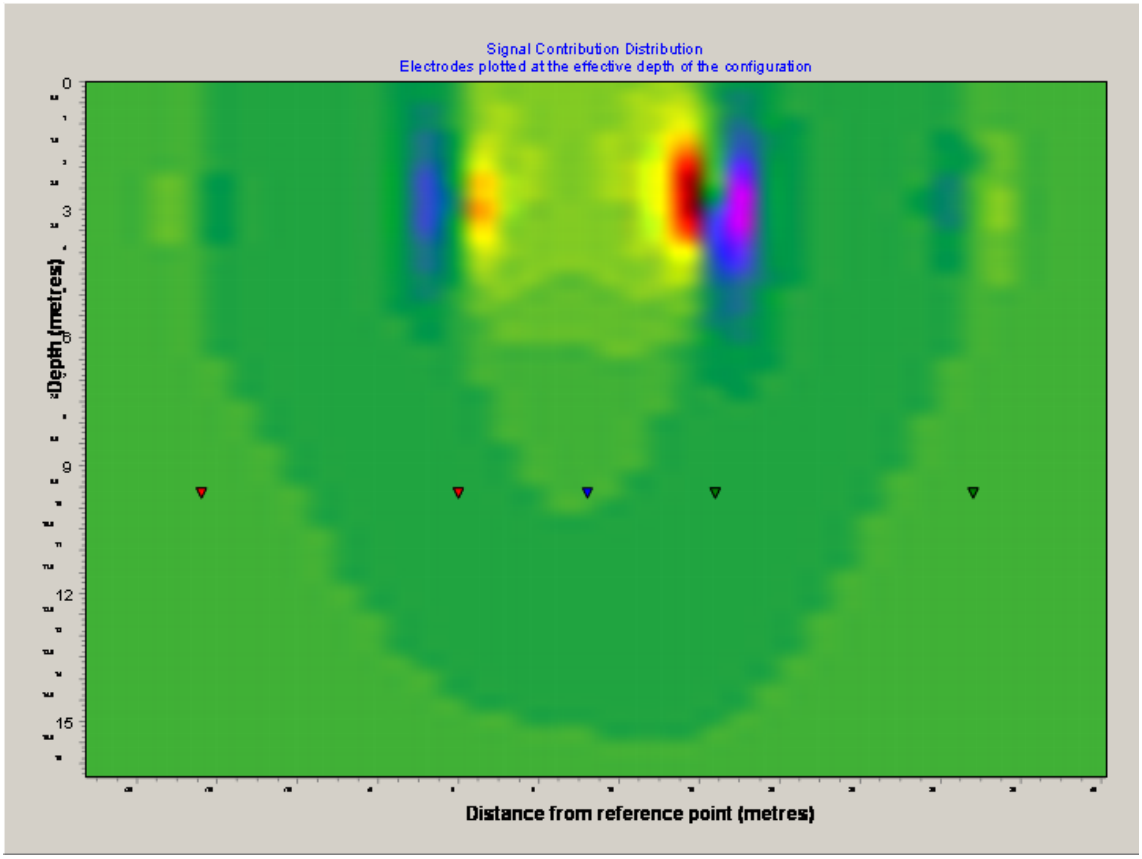

Figure 4.5 Signal contribution elements (eqn. 11) for the quadrupole shown at its effective depth (Triangles; Red=Tx, Green=Rx, Blue=Midpoint). The array is submerged 3m. The SCE image is in a plane 1m off the plane of the array because imaging on the plane of the array causes poor colour distribution. The slight asymmetry is a result of use of linear electrodes. Red indicates positive contribution. Observe how strong responses to 3D heterogeneities will only occur in the vicinity of the two inner electrodes.

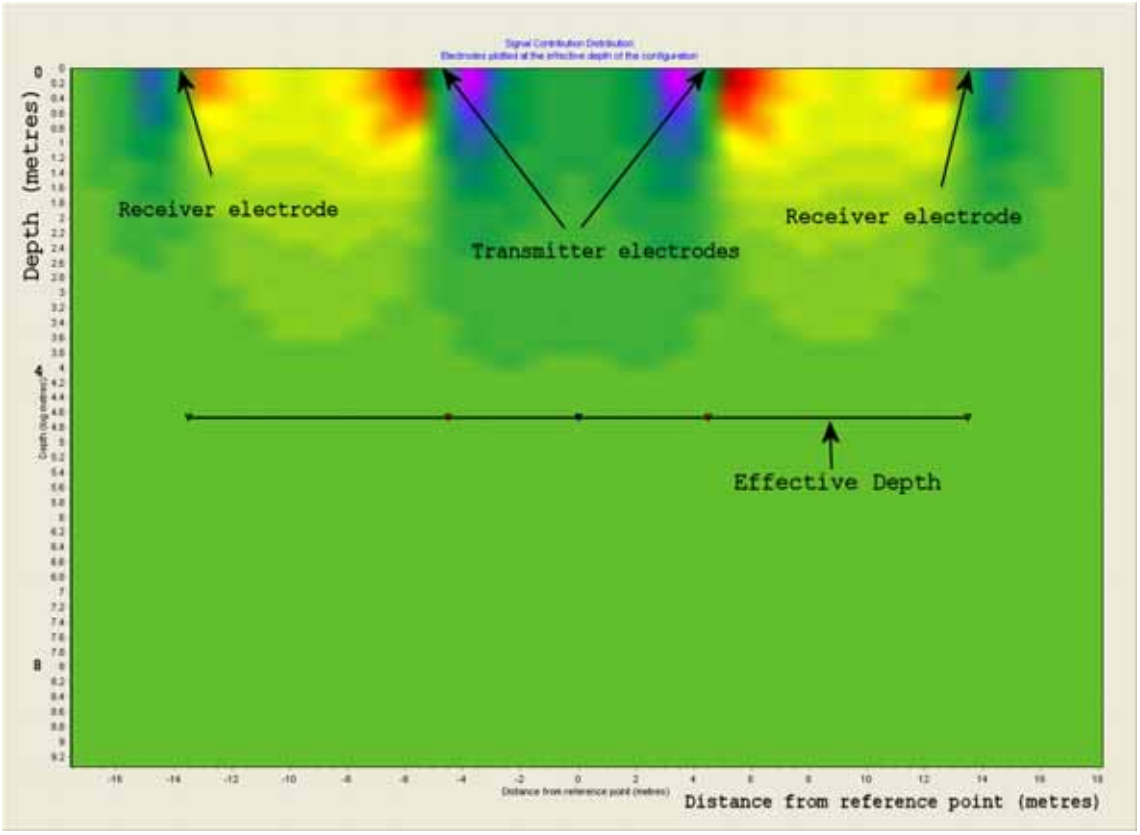

Figure 4.6 Signal contribution elements (eqn. 11) for a Wenner array on the surface with a = 9 metres. The SCE image is in a plane 1m off the plane of the array because imaging on the plane of the array causes poor colour distribution. Compare with Figure 4.5 and observe that this array is sensitive to 3D heterogeneity near all of its electrodes, not just the inner two. Red indicates positive contribution. Purple/blue indicates negative contribution.

4.7 Power consumption, electrode length and processing speed

Determination of an appropriate value for the segmentation constant c has been conducted by graphing a set of signal to noise ratio versus effective depth curves for a particular AXB array and various values of c. The results are presented in Figure 4-7. It can be observed that a reasonable degree of accuracy of approximation is attained once the value of c is reduced to 0.3 where the approximation is seen to be in error by only a few percent. At this value of c, the linear transmitter electrode of the closest transmitter/receiver pair only needs to be segmented into a few portions even though it is four times as long as its separation from the closest receiver electrode. Considering that near surface inhomogeneities cause large errors in the voltages at the very proximal

receiver electrodes for which segmentation errors also are largest, segmentation errors of a few percent are generally acceptable.

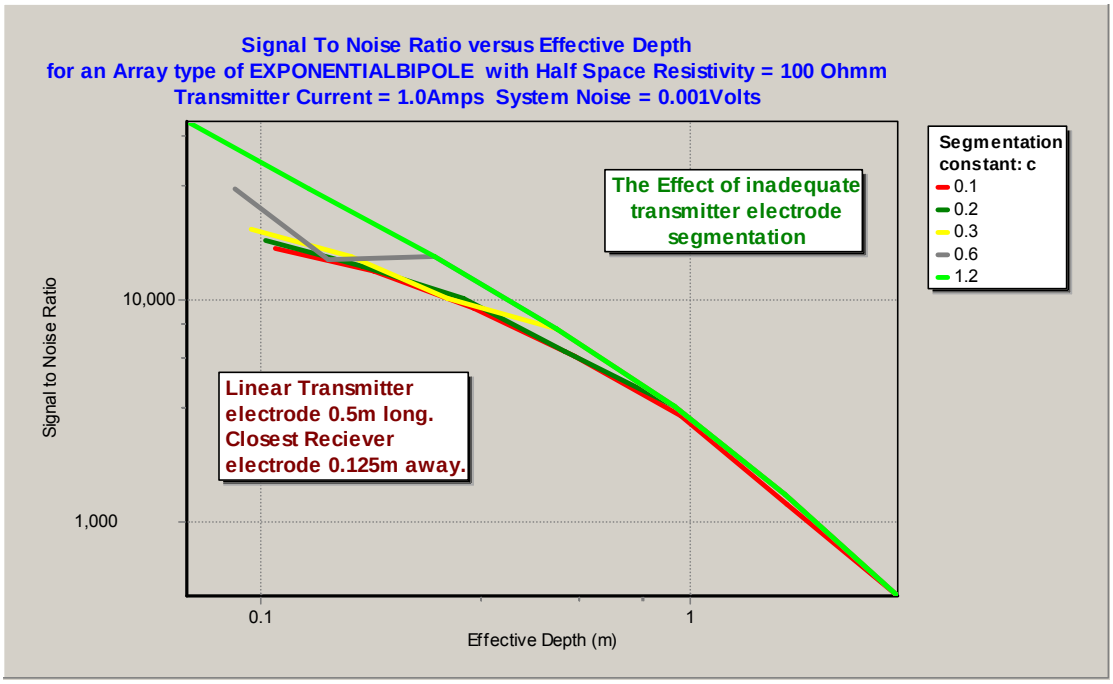

Figure 4.7 The effect of point source approximation of elongated electrodes using segmentation of transmitter electrodes with various segmentation constants (eqn. 27). The curve for c=1.2 is the equivalent point source geo-electric array solution. The curve for c=0.1 can be considered as a standard to which all the other curves should match. The curve for c=0.3 can be seen to match adequately for most surveys where near surface inhomogeneities typically disturb data by a few percent. Signal to noise ratio (eqn. 4) is plotted against effective depth (eqn. 19) to reveal approximation validity.

Processing speed can be reduced greatly if segmentation is conducted too finely, particularly if transmitter electrode lengths greatly exceed transmitter electrode to receiver electrode separation distances. However, Figure 4-8 shows that a segmentation constant of 0.3 for an array with the closest receiver electrode at ¼ of the transmitter electrode length would only increase data processing duration by 1.3 times that required for an equivalent point electrode array. With current readily available computational power (3.2 GHz Pentium 4) this is generally negligible while the advantages in survey performance and efficiency can be great.

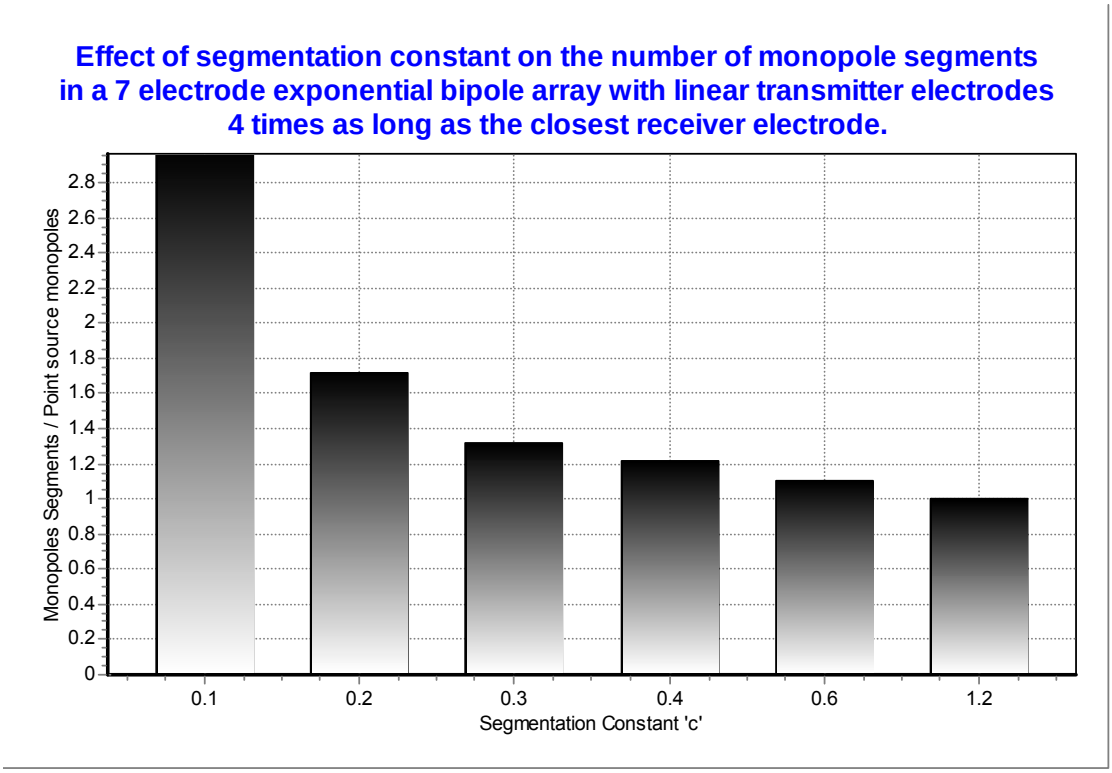

Figure 4.8 Increase in processing time with respect to segmentation constant 'c' (eqn. 27) for a 7 electrode exponential bipole array with linear transmitter electrodes 4 times as long as the distance between one transmitter electrode and the closest receiver electrode.

4.8 Floating array curvature effects

For simulation and other purposes a form within the program HydroGeoImager (Allen, 2006) is provided for entering exponential bipole bipole arrays such as the floating arrays used in this thesis. Because the array can curve around meandering rivers, provision for array curvature is provided on the form. Note that actual survey array configurations are not simple curves but are recorded as part of the survey path. The curvature affects the normalized depth of investigation curves (NDICs), geometric factors, effective depths and inversion. The effect is insignificant until curvature becomes tight. This is because the receiver bipoles of a curved array remain aligned near parallel to current flow lines eminating from the end of the transmitter bipole until curvature becomes tight.

Inter-electrode distances can be calculated for curved arrays just as they can for straight arrays. Then the NDICs, effective depths, geometric factors and inversion all can be

calculated the same way as for straight arrays. For field data, these distances are simply calculated using co-ordinate differences. For simulation purposes, they can be calculated using a radius of curvature as follows (see Figure 4-9 for clarification):

- Calculate the interelectrode distances as if the array was straight,
- Use the results and a radius of curvature to calculate true inter-electrode distances using the formula:

$$R_{CurvedArray} = 2r \sin\left(\frac{R_{StraightArray}}{2r}\right)$$

where:

r = radius of curvature of the array and Sine is calculated in radians,
R=Inter- electrode distance.

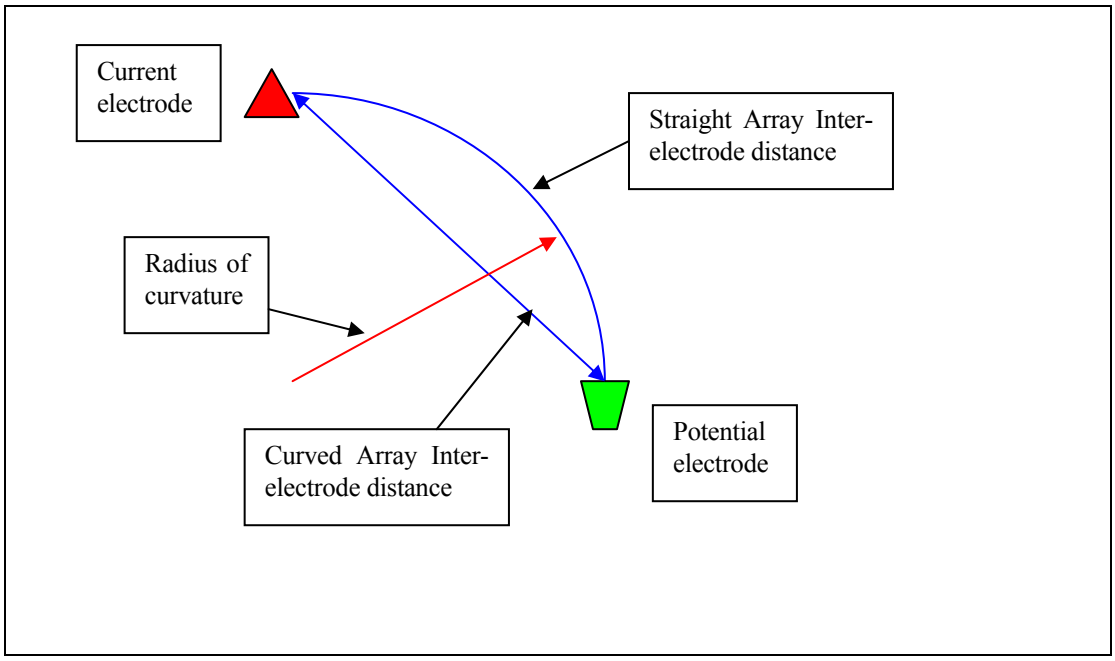

Figure 4.9 A schematic showing the effect of array curvature on a monopole voltage.

4.9 How much array curvature can be tolerated in field operations?

It is possible to generalize all equations to take into account array curvature using the recorded path of any towed array. Theoretical investigation of geometric factors and effective depths, given below, demonstrates however that this is an inappropriate waste of processing time. A better procedure is to add a data filter to the processing algorithm that totally rejects soundings with more than an acceptable amount of curvature. This is because the curved array performance very closely approximates that of a straight array until its length is curved around nearly 90 degrees of arc. When the array becomes curved more tightly than 45˚ of arc, it becomes extremely sensitive to positioning errors, noise and near surface and lateral inhomogeneities. Since none of these variables are measurable, data from such highly curved arrays should simply be discarded.

Analysis of the effect of array curvature on geometric factor and effective depth is given in Figure 4-10 using the response of curved arrays to a homogeneous half space.

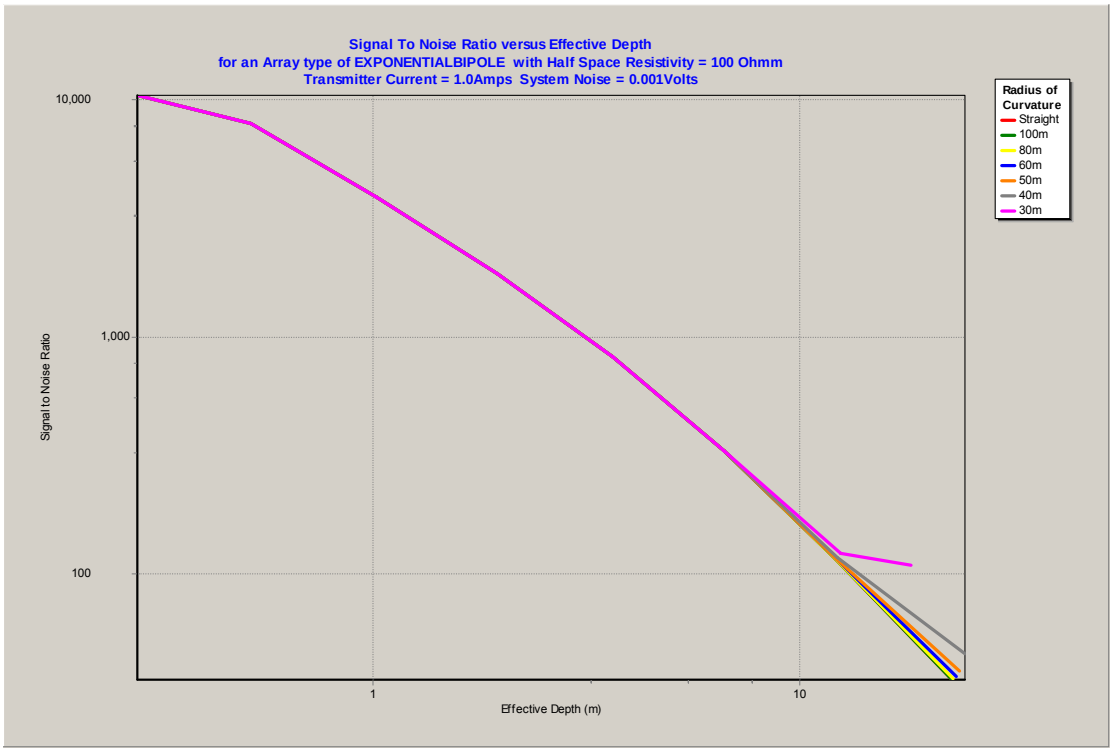

Figure 4.10 The effect of array curvature on the signal to noise ratio (which is proportional to the geometric factor – eqn. 3) and effective depth (eqn. 19) for an exponential bipole array with a Tx electrode separation of 16m and receiver electrodes from 0.5m to 128m from one Tx electrode in a homogeneous earth.

When surveying around bends in canals and rivers, the lateral effect of the wall of the canal can be very large. The effect is exhasebated in many canal cases by salt concentration in the banks caused by evapo-transpiration of seeping canal water. Chapter 11 discusses this situation.

4.10 The effect of variation of parameters of AXB arrays

Figure 4-11 shows the effect of lengthening the transmitter electrodes in an exponential bipole array. As the transmitter electrodes are lengthened, for constant current injection, signal level at the greatest effective depths does not vary but the problematic high signal levels obtained at shallow effective depths are reduced. Of course, with a constant voltage transmitter, current would actually increase as the length of the transmitter electrodes increases and signal levels would rise proportionally.

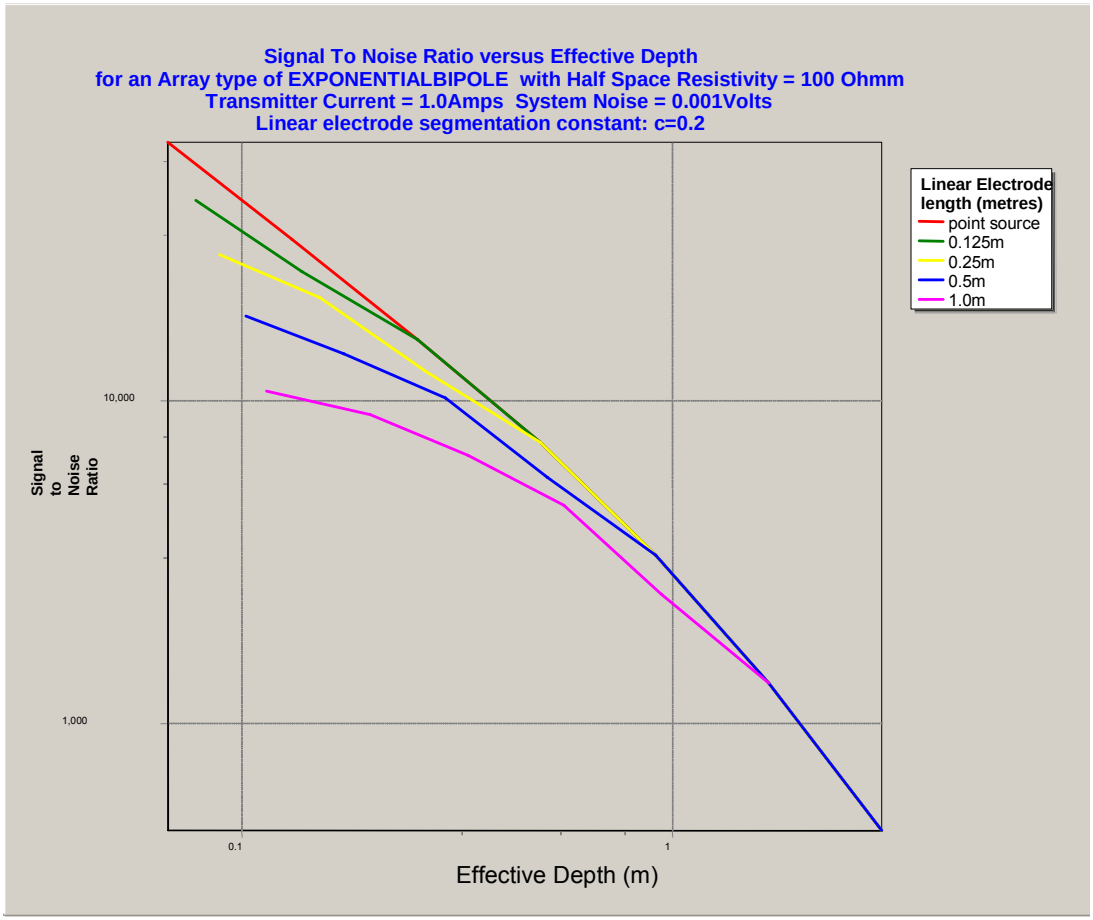

Figure 4.11 The effect of transmitter electrode length on the capabilities of an exponential bipole array with Tx Separation of 4m and Rx electrodes spaced at between 0.125m and 16m from one of the transmitter electrodes.

Similarly, Figure 4-12 shows that increasing spacing between the transmitter electrodes almost proportionally increases signal levels at great effective depths while not affecting signal levels at shallow effective depths.

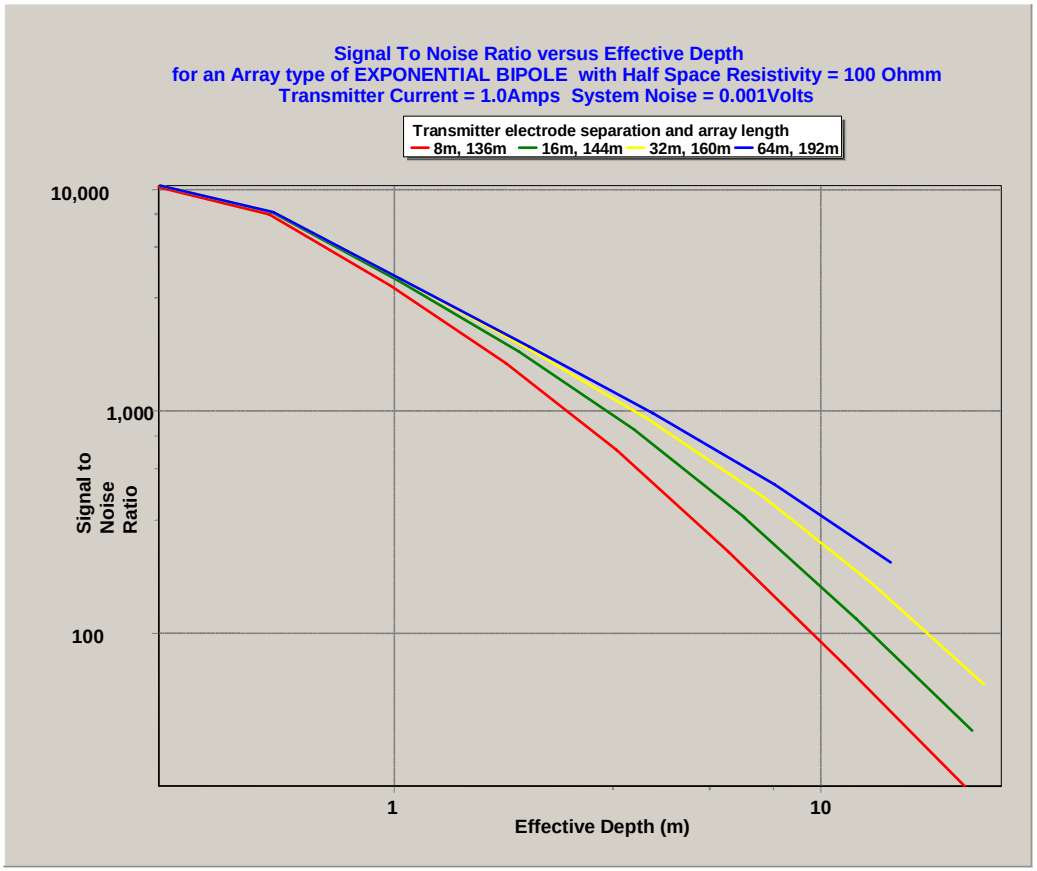

Figure 4.12 The effect of Tx Separation on the capabilities of a 144m exponential bipole array with Rx electrodes spaced between 0.5m and 128m from one Tx electrode. Signal to noise ratio (Eqn. 4) is plotted against effective depth (Eqn. 19).

4.11 Depth of investigation characteristic and two layer models

The effect of layering in a substrate on signal strength is probably best observed in depth of investigation characteristic (DIC) curves rather than normalized depth of investigation characteristic curves. For comparison, Figure 4-13 gives DIC curves for a homogeneous earth sampled by an AXB array. Figure 4-14 gives the DIC curves for the same array sampling a substrate with highly conductive basement. Note the deformation of the DIC curves and how sensitivity to changes in the conductive basement is extremely small. The exponential depth sampling capability of AXB arrays is very helpful when parameters of such conductive basement models need to be resolved.

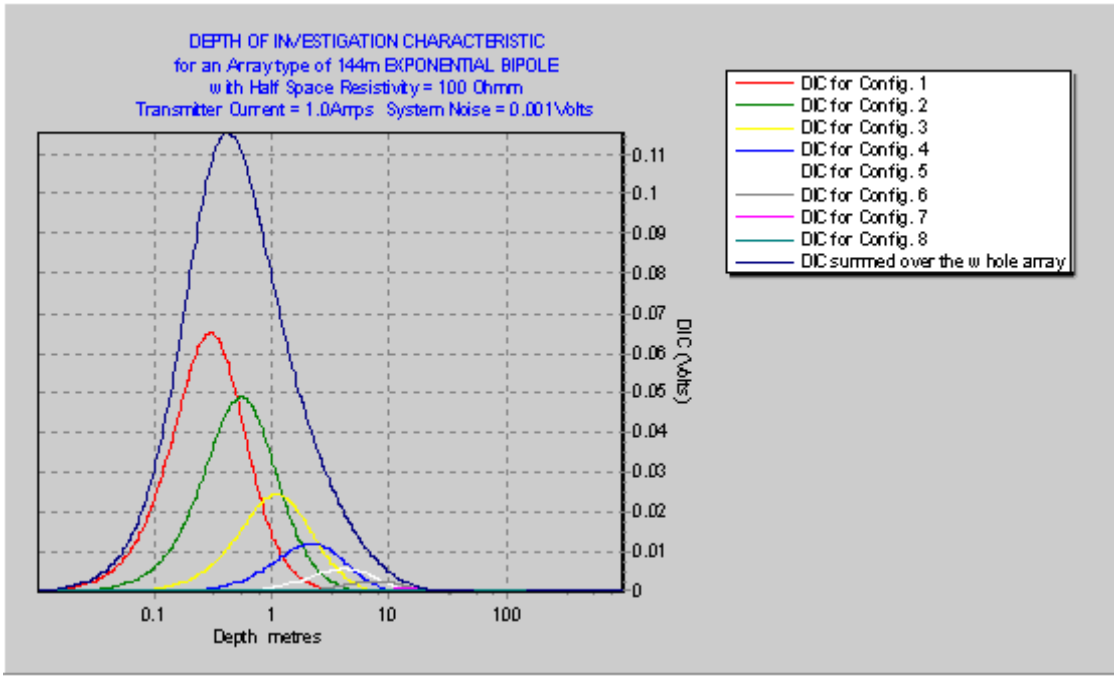

Figure 4.13 DIC (Eqn. 16) for a 144m XB array over homogeneous earth.

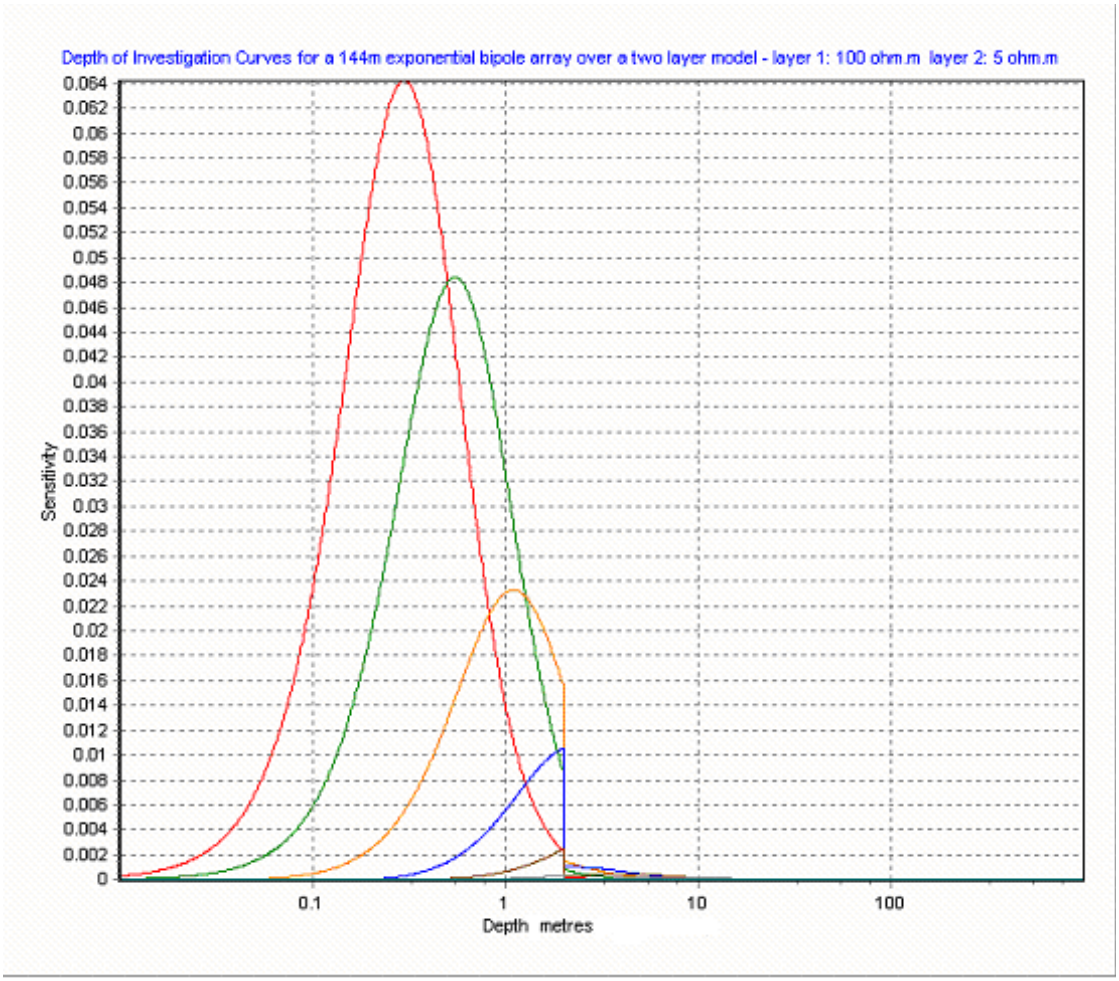

Figure 4.14 Two layer DIC curves (Eqns. 23 & 24) with a conductive basement.

4.12 The cumulative NDIC curves of an AXB array

Should cumulative normalized depth of investigation characteristic curves for an AXB array be plotted, effective depth would be evident as the ordinates of the intercepts of the curves with a normalized sensitivity level of 0.5. Similarly, resolution could be obtained from the difference between the ordinates for normalized sensitivity levels of 0.5 and 0.6. Extended effective depth could be obtained using the 0.1 normalized sensitivity level. In this thesis, all effective depths and associated parameters have been calculated by integrating under NDIC curves rather than by plotting cumulative NDIC curves and reading ordinates, in this manner, as this is computationally simpler.

4.13 Comparison of AXB arrays with some other arrays

AXB arrays are compared with a range of other arrays in Figures 4-15 to 4-20. Schlumberger, Wenner dipole dipole and the Aarhus Hydrogeophysics Group Pulled Array Continuous Electric Sounding Arrays have all been compared as follows. The configurations of each of these arrays is plotted with respect to their effective depths in those figures. Observe the distribution of sampled effective depths in each diagram, the ratio of array lengths to effective depths and the distribution of midpoints. The first four of these arrays have been selected because they have been designed and/or used for continuous towed surveying and because they attempt to sample a similar range of effective depths. The last two were selected because of their superior depth sampling distribution and signal strengths.

The first two arrays shown (AXB arrays) differ only by receiver electrode spacing. The first samples more densely than the second but would only be useful on surveys where vertical data density is highly valued because it contains twice as many electrodes, which adds to equipment costs, and it will receive slightly lower signal levels due to the electrodes being closer together which means that surveys need to be conducted with more power to get equivalent signal levels to surveys conducted with the second AXB array shown. It will also have slightly more complex response to heterogeneities due to the receiver electrodes being closer together.

The dipole-dipole array was chosen as it has been traditionally and widely utilized while the Aarhus array was chosen due to its extensive use as a towed array on ground. The

Aarhus array has a very complex and diverse response to 3D heterogeneities which means that data from it must be greatly smoothed horizontally prior to 1D (or even 2D) inversion. It does, however, obtain very high signal levels and uses a minimum number of electrodes. This is important when electrodes weigh 15 kg and contain costly electronics.

The Wenner array has superior signal strength but cannot be used in towed mode due to differing transmitter electrode locations in each configuration and it lacks fineness of depth resolution due to having so few configurations.

The Schlumberger array cannot practically be used in towed mode unless the transmitter and receiver electrodes are swapped and the transmitter electrodes are fixed rather than stepped as shown.

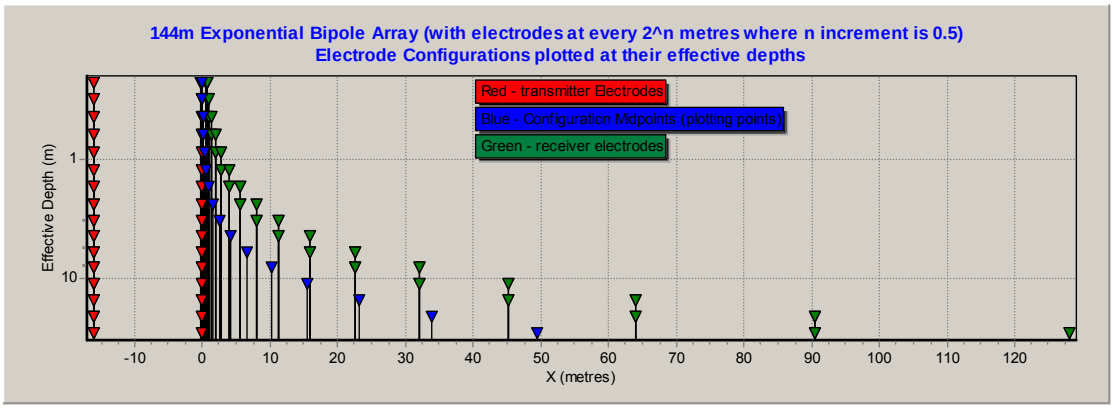

Figure 4.15 Electrode configurations of a 144m AXB array with 2^(0.5*n) receiver electrode increments plotted at their effective depths (Eqn. 19).

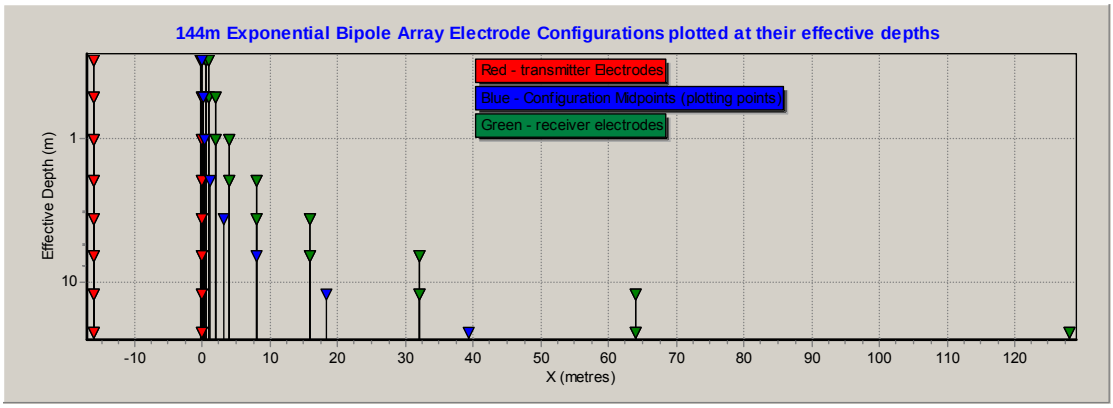

Figure 4.16 Electrode configurations of a 144m AXB array with 2^(n) receiver electrode increments plotted at their effective depths (Eqn. 19).

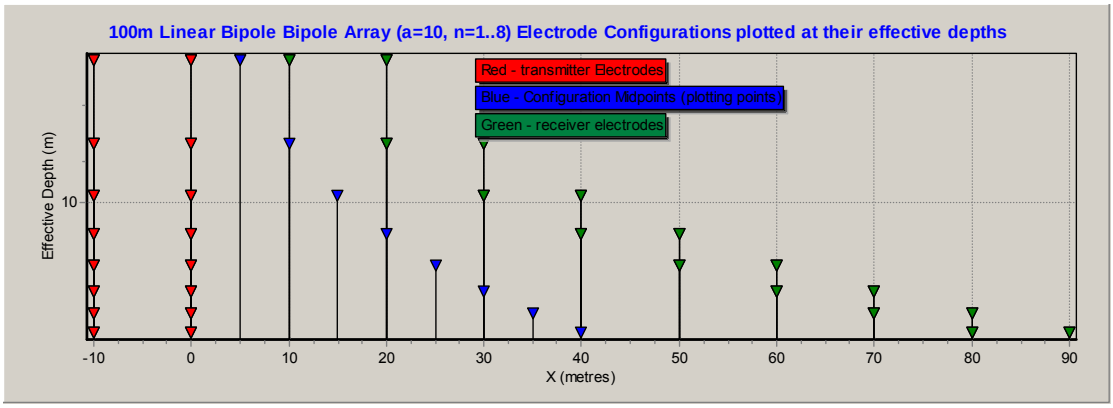

Figure 4.17 Electrode configurations of a linear dipole-dipole array with 10m dipoles plotted at their effective depths (Eqn. 19).

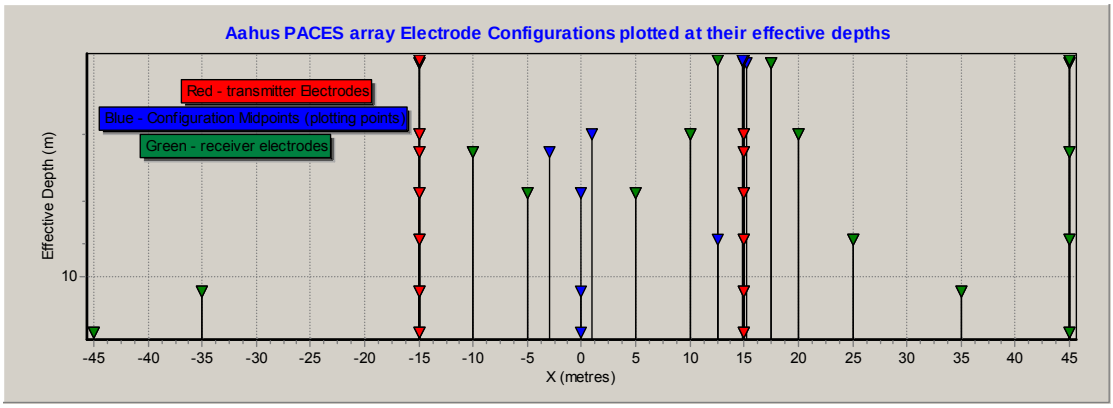

Figure 4.18 Electrode configurations of an Aarhus Hydrogeophysics Group Pulled Array Continuous Electric Sounding system plotted at their effective depths.

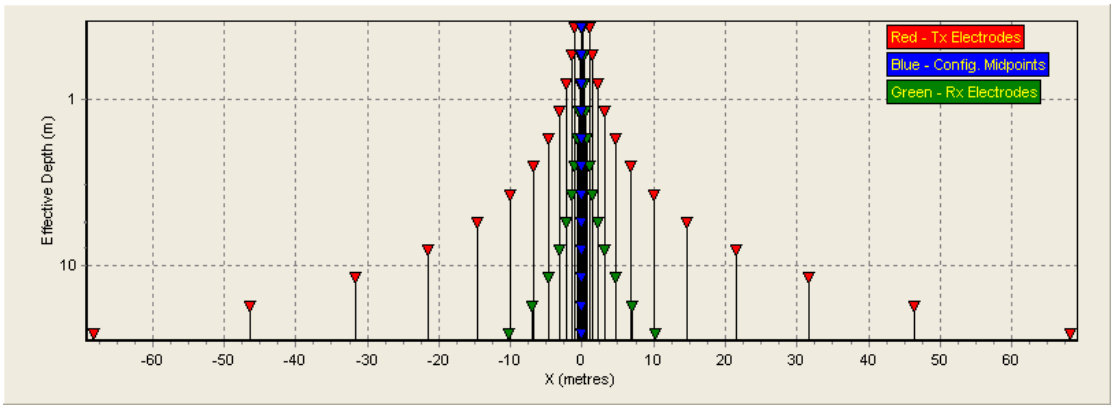

Figure 4.19 Electrode configurations of a Schlumberger Array with six configurations per decade plotted at effective depths (Eqn. 19).

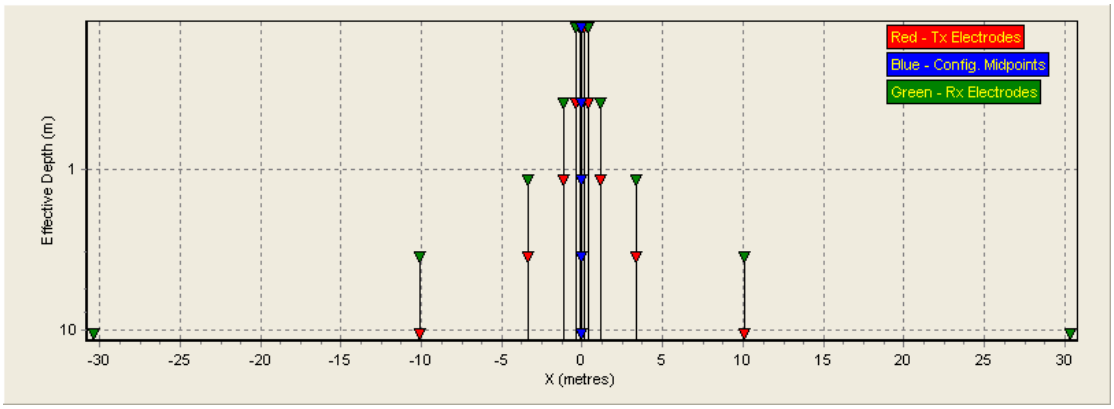

Figure 4.20 Electrode configurations of a Wenner Array, with a minimum 'a' spacing of 0.25m, plotted at their effective depths (Eqn. 19).

Normalized Depth of Investigation (NDIC) curves (see Chapter 3, Equation 17) for an AXB array and a dipole-dipole array have been displayed already in Figures 4-2 and 4-3. The normalized depth of investigation curves, used to obtain some other arrays are plotted in Figures 4-21 to 4-25. They reveal resolution of individual configurations within arrays. It can be seen that the dipole-dipole and Schlumberger arrays have configurations with narrowed higher resolution NDIC curves. When conducting 1D inversion, however, resolution is not just dependant on resolution of individual array configurations but, rather, is largely dependant on the sum of the portions of DIC curve areas that are above the noise level and that do not overlap DIC curves of other configurations in the array. Put another way, resolution of whole arrays is dependant not only on the resolution of individual configurations but on signal to noise levels and on the degree of overlap of DIC

curves. Resolution issues are even more complicated than that as DIC curves change shape over layered models. The complications will be dealt with in the next two chapters.

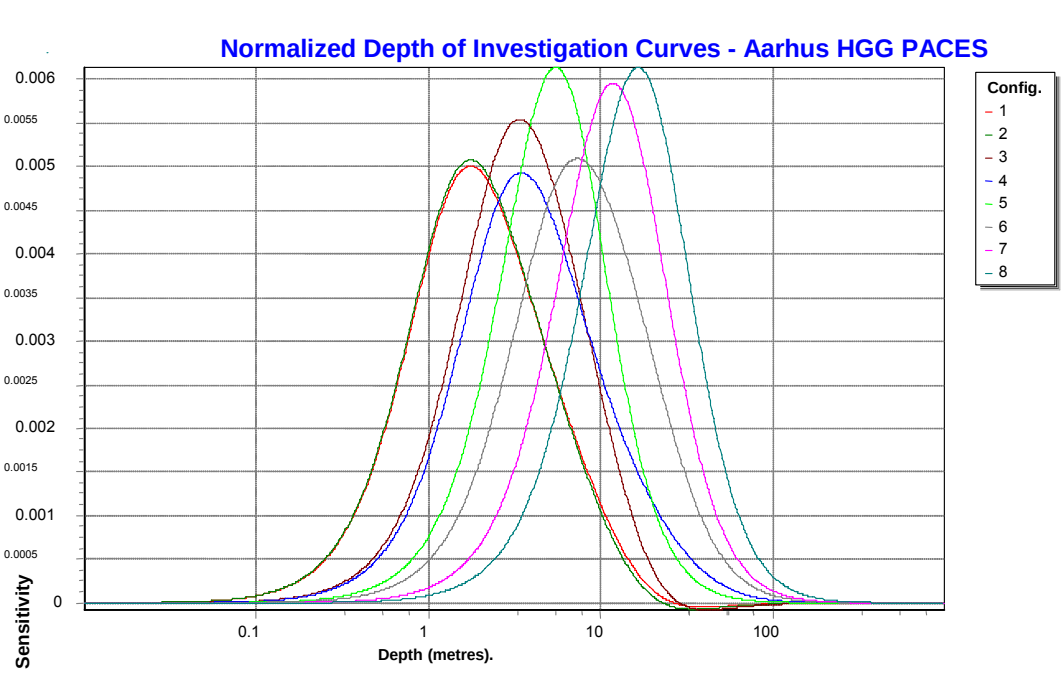

Figure 4.21 Normalized Depth of Investigation Curves (Eqn. 17) for the Aarhus University Hydrogeophysics Group Pulled Array Continuous Sounding device.

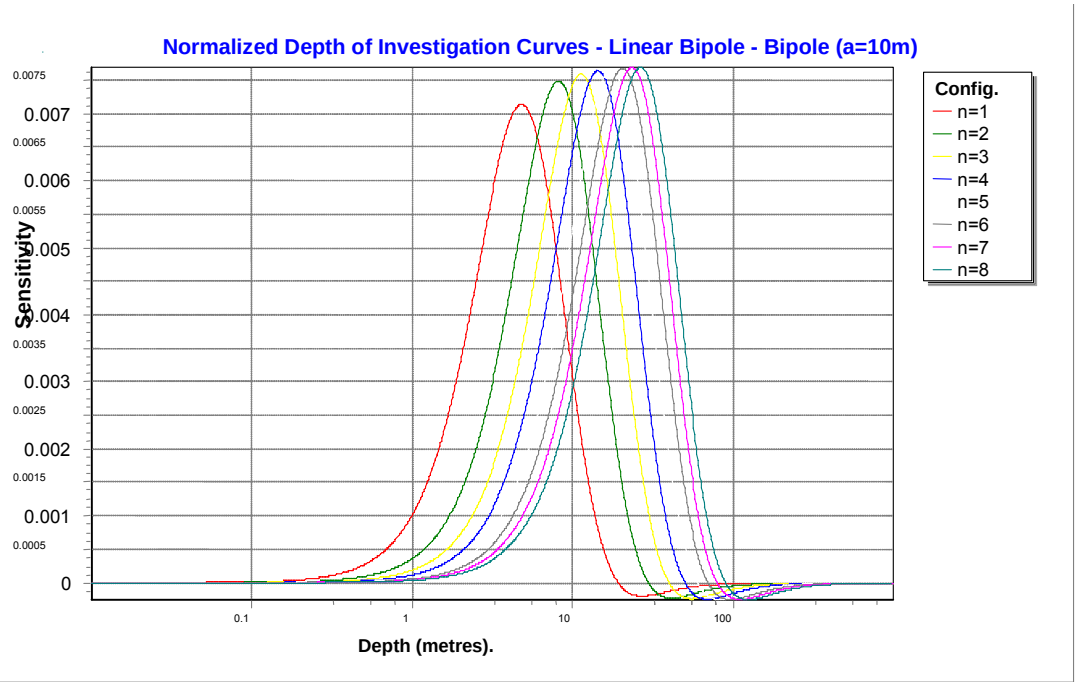

Figure 4.22 NDIC curves for a Linear Bipole Bipole Array with a=10, n=1 to 8

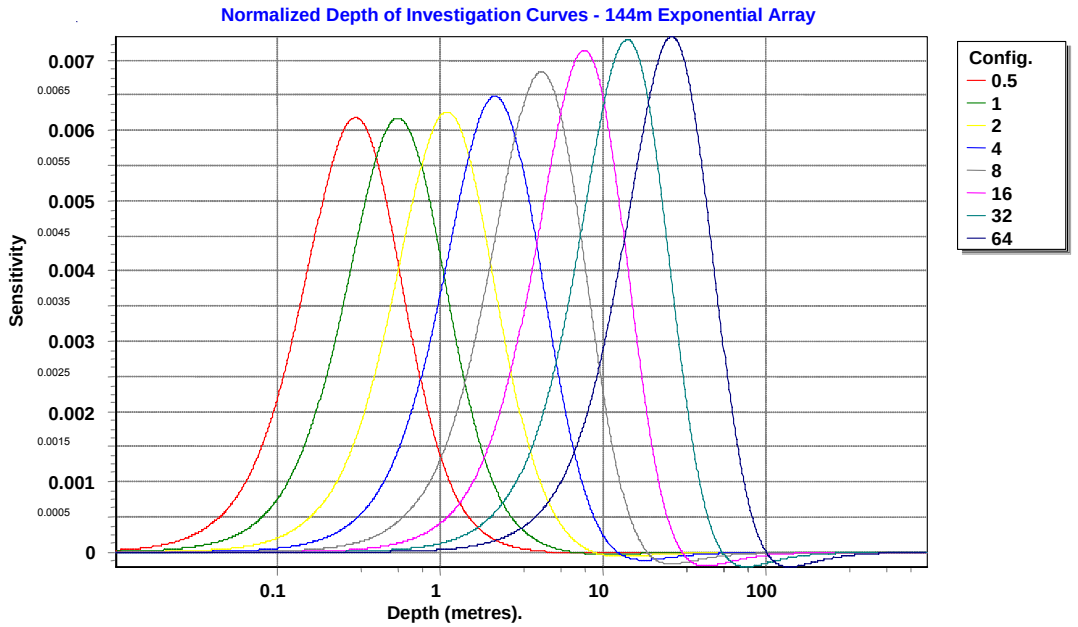

Figure 4.23 NDIC Curves (Eqn. 17) for an Exponential Bipole Bipole Array with TxSeparation=16m and RxElectrodes at 0.5m to 128m

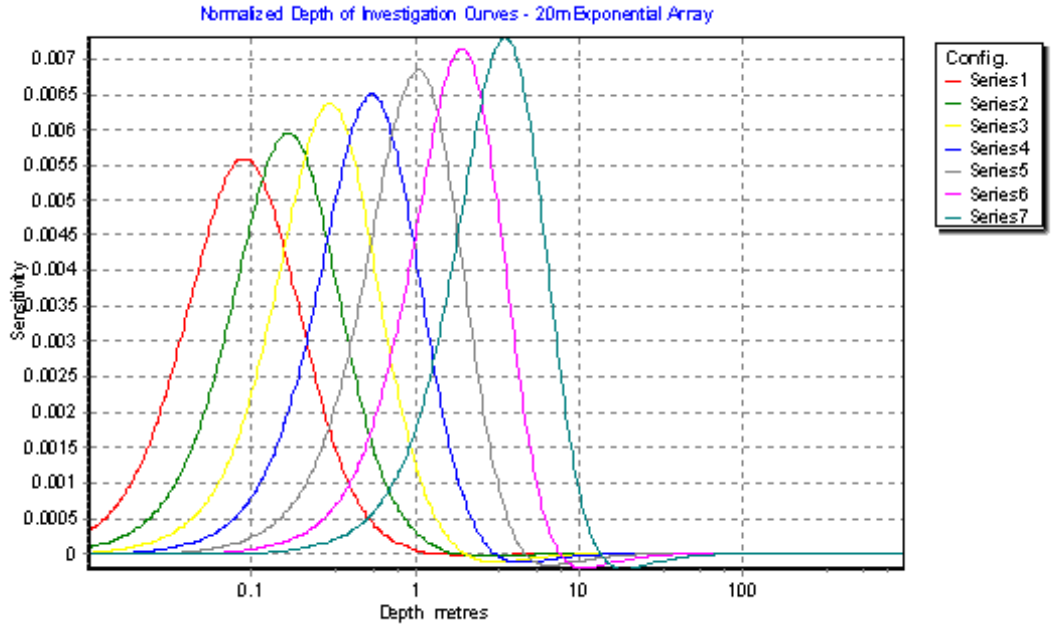

Figure 4.24 NDIC Curves (Eqn. 17) for a 20m long exponential bipole array – TxSeparation = 4m, RxElectrodes from 0.125m to 16m.

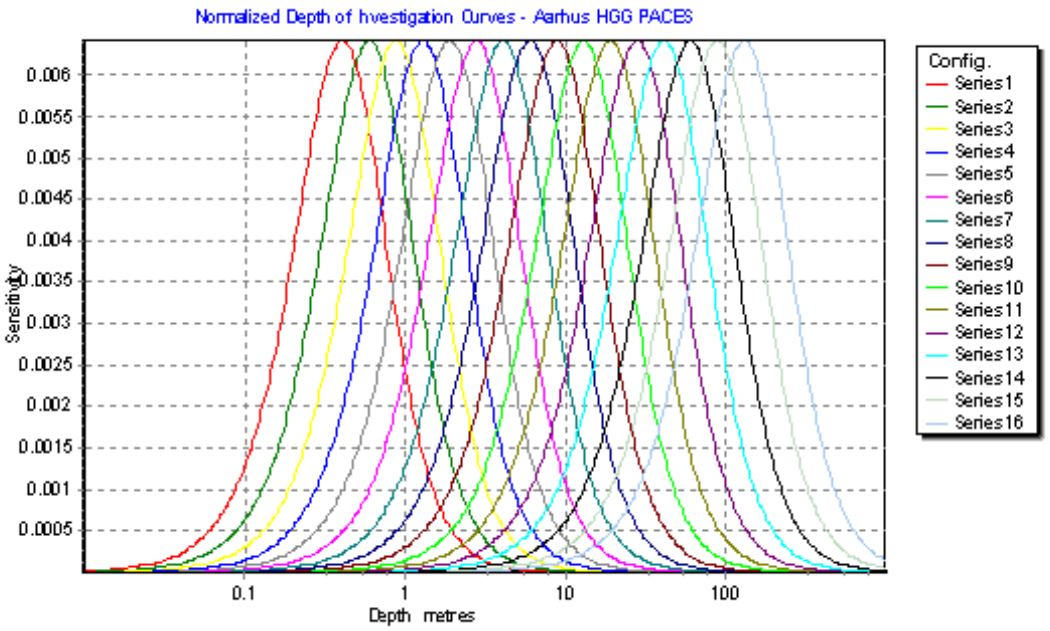

Figure 4.25 NDIC curves (Eqn. 17) for a schlumberger array with 6 configurations per decade.

4.14 Array comparison conclusions

Figure 4-26 shows the performance of various arrays. It can be seen that the AXB array is capable of detecting signal from a very large range of effective depths. The Linear dipole-dipole array is seen to be a very poor choice for sounding – it has poor distribution of effective depths (unless used to target ore bodies under a known thickness of overburden) and suffers severe loss of signal in the later dipoles. It is the shortest of the arrays shown but has good maximum effective depth however this is illusory as the signal levels at large effective depths obtained with this array are rarely sufficient to warrant use. The PACES system is seen to have excellent signal levels (due to pole-pole and Wenner type configurations) but a limited distribution of effective depth. The AXB array cannot compete with the PACES configurations for signal strength when current is kept constant however it can when its linear electrodes permit much greater currents to be injected. Its distribution of weight near the towing device permits it to have much greater length, and sample much greater effective depths, than a PACES array towed by a vehicle with the same pulling force.

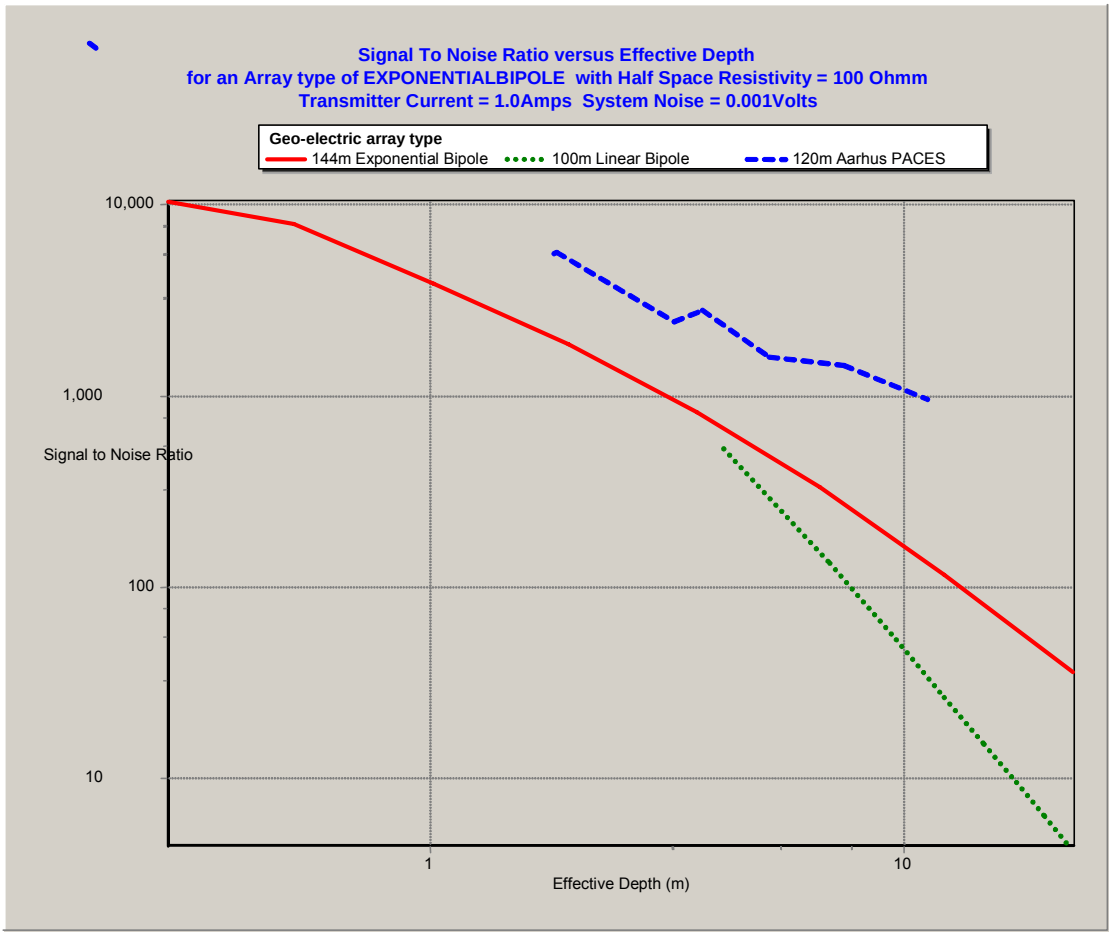

Figure 4.26 Comparison of the capabilities of various arrays viewed in Signal to Noise Ratio (Eqn. 4) versus Effective Depth (Eqn. 19) space.

4.15 Elaborate array combinations – multiple streamers

It is possible, using fractional signed monopole notation to facilitate multiple arrays surveying at the same time. The key in design of such systems of arrays is in ensuring that signal contribution concentrations of configurations in each of the arrays is well separated from signal contribution concentrations in the other arrays even though each array is receiving transmitted signal from the other. Multiplexing of operation of multiple arrays, so that interference would not be an issue is to be avoided when using towed arrays because it requires much slower surveying. There are two possibilities of merit:

1 - Parallel floating or submerged AXB arrays: On large rivers or canals, it is frequently desirable to measure gradient of electrical conductivity across the river while surveying along it. This can be done using parallel arrays. It is optimal, for collecting highest

possible quality data and for permitting direct comparison of data from each array, if both arrays can be transmitting and sampling at once. Fractional signed monopole notation would permit processing and inversion of such data. With both arrays running simultaneously, signal from each will interfere with the other resulting in a slight convergence of array footprints at deeper effective depths, however, if the arrays are sufficiently well separated, then data from receiver electrodes on each array may be inverted separately using fractional signed monopole notation based inversion software which could compensate for the transmitted signal coming from transmitter electrodes of the other array. The inverted models from each array could then be compared by making difference images as detailed in the processing chapter of this thesis. Pairs of parallel floating arrays towed from booms extending out each side of a boat are useful for determining from which side of a river saline inflow is coming. Sets of parallel submerged arrays are useful for combing ocean floor when looking for small metal objects such as unexploded ordinances. For such an application, use of two long transmitter electrodes perpendicular to, and spanning, the arrays of receiver electrodes would be appropriate.

2 - Simultaneous survey with floating and submerged arrays: In order to save time, floating and submerged array surveys could be conducted simultaneously using 2 transmitter electrodes (the first transmitter electrode on each array would be removed). The submerged AXB array would be towed very close to the boat with its transmitter electrode most distant from the boat and a suitable distance away from the beginning of the floating array. The floating array would follow at a distance so that interference would be minimal. Interference would be accommodated in the processing but it must be kept to a minimum because positioning errors between the arrays will not be small. Fractional signed monopole notation could then be utilized, along with forward modelling theory of Christensen (1994) mentioned in Chapter 5, to invert data from the two arrays. Accurate depth determination would be necessary. This concept would lead to towing of a floating array with a very long leader so its viability is questionable.

4.16 Capacitive resistivity line and plate antennae.

Towed geo-electric surveys are now being conducted over land using various capacitive electrodes devices, some of which are now commercially available. These devices use

either linear or plate electrodes that may not be accommodated by conventional inversion software (except by approximating the electrodes using point source electrodes). Fractional signed monopole notation based inversion software can, however, handle any linear or plate electrodes provided that segmentation of them is properly conducted (a one-off process).

CHAPTER 5 - HORIZONTAL LAYER FORWARD MODELLING

Figure 5-1 is provided as an example of some forward modelled data displayed by the software developed in conjunction with this thesis. The blue lines are the field data displayed as apparent resistivities and the red lines are the horizontal layer resistivities and boundary depths. The process for computing these models will now be explained.

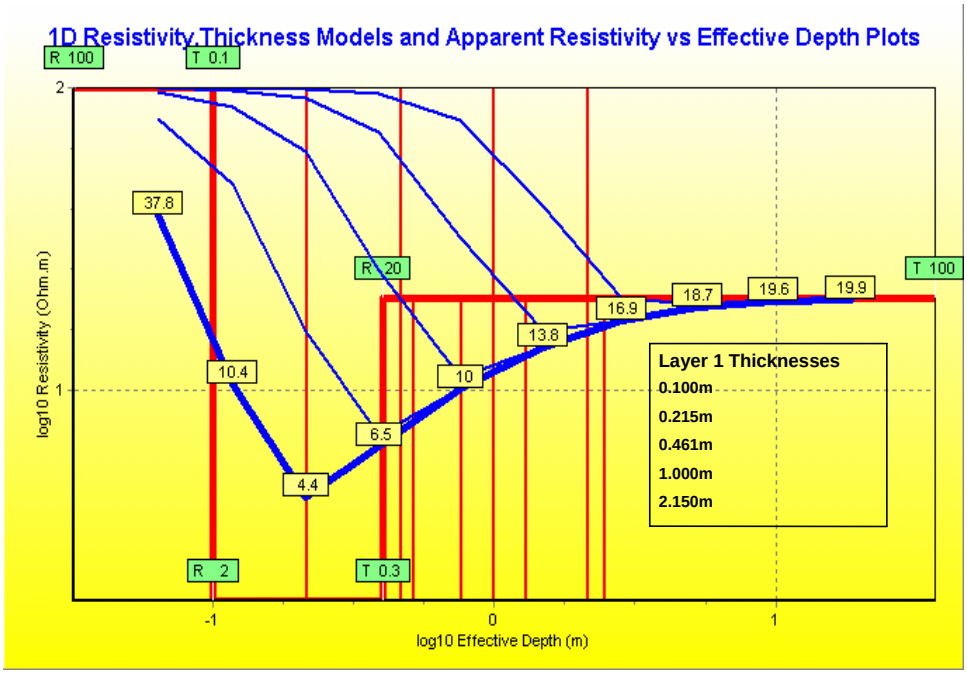

Figure 5.1 Some sample forward modelled datasets (Blue) and the horizontal layered models from which they were generated (Red). This forward modelling shows how apparent resistivity curves become insensitive to a thin (Thickness 0.3metres), conductive (Resistivity 2ohm.m) layer as it is overlain by increasing amounts of overburden. Labels give details of the first model in the set of 5.

Forward modelling is the process of generating field data from artificial models. In this thesis, the technique of modelling horizontally layer models will be explained even though some 3rd party software has been used to model some of the case study data in 2 dimensions. Because this thesis deals with high volume reconnaissance data, and because features of interest in that data are approximately horizontally layered, only 1D horizontal layer inversion will be investigated in detail. The fractional signed monopole notation of

Chapter 4 will be used to simplify and generalize the forward modelling procedure described by Davis (1979) for several field arrays.

5.1 Anisotropy

Isotropic resistivity is assumed in all modelled layers in the following derivations. Anisotropy (including unresolved macroscopic layering) distorts field data to represent equivalent isotropic models and therefore introduces undetectable error into field data interpretation. Merrick (1977) discusses this problem in detail. Electromagnetic method data does not suffer distortion from vertical anisotropy and so, when used in conjunction with geo-electric data by the process of joint inversion, can identify anisotropy provided that accurate calibration is performed.

5.2 Determining voltages obtained by floating arrays over known 1D models.

The following theory is taken principally from Davis (1979) and is presented here as a necessary introduction to the problem of a point current source over a stratified half space. Modifications and additions have been made, as indicated, to make it relevant to the algorithm and computer code presented as part of this thesis.

Current flow in stratified media will be examined first. Figure 5-2 introduces the scenario and the variables that will be used.

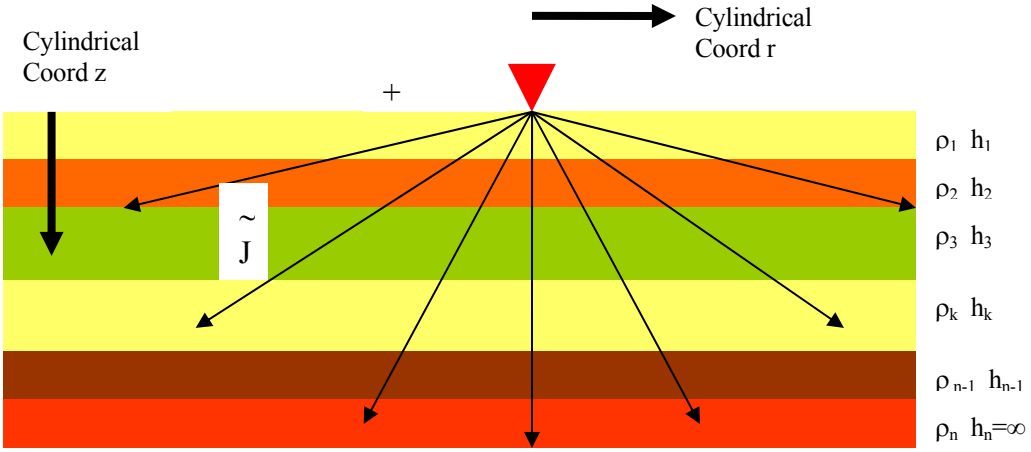

Figure 5.2 A current source on a stratified half space. Cylindrical co-ordinates, their origin at the current source, electric field vectors, layer resistivity and layer thickness variables are shown.

In source free regions of conducting media, the potential distribution satisfies Laplace's Equation:

$$\nabla^2 V = 0$$

In cylindrical co-ordinates centred on the potential source, V depends only on r and z so, on expanding Laplace's equation we get:

$$\nabla^2 V = \frac{\partial^2 V}{\partial r^2} + \frac{1}{r}\frac{\partial V}{\partial r} + \frac{\partial^2 V}{\partial z^2} = 0$$

By separating variables, the following equation is obtained:

$$V = A(\lambda)J_0(\lambda r)e^{-\lambda z} + B(\lambda)J_0(\lambda r)e^{\lambda z}$$

where

$J_0(\lambda r)$ = a zero order Bessel function of the first kind,

λ = an integration constant, and

r = the distance from the point source.

The Bessel function is defined as follows:

$$J_0(\lambda r) = 1 - \frac{\lambda^2 r^2}{2^2 (1!)^2} + \frac{\lambda^4 r^4}{2^4 (2!)^2} - \frac{\lambda^6 r^6}{2^6 (3!)^2} + \frac{\lambda^8 r^8}{2^8 (4!)^2} - .... \quad (28)$$

Choice of λ is completely arbitrary so for generality, all possible values must be included. This leads us to the general solution:

$$V = \int_0^\infty A(\lambda) J_0(\lambda r) e^{-\lambda z} d\lambda + \int_0^\infty B(\lambda) J_0(\lambda r) e^{\lambda z} d\lambda \quad (29)$$

The particular solution to this problem is obtained by applying the boundary conditions dictated by the physical problem. At each interface, potential and the perpendicular component of current density must be continuous. Davis (1979) continues, showing how these apply to the general solution for the Laplace equation.

The resistivity transform function (Koefoed, 1970) is defined as:

$$T_n(\lambda) = \frac{2\pi}{I} [A_1(\lambda) + B_1(\lambda)] \quad (30)$$

where:

n = the number of layers in a model (see Figure 5-2), and
subscript 1 refers to the solution of functions in the surface layer.

When substituted into the solution for potential at the half space surface, Davis (1979) obtains:

$$V_s(r) = \frac{I}{2\pi} \int_0^\infty T_n(\lambda) J_0(\lambda r) d\lambda \quad (31)$$

where:

$V_s(r)$ = potential at the surface.

This is the fundamental relation for a point source of current at the surface of a layered half space. Davis (1979) derives a solution to the transform function noting that potential in a uniform half space such as the bottom layer is given by:

$$V = \frac{\rho_n I}{2\pi} \cdot \frac{1}{\sqrt{r^2 + z^2}} \tag{32}$$

Davis (1979) makes this fit the form of equation 3 by use of the Weber-Lipschitz identity for the Bessel function:

$$\int_0^\infty J_0(\lambda r) e^{-\lambda z} d\lambda = \frac{1}{\sqrt{r^2 + z^2}} \tag{33}$$

The recursive solution for the transform function (Koefoed, 1970) described by Merrick (1977) using the nomenclature given in Figure 5-2 is finally given as follows:

$$T_1(\lambda) = \rho_n \tag{34}$$

(note: T_1 is only used for half spaces as normally recursion is started using T_2 as follows).

$$T_2 = \rho_1 \left(\frac{1 + \psi_{12} e^{-2\lambda h_1}}{1 - \psi_{12} e^{-2\lambda h_1}} \right) \tag{35}$$

$$T_{k+1} = \frac{T_k + T'_{n-k}}{1 + \frac{T_k T'_{n-k}}{\rho^2_{n-k}}} \tag{36}$$

where:

$k = 2,3,\ldots,n\text{-}1$ and represents layers as presented in Figure 5-2,

$\psi_{12} = \frac{\rho_2 - \rho_1}{\rho_2 + \rho_1}$ = the reflection coefficient for the boundary between layers one and two which ranges from -1 to 1 (37)

$$T'_{n-k} = \rho_{n-k} \frac{1 - e^{-2\lambda h_{n-k}}}{1 + e^{-2\lambda h_{n-k}}} = \rho_{n-k} \tanh(\lambda h_{n-k}) \tag{38}$$

T_n is obtained recursively starting with T_2,

The final resistivity transform is obtained by solving for $k=n$. Merrick (1977) presents equivalent forms of this equation published by others using different nomenclature.

As a result of the principle of super-position, using fractional signed monopole notation as described in chapter 4, the solution for apparent resistivity becomes:

$$\rho_{apparent} = K \cdot \frac{\sum_{i=1}^{n} p_i \cdot V(r_i)}{I} \tag{39}$$

where:

$\rho_{apparent}$ = Apparent resistivity for a surface array configuration.
K = the geometric factor for an array configuration
p_i = signed fractional monopole i
r_i = the transmitter electrode segment to receiver electrode separation
V = the voltage obtained using the fundamental relation for a point source of current given by equation 31.

We now have a solution to the forward modelling problem; however the Bessel function contained in the solution is not trivial to compute, let alone to numerically integrate along with the recursively obtained transform function. The Bessel function decreases as $(\lambda r)^{-1/2}$ for $\lambda r \to \infty$ and oscillates. Furthermore, Davis (1979) claims that it is difficult to obtain the error involved in numerical integration. A better approach to the problem involves use of linear filter theory.

5.3 Determining voltages obtained by submerged arrays in known 1D models.

Christensen (1994) has solved the fundamental relation for a point source of current within a water layer overlying a layered half space. The solution, of which the above solution is a special case, is as follows:

$$V_1(r,z) = \frac{I\rho_1}{4\pi}\int_0^\infty \frac{e^{(\lambda z_0)} + e^{(-\lambda z_0)}}{1-\gamma_1}\left\{\gamma_1 e^{(\lambda z)} + e^{(-\lambda z)}\right\}J_0(\lambda r)d\lambda \qquad z > z_0 \tag{40}$$

$$V_1(r,z) = \frac{I\rho_1}{4\pi}\int_0^\infty \frac{\gamma_1 e^{(\lambda z_0)} + e^{(-\lambda z_0)}}{1-\gamma_1}\left\{e^{(\lambda z)} + e^{(-\lambda z)}\right\}J_0(\lambda r)d\lambda \qquad z < z_0 \tag{41}$$

Where

$V_1(r,z)$ is the voltage in the water layer at depth *z* and radial distance *r* from the current source.

Z_0 = the depth of the current source.

ρ_1 = the resistivity of the water layer.

The coefficient γ_1 is determined using the recurrence relation:

$$\gamma_m = e^{-2\lambda h_m} \frac{\gamma_{m+1} + \psi_{m+1}}{1 + \gamma_{m+1}\psi_{m+1}} \tag{42}$$

h_m = the thickness of the *m*th layer where *m* is equivalent to *k* in Figure 5-2

$$\psi_{m+1} = \frac{\rho_{m+1} - \rho_m}{\rho_{m+1} + \rho_m} \tag{43}$$

recurrence is started with $\gamma_n=0$

For a submerged array that lies entirely in a horizontal plane, either equation 40 or 41 can be used to obtain a solution at the electrodes because the limit of validity of both equations is on that plane.

5.4 Convolution

Convolution as used in exploration geophysics is the change in wave shape as a result of passing through a linear filter (Dobrin 1988, p174).

$$h(t) = \int_{-\infty}^{\infty} f(\tau) g(t-\tau) d\tau$$

where:

f(t) and *g(t)* are two functions of time (or, in our case, radial distance from a current source), and

h(t) is the convolution product of the two functions.

This may also be stated using the symbol *, which means ‘convolved with’, as:

$$h(t) = f(t) * g(t)$$

Convolution theorem: The Fourier transform of the convolution of two functions is equal to the product of the transforms of the individual functions. This means that convolution in the time domain may also be accomplished by multiplication in the frequency domain (Dobrin 1988).

If $h(t) = f(t) * g(t)$ then $H(n) = F(n)G(n)$ where *H(n), F(n)* and *G(n)* are Fourier transforms of *h(t),f(t)* and *g(t)*.

The fundamental relation for a point source of current on a layered half space given in equation 31, or more generally for a point source in the top layer of a layered half space given in equations 40 and 41 is given as a Hankel transform of the potential field. Hankel transforms are equivalent to double Fourier transforms in which the function to be transformed has radial symmetry. The convolution theorem can therefore be applied to them.

O'Neill & Merrick (1984) state that equation 31 can be written as a convolution integral, by making the following changes of variable:

$$\begin{aligned} r &= e^{x} \\ \lambda &= e^{-y} \end{aligned} \tag{44}$$

Equation 31 then becomes:

$$\begin{aligned} V(r) &= \frac{I}{2\pi}\int_0^\infty T(\lambda)J_0(\lambda r)d\lambda \\ &= \frac{I}{2\pi}\int_{-\infty}^\infty T(y)e^{x-y}J_0(e^{x-y})dy \\ &= \frac{I}{2\pi}\int_{-\infty}^\infty T(y)f(x-y)dy \end{aligned} \tag{45}$$

O'Neill & Merrick (1984) explain that this means that the potential is given by the convolution of the transform function with a so called filter function which has the form

$$f(x-y) = e^{x-y}J_0(e^{x-y}) \tag{46}$$

5.5 Digital linear resistivity filters

O'Neill & Merrick (1984) state that the convolution of equation 45 may be expressed in discrete form as:

$$V(r) = \frac{I}{2\pi r} \sum_{j=-n1}^{n2} T(\ln r - \eta_j) \cdot C(\eta_j) \tag{47}$$

where:

j = the filter coefficient number,
η_j = the filter coefficient abscissae,
$C(\eta_j)$ = the digital filter coefficients,
n_1 = the number of coefficients to the left of the filter origin, and
n_2 = the number of coefficients to the right of the filter origin.

Continuing using fractional signed monopole notation described in Chapter 4 for the purpose of simplification, and so that linear electrodes can be accommodated, the potential difference between two potential electrodes is given by:

$$\Delta V = \sum_{k=1}^{n} V_k \tag{48}$$

where:

k = index for a particular fractional signed monopole,
V_k = fractional signed monopole voltage for index k, and
n = the number of fractional signed monopoles in the array configuration.

Using equation 47 this becomes, for array configuration i,

$$\Delta V^i = \frac{I}{2\pi} \sum_{j=-n1}^{n2} T_{ij} C(\eta_j) \tag{49}$$

where:

$$T_{ij} = \sum_{k=1}^{n} \frac{p_k T\left(\ln r_k^i - \eta_j\right)}{r_k^i} \tag{50}$$

T_{ij} may be referred to as the composite resistivity transform function, a term introduced by O'Neill & Merrick (1984). It is a function of the earth model parameters and of the inter-electrode distances.

Recall that, for an array on the surface:

$$\rho_a = K\frac{\Delta V}{I} \tag{51}$$

where:

ρ_a = apparent resistivity, and
K= geometric factor:

$$K = abs\left(\frac{2\pi}{\sum_{k=1}^{n}\frac{p_k}{r_k}}\right) \tag{52}$$

where
p_k= signed monopole fraction for index k.

Combining equations 49, 51 and 52 we obtain for the apparent resistivity, as measured by a generalized surface array with or without linear electrodes, the following:

$$\rho_a^i = \frac{\sum_{j=-n1}^{n2} T_{ij}C(\eta_j)}{\left[\sum_{k=1}^{n}\frac{p_k}{r_k}\right]_i} \tag{53}$$

For a 1D modelling of submerged array data, the same procedure applies. However, instead of using the transform function of equations 34 to 38, the transform functions embedded in equations 40 and 41 need to be utilized along with appropriate filter coefficients obtainable from Christensen (1990).

A slightly more complicated, but often faster, approach to forward modelling involves splining of the transform function. The Aarhus Hydrogeophysical Group have used this method in their inversion program – EM1DInv (Auken, 2005 personal communication). It

allows for reuse of calculated parameters but adds extra tasks and extra possible sources of error to the processing stream.

O'Neill & Merrick (1984) designed the digital linear filters used in the software written in conjunction with this thesis. They designed filters with three points per decade, six points per decade and 12 points per decade. The six point per decade filter has proved to be most appropriate for routine use due to its ability to handle all but exceptional resistivity contrasts without generating forward modelling errors in excess of data noise levels. The three point per decade filter should not be used unless real time streamed inversion is to required on very slow computers.

5.6 Forward modelling of induced polarization data

Seigel (1959) demonstrated that once the resistivity forward modelling solution is solved, the induced polarization forward modelling solution can also be solved. Dixon & Doherty (1977) showed that this may be done with linear filter theory such as presented above for apparent resistivity. They recommend a technique in which apparent chargeabilities are obtained using the difference between apparent resistivities calculated for both the resistivity model and the resistivity model perturbed by the induced polarization effect of the chargeability model. Readers are referred to the above literature for more explanation.

5.7 Forward modelling software

The above forward modelling theory has largely been implemented in the software made along with this thesis. The forward modelling sector of the program alone is immensely useful for educational and analytical studies. Multiple forward models can be plotted alongside each other easily as has been done in Figure 5-1. Facilities are included to allow any combination of stepped parameters and constant parameters to make up multiple forward models easily for comparison. These models can be output as actual datasets for inversion. Noise can artificially be added to such datasets in order to simulate natural conditions. As the original models can also be saved as if they were perfectly inverted data, inversions and original models can easily be compared.

The next chapter will explain the use of the forward modelling theory and code in the procedure of 1D inversion.

CHAPTER 6 - EFFECTIVE DEPTH CENTRED HORIZONTAL LAYER INVERSION

6.1 Introduction

Resistivity inversion programs attempt to determine automatically the resistivities of layers (or cells) that would most accurately reproduce the observed measurements. Some inversion programs additionally modify layer thicknesses in order to accurately model high contrast boundaries present in the earth. The author's experience with down hole resistivity logging and excavator pit examination confirms that in sedimentary environments that typically host canals and navigable rivers, a layered earth model with discrete horizontal layers of constant resistivity is appropriate under most circumstances. Rivers and canals, which range from semi-cylindrical to flat bottomed, also may be approximated by layered earth models because signal eminating out through a semi-cylindrical body co-axial with a geo-electric array will produce a response very similar to a layered model response.

The inversion scheme used in this thesis for routine use with towed waterborne systems attempts to decipher most of the information contained in the field data without adding geophysical artefacts to it (i.e. not putting false anomalous features in the data). Additionally, it does this without the need for user input on a sounding by sounding basis because such user input would be prohibitively costly for the volumes of data obtained typically with waterborne arrays. It is discrete layer inversion (not smoothed) as real geology generally has sharp boundaries particularly at the beds of canals and rivers. To more precisely model this sharp boundary and reduce artefacts that may occur from forcing data to fit a smoothed resistivity model across this boundary, one model layer boundary has been shifted to exactly match this boundary. However, if inversion detects that for some reason the water depth boundary has been incorrectly identified by depth sensors then it will attempt to move the boundary to the correct depth.

Inversion proceeds to try to improve the model primarily by adjusting resistivities, however it will also try to stretch the thicknesses of layers to match any sharp boundaries that may exist. The inversion software recognizes cases in which conductive basement,

that typically represents hyper-saline aquifers, has caused signal to drop below noise level and attempts to model such basement rather than reflect the instability of the noise.

Data are horizontally smoothed prior to 1D inversion in order to reduce noise (see Appendix 1 for the methodology).

6.2 Initial model selection

The inversion strategy is optimized for the AXB arrays or other exponentially spaced towed arrays such as inverse Schlumberger arrays. These arrays and the inversion strategy compliment each other with the result of near complete resolution of what is practically possible to resolve using a continuously towed geo-electric array travelling at reasonable speed. The initial models submitted to the inversion code are made of horizontal layers centred (on a log scale) on the effective depths of each configuration in the array. Two layer thicknesses are then adjusted in order to place one boundary onto the bed of the watercourses as measured by sonar or pressure sensors. Resistivities of the initial model layers are apparent resistivities.

An alternative approach in which the water layer is considered as a single layer rather than split up over configuration effective depths that happen to fall within it has been trialled but not put into routine use. This is because resistivity variations sometimes occur within the water column and, if not permitted to exist in models, sometimes forces artefacts into the ground layers as demonstrated by Day-Lewis, *et.al.* (2006). The variation may be due to temperature and salinity stratification within the water column, error in depth detection or to 3D undulations in the water depth. The original approach (mentioned above) permits variation to be modelled in the water layer which may be genuine or represent geophysical artefacts. Artefacts in the water layer are easy to dismiss however artefacts in the ground layer can confuse interpreters. Temperature stratification, as well as salinity stratification, can create large differences in EC with respect to depth in water bodies (Gippsland Lakes Board, 2007). Day-Lewis, *et.al.* (2006) have used theoretical models to demonstrate the perils involved with fixing the water depth to the value provided by sonar.

6.3 Inversion methodology adopted - Summary.

The inversion code written in conjunction with this thesis is extended from code DCINVERT (Schlumberger, Wenner and Dipole-Dipole 1D inversion code requiring manual initial model selection) and VESGEN (forward modelling code that follows the procedure of O'Neill & Merrick, 1984) both written by Merrick (1977 + later revisions).

Merrick explains the basic procedure utilized in DCINVERT documentation as follows:

> *'The inverse problem of determining layered model parameters from field resistivity data is solved by a least-squares iterative procedure. Iteration follows the Marquardt algorithm for determining an approximate generalised inverse of a matrix containing the derivatives of apparent resistivity with respect to each model parameter. The derivatives are found by convolving a digital filter with resistivity transform derivative data which are in turn defined by recursion formulas (*see previous chapter*). The matrix is inverted by orthogonal factorisation. The forward problem of calculating theoretical sounding data for a specified model is solved by linear filter theory (*see previous chapter*). Recursion formulas are used to calculate resistivity transform data which are convolved with a digital filter to produce apparent resistivity data.'*

Although Merrick was co-author of the paper by O'Neill & Merrick (1984) giving the algorithm for generating forward models for any 4-electrode array, he did not get to implement this algorithm within his inversion software – DCINVERT. Rather, restrictive older array-specific techniques of forward modelling were utilized that could minimize generation of transform functions and derivatives. Merrick's code was written in Ryan McFarlan FORTRAN which is now an outdated programming language. Software completed along with this thesis combines the general array forward modelling approach laid out in the VESGEN code of Merrick with DCINVERT code. Furthermore, it has been written in Delphi 7 (Object Pascal based language) in order to improve structure and

clarity and take advantage of improvements in programming language design. Problems related to parameter fixing have been removed and many enhancements made.

The process of effective depth centred horizontal layer inversion will now be explained in detail.

6.4 Least squares and least absolute deviation inversion criteria

Consider a set of *m* apparent resistivity field observations $\boldsymbol{\rho_a}^*=(\rho_{ai}^*)$, (i=1,2,…,m), and a set of *n* model parameters $\boldsymbol{P}^*=(P_j^*)$, *(j=1,2,...,n),* as defined in the previous section. We wish to find a model ***P*** that best fits the field data and that will therefore generate a set of observations, $\boldsymbol{\rho_a}$ that best fits the field data according to some criterion. The aim of the inversion is minimization of the criterion. Options of both least squares (L2) and least absolute deviation (L1) inversion are possible as well as a continuum of options with non integer (Lq) inversion criteria. L1 and L2 inversion have been implemented. The formula for general Lq inversion is:

$$\phi = \sum_{i=1}^{m} w_i \left| \ln\left(\rho_{ai}^*\right) - \ln\left(\rho_{ai}\right) \right|^q \tag{54}$$

Where

w_i = the weight associated with observation *i*.

q = the norm of inversion. Options of 1 and 2 have been facilitated.

The logs of the apparent resistivities have been compared in order to eliminate the scale dependence of the error measure.

If noise in the field data is normally distributed and the model is a smooth model rather than a layered model then L2 inversion would be appropriate. High contrast boundaries as well as outliers due to noise created by movement of electrodes through water and outliers due to lateral 3D heterogeneities are typical of waterborne geo-electric datasets, so L1 inversion, which is more robustness in the presence of outliers is more appropriate. Robustness is of high priority in automated inversion of large volumes of data.

L1 or L2 criteria are minimized by the inversion, however for verifying goodness-of-fit between model and field data, a normalized criterion must be used. Percent root mean square criterion, or its L1 equivalent is utilized.

In order to avoid normalization errors when model and field apparent resistivities are not in good agreement, the RMS parameter has been normalized by the average of the field and model data rather than just the field data as done by Merrick (1977). This approach is more computationally intensive but worthwhile for automated inversion of large continuously acquired datasets which routinely contain thousands of soundings with model and field data that are not in good agreement. With weighting added, the relevant parameters are given by the following equations in which RModel and RField stand for model apparent resistivity and field apparent resistivity respectively:

$$WeightSum = \sum_{i=1}^{nData} Weight[i]$$

$$SumOfAbsoluteDifferences = \sum_{i=1}^{nData} \left(abs\left(\ln\left(\frac{RModel(i)}{RField(i)} \right) \right) \times Weight(i) \right)$$

$$\%RMS = 100 \times \sqrt{\frac{\sum_{i=1}^{nData} \left(\frac{2(RModel[i] - RField[i])}{RModel[i] + RField[i]} \right)^2 \times Weight[i]}{WeightSum}}$$

$$\%NormalizedAbsoluteDifferences = 100 \times \frac{\sum_{i=1}^{nData} abs\left(\frac{2(RModel[i] - RField[i])}{RModel[i] + RField[i]} \right) \times Weight[i]}{WeightSum}$$

Note that WeightSum reduces to nData when all weights equal one.

6.5 Fixed parameters

The approach taken in this work differs from that of Merrick (DCINVERT) in that fixed parameters are not entered into the inversion routine. The set of parameters ***P*** that is utilized in the inversion code is therefore the non-fixed subset of the parameters traditionally also denoted as ***P*** in the forward modelling code. The forward modelling code must operate with the full set of parameters (resistivities and thicknesses). Because the inversion code passes parameters to and from the forward modelling code continually, sets of indexes were established to map fixed and variable parameters so that the variable parameters could be quickly extracted from and merged back into the full set of

parameters. Merrick had been fixing parameters by setting their transform derivatives to zero (the relevance of this is to be explained below). He had found that this caused some obscure problems and recommended the approach taken here.

6.6 Linearization and solution of non-linear inversion problems

If all parameters had independent effects on the inversion (a linear problem) then ordinary least squares inversion would be sufficient. Resistivity data inversion, however, is essentially a non-linear problem. Merrick (2000b) explains, as follows, the procedure used here to linearize this non-linear problem. This is a very long quotation but it is essential for explaining the approach taken in the software accompanying this thesis.

From Merrick (2000b) -

"A linear relationship can be forced by a Taylor's series expansion about the trial model with retention only of first order terms:

$$F_i(\mathbf{P}+\Delta\mathbf{P}) = F_i(\mathbf{P}) + \sum_{j=1}^{n}\left(\frac{\partial F_i}{\partial P_j}\right)\Delta P_j \tag{55}$$

$$\mathbf{F}(\mathbf{P}+\Delta\mathbf{P}) = \mathbf{F}(\mathbf{P}) + \mathbf{J}\Delta\mathbf{P} \tag{56}$$

$$\Delta\mathbf{F} = \mathbf{J}\Delta\mathbf{P} \tag{57}$$

The vector $\Delta\boldsymbol{F}$ consists of the differences between measured and computed values for the state variable (which in this case is apparent resistivity). The vector $\Delta\boldsymbol{P}$ consists of the corrections to the current model parameters. The vector $\boldsymbol{P}+\Delta\boldsymbol{P}$ is the next estimate of the earth model. The Jacobian matrix $\boldsymbol{J}$ quantifies the sensitivity of the *i*th observation to the *j*th model parameter in the vicinity of the current model.

The immediate problem is to find a model correction vector $\Delta\boldsymbol{P}$ which will give a better estimate of the model and will move towards the ultimate model $\boldsymbol{P}^*$. As we have linearized a non-linear equation, many small steps will be required to reach the destination. We find $\Delta\boldsymbol{P}$ by a generalized inverse method:

$$\Delta\mathbf{P} = \left(\mathbf{J}^{\mathsf{T}}\mathbf{J}\right)^{-1}\mathbf{J}^{\mathsf{T}}\Delta\mathbf{F} = \mathbf{J}^{+}\Delta\mathbf{F} \tag{58}$$

Because the geo-electric parameter identification problem is generally ill-posed, the generalized inverse $\mathbf{J}^+$ is unstable when one or more parameters is poorly resolved. The matrix **J** can have near-zero eigenvalues which make the matrix nearly singular. Overparameterised models are particularly susceptible to instability. The ill-posed nature of the problem means that solutions must be damped or regularized. One way of effectively stabilizing the inverse is to add a bias ($\varepsilon>0$) to the diagonal elements of $\mathbf{J}^T\mathbf{J}$. The ridge inverse is defined as

$$\mathbf{J}^+ = \lim_{\varepsilon \to 0} \left(\mathbf{J}^T \mathbf{J} + \varepsilon \mathbf{I} \right)^{-1} \mathbf{J}^T \tag{59}$$

Inversion by this method is known as *ridge regression* or *damped least squares inversion* (Inman, 1975). Marquardt (1963) developed an algorithm for varying ε as the inversion proceeds, the logic being to increase ε slowly when a solution is difficult and to decrease ε rapidly when a solution is easy. The bias effectively reduces the impact of near-zero eigenvalues by increasing the eigenvalues of $\mathbf{J}^T\mathbf{J}$ by an amount ε.

Orthogonal factorization (Jennings and Osborne, 1970) is an effective practical method for finding the ridge inverse."

-end of Merrick (2000b) quote.

Orthogonal factorization qualitatively measures parameter sensitivity using a partial derivative (Jacobian) matrix as opposed to singular value decomposition, which is not as efficient but does produce a quantitative sensitivity matrix.

6.7 The transform derivative

In order to invert data using the above optimized approach, transform derivatives are required for each layer parameter. Merrick (1977) derived the relevant transform derivatives for the surface array as follows:

"An earth model of n layers is characterized by $2n$-1 parameters (P_j *:j=1,2,..., n-1, n, n+1, ..., 2n-1)*. The first n-1 parameters are thicknesses (h_k*: k=1,2,..., n-1)* and the next n parameters are resistivities (ρ_k*: k= 1, 2, ..., n)*." The resistivity transform function is defined as in the previous chapter. Using the recursion formula for the transform function,

Merrick (1977) expresses the resistivity transform derivatives with respect to each model parameter as:

$$\begin{aligned} \frac{\partial T_{k+1}}{\partial P_j} &= \frac{1}{B}\left[A_1 \frac{\partial T_k}{\partial P_j} + A_2 \frac{\partial h_{n-k}}{\partial P_j} + A_3 \frac{\partial \rho_{n-k}}{\partial P_j} \right] \\ \frac{\partial T_2}{\partial P_j} &= C_1 \frac{\partial h_1}{\partial P_j} + C_2 \frac{\partial \rho_1}{\partial P_j} + C_3 \frac{\partial \rho_2}{\partial P_j} \end{aligned} \qquad \begin{vmatrix} k = 2,3,..., n-1 \\ j = 1,2,..., 2n-1 \end{vmatrix} \tag{60}$$

Where

$$\frac{\partial P_m}{\partial P_j} = \delta_{jm} = \begin{vmatrix} 0 & j \neq m \\ 1 & j = m \end{vmatrix} \quad \text{(the Kronecker delta)} \tag{61}$$

suffix *m* in the above equation denotes the index of any parameter.

$$B = \left(1 + \frac{T_i T'_{n-k}}{\rho^2_{n-k}} \right)^2 \tag{62}$$

$$A_1 = 1 - \left(\frac{T'_{n-k}}{\rho_{n-k}} \right)^2 \tag{63}$$

$$A_2 = \lambda \rho_{n-k} \operatorname{sech}^2(\lambda h_{n-k}) \left[1 - \left(\frac{T_k}{\rho_{n-k}} \right)^2 \right] \tag{64}$$

$$A_3 = \tanh(\lambda h_{n-k}) \left[1 - \left(\frac{T_k}{\rho_{n-k}} \right)^2 \right] + \frac{2 T_k T'_{n-k} \left(T_k + T'_{n-k} \right)}{\rho^3_{n-k}} \tag{65}$$

$$C_1 = \frac{-4\lambda \rho_1 \psi_{12} e^{-2\lambda h_1}}{\left(1 - \psi_{12} e^{-2\lambda h_1} \right)^2} \tag{66}$$

$$C_2 = \frac{(\rho_1 + \rho_2)^2 \left(1 - \psi_{12} e^{-4\lambda h_1} \right) - 4\rho_1 \rho_2 \psi_{12} e^{-2\lambda h_1}}{(\rho_1 + \rho_2)^2 \left(1 - \psi_{12} e^{-2\lambda h_1} \right)^2} \tag{67}$$

$$C_3 = \left(\frac{2\rho_1 e^{-2\lambda h_1}}{(\rho_1 + \rho_2)\left(1 - \psi_{12} e^{-2\lambda h_1} \right)} \right)^2 \tag{68}$$

The transform function approximately mimics, in a damped manner, the behaviour of apparent resistivity so transform derivatives approximate apparent resistivity derivatives. Inversion, however, is best carried out in the apparent resistivity domain in order to avoid exacerbation of errors in the field data during convolution and for other reasons (see Merrick 1977). In order to conduct inversion in the apparent resistivity domain it is necessary to convert the transform derivatives of models into apparent resistivity derivatives for those models. This is done using digital linear filters and convolution in a tag-along manner when conducting forward modelling using the transform function expressed in the previous chapter. Fractional signed monopole notation is incorporated into the tag-along solution for simplification and so that data from arrays with linear electrodes can be inverted.

For computational efficiency in a very speed critical part of the inversion program, two algorithms were generated. One generates both the transform function and the derivatives while the other just generates the transform function. When derivatives are not needed, the second algorithm is used.

6.8 Inversion Constraints

The inversion process utilized by Merrick in DCINVERT and modified in the software accompanying this thesis is now explained. Facilities for additional constraints have been added to the inversion code. Because we are conducting automated inversion which must be robust and automated in order to be useful, and because we are modelling the same number of layers as there are data values, we need to stabilize the inversion with additional constraint. We have an over-parameterized problem.

Recall that the inversion strategy involves creating an initial model with one layer per array configuration with each layer centred (on a log scale) on the effective depth of each configuration. This means that we have nearly twice as many parameters as data. At first an attempt was made to stabilize inversion by fixing all the layer thicknesses. This resulted in geophysical artefacts in situations where high contrast boundaries were not matched exactly by model boundaries. Running the inversion with no fixed parameters produced good results in some observed cases however layers tended to collapse or extend to large thicknesses resulting in chaos in other situations. Using fixed initial models with fewer layers proved to be inappropriate because a suitable initial model

picking procedure that produced meaningful results with few layers could not be found. Addition of a smoothness constraint and layer thickness stretch constraint finally solved the problems.

6.9 Stretch and Smoothness constraints

In order to float layer thicknesses when there is around one layer for every apparent resistivity/effective depth pair, additional constraint needs to be applied to inversion. Otherwise, layers could become excessively thick or thin pushing other layers out of range, resistivity overshoots and undershoots could get out of control or inversion could stop prematurely without changing the initial models optimally.

A parameter representing vertical roughness of resistivity and another representing the average degree to which layer thicknesses have been stretched from their initial model values must be added to the sum of squares or absolute differences for the inversion to take account of stretch and smoothness. Appropriate weighting also needs to occur. The additional parameters are as follows:

$$Roughness = \frac{wtVertSmooth \cdot \sum_{i=2}^{nLayers} \frac{2 \cdot abs(\rho_i - \rho_{i-1})}{\rho_i + \rho_{i-1}}}{nLayer - 1}$$

$$Stretch = wtOrigModel \cdot \sqrt{\frac{\sum_{i=1}^{nLayers-1} \frac{sqr(t_i - toriginal_i)}{toriginal_i}}{nLayer - 1}}$$

The roughness parameter is commonly used in inversion, however, the Stretch parameter may be a new concept. These constraints are added to the sum of squares or sum of absolute deviations as follows:

$$\begin{aligned} NewSumOfSquares &= SumOfSquares + WeightSum * (Roughness + Stretch) \\ NewSumOfAbsDev &= SumOfAbsDev + WeightSum * (Roughness + Stretch) \end{aligned} \quad (69)$$

Note that *sqr* may be interchanged with *abs* in both equations but *sqr* is always better in the *Stretch* equation because it is not desirable for the layers to stretch very far and also not desirable to unduly restrict small amounts of stretch. It is better for the layer above or below to start changing thickness in order to better match the data than for a layer to be

stretched so much that it overlaps the original boundaries of adjacent layers in the initial model. If *Stretch* has been calculated with *sqr* then, in order to weight the stretch constraint constantly with the L1 sum of squares goodness-of-fit of apparent resistivity model and field data, the square root of the sum term in the stretch equation must be taken.

wtOrigModel and *wtVertSmooth* may be varied from 0.001 to 10 in the software produced along with this thesis or may be set to zero in which case the respective weighting is disabled completely to save on processing time.

In order to resolve the many high resistivity contrast boundaries evident in towed waterborne data, it is important to keep *wtVertSmooth* as small as possible by compensating by increasing *wtOrigModel*. Stretch constraint alone cannot however stabilize the overparameterized models that are being generated. It has been found that, with an 8 configuration AXB array, a value of 0.01 for *wtOrigModel* and a value of 0.1 for *wtVertSmooth* (when conducting L1 inversion or 0.05 for L2) are optimal.

Smoothing constraint is largely needed to prevent inversion from over- and under-shooting. Such behaviour may well be more appropriately prevented using 2nd derivative smoothing rather than 1st derivative smoothing such as adopted here. Second derivative smoothing may have less impact on real high contrast boundaries.

6.10 Sub-noise data aware inversion

Highly conductive investigation targets such as sulfide ore bodies, aquifers containing hypersaline groundwater and thick saline clays often tend to consume almost all signal available to geo-electric arrays. Similarly, transient electromagnetic signals fall below noise at very early sample times when sensing resistive half spaces. The lack of signal does not imply that the data is useless but rather that the earth is very conductive if the data is geo-electric, or very resistive if the data is electromagnetic. This implication should be taken into consideration in inversion. Currently available inversion theory and software behaves erratically and erroneously with such data, particularly if the collection of effective depths of quadrupoles (geo-electric case) is sparse.

Sub–noise data aware inversion technique recognizes data that is below noise level and proceeds by constraining inversion to models that would create such sub-noise data. Such

an approach will honour data that is above noise level and invert it correctly while also modelling conductive anomalies to the minimum conductivity (geo-electric case) that would create data below noise level. The author suspects that this is a new concept.

The problem is more pronounced in cases where density of sampling of depth is poor such as with many pulled array surveys were electrodes have been spread widely in order to permit faster sampling. Existing algorithms inverting high vertical density geo-electric data are likely to model conductive features using data just above the features. If such algorithms were inverting data of low vertical density data then they will either just detect such conductive features or completely miss them.

Full explanation of the algorithm is as follows.

Least norm inversion (such as least squares inversion) tries to minimize a sum of errors between model and field data. It is common practice to weight such errors so that field data with low signal to noise levels has little influence on the sum of errors. In sub-noise data aware inversion, weights are dynamically adjusted not only depending on field data signal to noise ratio (SNR) but also on model data magnitude in relation to the field data noise level. To begin, a noise level is identified, either by an operator who has analysed a sample dataset or by an instrument that, theoretically, can automatically detect noise levels. Then, during the inversion process where an array of field apparent resistivities *RField(i)* is matched to models producing an array of simulated apparent resistivities *RModel(i)*, weights are applied to the data according to the following procedure:

For each sounding, the noise level is divided by current injected to give *NoiseDivCurrent.*

For each data point *i* within a sounding the following procedure occurs:

If *RField(i)<=NoiseDivCurrent*GeometricFactor(i)* then the field value is below noise level and the following procedure occurs:

> If *RModel(i)<=NoiseDivCurrent*GeometricFactor(i)* then the following occurs:
>
> > Difference between *RField(i)* and *RModel(i)* is recorded as zero so that the model is considered to be a valid model by the inversion criterion.
>
> Otherwise the following occurs:
>
> > Difference between *RField(i)* and *RModel(i)* is recorded as

*RModel(i)-(NoiseDivCurrent*GeometricFactor(i))* so that the inversion criterion only penalizes according to difference between the model data and the noise level.

Otherwise, normal inversion procedure occurs so that the difference between *RField(i)* and *RModel(i)* is recorded as the actual difference.

Using the differences calculated for all the data points, sum of squares or sum of absolute deviations is calculated and inversion proceeds.

Coded in pascal, the above algorithm appears as follows:

```
If SubNoiseInversion and (RField[i]<=
                        NoiseDivCurrent*GeomFact[i]) then begin
  If RModel[i]<=NoiseDivCurrent*GeomFact[i] then begin
    ModelMinusField[i]:=0;
  end else begin
    ModelMinusField[i]:=RModel[i]-NoiseDivCurrent*GeomFact[i];
  end;
end else begin
  ModelMinusField[i]:=RModel[i]-RField[i];
end;
```

The algorithm is presented as a flow diagram in Figure 6-1.

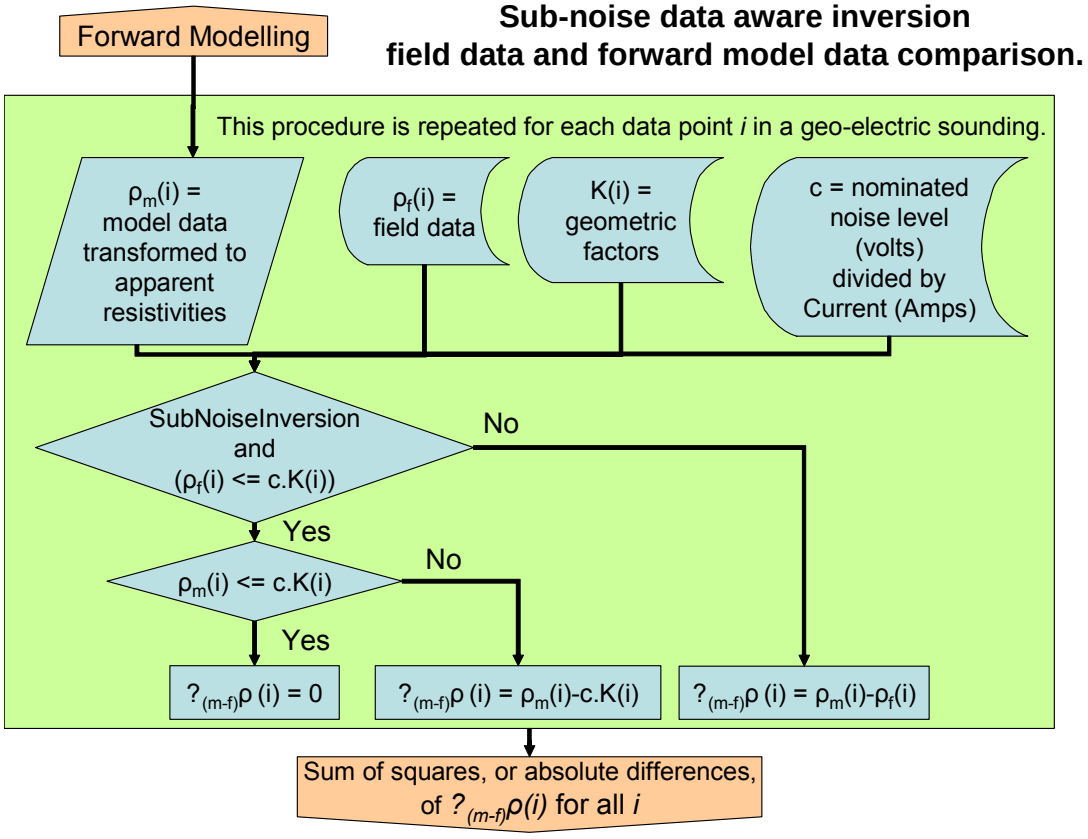

Figure 6.1 Flow diagram of sub-noise data aware inversion field data and forward model data comparison.

That is all that is needed to resolve conductive basement that is not detectable in the part of a geo-electric sounding that is above noise level but that has pulled some data below noise level. It is not possible to tell how conductive the basement is, however, just that it is conductive enough to force the field data to less than the noise level. The theoretical and saline inflow to rivers case studies given in later chapters will give examples of sub-noise data aware inversion.

6.10.1 Use of sub-noise data aware inversion with other inversion code

The inversion strategy of this thesis uses orthogonal factorization which will only provide a qualitative assessment of parameter sensitivity via a derivative matrix whereas many algorithms in modern inversion packages perform singular value decomposition in order to create sensitivity matrices and classify parameters. Sub-noise data aware inversion will, however, perform the same role if adopted in such algorithms as it does in inversion

algorithms based on orthogonal factorization. Without it, they would be able to do no more than mask out deep features that have pulled signal below noise level.

6.11 Weighting of data

6.11.1 Total rejection of data below noise level

In this thesis, parameters of each layer in initial models have been determined using the field datasets. If rejection of low SNR data is conducted prior to inversion then this results in models with different numbers of layers which may not compare well. Use of sub-noise data aware inversion rather than clipping of datasets prior to inversion will alieviate this problem. It will not, however, indicate at what level models should be clipped. This, instead, is the role of sensitivity analysis. Sub-noise data aware inversion can, however, be used even if datasets are clipped at noise level prior to inversion. In order for sub-noise data aware inversion to function with clipped datasets, clipped data points must be replaced with data at some arbitrary value less than noise.

For the purpose of creating initial models without excessive numbers of layers corresponding to data below noise level, options for rejection of data below a specified noise level and, optionally, rejection of subsequent data have been implemented and tested. The number of layers in the models changes as a result leading to inversions that cannot easily be compared. This strategy was then rejected for this reason. When weighting was applied to the data instead of rejection for data that fell below noise level, a minor improvement in inversion was noted.

6.11.2 Weighting of data depending on noise level

Facilitation for weighting of data was added and tested. Weights were observed by RMS and sum of square calculations within the inversion code. As all data remained, models calculated using the data kept the same number of layers and therefore were comparable. Reactions to signal level changes along the survey lines were gradual rather than abrupt as happened with the data rejection option.

Weighting was applied as follows:

The following parameters were input by the user:

WeightLimit (the maximum voltage at which weight is diminished),
Noise (the voltage at or below which minimum weight is applied),
WeightAtNoise (the weight at or below noise voltage),

Above WeightLimit, a weight of 1 was applied.

Between WeightLimit and Noise, a weight was applied linearly using -

$$Weight = WeightAtNoise + (1 - WeightAtNoise) \times \frac{V[i] - Noise}{WeightLimit - Noise},$$

Successive data points below *WeightAtNoise* were given half the weight of the points above them. This is because such data should theoretically have worse signal to noise ratios. Noise may have a significant systematic component (DC offsets) which appears like real geological features in stitched 1D presentations. Such noise must not be allowed to influence inversion so sub-noise data must be weighted minimally. Of course, if sub-noise data aware inversion such as described in the section above is conducted, then weights of data below noise level are insignificant. Weights of data just above noise level will, however, be significant and, if they are appropriate, will smooth and enhance inversion more than unweighted sub-noise data aware inversion.

6.11.3 Minimum and Maximum Apparent Resistivities

To further diminish the effect of erroneous data, a facility for removing input data with apparent resistivities that are above or below set values was added to the input filters. The facility helps strip out data collected when the array is pulled over obstacles or when the boat has stopped and the array has crumpled up against it.

If the inversion option to assume data has been clipped at noise level prior to, rather than during inversion is set and sub-noise data aware inversion is being conducted then this facility should not also be used as a conflict in noise handling will result.

6.12 Alternative methods of treating sub-noise data resulting from hypersaline basement or other signal consuming features

There are numerous other ways of coping with noisy data that the author believes are either inferior to, or compliment, the practice of sub-noise data aware inversion.

Alternative ways of treating noisy geo-electric array data and the consequences are as follows:

Include all the data: Deep features in the data appear, in some cases, as resistive anomalies as subsequent channels of positive data below noise level unrealistically elevate model resistivities. In other cases, sub-noise data will be negative requiring an exception to be triggered upon log transformation of that data or causing the inversion software to try to model infinitely conductive anomalies to non-transformed data.

A priori model constrained inversion: This technique will simply artificially replace conductive features with the *a priori* model resistivity. The information contained in the fact that some of the data are below noise level due to conductive features is lost. Results tend to confuse later users of the inverted data and very serious false interpretations may result. This technique is a default option in the Zonge package TS2DIP (MacInnes & Raymond 2002).

Clip off data below noise level: This option, at best, leaves non-anomalous parts of inversion models intact but leaves holes where conductive bodies should be. More frequently, the sites where the conductive features exist are modelled by extrapolation, conducted by gridding packages, from surrounding data resulting in no anomalies or resistive anomalies over the conductive features. Consider the case where some soundings in a profile contain very conductive basement highs that bring signal below noise level. Adjacent soundings will detect and model the edges of such conductive basement highs while the soundings over the highs will model relatively resistive basement.

Weigh the sensitivity of inversion to data depending on the signal to noise ratio of the data: This approach is an improvement on the previous approaches as it tends to dampen the effects of the poor signal to noise ratio data resulting in better inversion of resistive features while retaining some sensitivity to the conductive features. Even so, it still suffers the flaws, mentioned above, of the method of clipping data below noise level.

Any of the above with smoothing constraint: Smoothing will not help with the problem at hand. Rather it will just smooth both the correct and incorrect features of the inverted models.

Lateral constraint or smoothing, like the vertical smoothing constraint, will not help correct for noisy data due to conductive features. Rather, like vertical smoothness constraint, it will constrain anomalies over edges of conductive features correctly and erroneously constrain areas surrounding conductive features.

Cornacchiulo (2004) demonstrated the use of Kriging to replace noisy data. Like the smoothing constraint, this technique cannot identify lost sections of conductive basement unless they are very small and flanked by detected conductive basement.

6.13 Alternative inversion strategies.

In the process of development of the inversion technique employed in this thesis, numerous 3rd party inversion products were tested and assessed for use on data collected by towed waterborne arrays. Following is an assessment of those products/techniques.

6.13.1 Lateral constraint

Laterally constraining 1D inversions improves them if geology is clearly and discretely layered. Under Murray-Darling Basin canals and rivers, this was rarely encountered. A crude way of applying a pseudo-lateral-constraint is to horizontally smooth the data, particularly the data with larger effective depths. This method has been applied here (see Appendix 5.2) in preference to true 1D or 2D laterally constrained inversion, which has been solved by the Aarhus Hydrogeophysics Group (Auken 2004), simply because of cost and deadline limitations. Experimentation using up to 24 passes of a 17 point filter was conducted but up to 4 passes of a 9 point filter was found to be appropriate on data collected at 4 second intervals. The inversion algorithm presented in this thesis could easily be extended into true laterally constrained inversion following the approach of Auken (2004). The case studies section of this thesis gives examples of 1D laterally constrained inversion.

6.13.2 2D smoothed cells

Smooth model 2D resistivity inversion does not cope well with very fine layers at the surface and closely spaced electrodes that are designed to detect such layers. Horizontal ripple effect, where noise, or a geological feature, is modelled by a series of horizontal ripples rather than one peak, occurs in the inverted models almost invariably. Vast lengths

of data collected over predominantly horizontally layered geology results in an extremely ill-posed 2D inversion problem. Processing is excessively intensive and requires that data be cut up into small overlapping segments. The overlapping segments must then be stitched back together after inversion. End effects typically result in less than perfect stitching. Along rivers, features are generally horizontally layered with very sharp contrasts. Also, almost all horizontal variations along rivers are 3D rather than 2D so little improvement over 1D inversion may be achieved by 2D inversion. Often worse inversion occurs due to horizontal ripple, inappropriate smoothing effects and artefacts and less than optimal vertical variation, weighting and sampling. If one is looking for buried pipes or drums, then 2D inversion would be appropriate; however, such targets would be far better resolved using electromagnetic and or magnetic equipment than geo-electric arrays. This is because electromagnetic and magnetic features respond directly to isolated metallic features. Both Scott MacInnes' TS2DIP (2001) and Loke's RES2DINV were tested and the results are in the case study chapters. Both of these authors have recently been improving the ability of their software to handle very long marine resistivity datasets.

6.14 Alternative methods of selecting initial models and constraining inversion

The inversion scheme chosen permits any combination of layer thicknesses and resistivities as an initial model. Furthermore, any combination of those parameters may be fixed so that they are taken into account when forward modelling but ignored during inversion resulting in faster and more robust, but not necessarily more appropriate inversion. Not all combinations are sensible of course. Combinations of types of initial model selection and inversion constraint that have been tried are as follows:

1. *One fixed initial model may be selected for all soundings and inversion may be constrained by fixing of various parameters determined by the user* – This option has been facilitated but not favoured. Floating thicknesses can occasionally result in layers becoming infinitely thick or thin thus pushing other layers out of the range of sensitivity of the data. When hundreds of thousands of soundings need inverting, such behaviour cannot be tolerated. The option has been mainly rejected because input from the user wastes time in a production environment and requires well trained operators. Also, with long sections of data, it is unusual for one initial model to be applicable to the whole

section. A model with all layer resistivities equal would then possibly be the best fixed initial model that could be applied.

2. *Initial models may be created with one layer for the effective depth of each of the configurations in the geo-electric array. Thicknesses may all be fixed to assist in constraining inversion. Resistivities of the initial models may be set to the apparent resistivities of each configuration.* This option is good when data quality is good but gives no consideration to water depth. All the thicknesses are fixed as this option includes as many variables as the number of data values in the dataset, each variable carefully tied to a particular data value by sampling at effective depths so that no parameter becomes unstable. Addition of more variables will result in instability so it is important to keep the thicknesses fixed.

3. *Initial model creation and inversion constraint may be achieved as for case 2 but further constraint may be applied by imposing a limit on the number of layers.* This option is important because often data quality can become very poor at large electrode spacings. In such cases, the initial model must be forced not to include the deeper layers corresponding to data with large effective depths and poor data quality. This can be done by totally ignoring noisy data both in model picking and in inversion but this results in adjacent soundings inverting with models with different numbers of layers – the result is visually displeasing and very difficult to interpret. In many cases the number of layers changes back and forth repetitively. An alternative is to fix a maximum number of layers for the initial model and let the inversion code decide how much of the noisy data to use and how it will weight it.

4. *Initial model creation and inversion constraint may be achieved as for case 3 or 2 but all layers centred above the water depth may be replaced with one layer of resistivity equal to that of the initial first layer in order to further constrain inversion.* There are a few exceptions to be dealt with in this scenario such as when the water depth is not within the range of the effective depths of the array. Such exceptions are dealt with in code using simple logic. This option is viable but can cause hidden geophysical artefacts when water depth is extremely variable along the array length or laterally or when the river/canal water is not homogeneously conductive. Day-Lewis *et.al.* (2006) provide a very clear demonstration of what can go wrong when this approach is taken.

5. *Initial model creation and inversion constraint may be achieved as for case 3 or 2 but the layer boundary closest to the water depth may be shifted onto the water depth in order to create a more realistic initial model.* Again there are a few exceptions to be dealt with in this scenario such as when the water depth is not within the range of the effective depths of the array. Such exceptions are simply dealt with in code using simple logic. Significant geophysical artefacts are not created as may be in option 4. Rather, lateral or along-array water depth variations will result in small apparent variations in river water conductivity which can generally be rejected as artefacts. In some cases significant variation in river conductivity will exist and will still be measurable even in the midst of such small artefacts. Hydrographers routinely measure very small variations in river water salinities over time and tend to expect geo-electric arrays to be able to do the same. This is not possible because of the way signals from sediment below the river combine with signals from the river water in a way dependant very strongly on water depth. The signal resulting from extreme variations common in sediment overprint the signal from small variations in river water conductivity for all but the most shallow configurations.

6. *2D initial models of various types may be used with smoothness constrained 2D inversion.* Two dimensional inversion is not considered in detail here as it is not appropriate in layered sedimentary environments. Loke (2004) presents examples where 2D inversion has been useful for defining non-extensive highly important geological targets under watercourses such as proposed bridge pylon sites.

6.15 Detectability and Equivalence analysis using inversion of multilayer model geo-electric voltage response curves

The effective depth of a quadrupole, the 10% geo-electric array resolution criterion and the extended effective depth criterion of Merrick (1997) are useful for comparing performance of individual quadrupole in various geo-electric arrays but do not take into account signal to noise ratios or give any absolute information on ability of an array to detect change in a parameter. The ability of an array to resolve anything is also dependant on noise levels. Also, a combination of quadrupoles in a geo-electric array is much more able to resolve features than individual quadrupoles. The ability of an array to resolve variation in any model parameter can be obtained by conducting forward modelling using the base model with a set of small changes in the parameter of interest. A set of layered

models and associated type curves is developed. When two such curves vary at some point by more than the nominated noise level, then the parameter variation between them is detectable. This does not however mean that inversion will be able to attribute the measured variation to the correct parameter. A further problem called non-uniqueness produces additional ambiguity. Non-uniqueness, also, possibly erroneously, referred to as equivalence in geophysical literature occurs when there is more than a unique solution that will fit a particular dataset within the error bounds of that dataset.

Equivalence analysis is conducted by nominating a noise level and then making small variations in model parameters to see how much variation can occur before the noise level is exceeded on some datapoint or other. Detectability of features can roughly be determined by creating batches of forward models with minor incremental variations and adding noise to each of them. When the resultant datasets have been inverted, detectable variation will be evident in a stitched 2D section. If variations in the initial model parameter were fine enough, even if noise were not added, the effect of some equivalence will be evident in the 2D section as erratic changes in parameter combinations. For example, moving across a set of stitched together inversions, one may notice that a conductive layer underlies a resistive layer; however, some isolated soundings may indicate a very conductive thin layer overlain by that same resistive layer but underlain by a layer of moderate resistivity. Inversion is switching between two models that give equivalent data within the limitations of the initial model parameter variation, or noise specified. Because the inversion procedure recommended in this thesis involves generation of one initial model layer per electrode configuration, non-uniqueness could result in very unstable inversion solutions if constraints were not sufficient. By copying one forward model many times, adding random noise to each copy and inverting the resultant datasets, non-uniqueness, on its own, can be assessed in stitched 2D sections. The chapter on Theoretical Case Studies will present examples of 2D stitched sections exhibiting non-uniqueness and that are useful for determining what type of model variation can be resolved. Thorough equivalence analysis is a difficult process due to the way all variables must be considered in combination. It will not be considered further here. Readers are referred to Merrick (1977) or IX1D documentation (www.Interpex.com).

6.16 Summary

The technique used to produce initial models in this thesis has involved centring layers over the effective depths of each configuration in an array. The layer boundary closest to the water depth is then shifted to the water depth. Horizontal smoothing reduces noise levels in the data. During 1D inversion, Layer depths are treated elastically and minimal vertical smoothness constraint is applied. Data is weighted according to noise level and sub-noise data aware inversion is applied to resolve conductive basement.

Performance of the inversion strategy presented is demonstrated in both theoretical case studies, in Chapter 14, and case studies conducted on numerous water bodies, in Chapters 15 to 18.

CHAPTER 7 - EQUIPMENT FOR CONTINUOUS EC IMAGING

Equipment for EC imaging is composed of:

- either geo-electric arrays or loops of wire for generating electromagnetic fields;
- a mobile platform;
- position and water depth sensing equipment; and
- instrumentation.

Each of these will be considered in turn in this chapter.

7.1 Geo-electric arrays

Geo-electric arrays designed for continuous towed surveying require specialized design not only of electrode configuration but of cable and electrodes etc. Floating and submersible geo-electric arrays were especially designed and built, as part of this thesis, for application in inland rivers and canals. This chapter will look at physical (rather than configuration related) electrode array design criteria and then detail the way the author has dealt with these criteria in his electrode array designs. Towed array noise analysis will be discussed. Sample arrays are displayed in Figures 7-1 and 7-2.

7.1.1 Design Criteria

Good designs attempt to optimize the combination of the following features:-

- Low risk of physical wear resulting in leakage of voltage along array wiring;
- Minimal crosstalk between conductors in the array;
- Ease of current injection;
- Flotation of the entire geo-electric array, even when stationary;
- Minimal drag;
- Structural integrity;
- Wear resistance;
- Cost of construction;

- Ability to slide past fallen trees and other obstacles in the river without 'snagging';
- Fast setup and pack up;
- Facilitation of compact and robust shipping; and
- Visibility for navigation purposes.

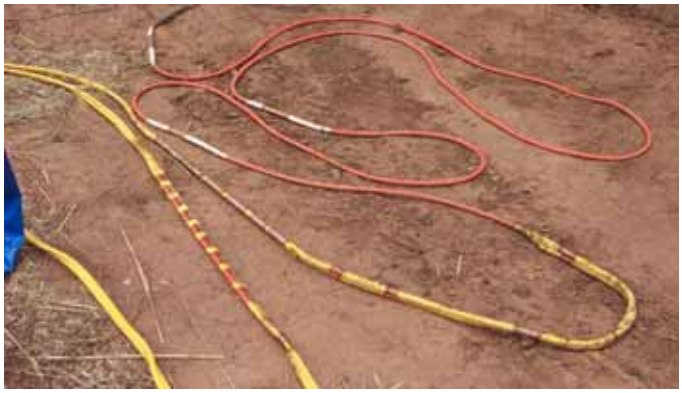

Figure 7.1 An early prototype submersible 20m geo-electric array (with 15m yellow leader).

Figure 7.2 A 144m geo-electric array deflated and packed for land transport. The last 64m of the array are seen at the top of the box (single wire in garden hose). The rest of the array consists of heavy gauge multicore cable glued to layflat hose.

More detailed analysis of each of the design criteria is as follows.

7.1.1.1 Insulation integrity and DC crosstalk

The first consideration when using waterborne arrays is robustness of insulation. A small defect anywhere along the insulation of a wire, in the presence of water will cause havoc since signal levels on adjacent wires tend to differ by many orders of magnitude. Dahlin (2005) states that PVC insulation absorbs enough water, when immersed, to become slightly conductive. Resistances of 2 megaohms between wet 100m lengths of adjacent PVC coated conductors have been measured by the author. When electrode contact resistances are of the order of 100 ohms, a 2 megaohm cable sheath resistance will result in a ratio of crosstalk signal pickup to genuine signal pickup of $100/200000=5x10^{-6}$. When signals from distant electrodes are very small, crosstalk from electrodes near the transmitter electrodes can be troublesome with such sheath resistance. Signals from distant electrodes may be 8 orders of magnitude smaller than power passing to transmitter electrodes through adjacent wires. Polyurethane insulation does not suffer from this problem and is therefore recommended. A megohmeter is most appropriate for testing geo-electric array insulation as an ordinary multimeter cannot create the large voltages required to conduct reliable high resistance tests.

7.1.1.2 Electromagnetic crosstalk

A similar consideration is that of electromagnetic crosstalk – this is particularly relevant when the transmitter signal is noisy. High voltage transmitters contain DC-DC converters which, if of poor quality, produce very noisy signal. If the cable is of very small diameter or if high signal wires are adjacent to low signal wires or if wires are not coupled so as to cancel noise, as much as is practical, then crosstalk can compromise the data quality. Appropriate use of twisted wires and/or shielding (which also needs to be fully insulated (including ends) when immersed in water) can further reduce noise and crosstalk.

7.1.1.3 Ability to slide past obstacles

The whole apparatus needs to be able to slide past obstacles without catching on them. It helps also if it is of low friction so that it is easy to pull and reduces build up of stress along the cable when it is towed in a zig-zag manner between several obstacles. For this reason it is best if electrodes can be of the same diameter as the cable. There is an

exception – when towing along ground, bulging electrodes can help as they can attain better ground contact than streamlined electrodes.

7.1.1.4 Ability to withstand towing forces

When the array does catch on something, it needs to arrest the motion of the towing vehicle before the limit of elastic strain of the array is reached. The cable strength required to stop a large boat or truck weighing several tonnes and travelling at 10 km/hr is immense if there is no high strain member at the attachment point. Even with a high strain attachment link between the array tethering point and the boat, such as a rubber strap or long spring, the array must still be strong enough to withstand the pulling force of the towing vehicle which needs to be considerable if the array is not streamlined. The pulling force can be restrained by the actual conductors in the cable if they are thick, or with a Kevlar strength member. Kevlar is a very strong, low strain material but it is not possible to completely prevent it from sliding within the cable and difficult to anchor it to electrodes. Steel cable strength members are of course not appropriate as electric current can leak along them.

7.1.1.5 Low Drag

Floating arrays, in particular, require low drag as with infinitely low drag they will follow in their path accurately while with high drag they will cut corners thus causing position errors and creating navigation havoc. Arrays of hundreds of metres of length with attainably low drag can easily be towed within metres of the towing vehicle's path even around corners of low tens of metres of radius.

7.1.1.6 Compact and practical shipping solutions

Additional design factors are equipment shipping dimensions and weight. Inflatable floating arrays have an advantage in this respect - for shipping, they can be deflated to save space. Inflation only takes a few minutes and is done using the mouth followed by a hand operated tyre pump. As inflatable arrays can be inflated with either water or air they can operate as dual purpose floating or submersible arrays even interchanging within survey transects when obstacles prevent towing during submersion.

7.1.1.7 Flotation of the entire geo-electric array, even when stationary

By adding float tube to the entire length of the array, it is prevented from sinking when stationary. Should the tube deflate to atmospheric pressure, there is still enough air in it to keep it afloat except near the heavy transmitter electrodes. This is important because, should the boat stop due to being snagged on a submerged obstacle, or for some other reason, the array will be caught up in the current and may be dragged across various obstacles. Towing of the array off the obstacles is generally very simple if it floats; however, if it sinks at some point, and this point is drawn by the current so that it drags the array through submerged obstacles such as trees then a disastrous situation eventuates.

7.1.1.8 Low electrode noise

When electrodes are towed through water, noise level increases drastically. It is believed that this behaviour is somehow dependent on ionic double layer breakdown. Electrodes optimally would be made of inert materials with stable non-polarizing fluid encompassing them; however this is not necessarily practical in towed arrays. During tests, the difference in noise in moving arrays with electrodes of copper, bronze and stainless steel could not be detected. However, good controlled tests were not conducted due to the cost of equipment rental. This is an important area for further work. Alternative electrode materials such as lead/lead oxide, graphite and silver/silver oxide are worth investigating.

7.1.1.9 Fast setup and pack up

Arrays of the designs selected could simply be pulled out of their packing boxes and laid out in a zig zag pattern on the river bank and then towed into the water. Packup simply involves lifting the array a little at a time back into the shipping box. Care must be taken not to bend the array around very sharp radii when packing as this puts great strain on the wires within it, particularly at their connection points to the rigid electrodes.

Where setup and pack up costs are critical, such as surveys involving many short lengths of canal or river, array length should be kept to a minimum as array length, and weight, proved to be the factors that most limited setup and pack up logistics.

7.1.2 Geo-electric array construction

A guide for constructing geo-electric arrays for towed use is included in Appendix 1. Also included in Appendix 1 are notes on designs that were rejected and electrode noise tests.

7.2 Towing devices, logistics and survey productivity

Towed geo-electric array survey productivity is almost entirely dependant on the towing device. The ability of the towing device to be quickly deployed and pass obstacles normally is much more important than its survey speed. Speeds of 5 to 10 km per hour are normal for geo-electric surveying. Faster surveys will suffer more from electro-kinetic noise.

Most waterbodies on which geo-electric surveys are warranted are not considered to be entirely navigable by conventional watercraft. Design and operation of suitable survey vehicles, in most cases, determines the practicality and viability of surveys. Such vehicles not only need to navigate through difficult watercourses but must do so productively, steadily and cheaply.

This rather pragmatic chapter is full of simple ideas that are critical for survey productivity and therefore are very important. Idling down a waterway in a boat towing some electronic equipment sounds rather straight forward; however most waterways are anything but the idealistic waterways with weir pools adjacent to towns and cleared of fallen trees, that people choose to boat on. Typical, obstruction filled waterways with currents do not allow one to stop if something goes wrong and are anything but straight forward to survey. Towed array surveys are useful at sites where canal seepage is problematic, where transmission losses from rivers need to be studied, and where saline inflow, acid inflow (from acid sulfate soils) or other pollution flows into rivers or drains. These sites rarely offer ideal navigation and innovative array towing solutions usually need to be implemented. Furthermore, launch sites rarely are good at survey locations, and, at some, there is not even public access. Survey budgets usually require that very efficient launching and landing be conducted under these non-ideal situations. Equipment used, including the geo-electric arrays, typically needs to be light, rugged and streamlined. Figure 7-3 presents some of the solutions implemented so far and Table 7-1 tabulates them.

Table 7-1 A summary of towing devices for geo-electric survey

Vehicle	*Use*	*Details*
Quad-bike with boom	Small canals, edges of flood & furrow irrigated land	A boom extending from the side of the bike normally tows the submersible array. The device is very limited by the length of boom that can extend from a quad bike.
Quad-bike with rice tyres	Flood irrigated land	The quad bike travels across flood irrigated land towing the array. This is very demanding on the quad bike.
Boom extending from a 4wd	Small and medium sized canals with continuous vehicular access along either bank.	A highly efficient way of surveying where vehicular access exists. A boom length of about 6 metres is practical which means that many canals can be surveyed from a track adjacent to the canal bank. Obstacles are simply driven past.
Canoe or boat with air propeller	Weed clogged canals and shallow waterways	A canoe or boat with an air propeller (like used on the everglades of Florida but on a much smaller scale) is lifted in and out of canals by a 4wd mounted crane and surveys straight through weed filled sections.
Dingy with paddlewheel	Weed clogged canals	A dingy equipped with a paddlewheel can slowly negotiate weed effectively but weed can wrap around the paddlewheel axle or jam under the guard.
Argo 6 or 8 wheel amphibious vehicle	Marshy rivers and swamps	6 or 8 quad-bike tyres propel a small boat. The device is limited in that it cannot drive in and out of canals and other waterways with steep slippery banks. It can operate with an outboard motor
Hovercraft	Not recommended	The hovercraft is a high speed device that lacks control that is crucial for towed array surveys.

Vehicle	*Use*	*Details*
Fully sealed radio-control watercraft	Not recommended except after much development work - Frequently obstructed canals.	Easy to lift over obstacles. Propelled by an air or water propeller or paddle wheel that will not be fouled by weed. Needs ability to easily reverse off obstacles which is important for unmanned craft. Power required for towing a submerged array is sufficient for propelling a man also, making this craft unviable except after much development work
Manned watercraft (canoe, dingy or boat)	Rivers and large canals	Limited by water depth, weed growth and frequency of obstructions. In canals, obstructions may be negotiated using a 4wd mounted crane.
Houseboat	Long stretches of very large rivers	Eliminates accommodation costs and transfer to and from the boat resulting in highly efficient surveying.
Dual watercraft	Obstructed rivers	A second watercraft is useful for moving the array past obstacles and fetching the land vehicle. The author tried it once and does not recommend it.
Aarhus Hydrogeophysics Group PACES	Towing specialized heavyweight geo-electric arrays across ground for aquifer characterization	A tracked hydraulically driven device similar to the Australian 'Dingo' earthmover is used to tow an array which is gouged into moist ground behind the vehicle. Special electronics and very heavy electrodes are needed to make the system work even in moist ground.
4wd or tractor mounted ripper and press wheel	A geo-electric array can be ripped into cultivated soil for soil studies.	A ripping tine is mounted on the tow bar of a 4wd or behind a tractor. the array is towed from a tube extending off the tine and soil is pressed onto it with a pressing wheel.

Figure 7.3 Equipment for towed geo-electric surveying from surface water bodies. Small watercraft such as canoes with outboard motors are appropriate in canals which typically contain numerous obstacles over which the craft must be lifted either by hand or with a small crane. In canals with lots of weed, which quickly stops outboard motors, a boom extending from a 4wd is most appropriate for towing arrays. Electronics suitable for operating the arrays is produced by Lund university combined with ABEM – Terraohm RIP924, Iris Instruments – Syscal Pro (lower left), Zonge – GDP32 (lower right) and AGI – Supersting R8 Marine.

Details and examples of productivity and logistics of numerous devices are given in Appendix 2.

7.3 Productivity of towed Geo-electric arrays versus towed TEM

Towed Zonge NanoTEM, described in chapter 3, can also be used for surveying under large water bodies. It requires towing of a large (approx 8 x 8 m) loop. This device is only practical on large open water ways. It takes about 1 day to set up and pack up but this could be improved a little. On land, towed TEM, or airborne TEM can achieve far better production (see the later chapter on surveying across land) than towed geo-electric arrays.

Survey speed of towed TEM and geo-electric arrays generally is similar on water.

7.4 Location and Water Depth Detection

Survey tracks were positioned using GPS, initially with differential corrections. Water depth was measured either with a ruler (early surveys), sonar or a pressure sensor. Data from the devices was time stamped for merging.

7.4.1 GPS and Sonar

Due to availability restrictions, the equipment used for positioning varied. The various GPS receivers used logged data to Notebook computers running Fugawi or, later on, to a PalmVx along with sonar data. Fugawi for Palm devices does not log sonar so a general purpose communications program was used with the PalmVx. The PalmVx proved to be very logistically appropriate due to its robustness, compactness, instant startup/shutdown, and screen suitable for viewing in daylight. With only 8Mbytes of memory, it permitted 7 hours of survey (enough for 60km of survey) between downloads. Early surveys used independent sonar depth sensors not capable of logging data so depths were logged against time manually every 30 seconds. Figure 7-4 is a schematic of such equipment while Figure 7-5 is a photograph of it. The system was set up in a small tool box so that it was modular and could be air-freighted.

The PalmVx only logged NMEA0183 codes rather than reformatting data. Codes were downloaded and reformatted in the office (see Appendix 8 - Processing). NMEA0183 codes are time stamped. Time stamping permits merging of the GPS and sonar data with geo-electric array data (if it is time stamped). The Iris Instruments Syscal – Pro geo-electric instrument directly logged the GPS data on one occasion but failed to due to CPU problems on a second survey. As that instrument does not time stamp yet, data merging had to be done using a pencil, note pad and wrist watch on that occasion.

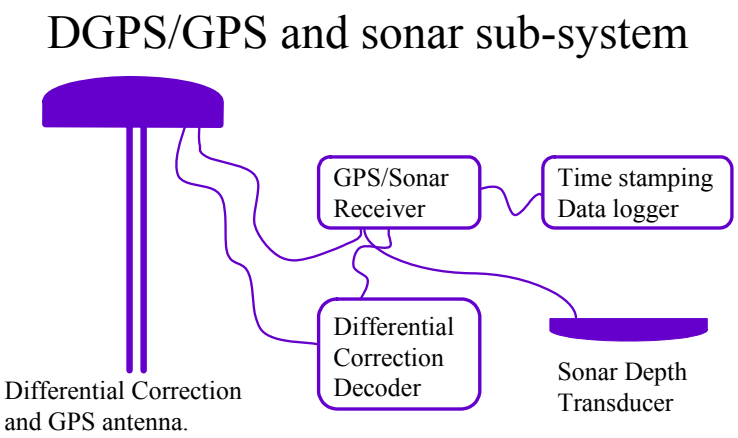

Figure 7.4 A schematic of a GPS sonar subsystem. On occasions a pressure sensor was used in place of sonar.

Figure 7.5 The GPS and sonar (Garmin GPSMap188) and data logger (PalmVx) subsystem

7.4.2 Differential GPS corrections

Differential GPS corrections were utilized on earlier surveys while selective availability was still implemented by the US military. After this was turned off, accuracy of GPS became about 5m (one standard deviation) and use of expensive differential GPS correction acquisition devices became unnecessary. New DGPS receivers do, however,

experience far fewer, and shorter, periods of unacceptable positioning accuracy than standard GPS receivers

7.4.3 Pressure sensors

Affordable commercial GPS – Sonar devices typically do not detect depths shallower than about 1.2 metres reliably. This limits their applicability. Use of a differential pressure sensor to measure depth is also possible. A Greenspan PS310 pressure/depth sensor (http://www.tycoflowcontrol.com.au/TES_Greenspan_Analytical/products/PressureLevel_Sensors) used on some surveys provided excellent depth control while being dragged along the bed of waterways along with the submersible array. The pressure sensor logged time stamped data all day and software later extracted relevant data for merging with geo-electric data. This sensor had a 40mm radius and included the logger at the actual sensor which meant that a rigidly encased foam padded enclosure had to be constructed to house it and drag it along the bottom. The sensor was chosen as it could be rented for a week at a rate that was affordable. For permanent use, a slimline sensor with a logger at the surface would be utilized. The sensor would be incorporated into the submerged array cable just before the reference transmitter electrode. These sensors require an air tube connection to the surface which is connected to a half filled bag of air in a rigid container. This allows pressure equilibration without electronics damage from condensing humidity entrained down the air tube. The pressure sensor setup utilized is evident in Figure A2-5, of the 4wd mounted boom in raised position. Later a more compact setup was achieved and it has been noted that, using the bubbler, or gas discharge, principle common in hydrographic installations that a far more compact setup is possible. Bubbler equipment that would need to be installed in the boat (gas bottle, course and fine regulators, etc.) would however be bulky.

7.5 Geophysical Instrumentation

Geo-electric arrays and transient electromagnetic loops must be operated with suitable geophysical instrumentation. A summary of instrumentation used with geo-electric arrays is given in Figure 7-6.

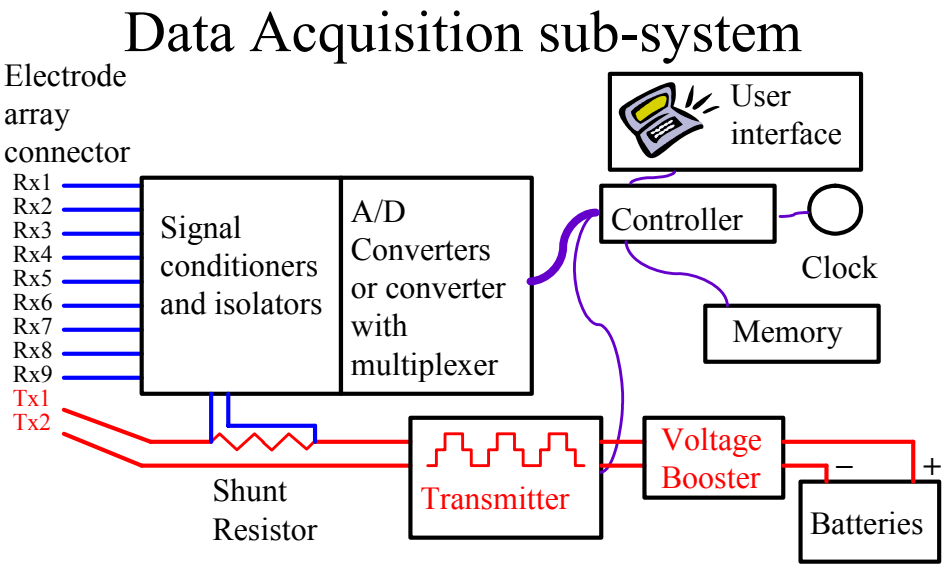

Figure 7.6 Geo-electric array instrumentation.

7.5.1 Geo-electric array instrumentation

A Zonge GDP32, a Zonge ZT30 and a Zonge power booster were used with two truck batteries and an isolation amplifier (for safe current measurement) for earlier surveys and large river surveys (see Figure 7-7). The ZT30 could transmit up to only 160 volts and drive only 600 milliamps through the transmitter electrodes thus transmitting only 100 watts. With a small routine modification which could not be afforded within the schedule of the surveys, the same transmitter would be able to transmit 400V and 1.5Amps. Better quality data could result from the modification.

Figure 7.7 Zonge GDP32 Receiver, isolation amplifier, shunt resistor, signal generator and voltage booster.

Should future surveys need to be conducted with very small boats or canoes, alternate light weight equipment is recommended. As all receivers and transmitters that are appropriate are used mainly for mineral exploration indefinitely on contracts lasting up to several months in remote locations (frequently in 3rd world countires), availability is unpredictable. The surveys conducted were only possible due to a period of minimal activity in the mineral exploration sector.

More compact equipment, the Syscal Pro with marine survey capability added, was designed by Iris Instruments after the initial trials demonstrated viability of the survey technique. This equipment was purchased by Geoforce of Western Australia for use in mineral exploration and rented by the author to conduct surveys on canals and constricted rivers. This equipment is displayed in Figure 7-8.

Figure 7.8 The EC data acquisition subsystem – Iris Syscal Pro (supplied by Geoforce) incorporated into a sealable water cooled box with GPS and sonar equipment.

Marine data acquisition software is available for use with the Syscal-Pro and an external logging computer. It was not used on any surveys due to lack of funding for purchasing the software and a suitable logging computer and lack funding for and practicality of operating a computer in the canoe. Computers now are available with a WiFi linked touchscreen that would be practical. Without the software, one must rely on internal data storage which was limited, and spot check quality control. This mode of operation proved to be very difficult and about one day in three had to be repeated due to unobserved quality control failures. Serious Syscal-Pro failures resulted in very low transmitted currents (driven by 12 or 25V in most instances) and other serious problems with DC offsets orders of magnitude higher than received signal strength. It is believed that these problems have been fixed.

The Syscal-Pro has a measurement range of +/-15V between electrode two and any other electrode (electrode 2 is used as a common ground). This means that dipoles one and two are measured in single ended mode while the remaining dipoles are measured in differential mode. Because the AXB array receives a very large variation in signal strengths with very high signal at electrodes one and two, the last electrodes measure

mainly common mode noise. If the array was connected in reverse, then the distant electrodes would be connected in single ended mode and problems with lack of instrumentation DC offset cancellation would result. A possible solution to this problem is to attenuate the large signals and buffer the ground (input 2) with greater percentages of distant electrode signals. This technique is presented in Figure 7-9.

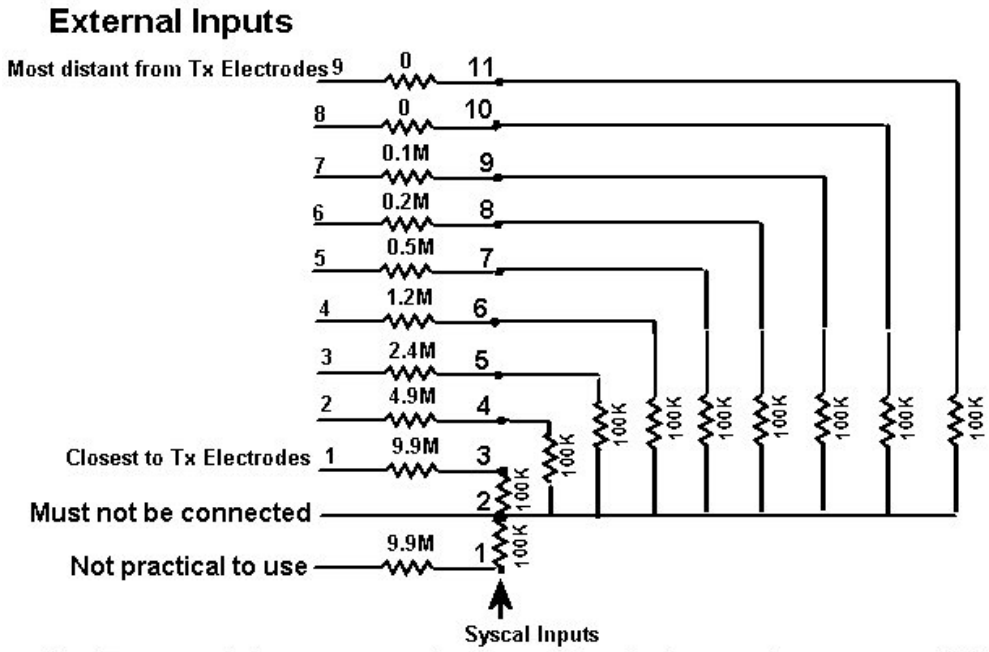

An External Attenuator for use of a 8 channel exponential bipole-bipole array with the Syscal Pro. Ground (input 2) is forced to a level near that of the most distant electrodes.

Figure 7.9 Attenuation of AXB array signals for input into a Syscal-Pro using a circuit of standard resistors.

As the input impedance of the Syscal-Pro is only 500 megaohms, the resistances of the voltage dividing resistors must be small. This means that the resulting system can only be used with arrays with very low contact resistances on all receiver electrodes. Submersible geo-electric arrays generally fit this criterion.

Another recently introduced instrument, the SuperSting Marine geo-electric transceiver is available from Advanced Geoscience Incorporated (www.AGI.com). This instrument has the same limitation of a common ground on input 2 as the Syscal-Pro, however, at the

time of writing it has an input range of only +/-5 volts. This renders it very unfavourable for use with arrays with very large signal ranges such as AXB arrays.

Instrumentation with isolated differential inputs and attenuation circuitry built in such as the Zonge GDP32 and the Lund University TerraOhm RIP924, which has just been designed, do not have problems with large signal ranges such as produced by AXB arrays. The RIP924 has been especially designed for continuous geo-electric surveying.

7.5.2 TEM Transmitter, Receiver and antennas

The Zonge Nanotem receiver and fast turn off ZT20 transmitter was used for all the TEM surveying. This equipment functioned very effectively. Ramp turn off time was 2 μs. Gates were measured between 5.14 μs and 1.014ms.

Zonge constructed a 7.5m square floating transmitter loop ($56.25m^2$) with a 2.5m square receiver loop ($6.25m^2$) in its centre. Their design followed on from a prototype they had constructed with assistance from Brian Barrett, a masters student at the University of Adelaide. As is standard practice, the receiver loop had an appropriate resistor included across its output wires for the damping of inductive ringing. The output wires were connected to terminals of a high quality fast sampling A/D (Zonge GDP32 nanotem card) and to instrument ground via appropriate resistors for signal stabilization. Both loops only contained a single turn of wire so that self inductance problems were minimized. The device when packed away just fitted on a trailer or Landcruiser roofrack. The loops were floated on a fairly rigid frame so that vibration (wobble) could not create significant noise due to the loop moving back and forth through the magnetic field of the earth. It took two people several hours to assemble and to pack up the device. As a result it always had to be either assembled or packed up on a separate day from when it was used for survey.

7.6 Safety, Legal and Environmental Assessment

Appendix 3 is a study of safety, legal and environmental issues of continuous EC imaging.

7.7 Complementary Investigation Techniques

EC images of aquifers beneath watercourses generally are only useful once they are interpreted in the context of other information. Appraisal of certain topical and/or promising investigation techniques has been conducted in Appendix 7 for this purpose. Examples of use of most of the techniques are given in the case studies in later chapters.

CHAPTER 8 - TERRESTRIAL MULTI-DEPTH EC IMAGING.

Vast amounts of single and dual depth EC imaging across land have been effectively conducted using Geonics EM34, EM31 and EM38 and related devices (Beecher, 2002). Tracing of aquifers across land from where they are connected to waterways is best done with multi-depth EC imaging devices because interpretation of single depth data can be ambiguous. Often, important features are missed altogether by single depth instruments due to inappropriate targeting of depth of investigation. Terrestrial multi-depth EC imaging devices include the following:

Towed frequency domain devices with multiple coil spacings and, in some cases, orientations.

Hammered stake geo-electic surveys

Geo-electric arrays towed by a ripping tine.

Aarhus University PACES system.

Towed capacitive geo-electric arrays

Manually laid loop TEM

Towed TEM

Airborne EM (Time or Frequency domain)

Two of these techniques, geo-electric arrays towed by a ripping tine and towed TEM, have been developed in this thesis. The rest have been included for brief discussion and comparison. Ranges of depth of investigation typical of each type of device are displayed in Figure 8-1. Notes on each of the techniques are as follows.

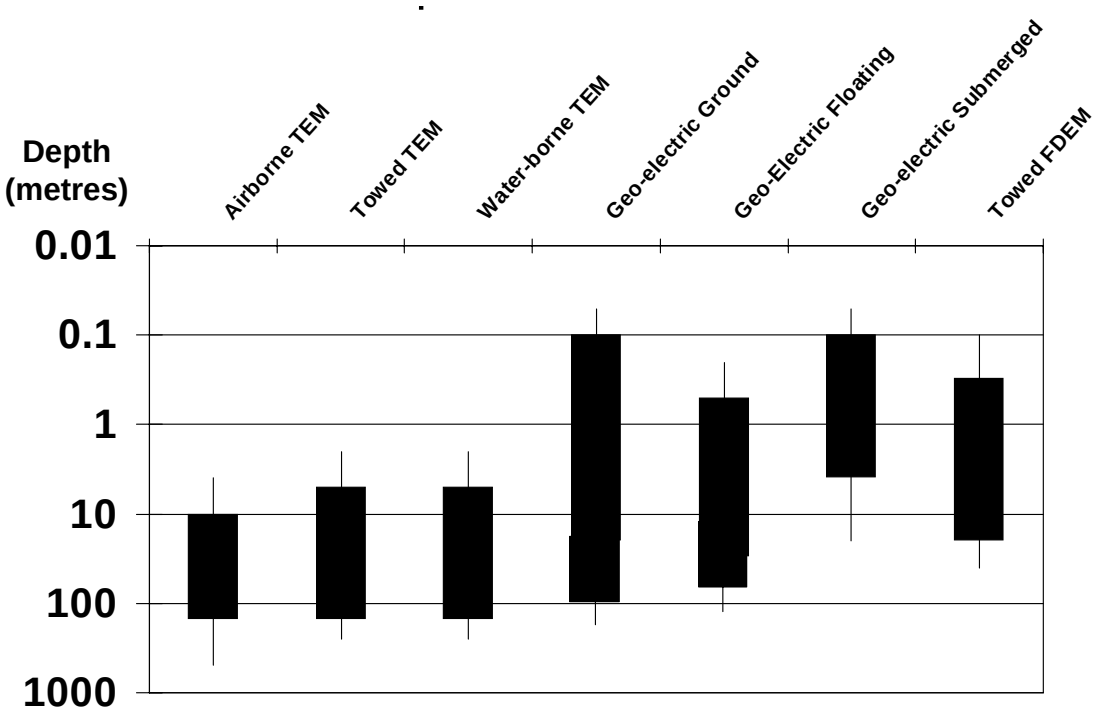

Figure 8.1 Ranges of detection of various types of EC imaging instruments achievable using budgets typical of environmental management. This is a subjective evaluation made after extensive equipment evaluation (Allen, 2005). The TEM techniques and airborne FDEM all have detection ranges that are dependent on conductivity multiplied by depth rather than depth alone. The other depth ranges are also dependent on conductivites in complex ways. Towed and waterborne TEM have not achieved the exploration depths indicated, to the authors knowledge, however the author believes that they could if sufficient development funding is applied.

8.1 Multi-spacing frequency domain electromagnetics (FDEM)

Frequency domain electromagnetic devices routinely used on land are single (or dual) spacing devices (eg Geonics EM38, Geonics EM31, Geonics EM34, Geonics EM38DD, Apex Max-Min, DualEM, etc). Manufacturers Geonics and DualEM are now beginning to to manufacture multi-depth FDEM. Such devices may be ideal for soil stratification mapping once commercially delivered. It may be possible to enhance the data from them using 1D inversion using software such as IX1D (www.Interpex.com). Multi-depth FDEM is limited by the necessity to make the instrument very rigid. A rigid 4m long

device can be towed easily and can image from about 0.2 to about 5 metres depth. FDEM instruments sense multiple depths using multiple coil orientations and spacings. Single spacing and orientation multi-frequency FDEM devices can be used for multi-depth EC imaging. However, Geonics (www.geonics.com, TN31) explain how limitations of practical frequencies of operation and the low induction number approximation render such equipment impractical for multi-depth hydrogeophysical applications.

8.2 Hammered stake geo-electric surveys

Various systems of automated geo-electric imaging systems using multi-takeout cables and hammered stakes are available that follow the design of Dahlin (2001). For routine use in search of aquifers, these techniques are not very popular due to their low productivity compared with FDEM techniques. The case study chapter on farm canal surveys contains a site where such surveys were done across rice cropping land (D'Hautefeuille, 2001) using a single channel Sting-Swift geo-electric transceiver. The Syscal-Pro used on some of the waterborne surveys in this thesis also is routinely used with multi-takeout cables terrestrially. In comparison to FDEM, this approach struggles with electrical contact resistance (see Figure 8-2). The solution used is hammering of stakes down into moist soil or wetting the ground contact. The following two techniques present alternate ways of dealing with high and variable contact resistances.

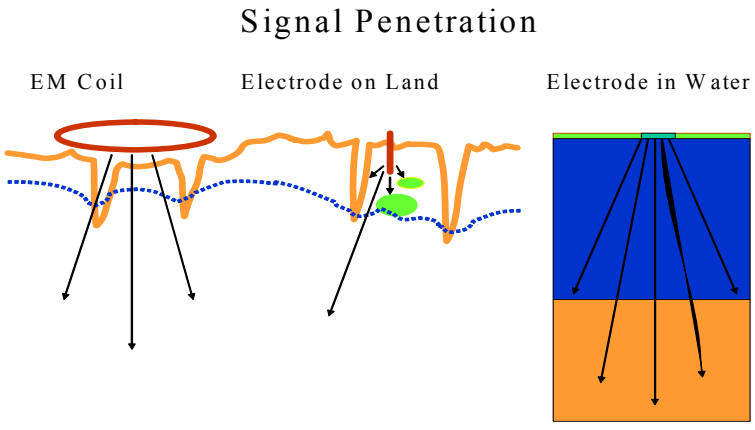

Figure 8.2 Schematic revealing how EM coils and waterborne geo-electric arrays can easily pass signal into the ground while terrestrial geo-electric arrays struggle to pass signal through the highly resistive and heterogeneous top of the unsaturated zone.

8.3 Towed capacitive geo-electric arrays

Towed capacitive geo-electric arrays have recently been developed. Electrodes make capacitive contact with the ground rather than galvanic contact. This enables them to cope with dry topsoil. The Corim device (www.IrisInstruments.com) and the Ohm-Mapper (www.geometrics.com) are examples that both have been very recently converted into multi-depth devices. The Ohm-Mapper (see Figure 8-6) is showing great promise due to its ability to collect good quality signal. It uses linear electrodes like the AXB array. Its receiver electrodes, as well as transmitter electrodes need to be linear so that they can detect sufficient signal. Fractional signed monopole based inversion and the AXB array design if utilized with this device, would be ideal for multi-depth terrestrial investigation over the dry topsoil found in Australia in the depth interval 0.2 to 15 metres. Capacitively coupled resistivity is limited by skin depth which means that in highly conductive, saline environments, it is not able to image very deeply.

Figure 8.3 The Geometrics Ohm-mapper capacitively coupled resistivity imaging equipment. Only one receiver dipole is shown. The linear electrodes are actually the cables, not the pods.

8.4 Aarhus University Hydrogeophysics Group PACES system

The pulled array continuous electric sounding (PACES) system was developed to reveal stratification in a depth range of 0.5 to 20 metres in Denmark. Data obtained has been in use determining the effect of aquitards on groundwater flow so that deeper groundwater

resources can remain unpolluted by infiltrating pollutants. In excess of 40 000 kilometres of traverse have been surveyed (Auken, pers. comm.). The configuration of this array was discussed in the chapter on the AXB array where it was compared with other array configurations. It is pictured in Figure 8-5. In the drier, hotter climate of inland Australia, this device is not particularly practical due to the high contact resistance of the dry surface of most Australian irrigation area soils whereas in Denmark, surface soil moisture is sufficient for electrodes to function. The device uses impedance transformers to cope with the high contact resistances and uses high speed selective stacking of data to cope with variable, intermittent contact.

Figure 8.4 The Pulled Array Continuous Electric Sounding (PACES) system imaging a depth interval from 0.5 to 20m in Denmark.

8.5 Ripping tine towed geo-electric arrays for soil stratification studies

The possibility of conducting towed geo-electric arrays across land exists but is immensely challenging. In the irrigated areas of Australia there exists a lot of cultivated land that can be easily ripped for insertion of an array in the soil at a depth sufficient to make contact with moist soil to create sufficient electrical contact. Accurate detailed soil

salinity stratification imagery could be generated after a great deal more research and development. Experimentation on this idea was commenced but did not show much promise. A ripping tine (Figure 8-3) was installed in the tow bar of a Landrover (Figure 8-4). A strong short geo-electric array cable was threaded through and anchored in a tube with a right angle bend in it just behind the tine. Half metre long transmitter electrodes separated by four metres were followed by receiver electrodes at 0.5m, 1m, 2m and 4m from the end of the second transmitter electrode. As survey progressed, water from a 200 litre drum was trickled into the ground. Clodding of earth resulted in poor electrode contact. When the earth behind the tine was pressed down, good contact could be attained but experimentation was done with only one person who had to both drive and press down clods which was not practical. Experimentation was abandoned because the author could not afford to rent the necessary electronics any longer. A press wheel would obviously need to be added to get the system working. Water from the drum only lasted about 1km but appeared not to be necessary provided that the tine ripped deep enough to contact ground moisture. The following photos show the trials.

Figure 8.5 The cable ploughing and irrigating prototype. Note - in order to prevent breakage on large survey jobs where obstacles would be encountered, a spring would need to be incorporated into this design. A press wheel also needs to be added to press down soil clods onto the cable.

Figure 8.6 Towing of a geo-electric array using a ripping tine. Slightly deeper ripping and addition of a press wheel is needed to prevent the array from leaving the ground as it does here.

8.6 Manually laid loop TEM

Theory on floating TEM has already been given and is identical to terrestrial TEM and therefore is not repeated here. Transient electromagnetic devices may use large loops of wire to transmit signal deeply and can readily image to depths of hundreds of metres in some terrains. Such large loops traditionally have been manually pulled into place by labourers. Productivity is limited to a few kilometres per day even when several labourers are employed. For this reason manually laid loop TEM has seen limited use in groundwater and agricultural applications. Examples of its use include Allen (1991) and Hatch, *et.al.*, (2002).

8.7 Towed terrestrial TEM

Geo-electric array systems can image to infinitely shallow depths whereas transient electromagnetic (TEM) systems cannot but are limited to imaging accurately at depths beneath about 2 metres at least. This means that they are useful for groundwater investigation and deep infiltration studies but not for root zone studies.

Time domain electromagnetic imaging is useful for imaging shallow groundwater resources for purposes such as tracing prior streams away from where they intercept surface water bodies, siting bores for tapping fresh water or for siting bores for drainage of saline groundwater away from sites where it is causing problems. These applications lower high water tables that cause crop waterlogging problems. Basic operating principles are summarized in Figure 8-7.

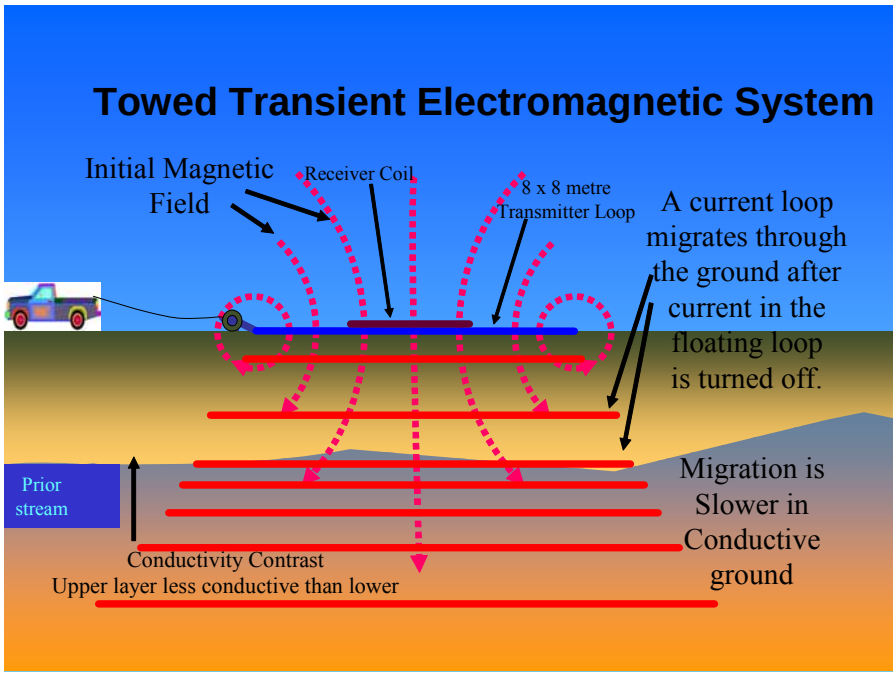

Figure 8.7 A schematic of a towed time domain electromagnetic system showing the effect of ground with different conductivities on current loop diffusion.

Time domain electromagnetic sounding requires a transmitter and receiver loop to be placed, generally concentrically, at consecutive positions along a profile line. The transmitter loop is connected to a 50% duty cycle square wave generator such as a Zonge NanoTEM transmitter which is synchronized with a receiver such as the Zonge GDP32 which is connected to the receiver loop. Metallic (or other highly conductive and/or

magnetic objects) must not be near the loops. The loops are sensitive to vibration and movement because movement of them through the magnetic field of the earth induces voltages within them. Transmitter loop dimensions are typically about half the desired maximum depth of investigation. Multi-turn transmitter loops can increase depth of penetration but suffer serious self inductance problems if their wires are placed close to each other. If the receiver loop is placed concentrically within the transmitter loop and the transmitter loop is small (less than 40m side length) there is a risk that electromagnetically induced polarization (IP) effects (see Geonics Protem 47 manual, www.Geonics.com) and primary field residual and loop self-transients (Kamenetsky & Oelsner, 2000) will dominate and de-validate the response of the instrument. An 8m wide transmitter loop combined with a concentric receiver loop may generate data dominated by IP effect on later channels rendering them difficult to interpret (personal experience).

Three towed time domain systems will be described here, the first two invented and developed as part of this thesis, and the last, developed by the Aarhus Hydrogeophysics Group.

8.7.1 Towed TEM on a plastic sheet

Multiple depth electrical conductivity imaging can be achieved productively across ground cleared of continuous cover of trees or large bushes using time domain electromagnetic transmitter and receiver loops towed on a sheet of plastic at a distance behind the towing vehicle and with the front edge of the sheet elevated by a non-conductive rod with a non conductive wheel at each end (see Figures 8-8 and 8-9). The elevation of the front of the sheet forces plants and other obstacles under the sheet as it travels. The light ground pressure of the sheet results in only very light abrasion and wear as the sheet travels over the ground.

In the same way that circuit boards make layout of circuits easy, the sheet makes layout of TEM loops and associated components easy. Because all the wires are fixed (by duct tape) to the sheet of plastic, none of them can catch on plants during motion of the device.

The towed sheet can easily be steered as it simply folds and crumples during the turn then lays out flat again once the corner has been negotiated. A crumpled TEM loop creates

anomalous data however this can be efficiently eliminated by a filter that analyses the track of the device (recorded by GPS in the towing vehicle) when post processing.

Multiple turn transmitter loops are good for increasing moment and therefore depth of exploration but if the turns are placed too close together and/or too many turns are added then self inductance increases turn on and off times too much to permit measurement of TEM decays resulting from changes in the ground. On the plastic sheet, multiple turn transmitter loops can be taped, each separated by an appropriate distance for reducing the effect of self inductance. Concentric loop turns can be placed to within 1m of the receiver loop, centred in the transmitter loops. The receiver loop can have multiple turns and noise shielding but in initial tests just a single wire loop was used due to budget constraints. Transmitter and receiver loop connector wires pass along the plastic sheet to the two tow ropes attached to the rod at the front of the sheet and then along the tow ropes to the tow vehicle. They pass as twisted pairs along each of the two tow ropes so as not to interfere with each other or the loops on the plastic sheet. Where they are attached to the tow vehicle it is essential that they do not wrap around or otherwise have close contact with conductive parts of the vehicle.

The device could be improved using a bucking loop around the receiver coil as part of the transmitter loop circuit. This bucking loop compensates for the primary field of the transmitter loop so that the receiver loop is not swamped with primary field which otherwise saturates amplifiers, causes other serious problems related to incomplete primary field removal and self-transients and requires that data be recorded at very low gains.

In order to avoid swamping the EM signal with EM induced IP effect and primary field residual, a reasonably large Tx loop is required (40 x 40 m is recommended by Geonics; however for towed loop some IP effect must be accepted and practical dimensions of about 8 x 8 m accepted). A 3 x 3 m receiver loop with a 100kOhm (Zonge specifications) resistor across the outputs for noise damping and dissipation of inductive ringing provides sufficient signal. The signal is measured across the high and low connections of an A/D converter channel with a 1kOhm resistor passing from each to ground (Zonge design). This arrangement centres signal around instrument ground and eliminates loss of amplification potential due to high proportion of common mode signal in the overall signal measured at the channel.

Further avoidance of IP signal can be achieved by adding a second receiver loop well behind or in front of the transmitter loop, using late channel data from it to merge with early channel data from the central receiver loop (See Geonics Protem 47 manual, www.Geonics.com). The out of loop receiver will however be strongly adversely affected by lateral inhomogeneities.

Shallow and deep data can be obtained by using a combination of single and multiple turn transmitter loops switched continuously from one to the other – an innovation of the Aarhus Hydrogeophysics Group (www.hgg.au.dk).

Plastic wheels placed at the 8m axle rod ends can appropriately be made of plastic 600 – 800 mm diameter plastic cable reels. The axle can be made of fiberglass encased bamboo with plastic pipe lengths and fittings placed at joins and ends. Joins placed next to the inward facing sides of the wheels permit quick removal of the wheels. Once the wheels are removed, length of the 8m rod is reduced to 6 m and the edges of the sheet can be folded inwards. Then the sheet can be rolled around the rod and easily lifted onto a roof rack for public road transportation. Next to the outside walls of the wheels, 90 degree elbow joiners can be fixed to the ends of the rod. From the elbows, pipe segments can extend backwards past the wheel radius and be terminated by 45 degree elbows and additional pipe segments that are long enough to keep the rod terminating pipe segments horizontal. The sides of the plastic sheet (with segments cut out to allow space for the wheels) are then fixed onto the pipe segments. The elbows and pipe segments have the additional role of preventing rotation of the axle and roll up of the loop due to axle friction.

Plastic sheet thickness should be sufficient to prevent it from being picked up by the wind. If it is too thick then it will be too heavy to man-handle. Initial tests were done using builders plastic (200 μm polyethylene) which proved to be unmanageable in strong wind. 1mm thick polypropylene is recommended due to its penetration and abrasion resistance and flexibility. Small weights added to the back corners or edges of the sheet can further help hold it on the ground in strong wind. Weights can be made of lay flat tubing containing sand, or, for the back of the plastic sheet only, rigid plastic pipe. The sides of the sheet need to be rolled for storage so rigid pipe cannot be fixed onto them.

Figure 8.8: Towed TEM on a plastic sheet

Figure 8.9: Towed TEM on a plastic sheet.

8.7.2 Towed TEM on a 4 wheel structure

A trial was also made of a 4 wheeled 8 x 6 m transmitter loop that could, unlike the plastic sheet device, withstand very strong wind during operation (Figure 8-10). The device is not recommended by the author due to trouble steering, trouble passing through gates and other narrow openings, lack of practical ways of implementing structural integrity and very involved set up and pack up procedure. A good understanding of the device can be gained by observing the photo provided.

Figure 8.10: A towed 8 x 6m TEM device set up on 4 wheels made of PVC pressure pipe and bamboo, numerous ropes and plastic (for the receiver loop). Front and back rods were held off the ground by wheels while the sides were allowed to droop – not being supported by wheels and bamboo. When cornering, transverse forces would distort the device so that turning circle diameter had to be limited to about 40m. Set up and pack up times were impractically large. This device is not recommended.

8.7.3 Aarhus PATEM

The Aarhus pulled array TEM device is a 5 x 3 metre, segmented, multi-turn transmitter loop pulled along on a wooden frame behind a tracked hydraulically driven hand tractor

(www.hgg.au.dk). The transmitter loop switches in and out segments alternately in order to get both high moment and fast turn off time data. The receiver loop is towed at a large distance behind the transmitter loop. The device can attain a moment of 4000 Am^2 which is considerably more than the 200 Am^2 obtainable with Zonge NanoTEM with the single turn towed TEM on a plastic sheet mentioned above. Although the device can see to over 100m deep and is relatively free of IP effect problems due to the out of loop configuration, it suffers from sensitivity to near surface 3D heterogeneities, again, due to the out of loop configuration. The Aarhus Hydrogeophysics Group have pursued airborne geophysics, as follows, in preference to refinement of their PATEM device, in part, because of land access and fence crossing problems.

8.8 Airborne TEM

Airborne devices such as the Aarhus Hydrogeophysics Group SkyTEM (www.SkyTEM.com) do the same type of survey from the air as towed TEM does from the ground. However, in inland Australia, ground based systems often have an economic advantage at least on small jobs due to mobilization costs and, in some locations, operating costs. They also have marginally superior near surface resolution. Older airborne TEM systems had very poor near surface resolution but some modern systems are capable of resolution almost equivalent to that of terrestrial TEM. Airborne systems can typically image to a depth in excess of 100 metres so they are good at deeper aquifer definition.

Airborne systems are not recommended for investigations beneath inland waterways because they can rarely compete with either the productivity or resolution of waterborne systems in such environments. Additionally, their data are very strongly affected by the incised topography typically found around rivers.

CHAPTER 9 - EC DATA MANAGEMENT AND PROCESSING

Geo-electric inversion procedure has been described in a previous chapter. There is much more processing necessary, however, for successful preparation of EC imagery than just inversion. In this chapter the numerous steps required to get from raw field data to EC imagery will be introduced. They are then described in detail in some Appendix 8 and even more detail in the Hydrogeo-imager documentation (on DVD). Appendix 8 also contains descriptions and derivations of peripheral algorithms essential to the processing stream. A schema is described in section 9.2 which sets the framework for the processing strategy adopted to cope with the large volumes of data processed in this thesis. Section 9.3 discusses the process of differencing EC datasets collected over similar paths while Section 9.4 details issues that arrise when time lapse imaging is attempted.

9.1 Waterborne geo-electric array data processing – an introduction

Towed EC data processing cannot be approached simply like traditional statically acquired EC data because it is so voluminous. A job containing a few hundred high value statically acquired soundings can be easily manually edited, however, a towed EC dataset containing tens of thousands of reconnaissance soundings cannot. Because waterborne surveying is conducted in a flowing current, the operator cannot stop whenever there is a problem to be dealt with. This results in numerous bad records and other defects in the data that must be largely automatically filtered out. Because tens of thousands of records are collected every day, manual removal of bad records is rarely practical and many elaborate filters must be applied. The filters do not remove all problems so interactive graphical interfaces also are essential for the cleaning of the data. The processing of data is described, in Appendix 8, in order of execution under the categories listed on the main menu of the software accompanying this thesis (see Figure 9-1). A sequential menu structure, although cluttered in appearance, was chosen because it acts as a checklist for the processor.

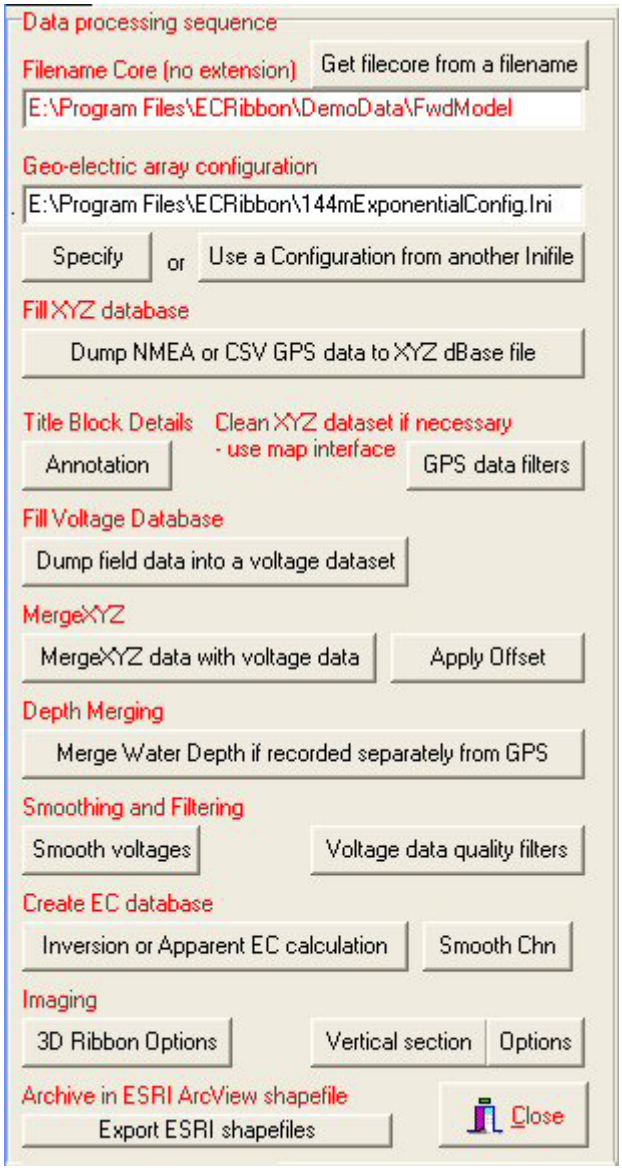

Figure 9.1 The data processing sequence menu, designed to act as a checklist, from the software produced along with this thesis.

9.2 Multi-depth EC data format

The various ground and airborne electrical conductivity dataset types acquired for the environmental, groundwater and agricultural sectors are largely incompatible. There is no common data repository or standard schema. A simple schema is proposed in Appendix 4, and summarized here, that allows integration of all this information. Many investigations may be conducted using a combination of EC imaging devices if a common format is available that facilitates efficient visualization of the data from multiple devices (Figure 9.2).

The schema records, along irregular transects, EC of stacked layers and depth to the bottom of each of those layers. As such, it is a useful medium for common archiving of:

- towed geo-electric array data, e.g. waterborne arrays, Geometrics Ohm-Mapper and the Aarhus University pulled array continuous geo-electric sounding system;
- geo-electric array data including systems that involve roll along cables such as the ABEM/Lund imaging system, the AGI sting swift system, the Zonge GDP32 roll along system, the Scintrex IPR12 and the Iris Instruments Syscal System;
- Frequency domain electromagnetic data such as the single and dual depth devices - DualEM 2 and 4, Geonics EM31 and EM38, the Geophex GEM2, L&R Instruments proposed FDEM device and the various multi-depth devices that are beginning to emerge;
- TEM soundings, eg. Protem, NanoTEM and TerraTEM;
- towed TEM such as the Aarhus University PATEM system;
- airborne EM. eg. SkyTEM, VTEM and Dighem; and
- summarized borehole EC logs (eg Geonics EM39).

The possibility of the proposed schema has arisen as a result of refinements in the way EC data is processed. Multi-depth EM and geo-electric data are now almost always converted to discretely layered EC data. Layer thicknesses are often allowed to float during processing so that they can match distinct EC boundaries within the ground accurately. Two and three dimensional modelling, often conducted on small datasets, also typically produces data that can be stored as layered models. Some data is converted to smooth layer models. This data can also be stored in the proposed schema. Lastly, some data such as EM31 data represents just a single depth range. By evaluating the signal contribution with respect to depth for such instruments, it is possible to specify a layer of thickness such that the bulk of the signal from such an instrument comes from that layer.

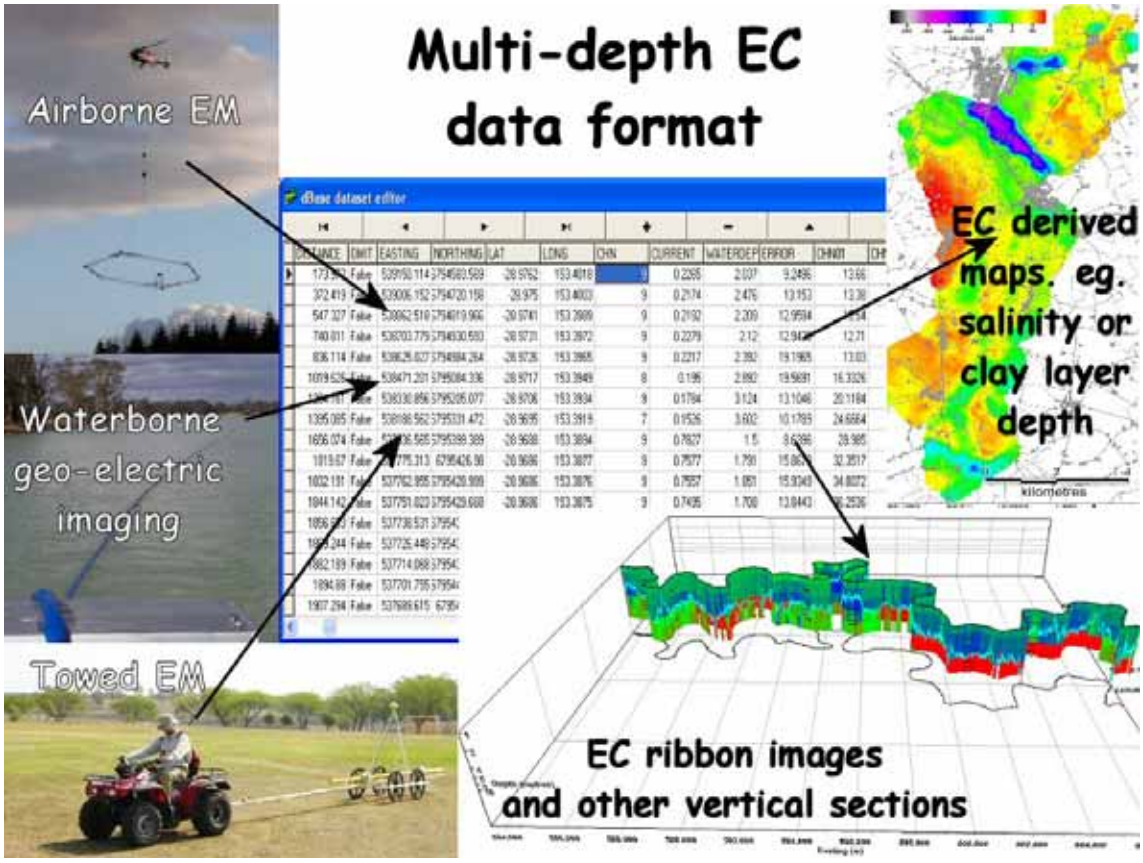

Figure 9.2 A summary of the concept of a common multi-depth EC data format for multiple instruments.

9.2.1 A Multi-depth EC data schema

A multi-depth EC data format has been formulated in which data is stored in layers of variable thickness along transects which may be irregular or may form grids. This matches the ways data now normally are acquired (with GPS) and converted into multi-depth EC (using inversion). In each data file, there are two columns for each layer, one giving resistivity as ohm.m (an SI standard for storing EC data) and the other giving the depth to the bottom of the corresponding layer. There are various other columns. One of those columns stores the number of layers in each record. Data format currently used is ESRI point shapefiles with redundant geographic information in the associated dBase attribute files. Metadata and projection files accompany the shapefiles. This format is used because it is almost universally supported by natural resource managers in Australia. Additionally, it can be indexed and accessed non-sequentially. A full description of the format, its design and its benefits are given in Appendix 4. From the perspective of the user with no special software, this data format may seem frustrating as, with many data

sets, viewing of EC at a particular depth requires a flow controlled, conditional, multi-column query. If multiple instruments are to be supported, full integrity of the processed data is to be maintained, and optimal software performance is to be facilitated, then this is necessary.

dBase and shapefile formats have been chosen for storing data records and accompanying INI files have been chosen for unique variable storage. All these formats are both human and machine readable using widely available interfaces. Conversion of the INI files to files compatible with a future extension of the exploration and mining markup language - XMML (Cox, 2004) would be straight forward. Documentation of these file formats is publicly available and the formats are extremely widely utilized. Creation of dBase files is widely facilitated; they can even be read and written by MS Excel. Because ESRI shapefiles are an elaboration of dBase files, conversion to ESRI point shapefiles is simple. Even once the conversion is made, the dBase part of the shapefile is still available to programs that cannot read shapefiles. The conversion is readily made in ESRI ArcView software or using freeware components. No information is stored in the ESRI shapefile that does not exist in the associated dBase file and therefore only the dBase file needs to be stored. The shapefile just makes the dBase file easier to use in a GIS system.

Table 9-1 gives all the necessary and optional columns in the schema along with units, field types and recommended field formats.

Table 9-1 A proposed schema for multi-depth EC dBase tables.

Field	Units	Field Type	Size.Decimals
Distance	Metres	Floating Point	12.3
Omit	n.a.	Logical	
Easting	Metres	Floating Point	12.3
Northing	Metres	Floating Point	12.3
Lat	Decimal degrees	Floating Point	15.10
Long	Decimal degrees	Floating Point	15.10
Chn	n.a.	Numeric	3
Time (optional)	Decimal days	Floating Point	12.7
Current (optional)	Amps	Floating Point	12.5
WaterDep (optional)	Metres	Floating Point	12.3
Elevation (optional)	Metres	Floating Point	12.3
Error (optional)	User specified	Floating Point	10.2
Chn##	Normally Ohm.m	Floating Point	10.2
.			
.			

Depth## . . Error## (optional) . .	Metres User specified	Floating Point Floating Point	8.3 10.2

A column headed ‘Depth00’ can be added to the datafile should a minimum depth for the first layer need to be specified. This is the case with some time domain electromagnetic transformations. If the column is missing, then the minimum depth shall be interpreted as zero or some fraction of ‘Depth01’ depending on the interpretation program.

The order of most of the columns is irrelevant since column indexes will be found by searching for their headers however the ‘Chn##’ and ‘Depth##’ columns need to be in contiguous blocks so that software can find the first of such columns and reference the remaining columns using the index of the first of those columns.

The ‘Error’ column may contain an averaged error over whole soundings while the ‘Error##’ columns may contain errors or sensitivities for each layer in a sounding. There is no consistency in the way errors are reported by different inversion and transformation software packages so units of error are left as user specifiable. The units of error must therefore be listed in the metadata file.

All depths are to be positive (increasing downwards).

All data should now be in GDA94 co-ordinates and an ESRI format projection file should accompany the data to document this co-ordinate system.

The filename, as well as the ini file should indicate what quantity type the file holds (eg Ohmm or Chargeability or Volt). The filename should include the quantity type as a suffix just before the .dbf in the filename (eg. *Ohmm.dbf, *Chargeability.dbf, *Volt.dbf). Datafiles of unprocessed voltages will not have ‘Depth##’ columns and the ‘Chn##’ columns should be replaced by ‘V##’ columns. Relevance of voltage columns should be stored in associated metadata files that record device configuration.

ESRI software facilitates geodatabases. The schema proposed here can logically be modified for use in geodatabases. However, the schema should be maintained, as is, for

transfer of data between parties, many of whom will not have the software and skills needed to operate geodatabases.

A previous schema for EM data storage was devised by AMIRA over ten years ago. It was an ASCII file format in which all data was stored in one file. The flexibility of the format made it very hard to support fully. Because the ASCII files had to be read sequentially, they could not be integrated into efficient geoprocessing and visualization solutions.

9.3 Differencing

Differencing between datasets collected over approximately the same path, either with a slight offset or at a different time, is sometimes considered to be appropriate. Offset surveys may show if saline inflow into a river is more pronounced on one side of the river while time lapse survey may indicate temporal change in groundwater properties. Differences in the paths of repeated surveys and of the effect of river depth on inversion is dealt with as best as is possible by the accompanying software.

Differencing of continuously acquired data requires the matching of soundings from different datasets that were conducted at similar locations. For this purpose, eastings and northings are compared to identify soundings where position matches most closely those of the other dataset. Some interpolation is then conducted to make additional improvement to the position matching. If a close match is not found, then differencing is not attempted.

On canals, differencing between datasets surveyed at different times can be fairly simple, however, on rivers differencing between datasets surveyed at different times is not as simple as it may first appear. Each survey is never conducted on exactly the same course and the water depth profiles below each course are often very different in a meandering river. As the conductivity contrast at the river bottom is often extremely large, good quality inversion is necessary for isolating the effects of waterdepth from the effects of variation in strata electrical conductivity. Excessive use of the smoothness constraint in the inversion process needs to be avoided in order to isolate the contrast at the river bed adequately.

Only once differences due to position mismatch and water depth variation are successfully minimized can differences, in strata, due to conductivity variation over time be determined. Even then, instrument calibration, and noise levels, will limit detectable variation.

Should there be any DC offset in data, or wire to wire leakage, then differencing results may again lack validity particularly at depth over highly conductive ground where signal levels will be very small. In such situations, one may still have confidence in lateral variation in the differenced data if it does not correlate directly with low conductivities (low signal to noise ratios) in the datasets.

Differencing may also be conducted between parallel datasets surveyed at similar times such as datasets surveyed next to each bank of rivers or datasets surveyed in parallel canals or furrows. Such parallel survey differencing does not suffer from most of the limitations mentioned above relevant to time difference surveys. Excellent quality parallel survey data can be collected using the simultaneously operated parallel arrays concept described at the end of the chapter on AXB arrays.

9.4 Survey management issues of periodic EC surveys

Use of waterborne EC imaging for long term monitoring requires rigorous data management. Very small changes in equipment parameters, faults and/or calibration, survey track, river level, and/or processing procedure can all affect time lapse imagery. When, over time, datasets are supplied with different equipment by different parties in different formats, the problems are compounded. On top of these problems with raw data, transparency (i.e. openness and clarity about the different steps involved in the analysis), and reproducibility of the processing steps taken to gain information from raw data are essential in such monitoring. Of course transparency and reproducibility are not sufficient if it is not economically viable to reformat all the data to a common format capable of documenting all the details of the various datasets and then reprocess and represent all the data in a uniform manner. For further discussion of such problems see Versteeg et al. (2004).

Datasets supplied here have been accompanied by INI files containing comprehensive documentation of the processing procedure. A uniform processing strategy has been

formulated for the geo-electric array data and TEM data. The two data types however cannot be directly compared for long term monitoring purposes due to different sensitivity to measured parameters. Histograms of datasets presented in Chapter 15 – 'River Case Studies' prove this point.

CHAPTER 10 - PRESENTATION

Presentation of multi-depth EC data can be conducted using plan images and vertical sections but it is most appropriate, in most situations, that it be conducted using 3D imagery – 3D EC ribbons.

10.1 3D EC ribbons - definition

3D EC ribbon images, such as Figure 1-1, are similar to stratigraphic fence diagrams however EC is presented instead of stratigraphy and soundings are so close together that they appear to the viewer as a continuum. Interactive viewing in an OpenGL interface further enhances usability of the data but, of course, interactive viewing cannot be presented here on paper.

10.2 The reason for development of a 3D EC ribbon viewer

Tens of megabytes of data can easily be collected by GPS tracked towed geo-electric arrays or towed TEM in a day. Presentation of that data is only feasible once it is in a form in which it can be efficiently geo-referenced by the viewer. Because of this, 3D ribbon imaging was developed by the author. 3D EC ribbon presentation differs from voxel 3D presentation such Slicer/Dicer in that it does not require memory to be allocated to a 3D grid of voxels. Voxel 3D presentation would be inappropriate, also, because the only data of value in waterway EC surveys is along the waterway whereas voxel packages are designed to image sections and isosurfaces through entire 3D grids of data.

Without a 3D viewer, required geographic cross-referencing with features of interest such as bores, geological boundaries and topography would be unmanageable. This is especially so on meandering rivers because, typically, anomalies in meandering rivers correlate with proximity to floodplain sides.

Although GIS packages typically used for evaluation of environmental data usually have 3D capability, none could be found that supported 3D surfaces that were not referenced to co-ordinates in a 2D plane. They all had an underlying database structure that did not permit any point in a surface to be plotted vertically above another. One could rotate data by 90 degrees before imaging so that segments of ribbons could be viewed but that was

hardly a viable solution for large datasets. Some GIS such as ArcGIS 3D extension could plot isolated voxels representing points in 3D space in such a manner that a 3D ribbon could appear to be generated if viewed from a sufficient distance, however, when one zoomed in on such a ribbon it would disappear as the voxels resized. High end geological imaging packages, such as Earth Vision, designed for petroleum exploration can, apparently do ribbon presentation, however, such software is beyond the budget of typical environmental scientists and is not tailored to EC imaging. Due to the apparent lack of an available GIS package capable of viewing EC ribbons effectively, one has been written which is called HydroGeoImager. It accompanies this thesis, equipped with a demo/educational licence suitable for processing and imaging small datasets. It is an OpenGL and Steema software COM based viewer and has many other features as well. Attempts at 3D ribbon visualization have been made using expensive general purpose packages by others but these viewers lacked either resolution and flexibility (Arcview 3D extension - where layers were represented by rows of individual voxels of equal size) or lacked mass production efficiency (geosoft Oasis in which the data had to be split into segments without common eastings and then plotted on their side). Packages designed for groundwater model visualization with ribbon imaging capability are beginning to emerge but, again, they are not specialized for the type of imaging done here.

10.3 Features of EC Ribbons

Electrical conductivity (or resistivity) ribbons presented in this document have the following features.

10.3.1 Log depth scale and marks

The depth scale used with EC ribbons should normally be a logarithmic scale because geo-electric and TEM resolution diminishes with depth. The dimensions of most features of interest in such data increase with depth and so suit a logarithmic scale. Spaced regularly along the ribbons are sets of log depth scale marks. There are 5 marks per decade. The end of each decade is evident from concentration of marks. Borehole logs are, however, one source of information that is traditionally plotted on a linear depth scale.

10.3.2 Equal area color

The colour scale representing EC (or resistivity or other properties) is stretched by transforming the data of the entire ribbon to the EC domain so that it can be plotted in a histogram. The colour scale then can be arranged so that equal area of each colour is evident in the histogram. The histogram is a valuable interpretation tool on its own and so is included with each ribbon image instead of just a colour bar. Equal area colour distribution optimally suppresses the effect of outliers and abnormal data distributions on the colour distribution. Typically, large areas of the ribbons are made up of river water which should be of constant EC so, if inversion has been successful, a peak on the histogram occurs representing river water EC. This peak causes the colour scaling to greatly enhance superficial variation in the interpreted river water EC. Aesthetically this is not pleasing, however, it is of use for understanding inversion quality and for instances where variation in river water EC actually is being effectively imaged.

10.3.3 Rotate, Zoom, Pan, Vertical Exaggeration

In HydroGeoImager, facilitation of rotation, zoom and pan of ribbons has been provided. As the datasets contain a great amount of high density data spread out in three dimensions, one single image is certainly not enough for full appreciation of the data. As a result of this the 3D viewer has been developed with interactive rotation, zoom, vertical exaggeration and pan facilities.

10.3.4 Background images

Geo-referencing requires layers of images of different data. Aerial photo images and topography form useful background images to ribbons. If the ribbons are presented in orthographic projection, then they can be superimposed exactly over plan maps without use of expensive software. Various effects can be utilized with the aerial photos such as overlay transparency variation and cut-away imaging. With a DEM, orthophoto imagery and ArcView 3D extension, the airphoto can be draped over the DEM and the EC ribbon added (although limitations on ribbon visualization in ArcView as described previously still need to be addressed). Should a data user wish to plot a ribbon image as a raster layer in ArcView without manipulating data or purchasing the ArcView 3D extension, then an option in HydroGeoImager can be activated which removes perspective and rotates the

ribbon so that it can be viewed from the south in orthographic projection. Such an image can be scaled to exactly overlay 2D datasets and orthophoto images. The overlay process is not limited to ArcView but can also be achieved in cheap photo editors such as Paint Shop Pro which was used to create Figure 1-1. Even photo editors distributed with computer magazines can be used for the superposition.

10.3.5 Graphs along the ribbons

It is practical to put graphs along the tops of the ribbons representing other run of river data such as salt load increase, seepage data, fitting errors or anything else of relevance.

10.3.6 Water depth (river bottom trace)

Superimposed on the ribbon images is the water depth trace. This line is crucial for interpretation as river bottom depths vary greatly and thus have an important influence on the ribbon images. In saline inflow investigations, it is important to be able to visualize how close saline hot spots are to the river bottom.

10.4 Vertical EC sections

Vertical EC sections such as the one in the software developed along with this thesis for viewing data during inversion are the clearest way to present EC data in isolation and out of geo-context. Such presentations are ideal for presenting snippets of data containing anomalies, however, for understanding and making routine use of huge volumes of EC data such as typically collected on routine surveys, 2D vertical EC sections are next to useless.

10.5 Map view colour scaled data

Although map view lacks the detail of the 3D view, it is frequently useful for presenting simplified presentations. The 3D viewer can first be used to determine what is appropriate to colour code in the 2D view. We have already seen colour coding in which devalidated data points were presented in grey while valid data points were presented in red. There is a wealth of other parameters that can be colour scaled.

Color scale can be simply and almost instantly applied to just the data location pointers or, somewhat slower, to the whole map by use of gridding. Many GIS packages permit such

operations. The Danish national multi-depth EC database – GERDA (http://gerda.geus.dk/introduktion/projektet.html) specializes colour scaling to multi-depth EC data.

A list of sensible features to image in a 2D colour scaled view, either gridded or not, are:

- EC of a particular layer;
- EC of a particular depth (An animated sequence of such images continuously cycling will give an indication of how things change with respect to depth. Such a presentation is appropriate for dense grid datasets such as terrestrial TEM surveys of paddocks or waterborne surveys of dams. An animated sequence can similarly be generated for EC of each layer in a model rather than each depth);
- Ternary images in which Red, Green and Blue, or Cyan, Magenta, and Yellow represent three different parameters such as conductivities of successively deeper layers;
- EC of a particular depth below a waterway bed;
- Depth of a waterway bed;
- Depth below the surface at which a data exceeding or less than a particular EC begins to occur (This is useful for salinity studies where high saline water tables are a problem);
- Depth below a riverbed at which a particular EC begins to occur (This is probably the most important feature for study of saline inflow into rivers. The proximity of saline groundwater to the river bed very closely corresponds to risk of and/or presence of saline inflow into rivers); and
- Thickness, or conductivity x thickness product of an interval exceeding a particular conductivity (This feature is particularly useful for definition of integrity of clayey aquitards).

CHAPTER 11 - INTERPRETATION

Multi-depth EC data is usually interpreted to find the following hydrogeological parameters:

- Potential for or presence of saline inflow into rivers and drains which is related to the proximity of high EC anomalies to river, or drain beds; and
- Seepage pathways under canals which generally create low EC anomalies due to freshwater flushing of more saline groundwater. Sometimes a dry layer is evident under canals with extremely low EC. Within such a layer, seepage will be evident as low EC within the otherwise extremely low EC layer.

The following notes explain some ways of interpreting EC imagery.

11.1 Background orthophoto images

EC Ribbons can be projected easily over orthophotos using just a photo editor if they are projected orthographically.

Orthophoto images and similar satellite imagery can greatly help with interpretation. Features such as geological lineaments that constrict groundwater flow are often evident. Floodplains and prior streams are often evident from variations in soil colour and in vegetation. Seepage sites sometimes are evident from presence of and/or vigour of deep rooted vegetation. Cultural features adjacent to, and affecting, EC ribbons such as, raised dams and irrigated agriculture with high infiltration losses are evident. River EC images usually show variation dependant on their proximity to sides of floodplains which are evident on orthophotos.

11.2 Saltwater interception bore locations

Saltwater interception bore locations posted onto the images are useful for showing any effect such bores have on the river.

11.3 Run of River salt load increase

Run of river salt load increase surveys plotted along ribbons show how much salt has actually entered into each kilometre of the river each day. These are surface measurements independent of the imaging survey and are not representative of salinity entering the river at that point but rather a little further upstream. As river water passes around bends it tends to flow in a corkscrew path similar to wind flowing over plains of longitudinal sand dunes. For this reason, sources of salt at the river bottom are likely to contribute to salinity variations at the river surface downstream at multiple locations as the helically flowing water surfaces and sinks. Correlation between surface salt load increases and anomalies in the EC ribbons upstream of those increases can be expected.

11.4 Action at the riverbed

By observing conductivities just below the sonar or pressure-logger water depth trace it is possible to get a good indication of sites of saline inflow and of risk of further saline inflow. These sites will be worth ground truthing using drilling and sampling from a barge in order to see how much other factors such as clay content affect the results.

11.5 Patterns in the riverbed

On EC ribbon images where sonar is sampled at 2 second intervals, the river bottom may be very irregular. Large sand waves dominate the river bottom in some locations and have been picked up by sonar. In other locations, the regular sandwaves are not evident and it is anticipated that there is rock there. The sonar can be used in this way to identify the type of sediment at the base of lengths of river.

11.6 Induced polarization

Induced polarization (IP) data is useful for discriminating between the effects of salinity and clay. IP data has a much lower signal to noise ratio than EC data and therefore is much more affected by signal-consuming high conductivity features. Where high conductivity saline basement consumes most of the signal from the transmitter, pervasive, minor induced polarization features present at a particular depth are not reliable but rather are likely to be systematic noise (DC offsets). A careful examination of those that vary horizontally is warranted. Under canals, sandy or gravely prior streams running through

otherwise clayey sediment may not be evident in EC data if they are full of saline water however they will have some effect on IP data.

11.7 Animation

Animation has been used in some examples to highlight features that could otherwise be masked. Three animation effects are useful:

- Overlay transparency can gradually be changed for airphoto comparison even using just a cheap photo editor such as Paint Shop Pro;
- The colour scale can be gradually vertically damped to show up important horizontal variations in the presence of extreme vertical conductivity contrast (e.g. River water overlying hypersaline groundwater). This involves creating a separate equal area colour histogram for each layer in an EC ribbon and then colouring each layer in the ribbon using a blend of the histogram for the overall ribbon and the histogram for each layer; and
- In an OpenGL interface for river imaging such as developed along with this thesis, 3D images can be rotated revealing blind spots and zoomed and panned revealing detail. Vertical exaggeration also can be altered.

11.8 Differencing

Difference images are subtraction of one image from another. Because the track of each periodic survey is different and the river depth under the various tracks varies greatly and sharply, and because DC offsets may cause shifts in deep data, time difference data is dubious. Unless time difference variation is so pronounced that it is evident from visual comparison of the un-differenced EC ribbons it will probably not be reliable in difference images. Bank to bank difference data does not suffer from these problems so it is useful. Variation in water depth is evident in the Error column of the data files and can be observed on images created from fixed layer inversions by comparing the aqua line taken from file two, with the layer boundary transferred from the water depth of file one.

11.9 Over-interpretation

As indicated, in some of the examples presented in later chapters inversion has fixed all layer depths. Should a sharp change in conductivity exist in the ground at a depth different to the layer boundaries, this change is smeared across 2 layers. For this reason, *at least two layers should be observed when looking at any anomaly in fixed layer data!* The water depth is a known sharp boundary so care has been taken to force layer boundaries to honour this. Should real conductivity contrast across the riverbed be negligible then the inversion will simply cause layers above and below the riverbed to have similar conductivities but if it is not, then the contrast will be revealed accurately rather than being smeared across two layers that are not correctly placed across the riverbed. In inversions conducted more recently, layer boundaries have been permitted to move up and down so single layer anomalies are reliable. Nevertheless, care must be taken as in some cases inversion overshoots with one layer and compensates by undershooting on the next giving the false impression of an isolated conductive layer.

11.10 Resolution, suppressed layers and equivalence

EC data loses resolution approximately exponentially with depth. Use of a log scale on the EC ribbons results in images that have similar resolution per pixel from top to bottom. This removes the necessity to explain resolution limitations to novice interpreters. Novice interpreters then typically do not assume the absence of suppressed layers that do not appear due to resolution.

Another problem plagues inverted EC data – the problem of equivalence. Given a certain degree of uncertainty in data, for TEM data, the conductivity times the thickness of conductive layers is the most determinable parameter and can be accurately determined while the separate conductivity and thickness of layers can be less well determined. This phenomenon is called equivalence and for geo-electric data it occurs in a similar manner but it is the resistivity times the thickness of resistive layers is the parameter that can be best determined. Interpreters must keep the possibility of equivalence in mind when interpreting data.

Further detailed explanation of these issues can be found in Merrick (1977a) and in Interpex IX1D documentation.

11.11 EC, salinity, clay content and rock texture

Discussion of EC, salinity, clay content and rock texture was included in sections 1.6 and 1.7. In this section, interpretation aids that help identify what has caused variations in EC at particular sites will be examined.

Histograms of EC have routinely been made when creating EC ribbons. Equal area colour has been applied using these histograms. The colour scale can then be transferred to approximate salinity scales relevant for various saturated soil textures using conversion factors derived from Slavich and Petterson (1993). An example is presented in Figure 11-1. Comparison of the histograms from various sites reveals a lot about conditions at those sites. The histograms form a summary of the types of features found at each site. For example, a site with unsaturated sands will have a peak EC of less than 100 μS/cm while a site with a hypersaline aquifer will have a peak EC greater than 10000 μS/cm.

The data scaled on salinity scales gives limits to what EC variation can be created by sediment texture variation. If variations in EC ribbons are observed to exceed the variation evident from sediment type then the interpreter can be confident that they have been created by either salinity (if conductivity is high) or dry soil (if the conductivity is extremely low) or to indurated rock. Interpreters then need to seek additional information in order to further interpret the data.

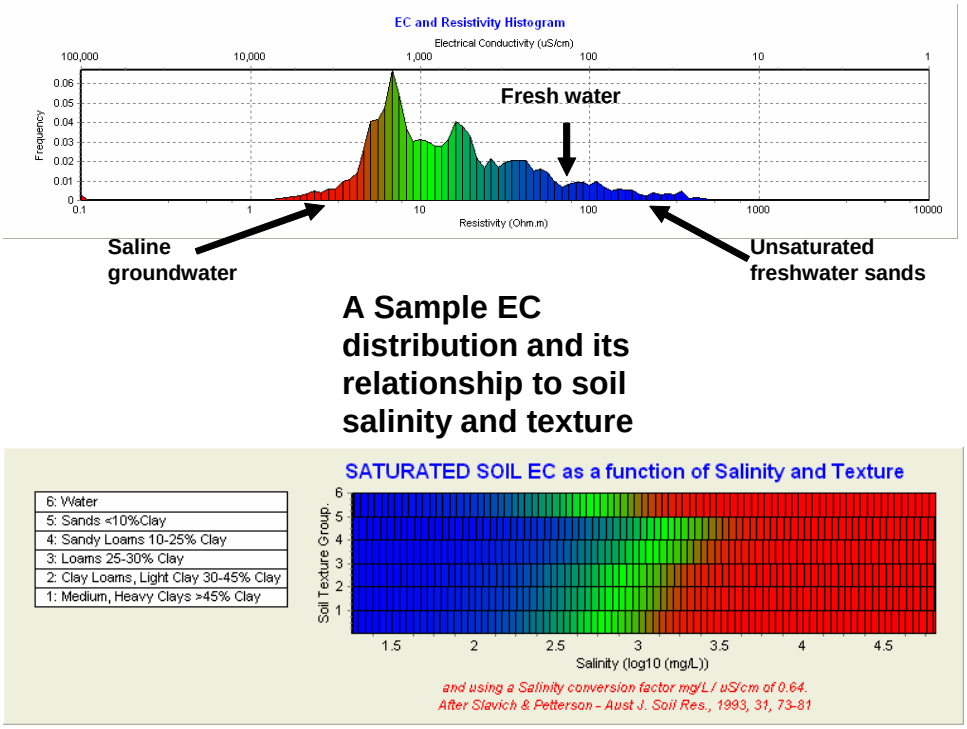

Figure 11.1 Use of an EC histogram to create equal area colour for EC ribbons and transformation of that colour scale to salinity scales for various soil textures.

Indurated rock is not encountered directly under much of the flatter parts of inland Australian rivers and canals where case studies of this thesis have been situated. Poorly cemented and indurated strata can be interpreted roughly with sediment texture corrections such as presented in Figure 11-1. Moderately or well cemented and indurated rock however behaves in a manner approximated by Humble's Law (Merrick 1977a) which is a refinement of Archies Law. Humble's Law is as follows:

$$F = \text{Formation Factor} = 0.62 \cdot \text{porosity}^{-2.15}$$
$$\sigma_{\text{Rock}} = \frac{\sigma_{\text{water}}}{\text{F}_{\text{apparent}}} \qquad (70)$$

Humble's Law is only strictly valid for sands in saline pore water. Much variation on this behaviour occurs in other environments, however, this is a large subject that will not be discussed further here because, in practice, sufficient porosity, permeability, and anisotropy data for precise quantitative correlation of EC imagery with individual aquifer properties such as pore water salinity and porosity rarely exist. Over solid rock, then, EC ribbons may exhibit anomalies related to porosity variations which, in turn, are related to

lithology or secondary cementation or dissolution along fractures. Because groundwater movement is typically constrained by such variations, salinity anomalies also will be likely to be incorporated into the data. Interpretation of such variations can usually be made by looking at the geometry and relative positions of anomalies but precise quantitative correlation with individual hydrogeological properties is rarely possible.

11.12 Soil moisture and texture relationship that leads to flushing of sands and salinization of clays

Much EC ribbon data shows up fresh deep flushed sandy soil and salinized clays. In order to understand why, consider that irrigation, floods, annual filling and emptying of canals and rainfall periodically apply water then let evapotranspiration concentrate salt in the soil. The soil moisture spectrum presented in Figure 11-2 shows how clays retain a lot of moisture while sands allow moisture to drain deeply away from where evapotranspiration can concentrate salts. The rapid deep drainage additionally flushes salt that is present in the sand. This behavior leads to clear EC anomalies in periodic recharge environments – the effects of soil texture and salinity add up to give enhanced clarity. Figure 11-3 summarizes this process. Even under canals that are permanently full, these enhanced anomalies may still be present if the canal has not thoroughly flushed salt from the underlying sediment.

In the next chapter, ways in which interpretation of EC ribbons are relevant to particular applications will be explained.

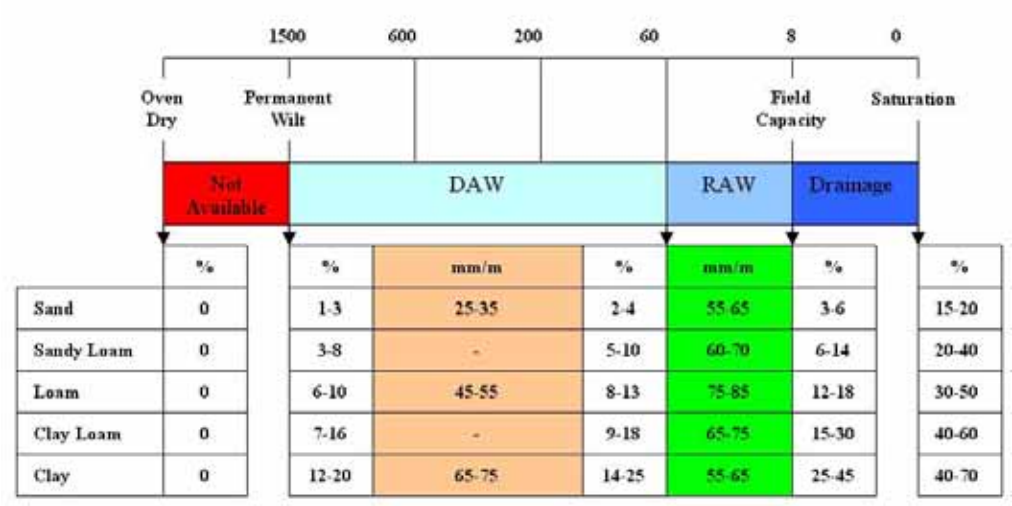

	%	%	mm/m	%	mm/m	%	%
Sand	0	1-3	25-35	2-4	55-65	3-6	15-20
Sandy Loam	0	3-8	-	5-10	60-70	6-14	20-40
Loam	0	6-10	45-55	8-13	75-85	12-18	30-50
Clay Loam	0	7-16	-	9-18	65-75	15-30	40-60
Clay	0	12-20	65-75	14-25	55-65	25-45	40-70

Figure 11.2 The soil moisture spectrum (Toome, 2004) shows how clay retains moisture while sand releases it quickly. DAW stands for Deficit Available Water. RAW stands for Readily Available Water. The top scale represents Kilopascals of soil suction. The other values in the image represent water content of the soil.

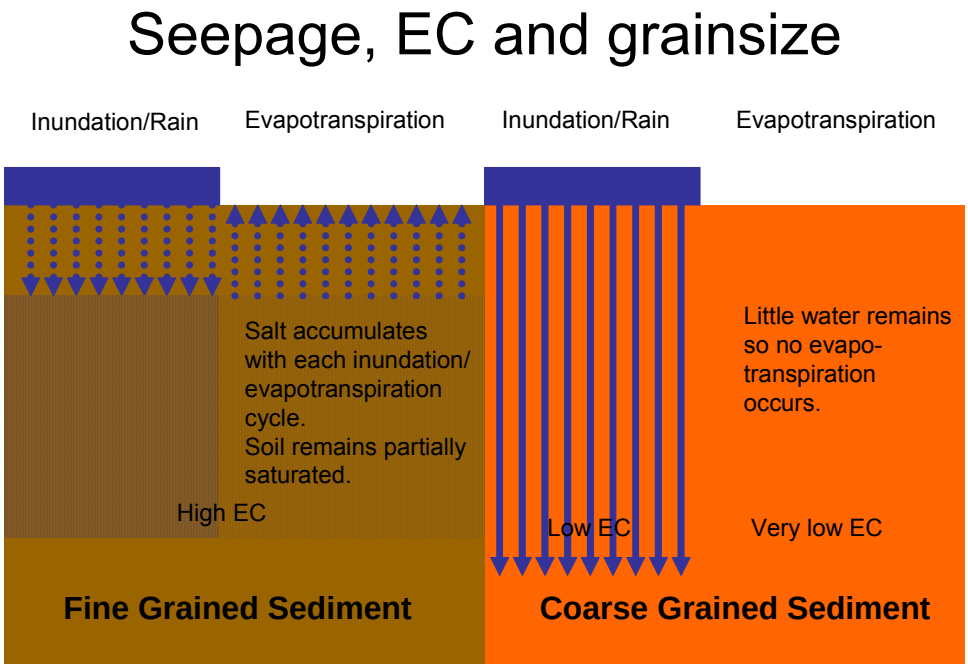

Figure 11.3 A schematic showing how, in a periodic recharge environment, clays concentrate salt while it is leached through sands.

11.13 Canal and river shape and curvature

Canal and river cross sections range from almost flat layer cases to semicircular. One dimensional (horizontal layer) assumptions used in interpretation of geo-electric data work ideally on the flat layered cases but also approximate the semicircular case reasonably well in a qualitative sense as the two cases interact with the fields coming from geo-electric arrays in qualitatively similar manners. The validity of this approximation may break down where canals and rivers curve sharply however. Canals and rivers typically contain numerous curves which often are sharp enough so as to require geo-electric arrays to curve sharply around them. Figure 11-4 indicates how equipotential lines conform approximately with the shape of a canal but part of the canal wall is anomalously sampled when negotiating sharp bends. Because evapotranspiration of lateral seepage in canal walls concentrates salt, canal walls often are of high EC, particularly at lateral seepage sites, and will create highly anomalous data if sampled inside canal bends.

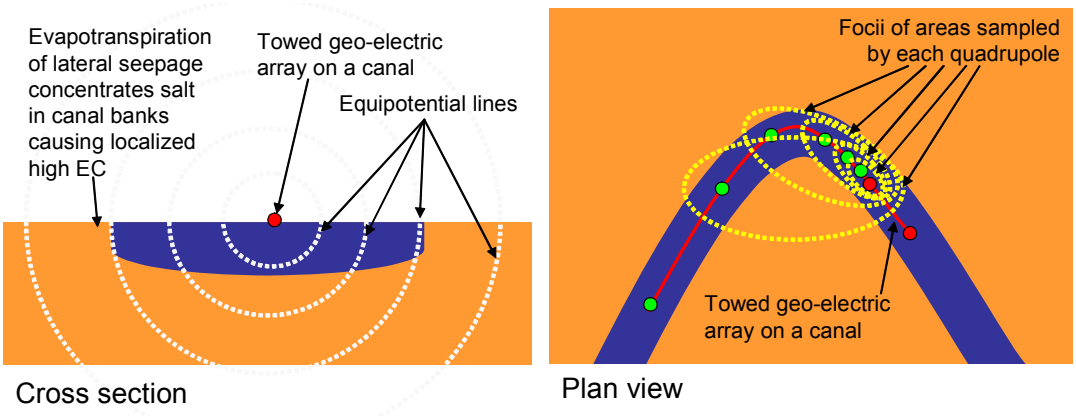

Figure 11.4 Demonstration of limitations of the validity of horizontal layer modelling of geo-electric array data.

CHAPTER 12 - APPLICATIONS

Applications of waterborne multi-depth EC imaging are as follows:

- Adding spatial detail to groundwater conceptual models;
- Seepage detection;
- Saline inflow detection and saltwater interception schemes management;
- Large scale river characterization;
- Modelling the effects of conjuctive surface and groundwater use;
- Groundwater recharge and recovery planning and management;
- Waterway pollution investigation;
- Salinity mitigation in flood and furrow irrigation schemes; and
- Mapping of hydro-stratigraphy beneath irrigation areas.

Applications of terrestrial multi-depth EC imaging are as follows:

- Adding spatial detail to groundwater conceptual models;
- 3D aquifer and aquitard definition leading to better groundwater recharge and recovery management and to recovery of infiltrating water that causes salinity problems; and
- Soil stratification studies involving identification of salt horizons resulting from evapotranspiration; and
- Shallow water table investigation.

These applications are examined in more detail below. Because EC imaging from watercourses is a new technique, supporting examples, including most of those from the few existing references, will be presented in subsequent case study chapters of this thesis.

12.1 Adding spatial detail to groundwater conceptual models

Perhaps the most significant criticism of groundwater modelling is that over-simplistic models tend to be used. EC imagery, calibrated to give groundwater model parameters

such as variable layer thicknesses and permeabilities, can be used to add spatial detail to groundwater models in a cost effective manner.

12.2 Seepage detection

Vertical EC images typically show low EC anomalies at sites where seepage has taken place but not necessarily is continuing to occur. These sites will have low EC due to lower clay content and also because the seeped water has flushed salt from the soil profile. This is not always what is observed; however; it is only over very dry sands, identifiably due to their extremely low EC where this trend does not occur. At such sites, the EC anomalies related to seepage tend to be of higher EC than the surrounding dry sand overlain by impermeable seals. In most established canals and irrigation districts however, water tables will have risen and silt will have sealed the bases of the canals and seepage will have slowed significantly if not drastically. The vertical sections will show some deep percolation pathways that are likely to be seeping away more canal water than the more closed-off shallow low EC anomalies that probably only collect seepage each time a canal is refilled.

Figure 12-1 presents most of the possible causes of anomalies beneath canals and reservoirs. At every investigation site, the interpreter needs to eliminate as many of these variables as possible using local knowledge or extra tests such as drilling before they can practically determine a relationship between EC ribbon anomalies and seepage. Even once they have done this, they will only have a spatially accurate but qualitative idea of where seepage has occurred. Quantitative seepage investigation will always require calibration with quantitative seepage measurements such as pondage tests (appropriate for typical Australian canals) or Idaho seepage meter tests (appropriate for canals on porous strata such as found in Nebraska). Figure 12-2 presents one such interpretation process.

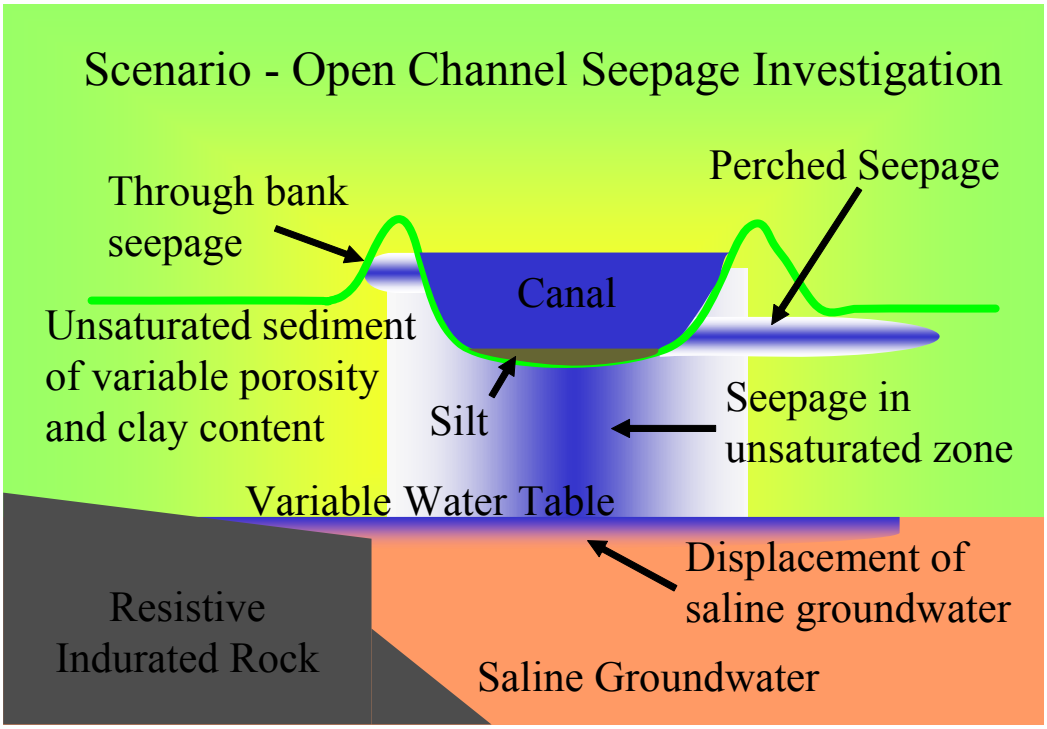

Figure 12.1 Factors affecting EC data collected beneath canals.

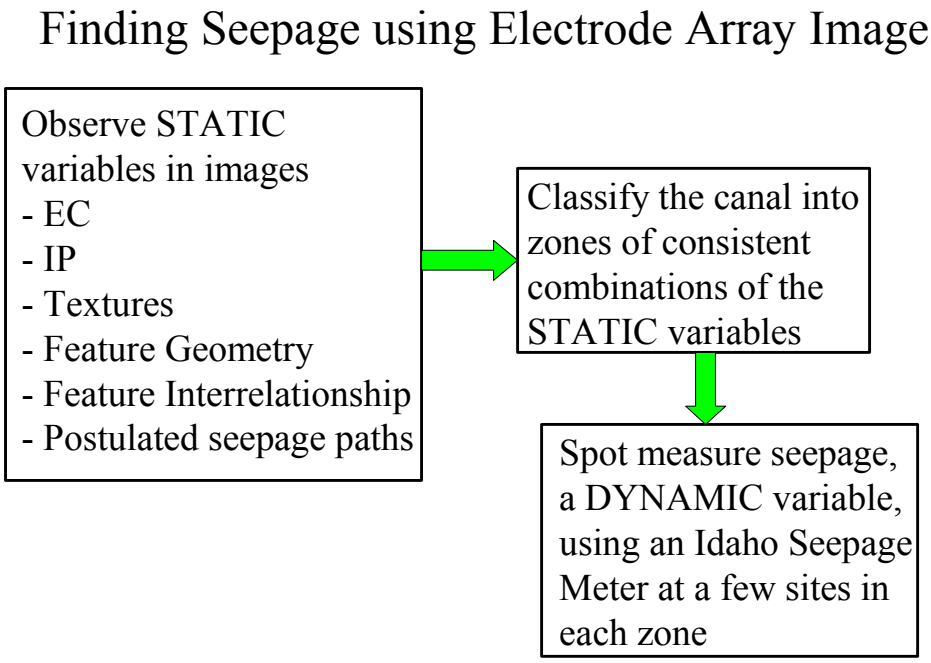

Figure 12.2 A procedure for quantifying seepage using EC ribbons. Note that for Australian canals, the Idaho meter tests typically need to be replaced by pondage tests.

Canal and river seepage have always been notoriously difficult to measure. Most seepage pathways become almost blocked with time after a canal has filled and a groundwater mound develops beneath it.

Farm canals and irrigation supply canals should be treated a little differently due to one type being generally full and the other type being generally empty. Seepage losses are of two types. The first is a large, short duration loss that occurs when a canal has just been filled and the canal saturates and seals ('silts') up underlying aquifers. The second is a continuous loss that occurs as water slowly seeps through underlying aquifers and gradually raises regional water tables to an equilibrium level. The farm canals suffer the first type of loss regularly due to regular refilling and emptying. Therefore they lose a lot more water (per unit area) than supply canals. Evidence for very small continuous losses after initial filling for Murray Darling Basin supply canals comes from CFC groundwater dating methods (see Appendix 7 – Complementary Investigation Techniques).

The many EC images conducted from canals, rivers and shallow drains (above regional water table levels) that have been ground truthed using shallow drilling show a good correlation between locations of low EC anomalies and low clay content, freshwater flushed sediment where complicating factors such as shallow indurated bedrock or dry sediment are absent. Correlation between EC anomalies and seepage however is not so clear. Very high seepage rates do correlate with low EC where there are no complicating factors but intermediate and low seepage rates have not correlated so well. It appears as if EC shows where seepage *has occurred* rather than clearly showing *how fast* it is occurring now.

It appears as if seepage is controlled in some permeable sites by limitations in the extents of the permeable bodies (eg. isolated point bar sands). Another control that may vary seepage over time is siltation that may have occurred over time after canals were originally formed. To detect such siltation, EC data must have very fine resolution at the canal bed.

As a result of the above, EC cannot be accurately correlated to current seepage rates. If silt and any clay lining from the bottom of a canal were to be scraped off and groundwater pumped from beneath it, and then, if the canal was refilled, then it is expected that the EC data would correlate well with seepage.

12.3 The saline inflow interpretation scenario

In the same way that the dynamic variable – seepage – can be evaluated along a canal with the assistance of dynamic test calibration of EC ribbon anomalies, saline inflow into rivers can also be evaluated by calibration of EC data using run of river salinity monitoring as shown in Figure 12-3. Run of river data may be accurate but it is offset downstream from where saline inflow occurred and does not have the ability of EC ribbons in determining sites of potential inflow. Correlation of EC ribbon anomalies with run-of-river salt load variation surveys is largely a matter of determining a downstream offset and removal of smoothing effects to convert EC ribbon anomaly ECs to salt load increases calibrated by the run-of-river data. Further calibration is practical using sediment samples obtained by a device using the design principle of a yabbie pump.

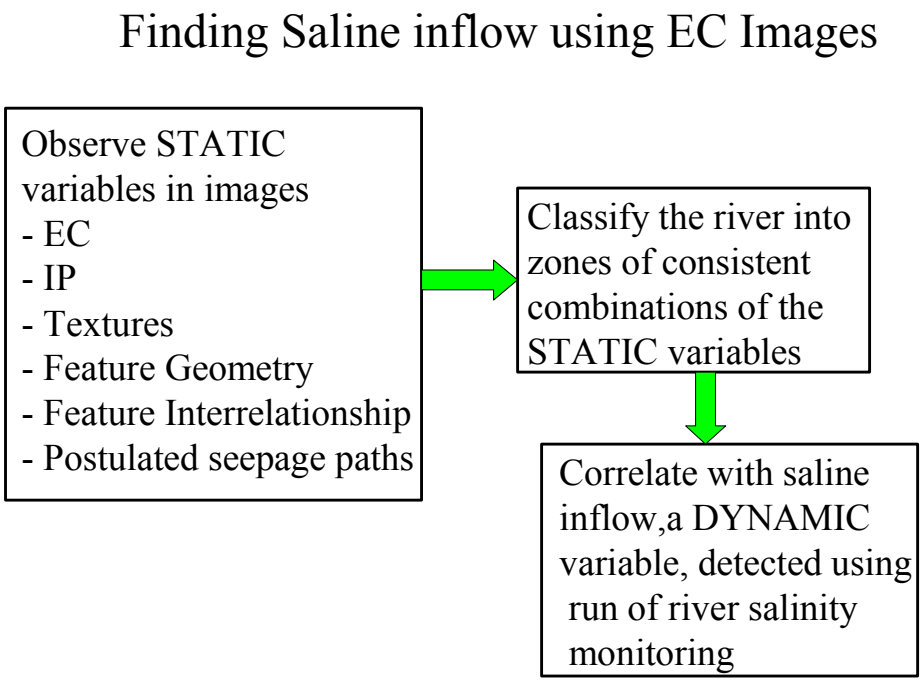

Figure 12.3 A procedure for investigating saline inflow to rivers using EC ribbons calibrated with run of river salinity surveys.

12.4 Large scale river characterization.

EC imaging beneath rivers can show, in most instances, if a river is recharging groundwater or being replenished by groundwater. This is principally because upwelling groundwater is normally more saline than recharging groundwater sourced from the river.

Within the EC imagery, overprinted on the salinity signature, distributions of clay, sand and rock under the rivers show up in three dimensions. Unsaturated zones beneath rivers show up as extremely low conductivity layers and indicate areas of lack of connectivity between groundwater and the rivers. EC imagery of vast lengths of river can be collected at a reasonable cost. A database of such imagery reveals a lot about rivers. Comparison of distant stretches of river often shows up clear EC and stratigraphy differences with significance related to geology, regolith weathering and salinity, palaeohydrogeology, river connectivity, transmission losses and transmission gains. Such EC differences and their relevance would be totally missed if small stretches of river were viewed in isolation. The author is promoting the setup and perpetuation of a national multi-depth EC imagery database because of the possibilities presented here. Terrestrial multi-depth EC imagery combined into such a database could provide information about floodplains rather than just the rivers themselves.

12.5 Conjunctive surface and groundwater use management

Most rivers in the Murray Darling basin are surrounded by bores that pump from the aquifers under the rivers. As features identified in EC imagery taken from rivers and canals, as well as terrestrially, strongly control groundwater flow, such imagery is highly useful for conjunctive surface water and groundwater management. Groundwater modelling of the effects of conjunctive water use may be severely inappropriate without detailed subsurface information on flow paths that can only economically be obtained by EC imaging in many instances.

12.6 Groundwater recharge and reuse management - Siting of drainage bores and artificial recharge sites for groundwater re-use under surface irrigation areas.

As demand for irrigation water increases, farmers are tending to use and recycle water of greater salinity. As a result, soil salinization rates are increasing and monitoring and soil reconditioning measures are becoming increasingly important. Farmers try to apply enough water to include a leaching fraction to take salt out of the root zone. In uniform soil, this practice could be valid, but it is not in non uniform soil where differential leaching quickly leaves clayey areas to become saline as a result of evapotranspiration

and sandy areas to become dry. FDEM instruments such as the Geonics EM31 are used currently to identify this leaching so that differential water application strategy can be applied (long period irrigation on the clays and minimal short period irrigation on the sands). Examples of the use of such surveys are posted on the United States Salinity Laboratory website (http://www.ussl.ars.usda.gov/CHMETRIC/ASSESS00.HTM). They also make up most of the content of the publication edited by Beecher (2002) and are the basis of numerous farm scale reports by Australian agricultural consultants (eg. Sustainable Soils Management and Dalcrom). Multi-depth EC imaging can see where deeply percolated water escapes through the sands (and generally does not become salinized) and can be tapped, pumped and reused. Multi-depth EC imaging such as Ohm-mapper or towed TEM can site useful pumping sites. Towed geo-electrical arrays used across a network of farm canals, furrows, drains and flooded bays also can be used for such bore siting. The recovered water may be moderately saline and only useful for salt tolerant crops. Pumping from deep sinks under the sands also decreases the water pressure under the clays which in turn causes increased leaching of salt to below the rootzone. This means that mult-depth EC used to site drainage bores could both solve salinity problems and water shortage problems in some irrigation areas.

Furthermore, evaporation losses from above ground water reservoirs can be reduced if an underground water storage site is designed into the reservoir as shown in Figure 12-4. Multi-depth EC imagery collected along existing canals, or over existing or potential reservoir sites can be sufficiently detailed to thoroughly delineate buried high permeability sands and gravels. The limits of extent of the sands and gravels can be identified in three dimensions and a decision on their suitability as underground storages of fresh water can be made. Assistance in such a decision can be gained by using the geophysics to inform groundwater modelling of pump tests at those sites. If the survey has been done over potential rather than existing reservoir sites, then the reservoir may be deliberately placed over a permeable feature so that it functions as an artificial recharge device. In Nebraska, geo-electric array surveys are being used to determine where canals should be cleaned in order to convert them to artificial recharge sites in order to develop underground reservoirs such as described here (Ball, L., 2005). In Australia, such schemes are generally demoted and discouraged because of potential ownership disputes between surface water and groundwater owners even though they potentially can save great quantities of useable land and water from evaporation and salinization losses.

Governing bodies seem to be very averse to the extra complications such management would add to their jobs and therefore strongly oppose rather than encourage this method of saving water and reducing salinity problems.

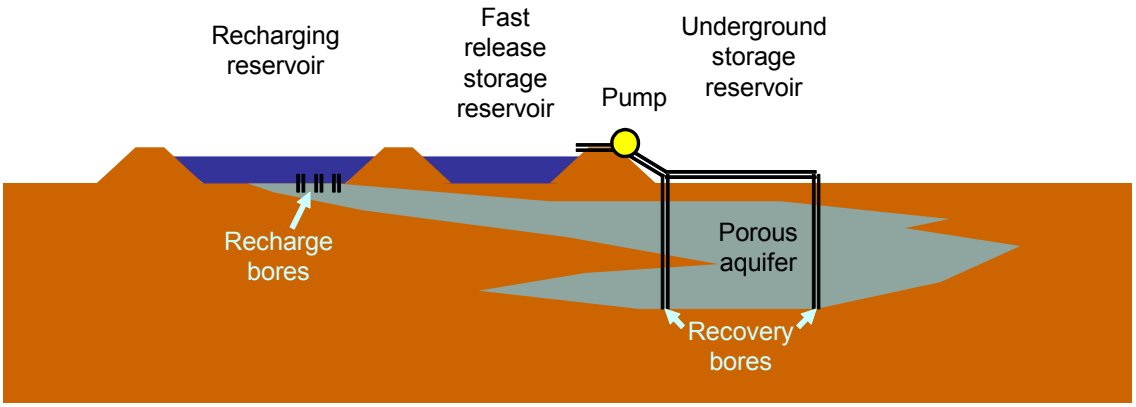

Figure 12.4 Aquifer recharge and recovery involving a ring tank and a porous shallow aquifer that could be mapped using multi-depth EC imagery.

12.7 Waterway pollution investigation

Pollutants from factories and other sources often enter groundwater and create plumes with anomalous EC. These can be detected under waterways using towed EC imaging systems. In built up environments, geophysics may be impractical on land due to clutter of conductive metallic objects, electrical noise sources and property access restrictions, however, on adjacent waterways no such nuisance objects typically exist. This may mean that it is much cheaper to identify a plume using towed EC imaging systems operating on water that is being intercepted by the plume and then trace it back across land using drilling and sampling.

Pollutants do not always produce detectable EC anomalies. Nevertheless, if they are flowing into a waterway, they will be flowing within a groundwater flow system constricted by sedimentary features evident in EC imagery. EC imagery conducted from the waterways and evaluated in the light of some additional information will then still offer best value for money as an investigation technique capable of isolating flow of the pollutant.

12.8 Salinity mitigation solutions

EC ribbon images created over networks of canals and/or rivers or over land reveal salinity concentration layers within the subsurface. Such imagery leads to understanding of the salinity problems which in turn permits management solutions to be applied precisely and appropriately.

Most salinity problems that may be observed using EC ribbons and that occur in irrigated land and waterways result from:

1. concentration of salt in the root zone resulting from evaporation/transpiration of irrigation water.
2. Shallow water tables causing waterlogging of the root zone AND reducing salt leaching rates from the root zone.
3. Upward groundwater flow through relict saline sediment with much greater salt content than present day environments.

12.8.1 Salt concentration due to evaporation

Concentration issues resulting directly from irrigation have been measured in several irrigation areas across Australia. Using the following details from the ANCID 2002/2003 Australian Irrigation Water Provider Benchmarking Report, we can calculate the significance of this concentration. We can use the figures provided for the Murrumbidgee Irrigation Area (MIA) as a guide as they are well documented. By considering salt balance in both groundwater and surface water it has been calculated that each year 92,100 tonnes of salt are retained in the 155 000 ha of intensively irrigated and 235 000 ha of stock land of the MIA. Assuming that the salt retention occurs primarily in the intensively irrigated land we can calculate that *60 grams of salt are retained annually in each square metre of land*.

Salt retained by rice farming in the MIA can be calculated using the following figures from the same source:

Salinity of irrigation water entering the irrigation area = 104EC*0.64=66ppm or mg/L or kg/ML,

Rice was irrigated with 14.1 ML of water per hectare on average in the MIA (less in the Coleambally Irrigation Area and Murray Irrigation Areas),

98% of salt entering the ground was retained (70 to 80% on average in other areas).

Salt retained as a result of rice farming in the MIA in 2003 is therefore

$$Concentration_{Salt} \approx 0.98 \times 1000 \times 104 \times 0.64 \times 14.1/10000$$
$$\approx 92 grams/metre^2$$

This figure does not take into account the fact that much of the applied water is evaporated not on the rice land but elsewhere as drained (often recycled) wastewater, so it is high. Rice farming has been chosen as an example because of the quality of data available for it.

Geophysics is being successfully used to reduce water infiltration rates from rice farming by relocating rice over less permeable soil, however, is yet to be used to work out the best locations for recovery of infiltrated water. If infiltrated water is recovered, the water table is drawn down and increased leaching of salt from the root zone occurs. Geo-electric array, towed multi-depth FDEM and towed TEM surveys combined with 3D ribbon presentation are promising to be useful in this task.

In all intensive irrigation, multi-depth EC imaging can be used to monitor root zone salt retention and to find groundwater pathways that lead to suitable pumping sites for recovery of shallow groundwater. Such pumping can be used to reduce water tables so that root zone leaching rates increase. Shallow groundwater pumping programs optimized using EC imagery also add the benefits of groundwater recycling (if groundwater is fresh enough) or efficient shallow groundwater disposal (due to extraction bores being sited in the most permeable sites).

Evaporative losses can further be reduced if geophysics is used to reduce canal seepage and irrigation infiltration losses. The result will be that less water will be transported and used and less fresh canal surface water will mix with salts in the ground and become useless. Waterlogging problems will also be reduced.

12.8.2 Waterlogging

Waterlogging occurs when water tables rise high enough to keep plant root zones saturated. This in turn results in evaporation and salt concentration in the root zone as well as decreased oxygen in the root zone (see Australian Government, 2004). When intensive irrigation is being conducted it occurs differentially over heterogeneous soil types. Geophysics can be used to plan and monitor precise site drainage. In most cases, multi-depth FDEM instruments are best used for such surveys.

12.8.3 Relict salt deposits

Relict salt deposits are more of a problem for deeply incised rivers and other low lying land than for irrigation land directly. Throughout history, salt has been delivered to low lying areas and left there as water evaporated. These salt deposits, now mostly buried, turn groundwater hypersaline as it passes through them. It then generally emerges in low lying water bodies (including the ocean) or low lying land. Waterborne EC imaging can delineate such phenomena in great detail very economically.

12.9 Mapping of hydro-stratigraphy beneath irrigation areas

Networks of canals and rivers crossing irrigation areas are frequently dense enough to allow long floating geo-electric arrays to be used on them to give a sufficiently dense dataset to reveal the hydro-stratigraphy beneath the irrigation area down to a substantial depth. As groundwater is usually used intensively from beneath irrigation areas, such information is highly valuable. Features likely to be evident are the spatial distribution and variation of aquifer and aquitard thicknesses as well as the quality of water within them and any unsaturated zones. Water tables will not be clearly evident in the multi-depth EC data because partially saturated sediment just above water tables will have almost the same EC as sediment just below the water tables.

12.10 Further notes on terrestrial EC Imaging applications

Features such as palaeochannels detected under waterways may be followed across land by terrestrial techniques to where they may or may not be intercepted by bore pumpers. Planning of groundwater recharge and re-use schemes requires terrestrial investigation normally. Soil stratification studies may be conducted using waterborne equipment in

furrows but normally will be conducted by terrestrial multi-depth EC imaging equipment such as multi-spacing FDEM or multi-depth Ohm-mapper. The same is true of shallow water table investigation. Multi-depth EC imaging for shallow water table investigation identifies EC increase at well above water tables but very little contrast at the actual water table. As salinization from shallow water tables results from the water drawn upwards from the water table by evapotranspiration, the depth at which EC increases due to saturation will in many cases be a better indicator of risk of salinization from shallow water tables than the actual water table depth.

Another application of terrestrial towed EC that could become very popular could be the siting of upland bores remote from irrigation areas. Related to this application is the determination of sustainable use of such bores. In many upland areas, appropriate siting of many bores could lead to saving of great quantities of fresh groundwater that would otherwise have become saline as it flowed through saline sediment further downstream in its groundwater flow system. If such water then would have polluted waterways, then the water quality in those waterways also could be improved.

CHAPTER 13 - CASE STUDIES - AN OVERVIEW

13.1 Contents

About 1000 km of geo-electric array and 300 km of TEM surveying were conducted as part of this thesis. It was through conduct of surveys that the most critical issues affecting the efficacy of EC imaging were identified. Solutions to those issues were tested in the numerous theoretical and field trials.

Around 500 images are displayed in Power Point presentations and various reports on the DVD accompanying this thesis. Although the images are valuable, they are not included in the main text due to their extensiveness and because some of them are animated sequences that can only be observed on Microsoft PowerPoint.

Case studies documented in the main document are as follows:

a) Introductory case study (Chapter 13):

- Murrumbidgee River and Sturt Canal.

b) Theoretical Models (Chapter 14):

- A range of typical three-layer models inverted using a variety of techniques; and
- Highly conductive basement models inverted with and without noise level aware inversion.

c) Rivers (Chapter 15):

- Murray Darling Basin - A comparison of lengths of rivers at selected locations within the Murray-Darling Drainage Basin;
- Waikerie - Waikerie saline groundwater interception scheme, Murray River;
- Mildura - Saline groundwater interception schemes near Mildura, Murray River;
- Gogeldrie Weir – Murrumbidgee River;
- Yanco Weir – Murrumbidgee River; and
- Border Rivers.

d) Coastal (Chapter 15):

- Tuckean Drained Swamp – Richmond River, NE NSW.

e) Irrigation Canals (Chapter 16):

- Coleambally Irrigation Area;
- Murray Irrigation Area;
- Murrumbidgee Irrigation Area; and
- Wimmera Mallee Irrigation Area.

f) Networks of farm channels and drains (Chapter 17):

- Farms 15 and 69 – Coleambally Irrigation Area;
- Farm 1576 – Yanco – Murrumbidgee Irrigation Area; and
- Whitton Clay Pan – Murrumbidgee Irrigation Area.

g) Reservoirs (Chapter 18):

- 30 ha reservoir - Jim Cattanach Rd – NW of Coleambally; and
- Dallas Clay Pan Reservoir.

h) Terrestrial EC imaging (Appendix 9):

- Coleambally - ploughed geo-electric array tests;
- Whitton Clay Pan – Murrumbidgee Irrigation Area – Transient EM; and
- Benerembah – Murrumbidgee Irrigation Area – Transient EM.

Case studies are ordered principally according to application rather than technique. Numerous examples of comparisons of inversion techniques, display techniques, and device application are interspersed through the case studies. The following list may be used as an index to case studies demonstrating various techniques and image features:

1. Comparison of dipole-dipole and AXB arrays;
    a. Figure 15-9 dipole array but with 5m, 10m and 20m dipoles – compare with AXB array river images.
    b. Figures 16-33 and 16-34 submerged AXB array data compared to dipole-dipole array (a=10m, n=1 to 6) data.
    c. Figures 16-34 to 16-44 are all dipole-dipole array data while all almost other data in this work are exponential Bipole array data.
2. Comparison of submerged and floating arrays;
    a. Figures 15-42 to 15-45 Tuckean Swamp (partly tidal).

   b. Figure 16-24 Submerged and floating array data plotted one above the other for the Coleambally main canal.
   c. Figure 16-19 A composite image using both submerged and floating array data to give more detail – Boona canal.
   d. Figure 16-17 Boona canal.
3. Comparison of Apparent resistivity, theoretical models and inverted images;
   a. Figure 16-17 Boona Canal.
   b. Figure 15-34 versus Figure 15-35 Murrumbidgee River.
   c. Figure 14-1, Figure 14-2 and Figure 14-5 Theoretical case studies.
4. Comparison of Fixed thickness and elastic thickness layer inversion;
   a. Figure 14-3 and Figure 14-5 Theoretical case studies.
   b. Figure 14-7 and Figure 14-10 Theorectical case studies revealing problems fixed by sub-noise data aware inversion.
   c. Figure 16-17 Boona Canal.
   d. Compare Figure 15-28 with Figure 15-24 Murray River.
5. Various third party inversion techniques;
   a. Figures 15-8 15-9 and 15-10 2D and 1D inversion at Waikerie.
   b. Figure 16-15, Figure 16-16 and Figure 16-17 Boona Canal. Inversion by EM-Model, Aarhus University and the author. 1D smooth model, 3layer and 3layer laterally constrained.
   c. Figure 16-18 Boona Canal. Res2dInv 2D inversion.
6. Induced polarization imagery;
   a. Figure 15-32 Murray River upstream of Mildura.
   b. Figure 15-36 Murrumbidgee River.
   c. Figure 16-18 Boona Canal and Figure 16-13 Bundure Canal (2D inversion).
7. Sub-noise data aware inversion of conductive basement;
   a. Compare Figures 14-6 to 14-13 Theoretical case study.
   b. Compare Figures 15-49 to 15-51 Murray River
   c. Numerous other examples, eg Figures 15-14 15-15 Murray River
8. Comparison of Geonics EM31 data and geo-electric data;
   a. Figure 16-8 Coleambally Channel 9
   b. Figures 16-34 to 16-42 Various canals.

c. Figure 18-4 Reservoir – Dallas Clay Pan study site.

9. Comparison of waterborne geo-electric survey with adjacent terrestrial TEM survey;
    a. Appendix 9 Figure 3 – Dallas Clay Pan study site.
10. Comparison of waterborne geo-electric and TEM survey;
    a. Figures 15-14 to 15-19 Murray River in the vicinity of Mildura.
11. Comparison of colour histograms;
    a. Figures 15-19 and Figure 15-20 TEM versus Geo-electric (beware of the effect of different depths sampled).
    b. Figures 15-44 and 15-45 Tuckean Swamp submerged and floating arrays.
    c. Figures 16-43 and 16-44 A collection of histograms over canals and rivers.
    d. Figure 15-3 A collective histogram for many images collected in the Murray Darling Basin.
    e. Figure 16-31 A histogram over sites with unsaturated sands.
12. Comparison of conventional and 100% vertically damped imaging;
    a. Figure 15-35 and 15-36 Murrumbidgee River.
13. 2D vertical imaging versus 3D ribbon imaging;
    a. Figures 15-50 and 15-51. Murray River.
14. Map imaging versus 3D ribbon imaging;
    a. Figure 15-24 compared to Figures 15-30 and 15-31 Murray River.
    b. Figure A9-1 and A9-2 Terrestrial towed TEM on the Dallas Clay Pan.
15. Differencing of images – time lapse;
    a. Figures 15-26 and 15-27 Chaffey Bend, Murray River, Mildura.
16. Differencing of images – left and right river banks;
    a. Figure 15-33 Mallee Cliffs, Murray River.
17. Data duplication;
    a. See the differencing of images references above.
    b. Figure 16-17 presents duplicated submerged array data on the Boona canal.
    c. Figures 17-3 and 17-4 Yanco Farm 15 farm canals surveyed a year apart with completely different arrays, transmitters and receivers.
18. Correlation with Salt water interception bore sites;
    a. Figures 15-9, 15-11 and 15-12 Waikerie SIS .

   b. Figures 15-21, 15-22, 15-23 and 15-24 Mildura, Buronga and Mallee Cliffs SIS schemes.

19. Correlation with seepage – pond scale;
   a. Figures 16-34 to 16-42. ANCID pondage test sites on canals.
20. Correlation with seepage – point scale – eg Idaho metre;
   a. Figures 16-16, 16-17 and 16-19 Boona Canal Idaho meter.
   b. Figures 16-26 and 16-27 Coleambally Main Canal SPOTs.
21. Correlation with lithology – eg bores, yabbie pump samples;
   a. The graphical bore lithology presentation method used in the imagery is described in section A7.3 and figure A7-1.
   b. Figures 16-7 to 16-13 Various Coleambally Canals and drill hole logging.
   c. Figures 16-20-16-22 and Table 16-1 Boona Canal augering, yabbie pump samples and drill hole logging.
   d. Figure 16-29 Argoon Canal Yabbie pump samples.
   e. Figures 16-32 to 16-34 Murray Irrigation canals with yabbie pump samples and drill hole logs.
   f. Figures 17-6 to 17-9 Dallas Clay Pan study site, augering.
   g. Figures A9-6 and A9-7 Benerembah towed TEM; drill hole logs.
22. Correlation with soil mapping;
   a. Figure 16-16 Coleambally canals.
23. Identification of palaeochannels;
   a. Figure 13-1 Sturt Canal.
   b. Figures 15-8 and 15-9 Beneath the Murray River, Waikerie.
   c. Figures 16-10 to 16-34 Coleambally and Murray Irrgiation Canals.
   d. Figures A9-1 to A9-9 TEM data.
24. Identification of dipping strata and faults controlling groundwater interaction with a river.
   a. Figures 15-14 to 15-24 Murray River, Mildura vicinity.
   b. Figure 15-32 McFarlanes Reef IP anomaly, beneath the Murray River.
25. Identification of hard indurated rock;
   a. Figure 16-35 Warburn canal adjacent to hard rock quarry.
   b. Figures 15-42 to 15-48 Tuckean Swamp.
26. Identification of sites suitable for recharge management and enhancement;

    a. Figure 13-1 and Figures 16-23 to 16-26 Murrumbidgee River and Tom Bullen Storage.
    b. Figure 16-12 Bundure Canal.
    c. Figures 16-34 to 16-36 Murrumbidgee River, Yanco Weir.
27. Identification of depth to and salinity of salt water beneath river beds;
    a. The entirety of Chapter 15 River case studies; Especially Figure 15-4 and Figures 15-30 and 15-31.
28. Identification of evapotranspiration concentrated salts resulting from irrigation and infrastructure;
    a. Figures 17-6 to 17-10 Whitton Clay Pan study site.
29. Waterbodies with unsaturated zones beneath them;
    a. Figures 15-34 to 15-36 Murrumbidgee at Yanco Weir.
    b. Figures 16-23 to 16-27 Murrumbidgee at Tom Bullen Reservoir.
    c. Figures 16-31 to 16-34. Denimein canals.
30. Imaging in tidal zones (salt water covered);
    a. Figures 15-42 to 15-48 Tuckean Swamp.

A comprehensive correlation of EC imagery against other methods may be impossible in view of the relative data density obtained from physical samples, however, in this research work, effort has been made to search out and survey past as many diverse, potentially-correlatable features and existing control data locations as was possible.

13.2 Introductory example, the Sturt Canal and Murrumbidgee River

Figure 13-1 presents an EC ribbon in 3D perspective plotted with a logarithmic depth scale evident in the bottom right corner and, also, at logarithmically spaced ticks along the ribbon. At first glance, the significance of the image may not be relevant, however, with a little local geological information, ambiguity in interpretation of the significance of electrical conductivity anomalies usually is resolved. Anomalies almost always correlate with groundwater salinity. Correlation with clay content is also common. Figure 13-1 presents a case where a submerged array has been used to suggest where water is seeping from a canal and river into buried river channels and other sediments. Comparison of EC under the canal and river shows that low EC exists under the river and therefore seepage (transmission losses) from the river can be assumed to be much greater than from the

canal. Under the river we can infer that sands and gravels exist from a time when the river was larger and deeper. Under the canal, minor variations in EC are evident suggesting that other river channels may have once existed there and now the resultant channels have been filled with silt. Yabbie Pump cores extracted from the canal bed at various sites along the canal suggest that the anomalies only relate to variation in clay rather than presense of sand. Thin layering near the canal bed suggest layers of canal lining and silt which has settled on top of that lining. EC distribution is indicated in a histogram below the image which suggests that none of the sediment is very saline. A large peak represents the canal/river water and a small low conductivity peak appears to suggest that the water under the river is from the river but has its bulk EC reduced by a sand porosity effect.

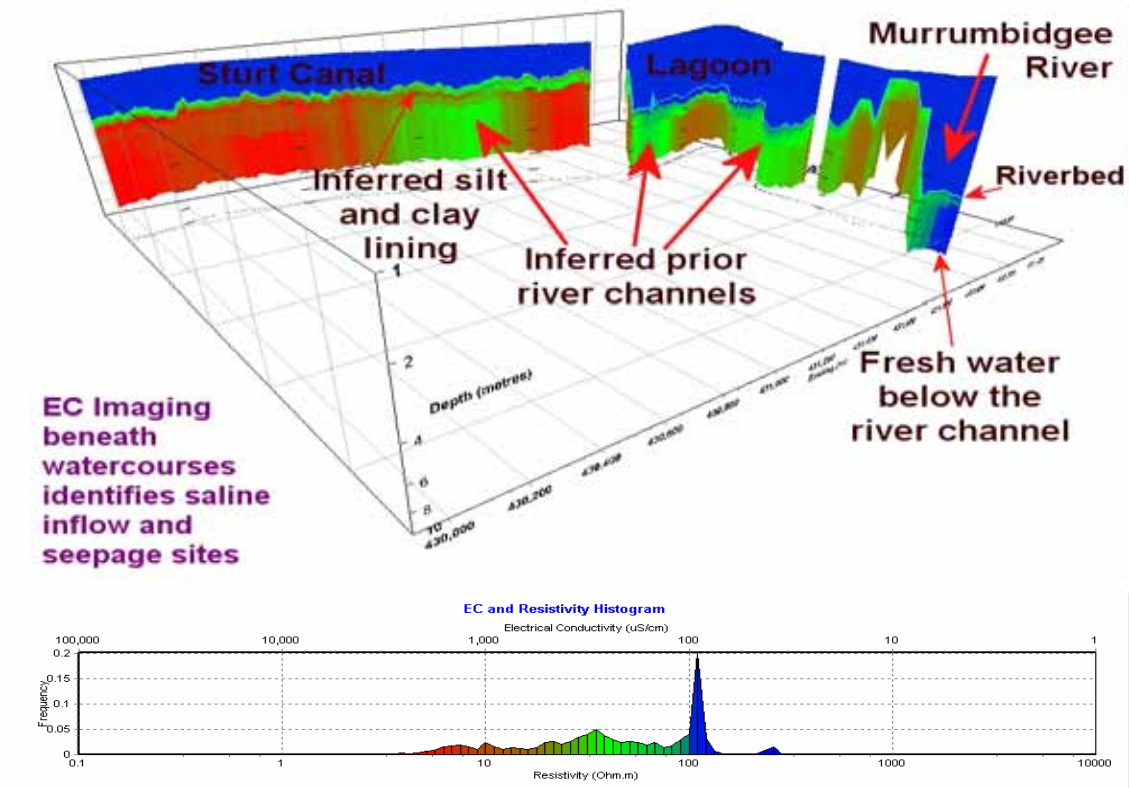

Figure 13.1 Sturt Canal - Murrumbidgee Irrigation Area – NSW – Australia. An example of submerged geo-electric array data with high resolution at the riverbed. Data was collected using an Iris Instruments Syscal Pro provided by Geoforce Pty Ltd. This data has been imaged simply by using an apparent resistivity formula for a submerged array in a half space along with sonar depth information, surface water resistivity and half space effective depths. The imaging procedure used is far from optimal however the level of detail produced is still impressive. Fast submerged array inversion is not yet available.

CHAPTER 14 - THEORETICAL MODEL CASE STUDIES

14.1 Effective depth centred layer inversion

Theoretical three-layer models were created for the purpose of testing inversion software following the methodology of Chapters 5 and 6. In order to reflect the types of models encountered under rivers, layer 1 was fixed at 100 Ohm-.m, layer 2 was varied from 1000 to 0.1 Ohm.m in five steps and layer 3 was fixed at 1 Ohm.m. For each of these five sets of layer resistivities, 11 variations of thickness one, 0.5 to 5m, were generated. Thickness two was set as 2 m and thickness three was infinite. All were plotted, stitched together, in a coloured vertical section as shown in Figure 14-1. For all of these models, simulated datasets were created for the 144 m long AXB floating array typically used in this work.

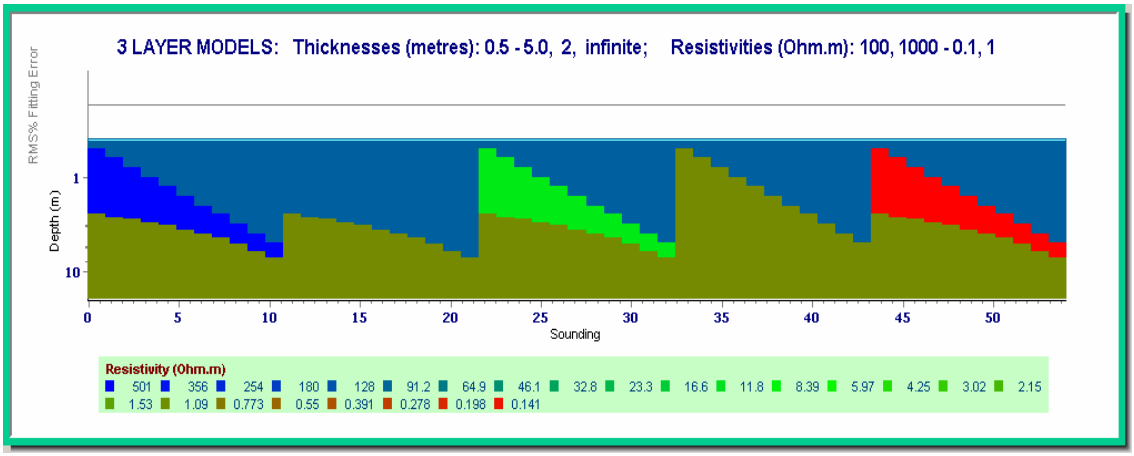

Figure 14.1 Stitched together layered models used for testing of 144m AXB array processing and inversion. Note well that the models are stitched together 1D models, not 2D, and the horizontal scale is 'Sounding', not distance.

The simplest and most robust way to present field data is to plot apparent resistivities against effective depths for each quadrupole in the geo-electric array. For layered-model presentation, a layer logarithmically centred on each effective depth is generated. The result (Figure 14-2) obtained from an array with a good distribution of effective depths such as the 144m AXB array typically is impressive and cannot be greatly improved.

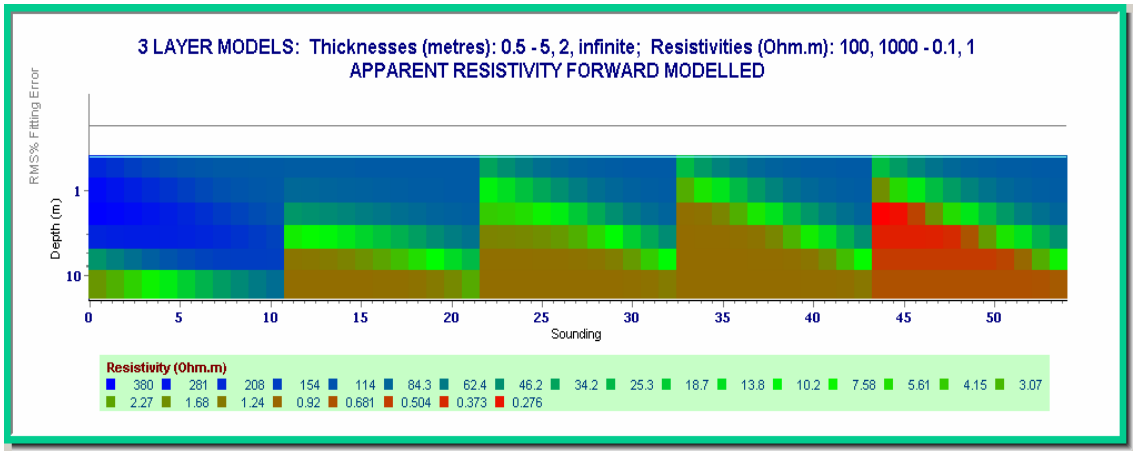

Figure 14.2 Apparent resistivities plotted with respect to effective depths for the models in Figure 14-1 and a 144m AXB array using the algorithm of Chapter 5.

In cases where strong resistivity contrasts exist, apparent resistivity images are not optimal. Sharp features are blurred and thicknesses of anomalously conductive or resistive layers appear incorrectly. In waterborne surveys, detail at the river bed (typically a high contrast boundary) is important and therefore inversion is recommended. Simple fixed layer inversion in which one layer is created for each effective depth in an array is shown in Figure 14-3. Fixed layer thickness inversion works well over smoothly varying layered models but, if the depth of a high contrast boundary does not match a fixed layer boundary exactly, fixed layer inversion creates excessively high or low resistivity layers (geophysical artefacts). In order to compensate for the mismatch of the depth of the high contrast boundary, resistivities of model layers above, straddling and/or below the real depth of the high contrast boundary take on extreme values. In Figure 14-3 an example of such an artefact exists and is clearly evident on the left side of the image as a high conductivity basement.

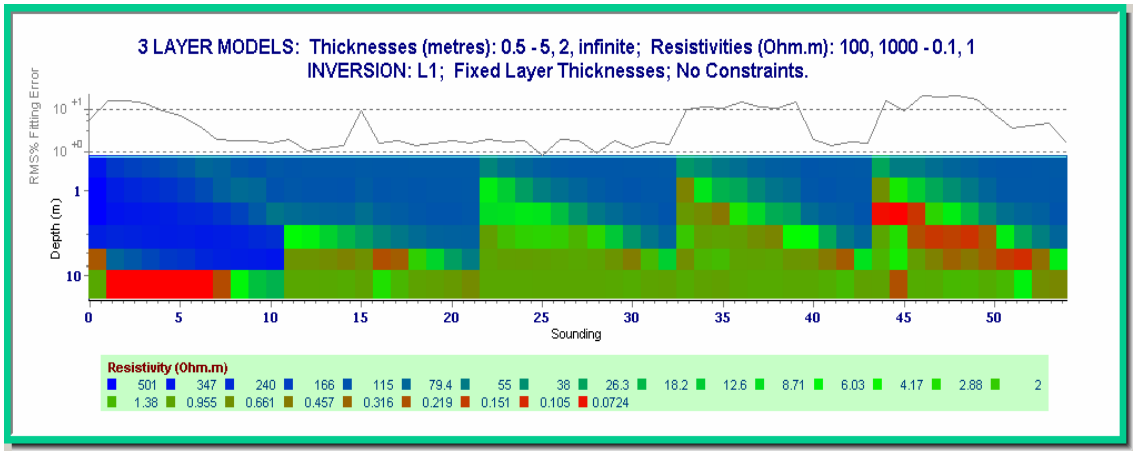

Figure 14.3 Fixed layer thickness inversion conducted using Chapter 6 algorithms with one layer per effective depth of the 144m AXB array and the models shown in Figure 14-1. Note the artefact of conductive basement near the left side.

Inversion becomes unstable when more variables need to be solved than the number of data-points in a sounding or when none of the data-points has significant sensitivity to one of the variables. The fixed-layer inversion utilized in Figure 14-3 ensured that each data-point has sensitivity to a particular layer by centring the layers on the effective depths of each array configuration. If layer thicknesses are to be varied, or if more layers are to be introduced, then additional constraint needs to be added to the inversion code to stabilize it. Unstable inversion code may operate well in many situations but not all. Most inversion specialists resort to creation of additional layers which they constrain using a vertical roughness parameter and sometimes a parameter giving departure from rather arbitrarily defined *a priori* values of resistivity. (Loke & Barker, 1996, Christensen, 2004, MacInnes & Raymond, 2001, www.Interpex.com). Arbitrary *a priori* values of resistivity may constitute a simple resistive or conductive half space. The author has observed that *a priori* constraint to a background value produces artefacts when the apriori values are wrong and therefore should never be used at all in production mode canal and river surveys where robustness of inversion is of paramount importance. Smoothness constraint blurs important high contrast boundaries such as river beds and the tops of saline aquifers and therefore should be minimized as much as possible. An example of smoothness constrained fixed layer thickness inversion is presented in Figure 14-4. One can see that the result differs little from an image of apparent resistivity plotted against effective depths.

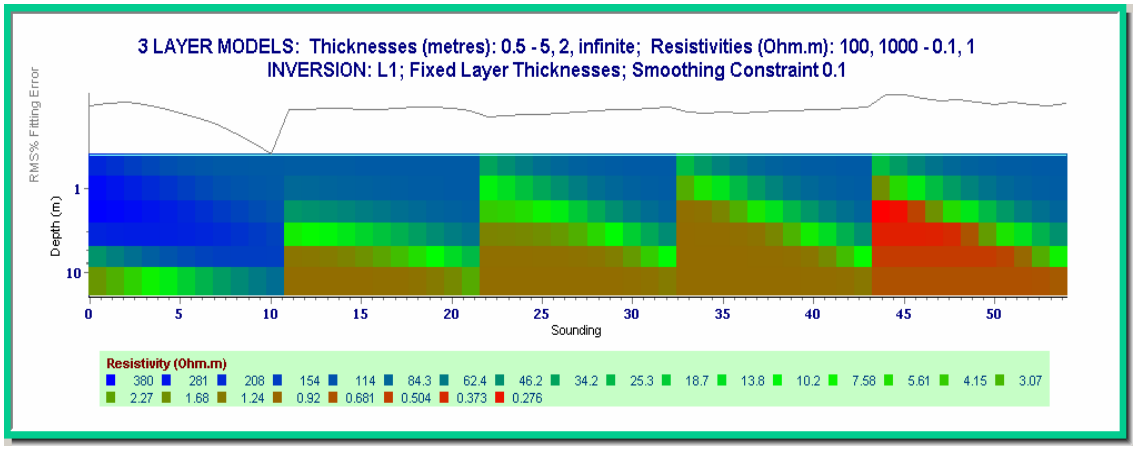

Figure 14.4 Smoothness constrained inversion with layers of fixed thickness centred on the effective depths of a 144m AXB array and for the models in Figure 14-1. Note the similarity with the apparent resistivity solution of Figure 14-2.

Rather than increasing the number of layers, the inversion code has been instructed to stretch thicknesses of modelled layers in order to fit data better. A stretch constraint was added and a little smoothness constraint was also added giving the result shown in Figure 14-5. Smoothness constraint was applied using L1 (least norm) inversion rather than L2 (least squares) inversion because L1 norm damps roughness outliers (high conductivity contrast boundaries) less.

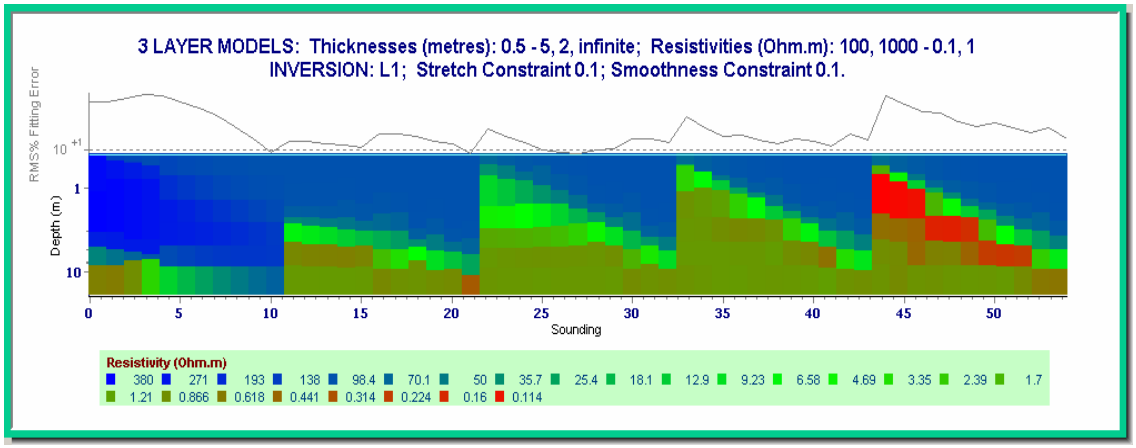

Figure 14.5 Stretch and smoothness constrained inversion of layers centred on the effective depths of the 144m AXB array and of the models presented in Figure 14-1. Seemingly random variations in the section are actually a result of instability resulting from the phenomenon of equivalence (Note that a resistive layer is resolved on the left side of the image but printed copies of this thesis may not have sufficient colour resolution to show it).

14.1.1 RMS Errors

Root mean square percentage errors plotted on the above graphs indicate how well inversions fitted data and the constraints; however; when plotting these graphs, smoothness and stretch constraint errors were inappropriately included in the error estimates resulting in much higher errors than just RMS error of fit of field and model data alone. After plotting these graphs, smoothness and stretch constraint errors were removed from the RMS error estimating algorithm used in the inversion code and typical errors dropped to around 2%.

14.2 Noise level aware inversion

Investigation of saline inflow into rivers involves another inversion challenge – extremely conductive basement which absorbs signal resulting in data that must be clipped at a noise level. The clipping of different soundings at different data-points creates instability in standard inversion software. Noise level aware inversion was used by the author to deal with this instability. The layered models shown in Figure 14-6 were produced to demonstrate the performance of noise level aware inversion.

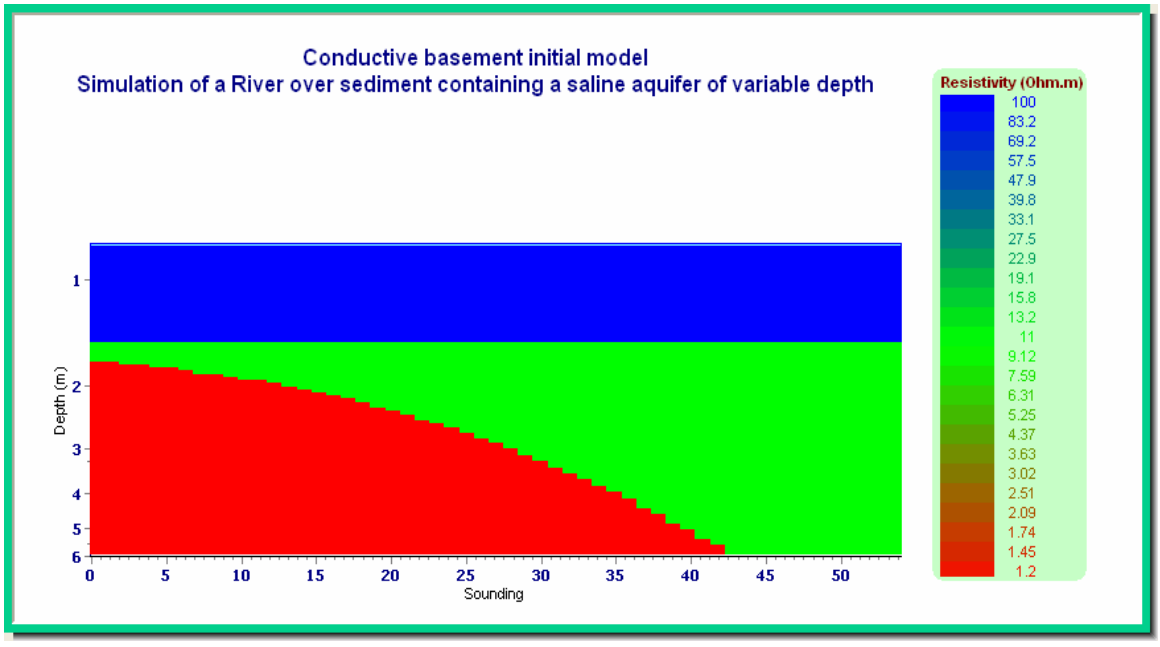

Figure 14.6 Stitched together 3 layer conductive basement models simulating a river over sediment containing a saline aquifer of variable depth.

The forward modelled datasets produced from these models were clipped at a noise level so that when plotted as apparent resistivity versus effective depth in Figure 14-7, it erroneously appears as if the conductive basement disappears on the left side of the image.

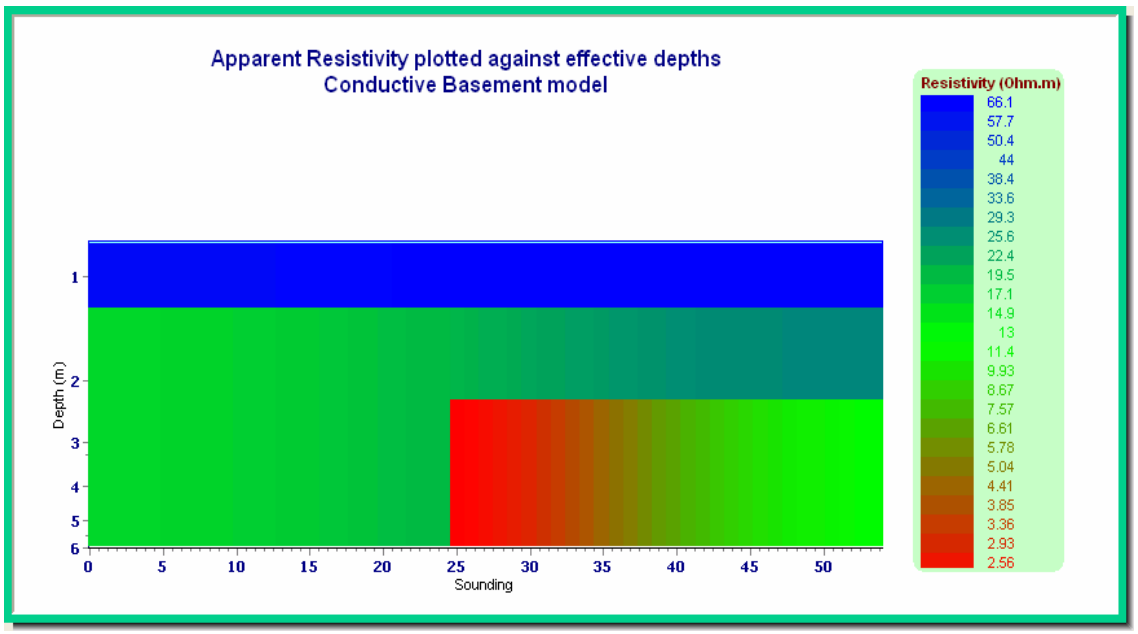

Figure 14.7 Apparent resistivity with respect to effective depth of data, clipped at noise level, collected with the 144m AXB array over the models of Figure 14-6. Note the highly disconcerting loss of detection of the conductive basement on the left. Data has been continued downward where clipped as it still has some validity at such depths. It could alternatively be clipped at a somewhat arbitrary depth but the visual effect would be very similar.

When the data, clipped at noise level, is inverted the serious geophysical artefact observed on the left side of Figure 14-7 may still exist or may even become enhanced as shown in Figure 14-8. When sparse discrete sampling of sounding curves (plotted with respect to effective depth) occurs and the curves are clipped at noise level, which is dependent on conductivity of various layers, conventional inversion will discretely either detect or completely miss deeper layers. Because the noise level is dependent on the conductivity of those layers the disconcerting behaviour evident in figure 14-8 frequently occurs. Sub-noise data aware inversion fixes the instability problem by ensuring that the inversion software fits only models that create voltages that drop into noise just as steeply, or steeper than the field data voltages.

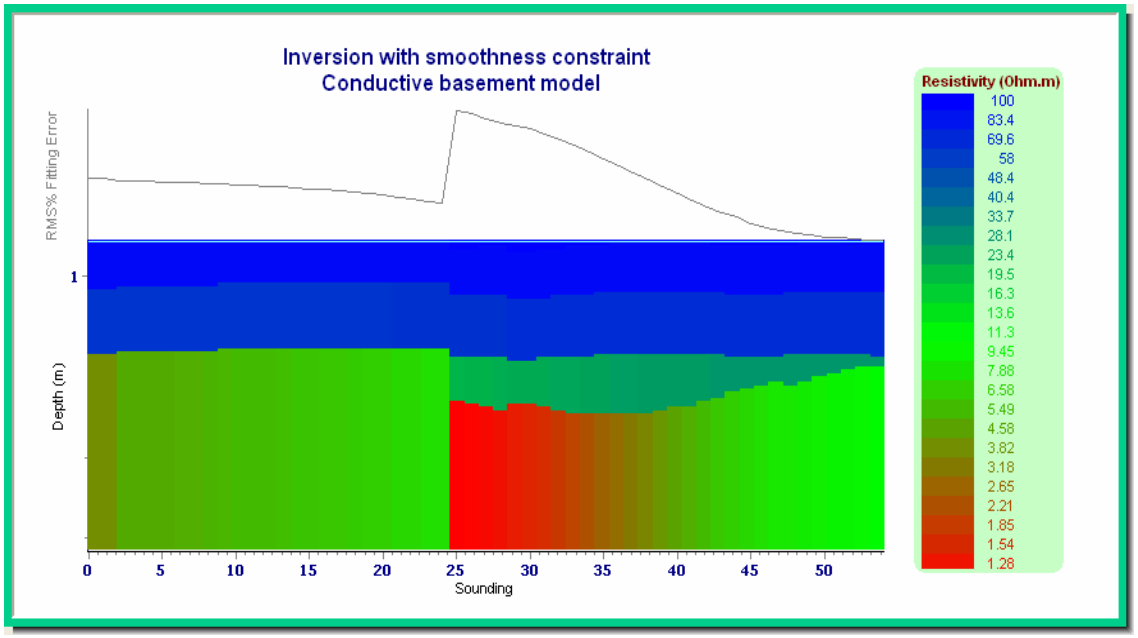

Figure 14.8 Inversion of data, clipped at noise level, collected over the models of Figure 14-6. Note again the disconcerting loss of detection of conductive basement on the left.

Sub-noise data aware inversion has removed artefacts in Figure 14-9, limiting conductivities to values that would generate data less than the noise level.

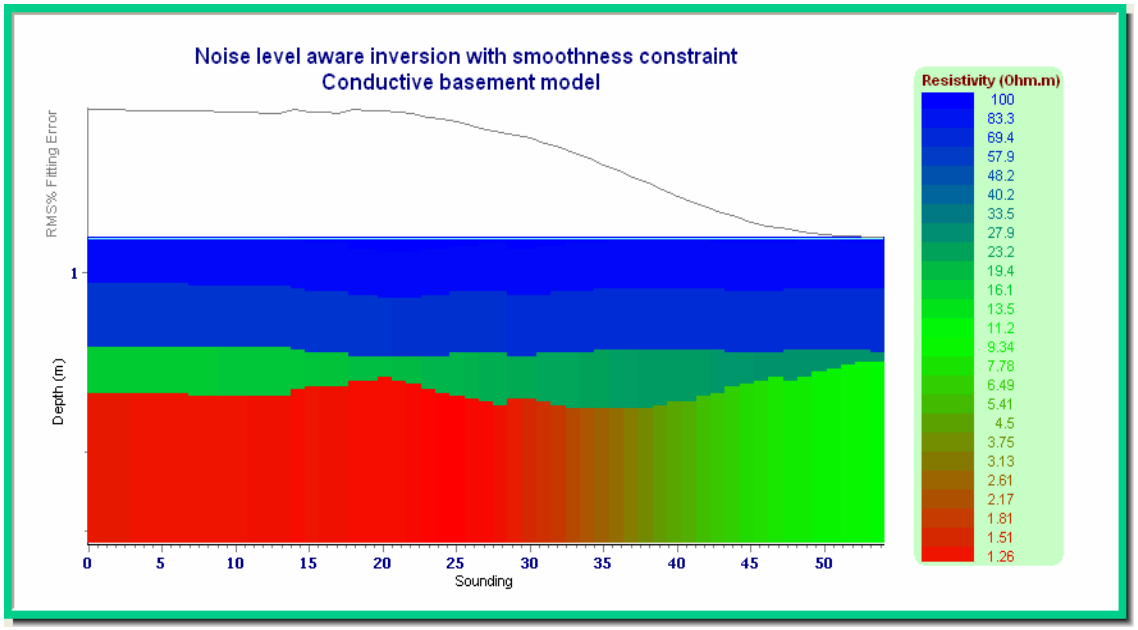

Figure 14.9 Sub-noise data aware inversion of data, clipped at noise level, collected over the models of Figure 14-6. See now that conductive basement is detected on the left.

If totally unconstrained, the result shown in Figure 14-10 occurs where the middle layer thickness goes to zero on the left side of the image.

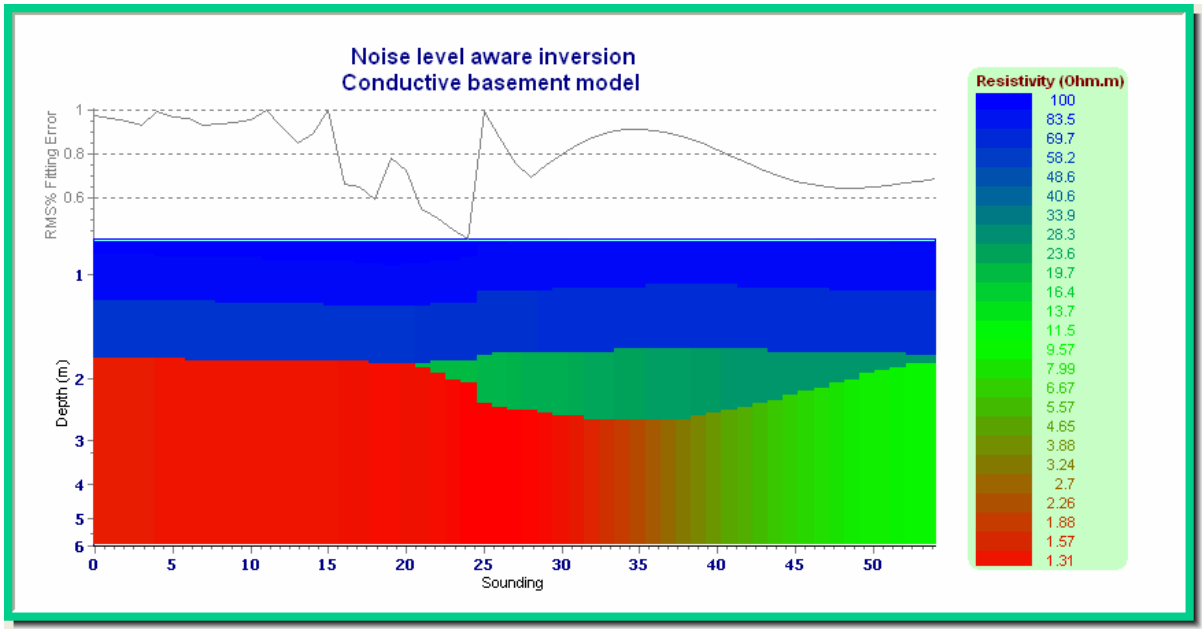

Figure 14.10 Sub-noise data aware inversion as for Figure 14-9 except without any stretch or smoothness constraint. Note that the middle layer disappears on the left – an example of inversion instability.

The same analysis can be done if we artificially add random noise to the forward modelled data before clipping it at the mean of the absolute values of the random noise. Standard inversion of such data would still result in an image with geophysical artefacts as shown in Figure 14-11.

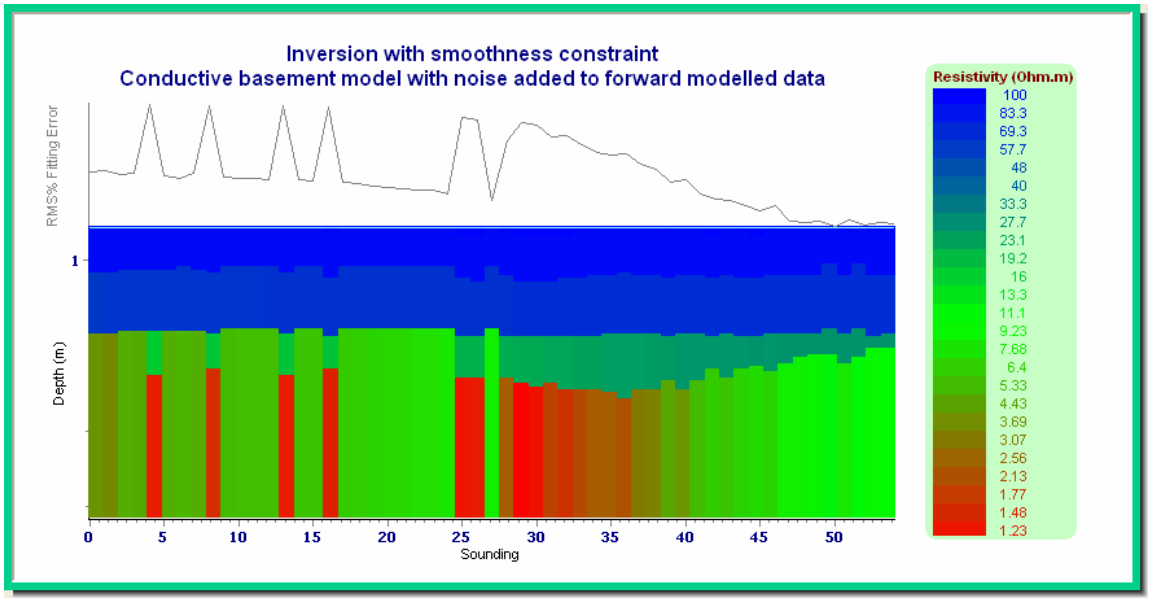

Figure 14.11 Inversion of data clipped at noise level as for Figure 14-8 but with noise added to the forward modelled data. Note again that the conductive basement is only sporadically detected on the left.

The problem is again fixed using sub noise data aware inversion as shown in Figure 14-12.

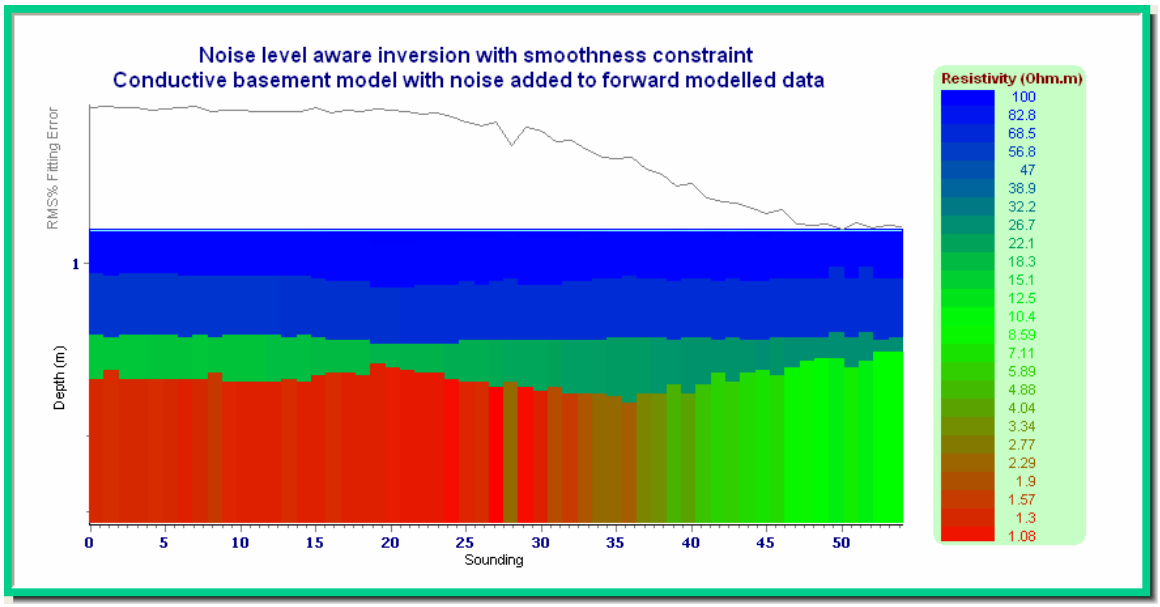

Figure 14.12 Sub-noise data aware inversion as for Figure 14-9 but with noise added to the forward modelled data. Note that the resulting image now clearly shows the conductive basement and is without confusing artefacts.

By increasing the layer thickness constraint and removing the smoothness constraint, a slightly better inversion was achieved as shown in Figure 14-13.

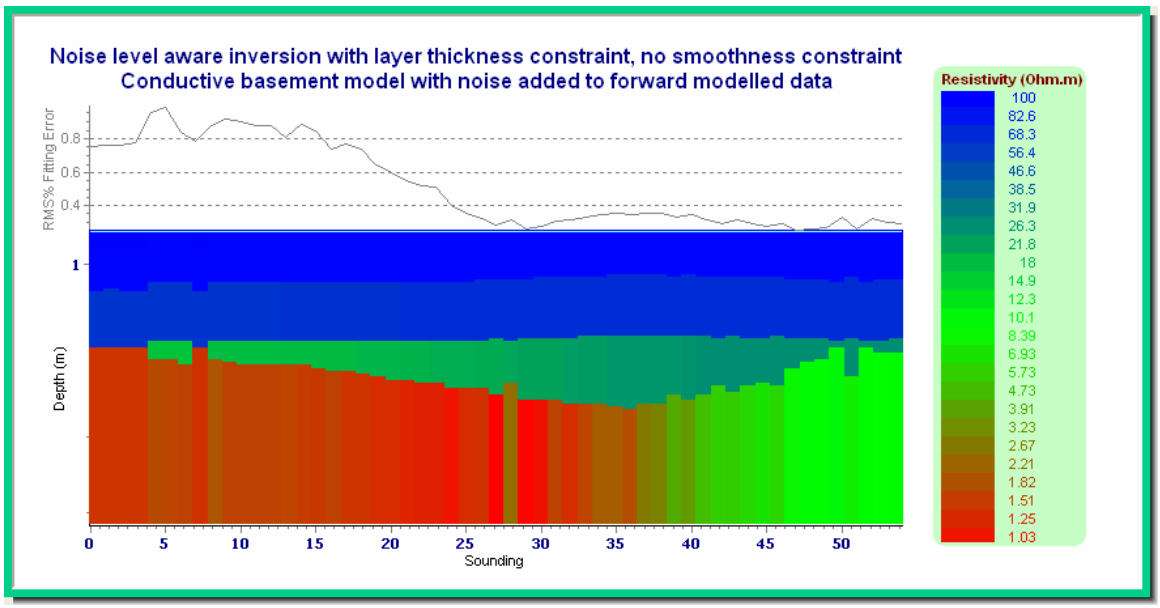

Figure 14.13 Sub-noise data aware inversion as for Figure 14-12 but with much stretch constraint and no smoothness constraint. The result is very similar to the initial models. Note that RMS errors are here only a fraction of a percent.

14.3 Detailed inversion analysis tools

Inversion can be analysed in greater detail than with the interactive 2D sections shown in the previous figures by using tools that are not appropriate for massive datasets such as those dealt with in this thesis. One such tool is a transform derivative and transform matrix. An example for the last iteration of inversion of one sounding is given in Figure 14-14.

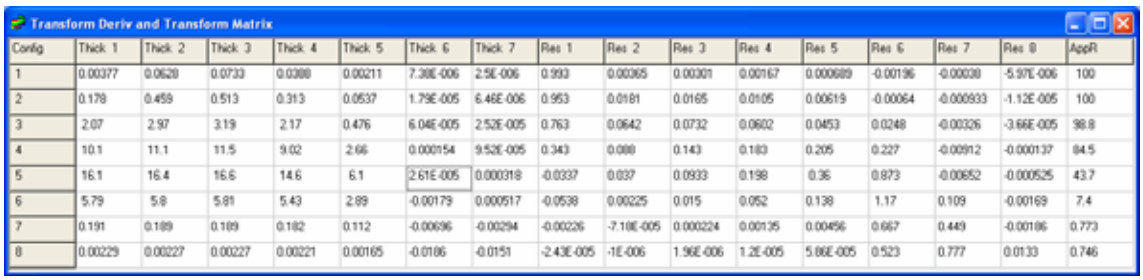
Transform Deriv and Transform Matrix

Config	Thick 1	Thick 2	Thick 3	Thick 4	Thick 5	Thick 6	Thick 7	Res 1	Res 2	Res 3	Res 4	Res 5	Res 6	Res 7	Res 8	AppR
1	0.00377	0.0628	0.0733	0.0388	0.00211	7.38E-006	2.5E-006	0.993	0.00365	0.00301	0.00167	0.000689	-0.00196	-0.00038	-5.97E-006	100
2	0.178	0.459	0.513	0.313	0.0537	1.79E-005	6.46E-006	0.953	0.0181	0.0165	0.0105	0.00619	-0.00064	-0.000933	-1.12E-005	100
3	2.07	2.97	3.19	2.17	0.476	6.04E-005	2.52E-005	0.763	0.0642	0.0732	0.0602	0.0453	0.0248	-0.00326	-3.66E-005	98.8
4	10.1	11.1	11.5	9.02	2.66	0.000154	9.52E-005	0.343	0.088	0.143	0.183	0.205	0.227	-0.00912	-0.000137	84.5
5	16.1	16.4	16.6	14.6	6.1	2.61E-005	0.000318	-0.0337	0.037	0.0933	0.198	0.36	0.873	-0.00852	-0.000525	43.7
6	5.79	5.8	5.81	5.43	2.89	-0.00179	0.000517	-0.0538	0.00225	0.015	0.052	0.138	1.17	0.109	-0.00169	7.4
7	0.191	0.189	0.189	0.182	0.112	-0.00696	-0.00294	-0.00226	-7.18E-005	0.000224	0.00135	0.00456	0.667	0.449	-0.00186	0.773
8	0.00229	0.00227	0.00227	0.00221	0.00165	-0.0186	-0.0151	-2.43E-005	-1E-006	1.96E-006	1.2E-005	5.86E-005	0.523	0.777	0.0133	0.746

Figure 14.14 An example Transform Derivative and Transform Matrix.

Each quadrupole of the array is listed on the left, model parameters are given at the top, the derivatives with respect to each of the model parameters are given in the Jacobian matrix (the matrix of all first-order partial derivatives of the transform function with respect to model parameters) and the transformed apparent resistivity is tacked on as the last column. This display indicates which data points in a dataset are sensitive to which parameters in a model.

Another tool is the textural inversion progress monitor. An example, for just one sounding is presented as subsection 14.3.1 of this chapter. The monitor indicates the efficiency and functionality of each iteration of the inversion process of every sounding in a dataset as well as numerous other details on the progress of inversions. The layout of the example monitor is derived from Merrick, (1977a).

14.3.1 An example of a textural inversion progress monitor:

```
Iteration 0
 Epsilon =  1.83E-001  Sum-of-Squares =  1.87E+000      20.34Percent RMS
 LAYER NO.     THICKNESS   RESISTIVITY    THICK*RES   THICK/RES
    1          0.382     100.126        38.242     0.0038
    2          0.343      99.831        34.274     0.0034
    3          0.687      96.626        66.408     0.0071
    4          1.264      77.857        98.376     0.0162
    5          2.256      33.394        75.325     0.0675
    6          4.063       3.890        15.807     1.0445
    7          7.639       0.707         5.398    10.8100
    8                      0.841       333.831    11.9526
Iteration 1
 Epsilon =  6.19E-001  Sum-of-Squares =  1.20E+000       8.44Percent RMS
 LAYER NO.     THICKNESS   RESISTIVITY    THICK*RES   THICK/RES
    1          0.998     100.124        99.916     0.0100
    2          0.343      99.830        34.274     0.0034
.
.
part removed for brevity
.
.
    7          7.020       0.378         2.652    18.5792
    8                      1.039       434.201    22.3528
Iteration 7
 Epsilon =  6.10E-002  Sum-of-Squares =  5.84E-001       0.79Percent RMS
 LAYER NO.     THICKNESS   RESISTIVITY    THICK*RES   THICK/RES
    1          1.633      99.802       162.951     0.0164
    2          0.343     104.525        35.886     0.0033
    3          0.687     107.254        73.712     0.0064
    4          1.264      90.574       114.445     0.0140
    5          2.256      18.215        41.087     0.1238
    6          1.601       0.301         0.482     5.3170
    7          7.033       0.387         2.719    18.1928
    8                      1.007       431.283    23.6736
 POINT      DISTANCE      RA(FIELD)      RA(MODEL)     PERCENT ERROR
  1         0.282        100.126        99.951         0.175
  2         0.516         99.831        99.725         0.105
  3         1.019         96.626        96.493         0.138
  4         1.959         77.857        76.811         1.353
  5         3.656         33.394        32.605         2.389
  6         6.653          3.890         3.935        -1.150
  7        12.162          0.707         0.701         0.821
  8        22.751          0.841         0.830         1.318
```

PERCENT RMS ERROR = 0.79 (CUTOFF SET AT 1.00)
INTERPRETED MODEL... : FIXED PARAMETER

---------- 0.00

RES = 99.80
THICK = 1.63
---------- 1.63
*
RES = 104.53
THICK = 0.34
---------- 1.98
*
RES = 107.25
THICK = 0.69
---------- 2.66
*
RES = 90.57
THICK = 1.26
---------- 3.93
*
RES = 18.22
THICK = 2.26
---------- 6.18

RES = 0.30
THICK = 1.60
---------- 7.78

RES = 0.39
THICK = 7.03
---------- 14.82

RES = 1.01

LAYER		T=THICK*RES	S=THICK/RES
1	,	162.951	0.0164
2	,	35.886	0.0033
3	,	73.712	0.0064
4	,	114.445	0.0140
5	,	41.087	0.1238
6	,	0.482	5.3170
7	,	2.719	18.1928
Total		431.283	23.6736

CHAPTER 15 - RIVER CASE STUDIES

This chapter presents EC ribbons under rivers of the Murray Darling Basin. First, regional scale EC ribbons will be used to present an overview of gaining and losing parts of that river system, then detailed EC ribbons will be used to present a scaled down view of detail at various sites. Lastly, we shall consider one case study of a coastal drained swamp site because it presents some contrast with inland rivers. River sites that have been investigated are displayed on a map of Murray Darling Basin rivers in Figure 15-1.

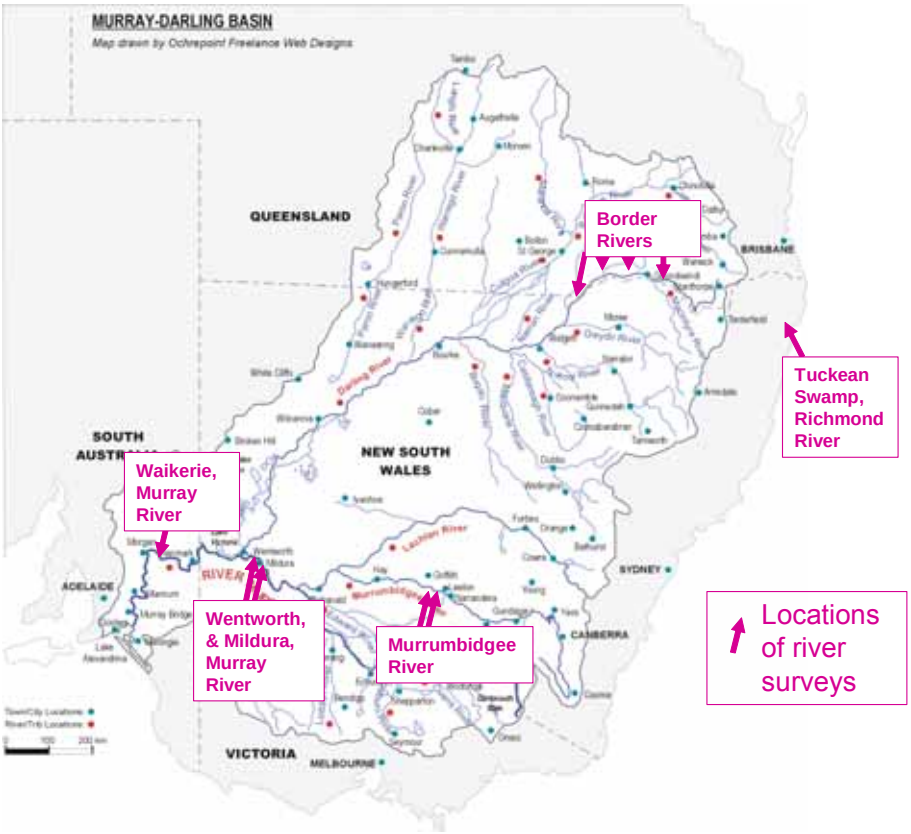

Figure 15.1 Locations of multi-depth EC surveys conducted from rivers of the Murray Darling Drainage Basin.

15.1 Catchment wide comparison of gaining and losing parts of rivers

EC Ribbon images are a good way of comparing gaining and losing parts of rivers in a comprehensive and detailed manner. In Figure 15-2, a losing part of the Murrumbidgee

River, is contrasted (using the same colour spectrum) with the gaining part of the Murray at Mallee Cliffs. One can see that at the losing site, EC beneath the river is almost the same as within the river due to the seeping river water flushing salt from underlying sediments. As water, lost from the river, passes though the ground, that water becomes salinized. Some of it re-enters rivers in the groundwater discharge regions of the Murray, and other, geological basins. One such discharge area is at the Mallee Cliffs site. At groundwater discharge sites such as Mallee Cliffs, the river is deeply incised into the terrain and therefore is at about the level of the water table. Features claimed (Brown, 1991) to be 'buried fossil groundwater discharge lake complexes' at such sites contain solid salt layers and hypersaline brine. In the EC ribbon data collected at that site, saline groundwater is evident as a high EC feature that rises vertically and abruptly is cut off by the river bed where the saline groundwater is being diluted as it is drawn away by the river.

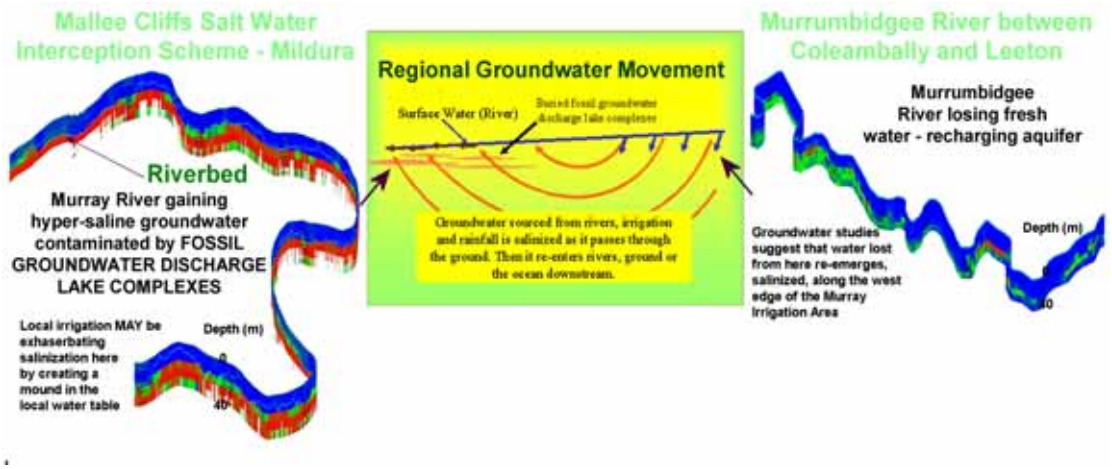

Figure 15.2 An example of contrast of recharge and discharge site EC ribbons.

Comparison of salinity beneath rivers adjacent to various irrigation areas and natural hydro-geological features is very significant to the future impact of those irrigation areas on river salinity. Areas where natural or irrigation driven groundwater flows up through natural salt stores beneath and adjacent to the rivers are high-risk areas where further irrigation expansion will increase river salinity. Water trading is likely to allow for such expansion however the costs to downstream water users (both human and other species) need to be considered as part of that trading. Government policy should be directed towards focusing further development onto sites that do not corrupt the quality of water being transported through them. EC imaging under rivers is possibly the best way of

indicating the current impact and potential future impact of irrigation adjacent to rivers and for indicating if rivers are gaining or losing. Extensive single pass EC imaging surveys covering large parts of river systems are strongly recommended as cheap and thorough transmission loss/gain and river/aquifer connectivity surveys.

The set of images of rivers scattered across the Murray Darling Basin presented in Figure 15-4 are plotted using one common colour scale (Figure 15-3) so that direct comparison of them is possible.

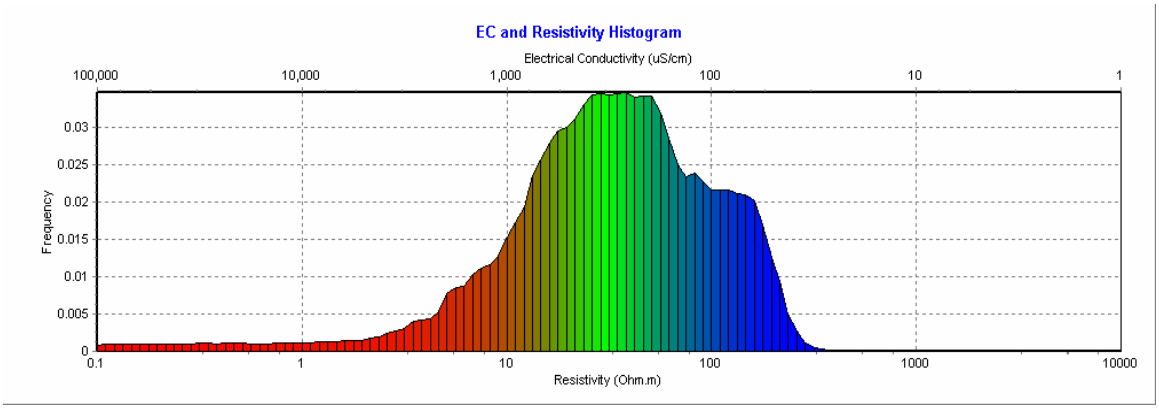

Figure 15.3 An equal area colour scale for Murray Darling Basin River EC images developed by summing histograms from numerous river segments.

The first river segment displayed in Figure 15-4, Waikerie, is subject to rapid inflow of moderately saline water (5000 µS/cm). Of great importance when looking at saline inflow into rivers is the proximity of saline water to the river beds, not just the salinity of water under the rivers. On the Waikerie image, one can see that saline groundwater is kept well below some parts of the River by salt water interception schemes. River water at Waikerie is seen to be much more saline (400 µS/cm) than river water at sites imaged further upstream.

The next river segment, Wentworth to Mildura, is subject to slow hypersaline groundwater upflow. Very high EC is evident right at the river bed. Some of this river segment, however, evidently is underlain by relatively fresh sediment. Groundwater upflow is therefore not present along the entire segment.

The next Murray River segment (starting at Mildura and extending upstream 60 km) includes the Mallee Cliffs salt water interception scheme. Hypersaline groundwater

upflow is present like downstream of Mildura. As mentioned before, the area contains fossil saline groundwater discharge lake complexes (Brown 1991) which are causal to the salinity of the local groundwater.

The Murrumbidgee leaves the Murray further upstream of that segment. A segment of the Murrumbidgee flanked by two canals is displayed in Figure 15-4d (Gogeldrie Weir). Under the river, very low salinity is evident, indicating transmission losses, however, away from the river, under the canals, EC rises. EC under these canals is not related to current day saline upflow like under the rivers. Rather, it is related to clay sediment over which the canals were built. The clay contains relict salt concentrated by evapotranspiration.

Further up the Murrumbidgee, more EC imaging was conducted (Figure 15-4e – Yanco Weir). Transmission losses are evidently occurring along this entire river segment.

The next three images (Figure 15-4f, g and h) are well up the Darling River system. The first is on the Barwon River and shows evidence of saline water that is generally not in contact with the river bottom due to lack of upward groundwater pressure. Upstream, near the NSW-Queensland border, the River becomes the MacIntyre River. Here we can see that the salinity of the lower groundwater has diminished and it still is not in contact with the river bed but rather is separated from it by an upper layer of fresh groundwater. Further upstream the river is called Dumaresq. Here it is beginning to rise up over shallow folded bedrock. EC under the river segment shown indicates transmission losses. These last three images collectively show the effect of passing from near a discharge site to a recharge site within a geological basin.

An in-depth study of these river surveys follows. Even more detail is provided in the various reports on the DVD accompanying this thesis.

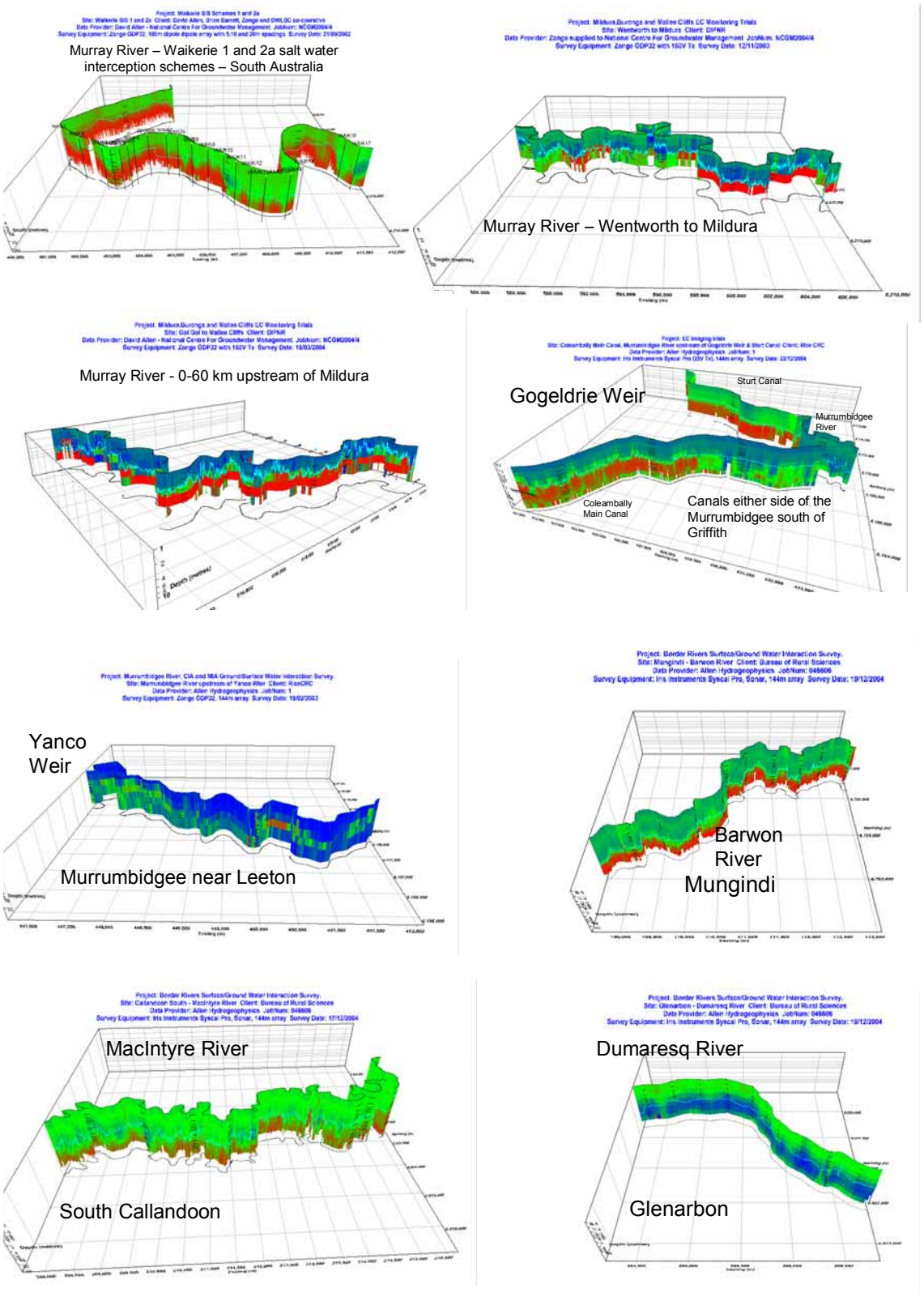

Figure 15.4 EC ribbons under eight Murray Darling Basin river segments plotted, using the common colour scale of Figure 15-3, in order from most downstream to most upstream ('a' to 'h' in horizontal direction first).

15.2 Waikerie salinity interception schemes – Murray River – South Australia.

The part of the Murray within the Waikerie saline groundwater interception schemes forms the first and most downstream case study within the Murray Darling Basin. Forward (2004) presents the scenario at the site (see Figure 15-5). The Woolpunda salt interception scheme is seen to be preventing natural regional groundwater flow from affecting the river, evident as a broad water table gradient on each side of the river. In contrast, the Waikerie schemes oppose groundwater flow driven by obvious groundwater mounds surrounding irrigation areas. The graph shows how the interception schemes have successfully reduced salt load, measured in tonnes per kilometre per day, entering the river. The multi-depth EC surveys conducted at the site were along both banks of the river within the extents of the Waikerie salt interception scheme and Waikerie phase IIA salt interception scheme. At the time of the survey, Waikerie IIA had not started operation.

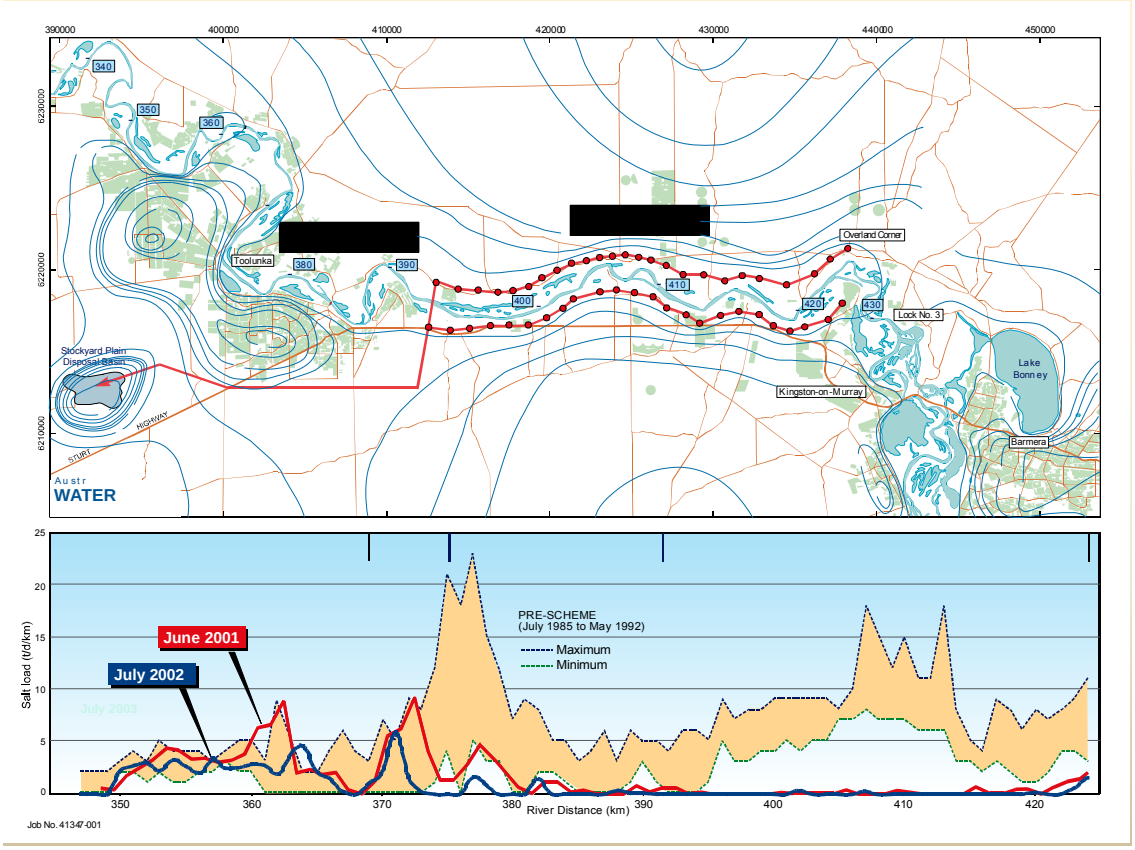

Figure 15.5 Salinity entering the Murray around Waikerie and the location of saltwater interception bores (from Forward, 2004)

The effect of irrigation induced saline groundwater upflow on the river flats, which are surrounded by cliffs and uplands, is evident in Figure 15-6.

Clark's floodplain - Bookpurnong

Figure 15.6 Visual evidence of the ecological damage caused by saline groundwater intrusion into the lower Murray river floodplains and river (from Forward, P. 2004)

Woolpunda and Waikerie schemes are now removing 250 and 100 tonnes of salt per day respectively leaving 10 tonnes of salt entering the river at each site every day (Forward 2004)

Figure 15-7 shows a geo-electric array being used to image EC beneath the Murray at Waikerie. Notice the salt scald, on the cliff, which has resulted from groundwater outflow resulting from irrigation directly above that portion of the cliff.

Figure 15.7 Geo-electric survey on the Murray at Waikerie. A salt scald, demonstrating the localized effect of irrigation, is evident as a light patch in the cliff.

The Waikerie survey was conducted in September 2002 when the Waikerie scheme had only recently started pumping. It is believed that because the bores there are very close to the river, and because the geological strata there, that the river has incised, are permeable, distinct anomalies exist around the bores.

The ribbon image in Figure 15-8 is a heavily smoothed 2D inversion conducted using software written by Scott McInnes (TS2DIP - Zonge Engineering and Research Organization, 2002). This inversion software is very similar to Loke's Res2DInv. Figure 15-9 presents a subset of Figure 15-8 inverted using the 1D inversion software written along with this thesis. The results are very similar once the 2D inversion has been horizontally smoothed to remove a resonating artefact (horizontal ripple) in the 2D inversion. The time taken to conduct the inversion however is not similar – the 1D inversion can be completed in seconds while one watches it being progressively imaged on a computer screen however the 2D inversion takes 10's of hours to complete. For

exponentially spaced arrays such as used throughout most of the fieldwork of this thesis but not at Waikerie, the time taken to complete a 2D inversion increases markedly. It was only because the Waikerie data was completed using a linearly spaced dipole – dipole array that rational comparison of 1D and 2D inversion was possible. Such an array has poor signal to noise ratios at greater depths and a poor distribution of effective depths as is evident in the layering in Figure 15-9. The groundwater is not highly saline at Waikerie so signal to noise ratios were reasonable. Figure 15-10 is a close-up comparison of the 1D and 2D inversion results both presented without horizontal smoothing to clarify the differences between them. Figure 15-8 is made up of many small overlapping 2D inverted data segments, such as the one in Figure 15-10, but with the end effects removed.

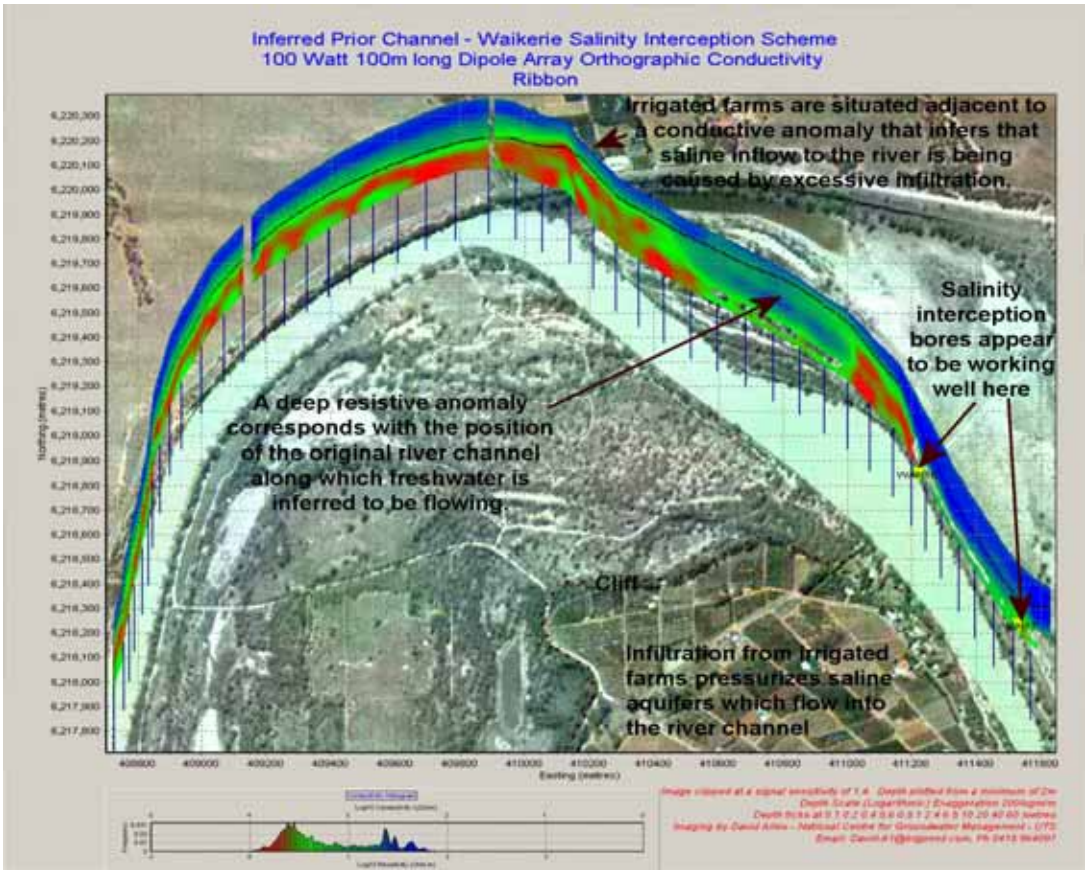

Figure 15.8 Part of the Murray River within the Waikerie salt water interception scheme in which there is evidence of saline inflow related to irrigation near the river (top), a deep, buried, fresh/brackish water filled prior river channel (centre right) and freshwater flushing of strata beneath the river in the vicinity of SIS bores (far right). Note how the cliff intersects the river at the edge of the prior river channel anomaly. See Figure 15-9 for close up views of the anomalies. This ribbon was inverted using a 2D algorithm.

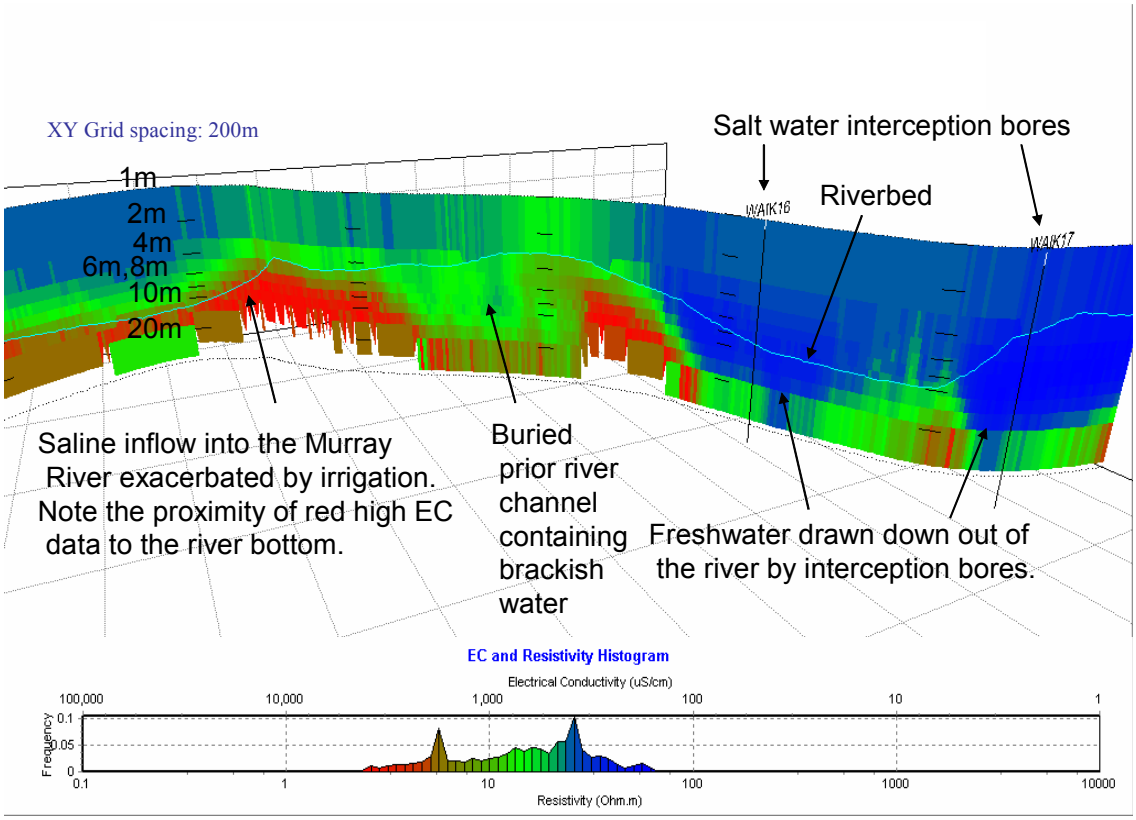

Figure 15.9 The far right part of Waikerie SIS scheme shown in Figure 15-7. A close-up of anomalies resulting from a palaeochannel, and Waikerie SIS bores 16 and 17 (shown as vertical black lines). This ribbon image was generated using 1D inversion – contrast it with the 2D inversion in Figure 15-7. Note the thick surface layer that is a result of the poor near surface resolution of linearly spaced dipole–dipole arrays such as used at Waikerie. Note how the riverbed (aqua line) does not correspond with the base of the blue low EC anomaly near the SIS bores – the bores appear to have drawn freshwater downwards from the bottom of the river in the vicinity of the bores.

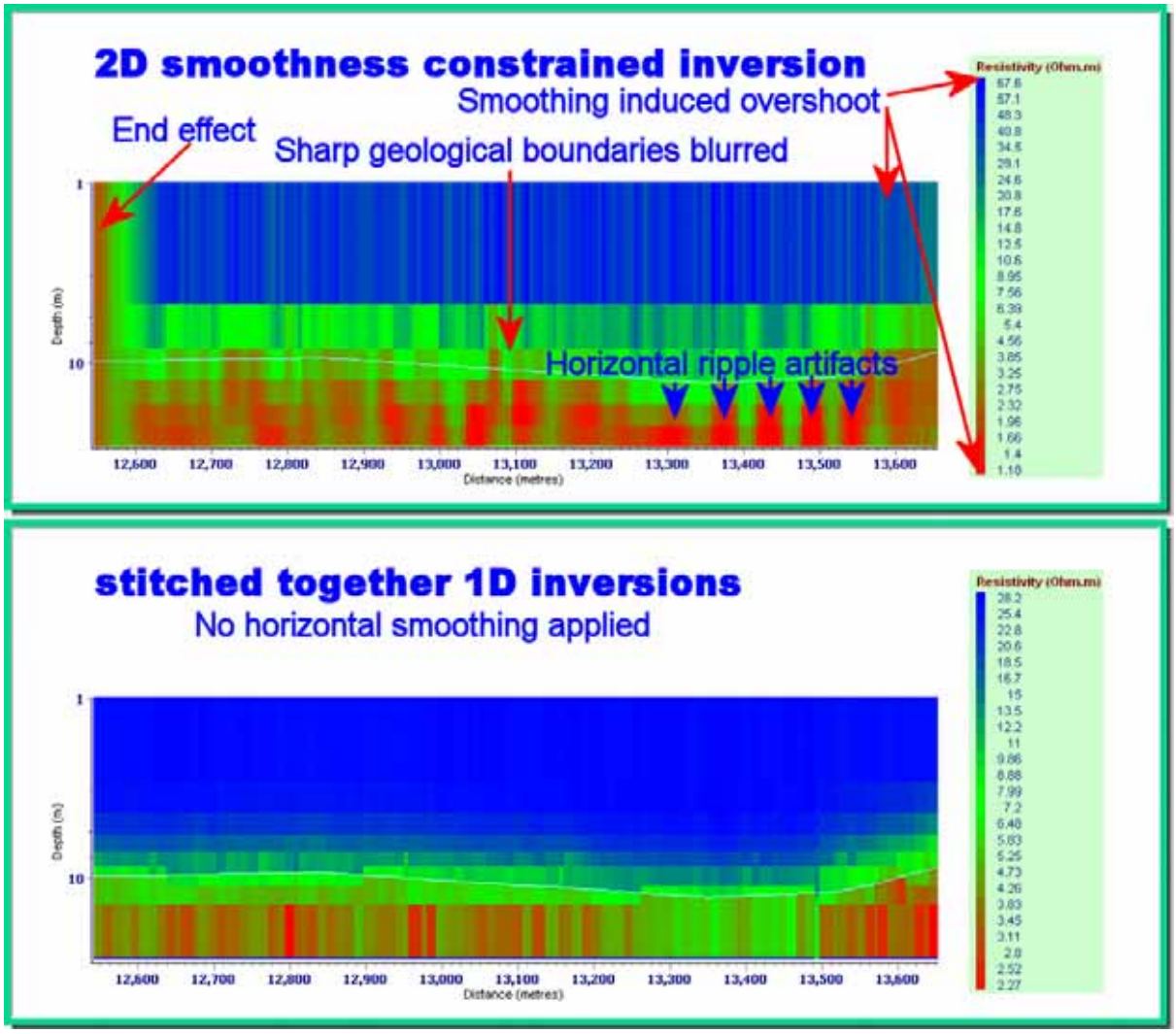

Figure 15.10 A comparison of 2D and 1D inversion of one 1km long segment of riverborne geo-electric data collected with a dipole-dipole array. An aqua line represents the approximate depth of the river bed. 1D inversion works more effectively with an AXB array but 2D inversion of data collected with such an array is not practical. For comparison purposes, inverted data has not been horizontally smoothed as would normally be done to reduce the effect of noise.

As EC reflects groundwater salinity rather than rate of saline flow, in most cases, in the vicinity of SIS bores, EC anomalies are not expected unless the SIS bores have been pumping sufficient flows to reverse the vertical groundwater flux under the river so that river water is drawn into the SIS bores. As soon as that occurs, the strata under the river become flushed with fresh river water rather than up-welling saline groundwater and a distinct EC anomaly occurs. The EC anomaly then shows the extent of flow reversal causal influence of the SIS bore which in many cases is distorted by geological variations

such as prior river channels. Distortion of drawdown around an interception bore location (Waik 7b) by a prior river channel location is clearly evident in Figure 15-11. Numerous good examples of such anomalies exist at Waikerie SIS. Figures 15-8, 15-9 and 15-11 show such anomalies as well as another good anomaly believed to be resulting from a buried deep river channel which is evident in the airphoto in Figure 15-8. The history of the river is evident from the presence of the buried deep channel. You may correlate, on the airphoto of Figure 15-8, the location of this deep channel with evidence of its path, which has determined some of the cliff locations as well as lagoon locations, on the airphoto. Cliffs flanking the river are separated by only about 1 kilometre. The river has created cliffs as it has flowed. Greater flows probably occurred in the past than the present because the buried river channel evident in the imagery is much deeper than the current river channel. The flow of the river does not appear to have lasted for long however because only one deep buried river channel is evident. The age of the river is probably limited by the amount of time it would have taken for the river to have eroded, rapidly at first, just to the bottom of the buried river channel and then out to the current cliff locations.

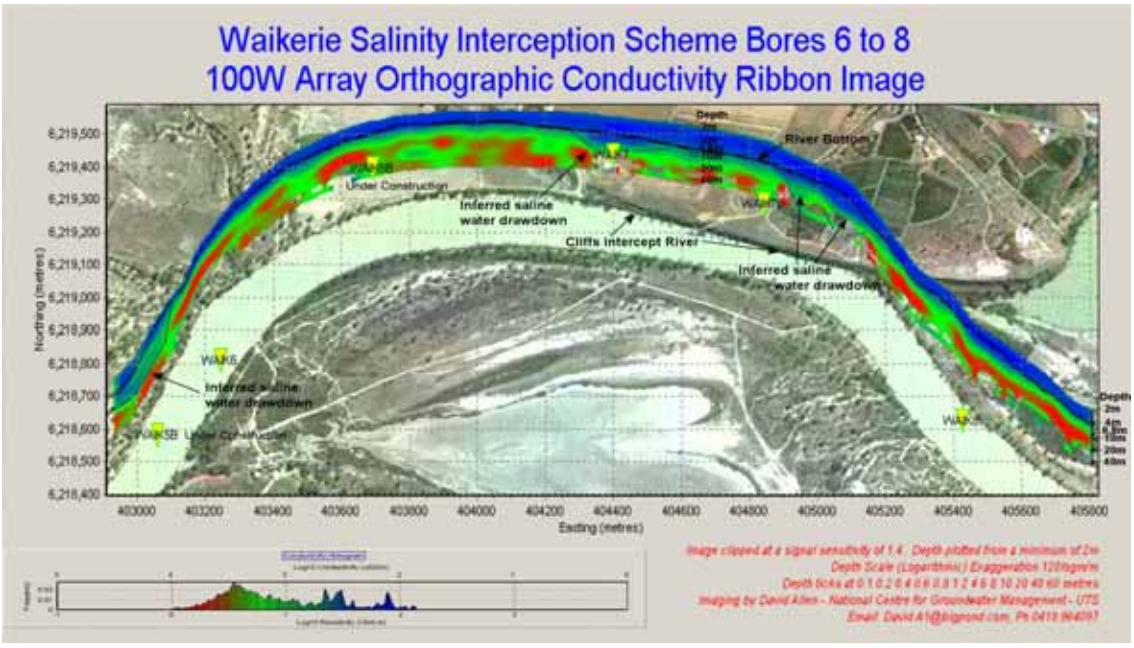

Figure 15.11 Freshwater drawdown cones evident around salt interception bores Waik5, Waik7, Waik7b and Waik8. Note the offset of the cone around Waik7b which is caused by the prior river channel, the location of which is evident from the cliff in the airphoto.

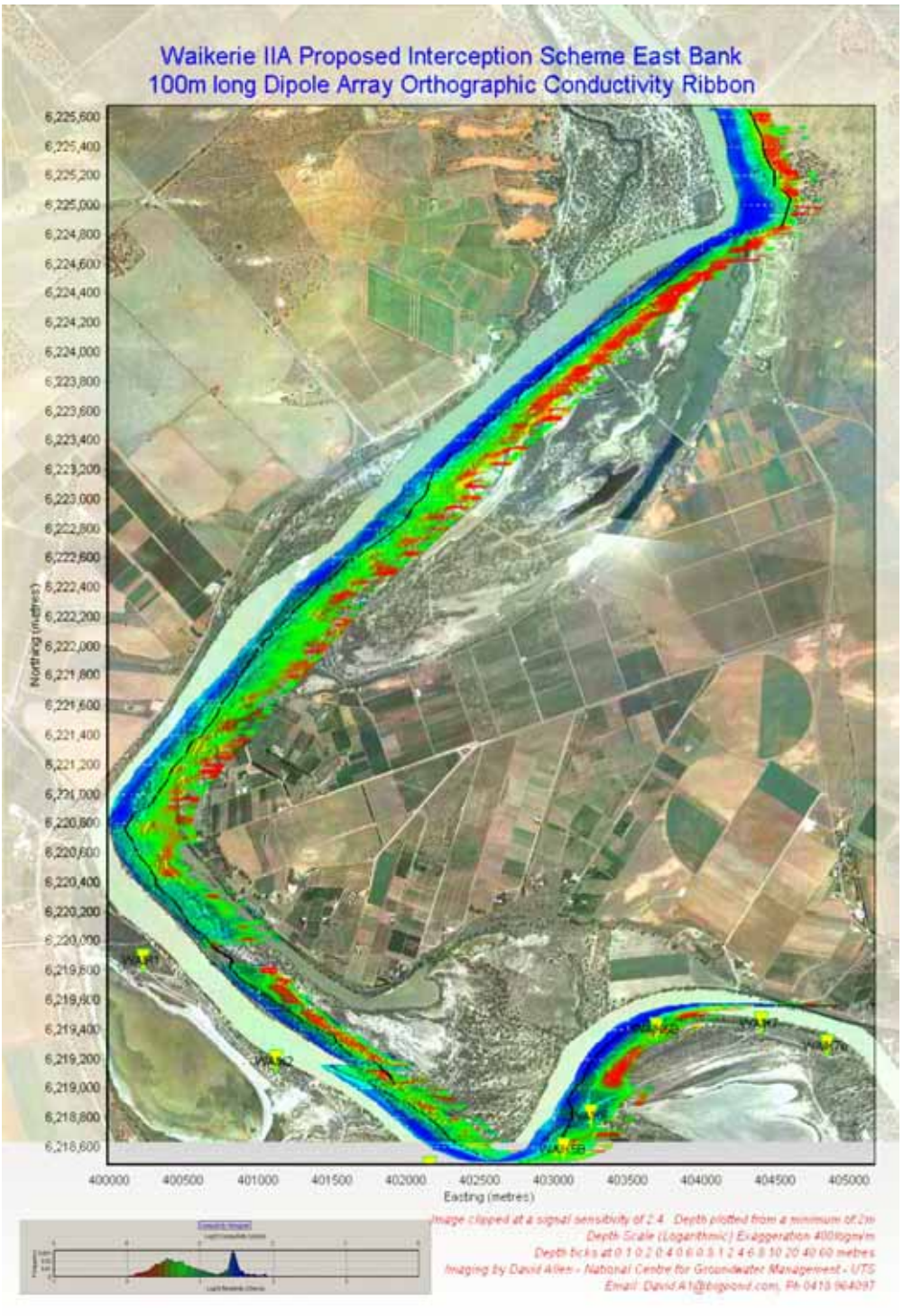

Figure 15.12 Waikerie IIA before commencement of pumping. The 3D EC Ribbon is to be viewed from the east and is overlain by a semi-transparent airphoto. Inversion was conducted using TS2DIP. Note the increase in EC towards the north away from the bores of the existing Waikerie salt interception scheme. Note the deep hole at the river bend in the north that cuts deep into saline sediment.

EC imaging was done along both banks of the part of the Murray within the Waikerie IIA scheme. As the scheme had not commenced operation when the survey was conducted, we only see pre-pumping conditions. It is evident that saline groundwater makes good contact with the river in deep holes such as in the north east corner of Figure 15-12. Where the river is shallow, a lens of fresher sediment separates the river from the saline sediment. The separation increases with proximity to the Waikerie salt interception scheme in the south east.

15.3 The Murray River in the vicinity of Mildura, Victoria/NSW border

15.3.1 The problem of saline inflow into the Murray River near Mildura

The Murray River around Mildura may look very tranquil and healthy, yet just beneath the river flows an expanse of pressurized hyper-saline groundwater. Pressure has forced the groundwater to flow through what may be fossil buried saline discharge lake deposits and become hyper-saline. From there it seeps gradually into the river from below. Raised water tables resulting from irrigation adjacent to the river increase pressure on the hyper-saline groundwater under the river. As a result, upward flow of that water into the incised Murray River channel has increased. Weirs have raised the river water level and thus provided significant opposing pressure on groundwater trying to enter the river resulting in an improvement on natural river salinity levels. At each weir, there is however a sharp pressure gradient acting on the groundwater beneath the river which causes increased upward flow of groundwater downstream of the weirs. As the deeper groundwater is more saline, higher river salinity can be expected downstream of weirs. The hydro-stratigraphy and the effect of salt interception pumping on the scenario at the river is presented in Figure 15-13.

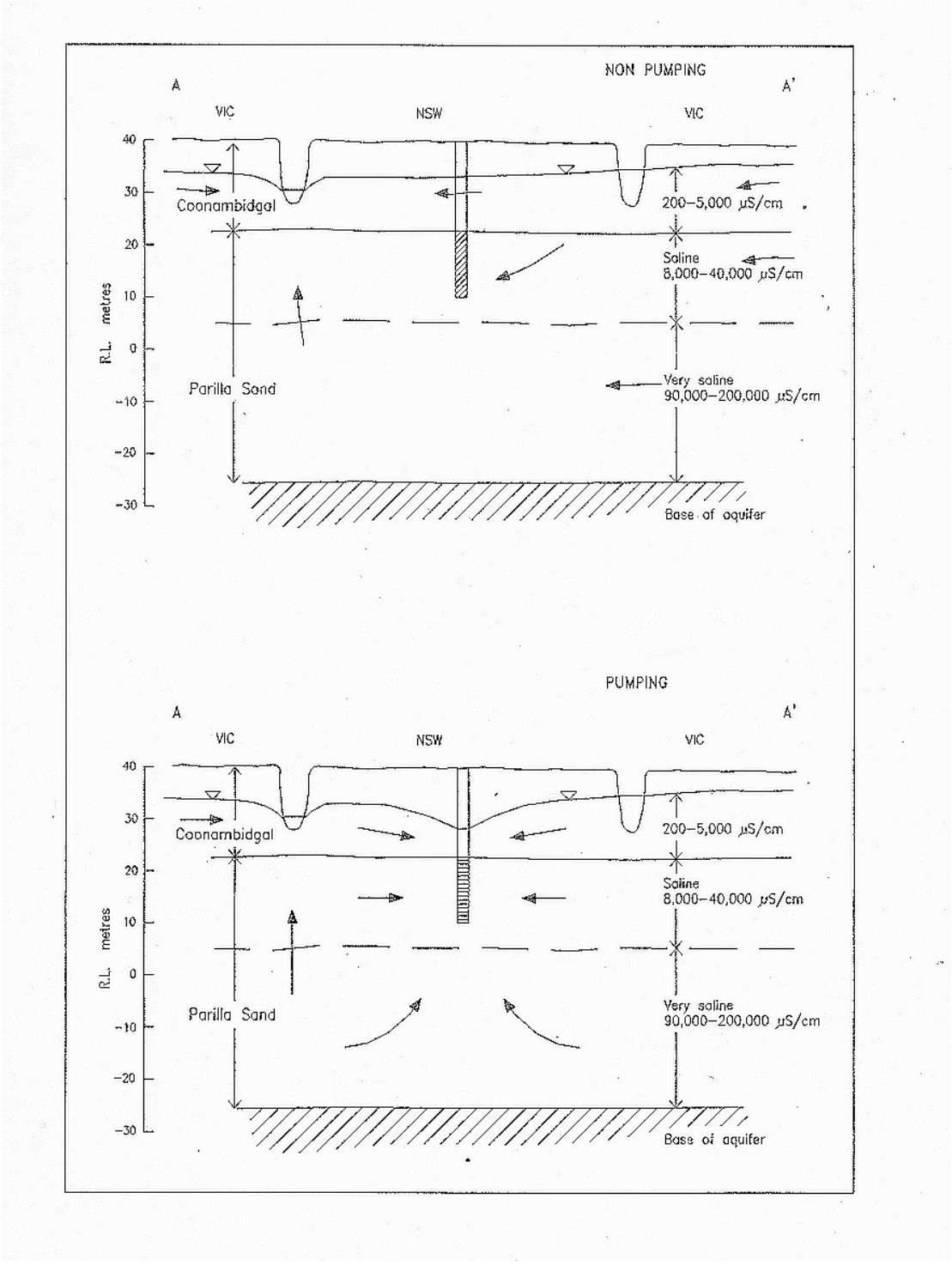

Figure 15.13 Hydro-stratigraphy in the vicinity of Mildura and groundwater flow before and during salt interception bore operation (from Merrick 2002, taken from Williams and Erny – date unknown).

15.3.2 Assessment of saline inflow using EC imaging

Electrical conductivity (EC) imaging has delineated sources of salinity and the salt concentration of groundwater flowing in and out of the riverbed. 3D presentation of the imagery was used to observe how the sources of salinity connect to geological and geographical features around and under the river.

15.3.3 Surveys conducted

Electrical conductivity imaging of sediment under the Murray River from Wentworth, upstream through Mildura and Mallee Cliffs salt interception schemes was conducted. A set of seven time lapse surveys was conducted between March 2003 and March 2004. Surveys were conducted using both a 144m long floating AXB geo-electric array and a 7.5m square floating transient electromagnetic (TEM) loop device.

15.3.4 Survey Results

EC ribbon images of the most successful geo-electric array surveys are presented in Figures 15-14 and 15-15. In Figures 15-16 and 15-17, the most successful transient electromagnetic surveys are presented. Blues represent low EC while reds represent high EC. An aqua line represents the river bed. Depth scale is logarithmic and depth ticks are evident on the ribbon in some places with ticks at 1,2,4,6,8,10 and 20 metres. Purple discs are plotted at each kilometre marker along the river. The radii of the disks are proportional to salt load increase in the river water within each kilometre measured by independent run of river water salinity and flow surveys. The salt load increases are graphed in tonnes per kilometre per day in Figure 15-18. Large increases in salt load are evident downstream of where the river bed intersects saline hot spots. The salt load increase is especially pronounced downstream of deep holes, in the riverbed, that penetrate deep into saline aquifers. Salt load increase is least just upstream of weirs where pressure of the river on underlying aquifers is greatest.

15.3.5 Comparison of Geo-electric Array and TEM data

Images created by both devices have clearly picked up the same salinity concentrations under the river. The geo-electric array has accurately picked true electrical conductivities except in extremely saline spots where signal strength is low. The geo-electric array used has good resolution at and just below the riverbed. The TEM device has clearly resolved

the horizontal extent of the extremely saline hot spots but has not been able to resolve low EC (low salinity) features and features at or above the riverbed so well. In Figures 15-19 and 15-20, the colour histograms for the geo-electric and TEM images are presented in units of both EC and resistivity (the inverse of EC). They have been generated as a by product of painting the images with equal area color distribution. The geo-electric histogram has a large peak representing the river water and a long flat tail representing the saline sediments under the river. Because of the river water peak, the superficial variations in river water EC have been exaggerated in the geo-electric array imagery which has very high data density in the actual river water. These visually enhanced superficial variations in the river water EC probably largely represent geophysical artefacts. The peak of the TEM histogram representing the river water is not where it should be due to mathematical approximation limitations of TEM processing at shallow depths however the histogram covers a tremendous range due to higher data density beneath the river and indicating better resolution of conductive features. The mean depth of signal contribution received by the first useable time gate of the TEM system was about 10 metres whereas the geo-electric data starts at about 10 centimetres deep and extends to only about 20 metres deep at this site.

Note that the scales on the histograms (Figures 15-19 and 15-20) cover 5 orders of magnitude. Contrast this to the scale of typical river water salinity variation surveys that may cover a fraction of one order of magnitude of EC variation.

15.3.6 Effects of Weirs

The effect of weirs at Wentworth and Mildura is evident in Figures 15-14,15-15,15-16 and 15-17 as low EC just upstream of the weirs and high EC just downstream of the weirs. The weirs are at the extremities of the ribbon images in Figures 15-14,15-15,15-16 and 15-17 – ie. at river kilometre markers 832 and 886.

15.3.7 Effects of SIS bores

Salinity interception schemes have been set up to draw salt water out of aquifers under the river before it gets a chance to flow into the river. The bores in the schemes appear to have not been pumping sufficiently to totally arrest saline inflow and therefore the effect of them is not evident in the EC ribbons. This is because they are too far from the river (except PS3) Contrast this imagery with imagery around bores at Waikerie that have

pumped sufficiently (or excessively) and have anomalously low EC surrounding them on the ribbons. Effects of the pumping at schemes near Mildura appear to be spread widely, probably due to horizontal stratification of aquifers and aquitards. As a result, anomalies on the ribbons due to SIS pumping are not always easy to identify at these sites.

As the images respond to salinity of groundwater rather than the rate at which it moves into or out of the river, significant anomalies around SIS bores are not expected unless a complete reversal of flow occurs under the river near the SIS bores and water begins to be drawn out of the river, into the ground, and ultimately away through the SIS bores. The SIS bores therefore need to be drawing river water into the ground before significant anomalies can be expected in the ribbon images.

Figures 15-21, 15-22 and 15-23 show the locations of SIS scheme bores and the effect of them. Low EC anomalies just beneath the riverbed are evident around Buronga bores 5 and 4 (just off the edge of the image east of bore 5) and around the Mallee Cliffs bores. A comparison of Mallee Cliffs between March 2003 and January 2004 is included. A difference in impact is most evident by comparing the impact of the bores with the un-pumped strata upstream and downstream of the SIS bores. No text book quality anomalies, such as exist further downstream near the Waikerie SIS scheme bores are evident around any of the bores studied near Mildura.

15.3.8 Effects of geology

Because the ribbons are plotted in 3D, the effect of the river floodplain is evident. As the river meanders close to the sides of the flood plain, saline strata are seen to rise up closer to the riverbed. At some points in the floodplain, evidence of deep fossil river channels exists. Examples of these features are evident in a cross section across the floodplain between Merbein and the Coomealla pumping station at Dareton. The grey soil of the southern end of the floodplain is evident in the airphoto overlay on Figure 15-24.

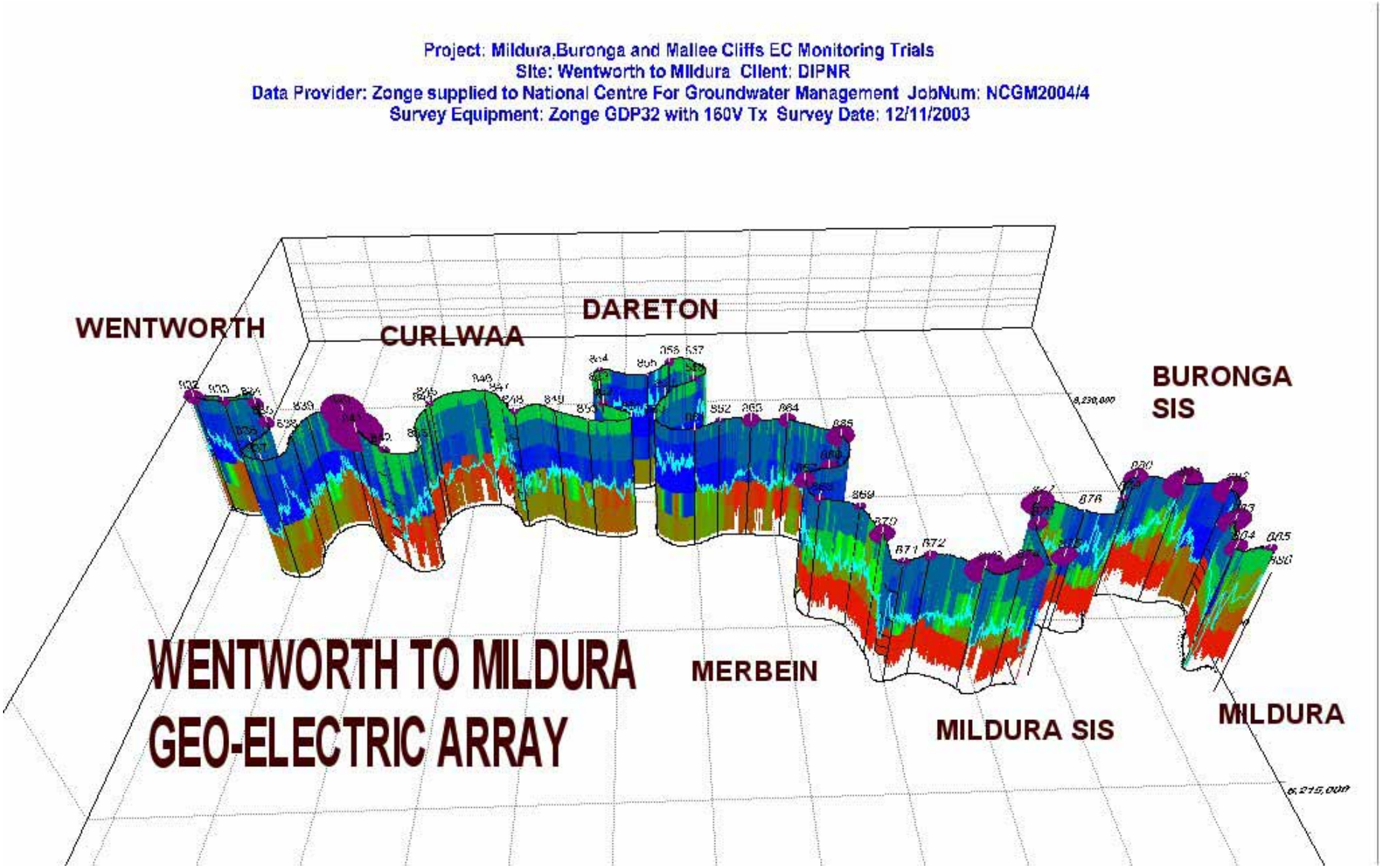

Figure 15.14 Geo-electric array EC Ribbon between Wentworth and Mildura

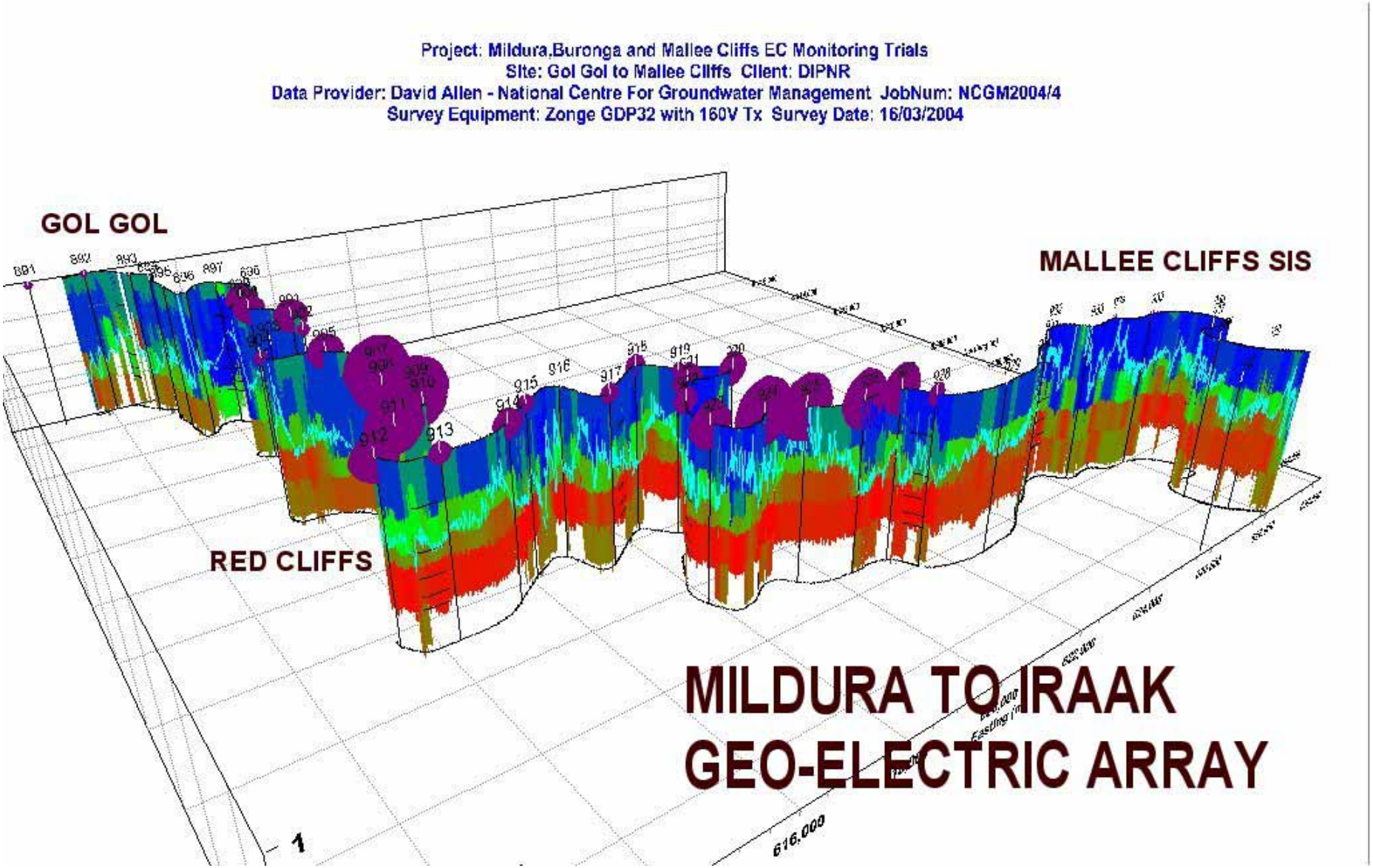

Figure 15.15 Geo-electric array EC Ribbon between Mildura and Iraak.

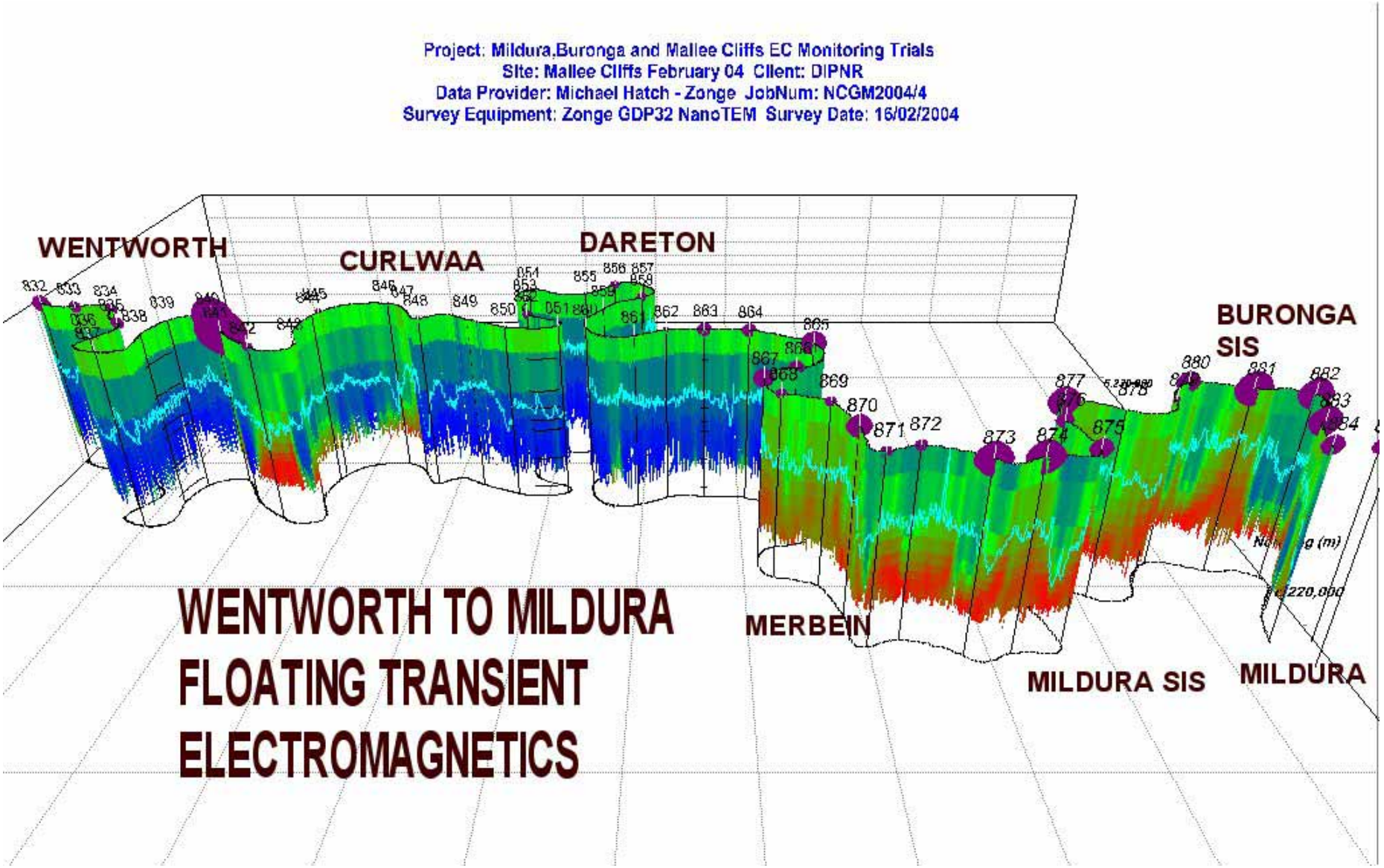

Figure 15.16 TEM EC Ribbon between Wentworth and Mildura

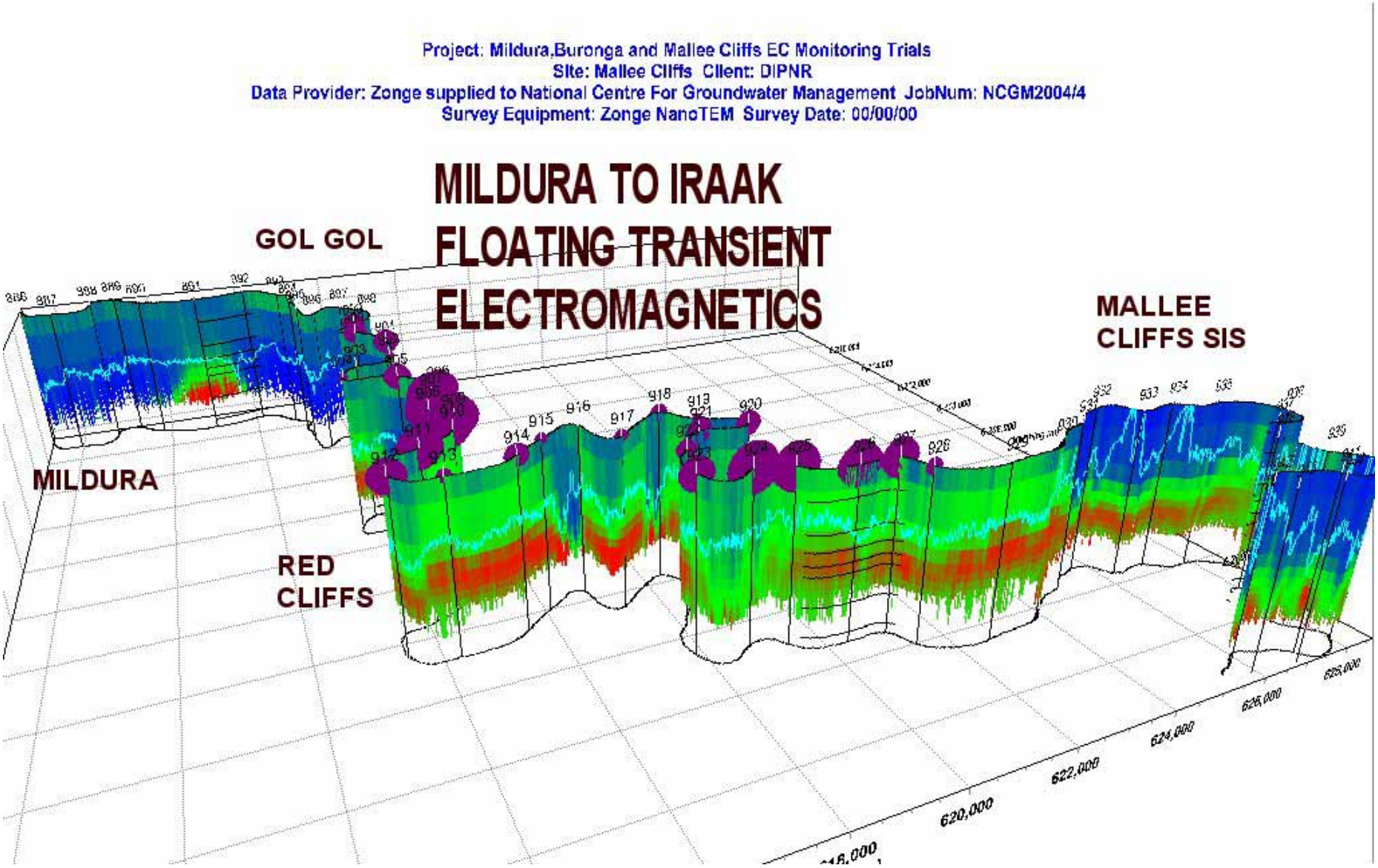

Figure 15.17 TEM EC Ribbon between Mildura and Iraak

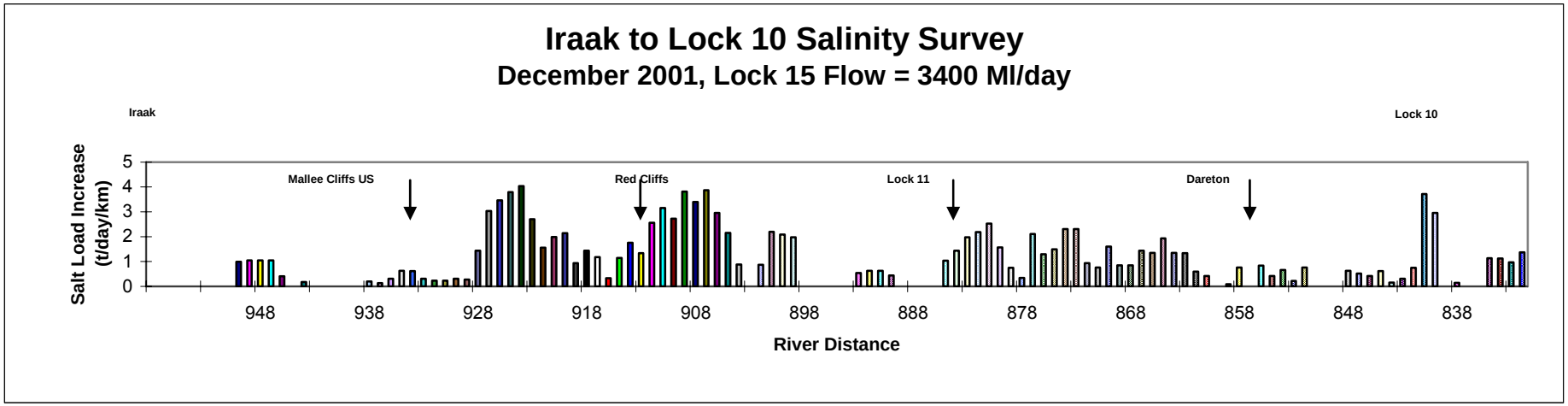

Figure 15.18 Murray river salt load increase between Wentworth and Iraak. (Allen 2004)

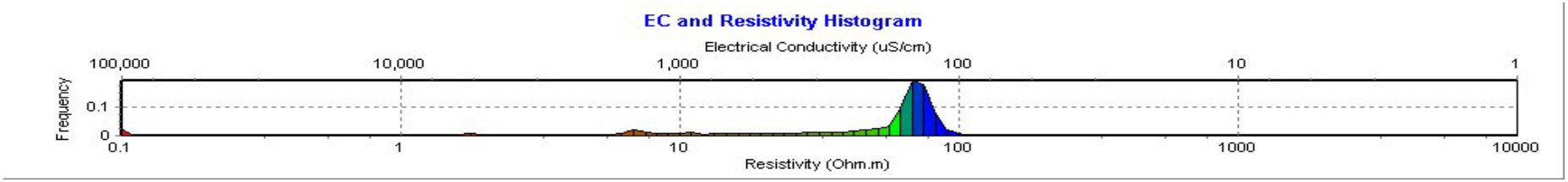

Figure 15.19 Color Histogram generated for the geo-electric array EC Ribbons.

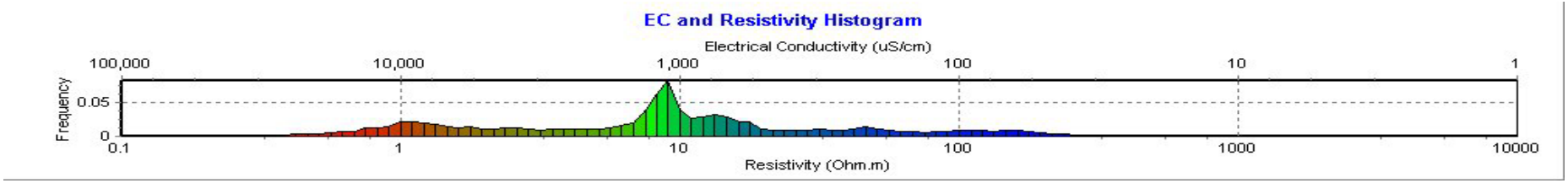

Figure 15.20 Color Histogram generated for the TEM EC Ribbons.

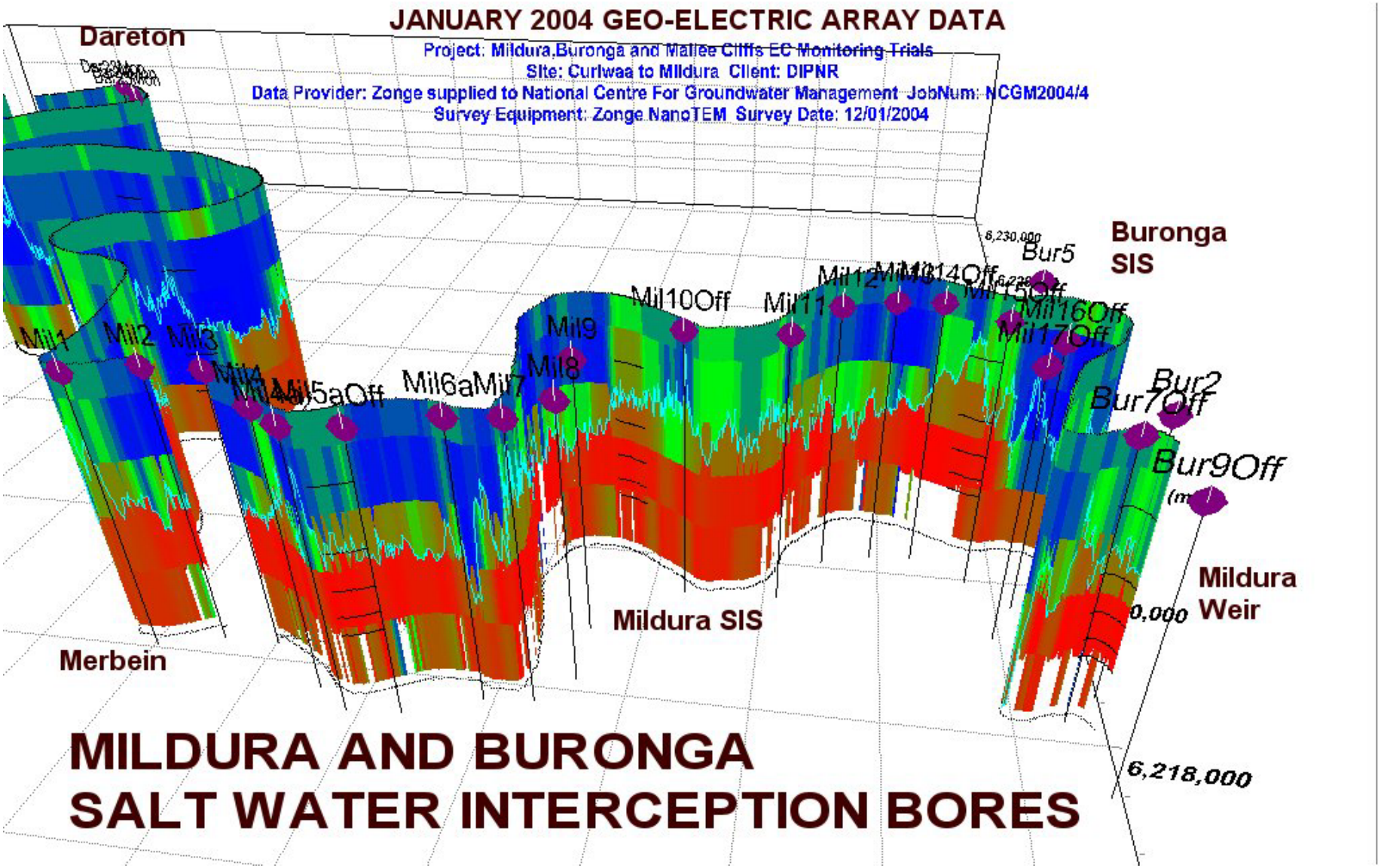

Figure 15.21 Locations of Mildura and Buronga saltwater interception bores and their effect on sub-river sediment presented in an EC Ribbon.

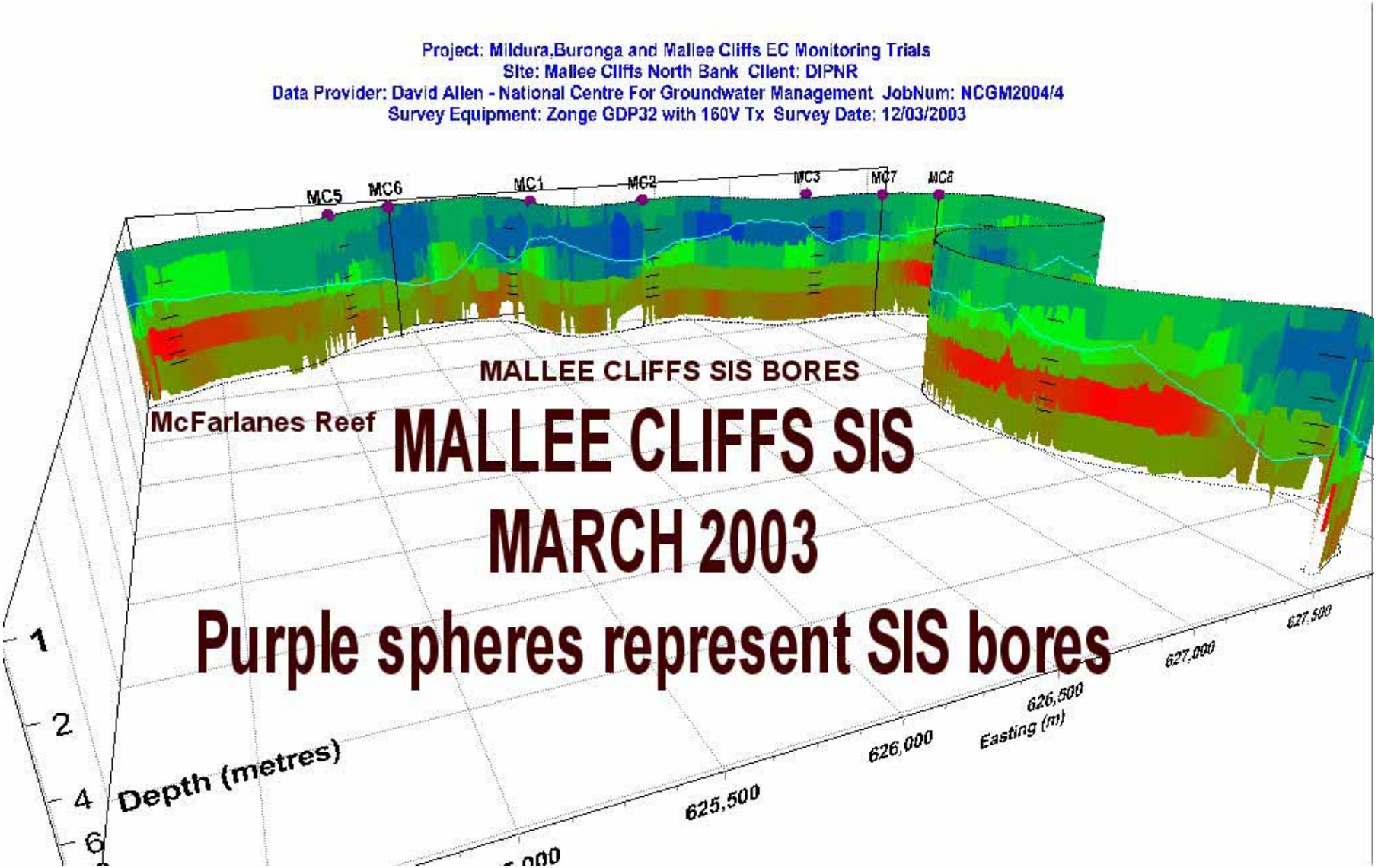

Figure 15.22 Locations of Mallee Cliffs SIS bores and their effect on sub-river sediment presented in an EC Ribbon. March 2003 - compare with Figure 15-23.

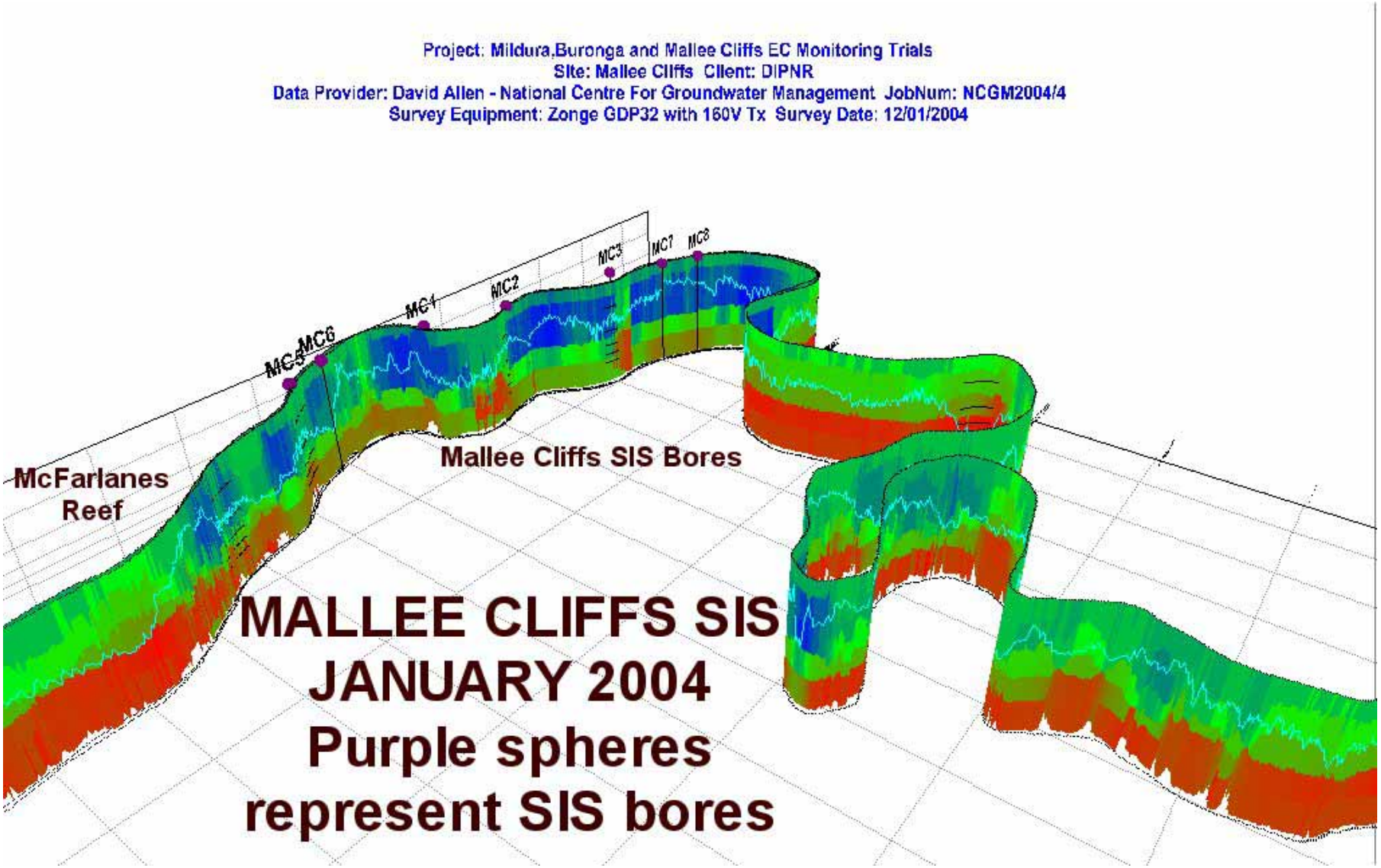

Figure 15.23 Locations of Mallee Cliffs SIS bores and their effect on sub-river sediment presented in an EC Ribbon. January 2004 - compare with Figure 15-22.

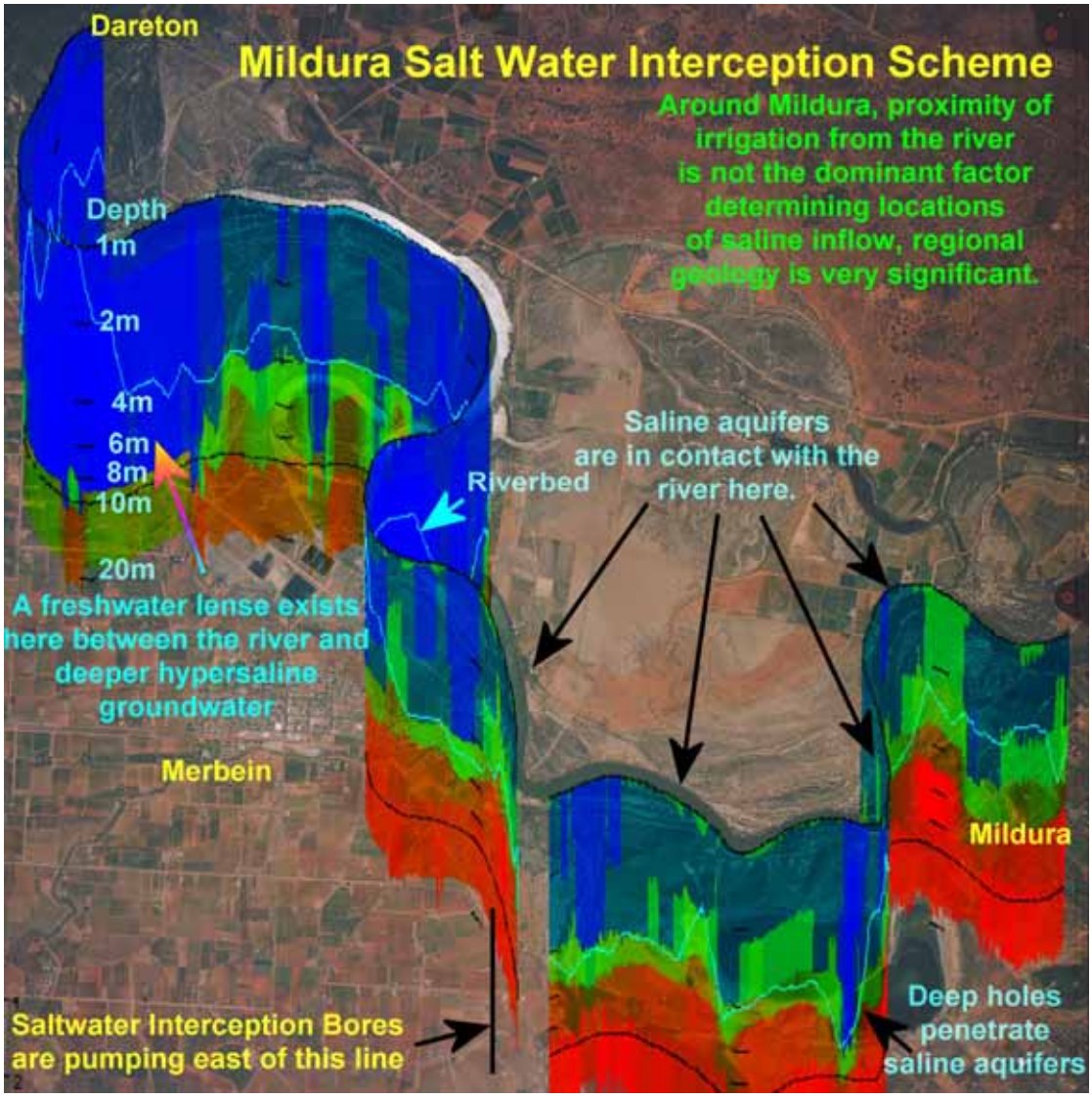

Figure 15.24 Airphoto overlay of a Murray River EC Ribbon (March 2003) at Merbein

15.3.9 Long term monitoring

Time lapse imaging around SIS schemes may show large changes in impact of the schemes as they pump. If the changes are not large then they may be overprinted by complications of 3D variation such as water depth along the slightly different path taken by each survey along the river. These effects will become more evident once a history of images is built up for comparison. Detection of change is made much more difficult by the high salinity groundwater around Mildura that consumes signal thus enhancing any systematic error in the data. Systematic error is likely to be evident in difference images as consistent single layer anomalies. As high salinity groundwater enhances rather than

degrades TEM signal, TEM has better capability of detecting change in the salinity of but not the depth to saline aquifers that are typical around Mildura.

After ten months of periodic survey and pumping of the Buronga SIS scheme, a low EC region appeared at Chaffey Bend as displayed in Figure 15-25.

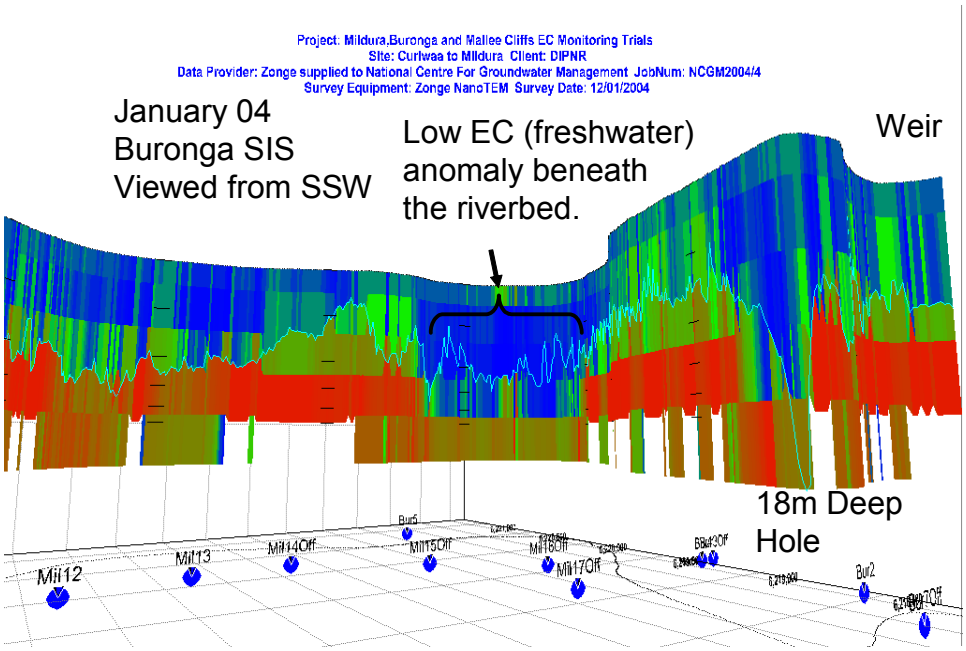

Figure 15.25 A low EC anomaly at Chaffey Bend (Buronga) that appeared in geo-electric array data in January 2004.

In Figure 15-26, time difference comparison of the January 2004 data with the March 2003 data is presented. Colour scale on the difference images represents the following:

- Blues represent decreases in salinity (increase in resistivity).
- Reds represent increases in salinity (decreases in resistivity).

As a result of the different tracks of the surveys that passed over water of different depths, the difference images are rather dubious however one feature is evident that the author has confidence in because it is represented in multiple layers and has caused clear horizontal variation. It is a drop in salinity at Chaffey Bend which is likely to have been caused by SIS pumping from Buronga bores 4 and/or 5.

Difference images for both TEM and geo-electric data have been included for two different date pairs (ie. Figure 15-27 and Figure 15-26 again). In the TEM difference image, the variation at Chaffey Bend shows up incorrectly as an increase in river water salinity. This is because TEM inversion cannot effectively remove the effects of mid depth strata from shallow strata (<5m) and river water and vice versa. The difference is real but is represented incorrectly. The TEM data, originally plotted in microseconds after turn off must be converted to conductivities and depths. Data at later times is easily converted to EC for deeper depths but the data at early times relates somewhat ambiguously to EC variations at shallow depths.

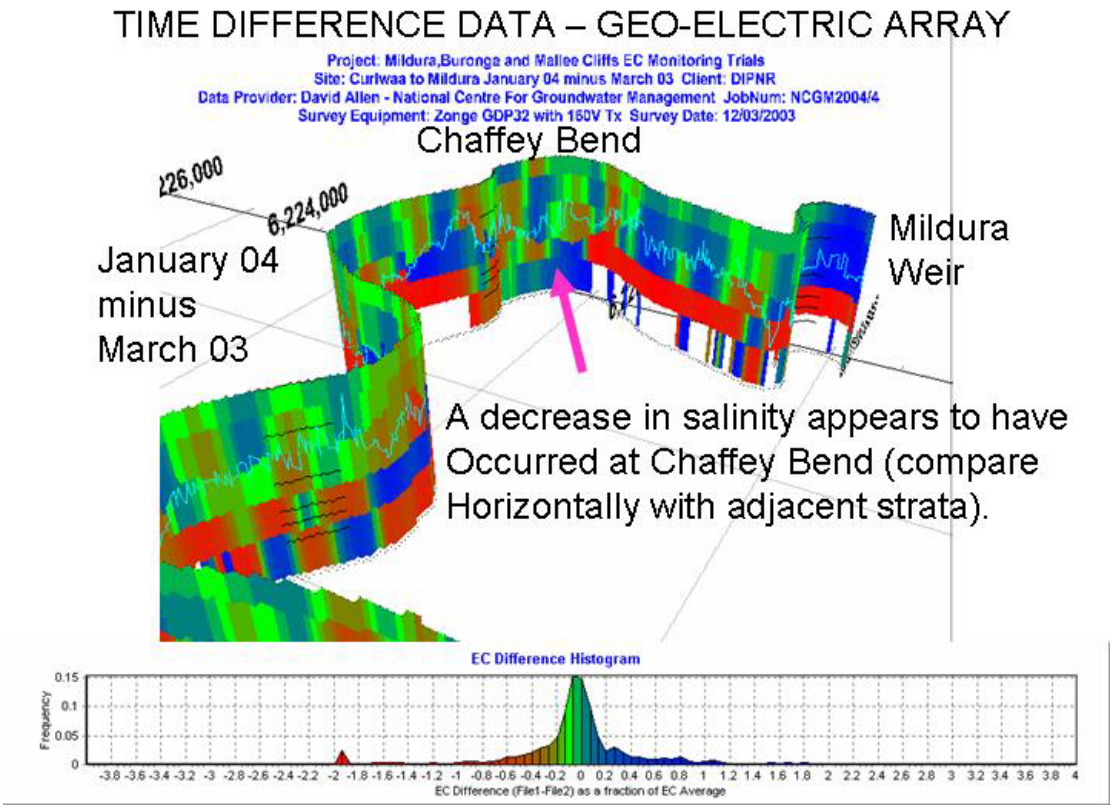

Figure 15.26 Time Difference data at Chaffey Bend collected using a geo-electric array. Reds should represent salinity increases. Blues should represent salinity decreases.

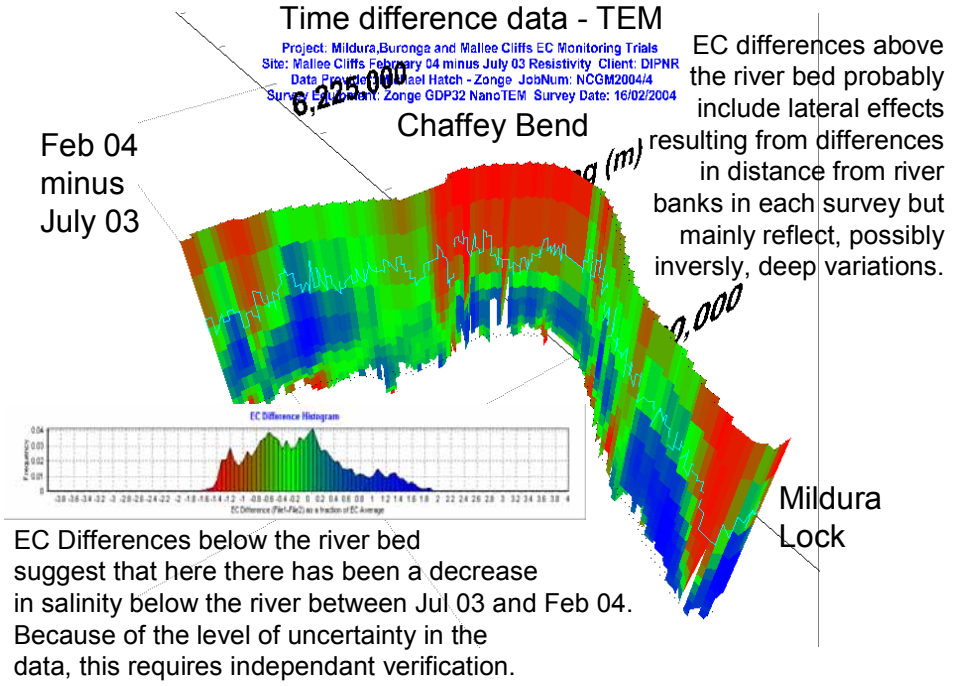

Figure 15.27 Time Difference data at Chaffey Bend collected using TEM. Reds should represent salinity increases. Blues should represent salinity decreases.

15.3.10 Airphoto overlay for geomorphological and geographical comparison, Vertical 2D Imaging

Figure 15-28 has an airphoto overlying an EC ribbon. It is the same as Figure 15-24 but with vertical exaggeration reduced so that features on the airphoto can be seen. The airphoto is useful for comparison of anomalies with the locations of prior river channels, geological structure and irrigation. Along the salinity interception scheme we can see saline/ hypersaline aquifers just below the riverbed. Deep holes in the riverbed are observed to penetrate into, or close to, the saline aquifer. The riverbed in the part of the river in the northwest of the image immediately overlies fresh water. No direct relationship between immediate proximity of irrigation and saline inflow is evident. Along this survey, geological structure appears to determine which sites are susceptible to saline inflows.

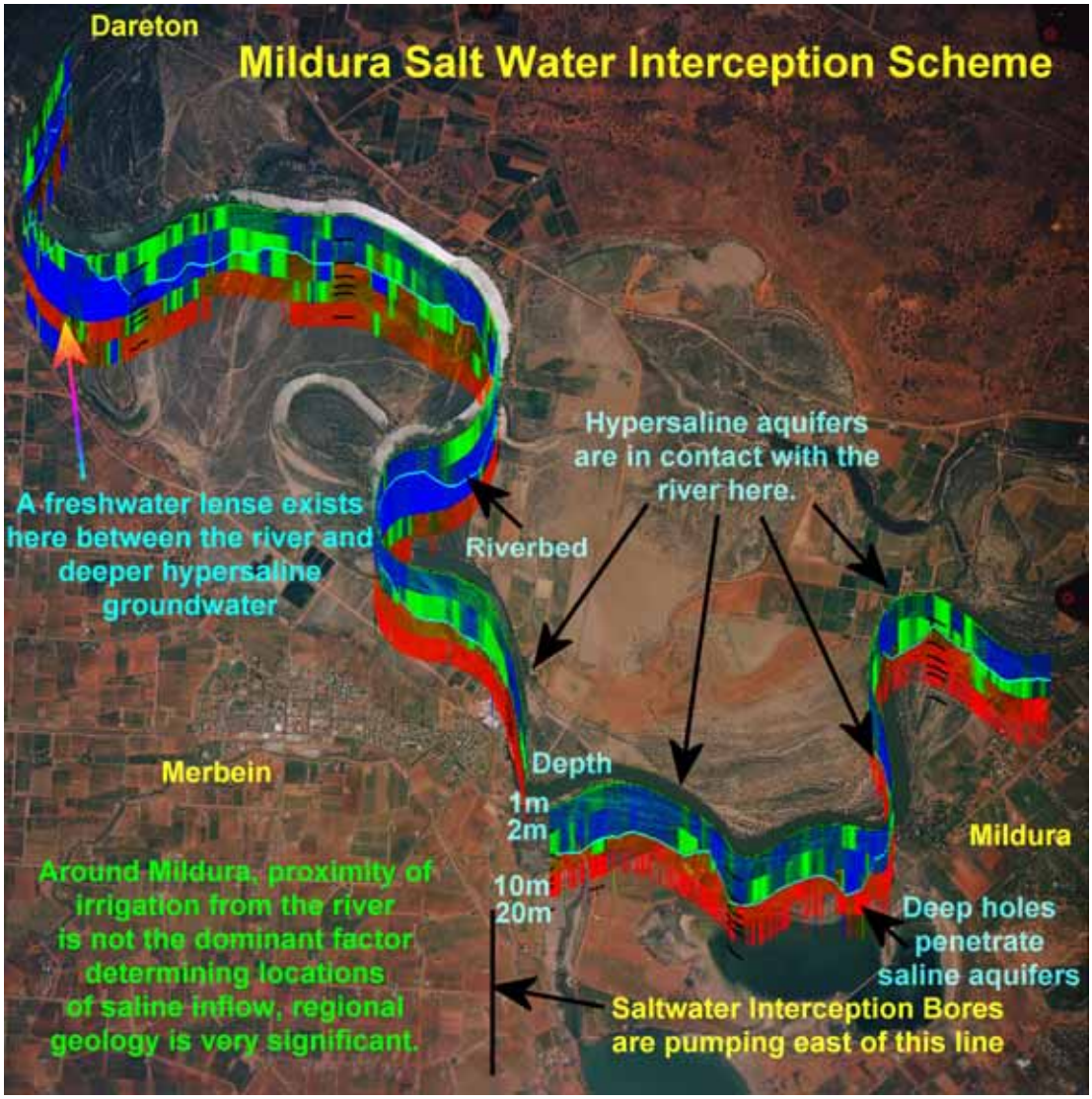

Figure 15.28 Mildura Saltwater Interception Scheme – Fixed layer inversion (compare to Figure 15-24 with stretch and smoothness constrained layer inversion).

The EC ribbon in Figure 15-28 was inverted with fixed layer thicknesses. Compare it with Figure 15-24 and Figure 15-29 which contains the same data inverted with thickness stretch constraint and smoothness constraints rather than fixed layers. Figure 15-29, being a 2D vertical section demonstrates the frustration that can arise if attempting to geo-reference data without a 3D presentation solution. In Figure 15-29, clipped logarithmic color distribution has been applied rather than equal area colour distribution such as was used in Figure 15-24 and Figure 15-28. Observe that all the variation in the water layer disappears – it is only superficial (in geo-electric array data) but is emphasised by equal area colour distribution. Remember the different distributions in the equal area colour

histograms for the geo-electric and TEM data (Figure 15-19 and Figure 15-20). Remember how there was a peak corresponding to river water in the geo-electric array data but not in the TEM data. Much of the difference in the appearance of the geo-electric array and TEM data results simply from the presence or absence of this peak in the histogram. In Figure 15-29, since clipped logarithmic colour scaling has been applied, it is as if the peak has been removed and the river water suddenly appears uniform and the sub-river-bottom data starts appearing similar to the TEM data (Figure 15-15).

Equal area colour distribution is recommended for quick automated viewing and for enhancement of subtle anomalies but can confuse novice image interpreters by making subtle anomalies appear to be as significant as major anomalies. Logarithmic colour distribution (with manually adjusted maximum and minimum) is recommended for processing intensive real time viewing and for some presentations to novice audiences. Whatever colour scale is used, some feature or other will not be clearly evident in the data so it is recommended that different options are tested and that the images are always interpreted with due regard to the colour histogram/scale.

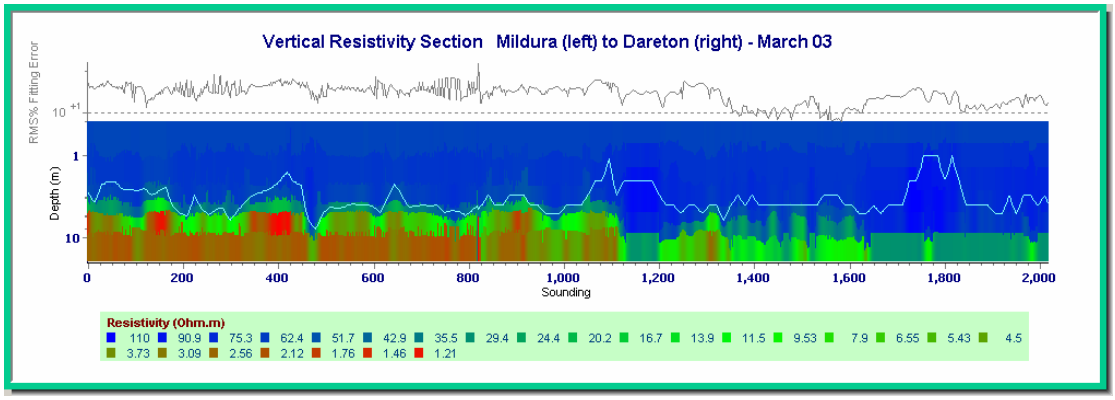

Figure 15.29 Vertical 2D imaging with clipped logarithmic rather than equal area color distribution. Data is from the EC ribbon in Figure 15-28 (Sounding 0 is upstream).

15.3.11 Images of EC at a fixed depth below riverbeds

Depth slices in which EC at a particular depth is presented on a map are a simple form of presentation which, in some situations, is useful. When dealing with rivers, however, we usually want to present images of EC at a particular depth below the river bed. Such images show up, in a simplified manner, what parts of the river are most at risk of saline

inflow. High EC (salinity) anomalies in the deeper images present less risk of saline inflow to the rivers than the high EC anomalies in the shallower images. Figures 15-30 and 15-31 present a shallow and deep image of this type, of the Mildura and Buronga Salinity interception schemes.

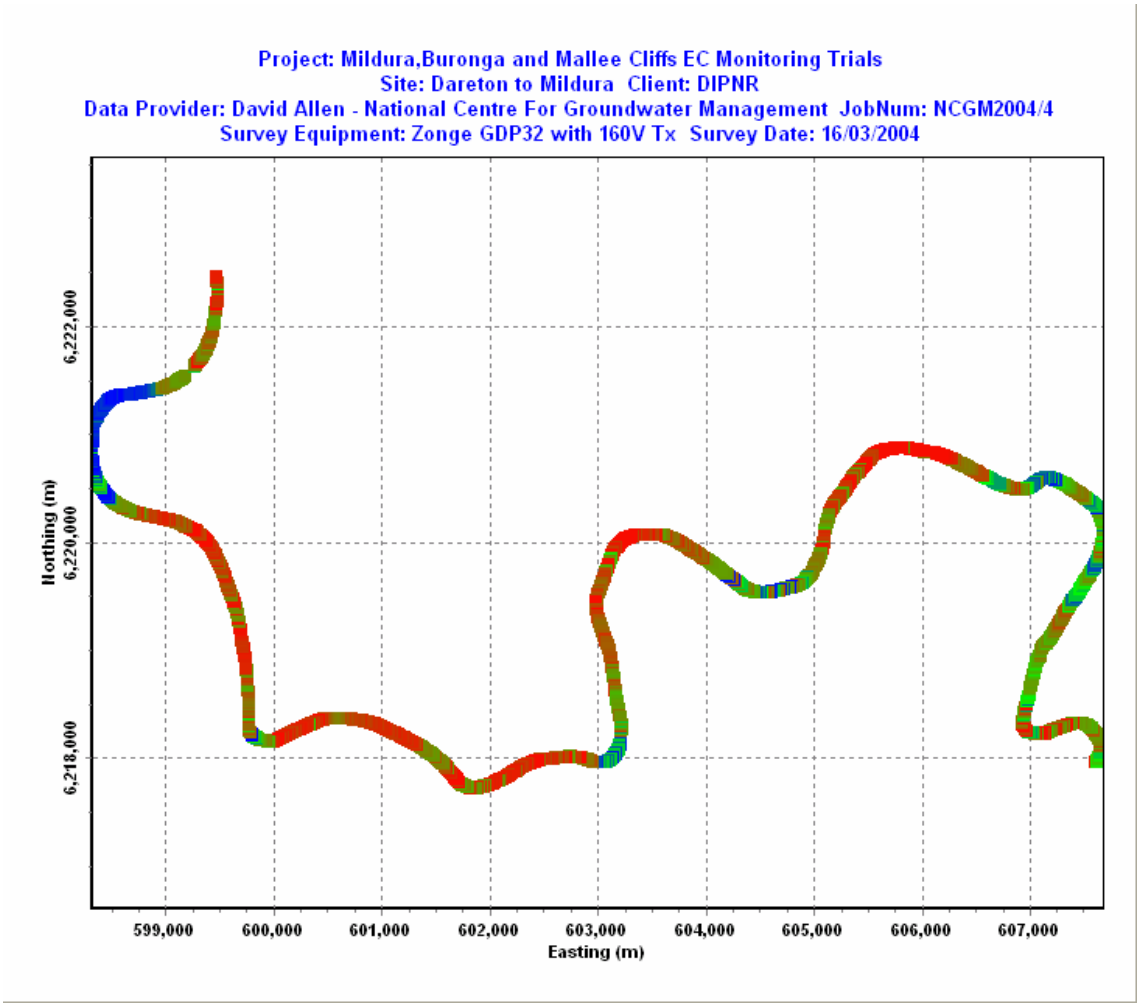

Figure 15.30 EC 0.5 metres below the Murray riverbed downstream of Mildura (March 2004). Observe that saline groundwater is separated from the river within the Buronga interception scheme on the east side of the image (ie. east of 606500E). Low EC west of 599000E is probably due to a change in dip of strata that the river has incised.

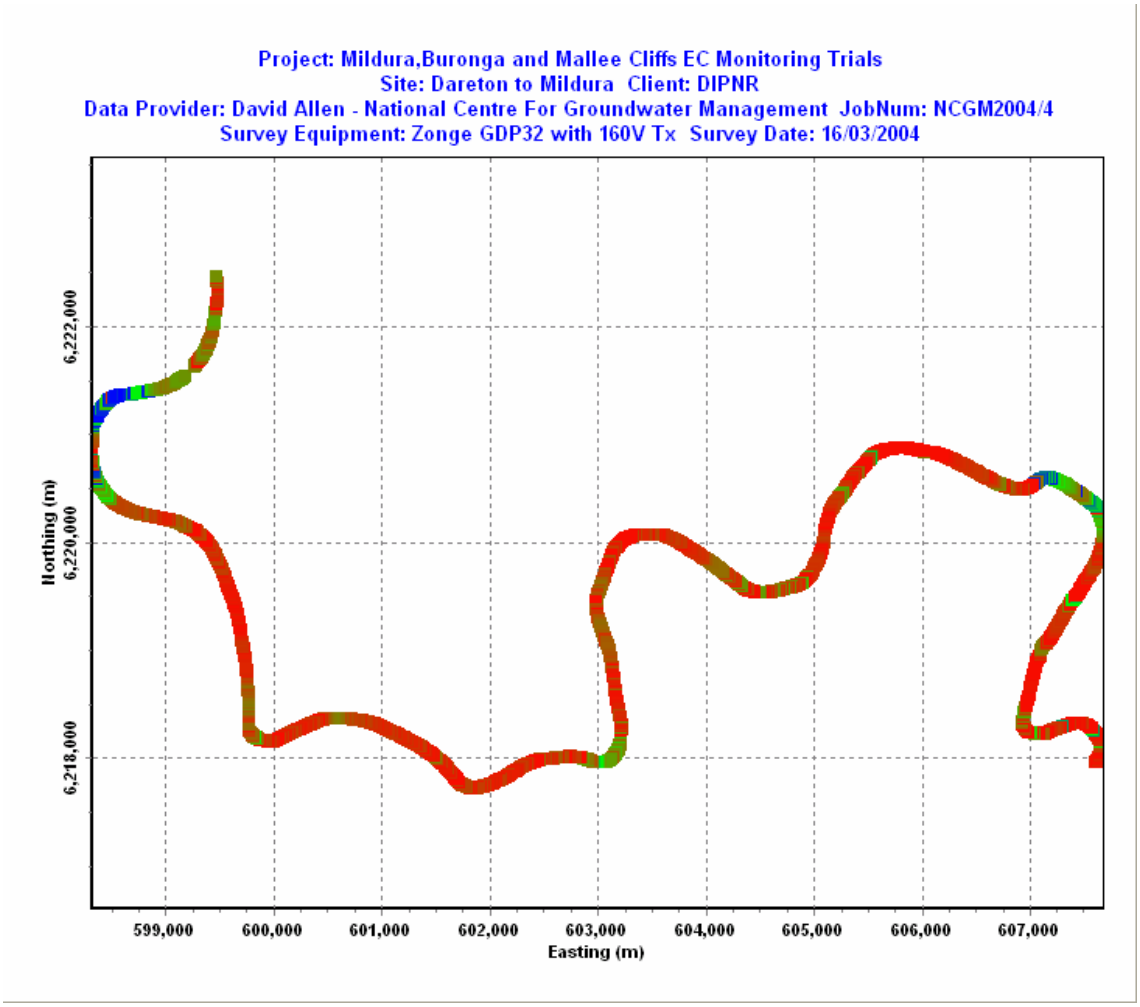

Figure 15.31 EC 3 metres below the Murray riverbed downstream of Mildura (March 04). Compare this with the previous image observing that there is little influence from the Buronga Interception scheme at a depth 3 metres below the river.

15.3.12 Induced polarization

Electrode arrays can also detect the property called induced polarization. This is a capacitance effect which is common in clays and is only detectable with adequate signal-to-noise levels.

Figure 15-32 is an example of induced polarization data that shows variations relating to clay content of sediment. A notorious rock outcrop, responsible for sinking of river steamers, is seen to cause an IP anomaly. The outcrop is probably a chemically altered geological fault. It may be confining groundwater in such a way that it works as a boundary controlling saline inflow into the Murray. The variation along the rest of the

image is likely to reflect the thickness and clay content of geologically recently deposited sediment in the river bed. Even though the induced polarization data has not been inverted due to its poor signal to noise ratio, it is seen to largely honour the depth of the river bed. Very low IP effect is expected over saline sediment but signal to noise ratios of data representing such sediment are also very low leading to inconclusive results in such sediments in Figure 15-32.

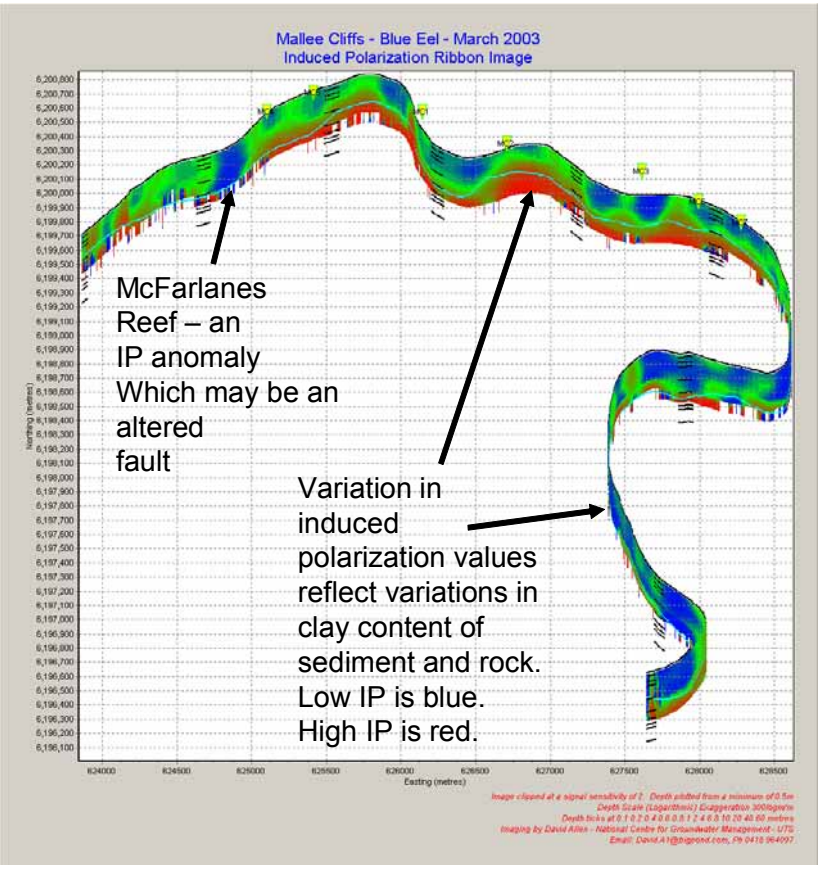

Figure 15.32 Induced Polarization anomalies at Mallee Cliffs SIS.

15.3.13 EC difference between parallel ribbons

Unlike time difference images in rivers, images of difference between parallel survey lines, such as may be conducted along each bank of a river, usually are robust and meaningful. Calibration and DC offset problems are cancelled out and the difference in track is generally not troublesome. On occasions, tracks that supposedly are meant to be along each bank of a river cross over due to navigation complications such as reefs or wayward traffic that must be avoided. Figure 15-33 is one example of such imaging. Around the Mallee Cliffs salt interception scheme, we can see that EC is higher under the

south bank. This may be because the SIS bores are on the north bank or may be co-incidental.

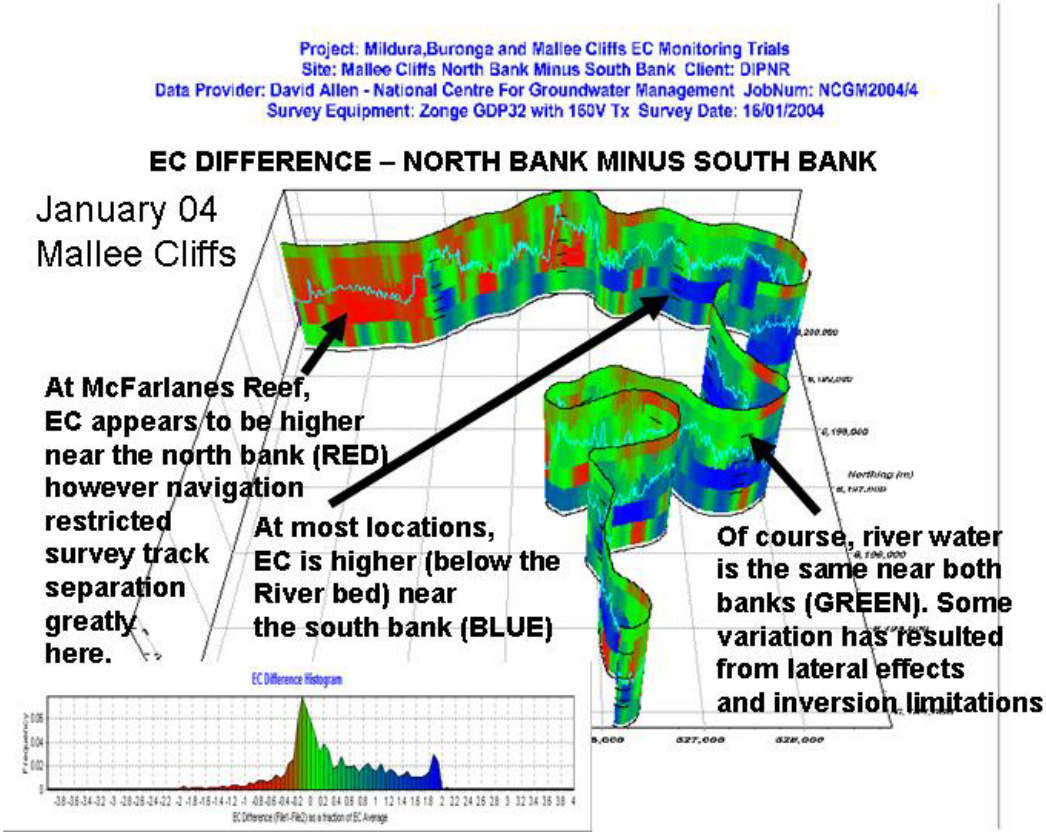

Figure 15.33 Difference between EC near the north and south banks of the Murray at Mallee Cliffs.

15.4 The Murrumbidgee River at Gogeldrie Weir

The site of the Murrumbidgee River at Gogeldrie Weir will be studied in detail in the chapter on irrigation canals (Chapter 16) because the dataset there consists mainly of canals.

15.5 The Murrumbidgee River upstream from Yanco Weir

Eleven kilometres of river was surveyed upstream of Yanco Weir. Figure 15-2 and Figure 15-4 showed how the common colour scale of Figure 15-3 revealed that this site is clearly a site where river transmission losses are occurring. Let us now look at the site in more detail. Figure 15-34 presents the river segment re-coloured with equal area colour so that features can be seen. It is presented in apparent resistivity. Figure 15-35 shows the same

segment subject to 1D fixed layer thickness inversion. Note that there is no water depth data for this dataset. Water depth ranged from 200 millimetres to about 1.5 metres. Figure 15-36 shows the induced polarization data collected at the site. Because there was a strong vertical gradient in the induced polarization data, it has been vertically damped in bands to enhance visibility of horizontal variations in induced polarization.

In Figures 15-34 and 15-35, we can see that a relatively conductive anomaly exists adjacent to a flood irrigated crop (probably rice, centre left). In this case, this anomaly has been tentatively attributed to increased clay in the vicinity of the crop. Flood irrigated crops typically are grown on clayier sites. Flood irrigation high above the river is likely to be causing saline inflow into the river but, at this site, this is not apparent because the EC is too low (see the histogram on Figure 15-34) and an IP anomaly, suggesting clay, corresponds with the EC anomaly. Another relatively conductive anomaly exists in the mid-right of the image. One can see that treeless ground flanks both sides of the river there. Trees such as seen here grow in the permeable sediment that is fed by river transmission losses. The lack of trees on both sides of the river at this site therefore indicates that a competent non riparian geological feature is cut by the river at this point. It is likely to be a barrier to groundwater flow. The induced polarization data contains various clear features that the author cannot decisively interpret due to lack of controlling geological information at the site. Most correspond with EC anomalies suggesting that they represent clay. Anomalous layering on the right side of the Figures 15-35 and 15-36, both in the inverted EC data and the IP data is as yet unexplained.

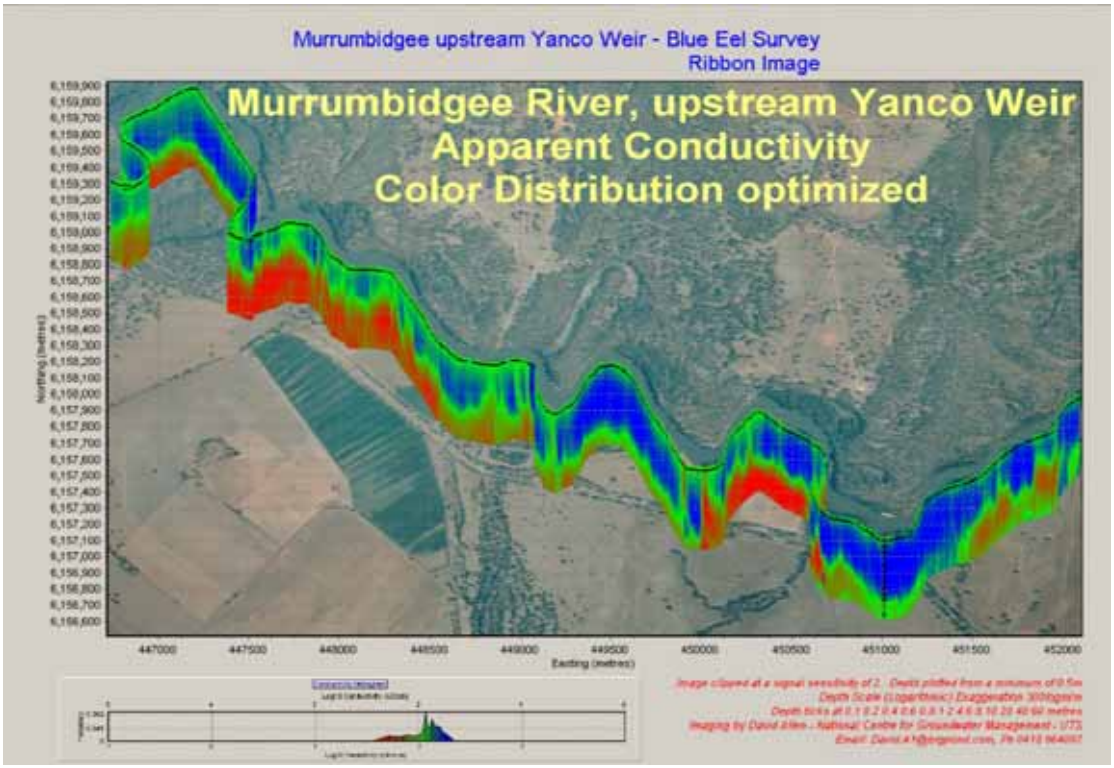

Figure 15.34 The Murrumbidgee River upstream of Yanco Weir – Apparent Resistivity 0.5 to 30 metres deep.

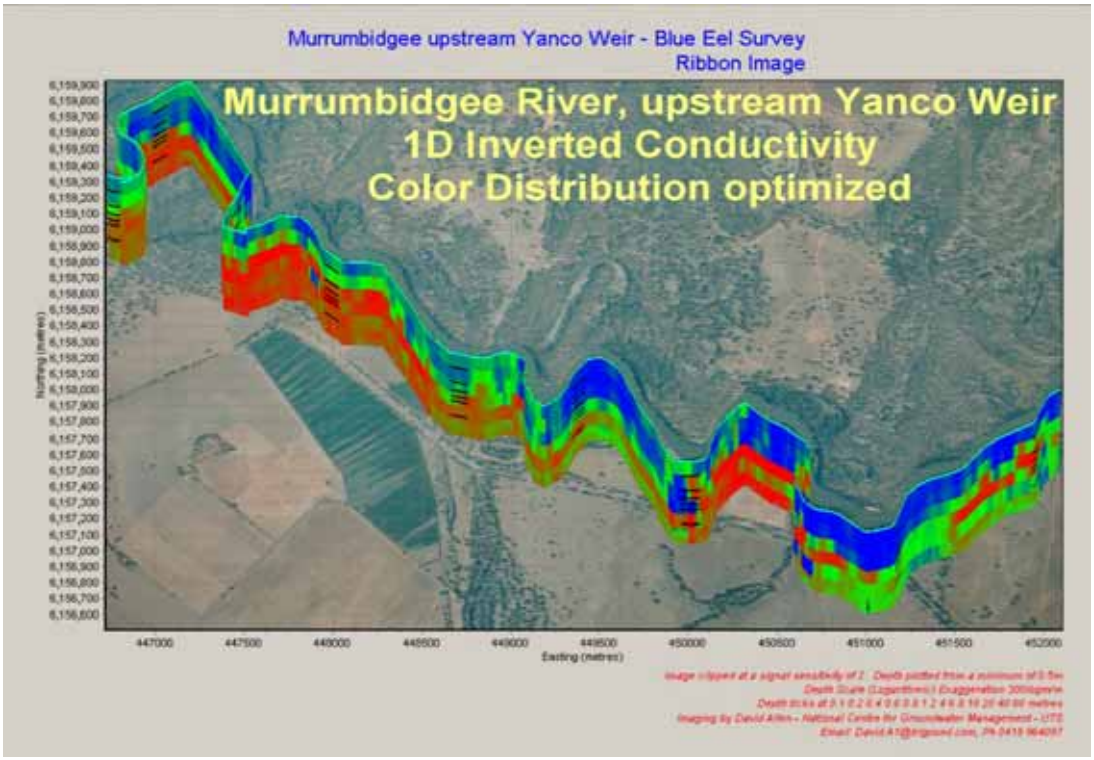

Figure 15.35 The Murrumbidgee River upstream of Yanco Weir – 1D fixed layer thickness inversion 1 to 40 metres deep.

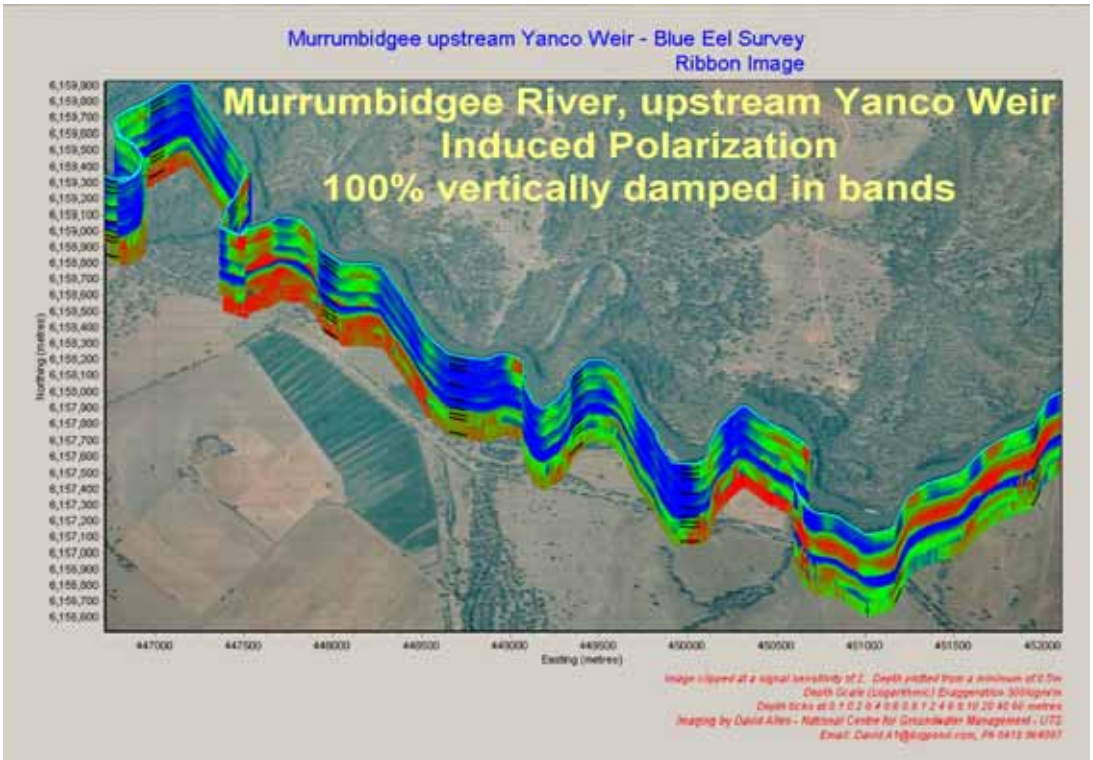

Figure 15.36 The Murrumbidgee River upstream of Yanco Weir – Induced Polarization 0.5 to 30 metres deep with vertically damped colour scaling.

15.6 The Border Rivers

EC imaging beneath the Border Rivers is useful for densely delineating the proximity and salinity of saline groundwater to the base of the rivers at numerous sites along the rivers. Sites long enough to average out isolated variations can be surveyed. The rivers are blocked by too many fallen trees, however, to allow economical continuous surveying where public river access points are sparse. EC imaging of sediment under lengths of the Dumaresq (pronounced Dumerick), MacIntyre and Barwon Rivers was conducted as shown in Figure 15-37.

The conditions under the rivers are very uniform. A distinct increase in salinity occurs in the downstream direction. Depth to saline groundwater varies with influence of local geology such as recently buried river channel locations. Depth to saline groundwater is around 6m at Mungindi and increases going upstream. A major change occurs west of Glenarbon where no saline or brackish groundwater was evident. Proximity of cotton irrigation and water storages to the rivers does not correlate clearly with EC hot spots

under the rivers except near Mungindi where high EC sediments appear to be slightly closer to the riverbed very close to storage dams.

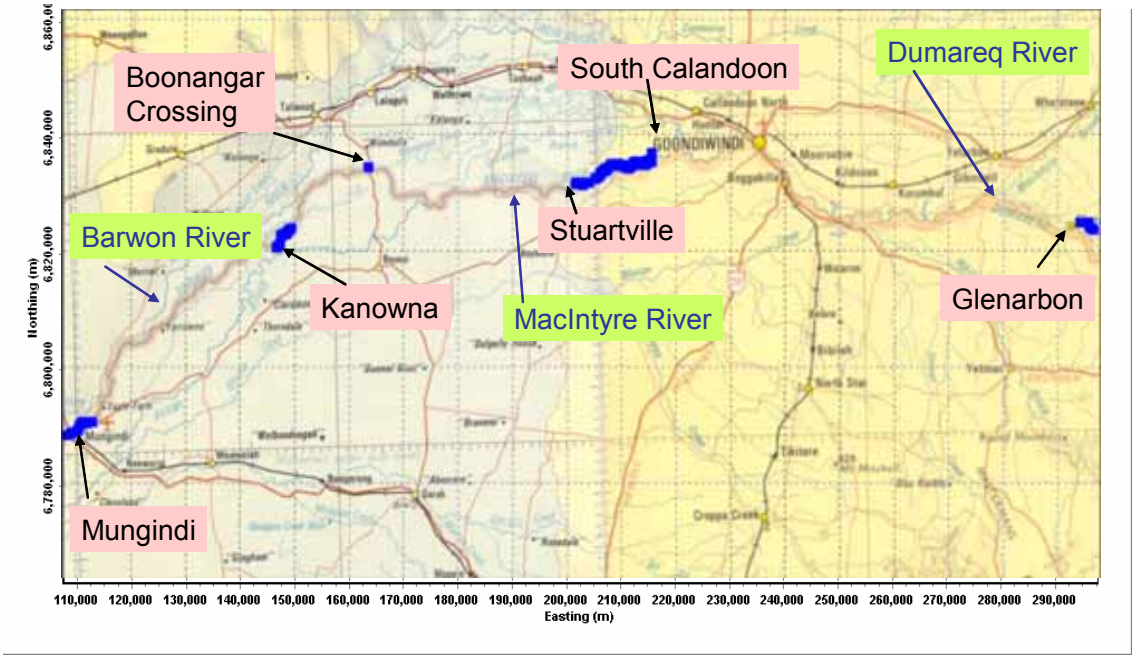

Figure 15.37 Location of EC imaging conducted from the Border Rivers, NSW/Queensland Border (highlighted in blue).

15.6.1 Ground water interaction with the Border Rivers

Water quality in the Border Rivers may suffer from inflow of saline groundwater. The rivers flow across a vast plain of self mulching clay soil of low permeability and moderate salinity. Where the groundwater is in contact with rivers, interaction occurs. Heavy use of water from the rivers, and from sub-artesian aquifers beneath the rivers is made for the purposes of cotton, and other, farming along the river margins. This farming, in turn, is altering the watertable level in the proximity of the rivers and the rate of saline flow of groundwater into the rivers. The farming involves: clearing of trees, application of water to the riverine plains and extraction of groundwater. It is in the collective interest of the local farmers and other natural resource users and downstream water users to understand and manage this situation.

Images created have clearly picked up salinity concentrations under the rivers. A steady increase in groundwater salinity beneath the rivers can be observed in a downstream direction. At Glenarbon, upstream of Goondiwindi, river recharge appears to be the

primary source of underlying groundwater because it has very low EC. Salinity increases progressively downstream of Goondiwindi. Comparison with sites displayed on other Murray Darling Basin Rivers places the Border Rivers into basin-wide context. The MacIntyre/Barwon River is evidently lying on very uniform sediment in comparison with the other rivers. Some minor conductivity variation is evident under it. Most transverse variation is evident in the South Callandoon Image where the river intersects, at numerous locations, the sides of a swath of recent river palaeochannels which are recessed into the broad scale floodplain.

Beneath the rivers there exist layers of variable thickness and salinity which can be summarized as follows. Three layers are evident – the first includes the river water and any sediment beneath it that has the same EC as the river water. The next is thought to be a transitional layer where groundwater and river water have mixed giving transitional ECs. The deepest layer is thought to be moderately saline groundwater possibly undiluted by river water recharge. The measured ECs do not exactly reflect true groundwater ECs – some calibration is necessary. The following table presents a summary of the layers going from Mungindi upstream:

Survey	Fresh top Layer (including river)	Mixed water origin layer	Ground-water layer	Top layer EC uS/cm	Middle layer EC uS/cm	Ground-water layer EC uS/cm
Mungindi	0-6m	2-6m	>6m	150-500	150-500	>2000
Kanowna	0-4m	2-4m	>2-10m	400-600	600-1000	>1000
Boonangar	0-8m	2-8m	>6-8m	600-800	600-1000	approx 1000
Stuartville	0-10m	2-10m	>20-40m	300-500	500-800	>800
South Callandoon	0-40m	2-40m	>4-40m	200-500	200-500	600-1000
Glenarbon	0-3m	3-40m	>40m	approx 300	approx 100	approx 100

Table 15-1 Inferred hydro-stratigraphy below segments of the Border Rivers.

When interpreting the data it should be kept in mind that the survey was conducted 2 weeks after a flood event.

Many of the sites surveyed are presented below in Figure 15-38, Figure 15-39, Figure 15-40 and Figure 15-41. All the figures use the composite Murray Darling Basin colour scale

of Figure 15-3 which is reproduced on the top of Figure 15-38. The most upstream site, Glenarbon, is displayed only in Figure 15-4.

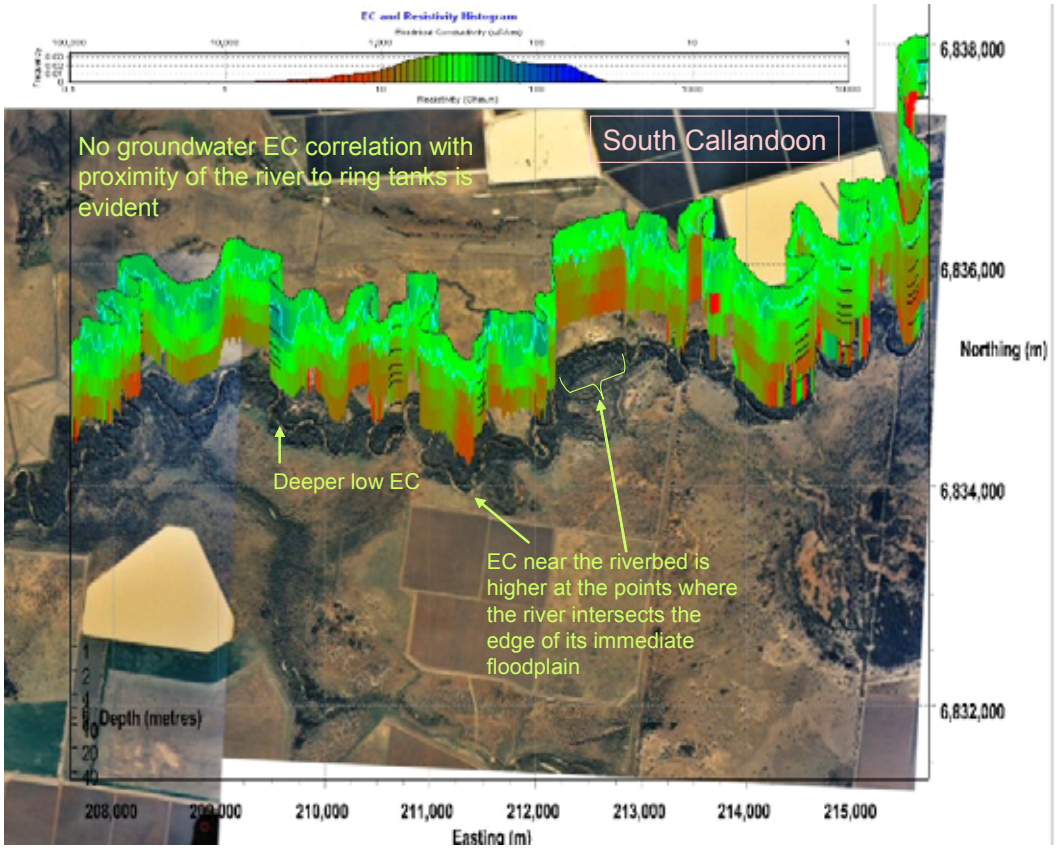

Figure 15.38 MacIntryre River – South Callandoon.

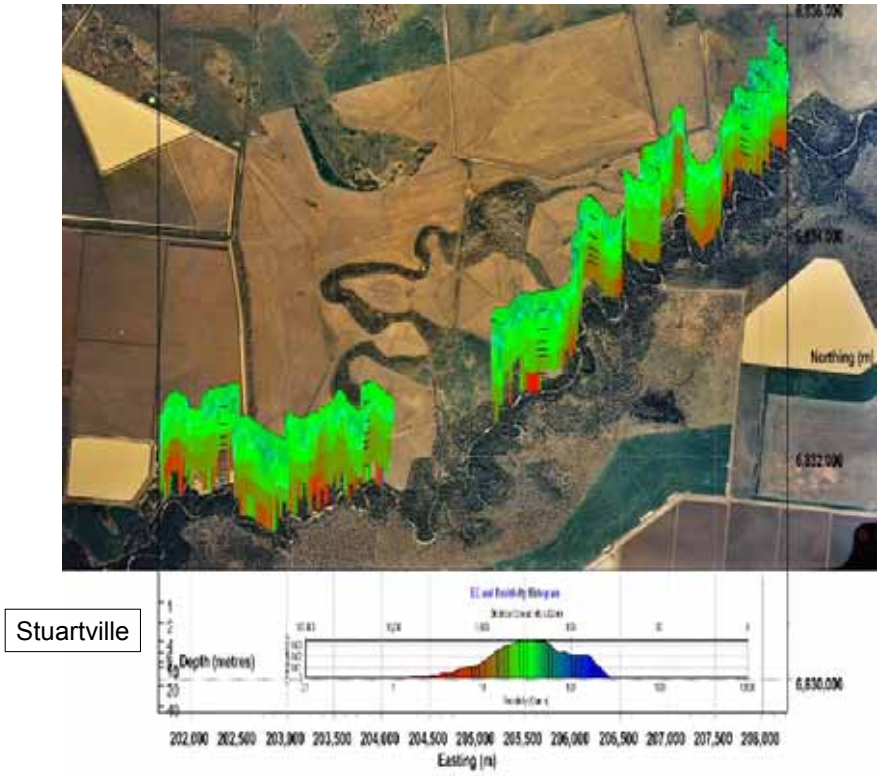

Figure 15.39 MacIntyre River – Stuartville.

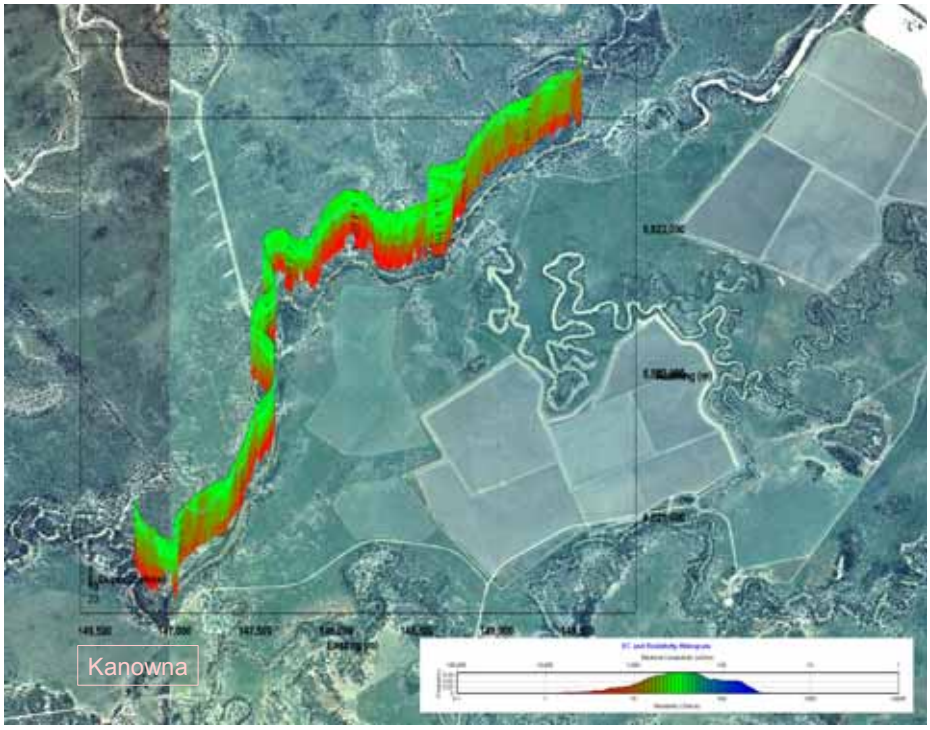

Figure 15.40 MacIntyre/Barwon River – Kanowna.

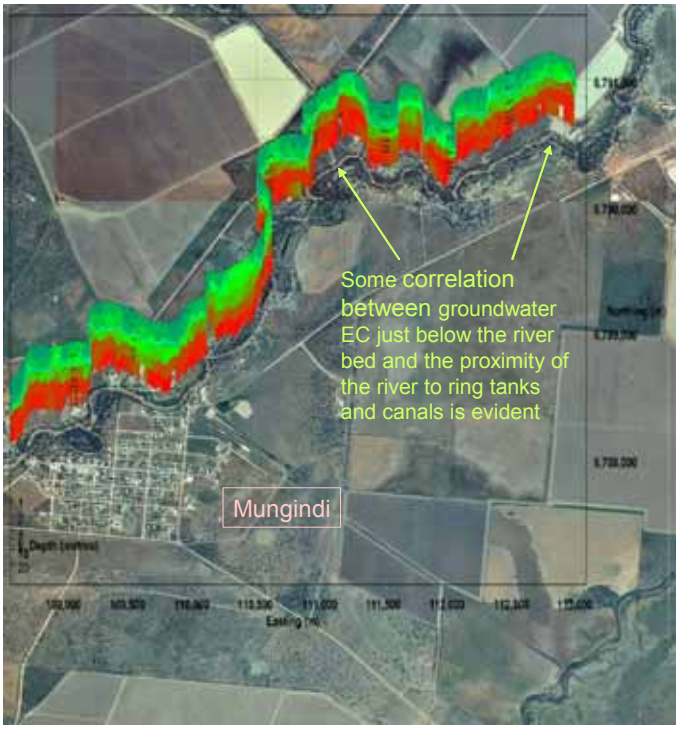

Figure 15.41 Barwon River – Mungindi.

Interpretation of Murray Darling Basin Rivers is now concluded. The next section investigates somewhat different issues on a coastal river backswamp.

15.7 Tuckean Swamp drains – Richmond river – NE NSW

15.7.1 The problem of acid sulphate soil leaching in the Tuckean Swamp – lower Richmond River – NE NSW

The Tuckean 'Swamp' was once a large tidal swamp. The anaerobic environment of the swamp resulted in pyrite in the soil. The swamp was drained to create land for cattle. Now the pyrite is leached by groundwater flowing into the drains. In solution, the pyrite oxidizes and forms sulphuric acid. The acid pulses out of the swamp into the Richmond River as concentration and release of the acid is influenced by the tide and floods. Much aquatic life cannot survive the acid particularly when it arrives in a sudden pulse.

15.7.2 Delineation of acid inflow using EC imaging

Electrical conductivity (EC) imaging which probes through the drain water right down into the sediment below the drains can delineate sources of salinity and the salt concentration of groundwater flowing in and out of the drain beds. 3D presentation of the

imagery is then used to observe how the sources of salinity connect to geological and geographical features around and under the river. Correlation between salinity and acidity under the drains is suspected because the sediment in which the acid producing pyrite formed are believed to have been submerged in saline water prior to draining of the swamp.

15.7.3 Surveys conducted

EC imaging of sediment under the most problematic large drains within the Tuckean Swamp was conducted. Surveys were conducted using two geo-electric arrays: a 144m long floating geo-electric array and a 20m long submersible array. The survey was conducted for the Bureau of Rural Sciences and funded by an Australian Research Council grant to the Australian National University.

15.7.4 Survey Results

EC ribbon images of the geo-electric array surveys are presented in Figure 15-42 and Figure 15-43. The colour scales for the images are presented in Figures 15-44 and 15-45. Each survey covered a slightly different combination of drains but common drains are evident from their geometry. Blues represent low EC while reds represent high EC. An aqua line represents the drain bed on the 144m array data (Figure 15-43). This data extends to a depth of about 40m. The 20m submerged array data is plotted from the drain beds downwards about 4m. Depth scale is logarithmic and depth ticks are evident on the ribbon in some places with ticks at 0.1,0.2,0.4,0.6,0.8,1,2,4,6,8,10,20 and 40 metres for the 144m array data. Figures 15-46, 15-47 and 15-48 present the floating array data superimposed on an airphoto with representation of pH, EC and dissolved oxygen of the drain water.

15.7.5 Comparison of floating and submerged Geo-electric Array data

Images created by both devices have clearly picked up the same salinity concentrations under the drains; however resolution and depth penetration are different. The floating geo-electric array data has been resolved using the process of simulating layered geological models that may fit the measurements and then determining which model best fits the data obtained (the inversion process). The submerged array data has simply been converted to apparent EC assuming ground uniformity beneath the drains and that the drain water is

much more resistive than the sediment beneath. Where these assumptions are not valid, the apparent EC departs from true EC; however a very useful image still results. Validity of the assumptions is tested by observation of the surface water EC and depth.

The floating geo-electric histogram is bimodal. One peak represents the drain water and the other the sediment beneath the drains. The submerged geo-electric histogram is unimodal because it merges what it sees both above and below it into one image – depth on the image really represents averaged EC from above and below the array at the specified depth (distance from the drain bed).

15.7.6 Interpretation

Sites where acid is being leached out of soil into the drains are expected to coincide with sites of high sediment salinity. Several such sites are evident on the images. Within the drain water, sites with high salinity are also present – they result from a combination of groundwater inflow and tidal input of sea water. Where Marom drain (the west most drain) enters the main drain, it adds freshwater to the main drain, which at the time of the survey, cut off a site of more saline water further upstream in the main drain that had probably resulted from recent tidal inflow.

Basalt flows and other low porosity rock forms a basement to the swamp basin and are evident as low EC at depth in the north parts of the drains – particularly the top of Marom drain (submerged array data only) where the drain is cut directly into basalt.

Submerged array data in Henderson drain (the drain in the centre-north of Figure 15-42) suffers from poor signal strength (due to transmitter problems) and therefore is noisy at depth.

It is proposed that acid inflow to the drains is occurring at all points where high salinities are evident right at the drain bed. The rate of inflow however is probably not even across all such sites nor proportional to EC.

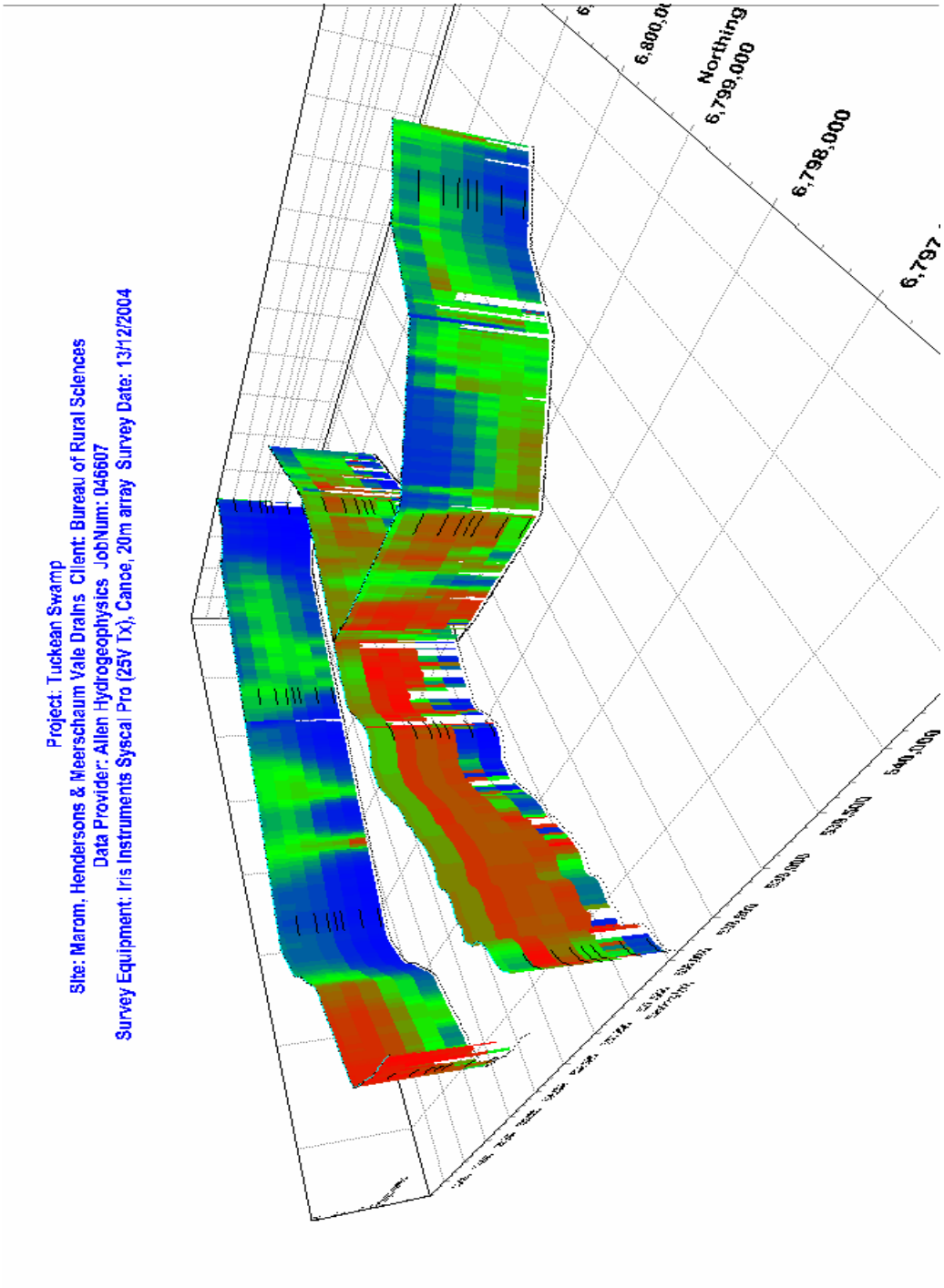

Figure 15.42 : Submerged array EC ribbons -Depth 0.1 to 4m beneath the drain beds.

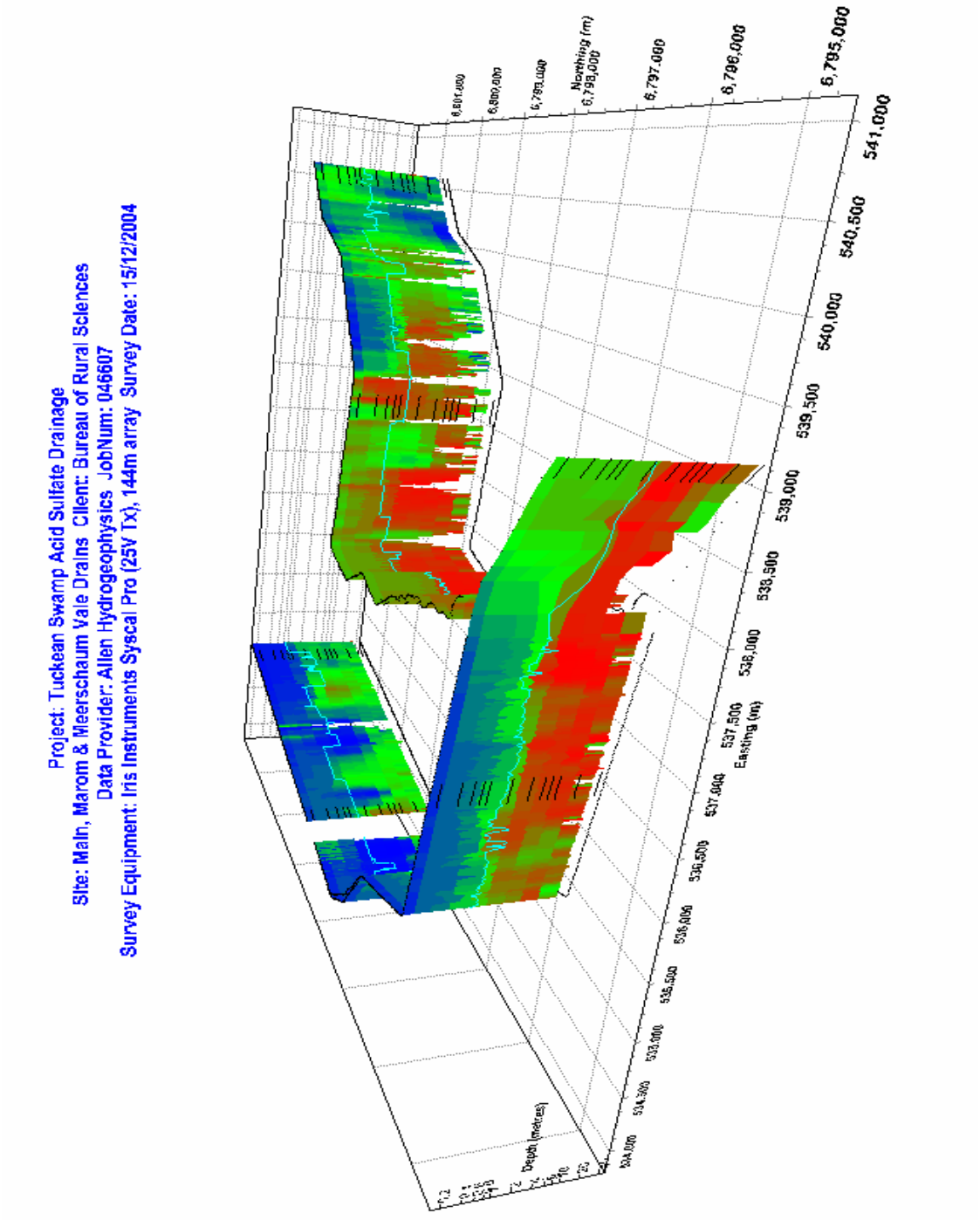

Figure 15.43 : Floating array EC ribbons - Depths 0.1 to 40m below drain water surface.

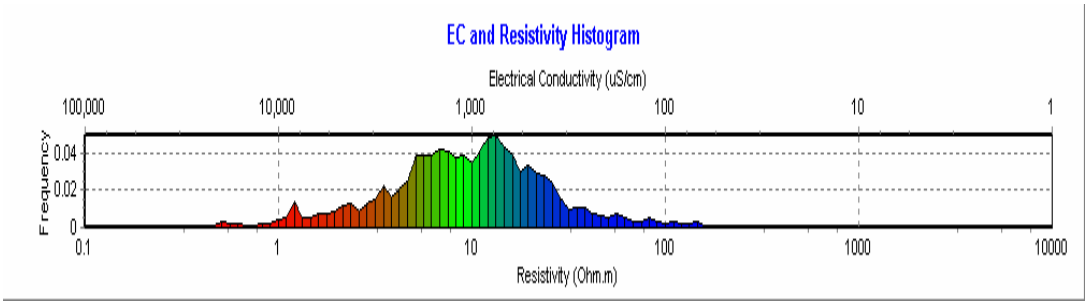

Figure 15.44 Color Histogram generated for equal area color distribution of the submerged geo-electric array data (0.1 to 4m deep data).

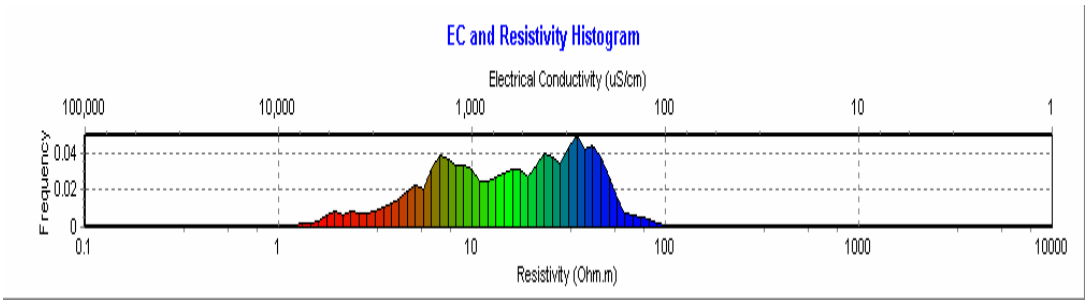

Figure 15.45 Color Histogram generated for equal area color distribution of the floating geo-electric array data (0.1m to 40m deep data).

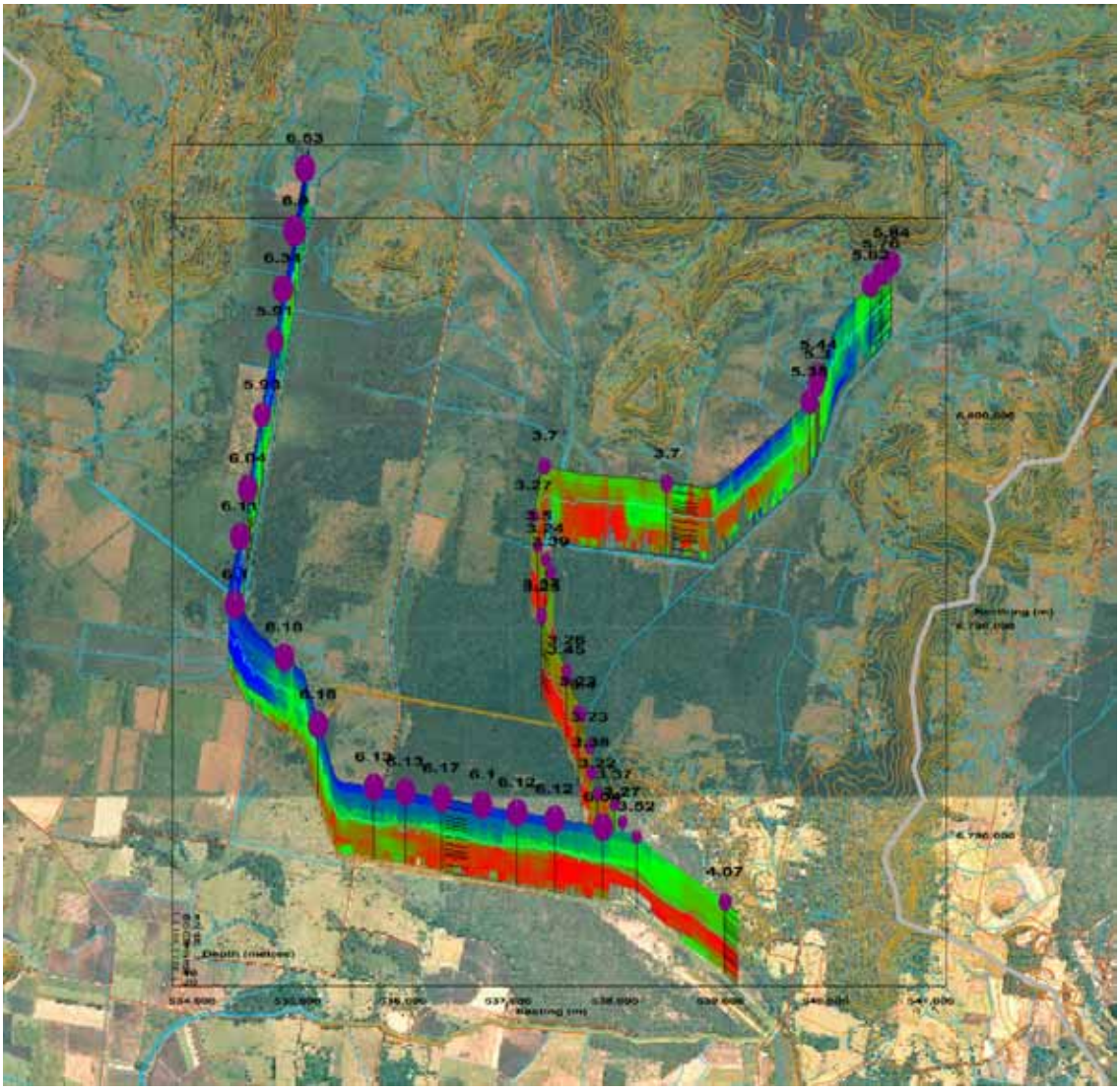

Figure 15.46 Floating Array EC Ribbons (0.1 to 40m deep) and proportionally sized spheres representing drain water pH superimposed on an airphoto of the drained Tuckean Swamp.

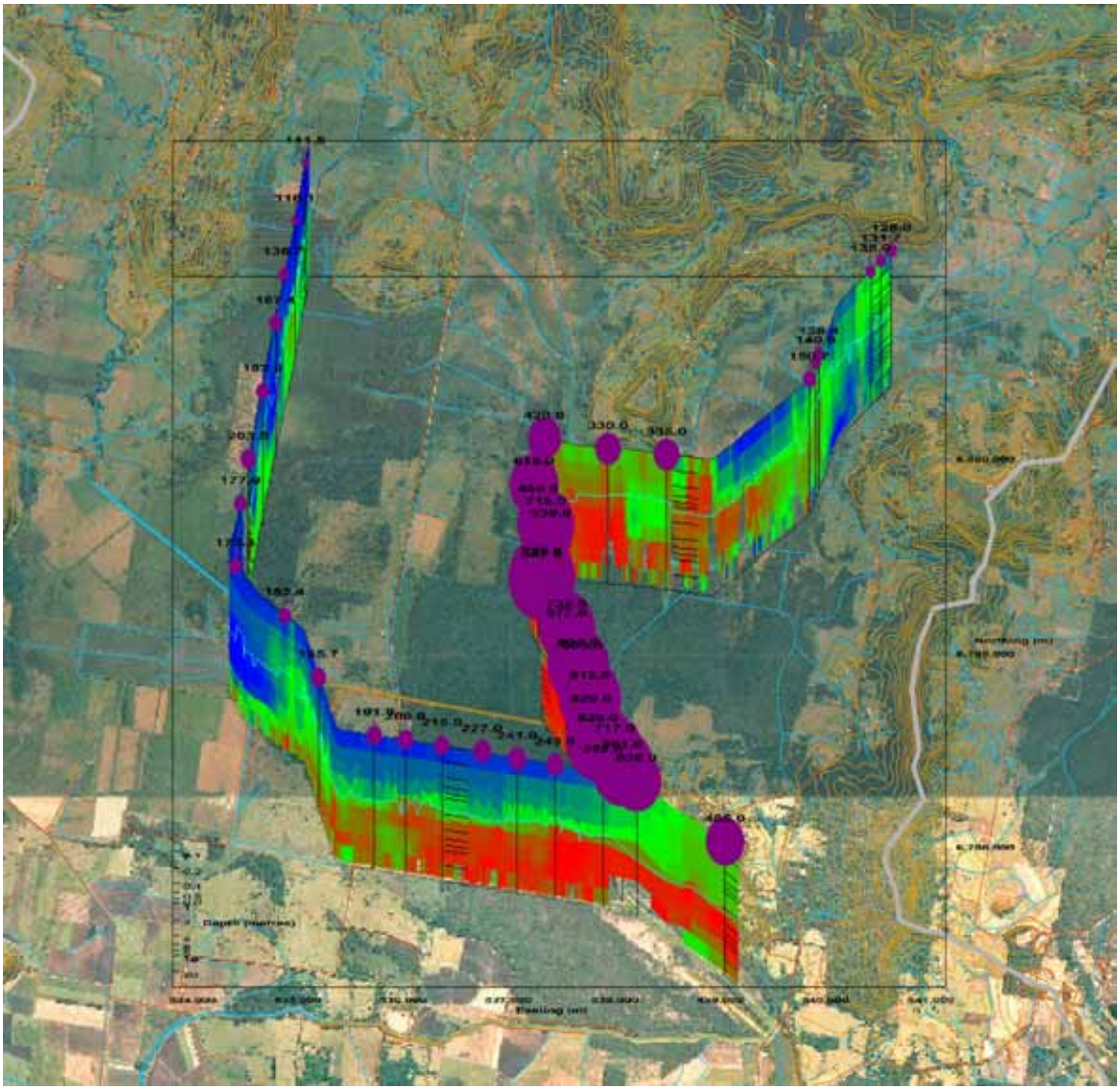

Figure 15.47 Floating Array EC Ribbons (0.1 to 40m deep) and proportionally sized spheres representing drain water EC superimposed on an airphoto of the drained Tuckean Swamp.

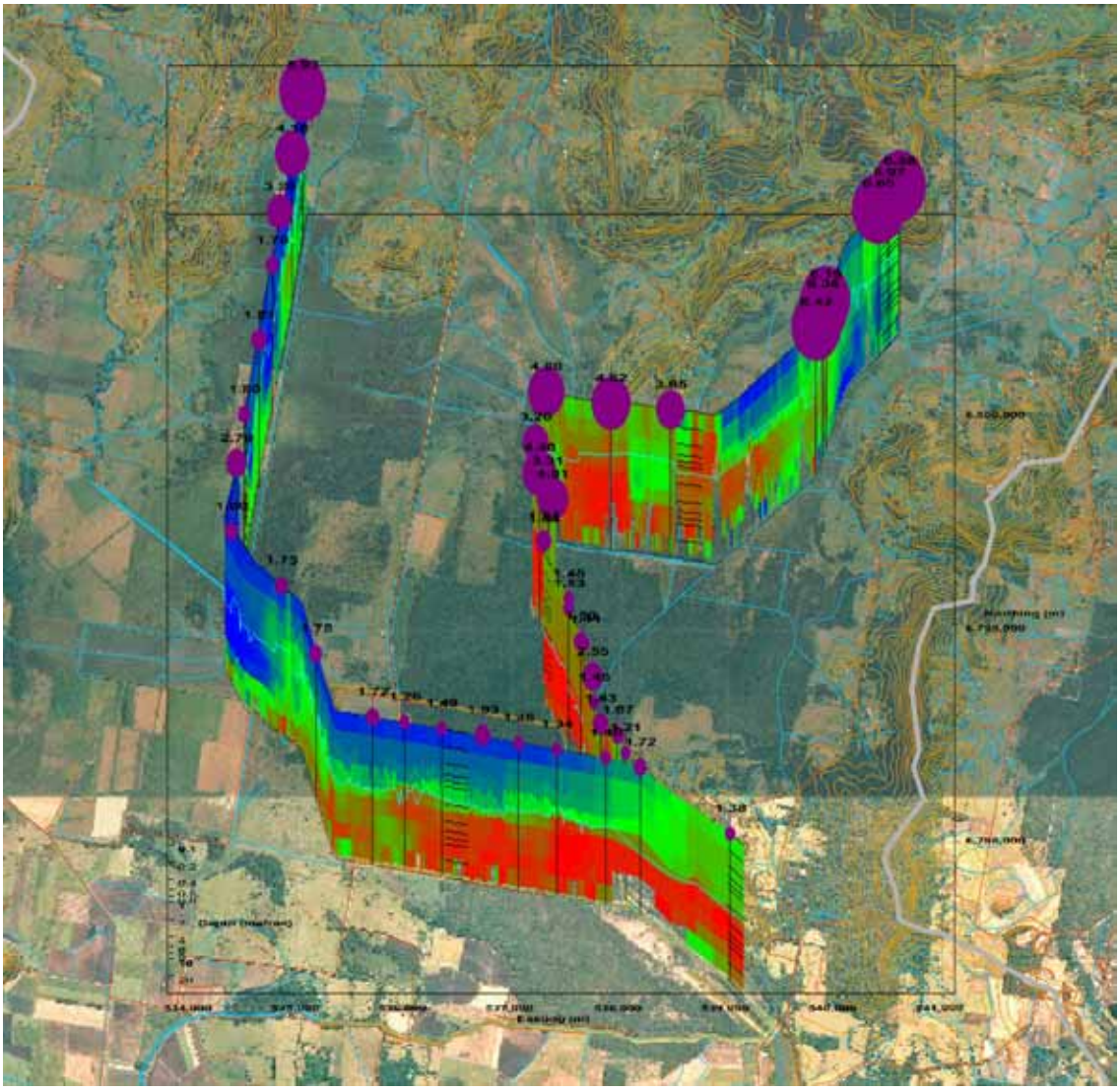

Figure 15.48 Floating Array EC Ribbons (0.1 to 40m deep) and proportionally sized spheres representing drain water DO superimposed on an airphoto of the drained Tuckean Swamp.

15.8 Noise-level aware inversion on the Murray River at Mildura

Geo-electric data, collected along a part of the Murray River near Mildura that overlies upward flowing saline groundwater, was inverted both with, and without noise level awareness invoked. Figure 15-49 shows the result without noise level aware inversion and is greatly affected by artefacts as is evident from comparison with Figure 15-50 which was inverted with noise level awareness invoked. Figure 15-51 shows the Figure 15-50 data wrapped along the river course in 3D so that it is clear that the anomalies in the inverted data relate to locations of real geological and cultural features.

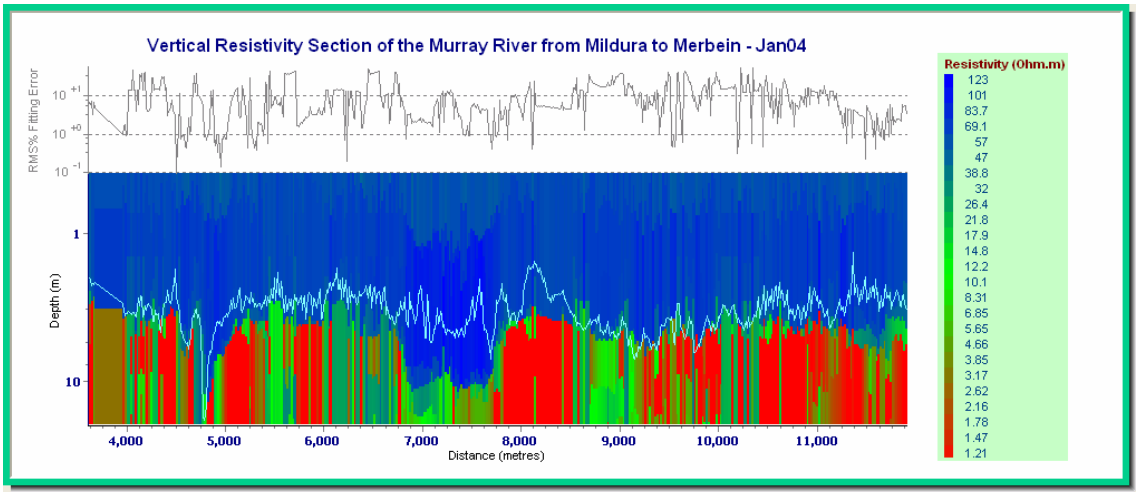

Figure 15.49 An example of inverted geo-electric array data collected at a part of the Murray River where hypersaline groundwater is just below the river bed. The hypersaline groundwater has consumed signal and resulted in artefacts in the data where inversion has been destabilized by low signal to noise ratios and data clipping.

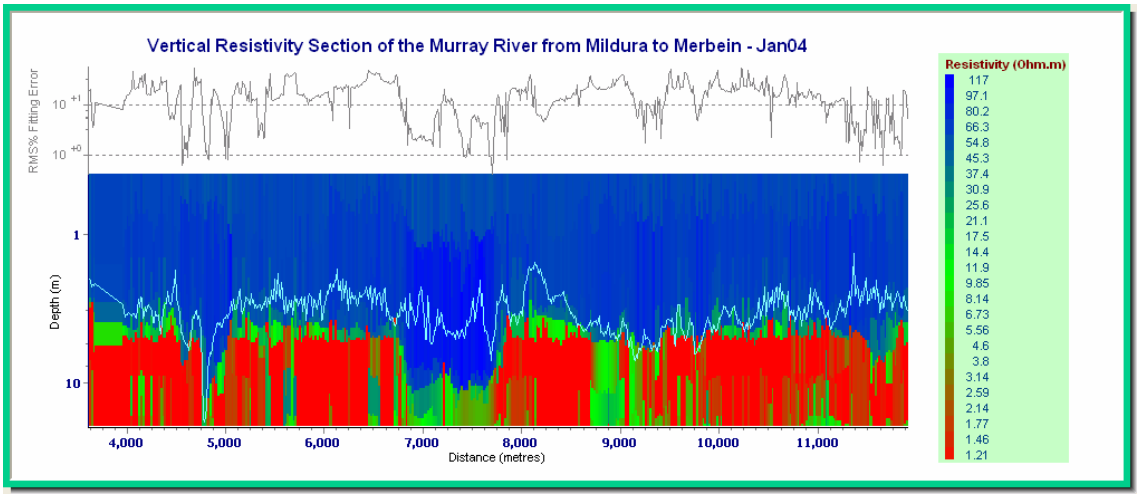

Figure 15.50 The same data as Figure 15-49 re-inverted using noise level aware inversion. Most of the artifacts are now eliminated.

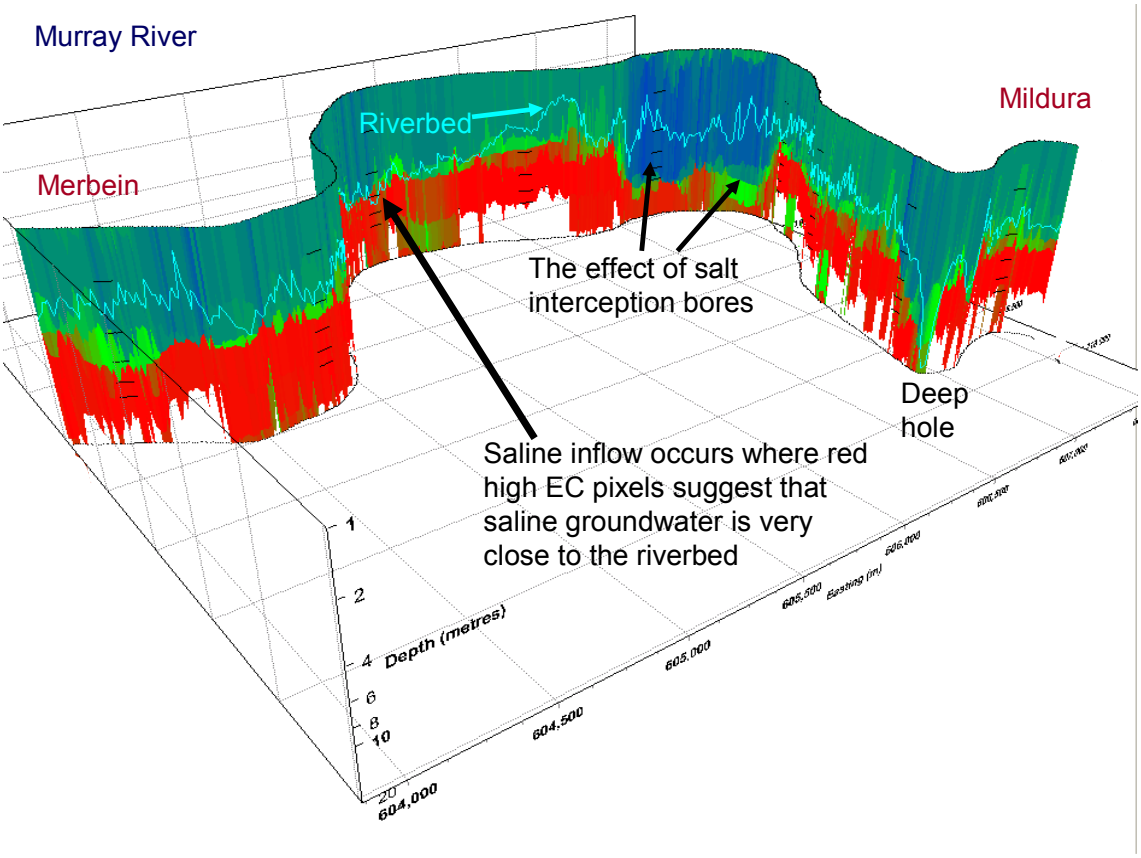

Figure 15.51 Three dimensional presentation of the data in Figure 15-50. This presentation method shows that anomalies present in the plain vertical section of Figure 15-50 correlate with the locations of known geological and cultural features.

15.9 River case studies concluding summary

Geo-electric EC imaging is useful for spatially dense, cost effective detection of ground salinity and texture at numerous depths beneath rivers. In lengths of river that are at risk of saline inflow, proximity of and salinity of saline water to river beds can readily be identified. In other areas, rivers recharge aquifers. The dominant recharge flow paths tend to be evident as regions of low EC in imagery. In some recharge areas, riverwater percolates downwards through an unsaturated zone that appears as a particularly low EC anomaly.

Floating geo-electric arrays are most practical for imaging a range of depths while submerged arrays give vertically dense information just below the river bed. Transient electromagnetic devices may be used to similarly image beneath rivers but cannot resolve shallow features that are useful to the study of interaction between rivers and the substrate.

CHAPTER 16 - IRRIGATION CANAL CASE STUDIES

16.1 Coleambally Irrigation Area

Multi-depth electrical conductivity (EC) imaging was conducted beneath numerous canals in the Coleambally Irrigation Area during development and refinement of EC imaging equipment and software. The data was compared with soil and groundwater data using the software (hydro-Geo Imager) and revealed isolated seepage sites, and salinity distribution within the groundwater beneath the canals. Numerous sites were also identified where shallow fresh groundwater pumping could be attempted to lower water tables, increase leaching of salt from the root zone and re-use infiltrated water. Such pumping can increase canal seepage resulting in water ownership disputes but also provides nil evaporation loss by storing water underground. Water ownership disputes would have to be solved by cooperative groundwater and surface water management.

Isolated seepage sites were identified under the Coleambally Main Canal, Bundure Main Canal, Argoon Main Canal and Boona Main Canal. Although seepage is notoriously hard to measure quantitatively, good correlation was obtained with sediment samples extracted from canal beds using a yabbie pump and with seepage indicators such as clusters of deep rooted trees and piezometer level changes that occur when canals are filled.

Use of a submerged 20m Allen Exponential Bipole Geo-electric array towed using a 4wd mounted boom for EC imaging proved to be efficient where access along canal banks was maintained. This device resolved EC in a depth range of 0.05 to 6m beneath canals. A survey speed of 7 km per hour was practical and 15 to 30 km of canal obstructed by frequent fences, trees and regulators could be surveyed per day. Use of a canoe or boat to tow the array on small canals was precluded by weed growth which fouls outboard motor propellers. Deeper (0.1 to 40m) imaging was conducted using 80m and 144m long floating arrays which could be towed efficiently but took longer to feed over obstacles.

Results were interpreted in the context of existing data available on EC, sediment types, permeability and seepage rates. Idaho Seepage Meter data, bore logs, vegetation observations, EM31 data, aquifer salinity distribution data, airphotos, piezometer data, satellite imagery and soil maps were already available. At some sites, additional

information was gathered at targeted locations using a 3m penetrating hand auger, a bladder type seepage meter and a yabbie pump.

Geology of the CIA relevant to these case studies is presented in Figure 16-1. Figure 16-2 presents an understanding of some of the potential groundwater percolation pathways and sinks. Braided stream deposits do not dominate the CIA but are congregated under certain parts of it. Hulme (2002) presents alternate stream deposit types of more isolated nature which he has identified further north. Identification of percolation pathways is important for seepage studies and, more lucratively, for siting groundwater reuse schemes.

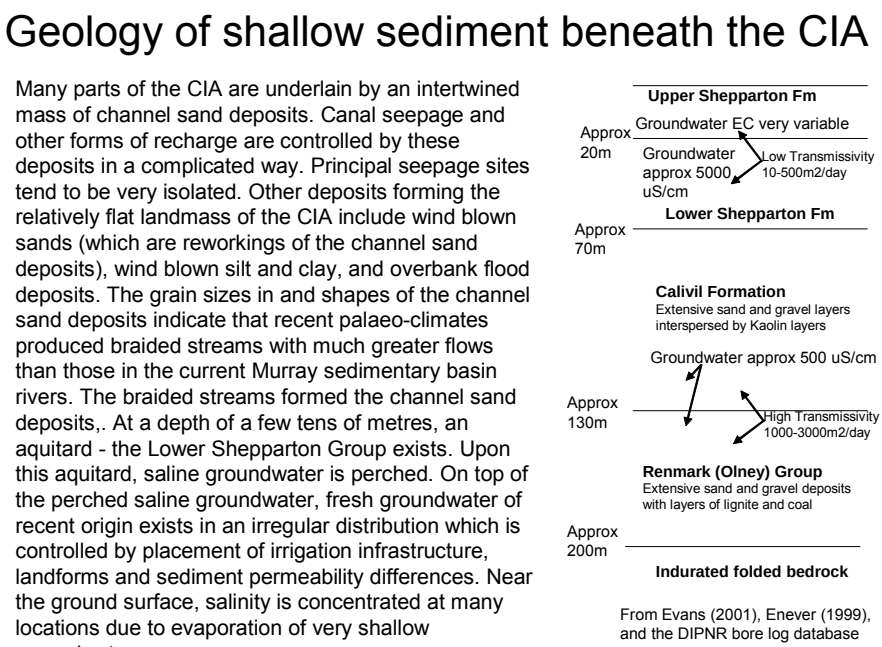

Figure 16.1 Geology of the Coleambally Irrigation Area.

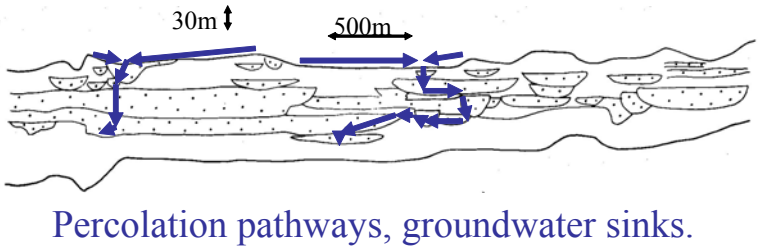

Figure 16.2 A vertical section through channel sand deposits formed by braided streams showing potential percolation pathways and groundwater sinks.

16.2 Coleambally Floating Geo-electric Array Results

The principal purpose for using floating geo-electric arrays in the CIA was imaging of sites of fresh groundwater accumulation suitable for pumping and conjunctive use in irrigation. Data is also useful for seepage site identification.

Floating geo-electric array surveys were conducted on canals spread across the CIA (see Figure 16-3). These surveys revealed both anomalous seepage sites as well as detailing groundwater salinity at multiple depths down to as deep as 40m.

Figure 16-4 presents an overview of the floating array EC ribbons. It seems to show, principally, a hint of the distribution of vadose zone salinity and shallow groundwater salinity across the irrigation area. Detail is not evident at this scale, and extreme vertical exaggeration.

Salinity under the CIA at various depths can be assessed using geo-electric arrays. It has been compared, in Figure 16-5, with salinities found from sampling piezometers of various depths. Due to confidentiality, the piezometer data has been smoothed. This has impared proper comparison. The geo-electric array data respond more to vadose zone salinity than do the piezometers and have a much greater sampling density than them. These differences impair correlation between the two datasets. It is a subject of debate whether one or the other relates more to salinity problems of various sorts. Soil salinity problems are very dependent on vadose zone and shallow perched groundwater that are not detected by borehole water samples but are imaged with great clarity by geo-electric arrays. Soil texture, however, complicates interpretation of geo-electric data and time lapse interpretation may be complicated by factors such as canal water depth and survey path duplication accuracy.

Correlation between the EC imagery and soil classifications was investigated in Figure 16-6 and the results are discussed there. In summary, correlation is poor because surface soil is often very thin and does not necessarily bear resemblance to underlying hydrogeological features evident under the incised canals.

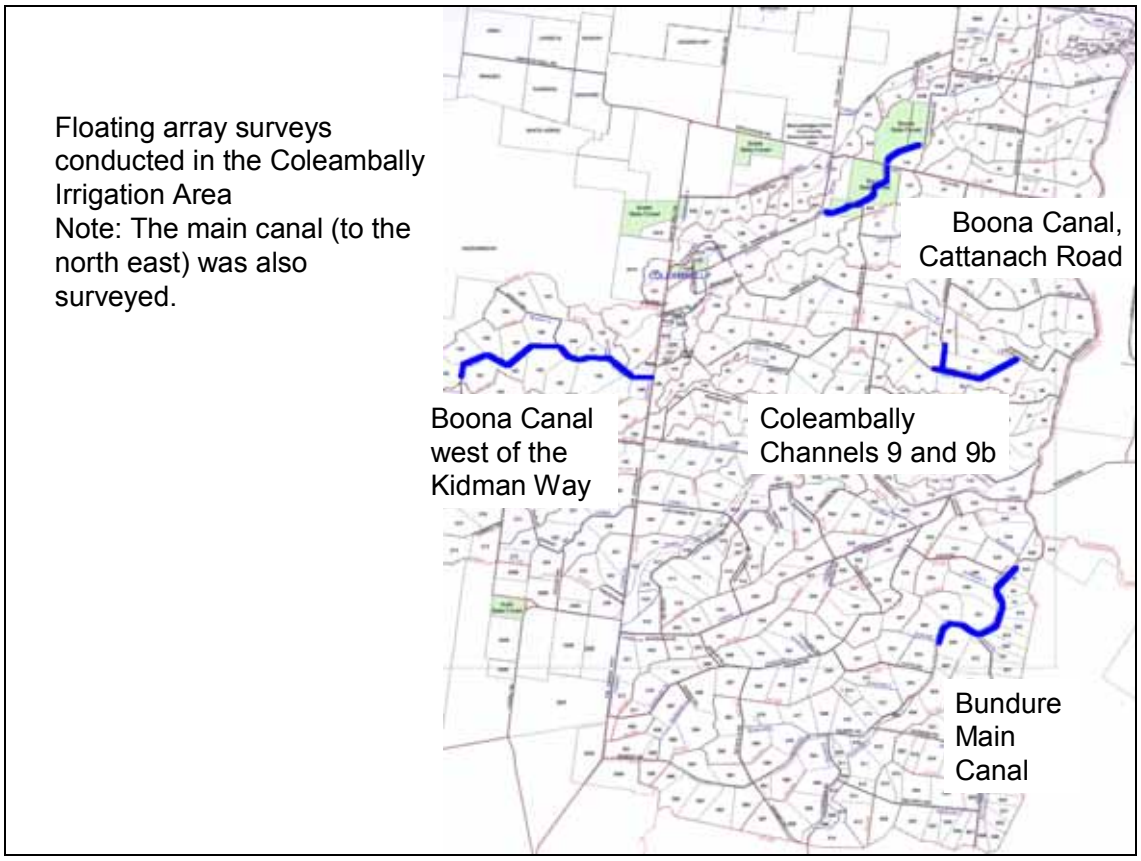

Figure 16.3 Floating array surveys conducted in the Coleambally Irrigation Area.

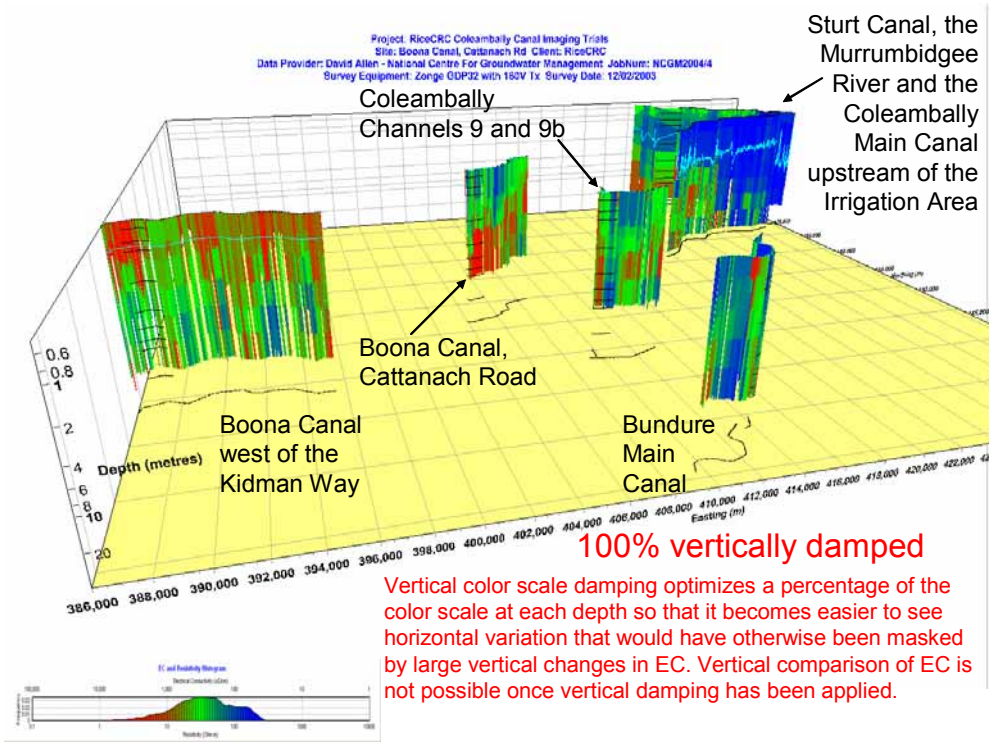

Figure 16.4 An overview of EC imaging conducted with floating arrays contrasts variation in salinity at various depths under canals.

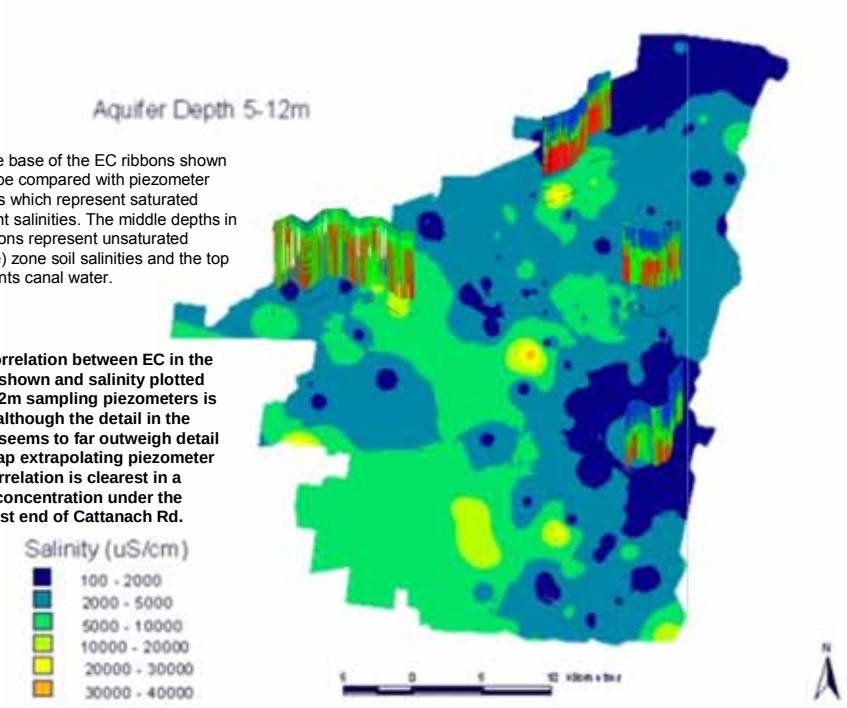

Figure 16.5 Comparison of EC ribbons and Salinity of bore water in shallow bores.

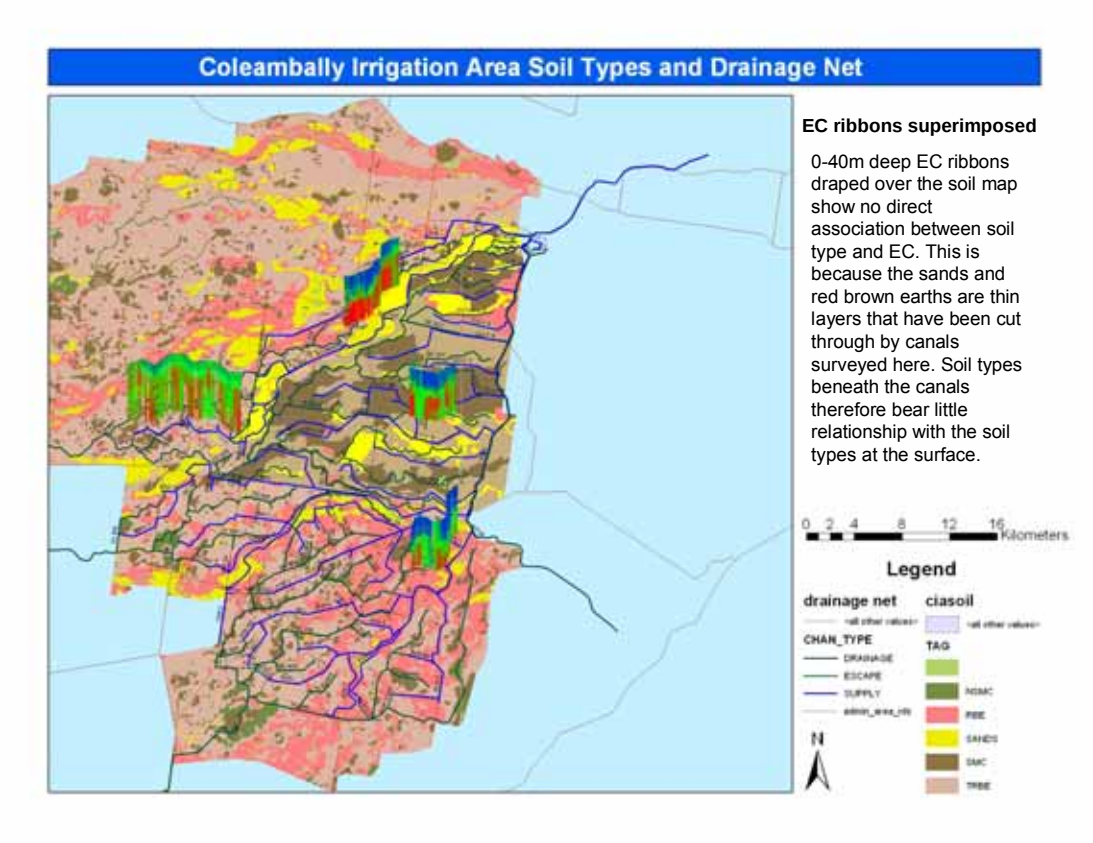

Figure 16.6 EC ribbons and soil types.

16.2.1 Boona Canal – Cattanach Road

This section of canal is situated along the edge of a sand hill. Drilling results superimposed on the EC image (Figure 16-7) show that the canal has been cut deep enough at most places to intersect clay. Seepage through the canal floor therefore does not appear to be a major problem. Seepage through canal walls may be a problem but cannot be identified using a geo-electric array in the canal. The southern end of the canal (left side) passes over particularly conductive ground – probably shallow saline groundwater in clay (partially or fully saturated).

At sites such as near borehole 868 (mid-right), which is almost entirely sand, and at the NE end of this canal section, low EC is evident directly below the canal. It is possible that sand was not entirely excavated from beneath such sites and that seepage is occurring there.

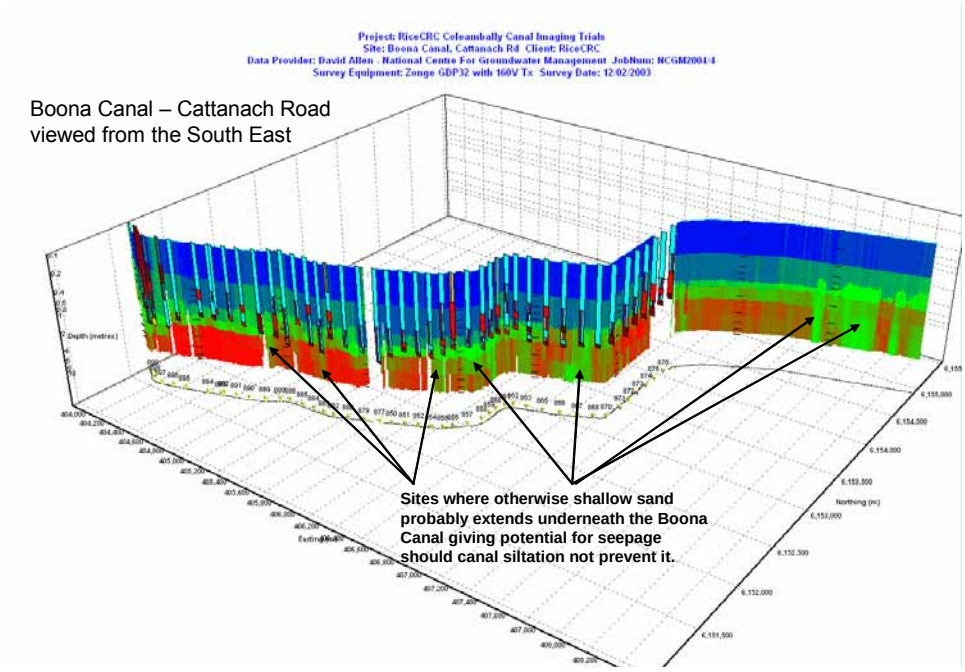

Figure 16.7 Boona Canal, Cattanach Road EC ribbon 0.1 to 10m deep. Borehole logs from holes adjacent to the canal are graphically displayed using the colour scheme of Figure A7-1 (aqua = sand, red = medium clay, purple = clay, brown = heavy clay, yellow = light clay, and grey = loam).

16.2.2 Coleambally Channels 9 and 9b

These canals were surveyed to check a marked contrast in EC, as measured by an EM31 survey, between the two canals. Results are presented in Figure 16-8 and Figure 16-9. The geo-electric array survey showed that the EM31 survey had responded predominantly to differences in the water depth and/or salinity of water in the two canals rather than any variation in the ground under the canals (see the contrast in EM31 data at the junction of the canals).

Although much variation in EC is evident along the canal, no isolated anomalous seepage sites deemed to be worth fixing were identified. The lower EC sites, particularly the one next to a bore containing gravel, could be targeted for shallow groundwater pumping.

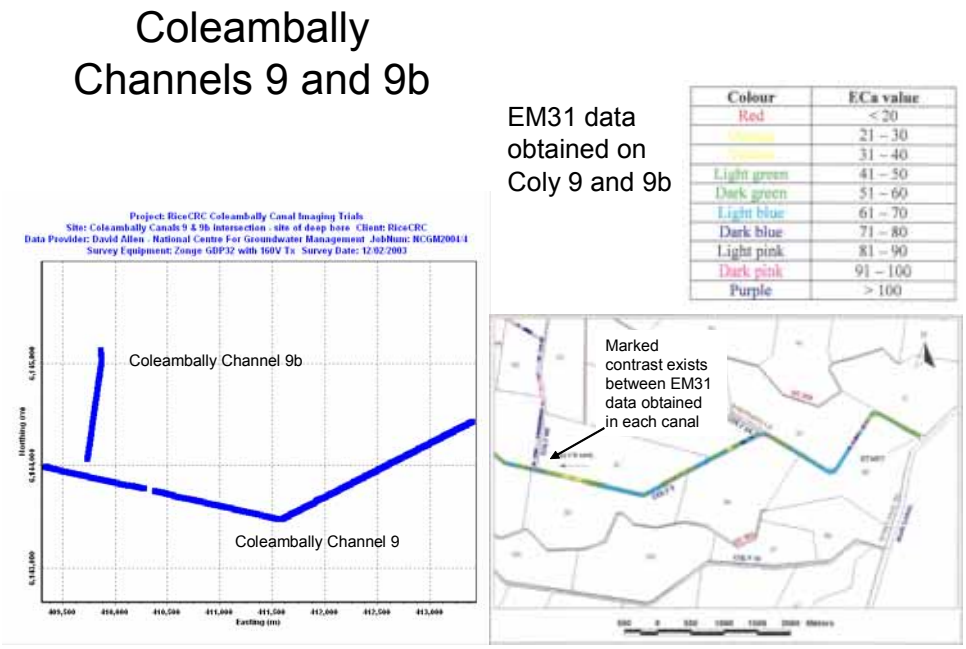

Figure 16.8 Coleambally Channels 9 and 9b EC ribbon location (blue line figure) and EM31 survey results from Harding (2002).

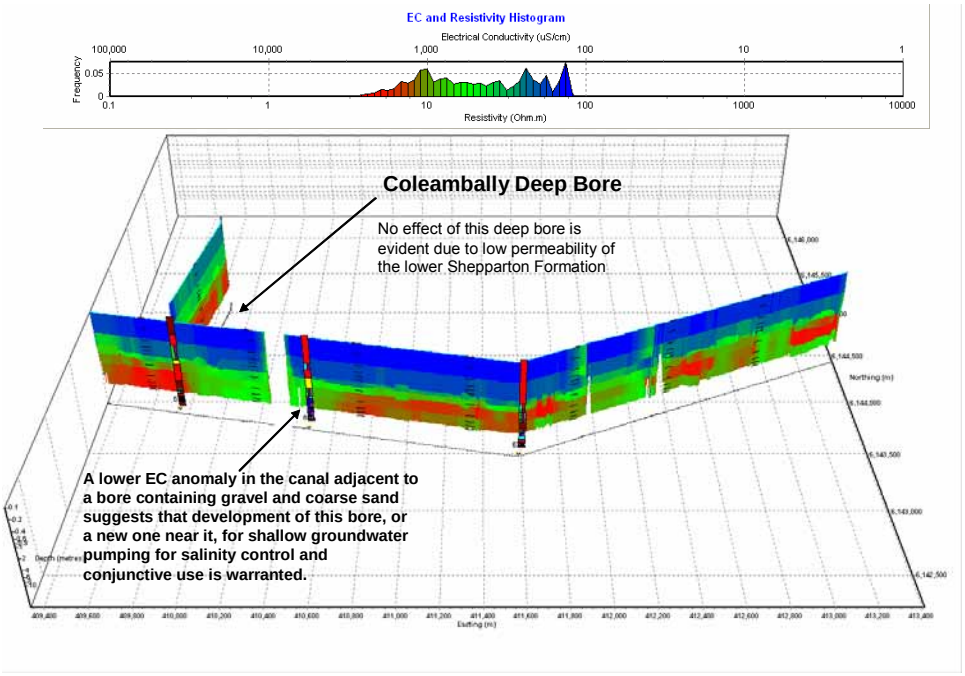

Figure 16.9 EC ribbon – Coleambally Channels 9 and 9b.

16.2.3 Bundure Canal

Bundure canal (Figure 16-10) passes over stringer sands of a prior braided stream. One sand/gravel in particular, near bore 4137, has a distinct deep low EC anomaly (Figure 16-11 and Figure 16-12). This sand/gravel would probably be ideal for shallow groundwater pumping. It is believed that bore 4137 missed the sand. Two auger holes (999201 and 999202) were sunk but did not reach the sand.

EC directly beneath the Bundure canal is less than at other surveyed canals. This suggests that the saline water elevation (saturated or unsaturated), not the water table, also is lower there.

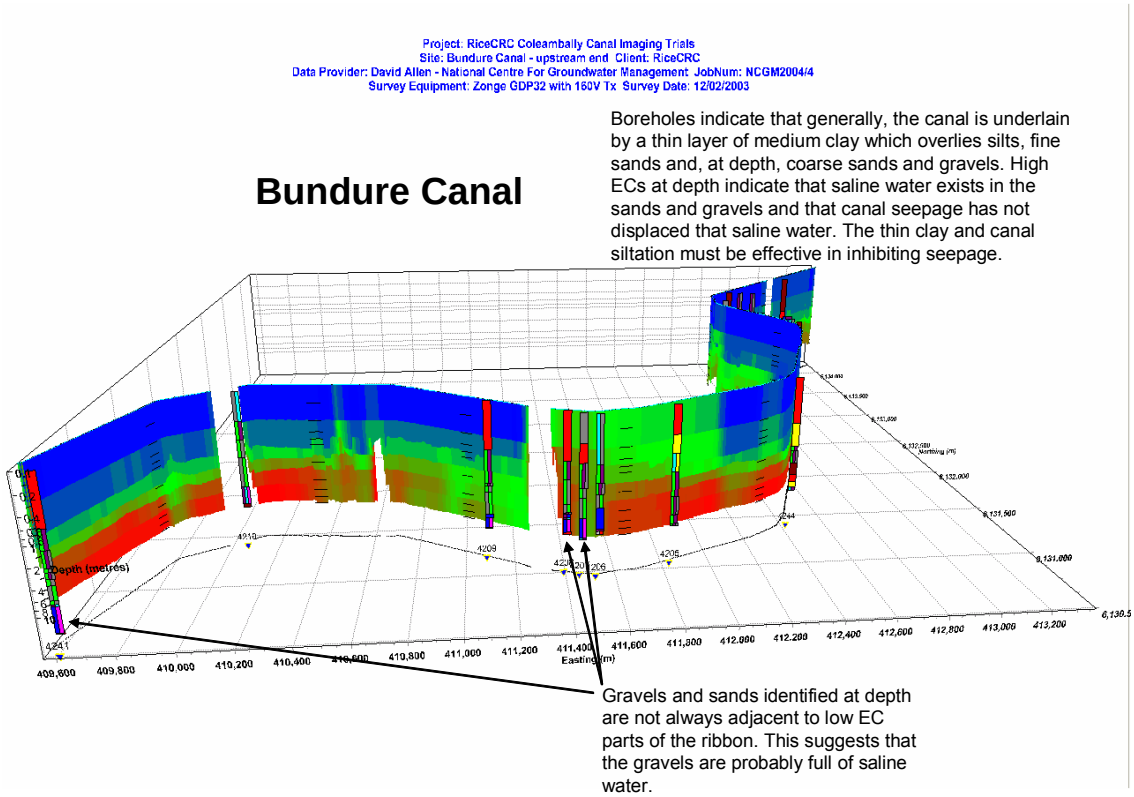

Figure 16.10 Bundure canal 0.1 to 10m deep EC ribbon and bore logs.

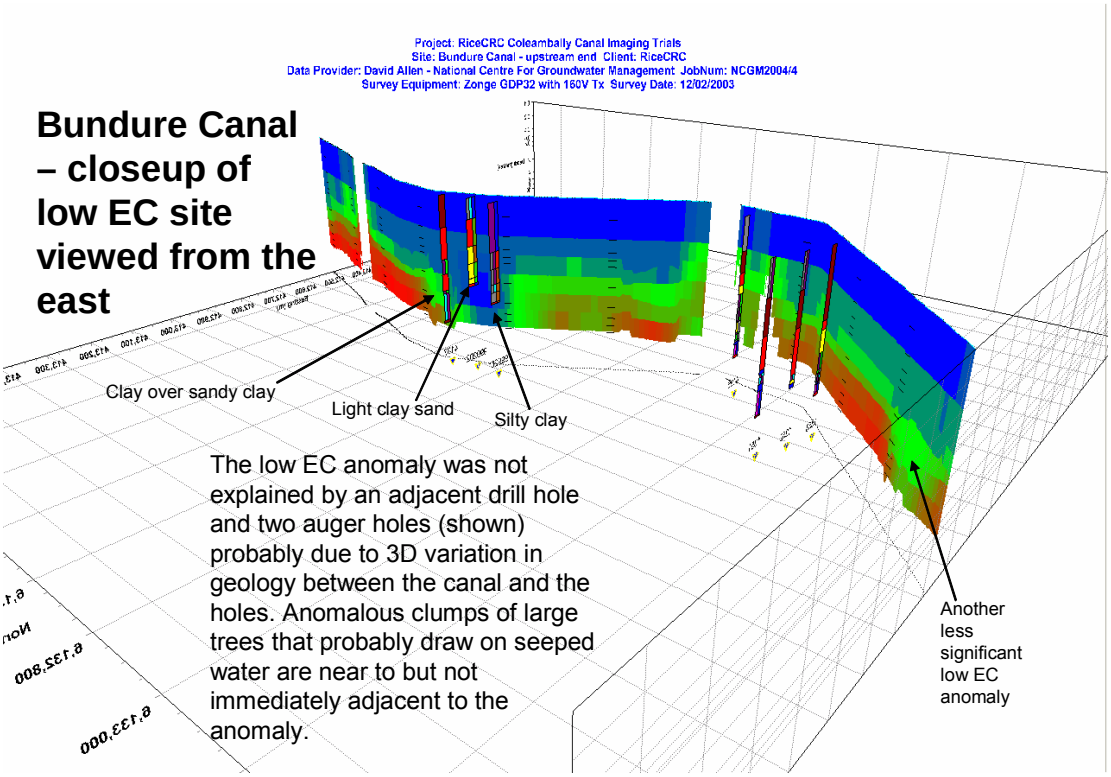

Figure 16.11 A close-up view of a clear low EC anomaly under the Bundure canal (looking from the NE).

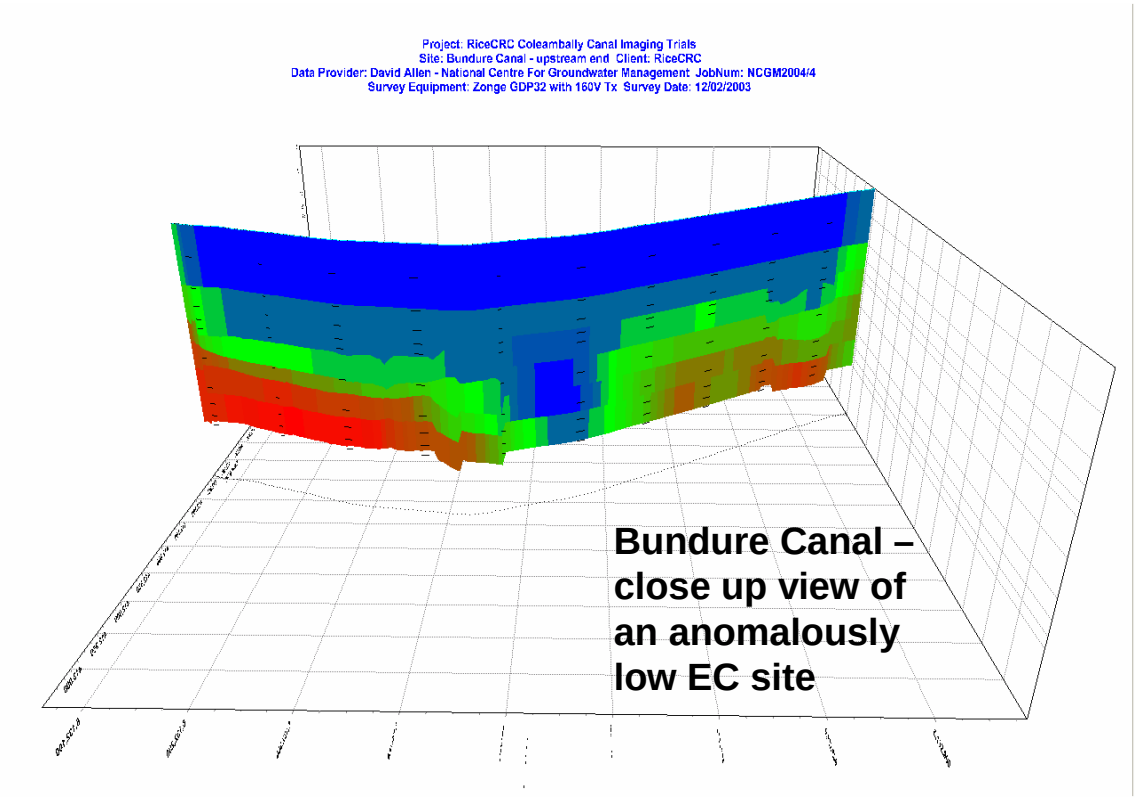

Figure 16.12 An uncluttered display of the anomaly of Figure 16-11.

Numerous boreholes along the canal show that gravels exist at depth. EC at depth is not low however. It appears that these deeper gravels must be filled with saline high EC water. A PhD student at Monash University - Viezolli (2005) inverted resistivity and IP data acquired by the author, using Res2DInv, from a segment of this dataset surrounding easting 411500 (see Figure 16-10). The anomaly there seems to represent gravel containing fresh water (probably overlying saline water) and so should be a good low IP anomaly. Viezolli's results are reproduced in Figure 16-13 for reference. When comparing images note that Viezolli's depth scale is linear. Viezolli's 2D inversion has a horizontal ripple in it at depth that is probably a geophysical artefact but results above 7m look reliable. Viezolli claims that by multiplying the EC and IP images one gets a superior indicator of seepage pathways. He adds evidence to this claim with Figure 16-13c. The signal level advantages of the AXB arrays have, as a by-product, permitted good detection of IP data at sites such as the Bundure Canal as demonstrated by Viezolli. Very good quality IP data may be obtained once a capable receiver is connected to a submersible AXB array.

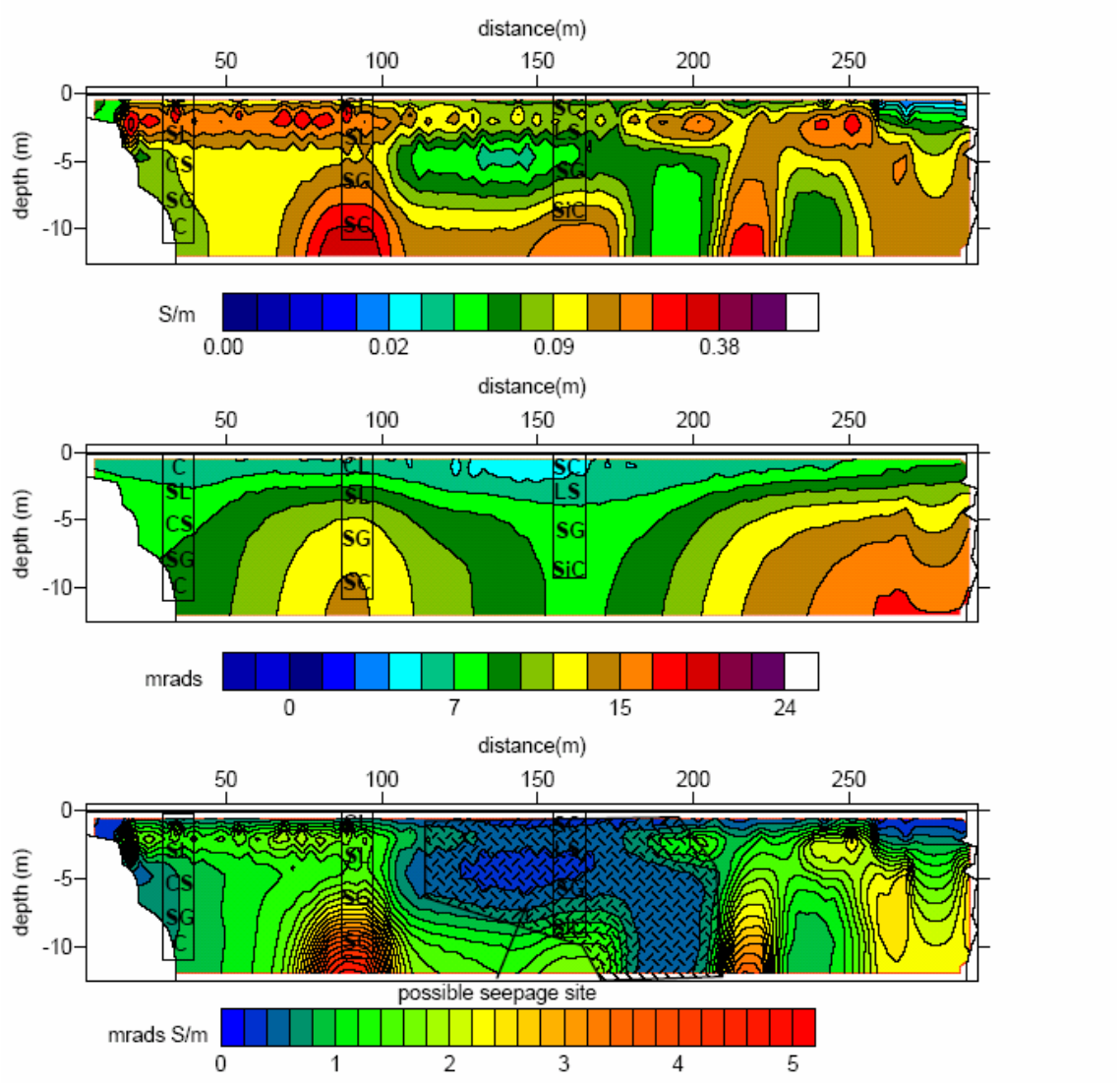

Figure 16.13 (from Viezolli 2005) Conductivity (top, Figure 16-13a), chargeability (middle, Figure 16-13b) and normalized chargeability (bottom, Figure 16-13c) cross sections for section # 2 are presented. Lithology logs from neighboring boreholes are superimposed to the sections. Letter codes are as follow: S=sand, C=clay, G=gravel, L=loam, Si=silt, LC=light clay, HC=heavy clay. Note that CL= clay loam, SC=sand clay, etc. Possible seepage sites locations are indicated.

16.3 Coleambally submerged and floating geo-electric array results.

16.3.1 Boona Canal – west of the Kidman Way

This section of canal was surveyed because it is flanked by salinised depressions (see Figure 16-14). In the original plan of the Coleambally Irrigation Area, these depressions were marked as sites that should not be farmed due to their low elevation however in later years, the depressions were farmed and turned into salinas. Farming then obviously had to stop. Rehabilitation works have been commenced. It has been suggested (CIL discussion) that canal seepage caused water tables to rise which caused the salinization. This could be partly true. Anomalous seepage sites were found on the canal as shown (Figure 16-15).

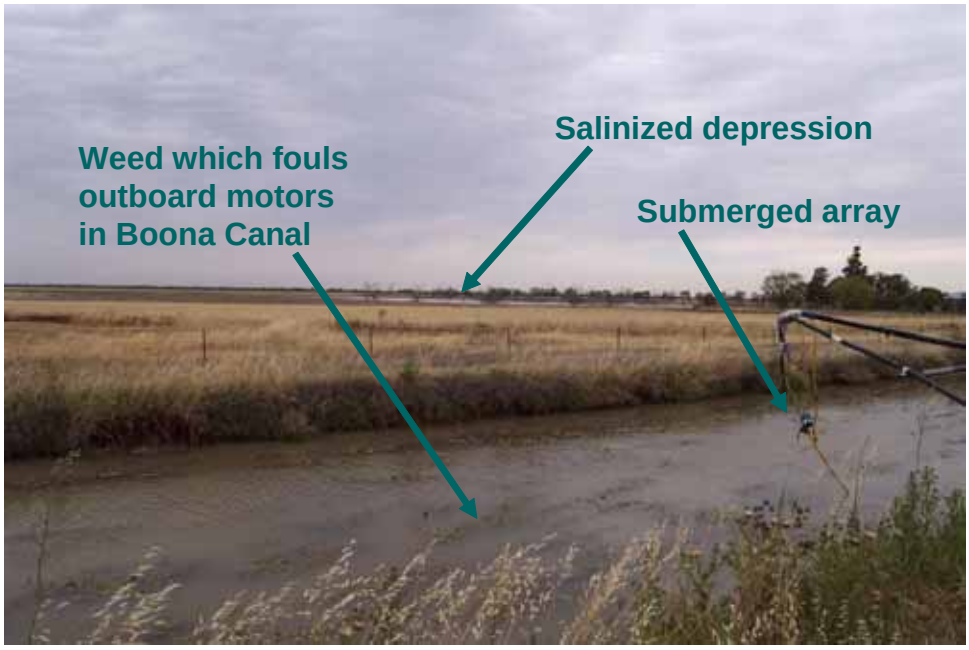

Figure 16.14 A salinized depression near the Boona Canal. Also evident is canal weed which fouls outboard motors. This problem lead to development of the boom seen towing a submerged array.

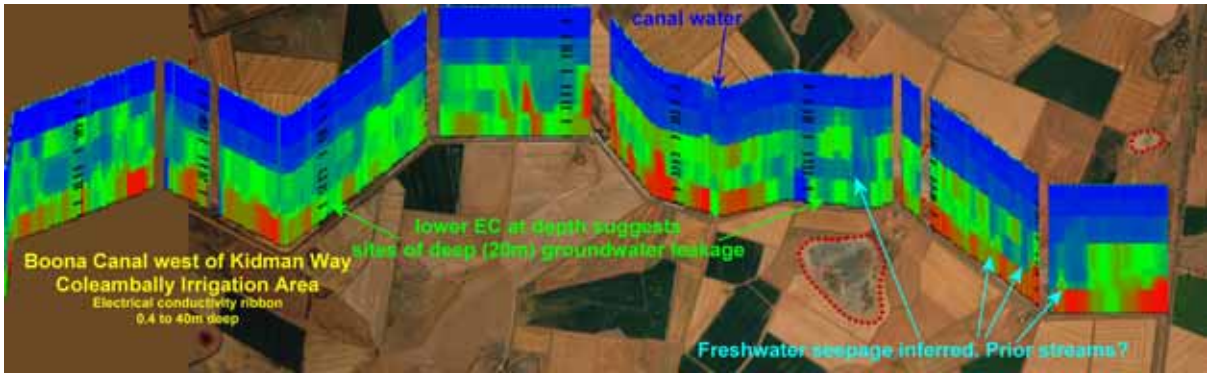

Figure 16.15 The Boona Canal west of the Kidman Way. Inverted data showing various anomalous features related to groundwater movement. Twenty layer smoothed model inversion conducted by Christensen (2004). Note that the canal water (blue) extends to about 0.9m.

The Boona Canal, west of the Kidman Way, was used as a test site for numerous inversion techniques and both floating and submerged geo-electric arrays. In particular, the eastern kilometre of this segment was intensively studied. Sands exist there and seepage is known to be a problem there. Unlike the Bundure Canal, the anomalies corresponding to seepage sites under the Boona Canal are small and irregular and therefore present a challenge to inversion techniques. It may be true that if an inversion technique can define seepage on this segment of canal then it should work in most places.

Figure 16-16 presents a map of the canal segment and EC ribbon images of floating 80m long geo-electric array data inverted in six different ways. Detail is difficult to see on Figure 16-16 so Figure 16-17 presents a blow-up of the eastern 1 kilometre of the EC ribbons of Figure 16-16 as well as some submerged array data collected over that length of canal. The depth scales on many of the images are not the same due, in part, to different amounts of extrapolation of the different inversion techniques. Finally, Figure 16-18 presents the middle 600m of that 1 kilometre segment as inverted by Viezolli (2005) using Res2DInv to give both resistivity and induced polarization images. Some of the inversions have been conducted by the Aarhus Hydrogeophysics Group, others by Niels Christensen (EMmodel) and others by the author (using HydroGeoImager). It can be seen that the laterally constrained 1D inversion samples may be ideal elsewhere but here they suffer from simplification of models to three layers and from in-appropriately excessive horizontal constraint.

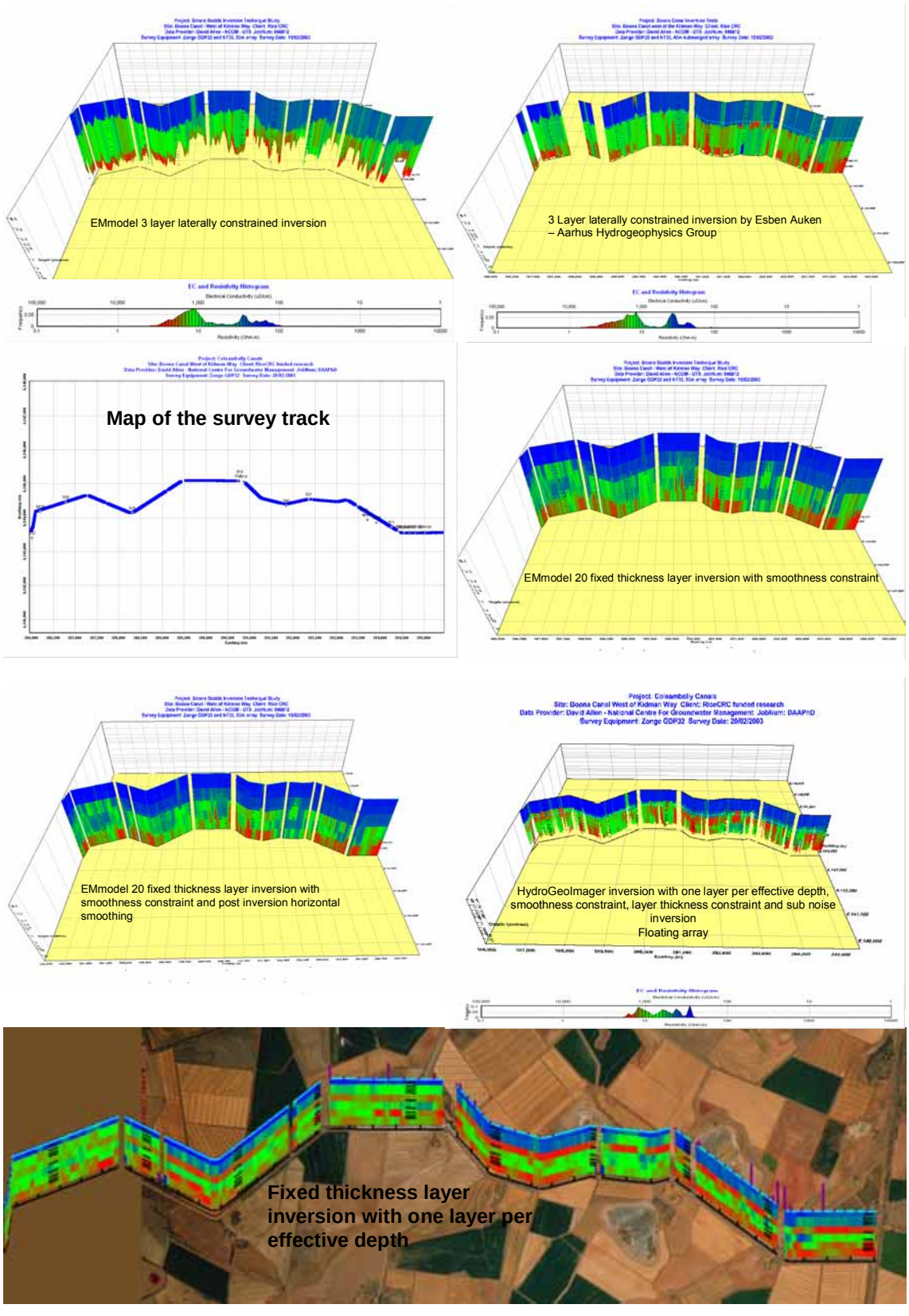

Figure 16.16 Boona Canal inversion tests

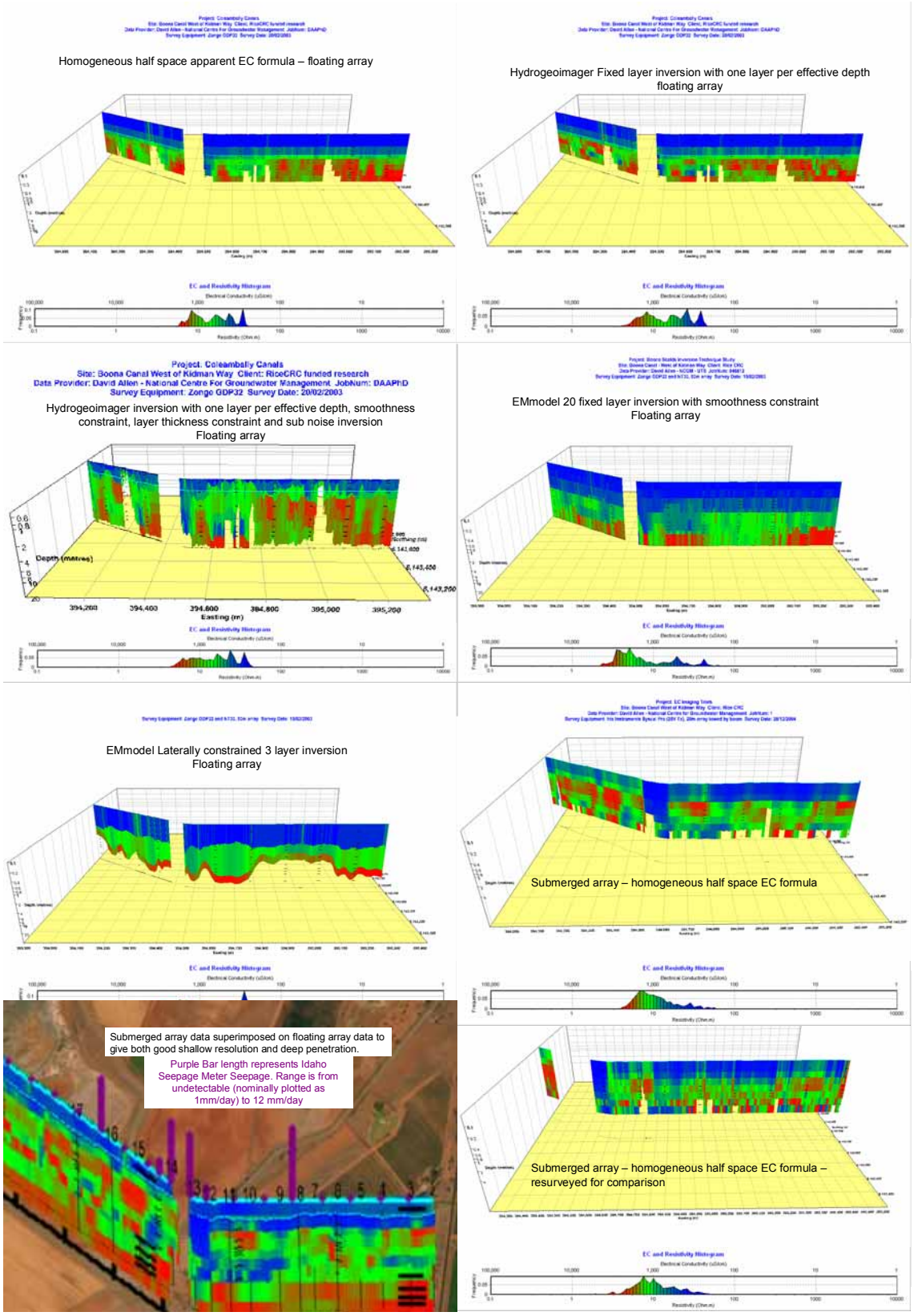

Figure 16.17 Boona canal inversion tests 2. Note that the submerged array data is all collected with an injected current of only 12 Volts.

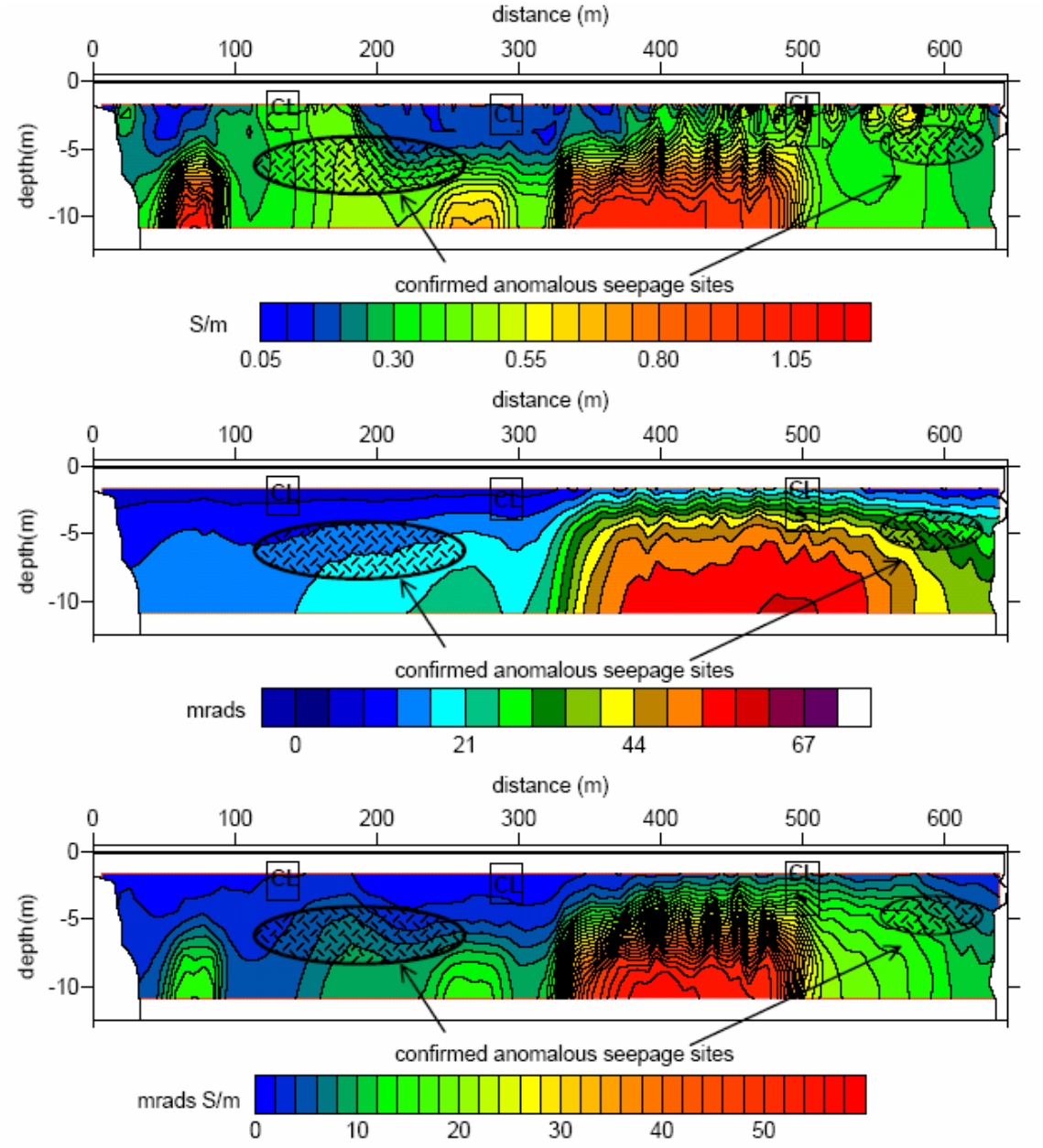

Figure 16.18 (from Viezolli, 2005) Res2DInv inversion, for comparison with Figure 16-17, of the Boona Canal east of the regulator that has created the gap in the images in Figure 16-17. Conductivity (top, Figure 16-18a), chargeability (middle, Figure 16-18b) and normalized chargeability (bottom, Figure 16-18c) cross sections. Lithology logs from neighbouring boreholes are superimposed on the sections. Letter codes are as follow: S=sand, C=clay, G=gravel, L=loam, Si=silt, LC=light clay, HC=heavy clay. Note that CL= clay loam, SC=sand clay, etc. Locations of seepage sites obtained from seepage-meter measurements are shown.

It can be seen that the 20 layer 1D smoothness constrained inversion is very stable and replicates most detail but in a blurred manner. It is particularly challenged by high contrast boundaries such as the base of the canal and clay/sand boundaries. The apparent resistivity versus effective depth image is even more robust than the 20 layer smoothness constrained inversion but lacks resolution. The HydroGeoImager inversion with one layer per effective depth, a little smoothness constraint and stretch constraint can be seen to have ability to clearly and accurately define major high contrast boundaries such as the canal bed and also detect minor details in the data. The technique's stability is typically less than the 20-layer smoothness-constrained inversion. Its stability is dependant on having sufficient smoothness constraint and only an appropriate amount of stretch constraint. Too much stretch constraint will produce overshoots and undershoots at poorly matched high contrast boundaries and too little will lead to various layers blowing out or disappearing. Finally, the example of fixed layer thickness inversion with the airphoto background demonstrates the undesirable artefacts caused by fixing boundaries so that they cannot match real high contrast boundaries – overshoots and undershoots occur.

The submerged array data in Figure 16-17 were not inverted but simply plotted as apparent resistivity with respect to surface array effective depths. Note that the water layer is not imaged in that data. Two submerged array surveys were conducted along the same stretch of canal. The two may be compared to reveal repeatability. Figure 16-17 also contains an image of submerged array and floating array data super-imposed revealing that the two datasets match as well as could be expected considering resolution of each.

The Res2DInv inversion of resistivity and induced polarization data conducted by Viezolli (2005) collected with the floating array shown in Figure 16-18 also can be compared with the other inversion techniques if one takes into account the very different color stretch and vertical scale applied. Anomalies broadly match those obtained with the other techniques but are superimposed by horizontal ripple. As with the Bundure Canal, the IP data appears to be useful.

After assessing the difference various inversion algorithms could make to the Boona Canal data, it is appropriate to examine how that data relates to seepage losses and the salinization surrounding the canal. Figure 16-19 presents the east end of the canal where salinization has occurred in depressions near the canal.

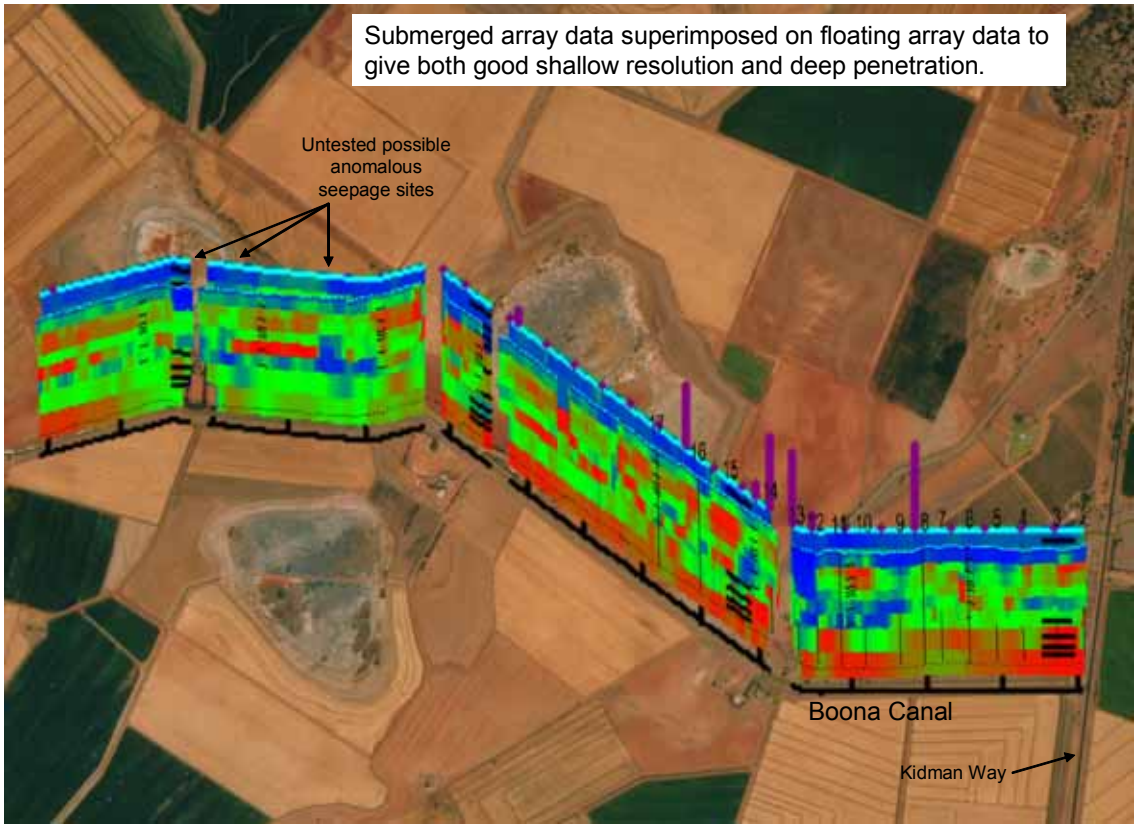

Figure 16.19 Boona Canal west of the Kidman Way – Submerged and floating array superimposed EC ribbons showing Idaho meter seepage (from undetectable up to 12mm/day) as a purple bar graph and possible untested seepage sites in the vicinity of salinized depressions which may or may not be related.

Figure 16-19 presents the seepage sites already discussed as well as some untested probable seepage sites in the midst of the salinized depressions. Figure 16-20 presents a close-up of these probable seepage sites along with a bore log in which gravel is indicated (a likely high velocity prior stream).

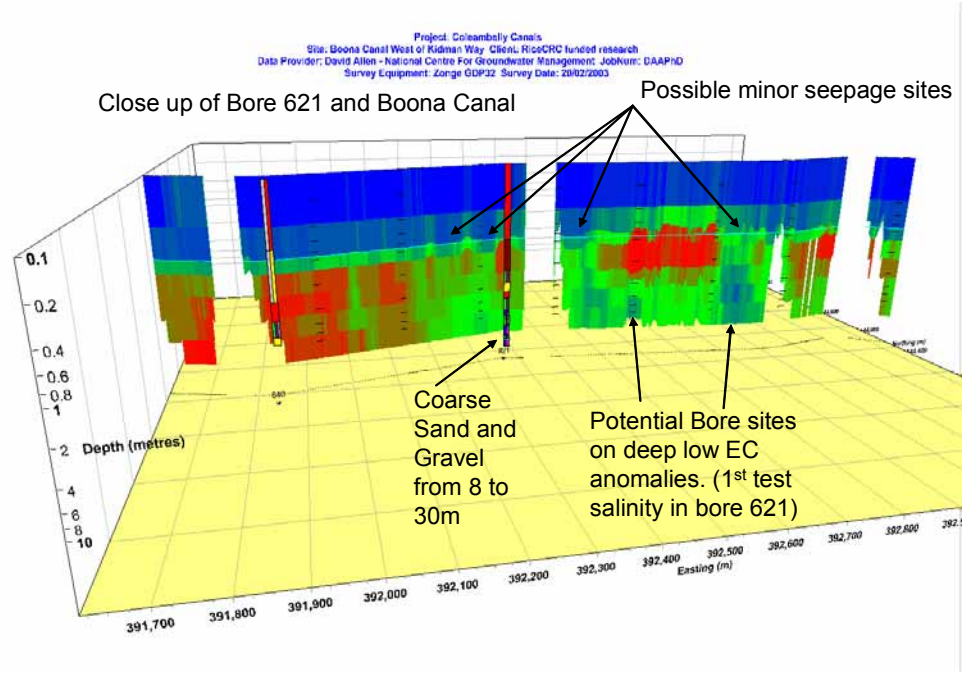

Figure 16.20 Sites on the Boona Canal where seepage is possibly occurring resulting in salinization nearby. As the water causing the shallow water tables appears to be fresh under the canal, potentially bores could extract it and use it to eliminate the problem. An existing bore has struck gravel indicating good permeability in a prior stream.

Figure 16-21 presents auger samples with EC_a logs and lithology logs as well as Yabby pump penetration depths along the canal (the penetration is typically proportional to permeability). Evidence for seepage came from low EC water in sandy auger samples. Seepage was then confirmed when the Landrover used for survey became bogged next to the canal at the low EC site seen in the EC ribbon.

The Yabby pump samples numbered on Figure 16-21 have lithology as per Table 16-1.

Figure 16-22 shows what four of the Yabby pump samples looked like and their relevance.

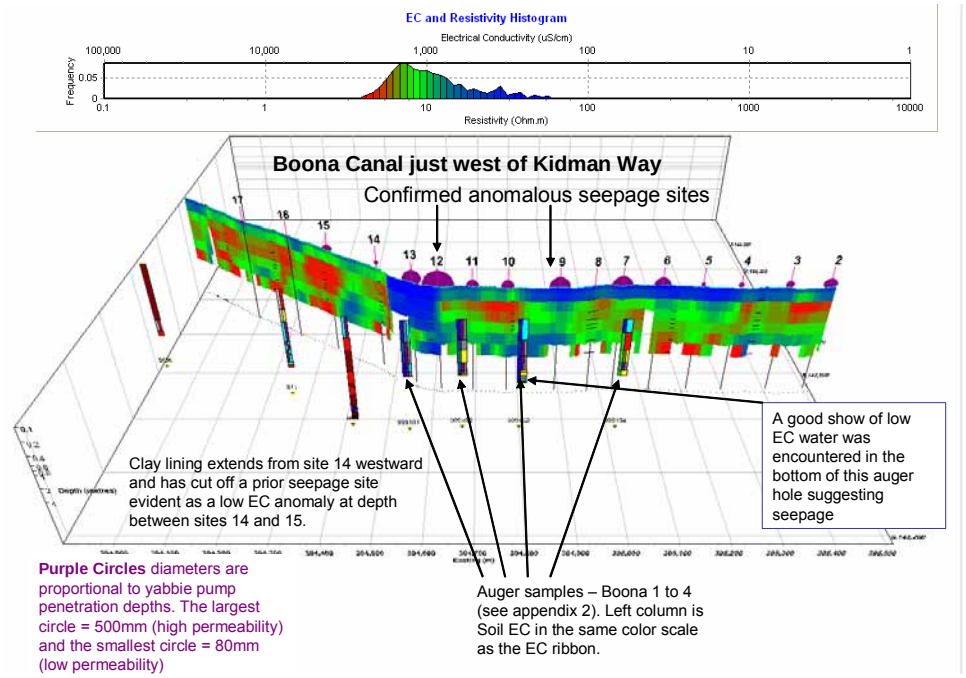

Figure 16.21 Boona Canal west of the Kidman Way indicating Yabby pump penetration depths and auger sample lithological and EC_a logs.

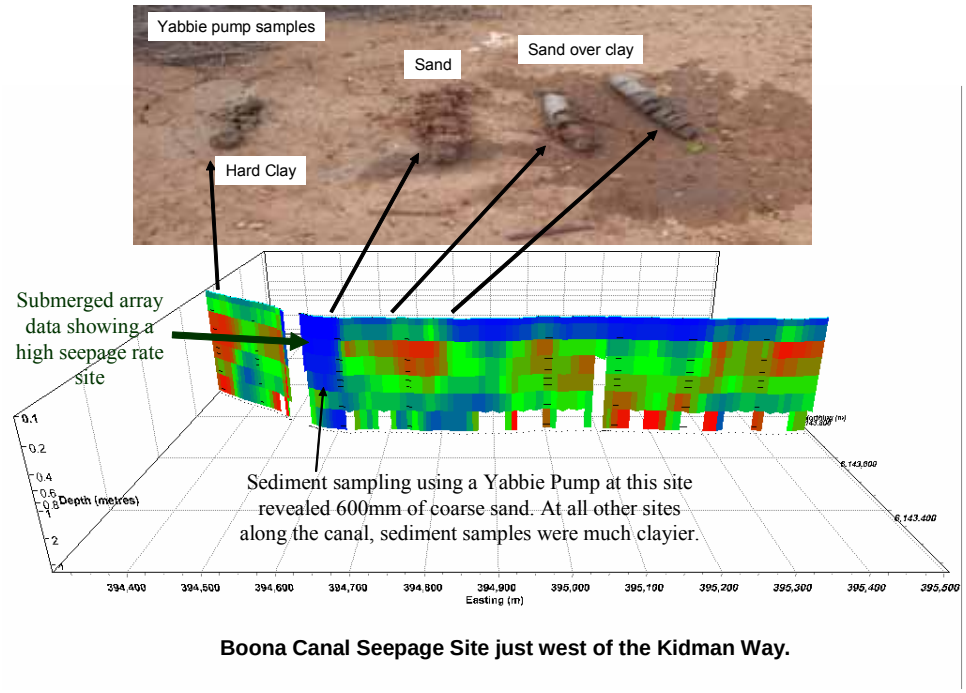

Figure 16.22 Some Yabby pump samples and their relevance to anomalies on an EC ribbon of part of the Boona Canal.

Site	Penetration	Sediment type	Zone 55 WGS84	
Number	(mm)	Log top to bottom (depths in mm)	E	N
1	200	80 soft sandy clay over 120 clay(ribbon 50)	395609	6143883
2	220	100 soft sandy clay over 120 clay(ribbon 50)	395498	6143730
3	140	20 soft sandy clay over 120 clay(ribbon 50)	395406	6143729
4	100	20 sand over 80 gritty clay (ribbon 30)	395298	6143727
5	80	80 clay (ribbon 60) Weed	395212	6143728
6	250	30 silt over 120 coarse sand over 100 clay (ribbon 30)	395121	6143728
7	310	300 sand over 10 clay	395031	6143726
8	60	10 sand over 50 clay (ribbon 20)	394970	6143724
9	320	200 sand (red at top) over 120 silty clay (ribbon 15)	394890	6143722
10a	300	20mm soft sandy silt; 100mm silty moist clay	394774	6143723
10	200	150 wet silt over 50 dry compacted silt (ribbon 5 sticky)	394774	6143723
11a	300	20mm soft silt; 70mm coarse sand; 100mm medium moist clay	394694	6143725
11	200	150 clayey sand over 50 silty dry clay	394694	6143725
12a	500	20mmSoft silt; 500mm coarse well sorted sand; 30mm silty sand	394616	6143727
12	160	120 red sand over 40 dry sandy clay	394616	6143727
13	300	Upstream of Regulator - 200 sand over 100 moist silt	394555	6143758
14a	100	20mmSoft silt; 100mm heavy grey clay - pressed dry at base	394466	6143842
14	80	80 clay (ribbon 40)	394466	6143842
15	150	150 clay	394339	6143923
16	60	60 clay (ribbon 50)	394231	6143988
17	80	80 clay (ribbon 30)	394099	6144086

Table 16-1 Boona Canal Yabby Pump Sediment Samples. Site numbers are posted on Figure 16-21 along with penetration depths.

16.3.2 Coleambally Main Canal - CIA, Gogeldrie Weir – Murrumbidgee River and Sturt Canal – MIA

This next case study is of a cross and long section of the Murrumbidgee palaeochannels between the Coleambally Irrigation Area and the Murrumbidgee Irrigation Area. The Coleambally Main Canal, the Murrumbidgee River and the Sturt Canal were used to conduct both floating 144m AXB geo-electric array survey and submerged 20m AXB geo-electric survey. Likely seepage of high economic significance appears to be occurring beneath the river and the Coleambally Canal. Various parties (the Pratt Group, and CIA) are preparing cases for remediation works. As this thesis is being written, expensive pondage tests are being conducted on the main canal at sites determined using data presented here. Political complications surround the case because the water in the canal is property of CIA but once seeped is the property of DNR. The seeped water is in aquifers connected to the river so any removal of the seeped water depletes the river. As the river water and groundwater are managed separately, more complications arise.

The floating array data collected for this case study is presented in Figures 1-1 and 1-2 (Chapter 1 'Introduction'). Figure 1-1 projects the EC ribbon upwards from the airphoto while Figure 1-2 projects it downwards. That way airphoto features on both sides of the canals and river can be compared with the EC ribbons. One can see how there is a distinct low EC zone surrounding the river and extending deeper than 30m (the limit of detectability of the array). This suggests that the river could be recharging the lower Calivil formation aquifer not typically thought to be connected to the river due to the general low permeability of the Lower Shepparton Formation (see Figure 16-1 of this chapter for geological explanation). One can see how this sort of data could be very important to groundwater flow modelling from this case study. Various prior streams are evident on Figures 1-1 and 1-2 as low EC anomalies in the EC ribbons and as deep rooted vegetation anomalies on the air photo. The depths of the prior streams also are evident. The zone of prior streams abruptly changes to higher EC (higher clay content) sediment part way along the Coleambally Canal. Obviously, bore pumping on either side of this abrupt change will have very different consequences. Again this means that the data are very valuable for correctly constraining groundwater modelling. The potential for a terrestrial system such as towed TEM is emphasized by this example because canals are not available everywhere for hydrogeophysical surveying.

Figure 16-23 presents the same dataset, somewhat extended, superimposed on satellite imagery. In Figure 16-23 the EC ribbon is projected downwards from the canals and rivers while in Figure 16-24, it is projected upwards. In Figure 16-24, the submerged array data has been projected upwards above the floating array data but on a different depth scale due to its different range of exploration depth. The submerged array data for the start of the Sturt canal and the River were presented as an introductory case study in the case studies overview chapter. Explanations of numerous geomorphological features and related groundwater recharge pathways are annotated in the various images. Figure 16-25 presents the entire submerged array dataset at this site. A lot of farm canals and drains were also surveyed as part of this dataset. Their significance will be later explained as part of the Dallas Clay Pan case studies. In Figure 16-25, there is a large contrast between the salinity under the farm and main canals due to different durations of inundation and resultant evapo-transpiration.

Cross and long section of the Murrumbidgee River at Gogeldrie Weir between the Coleambally and Murrumbidgee Irrigation Areas

Floating array 1 to 40m deep

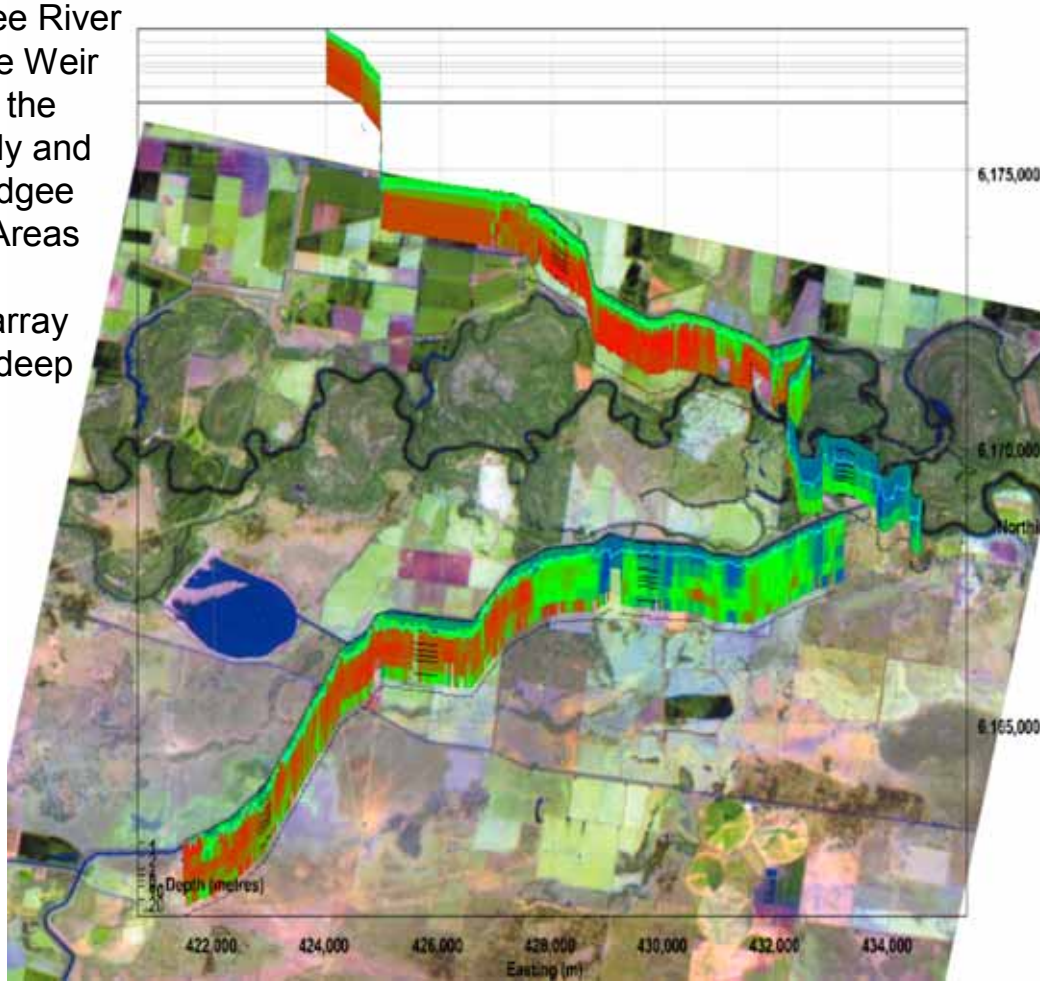

Figure 16.23 1 to 40m deep floating array EC ribbons around Gogeldrie Weir superimposed on false colour satellite imagery obtained from Coleambally Irrigation.

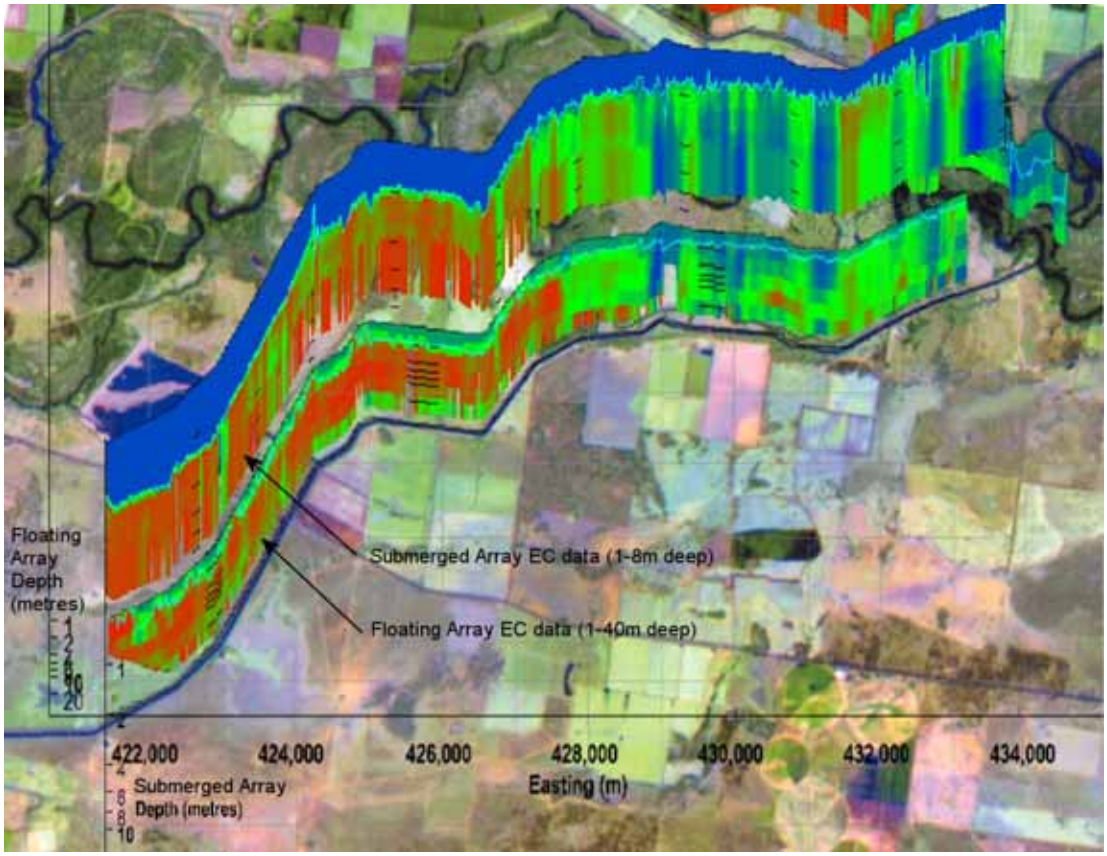

Figure 16.24 Floating array EC imagery as per Figure 16-23 but projected upwards rather than downwards from watercourses so that features on the other side of the watercourses can be compared with the ribbons. Submerged array EC data has been added above the floating array EC data for comparison.

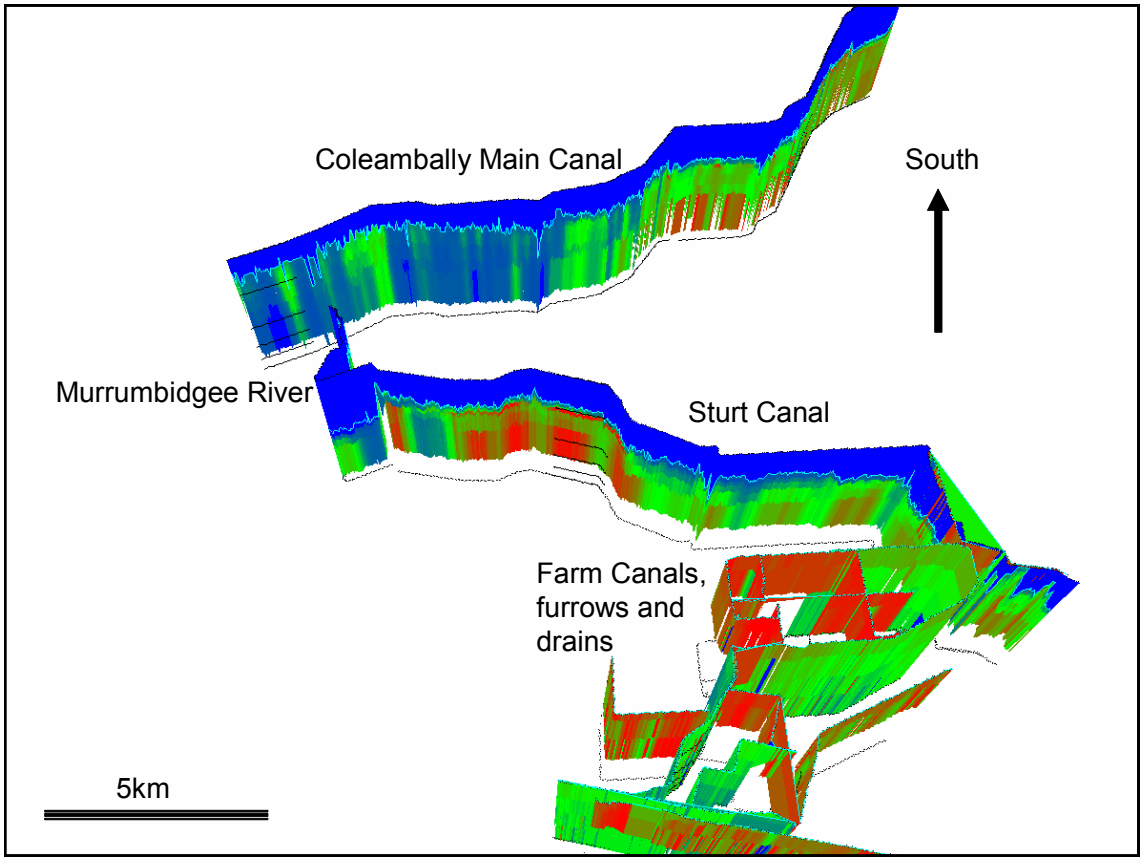

Figure 16.25 Submerged array EC data collected around Gogeldrie Weir and the Dallas Clay Pan on supply canals, the river, farm channels and drains.

Vertical pipe infiltrometers were installed, using EC imagery as a guide, along the Coleambally Main Canal and other Coleambally Canals (Allen, 2005b). Seepage was detected at some of the low EC anomalies and not others. An anomaly just downstream of the main canal offtake was of particular interest – the results are presented in Figure 16-26 while Figure 16-27 shows how seepage for the whole canal was calculated by dividing the canal area up into segments centred around each vertical pipe infiltrometer.

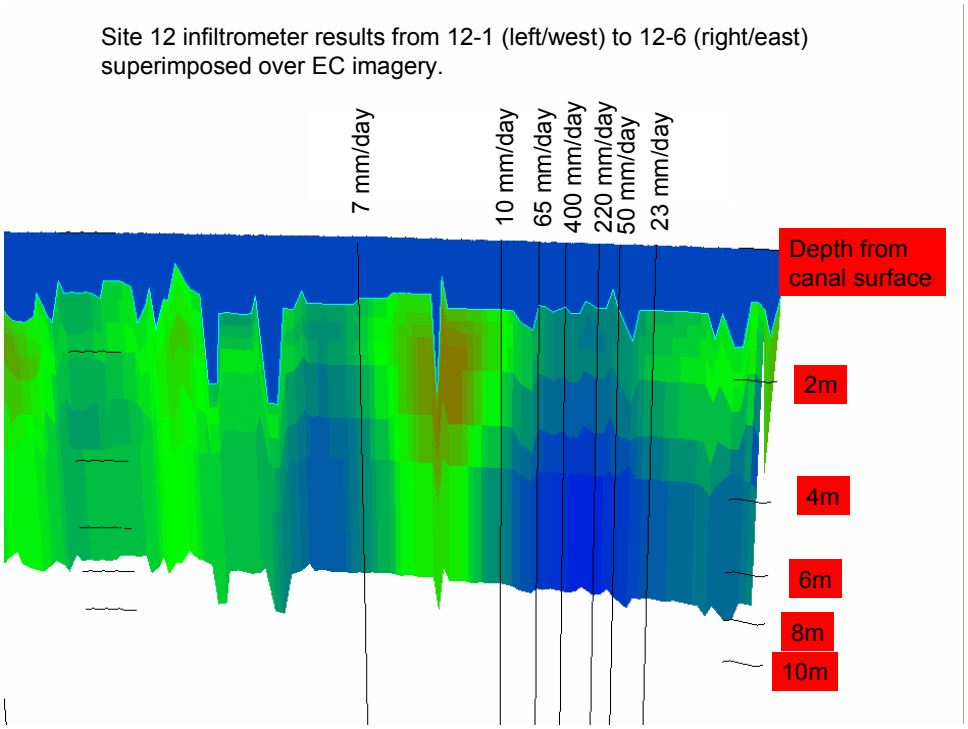

Figure 16.26 Vertical pipe infiltrometer results at an EC anomaly just downstream of the offtake for the Coleambally Main Canal. An alarming 400mm/day of seepage was detected in the centre of the anomaly even though it is just hundreds of metres downstream of the offtake.

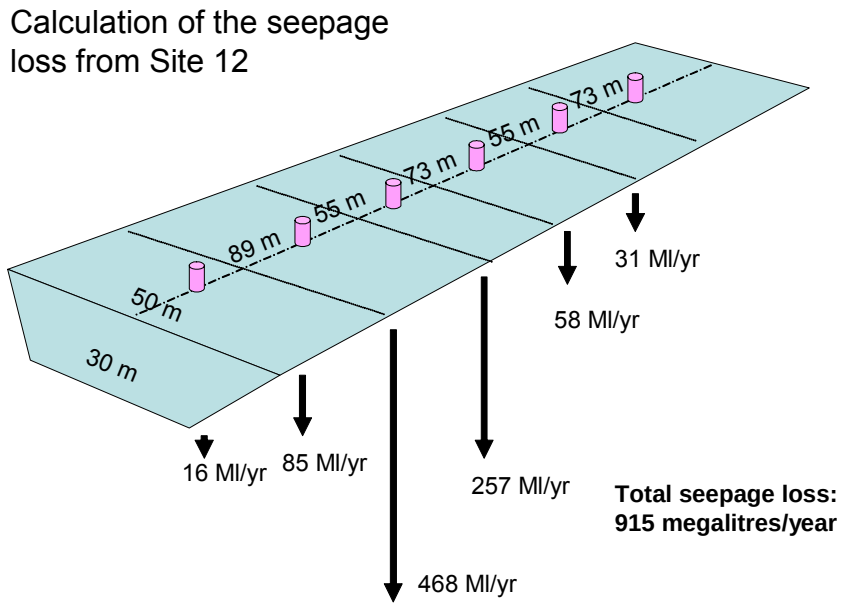

Figure 16.27 Calculation of yearly seepage losses just downstream of the Coleambally Main Canal offtake using vertical pipe infiltrometers placed along the length of the low EC anomaly that exists there. Beware that the infiltrometers disturbed the canal clay lining, found to only inches thick at this site, so are highly unreliable. Because of the unreliability of the seepage measurements, dependence of seepage on unmeasured variables and lack of data, a precise correlation between EC and seepage has not yet been established.

16.4 Coleambally submerged array EC ribbons

On the Coleambally and Murrumbidgee irrigation areas, at some sites, only submerged array data were collected. All submerged array data collection sites are displayed on Figure 16-28. Most of these sites are farm canals and therefore will be discussed in the next chapter however one that has not already been discussed, the Argoon/Yamma main canal will be discussed here.

16.4.1 Argoon/Yamma Main Canal anomalous seepage site

A site on the Argoon Main Canal was investigated to isolate a seepage hot spot suspected due to growth of deep rooted vegetation near the canal. Figure 16-27 shows the part of the

submerged array EC data collected there along with Yabbie pump samples. The seepage sites are clearly evident as low EC anomalies.

Figure 16.28 Submerged array surveys, marked as blue lines, conducted in the Murrumbidgee Irrigation area and the Coleambally Irrigation Area

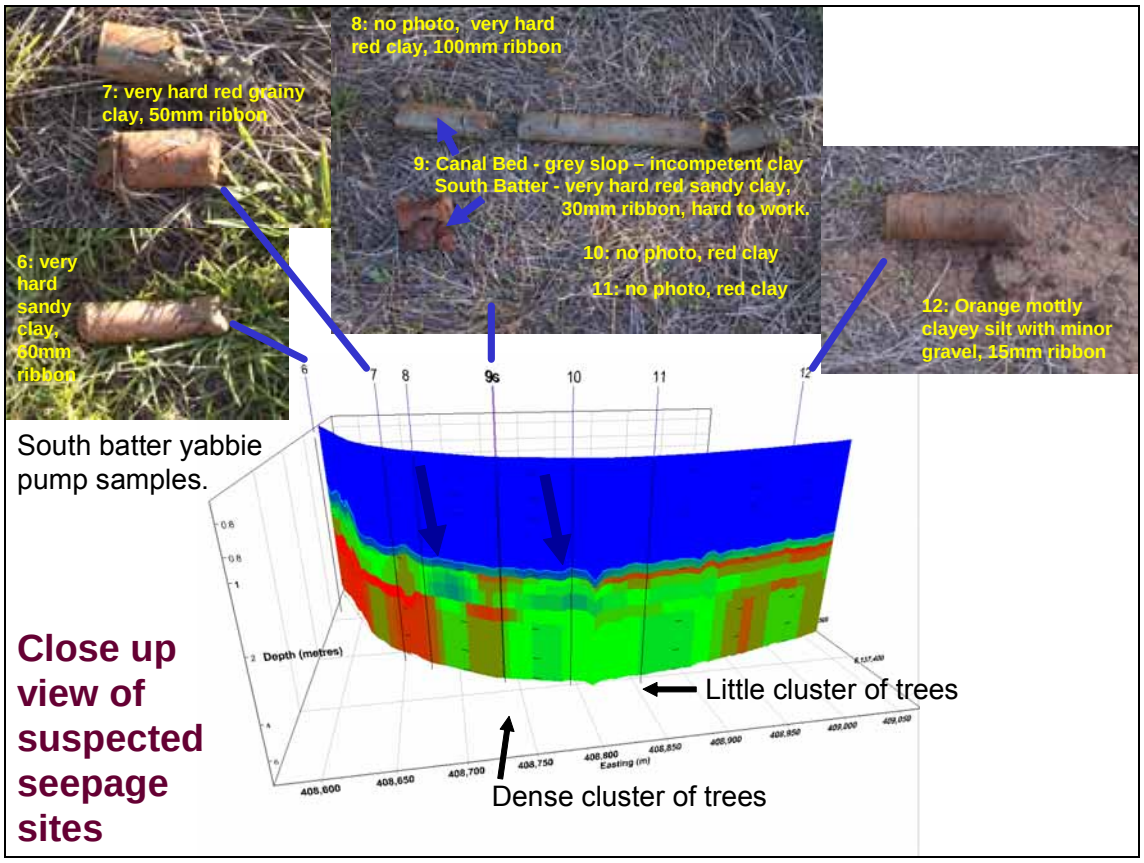

Figure 16.29 A suspected seepage site on Argoon Main Canal revealed in submerged array EC data. Site 9 was sampled on both the canal bottom (700mm penetration) and the south batter (60mm penetration)

Yabby pump sediment core sampling was conducted on the south batter of Argoon Main Canal rather than the bed because sampling under 1.9m of flowing water is more difficult than under 0.8m of water. Under 1.9 m of flowing water, it is difficult to press down on the pump as the operator keeps being pulled away by the current and their submerged eardrums are impacted when the pump pops out of the sediment. Therefore, canal bed sampling should be left until the canal is just emptied.

At site 9, the canal bed was sampled because it was obvious that sediment in the batter at that site did not explain the low EC and clump of trees at that site. A 700mm sloppy, incompetent, clay sample was obtained from the canal bed at that site suggesting that seepage occurs there through low exchangeable sodium percentage clay. Submission of the sample for ESP analysis is recommended.

Between sites 4 and 12 there exists a very hard red grainy clay in the south batter which appears to be impermeable. In some places it is sandy but still clay matrix supported. This layer is not indicated directly by the EC image which is imaged from the canal bed 1 metre below the batter. The sample taken in the canal bed at site 9 confirms that the clay layer is less than 1 metre thick and does not extend under the canal bed at that site.

Generally, the south batter core suggests that the site is highly stratified with little similarity in sediment between the canal batter and canal bed levels.

Seepage is indicated by continuous low EC paths from the bed of the canal downwards near sites 8-9, 10. Clusters of trees at sites 9 and 11 suggest destinations of seeped water which are close to source sites (8-9 and 10).

16.5 Murray Irrigation Canals

Electrical conductivity (EC) imaging was used to identify lengths of irrigation canals with anomalously high seepage rates in the Denimein part of the Murray Irrigation Area in the summer of 2004/2005. Good correlation was obtained with sediment samples extracted from canal beds using a yabby pump. Absolute seepage measurements of about 10mm/day were obtained previously using pondage tests at an anomalous site. Point seepage measurements were conducted using Idaho seepage meters and bladder type seepage meters. Almost all of these measurements indicated undetectable seepage rates. This undetectable seepage was probably partly a result of record rainfall that occurred the week before the trials. It is believed that seepage in the tested canals is negligible and predominantly through canal walls – the beds of the canals having silted up over tens of years. An attempt was made to measure sediment permeability at selected sites adjacent to the canals using a Guelph Permeameter. Cracks in the clayier soil lead to questionable results; however, seepage of 10^{-3} cm/sec was obtained on the sandier site and about 10^{-6} cm/sec on the clayey sites (see Allen 2005a, included on the thesis DVD, for full details). Use of a submerged 20m Allen Exponential Bipole Geo-electric array towed using a 4wd mounted boom for EC imaging proved to be efficient. A survey speed of 7 km per hour is practical and 15 to 30 km of canal obstructed by frequent fences, trees and regulators could be surveyed per day. Murray irrigation canals are crossed by numerous fences, unlike canals of some other companies, but they do typically have good vehicular access next to them. Use of a canoe or boat to tow the array should be avoided on small canals

due to the problem with the fences and weed growth which fouls outboard motor propellers and is only practical with the assistance of a 4wd mounted crane for lifting it over the numerous fences crossing the canals.

16.5.1 Early ANCID funded surveys

Murray Irrigation Limited funded seepage measurement trials on the Dahwilli Main canal as part of a study by ANCID in 2002. Pondage tests were conducted to get absolute values for seepage at a few sites and various methods of measuring electrical conductivity were used to get low cost spatial detail indicative of seepage rates. Most of the selected sites were very similar and anomalously sandy. One heavy clay soil site appeared to be useful as a contrast but pondage test results indicated a similar seepage rate to the sandy soil sites. As a result, poor correlation between electrical conductivity and pondage test seepage rates was observed.

16.5.2 Rice CRC and Murray Irrigation funded trials

RiceCRC and Murray Irrigation funded work in the summer of 2004/2005 in order to re-attempt to measure seepage at one trial site and some clayey soil control sites. The locations of the more recent surveys are presented in Figure 16-30.

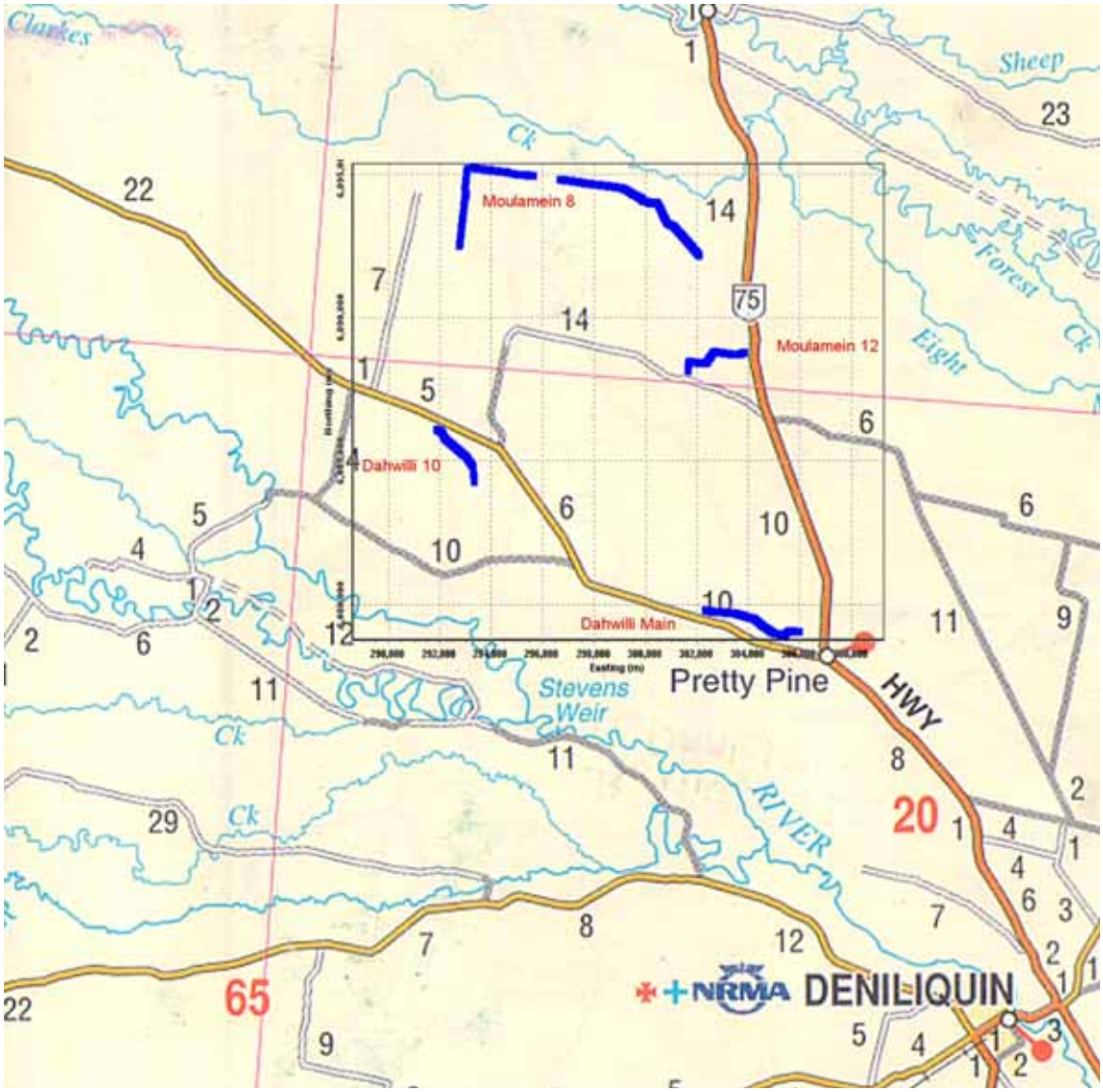

Figure 16.30 Location of Denimein EC imaging trials. ANCID trial sites are not shown but were on Dahwilli Main Canal.

The distribution of EC within the images produced is evident in Figure 16-31. A significant component only attributable to unsaturated sands is present in the histogram due to its very low EC. The results from all the Denimein Canals are presented in Figure 16-32 along with photos of yabby pump samples. More magnified images of the individual segments are available in Allen (2005a) however the Dahwilli main segment has been reproduced here as Figure 16-33. This segment is anomalously sandy throughout and therefore appears entirely blue in the colour scale on the main image (Figure 16-32). For this reason, no significant correlation between seepage and EC could be detected within the site by Street (2001). Figure 16-33 does however show variation within the site. Figure 16-34 shows the results of the ANCID trials conducted previously at the site

on which Street (2001) reported. Note the difference in detail between the submerged array data and the dipole-dipole array data collected earlier. The 20m submerged array detected detail accurately but, being a short high efficiency array, could not attain the effective depth of penetration needed to pick up the water table detected by the dipole-dipole array previously.

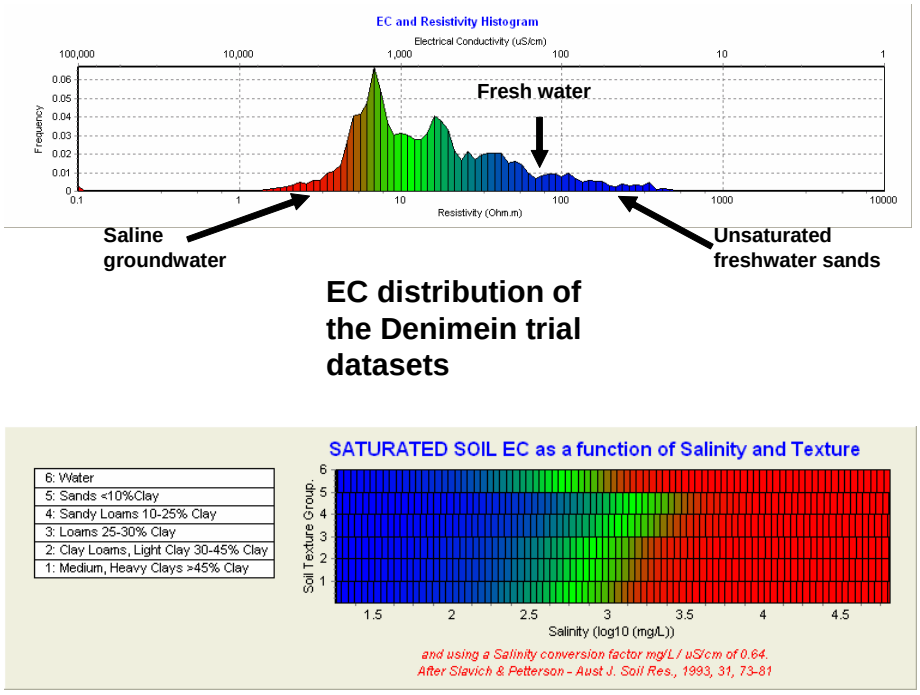

Figure 16.31 EC distribution of the Denimein trial datasets.

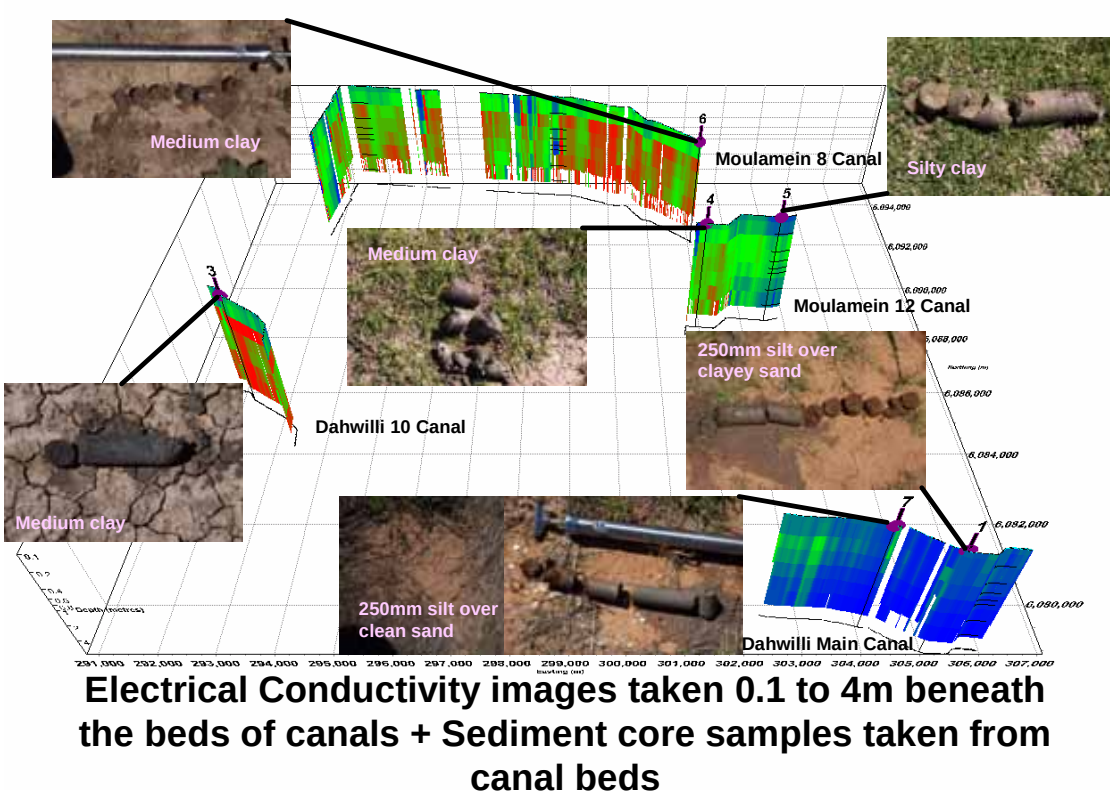

Figure 16.32 Denimein canal submerged array EC images and canal bottom sediment cores.

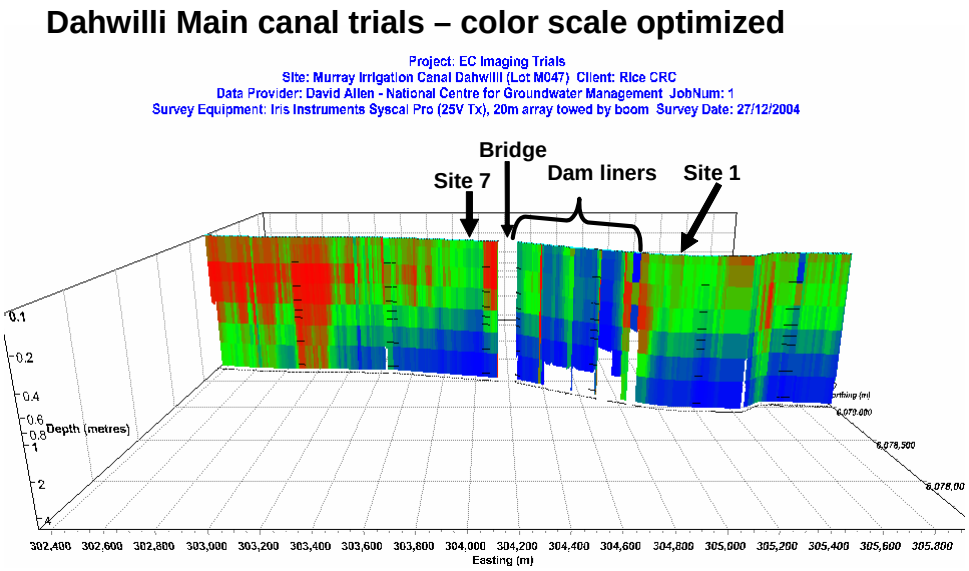

Figure 16.33 Dahwilli Main Canal submerged array data with color scale optimized (compare Figure 16-32 – SE corner). Dam liners trials and numerous seepage tests have been conducted at this site.

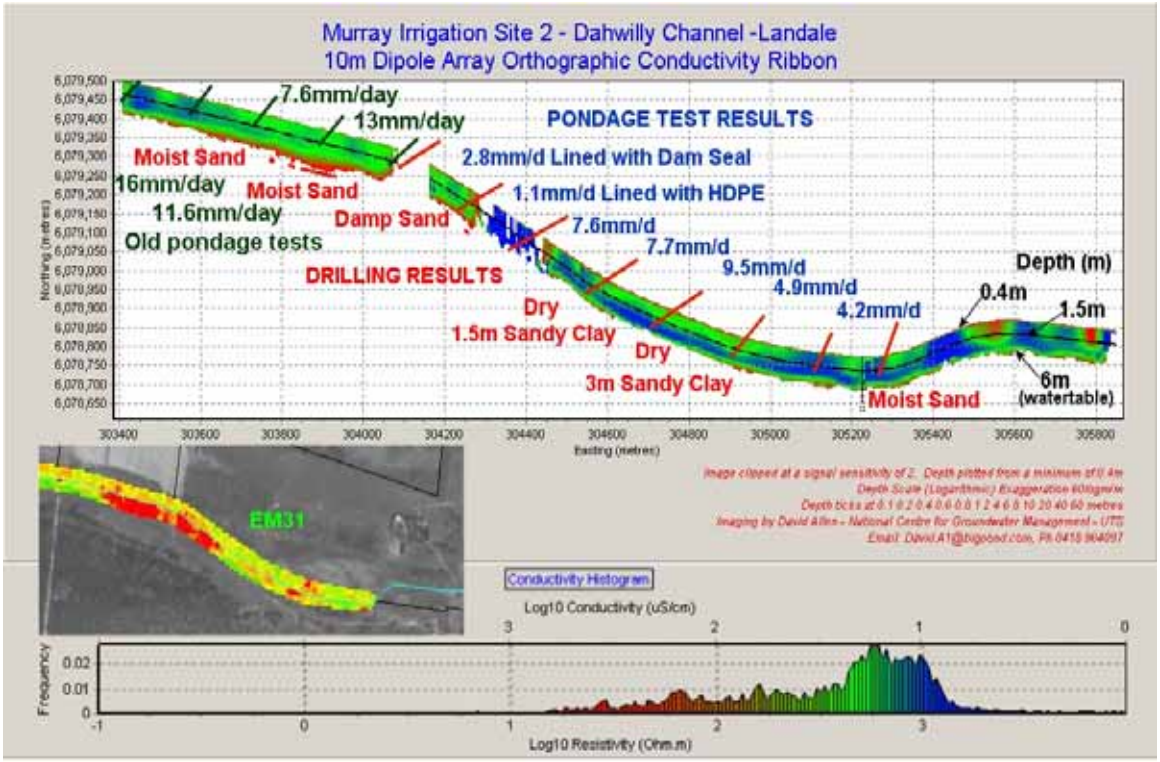

Figure 16.34 The Dahwilli Main Canal site of Figure 16-33. Data collected using an EM31 and ANCID floating dipole-dipole array with 10m dipoles compared to pondage test results and drill core summaries. Beware – the EM31 colour scale is the inverse of the geoelectric array colour scale.

Note that the 250mm of silt at the bottom of the Denimein Main Canal has not been detected by the submerged array due to lack of EC contrast with the underlying sand. The pondage tests of Figure 16-34 show no significant correlation with EC due to lack of a low seepage control site. Seepage there appears to be abated by the 250mm of silt on the canal bed so it is probably principally through the lower parts of the canal walls that Idaho meters could not test due to the steep slope of the walls. The EM31 data is seen to correlate with the geo-electric data but, since it is collected only at one depth, is much more difficult to interpret.

In summary, the 20m submersible EC array is a device capable of correlating with clay content under Murray Irrigation canals very effectively. Use of much longer arrays on Murray Irrigation canals should be avoided because of the numerous fences crossing the canals.

16.6 Murrumbidgee Irrigation Canals

A great number of Murrumbidgee Irrigation Canals were surveyed within the Dallas Clay Pan as located in Figure 16-28 and displayed in Figure 16-25. These will be studied in more detail in the next chapter on farm channels and drains. In earlier ANCID trials, other canals were surveyed using a floating dipole-dipole array. They were located (see Figure 16-28) north of Griffith, one north east of Lake Wyangan along a hillslope, one north of Lake Wyangan beside a valley experiencing waterlogging problems, one adjacent to the Warburn hard rock quarry and one on the banks of Lake Tabbita. With the exception of the Warburn survey, the 2002 surveys were conducted on sites with little sediment contrast and marginal variation in seepage and therefore are not very interesting. Because they were subject to pondage testing as well as EM31 survey, they have all been presented here as case studies.

The Warburn quarry site overlies hard rock with fractures in it. Adjacent to the canal there is a deep quarry which permits free drainage of the fractures. The canal has been clay lined. The clay lining is not evident in the EC imagery because the floating dipole-dipole array lacks the necessary resolution; however the hard rock distribution is clearly visible (Figure 16-35). The other three sites are presented in Figures 16-36, 16-37 and 16-38. All of these sites, surveyed with five and ten metre dipole dipole-dipole arrays were inverted by Zonge using TS2DIP and are a good example of such inversion, yet also, a good example of the limitations of the dipole-dipole array. The geophysics seems to have reliably shown consistent conditions under the canals as they should have considering that the drilling results and pondage test results also are very consistent. Beware – the EM31 colour scale is the reverse of the geo-electric array colour scale.

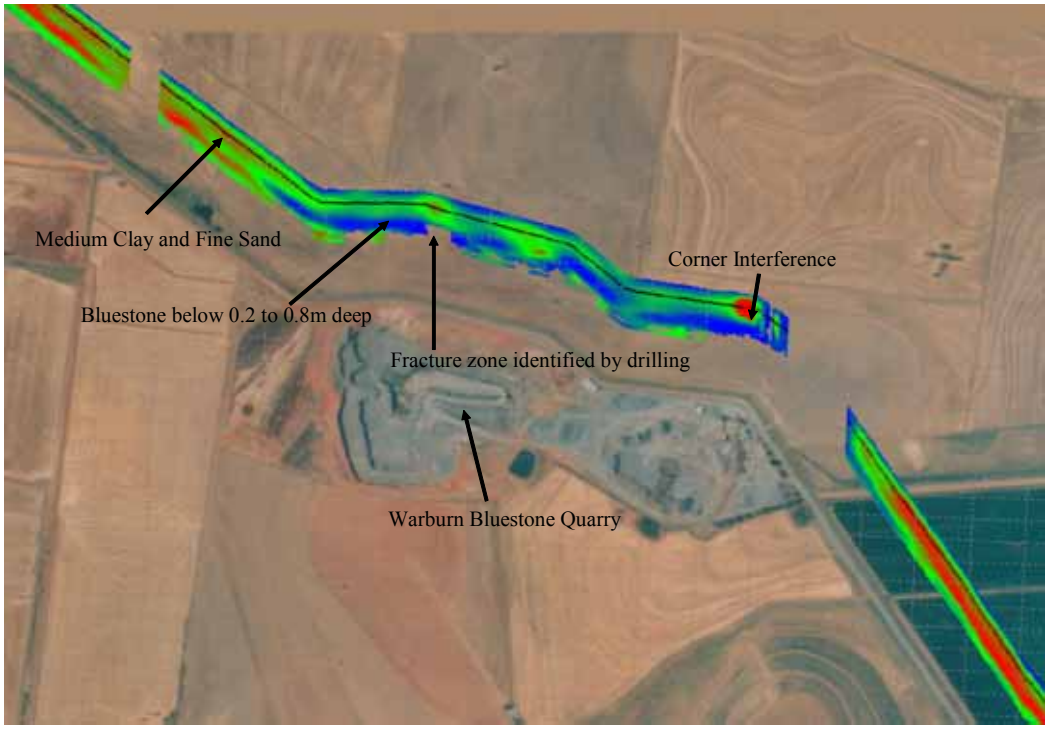

Figure 16.35 Warburn Hard Rock Quarry NW of Griffith, MIA. An example of hard impermeable, but fractured, rock beneath an irrigation canal.

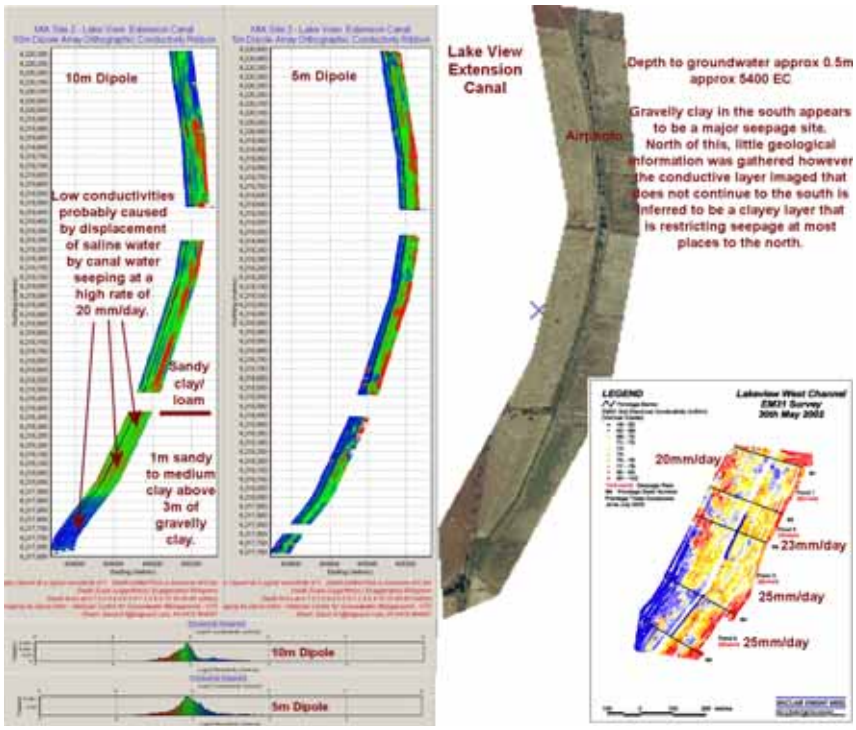

Murrumbidgee Irrigation Site 2 Sloping valley with shallow water table

Figure 16.36 Five and ten metre dipole-dipole array, EM31, drilling and pondage tests conducted on Lake View Extension Canal.

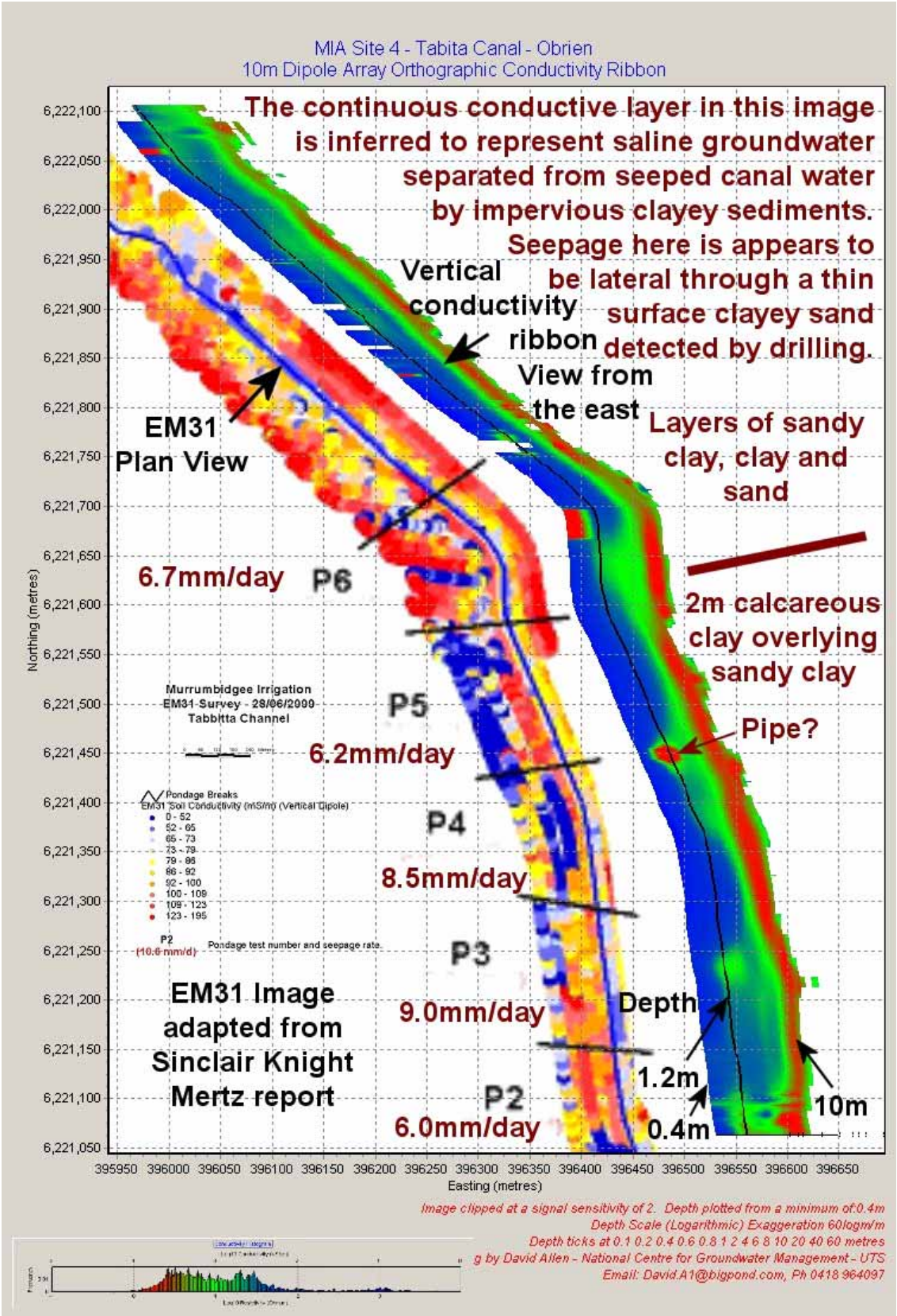

Figure 16.37 Ten metre dipole-dipole array, EM31, drilling and pondage test data on Tabita canal, MIA. Note that the EC ribbon is projected from the east.

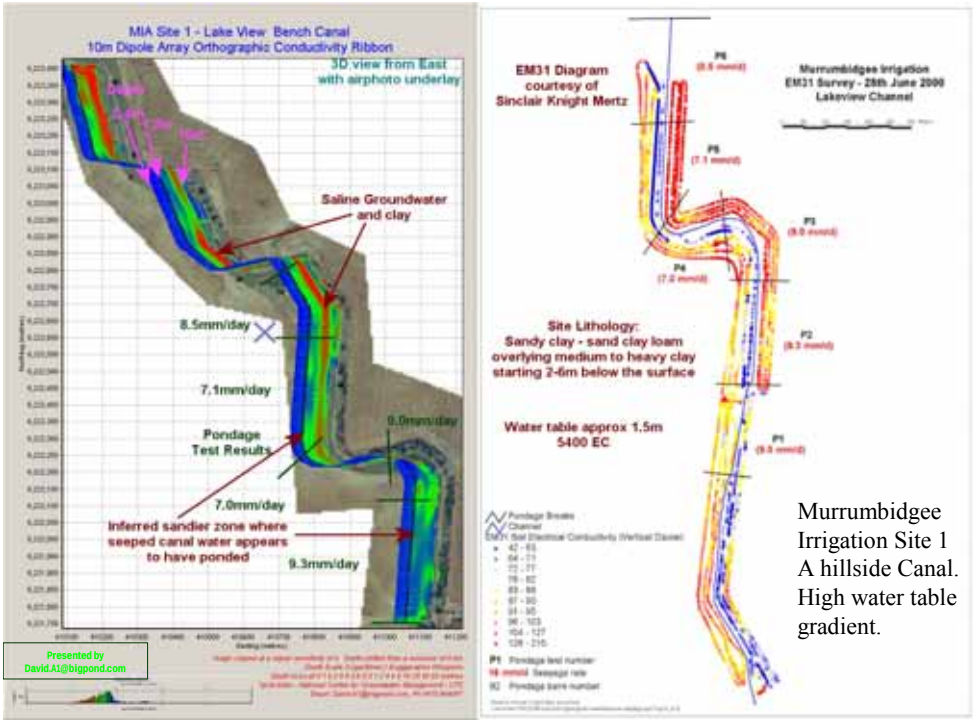

Figure 16.38 10m dipole-dipole array, EM31, drilling and pondage tests conducted on the Lake View Bench Canal north of Griffith. Note that the EC ribbon is projected from the east (ie. as if the view was looking down from east of the image).

16.7 Wimmera Mallee Irrigation Area Canals

Wimmera Mallee Irrigation Area in north west Victoria has canals running across broad undulating hills containing a lot of permeable geological units. Losses from the canals have been quoted as 80 – 90% (ANCID seepage report, 2003). The canals are rarely filled so most loss is likely to be occurring upon wet-up of the canals. Three sites on the Toolondo canal were surveyed using 5 metre dipole-dipole arrays as part of ANCID seepage detection trials. The locations of the trails are displayed in Figure 16-39. Results are presented in Figures 16-40, 16-41 and 16-42. Notice that at the west site (Figure 16-40) that pondage tests were centred over an EM31 anomaly (note that the EM31 colour scale is the opposite of the geo-electric colour scale). The EM31 anomaly only represents a surficial low EC anomaly at this site and, therefore, seepage at this site is not impressive. If the geo-electric array data had been available for siting pondage tests, then the deep low EC anomalies at the other end of the site would no doubt have been picked as prime high seepage rate sites that should be pondage tested.

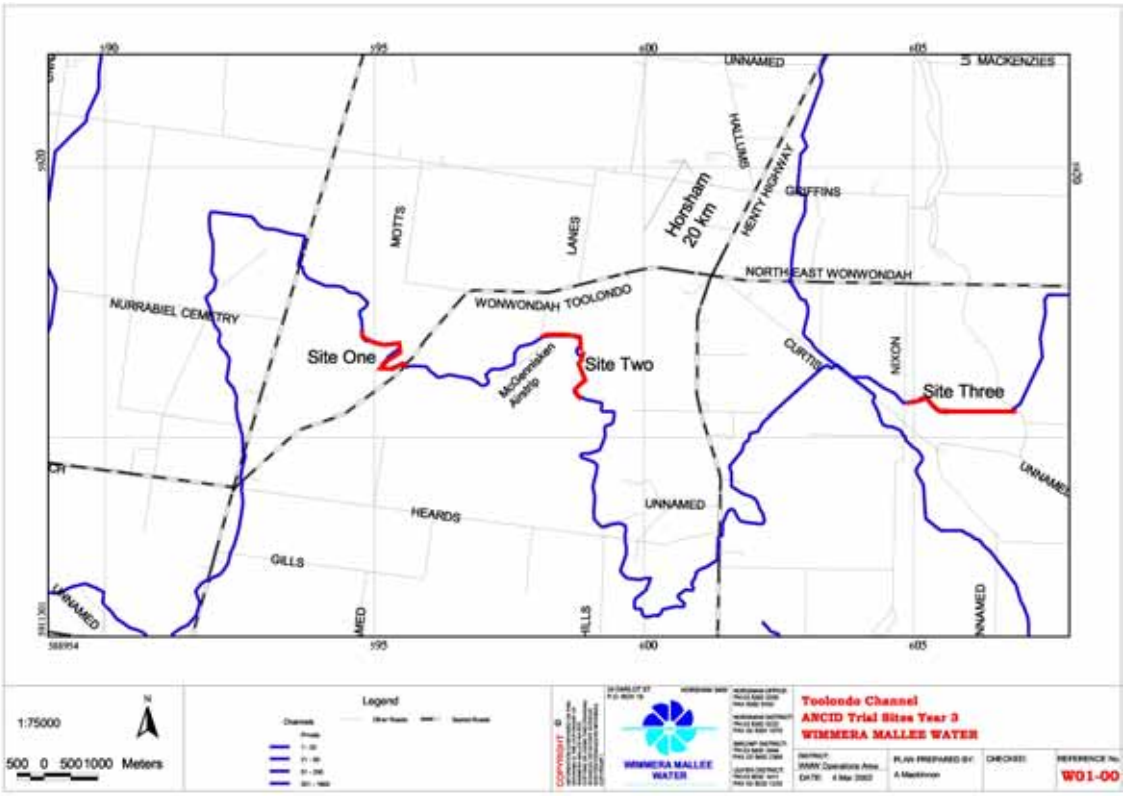

Figure 16.39 Locations of Wimmera Mallee EC imaging trials on the Toolondo Channel south of Horsham.

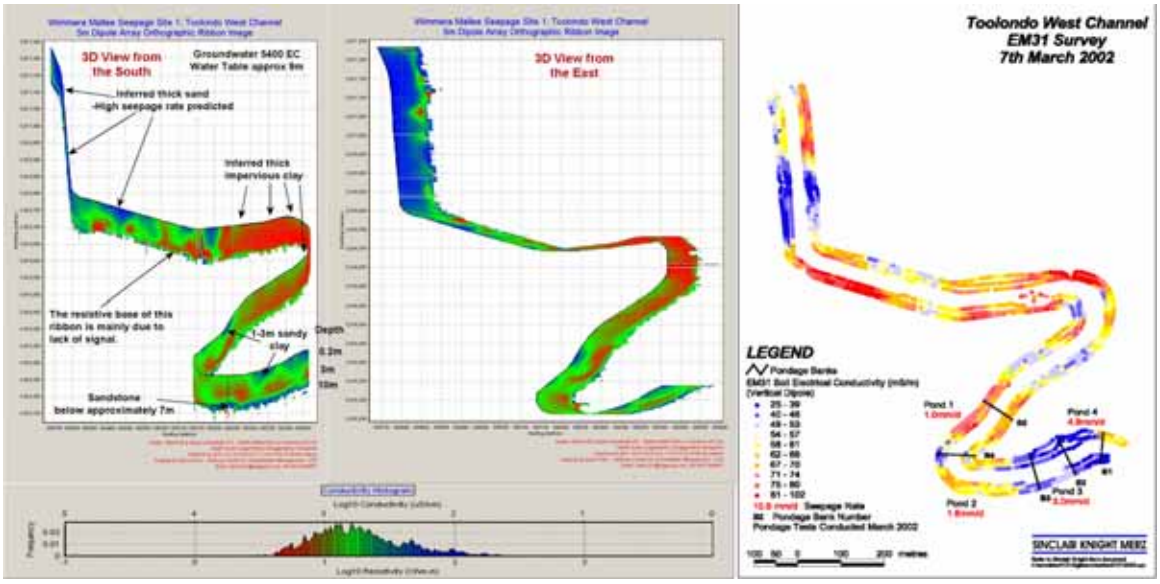

Figure 16.40 Toolondo Channel west EC imaging site. Dipole-dipole array, EM31, and pondage test data.

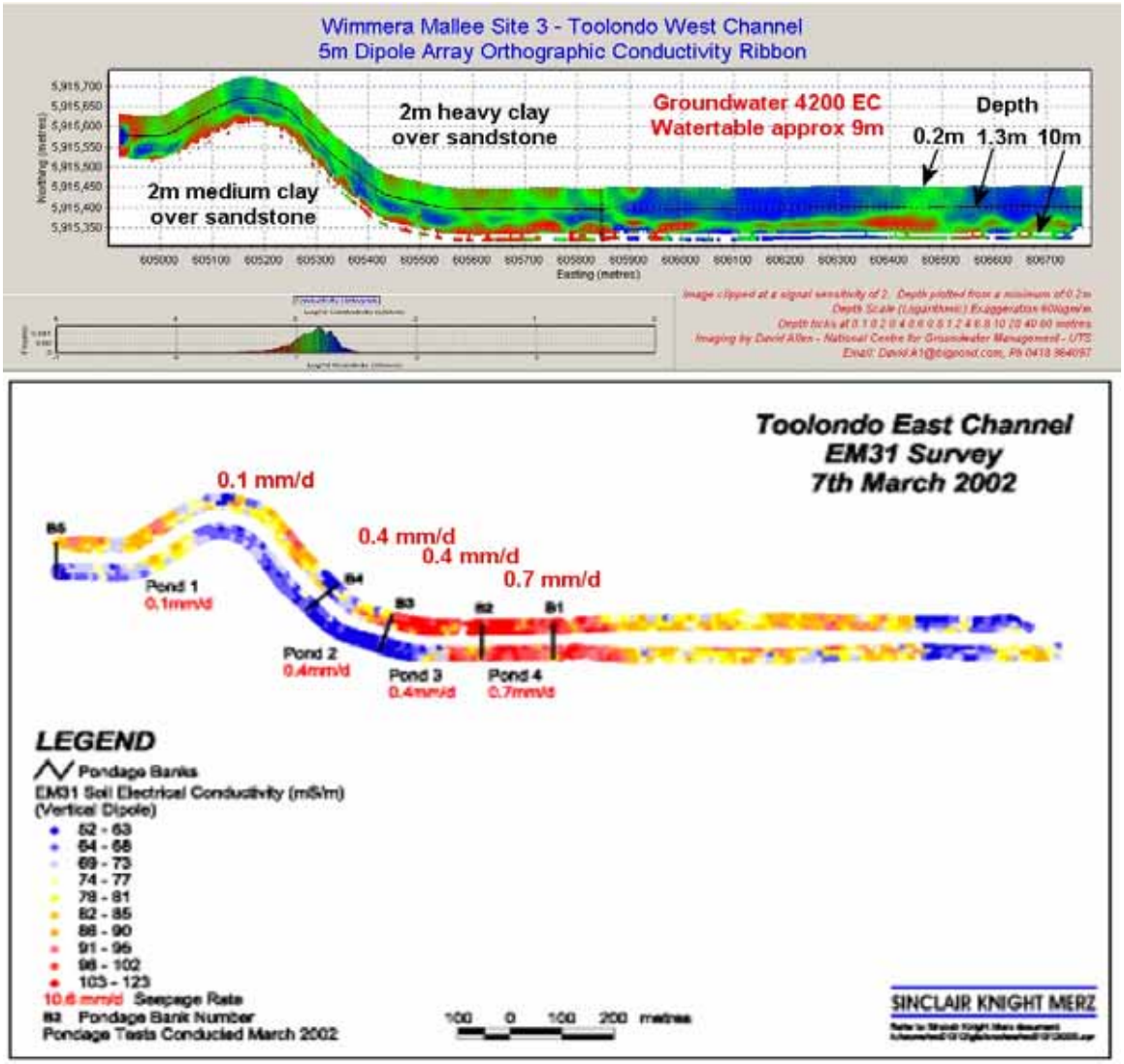

Figure 16.41 Toolondo Channel east site. 2m heavy clay over sandstone. Seepage rate here is unanimously low. Higher EC seems to relate to increased seepage probably due to saturation differences in the clay beneath the canal.

The central site (Figure 16-42) has comprehensive pondage testing and drilling conducted along it. Correlation between sandy channels and low EC anomalies is obvious once we consider that drilling adjacent to the canal sometimes does not target what is under the canal adjacent to the drill hole. Seepage also correlated well except in one pond with a seepage rate of 1.1mm per day. This pond seems to be underlain by low EC sand that is cut off all around by clay.

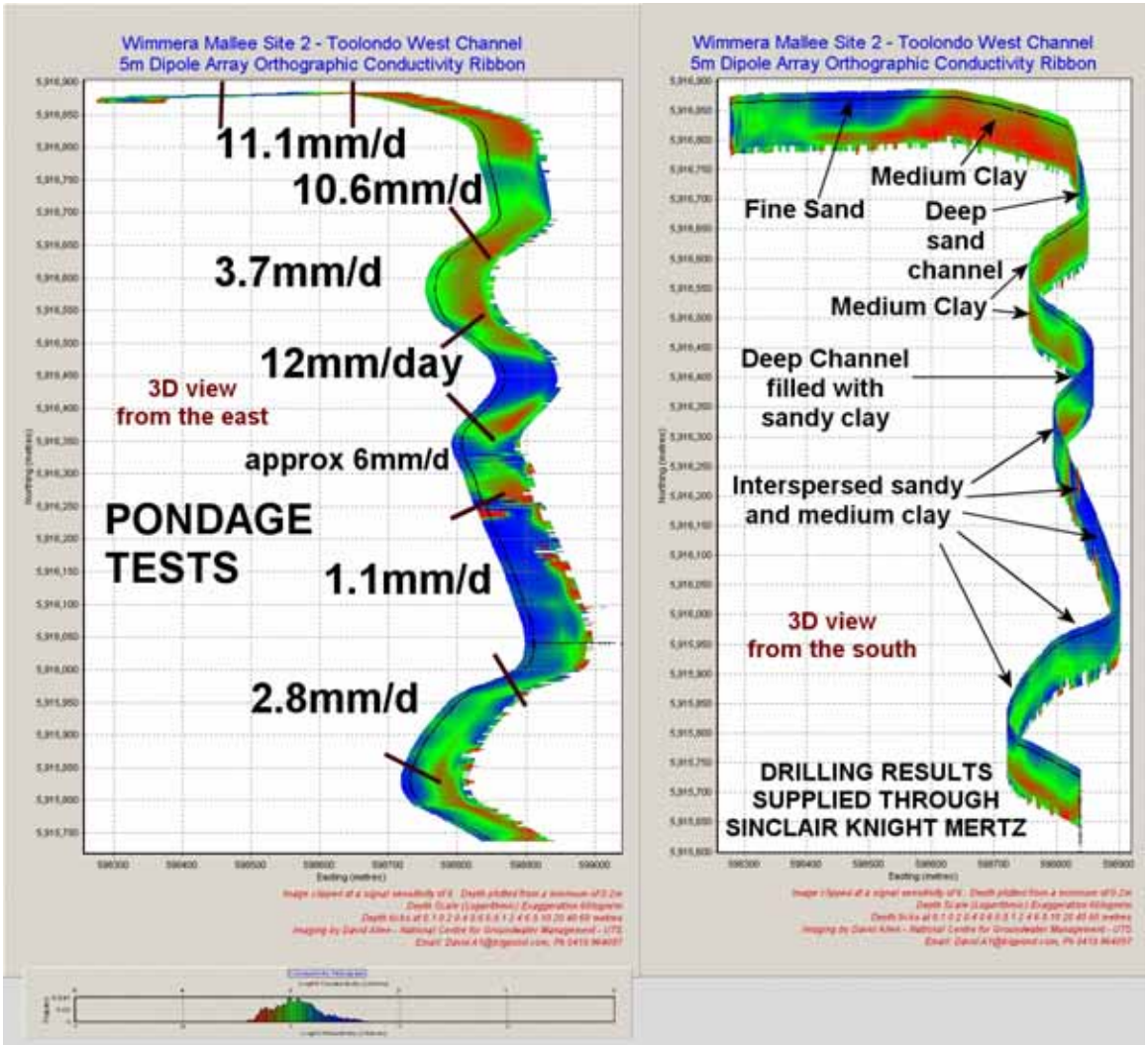

Figure 16.42 Toolondo Channel central site showing 5m dipole-dipole array data, pondage tests and lithology adjacent to the channel.

Comparison of entire survey sites with each other can be effectively conducted using the EC histograms from each site. Figure 16-43 presents a comparison of the Landale site on the Dahwilli Main Canal in Murray Irrigation (see Figure 16-34) with the Toolondo canal sites. Annotation at the top of the histograms shows how the different sites have different proportions of salinity, saturation and clay content. Recall that the Landale site is over unsaturated sand. Figure 16-44 then presents some Murray River Histograms overlying saline and hypersaline groundwater. They are included here for the purpose of comparison with Figure 16-43.

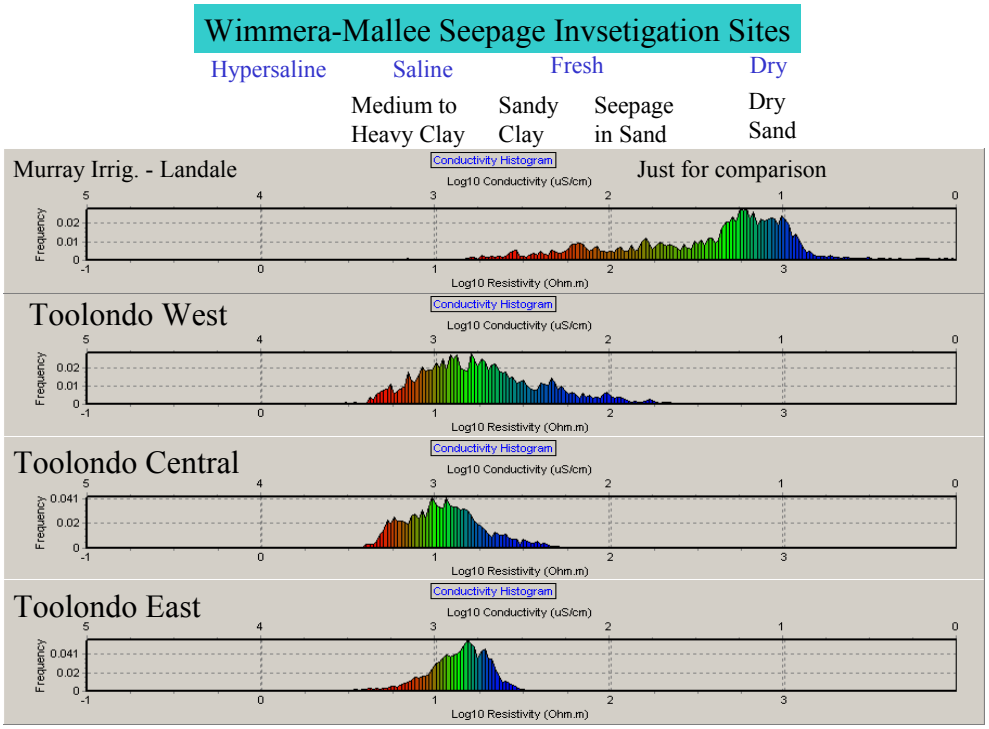

Figure 16.43 Murray Irrigation and Wimmera Mallee Irrigation seepage site EC histograms.

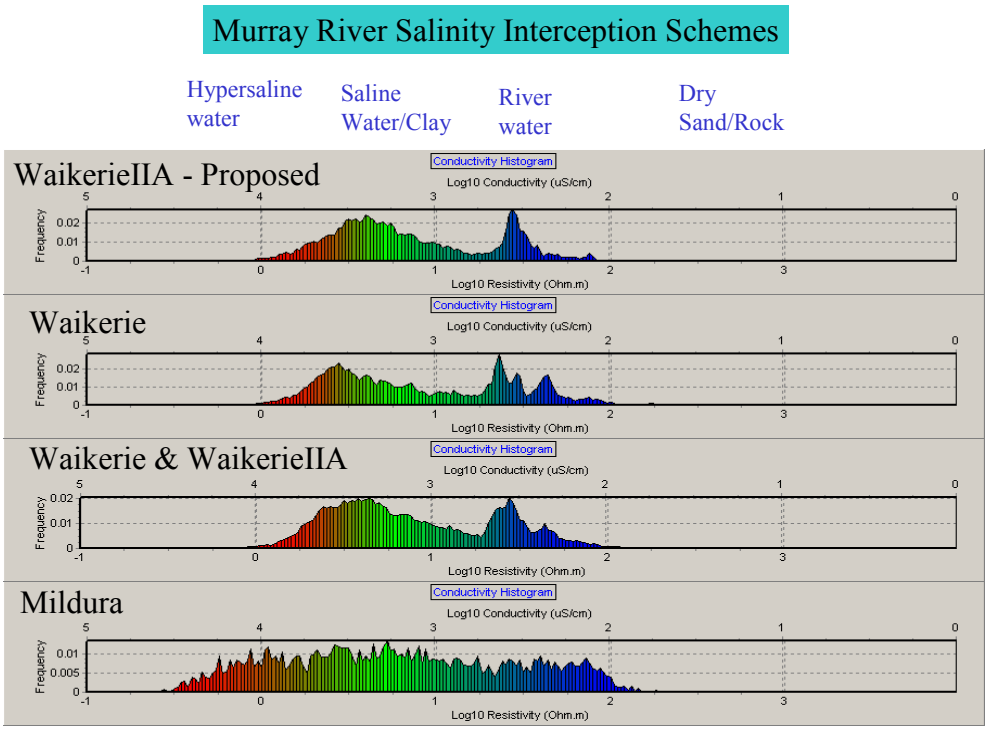

Figure 16.44 Murray River saline inflow site EC histograms for comparison with Figure 16-43.

16.8 Concluding summary on geo-electric survey of supply canals

Electrical conductivity survey of sediment beneath supply canals is useful for identifying seepage pathways beneath the canals. Lateral seepage from canals can be detected in other ways including observation of vegetation. Prolific seepage, however, typically occurs downward through seepage pathways that lead to deep aquifers. Multi-depth EC imaging can confirm where pathways extend to great depth. The pathways normally are characterised by low EC due to fresh water flushing of sediment, typically of minimal clay content, although in places clay with granular appearance forms the seepage pathway. Unsaturated sediment and hard rock may complicate interpretation at some locations. Once deep seepage pathways are found then canals can be remediated strategically just at prolific seepage sites. Additionally, some of the pathways may be ideal for managed aquifer recharge and could be investigated further.

Canals are best surveyed with a submerged array due to the need to have high vertical resolution near the canal bed combined with a pragmatic survey solution. Submerged arrays do not have to be as long as floating arrays in order to image to the same depth which means that they can more readily pass over the numerous obstacles that exist along canals.

Seepage requires more than just a pathway. A thin fragile silt and clay clogging layer just under the canal can drastically inhibit seepage until disturbed or left to dry and crack. Additionally, the water needs to have somewhere to go and many aquifers may be quickly filled by seepage. For these reasons, correlation between seepage and EC alone, even a combination of EC at multiple depths, is not perfect.

CHAPTER 17 - NETWORKS OF FARM CANALS AND DRAINS - CASE STUDIES

Farm canals nearly always seep much more than major supply canals because they are only temporarily saturated. This is demonstrated on the following EC ribbon images by Idaho seepage meter readings supplied by Saud Akbar of NSW Agriculture. One of the farms is in the CIA and the other is in the MIA near Yanco (refer back to the map of submerged array survey sites – Figure 16-28). The EC histograms for the farm canals are much more conductive than those for major supply channels. This is because farm canals are shallow and therefore the beds of them include soil layers where a large concentration of salt has built up via evapotranspiration. Farm canals can be surveyed quickly and, therefore, cheaply using a submerged array towed by a 4wd mounted boom because farmers typically maintain good vehicular access along their canals and drains.

Figures 17-1 and 17-2 present farm canals with very uniform but high seepage rates. The uniform seepage rates are reflected by uniform EC images. There is a very distinct vertical gradient in EC at this farm so Figure 17-2 has been provided as a 100% vertically damped EC ribbon duplicate of Figure 17-1. With the vertical colour scale damping, one can see that lower EC correlates, at least a little, with higher seepage even though variation is minor.

Figures 17-3 and 17-4 present farm canals overlying both sands and clays. They represent surveys repeated 1 year apart. The first was conducted with a canoe and took 2 days due to obstacles along the canals. The second was conducted with a boom extending from a Landrover and took only 3 hours even though several extra canals were surveyed. Figure 17-4 (but not Figure 17-3) includes some of the Murrumbidgee Irrigation Main Canal (in the foreground) which seems to have EC beneath it that is very similar to beneath the adjacent farm canal. At this farm, there seems to be good correlation between low EC and high seepage but moderate and high EC seems to relate to variable moderate seepage rates possibly due to presence of structured permeable clay. Under the canal in the lower right of Figure 17-3, we can see moderate to low EC but very low seepage rates. This was because the water in that canal was only a few centimeters deep and therefore did not have sufficient pressure to cause much seepage. In Figure 17-3 shallow EC is consistently

high possibly due to salt concentration via evapotransiration while the canal was empty but, at this site, as well as the site in Figure 17-1, equipment calibration error is suspected.

Data collected at the previous three locations was collected for comparison with seepage data that was being collected there.

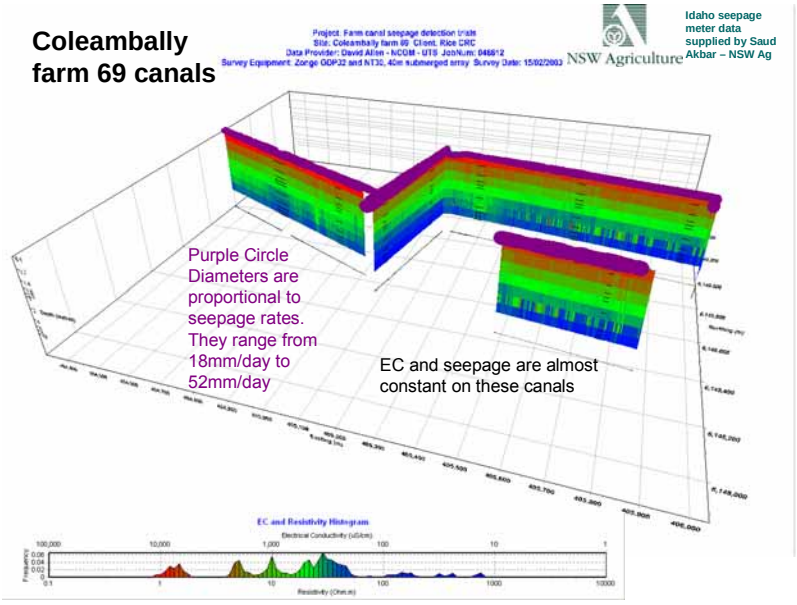

Figure 17.1 Coleambally Farm 69 canal EC ribbons with Idaho Seepage Meter seepage rates collected by Saud Akbar (NSW Agriculture).

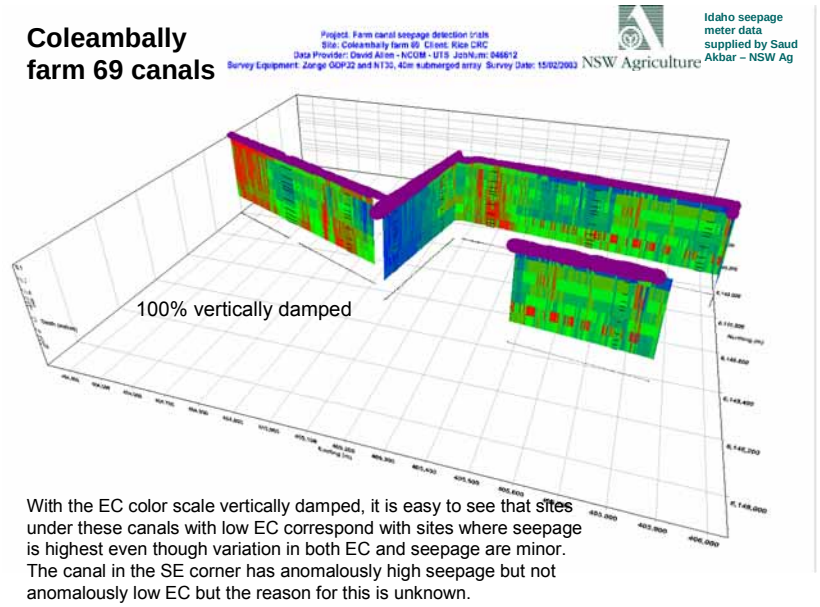

Figure 17.2 A copy of fig. 17-1 100% vertically damped showing up horizontal EC variation that correlate with seepage rates.

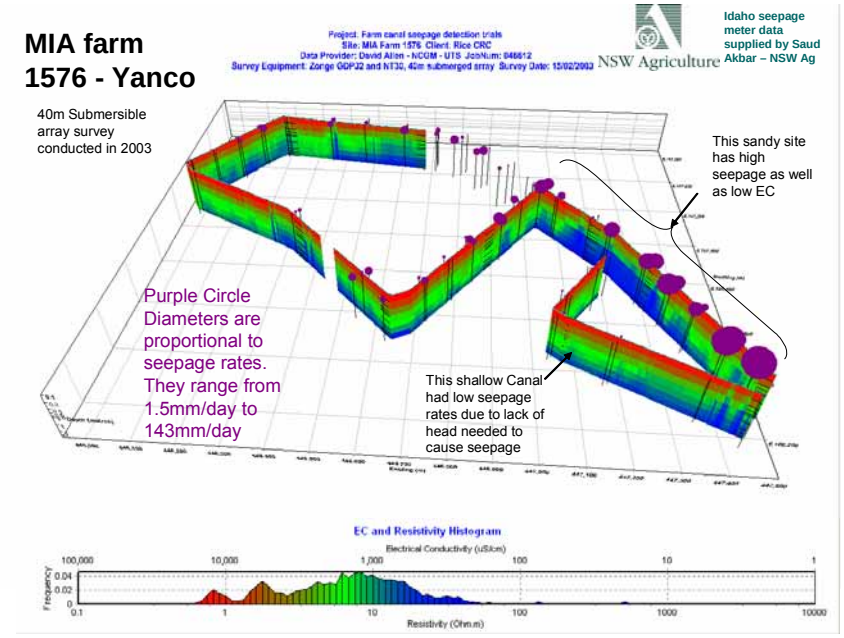

Figure 17.3 MIA farm 1576 EC ribbons and Idaho seepage rates (measured by Saud Akbar, NSW Agriculture). 2003 survey.

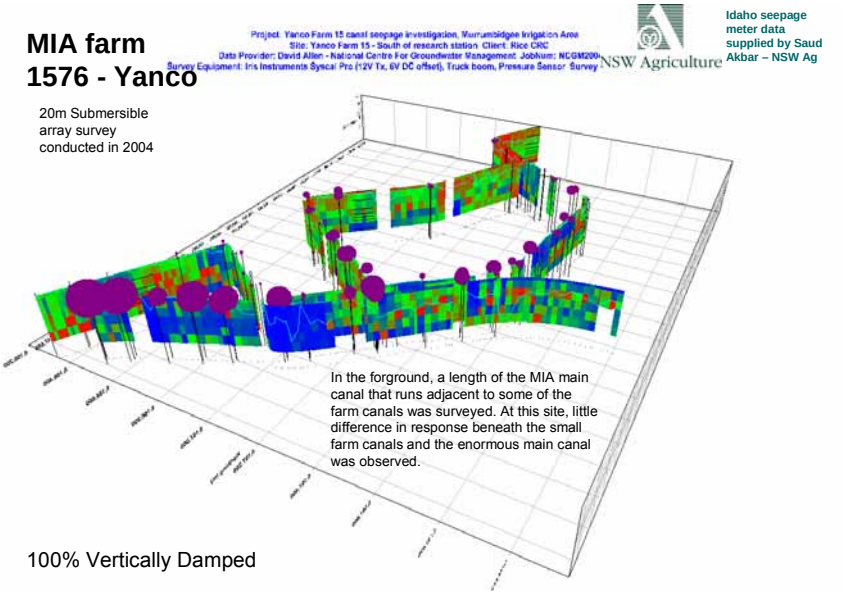

Figure 17.4 MIA farm 1576 EC ribbons (100% vertically damped) and Idaho Seepage rates (measured by Saud Akbar, NSW Agriculture). Note rotation angle compared with Figure 17-3. The MIA main canal in the foreground has EC very similar to the adjacent farm canal. 2004 survey conducted rapidly (3 hours including setup and packup).

The next case study is of canals and drains on the Dallas Clay Pan. This site was surveyed as it is a site used for investigation of the effect of rice farming on groundwater and salt movement. Figure 17-5 presents the 20m AXB submerged array data. In the foreground, we can see an EC ribbon commencing in the Murrumbidgee River and moving along Sturt canal. Contrast in soil types along that canal and then within the farm canals is evident. some of the farm canals are very shallow and are on the edge of flood or furrow irrigated land. Beneath those canals EC is extremely high due to saline water being pushed out from under the irrigated paddocks. Evaporation of that water in the vicinity of the shallow canals has led to concentration of salts under those canals.

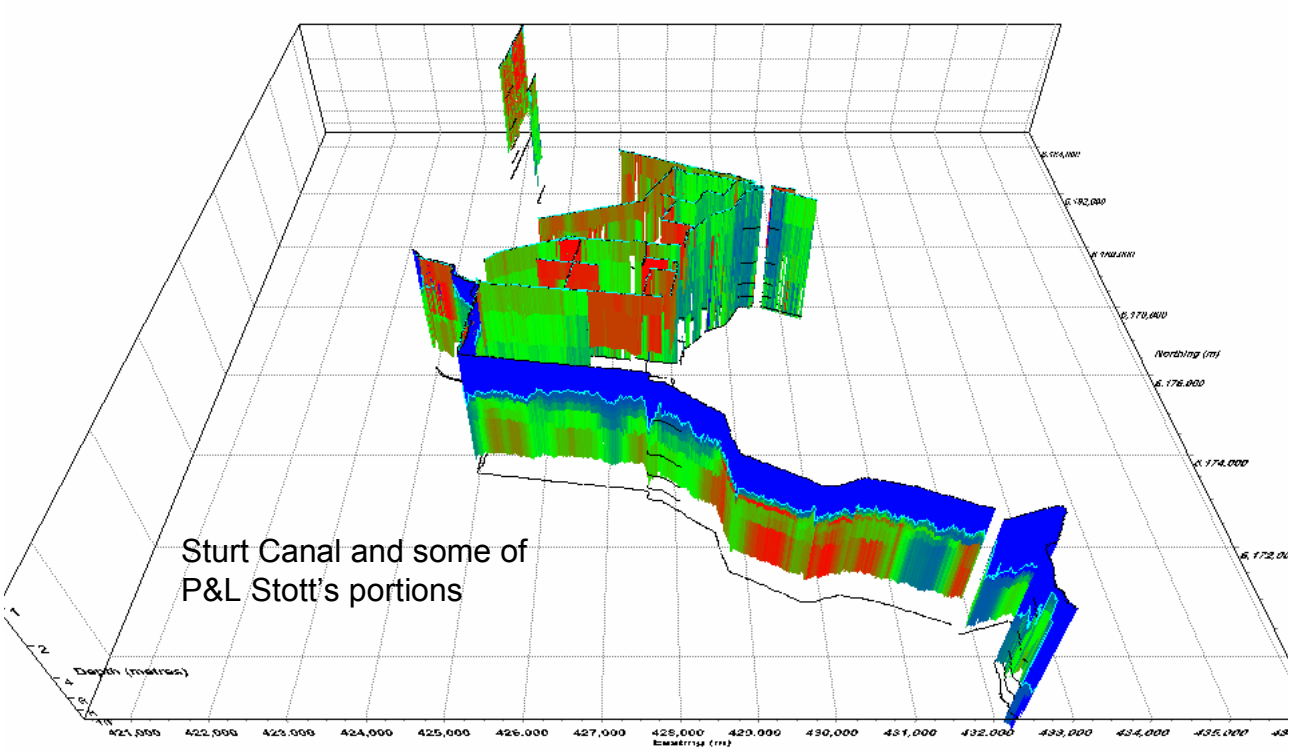

Figure 17.5 Submerged array EC imagery on canals and drains stretching from the Murrumbidgee River in the south 15 km across the Dallas Clay Pan to beyond Whitton. Contrast results from sediment types with resultant infiltration differences and salinity differences as well as canal/drain types which are more or less susceptible to evapo-transpiration driven salinity concentration from adjacent crop irrigation.

Figure 17-6 presents canals and deep drains surveyed with a 36m submersible and 80m floating array. Under most canals and drains it can be observed that there is typically a

salinity concentration near the bed but EC otherwise is fairly constant with respect to depth. In the north-east corner there is a distinct exception where a distinct low EC layer overlies a high EC layer. Augering revealed that about 2 metres of sand overlies clay there. Contrast this site with the low EC anomaly, which extends to great depth, further down the Gogeldrie South Drain and under much of the dam. That low EC anomaly corresponds with a 'tight' sand clogged with clay.

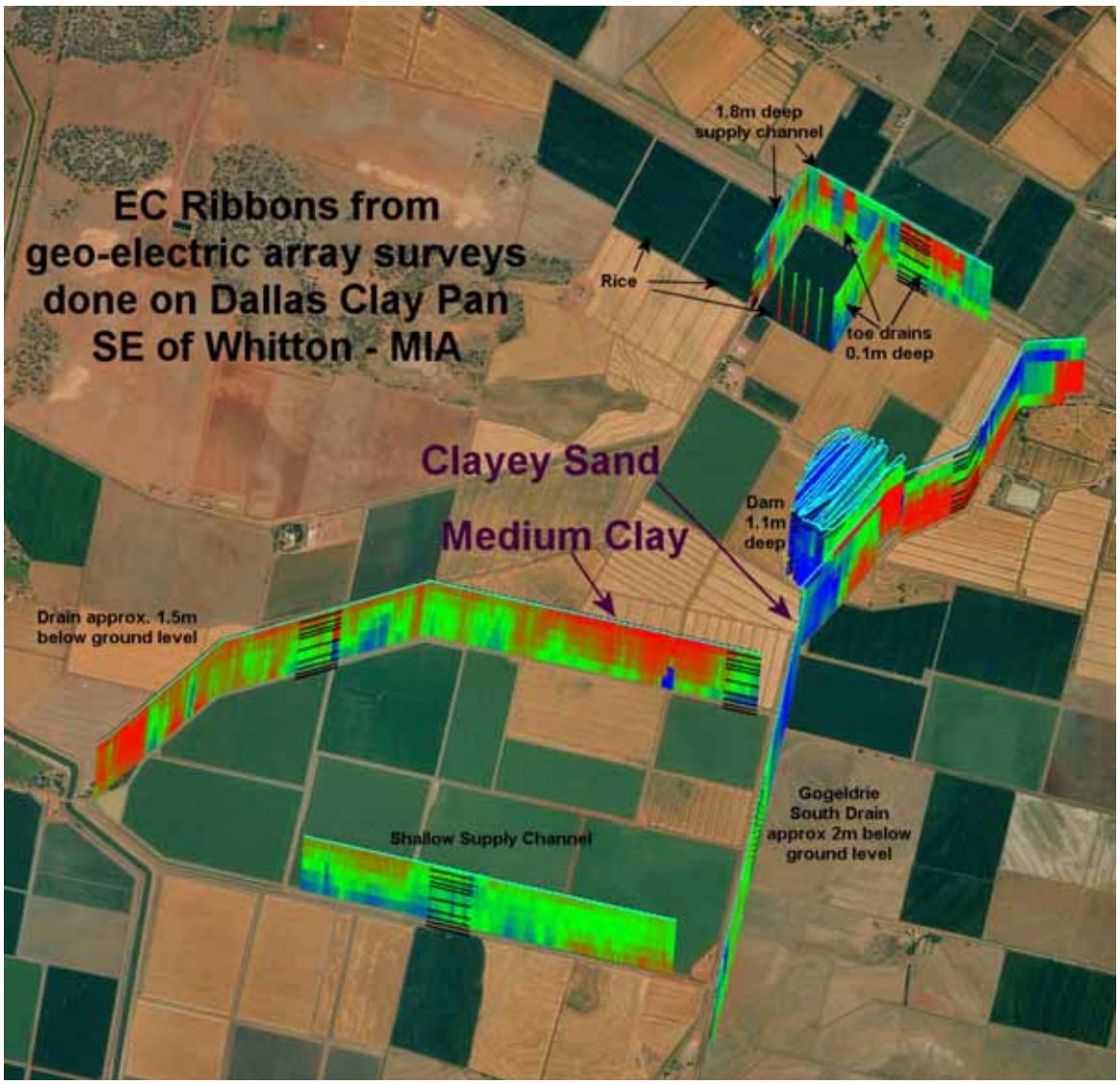

Figure 17.6 EC ribbons, some 0.2 to 8m deep, others 0.2 to 15m deep, imaged from drains, a dam, supply channels and rice toe drains on the Dallas Clay Pan. Under the Gogeldrie South Drain, notice that one low EC anomaly is only 1.5 metres deep while another is over 15m deep.

After the data presented in Figure 17-6 were collected, the 4wd mounted boom was invented and the site was very quickly resurveyed extensively using that device with a 20m long submersible AXB array in order to prove the potential of that boom. Figure 17-7 presents the comprehensive resurveying, completed in 12 hours, as well as the sites of Auger samples and one 6m deep excavator pit (999007). All the auger sample details are presented in Appendix 2. The samples showed a good correlation between EC_a and $EC_{1:5}$ as well as between EC_a and clay content. Figure 17-8 and Figure 17-9 present that data, along with bore logs, viewed from different angles.

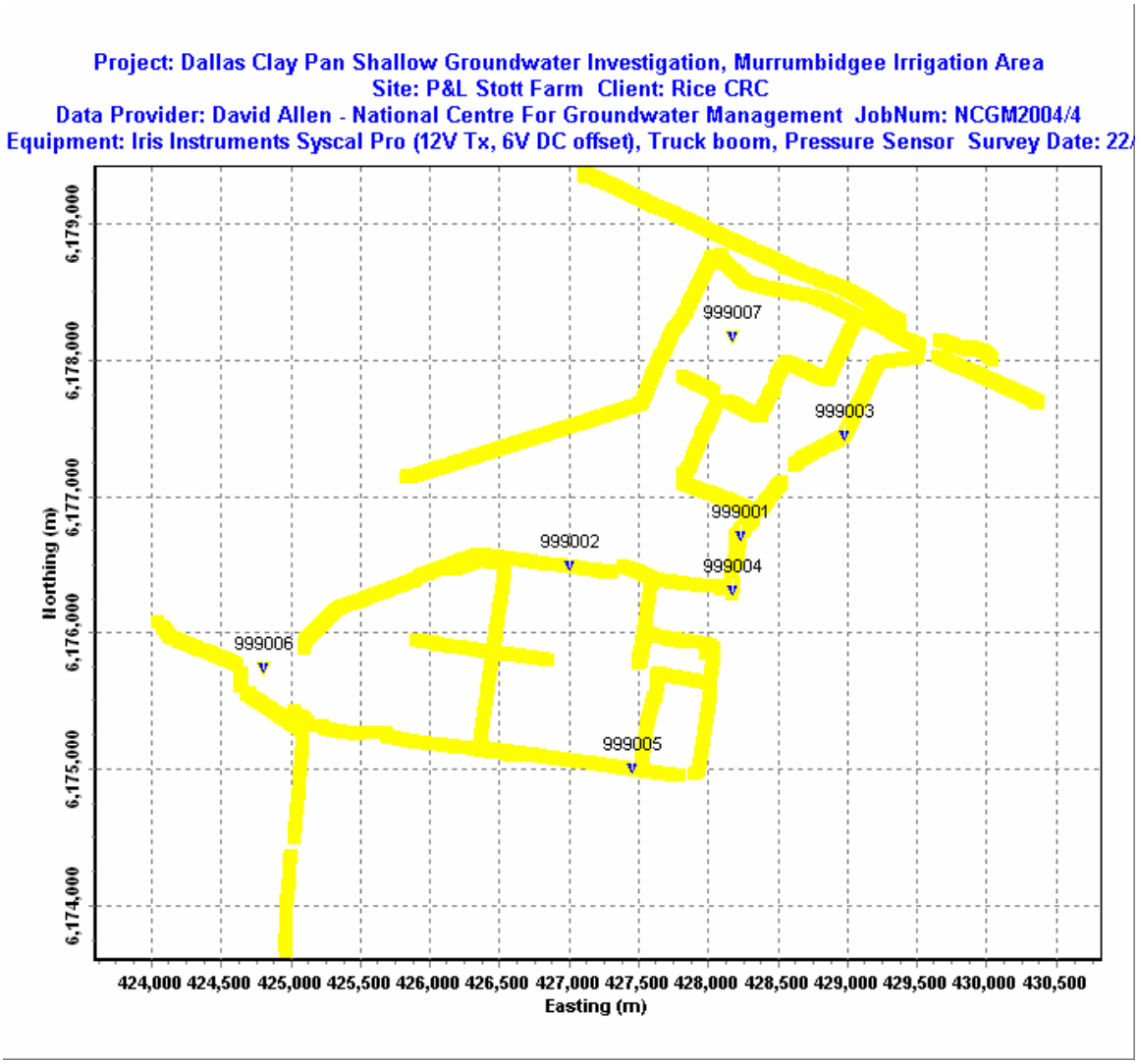

Figure 17.7 Submerged array surveys and auger sample sites on the Dallas Clay pan (south east of Whitton).

In Figures 17-8 and 17-9, the blue upper layer is the canal and drain water with a depth measured using a towed submerged pressure sensor. Although clay percentage greatly

influences the EC in the supply canals and drains, salinity has certainly dominated the EC response in the shallow canals and furrows. Watercourse type has been annotated on Figure 17-9. One can see that beneath some of the furrows and small canals the soil is extremely saline due to the effect of frequent irrigation of adjacent crops flushing salt from beneath the crops but concentrating it, through evapo-transpiration around the crop margins where the canals and edge furrows lie. This data is therefore further evidence of the theory presented by D'Hautefeuille (2001) in her interpretation of time-lapse animated EC variation with respect to time beneath rice fields.

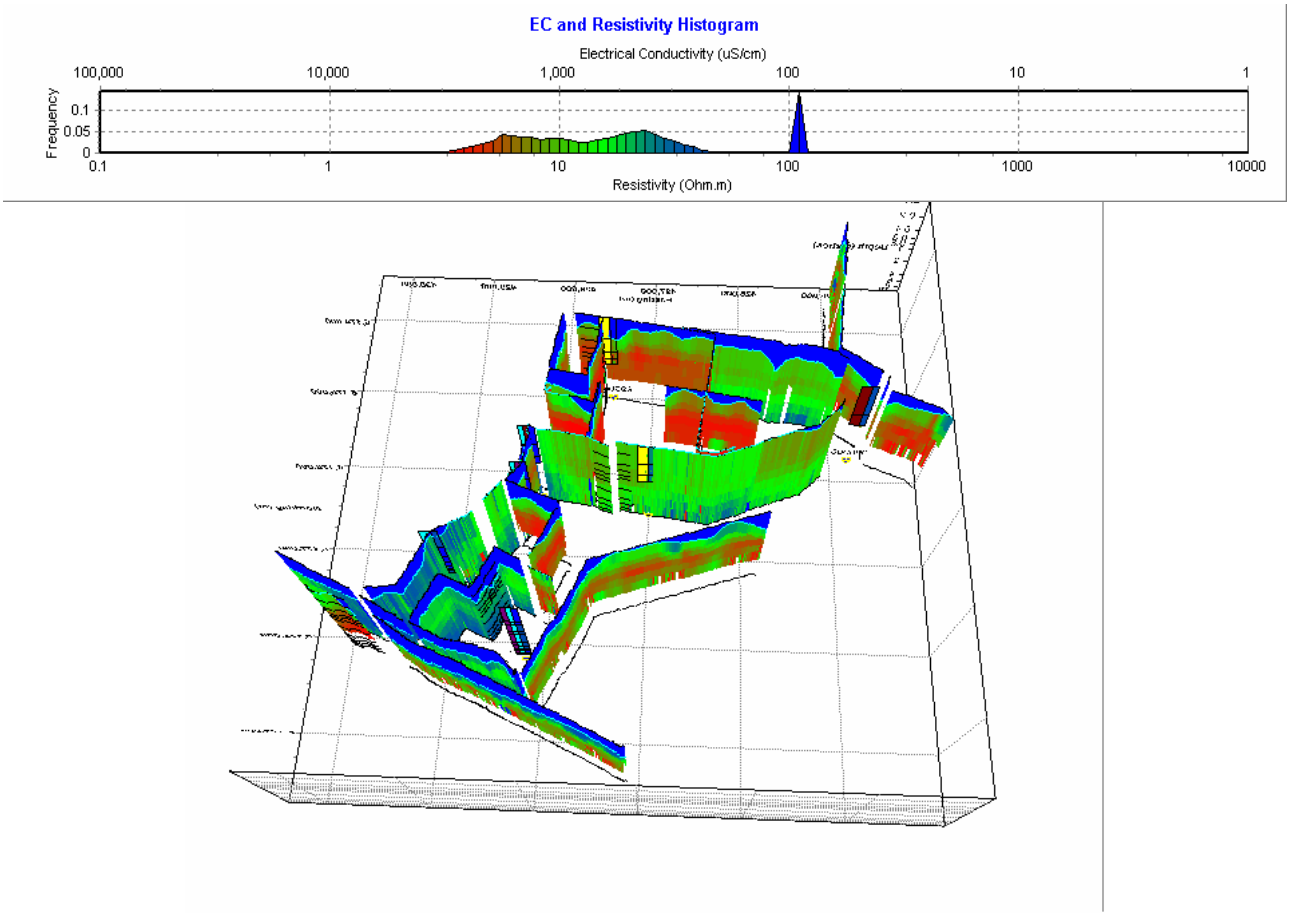

Figure 17.8 Dallas Clay Pan 20 m submerged array data collected along farm drains and canals of various sizes. Auger logs are added. View is from the north. Depth scale is from 0.1m to 8m.

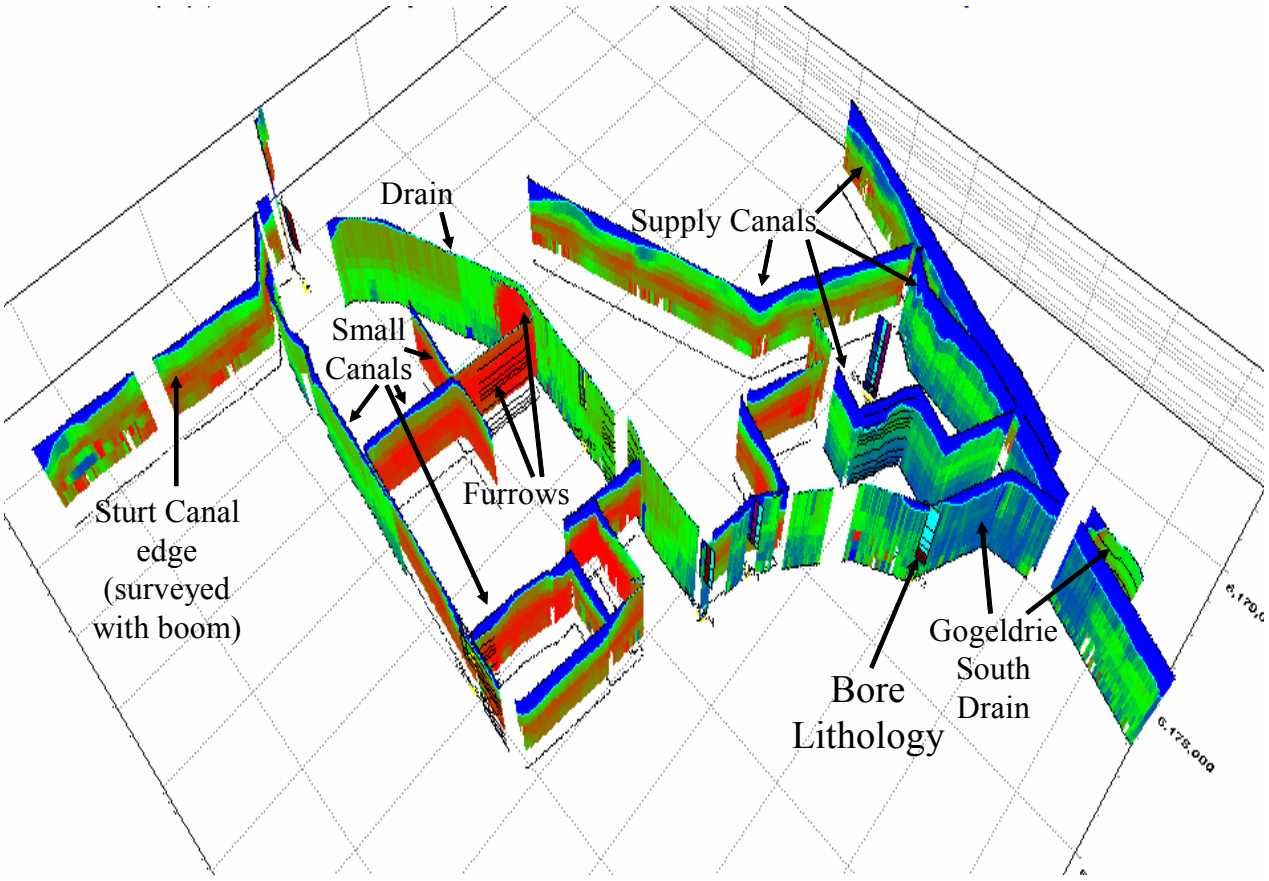

Figure 17.9 Dallas Clay Pan 20 m submerged array data collected along farm drains and canals of various sizes. Auger logs are added. View is from the SE. Depth scale is from 0.1m to 8m.

Figure 17-10, a close-up of some of the data at the north of the survey area, displays the effect of evapo-transpiration around crops even more clearly. Rice pond toe drains, and small farm canals are surrounded by a deep supply channel which is separated from them by a roadway. In less permeable sediment, very high EC, related to high salinity, has built up under the small waterways but not the supply channel. It has done this principally near the surface. Under more permeable parts of all the canals and drains, the salinity build-up is either not evident or not very pronounced. The south-east corner of the rice fields in Figure 17-10 is one such site. Just south of this site, a 6 metre deep pit was dug and soil was inspected. The profile is displayed in Figure 17-11. The soil is clayey with a gypsum horizon but was very permeable due to structure in the clay. The clay had aggregated into grains between which water could flow. Once the pit was dug beyond 5 metres deep, the rate of water infiltration was so high that it could not be continued.

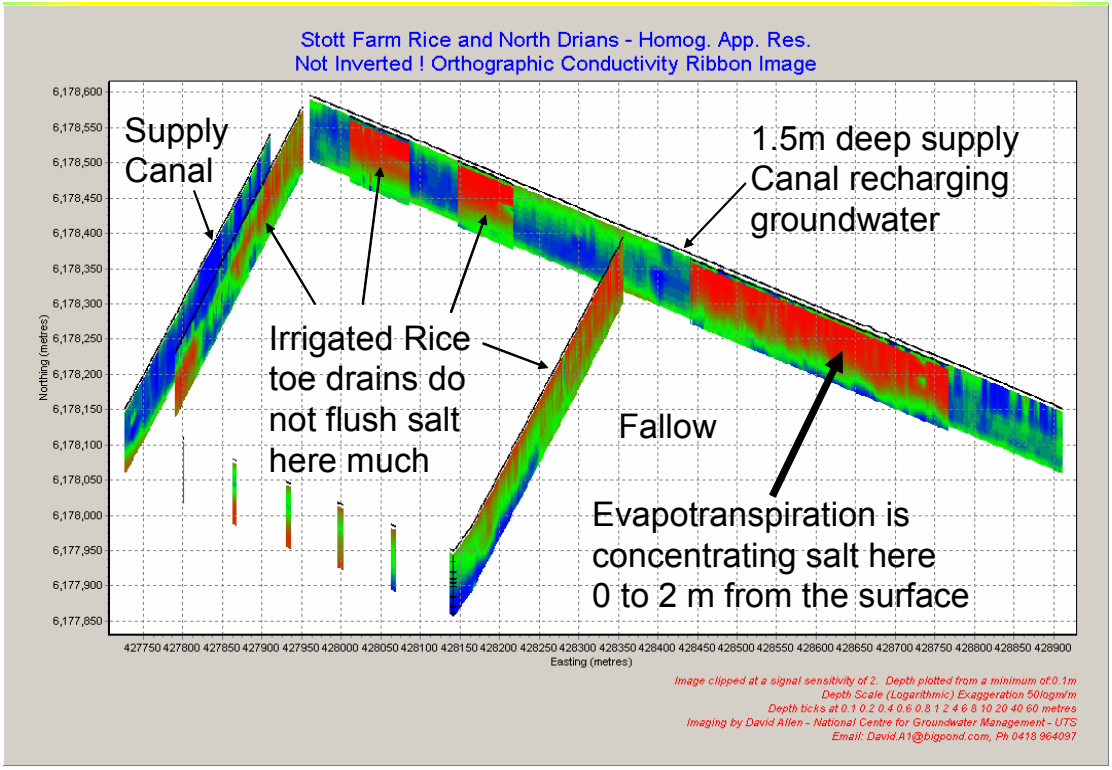

Figure 17.10 The effect of evapotranspiration on 36 metre AXB submerged arrays pulled along deep canals compared to shallow farm canals and toe drains.

Figure 17.11 Mike Nalore examining soil investigation trench site 7. Note the base of the red soil where some gypsum exists. Once this trench was extended past 5m deep, so much water was gushing in that it had to be abandoned. Permeability exists there in clay structure. The clay had aggregated into grains between which water could flow.

17.1 Concluding summary on geo-electric survey of farm canals

Unlike supply canals, farm canals and drains are usually empty and often receive saline groundwater discharge from adjacent crops. When dry they crack deeply where passing through self mulching clays. For these reasons, seepage from them and EC beneath them can both be much more spatially and temporally erratic than for supply canals. Correlation between seepage and EC is likely to be poorer.

Because farm canals are generally well maintained with access tracks alongside them, survey using a submerged array towed by a vehicle mounted boom can be very cost effective.

CHAPTER 18 - RESERVOIR CASE STUDIES

18.1 Thirty hectare reservoir – West end of Jim Cattanach Road – Coleambally

Reservoir survey using geo-electric arrays has proved to be very efficient as, once a watercraft is launched onto the reservoir, a survey may proceed at full speed without interruption. The example presented here in Figure 18-1 was surveyed in just 3 hours using a 20m long submersible AXB array. Interpretation is as posted on Figure 18-1. The low EC anomaly on the NE corner of the dam has since been investigated. A backhoe pit revealed pure white sand to a depth of 3 metres. It has been noticed that pine trees (that cannot cope with waterlogged roots) near the NE corner of the dam are dying. Figure 18-2 presents the same information as depth (below the dam bed) slices.

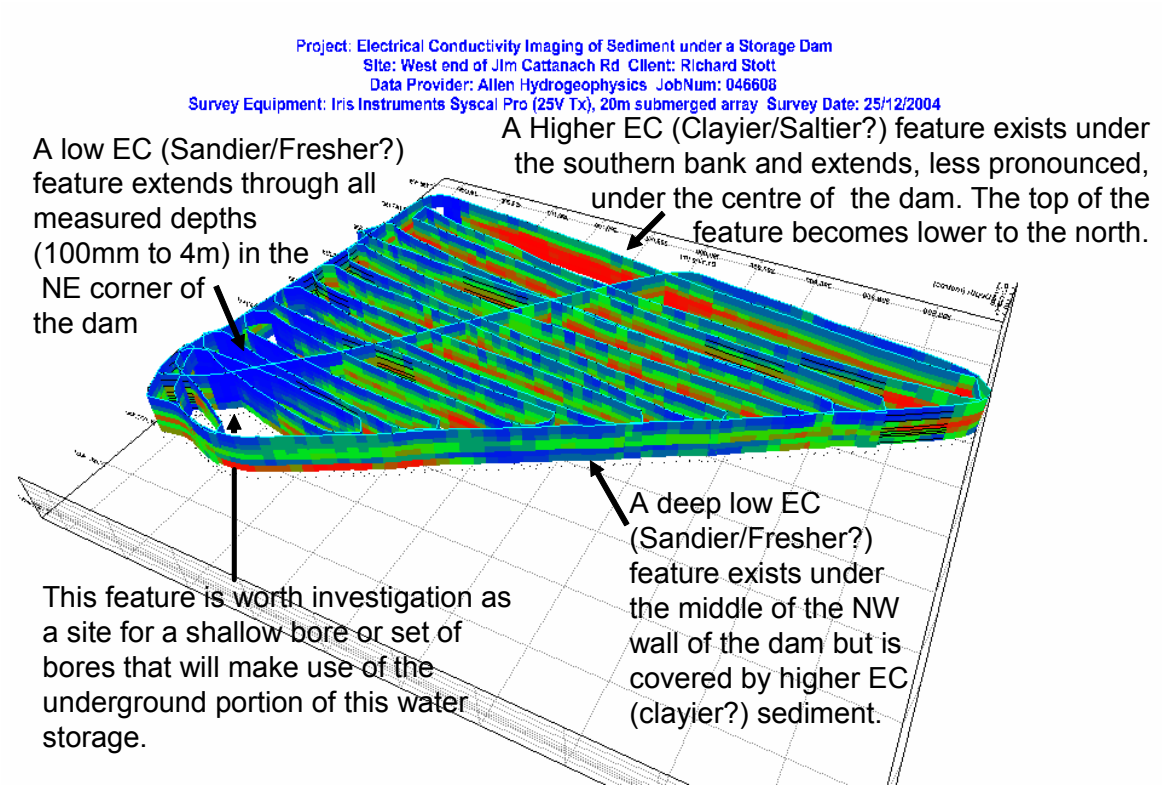

Figure 18.1 Submerged array survey of a 30 hectare reservoir. Line spacing is approximately 20m. Depth scale extends from 0.1m to 4m below the bed of the reservoir. View is from the northwest.

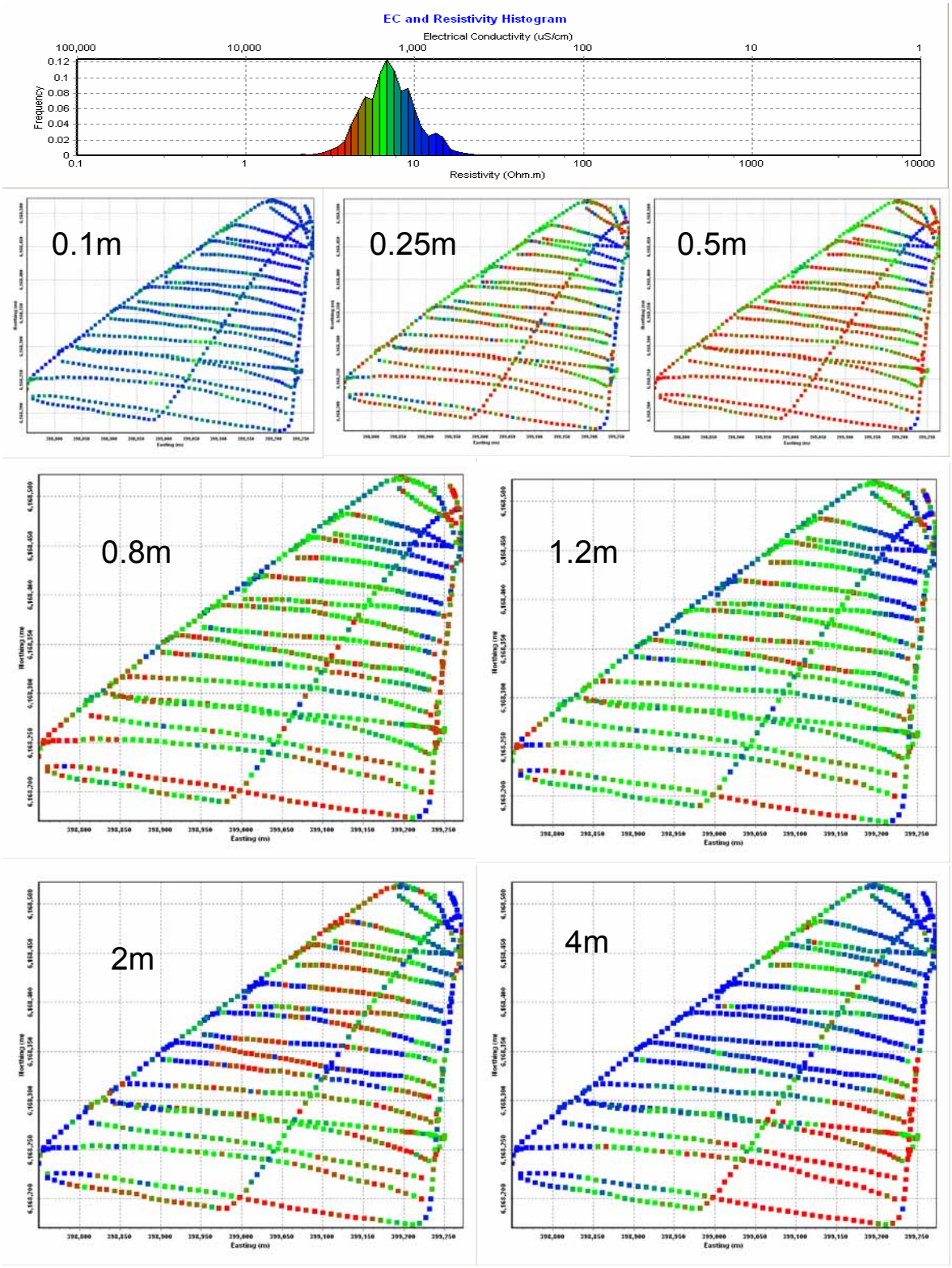

Figure 18.2 Depth (below dam bed) slices showing how a low EC feature in the NE corner spreads out 4m below much of the dam.

18.2 Dallas Clay Pan Reservoir (15 Hectares)

A 15 hectare reservoir, was surveyed using an 80 metre long floating AXB array. This was one of the first surveys ever conducted and no navigation aids were used so line spacing is erratic. Nevertheless, the reservoir was successfully surveyed within 3 hours. A low EC layer 3-7 metres under the west side of the reservoir was identified and is thought to be permeable. The layer appears to connect with an inferred prior stream to the southwest. Other evidence of the 'prior stream' is evident in the rest of the Dallas Clay Pan case studies. It seems plausible that spear points may be installed in the 'prior stream' in order to recover water, in times of water shortages, lost from the surface reservoir. Figure 18-3 presents the colour scale used to image the reservoir while Figure 18-4 presents the data collected from the reservoir both as EC ribbons and as depth slices. No depth slices shallower than 1.5m are supplied because the reservoir was 1.1 metres deep. EM31 data, supplied by the farmer, is included for comparison with the 3 metre deep depth slice. Beware that the colour scale on the EM31 data is the inverse of the color scale on the geo-electric array data. The effective depth of the EM31 data is approximately 2.5 metres from the lake bed while the depths of the geo-electric array data are referenced to the Lake surface.

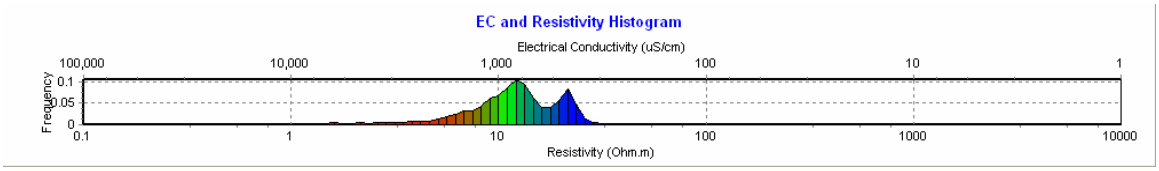

Figure 18.3 The colour scale used to present EC on Figure 18-4.

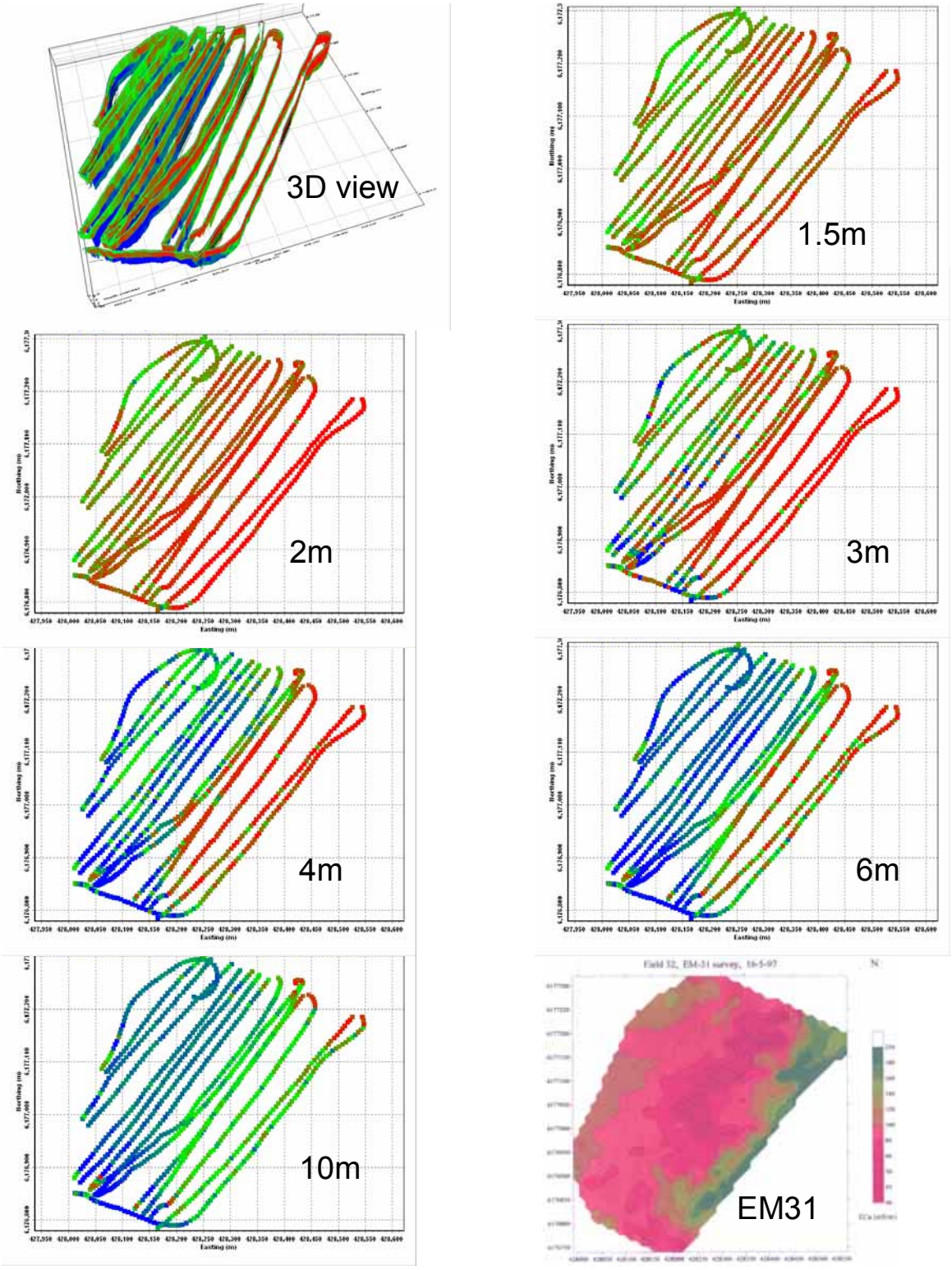

Figure 18.4 EC ribbons and depth slices of inverted floating array data collected from a 15 hectare reservoir. EM31 data, collected prior to construction of the reservoir has been supplied for comparison. Beware of the inverse colour scale on the EM31 data.

18.3 Concluding summary on geo-electric survey of reservoirs

Geo-electric surveys of reservoirs may be interpreted in a very similar manner to supply canal surveys although the dense 3D coverage that is possible is better presented as depth slices rather than vertical sections. Good rejection of data collected during u-turns is required. Provided that a boat capable of navigating the shallow parts of the reservoir is available, survey may be extremely cost effective. Dam topography and volume survey may proceed at the same time if GPS and depth measuring equipment is of suitable quality.

Many reservoirs with seepage problems may be suitable for use as managed aquifer recharge sources. The imagery attainable beneath the reservoirs can indicate where the seepage goes so that a groundwater extraction licence can be obtained (government permitting) and a bore sunk to re-extract the seeped water. Since evaporation losses from storages typically are considerable, such ventures are likely to be a cost effective method for saving water and facilitating additional long term water storage. EC imaging in the vicinity of the reservoir would also be required to identify seepage pathways from some reservoirs. Such survey could be readily conducted using towed TEM equipment.

CHAPTER 19 - CONCLUSION

This thesis focuses on identifying and removing obstacles to the routine use of geo-electric and electromagnetic EC surveying of aquifers connected to watercourses. It has presented numerous case studies taken from throughout the Murray Darling Basin, Australia that demonstrate progress in solving problems associated with numerous production scale applications of EC imaging.

In summary, original contributions by the author and advances developed during the course of the study include the following:

- Continuous mode operation for geo-electric surveying (Allen, 1991)
- 3D animatable EC ribbon presentation with log vertical scale for equal visibility of all resolved features, water depth trace, depth ticks and other features.
- Development of fractional signed monopole notation. A generalization and simplification of geo-electric equations resulted. The new notation prepared the way for facilitation of diverse geo-electric arrays in general processing algorithms.
- Exponential Bipole and AXB geo-electric array development optimized shallow investigation resolution and signal strength as well as array weight and handling. The AXB array is defined as two linear transmitter electrodes followed by an array of receiver electrodes spaced at 2^n from the end of the second transmitter electrode where n increments constantly.
- Linear electrode theory facilitated both high signal output necessary for deep imaging and shallow imaging involving electrodes separated by much less than their lengths.
- Effective depth centred layer inversion was written so that robust, fast inversion of massive datasets could be achieved that could resolve high contrast boundaries. This inversion was constrained by a combination of layer stretch constraint and smoothness constraint.
- Submerged array equipment and theory was developed for the resolution of fine layered features just beneath watercourse beds such as clay lining preventing seepage and proximity of saline aquifers threatening to contact and flow into watercourses.

- A data schema and data management strategy for utilization of large volumes of multi-depth data collected along irregular tracks was developed and tested.
- Survey propulsion solutions including a 4wd mounted boom, lightweight watercraft with 4wd mounted crane support and airboats were developed to negotiate, in an economically viable way, the numerous obstacles and water weed typically encountered on watercourses to be surveyed.
- Geo-electric arrays were constructed of a streamlined nature that could easily slide past the numerous obstacles encountered in routine survey of watercourses.
- Trials of land-based arrays for use behind a ripping tine were developed but the Ohm-mapper multi-dipole device was developed by Geometrics simultaneously and proved to be a better solution to shallow terrestrial imaging. The ability of the Geometrics device is enhanced by AXB type array design and the inversion software developed as part of this thesis.
- Sub-noise data aware inversion was developed to deal with problems of reliably inverting hypersaline and very saline aquifers that consume all available geo-electric signal.
- Towed TEM survey using a plastic sheet was developed as an extremely productive and simple way of EC imaging across land.
- Conduct of numerous surveys proved up application of EC imaging to:
    - transmission loss and seepage studies;
    - conjunctive water use investigations;
    - isolation and monitoring of saline inflow to rivers and drains;
    - isolation of acid sulphate groundwater pollution from drained swamps;
    - reservoir seepage studies that could lead to conjunctive water storage in both reservoirs and aquifers beneath them; and
    - terrestrial multi-depth aquifer definition.

19.1 Comparison of TEM and geo-electric arrays.

Multiple depth EC data was collected with both transient electromagnetic devices and geo-electric arrays. Table 20-1 presents a comparison of the capabilities of each of these techniques.

Geo-electric array equivalent	*Electromagnetic equivalent*
Resistor thicknesses well defined	Resistor thicknesses (such as water depth) poorly defined by TEM. Conductive layers well defined by TEM.
Good, very shallow investigation	Investigation above 2m impractical with TEM but well supported by FDEM. However no suitable instrument for good multidepth single pass FDEM surveying had been developed by the completion of this thesis (DualEM and Geonics will construct upon demand).
Deep investigation restricted by length of cable that can practically be towed.	Deep investigation is limited by signal to noise that can practically be obtained by towable EM loop systems. Switching single turn / multi turn TEM loop systems can see deeper but require careful design for accommodation of high self inductance of multiturn TEM loops and complete removal of primary field. FDEM deep investigation is restricted as for geo-electric arrays, by the practical length of towable devices.

Table 19-1 A comparison of the features of geo-electric and electromagnetic systems for continuous multi-depth imaging of aquifers connected to watercourses.

19.2 Future work

Further geophysical equipment and software development recommended includes:

- terrestrial towed TEM platforms;
- towed multi-spacing FDEM development (hardware and software);
- application of the inversion and imaging techniques with capacitive resistivity line and/or plate antennae devices such as the Geometrics Ohm-Mapper TR5.
- analysis of the effect of water flowing past various types of electrodes; and
- development of the ripping tine towed geo-electric array.

Future theoretical advancements recommended include:

- Calculation of the depth of investigation equation and effective depths for submerged arrays; and
- extension of the forward modelling, and inversion, technique of this thesis to submerged array data.

Future logistical advancements recommended include:

- Commencement of a national multi-depth electrical conductivity database using an elaboration of the data schema detailed in Appendix 4. This database could be served via the world wide web to customers with specialized viewers.

19.3 Recommendations for seepage investigation

Recommendations for future seepage investigations are:

- EC imaging is the most cost effective method of targeting seepage remediation accurately but cannot give absolute seepage rates without external calibration using other tools. No tools exist that accurately and economically can detect absolute seepage rates. Pondage tests are the only reasonable way of measuring absolute seepage rates but are expensive and require good evaporation loss corrections.

- Remediation programs should be conducted after identifying troublesome seepage sites using EC imaging combined with detailed site investigation (anomalous vegetation identification, piezo monitoring etc), yabbie pump sampling of sediment from canal beds and occasional pondage tests (for calibration).

- EC imaging should be conducted using a 20-36 m long submersible Allen Exponential Bipole Geo-electric array towed from a 4wd mounted 6m reach boom. On larger canals the array should be towed using a canoe or boat which could be lifted over obstacles using a large 4wd or trailer mounted crane. The watercraft should have a propulsion mechanism, such as an air propeller, capable of functioning in water weed.

- A 3D capable EC data processor/presenter software package is essential for economically managing and understanding the EC data.

- Seepage remediation could be viable at numerous isolated sites in the Murray Darling Basin if the cost of elevated water tables caused by seepage is considered.

19.4 Recommendations for conjunctive surface water and groundwater management

EC imaging using a streamlined AXB floating geo-electric array 144m long is practical on all canals and rivers that can be navigated with any craft. Such an array can probe from 0.1 to 40m deep revealing significant information on shallow groundwater salinity and levels as well as revealing sites of anomalous seepage from canals and rivers. Such an array may be used to reveal lengths of rivers or canals where groundwater pumping will result in surface water depletion or vice versa. It can be useful for assessing the impact of bores that already pump from connected aquifers. Aquitards beneath a river or canal may be evident in the EC imagery. Management of groundwater pumping adjacent to the river can then take this into account.

Use of EC imaging could revolutionize shallow groundwater pumping for salinity control and conjunctive use. At present, farmers are unwilling to initiate shallow groundwater pumping, preferring to pump from large permeable deep aquifers, largely because of lack of commercial pumping technology designed to tap low yield shallow aquifers effectively and partially because until now, little technology suitable for siting bores in pockets of freshwater was commercially viable. Legislation that locks up shallow groundwater in an effort to prevent it from depleting connected surface water resources is hampering use of shallow groundwater that could alleviate shallow water table problems and minimize the need for surface reservoirs with high evaporative losses. Such legislation tries to make up for lack of knowledge about connectivity by preventing use of groundwater. EC imaging can help identify the connections so that water trading can take place and surface waterways, as well as land currently suffering from shallow water tables, can be preserved.

19.5 Recommendations for development of underground water storage facilities.

Shallow permeable aquifers, whether empty or full, can be used as underground water storages if water loss to inaccessible realms and to salinization can be brought to acceptable levels. Similarly, where seepage pathways extending to deeper, more extensive aquifers are clear, storage in those aquifers may also be augmented using managed recharge from especially developed surface reservoirs. Extensive aquifers in some locations are also useful as an alternate bodies for water conveyance.

Terrestrial EC imagery can be used to identify permeable aquifers, where to drill, and how deep to drill in order to emplace and remove most fresh water from those aquifers. Some such aquifers will be significantly connected to watercourses, while others will not. Connected aquifers typically are already being depleted by pumping and the connections need to be established so that conjunctive water management can be implemented fairly. Those freshwater aquifers that are not well connected to rivers, or are connected in such a manner that they usually drain into the rivers, will, if depleted, need artificial replenishment by siting of reservoirs above them with connecting, non-clogging interfaces. As farmers will lose water from their reservoirs to the ground, they will want to know that their recovery losses will be less than the evaporation losses they otherwise would encounter on the surface. They will also want to know whether their underground water storage will become unacceptably salinized. EC imaging will be an essential tool, combined with drilling, pump testing and groundwater modelling, for identifying and dealing with any leakage pathways from the underground water storages. Some leaks will be dealt with using appropriately placed recovery bores while others, such as long prior streams, will be dealt with by excavating and sealing.

19.6 Recommendations for saline inflow management

As the salinity of groundwater under saline inflow sites is typically very high, it is reasonable to suggest that the EC ribbon images of those sites correspond almost directly to salt storage (salinity x porosity x volume) under the river. High EC anomalies adjacent to the river bed are believed to associate with saline inflow. This is most common in many of the deep trenches in the rivers. Additionaly, proximity to floodplain banks and routes

of prior river channels beneath existing rivers complicate saline inflow. Interpretation of such features requires that EC imagery be viewed in a 3D interface.

It is recommended that presence of saline inflow in lengths of river first be identified by run-of-river salt load difference surveys. It then can be isolated using EC imaging. EC imaging can also then show up sites where saline groundwater is dangerously close to river bottoms. EC imaging should first be conducted with a long floating EC array so that deep and rapid imaging is possible. Follow up surveying using a submersible array can isolate saline inflow. Sediment sample logging using an extended Yabbie pump can enhance the usefulness of EC imagery at saline inflow sites as can study of groundwater mounds adjacent to the sites.

Salt interception bores will produce low EC anomalies wherever they draw river water downwards from river beds. Such drawdown can be EC imaged. The imagery can help with scheme monitoring by indicating if pumping is inadequate or excessive.

19.7 Summary of applications

In conclusion, application of electrical conductivity imaging of aquifers connected to watercourses is capable of facilitating:

- development of spatially detailed groundwater/surface-water conceptual models for conjunctive water use management;
- cost effective survey of canals for seepage hot spot isolation;
- planning of low evaporation loss, water storage solutions involving groundwater recharge and reuse management; and
- optimal positioning, refinement and monitoring of salt water interception schemes.

LIST OF REFERENCES

Note that most of the references listed have been included in the REFERENCES directory on the DVD accompanying this thesis. Software has been listed separately at the end of the list of references.

Adams, R., 1987, *Calculus of Several Variables*. Addison Wesley, Don Mills, Ontario. 456 pages.

Advanced Geosciences Incorporated, 1997, *Marine channel submerged survey*, AGI STING/Swift case study 6. http://www.agiusa.com/marine.shtml,

Akbar, S., Beecher, H.G., Cullis, B. & Dunn, B., 2002, Channel Seepage Estimation and Identification using two Techniques, Proceedings of a conference held at Yanco in 2001 - *Electromagnetic techniques for agricultural resource management* – ed. Beecher, H.G., Australian Society of Soil Science, Inc. Riverina Branch.

Allen, D.A., 1991, *Use of electrical geophysics for the location of saline groundwater inflow to the Barwon, Darling and Bogan Rivers.* BScHonours Thesis, University of New South Wales, School of Applied Geology.

Allen, D.A., 2002, Resistivity Imaging from Rivers. *Proceedings of a conference held at Yanco in 2001 - Electromagnetic techniques for agricultural resource management* – ed. Beecher, H.G., Australian Society of Soil Science, Inc. Riverina Branch.

Allen, D.A. & Merrick, N.P., 2003, A floating electrode array for continuous geo-electric imaging. Extended abstract – *Proceedings of the Aust. Soc. of Exploration Geophysicists 16th Geophysical Conference and Exhibition, Adelaide.*

Allen, D.A. & Merrick N.P. 2004, Identifying fresh and saline water using hydro-geophysical imagery of strata beneath watercourses. *Paper and posters presented in*

the proceedings of the 9th Murray Darling Basin Groundwater Conference – Feb. - Bendigo.

Allen, D.A. & Merrick, N.P., 2004 *Comparison of electrical conductivity ribbon images surveyed in 2003 and 2004, of strata beneath the Murray River, in the vicinity of Mildura*. National Centre for Groundwater Management, Univ. of Technology, Sydney research report NCGM 2004/4 prepared for the NSW Department of infrastructure, planning and natural resources, Buronga, NSW.

Allen, D, 2005, *EC Imaging for seepage investigation – a trial in the Murray Irrigation Area.*. Murray Irrigation internal report.Murray Irrigation Ltd. Deniliquin, NSW, Australia.

Allen, D., 2005, Electrical Conductivity *Imaging under Coleambally Irrigation Canals. A feasibility study for canal seepage and shallow groundwater investigation* - Allen Hydro-Geophysics. Coleambally Irrigation Incorporated internal report.

Allen, D.A. & Merrick, N.P., 2005, Towed geo-electric arrays for analysis of surface water groundwater interaction. *Proceedings of the Sympos. on Applications of Geophy. to Engineering and Environmental Problems conference* – April – Atlanta, USA, ISSN 1554-8015.

Allen, D.A. & Merrick, N.P., 2005, Imaging of aquifers beneath watercourses. Referreed proceedings of the Int. Ass. of Hydrogeologists – Australasia conference, Nov. Auckland, NZ.

Allen, D.A., 2006, HydroGeoImager. Software accompanying this thesis also available from www.GroundwaterImaging.com

Allen, D.A., and Merrick, N.P., 2006, Aquifer and watercourse interaction in the Murray Darling Basin elucidated using electrical conductivity imaging. Extended Abstract - *Proceedings of the Australian Earth Sciences Convention* (including ASEG), July.

Allen, D.A., and Merrick, N.P., 2007, Robust 1D inversion of large towed geo-electric array datasets used for hydrogeological studies. *Exploration Geophysics*, Vol 38 No 1, ISSN0812-3985; Butsuri Tansa (Japanese) 60.1; and Mulli-Tamsa (Korean) 10.1.

Ankeny, M., Harbour, J., Heath, G., Kostelnik, K., Mattson, E., Moor, K., Richardson, A., and Wangerud, K., 2004, A structured approach to the use of near surface geophysics in long term monitoring, *The Leading Edge*, Vol. 23, No. 7, (July).

Auken, E., Breiner, M., Nebel, L., Pellerin, L., Thomsen, P., and Sørensen, K. I., 2001, EMMA - Electromagnetic modelling and analysis. *EEGS Birmingham Proceedings.* Birmingham, U.K.:EEGS. 114-115, 2001. JED.

Auken, E., and Christiansen, A.V., 2004, Layered and laterally constrained 2D inversion of resistivity data. *Geophysics*, Vol. 69, No. 3, (May-June), p. 752-761.

Auken, E., Nebel, L., Sørensen, K., Breiner, M., Pellerin, L., and Christensen, N., 2002, EMMA – A Geophysical Training and Educational Tool for Electromagnetic Modelling and Analysis. *Journal of Engineering and Environmental Geophysics*, Vol. 7, Issue 2, pp. 57-68, (June).

Australian National Committee on Irrigation and Drainage., 2003, *Open Channel Seepage & Control Vol 1.5 – Channel Seepage Identification and Measurement – Final Report, Compiled by Wimmera Mallee Water.,* www.ANCID.org.au

Australian National Committee on Irrigation and Drainage., 2004 (May), *Australian Irrigation Water Provider Benchmarking Report for 2002/2003.* ANCID

Ball, L., *et.al.* 2005, Determination of canal leakage potential using continuous resistivity profiling techniques in Western Nebraska. Proceedings of the Geological Society of America Annual General Meeting, Salt Lake City. Paper 66-10. (http://gsa.confex.com/gsa/2005AM/finalprogram/abstract_95058.htm).

Barret, B., Hatch, M., Heinson, G., and Telfer, A., 2003, Salinity monitoring of the Murray River using a towed TEM array: *Aust. Soc. of Explor. Geophysicists 16th Geophysical Conference and Exhibition, Adelaide*.

Becker, J. 2003, Constructional Project - Earth Resistivity Logger – *Everyday Practical Electronics* – Part 1 in April 2003, pp 288-295 and Part 2 in May 2003.

Beecher, H.G. (editor), 2002, Electromagnetic Techniques for Agricultural Resource Management., *Proceedings of a conference held at Yanco Agricultural Institute, Yanco*, NSW, July 2001, Australian Society of Soil Science, Inc. Riverina Branch.

Braaten, R. & Gates, G., 2001, *Groundwater – surface water interaction in inland New South Wales: a scoping study.*, Department of Land & Water Conservation, GPO Box 39, Sydney NSW 2001, Australia.

Brown, C.M. & Stephenson, A.E., 1991, *Geology of the Murray Basin, Southeastern Australia, BMR Bulletin 235.*

Christen, E.W., Prasad, A. and Khan, S. (2000) *Spatial analysis of shallow groundwater pumping for salinity control and potential conjunctive use: A case study of the Coleambally Irrigation Area.* Technical Report 40-00. CSIRO Land and Water, Griffith, NSW.

Christensen, N.B., 1990, Optimized Fast Hankel Transform Filters, *Geophysical Prospecting* 38, 545-568.

Christensen, N.B., 2001, *The direct current geoelectrical problem*, Lecture notes – Geofysisk Afdeling, Geologisk Institut, Aarhus Universitet, Finlandsgade 8, DK-8200 Aarhus N, Danmark. Email nbc@geo.au.dk.

Christensen, N.B., 2004, personal communication – a report containing various types of inversion of geo-electric array data on a Coleambally Irrigation Canal. Included on the Thesis DVD.

Cornacchiulo, D. and Bagtzoglou, A.C., 2004, Geostatistical reconstruction of gaps in near-surface electrical resistivity data – *Vadose Zone Journal* 3:1215-1229

Corwin, R.W., and Butler, D.K., 1989, *Geotechnical Applications of the Self-potential Method, Report 3, Development of Self-potential Interpretation Techniques for Seepage Detection*: Technical Report REMR-GT-6. US Army Corps of Engineers, Washington, DC.

Cox, S.J.D., 2004, XMML – a standards conformant XML language for the transfer of exploration data. Extended Abstract, *Proceedings of the Australian Society of Exploration Geophysicists Conference* (August), Sydney.

Craig, I. & Hancock, N., 2004, Methods for Assessing Dam Evaporation – An Introductory Paper. *Irrigation Association of Australia 2004 Conference proceedings – Barossa Valley.*

Dahlin, T., 2001, The development of DC resistivity imaging technology. *Computers and Geoscience*, Vol 27(9) pp 1019-1029.

Dahlin, T and Allen, D., 2005, *Noise test of a submerged towed geo-electric array with the RIP924*, personal communication included in the references directory on the Thesis DVD.

Dahlin, T., 2005, *Specifications for a resistivity and IP receiver – RIP924* - personal communication, Engineering and Env. Geophysics, Dept of Geotechnology, Lund University, Sweden Torleif.Dahlin@tg.lth.se

Daniels, J.J., 1978, Interpretation of buried electrode resistivity data using a layered earth model., *Geophysics*, Vol. 43, No. 5 (Aug); pp 988-1001.

Davis, J.C. 1986, *Statistics and Data Analysis in Geology – 2nd Edition*. John Wiley and Sons, New York. 645 pages (Smoothing algorithm – pp268-270).

Davis, P.A., 1979, *Development and Application of Resistivity Sounding Inversion for Several Field Arrays*, MSc Thesis, University of Minnesota.

Davis, P.A., Greenhalgh, S.A. & Merrick, N.P., 1980, Resistivity Sounding Computations with Any Array using a Single Digital Filter, *Aust. Soc. of Exploration Geophysicists – Bulletin*, Vol. 11 No. 1/2. pp54-62

Day-Lewis, F., White, E., Johnson, C., and Lane, J., 2006, Continuous resistivity profiling to delineate submarine groundwater discharge – examples and limitations. *The Leading Edge*. June, pp 724-728.

D'Hautefeuille, F., 2001, *Heterogeneity of a Field Site using 3-Dimensional Resistivity Imaging*, MSc Thesis – National Centre for Groundwater Management, University of Technology, Sydney. (includes a CD of animated 3-D EC imaging).

Dixon, O. & Doherty, J.E., 1977, New interpretation methods for IP soundings. *Bull. Aust. Soc. Explor. Geophysics*. Vol 8, No. 3., pp 65-69.

Dobrin, M.B. & Savit, C.H., 1988, *Introduction to Geophysical Prospecting*. Fourth Edition. McGraw-Hill, New York. ISBN 0-07-100404-1, 446 pages.

Edwards, L.S., 1977, A modified pseudosection for resistivity and IP., *Geophysics*, Vol 42, No. 5 (August 1977); P. 1020-1036.

Enever, D., (1999) *Coleambally Irrigation Area groundwater simulation model: Model calibration and analysis of scenario results.* Consultancy report 99-6. CSIRO Land and Water, Griffith, NSW.

Fetter, C.W., 1988, *Applied Hydrogeology*, 2nd Edition. Merrill Publishing Co. (http://www.vonl.com/CHIPS/apphyd4.htm), ISBN 0-675-20887-4, 598 pages.

Forward, P., 2004, SA's River Murray salt interception schemes' successes so far and challenges for the future – *9th Murray Darling Basin Groundwater Conference - Powerpoint presentation – conference proceedings*, Feb. Bendigo.

Gibbs, Simon, approx. 2001, *Horticultural Salt Bag – Water and soil salinity monitoring kit*. NSW Agriculture – Salt Action. www.agric.nsw.gov.au/reader/16

Gippsland Lakes Board. 2007, Why is stratification a problem, Gippsland Lakes Environmental Study – Fact sheet No. 5. http://www.gcb.vic.gov.au , Gippsland Coastal Board, Bainsdale, Vic. Australia.

Hatch, M., Barrett, B., Bennetts, D., Heinson, G., Telfer, A., and Roberts, C., 2002, Improved near surface mapping in groundwater studies: Application of fast-sampling time-domain EM surveying methods. *ASEG Preview*, (Feb) pp. 25-29.

Harding, J., 2002, *Investigation of channel seepage in the CIA using EM-31 technology – Coleambally Irrigation Summer Vacation Program*. CIA internal document.

Heslop, W.A. & Murphy, T.J., 2002, Evaluation of the EM-31 to identify areas subject to channel seepage. *Proceedings of a conference held at Yanco in 2001 - Electromagnetic techniques for agricultural resource management* – ed. Beecher, H.G., Australian Society of Soil Science, Inc. Riverina Branch.

Hodson, A., 2001, *Groundwater Flow and Solute Transport Emulation Model at Stott's Farm, MIA*, MSc Thesis, Universtity of Technology, Sydney.

Hornbuckle, J. & Christen, E., 1999, *Physical properties of soils in the Murrumbidgee and Coleambally Irrigation Areas*, CSIRO Land & Water, Griffith, Technical Report 17/99

Hotchkiss, P.E., Wingert, C.B. & Kelly, W.E., 2001, Determining Irrigation Canal Seepage with Electrical Resistivity., *J. of Irrigation and Drainage Engineering*/ Vol. 127, No. 1, Jan/Feb.

House of Representatives, House Standing Committee on Science and Innovation, 2004, *Science overcoming salinity: Co-ordinating and extending the science to address the nation's salinity problem.* Parliament of Australia. ISBN 0 642 78468 X http://www.aph.gov.au/house/committee/scin/salinity/report.htm.

Hughes, J.D., *Southern Irrigation SOILpak – For irrigated broad area agriculture on the Riverine Plain in the Murray and Murrumbidgee valleys.*, Editor Evans, L.H.

Inman, J.R., 1975, Resistivity inversion with ridge regression. *Geophysics*, vol. 40, no. 5. pp. 798-817

Jennings, L.S. & Osborne, M.R., 1970, *Applications of orthogonal matrix transformations to the solution of systems of linear equations.* Aust. Nat. Univ. Computer Centre, Canberra, Tech. Report No. 37, 45p.

Kamenetsky, F. and Oelsner, C., 2000. Distortions of EM transients in coincident loops at short time-delay. *Geophysical Prospecting*, 48: 983-993.

Kelly, W.E., 1985, Electrical Resistivity for Estimating Ground-Water Recharge. *J. of Irrigation and Drainage Engineering*, Vol 111, No. 2, pp. 177-180.

Koefoed, O., 1970, A fast method for determining the layer distribution from the raised kernel function: *Geophys. Prosp.*, v. 18, p. 564-570.

Koefoed, O., 1979, Geosounding Principles. In: *Methods in Geochemistry and Geophysics ; 14A- Resistivity sounding measurements*. Elsevier, Amsterdam. ISBN 0-444-41704-4

Kuras, O., Beamish, D., Meldrum, P., and Ogilvy, R., 2006, Fundamentals of the capacitive resistivity technique., *Geophysics*. Vol. 71, No. 3; pp G135-G152. 10.1190/1.2194892

Lane, J., 2003, *Continuous Resistivity Profiling*, Office of Groundwater, Branch of Geophysics, USGS, URL: http://water.usgs.gov/ogw/bgas/crp/

Leany, F., and Harrison, A. 1998, Estimation of Leakage from Irrigation Channels Using Hydrochemical Techniques, *Australian Committee on Irrigation and Drainage Conference 'Are your channels leaking' workshop – Moama*. Graphs and notes refined from overhead transparencies after discussion with the principal author.

Leeder, M.R., 1982, *Sedimentology Process and Product*, Allen and Unwin, (p152 fig 15.19). London, Boston. 344 pages.

Loke, M. H., and Barker, A. D., 1996, Rapid least-squares inversion of apparent resistivity pseudosections by a quasi-Newton method: *Geophysical Prospecting*, **44**, 131-152.

Loke, M.H. and Lane, J.W. 2004, Inversion of data from electrical imaging surveys in water-covered areas, Extended abstract (and paper submitted for publication in *Exploration Geophysics*), *Proceedings of the Australian Society of Exploration Geophysicists Conference* (August), Sydney.

MacInnes, S., 1999 *Notes on Resistivity/IP Array Sensitivity*. Zonge Engineering and Research Organisation Document unpublished at time of contact. Tucson, AZ, USA.

MacInnes, S., and Raymond, M., 2001, *TS2DIP – Smooth-Model Resistivity and IP Inversion with topography version 4.00,* Zonge Engineering and Research Organization, Inc. zonge@zonge.com , Tucson, AZ, USA.

MacInnes, S., 2005. STEMINV: Smooth model TEM Inversion. Zonge Engineering, Tucson, AZ, USA.

Marquardt, D.W., 1963, An algorithm for least-squares estimation of non-linear parameters: *J. Soc. Ind. & Appl. Math.*, v. 11, p. 431-441.

Marsden Jacob Associates, May 2003, *Improving Water-use Efficiency in Irrigation Conveyance Systems: A Study of Investment Strategies*, Land and Water Australia, Product Number PR030516, ISBN 0642 760 993 (print) 0642 761 000 (web) www.lwa.gov.au

McLachlan, M., 2000, *Data Collection Report for the Modelling of Groundwater Dynamics and Salinity at Stotts Farm, M.I.A.* , MSc Thesis – National Centre for Groundwater Management, University of Technology, Sydney.

McNiel, D., 1980, Geonics Limited Technical Note TN-6 "*Electromagnetic Terrain Conductivity Measurement at Low Induction Numbers*", www.Geonics.com

Merrick, N.P., 1974, The pole-multidipole method of geoelectrical sounding. *Bull. Aust. Soc. Explor. Geophys.*, Vol.5, No.2, 48-64.

Merrick, N.P., 1977, *Resistivity Sounding for Groundwater.* MSc Thesis – Univ. of Sydney.

Merrick, N.P., 1997, A new resolution index for resistivity electrode arrays. *Exploration Geophysics*, 28, 106-109

Merrick, N.P. and Williams, R.M., 1998, *Whitton Geoelectrical Survey*: October 1998, NSW Department of Land and Water Conservation, Sydney, CNR 98.033.

Merrick, N.P., 2000, *Groundwater Geophysics Course Notes*, UTS, unpublished.

Merrick, N.P., 2000, *Optimisation techniques for groundwater management*. PhD Dissertation, University of Technology, Sydney. Unpublished, 551p

Merrick, N.P., 2002, *Buronga Saltwater Interception Scheme optimisation.* National Centre for Groundwater Management. Access UTS report – project number C01/44/007 for the Department of Land and Water Conservation – NSW.

Nabighian, M.N., 1987, *Electromagnetic methods in Applied Geophysics – Theory*, Volume 1, Series: Investigations in Geoph. Vol. 3. SEG ISBN 0-931830-51-6.

New South Wales Canoe Association, 1998, *Canoeing Guide of N.S.W. Rivers Waterways.*, McLaughlin, Sydney., 122 pages.

O'Neill, D.J. & Merrick, N.P., 1984, A Digital Linear Filter for Resistivity Sounding with a Generalized Electrode Array, *Geophysical Prospecting* 32, 105-123, 1984.

Panissod, C., Dabas, M.., Hess, A., Jolivet, A., Tabbagh, J., and Tabbagh, A., 1998, Recent developments in shallow-depth electrical and electrostatic prospecting using mobile arrays. *Geophysics*. Vol.63, No. 5, (Sept-Oct) p. 1542-1550.

Parasnis, D.S., 1986. Principles of Applied Geophysics. Chapman and Hall, New York, 402 pp.

Pels, S., 1964, Quaternary Sedimentation by Prior Streams on the Riverine Plain, South-west of Griffith, N.S.W., *Journal and Proceedings, Royal Society of New South Wales*, Vol. 97, pp. 107-115.

Reitz, J.R., Milford, F.J. & Christy, R.W., 1980, *Foundations of Electromagnetic Theory* – Third Edition, Addison Wesley Publishing Company, New York. 640 pages, ISBN 0201526247.

Rhoades, J.D., Chanduvi, F. & Lesch, S., 1999, *Soil Salinity Assessment, Methods and interpretation of electrical conductivity measurements*, FAO (Food and Agriculture Organisation of the United Nations) Irrigation and Drainage Paper 57.

Rosenberry, D.O. and Morin, R. H., 2004, Use of an electromagnetic seepage meter to investigate temporal variability in Lake Seepage. *J. of the Assoc. of Groundwater Scientists and Engineers*, a Div. of N.G.W.A. Vol 42, No. 1, pp68-77.

Roy, A. & Apparao, A. 1971, Depth of investigation in direct current methods., *Geophysics*, Vol. 36, No. 5 (October 1971), p. 943-959.

Shaw, C. 2002, *Infiltration on common rice soils within MIL*. chriss@murrayirrigation.com.au; Murray Irrigation, Deniliquin, NSW, Australia

Seigel, H.O., 1959, Mathematical formulation and type curves for induced polarization. *Geophysics*, 24, pp. 547-565.

Singh, S.K., 2003, Flow depletion of Semipervious Streams Due to Pumping, *J. of Irrigation and Drainage Engineering*, Vol. 129, No. 6, pp.449-453

Sjostrom, K.J. and Hotchkiss, G., 1996., Seepage Detection Along the Chicago Sanitary and Ship Canal Near Lockport, Illinois. *Proceedings of the Syposium on Application of Geophysics to Engineering and Environmental Problems*, Keystone, Colorado, April 28 - May 2, 1996. Published by: Environmental and Engineering Geophysical Society, 10200 W. 44th Ave #304 Wheat Ridge, CO USA 80033, April 1996, p377-386.

Slavich, P.J. & Petterson, G.H., 1993, Estimating the Electrical Conductivity of Saturated Paste Extracts from 1:5 Soil:Water Suspensions and Texture, *Aust. J. Soil Res.*, 31, 73-81.

Smith, R.J., and Turner, A.K., 1982. Measurements of Seepage from Earthen Irrigation Channels. *Civ. Eng. Trans.*, Inst. Eng. Aust., CE24(4): 338-345. - refers to incomplete reference - Wantland, D. and Goodman, D.L., 1962. Electricity Detects Canal Seepage. The Reclamation Era.

Snyder, D.D., and Wightman, E., 1999, *Application of Continuous Resistivity Profiling to Aquifer Characterization*. (Report on a dipole dipole survey on the Ohio River, KY). Available from Zonge Engineering and Research Organization. www.Zonge.com

Snyder, D.D., MacInnes, S.C., Raymond, M.J. and Zonge, K.L. 2001, Continuous Resistivity Profiling in Shallow Marine and Freshwater Environments, Zonge Engineering and Research Organization, Tucson, AZ, SkipS@zonge.com, *Proceedings of the Syposium on Applic. of Geoph. to Eng. and Env. Problems.*

Soil Moisture Equipment Corp. 1986, *2800KI Operating Instructions – Guelph Permeameter Rev 8/86.* obtainable from Construction Materials Technology Network – www.QCQA.com

Song, S., Song, Y., and Kwon, B., 2005, Application of hydrogeological and geophysical methods to delineate leakage pathways in an earth fill dam. *Exploration Geophysics* (2005) 36, 92–96; also published in *Butsuri-Tansa* (Vol. 58, No.1); *Mulli-Tamsa* (Vol. 8, No.1)

Sørensen, K.I., 1995, Pulled array continuous vertical electric sounding (PA-CVES). *Proceedings of the Symposium on the Application of Geophysics to Environmental and Engineering Problems*, Orlando, 1995, p893-898.

Sørensen, K.I. and Auken, E., 2004, SkyTEM, a new high-resolution helicopter transient electromagnetic system., *Exploration Geophysics* Vol 35, No. 3. pp 191-199.

Spies, B., 1989, Depth of Investigation in Electromagnetic Sounding Methods. *Geophysics*, Vol. 54, No. 7, (July), p. 872-888.

Standing Committee for Fisheries and Aquaculture, Australia, 1997, *Australian Code of Electrofishing Practice*, NSW Fisheries Management Publication No. 1, ISBN 0 7310 9412 3

Stevens, R. 1998, *Ready-to-Run Delphi 3.0 Algorithms – Time Saving Blueprints for Developers*. Wiley, New York. 398 pages (p266 - Binary Search Algorithm).

Stewart, B. 1994, *Coleambally Irrigation Area Channel Seepage Report*. Coleambally Irrigation Co-operative Limited, Coleambally, NSW.

Stewart, B. 1996, *Coleambally Irrigation Area Channel Seepage Report*. Coleambally Irrigation Co-operative Limited, Coleambally, NSW.

Street, G. J., Parson, S., Allen, D., and Hatch, M., 2003, Irrigation channel seepage investigation: *Proceedings of the Aust. Soc. of Explor. Geoph. 16th Geophysical Conference and Exhibition*. Expanded Abstracts, Adelaide.

Telford, W.M., Geldart, L.P. & Sheriff, R.E., 1990, *Applied Geophysics*, 2nd Edition, Cambridge University Press, Cambridge. 770 pages.

Thomsen, R., Søndergaard, V.H., & Sørensen, K.I., 2004, Hydrogeological mapping as a basis for establishing site-specific groundwater protection zones in Denmark. *Hydrogeology Journal* vol12, no. 5:550-562

Toome, P., 2004, An Alternative Measurement System for Soil Moisture Tension – *Proceedings of the Irrigation Association of Australia Conference*, Adelaide, May.

Roelof Versteeg, R., Ankeny, M., Harbour, J., Heath, G., Kostelnik, K., Mattson, E., Moor, K., and Richardson, A., 2004, A structured approach to the use of near-surface geophysics in long-term monitoring. *SEG - The Leading Edge* Vol 23, No.7, July, ISSN 1070-485X. pp 700-703.

Viezzoli, A. & Cull, J.P., 2005, Induced Polarization measurements applied to irrigation canals freshwater seepage detection, Submitted to *Near Surface 2005* – Palermo, Italy, Sept.

Volmer, B., Hatch, M., Wilson, T. and Hill, T. 2004, River-borne NanoTEM survey for location of salt accession to the River Murray at Loxton, Extended Abstract, *Proceedings of the Australian Society of Exploration Geophysicists Conference* (August).

Wright, M., 2002, *River Murray Charts – Renmark to Yarrawonga (includes 60km of River Darling)*, Seventh Edition (http://www.rivermurraycharts.com.au/).

Zhadanov, M.S. and Keller, 1994, *Methods in Geochemistry and Geophysics, 31 – The Geoelectrical Methods in Geophysical Exploration.* Elsevier, ISBN 0-444-89678-3

AERIAL PHOTOS

Land and Property Information Centre, NSW Department of Lands, Bathurst., www.lpi.gov.au

SOFTWARE SOURCES

Search these sources via a web search engine for latest releases unless specified otherwise.

Aarhus Hydrogeophysics Group software for geo-electric and electromagnetic device evaluation – EMMA, Pulled Array Continuous Electric Sounding, continuous

electromagnetic sounding – both pulled and airborne – SEMDI, SEMVI, Workbench and Electrical Conductivity database facilitation – GERDA.

Allen, D.A., 2006, HydroGeoImager. Software accompanying this thesis also available from www.GroundwaterImaging.com

Delphi 7 www.Borland.com

EM31 www.Geonics.com

ESRI ArcView 8.3 www.ESRI.com

Exploration and Mining Markup Language (XMML), Geographic Markup Language (GML) – http://www.seegrid.csiro.au/xmml

Geoscience Australia (was AUSLIG) web site – excel spreadsheet facilitating conversion of latitude and longitude to UTM coords.

MacInnes, S., and Raymond, M., 2001, *TS2DIP – Smooth-Model Resistivity and IP Inversion with topography version 4.00,* Zonge Engineering and Research Organization, Inc. zonge@zonge.com

MacInnes, S., 2005. STEMINV: Smooth model TEM Inversion. Zonge Engineering, Tucson, AZ.

Merrick, N.P., 1977, DCInvert - 1D inversion software and updates – nmerrick@uts.edu.au

Merrick, N.P., unpublished Normalised Depth of Investigation Equation for the Geonics EM31 – Excel Spreadsheet – Validity confirmed by Geonics TN-6. nmerrick@uts.edu.au

Paint Shop Pro v7, 8 and ProX. – Corel.

Shapefile support code :- http://gdal.velocet.ca/projects/shapelib/shapelib.html

Res2Dinv – algorithms by Loke (www.geoelectrical.com).

Slicer - Fortner Research LLC, 1996, SLICER 3D for Windows version 1.1, Fortner research LLC, USA.

Steema Software TeeChartPro version 7 www.steema.com

Surfer - Golden Software, 1995, SURFER Versions 5 Surface Mapping System, Golden Software Inc. Colorado.

APPENDIX 1 - GEO-ELECTRIC ARRAY DESIGN AND CONSTRUCTION GUIDE

Taking the design factors of Chapter 7 into consideration the following arrays were designed. First, the most favoured designs will be examined and then, many designs that have been tried and rejected will be discussed. Photo montages (Figures A1-1 and A1-2) graphically present many steps referred to in the text by photo numbers.

A1.1 Small submersible array design

Very cheap and sufficiently strong arrays can be constructed using 1.5mm^2 conductor 5 core 15Amp cable which is readily available for use in 3 phase factory wiring. It is durable enough to take pulling forces applied in most surveys with the exception of submerged seawater surveys where huge survey craft are used. It must be used in conjunction with an appropriate high strain tethering device such as a long spring, rubber strap and/or flexible fibreglass encased boom. Joining of two 5 core cables, side by side, by plastic welding or gluing with PVC glue allows for weight and cross section area reduction at a point along the cable length where one of the cables is no longer needed. Joining of separate cables also permits good separation of high and low level signals and cancellation of major noise problems by twisted wire methodology. The 2 lowest signal pairs of wires are twisted into one cable while the highest signal (and power) pair (the transmitter wires) is twisted into a separate cable.

Electrodes are made of thin pipe (copper) of exactly the same (or a fraction of a millimetre more) ID as the OD of the cable. They can be cut with neat rounded ends using a standard pipe cutting tool (1).

The edge of the part of the electrode that is to be exposed (typically 40mm or more from the end) scribed with the cutting tool for later reference (2).

The photo montages (Figures A1-1 and A1-2) show a technique where a small hole is drilled 4mm from a pipe end (3). Additionally, a recess in the pipe end is cut and filed. If the hole is drilled too close to the end, then the wire that is to be soldered onto it will have its rigid soldered end poking out the end of the electrode where it can catch on things and cause waterproofing problems. If it is drilled too far from the end then it will be difficult

to clean off solder dags to allow the electrode to slide along the cable. The part of the electrode at the hole is crimped inwards 0.5 mm. A short (100mm) joining wire of 0.5mm^2 CSA is soldered onto it (4) (note that a braising torch is needed to supply enough heat for this operation as the copper electrode quickly conducts away heat). To make the soldered join both streamlined and strong, the wire is fed through the electrode from the far end, up into the drilled hole and then the end of it with insulation removed is recessed into the crimped part of the pipe where soldering is done (note solder should also fill the drilled hole). The electrode is then finished by sanding and filing off excess solder and the curved in edges of the pipe that would otherwise dig into the cable as one attempts to slide the electrode over the cable. The technique shown in the diagrams now has been modified because cable flexing near cable ends can result in breaking of the soldered connecting wire. Additionally, when the connecting wire is spliced into the cable and then the splice is slid into the electrode, flexing and bunching of the connecting wire weakens it. As solder seeps along it during the soldering process, stiffening it, it can only withstand a very limited amount of flexure. Connecting wires are now connected to small hole drilled at the end of a groove in the middle of the electrodes where flexure is less of a problem. The electrode is splayed open during the spicing operation and then crimped shut afterwards. The groove is then filled with resin.

Many of the electrodes have two or more cables passing through them. These electrodes need to be made of two or more pipes soldered together using the braising torch (5). If three pipes must be soldered together then they should be soldered in a plane rather than in a triangular bunch as shown. This is because flexure, around a tight radius of curvature, of the cable at the end of a triangular bunch electrode results in great cable strain.

The cables are then marked out with distances to electrodes (6). Eighty millimeter lengths of good quality heat shrink with the inner surface coated with resin are cut to cover each end of each electrode.

Using ‘Slippery Lube’, and by anchoring one end of the cable to a strong anchor point, it is then possible to slide all the electrodes and heat shrink onto the two cables (7,8,9). Heat shrink lengths are placed in order with the electrodes and fed sequentially along the cable. Once nearly in position, it is then time to cut windows into the cable sheaths.

Electrodes are added over small windows cut into the outer sheath of the cable which needs to be carefully removed a little at a time using a sharp knife. A mistake made in this operation will be difficult or impossible to remedy so immense care is needed. After cutting the hole in the outer sheath, enough insulation on the appropriate wire within is removed with a sharp knife, again exercising immense care. The small wires attached to the electrodes are spliced into the appropriate wires in the sheath windows. Then the splicing points are soldered (10). Insulating resin is then melted back around the wires within the window taking care to ensure that no water can enter even if the window is stretched or flexed slightly. Care must be taken to ensure that the cable cross section is not greatly altered at the windows by messy splicing and gluing. While the resin is still molten, the electrode is heated with a heat gun and slid over the splices flexing the attachment wire back into the electrode in the process (11). Recall, however that splices are now being conducted in grooves within electrodes which results in slight modification of this process involving less connecting wire flexure. This flexure is not a significant risk as the window will be covered by the rigid electrode however during stretching, individual conductors can slide along inside the cable sheath and the wire joined to the electrode will break off if the conductors are not bound together with the sheath at the windows by the meltable glue. If no faults in the cutting operation occurred then a break in the melted resin insulation will have no effect except in one case – at the cable end.

As it is necessary for wires to be spliced into rather than cut and joined, they continue on to the cable end where they can leak voltages if not sealed well. They are continued as they are needed for cable strength and integrity. Also cutting them would still leave the excess length of each wire in the cable and if the ends of them were not sealed well then those lengths could leak current if water enters the cable sheath. After sealing the window, ‘Slippery Lube’ is again applied under the electrode until it slides and then the electrode is heated to the point where it just does not melt the PVC cable sheath. More glue is applied from the melting glue gun over the window and the electrode is quickly slid over the window ensuring that the joining wire disappears under the electrode end and that the window is thoroughly covered. In order to ensure that a watertight seal is attained, one must be careful to bring the cable sheath to melting point where it contacts the glue gun glue. The heat shrink end covers are brought over the electrode and shrunk on using the heat gun (11). Electrical tape can then be applied over the heatshrink to increase its abrasion resistance and to supply a layer that can be easily maintained as abrasion occurs.

Once the electrode cools, because it is glued to the cable sheath, it will not be moved along the cable if it is caught on any obstacle.

It is sensible to make the cable to the last one or two electrodes thinner as it carries fewer conductors (1 or 2). This involves a cable join conducted in a similar manner to the electrodes. At the end of the cable or at cable joins, each conductor should be terminated in a staggered manner and insulated separately (12). The last electrode can be made simply by stripping windows into the last metre or so of the sheath of its wire. A significant length of conductor can be windowed (to increase exposed surface area and thus reduce contact resistance) as the electrode position is not critical at such a distance. The result does not look strong but certainly is most efficient in avoiding 'snagging' and thus the need for strength. It can also be cheaply replaced by wire replacement (but with care taken when joining). The author has never experienced any problem with these crude simple electrodes at array ends and so highly recommends them. As stress along the cable is multiplied as one approaches the anchoring point, the effect of reducing cable diameter near the cable end is that of greatly reducing stress at the anchoring point. This is very important if the towing vehicle has little power. It is also very important for reducing abrasion and stress along the cable.

Once each individual cable is constructed, it is attached to the other cables by gluing, taping or plastic welding (16). Taping is a cheap but poor solution as tape gets scraped off and then 'snags' catch under the remaining tape. A design modification for increasing electrode surface area is to add electrodes to both cables at every point where an electrode is connected into one of the cables (5). If this design modification is present, then when joining cables together, these electrode parts must also be joined together. They can be soldered together (5). The solder join is strong enough to endure a great deal of wear and tear.

In order to get the cable to remain submerged when traveling at speed, a length of hose about 3 times the intended depth of usage and containing lead shot is attached to the leading end of it just before the leading current electrode. Alternatively, an insulated copper earthing rod can be attached. This part of the cable drags transversely through the water and must be both streamlined and heavy to keep the cable on the water bottom. By adding length to the lead in section, the weight required in the lead shot filled tube is reduced. 15m of lead in allows for practical operation in 3m of water.

At the anchor point end of the cable, an anchoring device and stretch section must be added. The anchor is normally a device through which the cable zigzags enough to prevent it from sliding. The cable past the anchoring device is then loosely attached in loops along the stretch device (such as a thick rubber strap) which is firmly anchored to the towing vehicle.

The cable is terminated by a group of durable banana plugs (13), selected because they can be fed through cable glands and other small openings of approximately the same diameter as the cable. Also, when they are harshly treated or immersed in water, they generally survive. Slimline multiconductor connectors were tried but rejected because of cost, lack of design for 2.5mm^2 CSA conductors and, importantly, because, when accidentally waterlogged or poorly joined, diagnosis of faults within them takes a lot of time. Even high quality military specification Bendix connectors were rejected for this reason. With 4mm plugs, the cable then can be attached directly to instruments or to extension cables (14) and/or to short cables sitting permanently through cable glands for the purpose of waterproofing equipment while maintaining easy equipment setup and pack up (13, 17).

If the cable is to be used in shallow water, then cheap commercial sonar will not be adequate for depth determination and a pressure sensor will be required. This sensor is also bundled with the cable. It is best placed just before the second transmitter electrode (near the sounding reference point) but must at least be placed after the lead in section. A Greenspan 4-20mA sensor is appropriate (of small diameter and robust design). Its cable contains an air tube which needs to be terminated at the surface using a flexible membrane that allows pressure but not humidity transfer. The membrane is housed in a small box alongside the banana plug connectors.

An alternate way of detecting pressure, and therefore depth, is via the use of the ‘bubbler’ principle in which bubbles are fed slowly down a tube with an orifice at the measuring depth while pressure is detected at the other end above water. Equipment such as the OTT Nimbus is designed for this task.

A finished submersible array is shown in (19). Electrical tape is observed at electrode ends. This is replaced periodically as abrasion occurs.

A1.2 Floating array design

Floating cable design is the same as for the submerged cable however a float is added along its length using PVC glue (16). The glue is readily available for gluing UPVC sewer pipes together and forms a very strong bond even on flexible PVC such as layflat tubing and 3 phase power cable sheathing. For a 144m array, about 8 litres of glue is necessary. The glue is best applied using a bottle with a nozzle (16). First the cables and layflat tubing are laid out and tack glued together (at places assisted with pegs that temporarily hold them together). Then gluing is done in several passes until a flange is built up between the layflat tubing and the cables. Layflat tubing makes a very good float as it slides past obstacles easily, being of constant CSA, and can be deflated in order to make shipping and storage practical. If deflated or filled with water, the floating array is easily converted to a submersible array. This change can be made easily during a survey if a pressure release valve is added to the far end of the array. Inflation using air can be done with a few breaths into a mouthpiece. Greater rigidity, which results in less 'snagging' can be added by inflating further using a few pumps on a car tyre pump. The tubing usually becomes leaky due to puncturing by sticks, knives and barb wire just like when it is used in irrigation and therefore, once old and worn requires regular repressurizing. Layflat tubing leakage does not eliminate its practicality since once an array is in motion, atmospheric pressure within the tubing is sufficient to keep the cable afloat. On occasions it can be repaired using patches or it can simply be regularly pumped up. Twenty to fourty millimeter diameter layflat tubing has been used depending on array weight. The lengths of cable extending to the last two electrodes on an array (which add about half the length of the array) may be held up by 13mm garden hose which is more compact than minimum diameter layflat tubing. The cable for these electrodes can even be laid within the hose after a fishing wire attached to a sinker is blown down the hose as a leader onto which the other wires can be attached. If this is done, the wires and its connections must be strong enough to take the stress of the hose being caught on obstacles.

Floating arrays need to be visible to other boat traffic and so need fluorescent floats along their length. Such floats can be attached by weak string to the array and must be streamlined in order to prevent navigation havoc that results when high drag devices are attached to the array. The string attachment should be weak so that the float will break off without causing further damage when it becomes 'snagged' in obstacles.

An alternative way of making arrays float in open water is to add clip over plumbing insulation lengths. The foam insulation does not slide easily past obstacles but is reasonably streamlined. It typically comes in 1.2m lengths. The lengths are only needed near electrodes and at wide intervals between distant electrodes in order to keep the array afloat once it is in motion. Such floats offer an alternate, quick and troublesome way of getting an array to float.

A finished 144m long deflated floating array is displayed in (18) packed into a shipping box. The packed array is best used with a small trolley as shown so that it can be handled by one person.

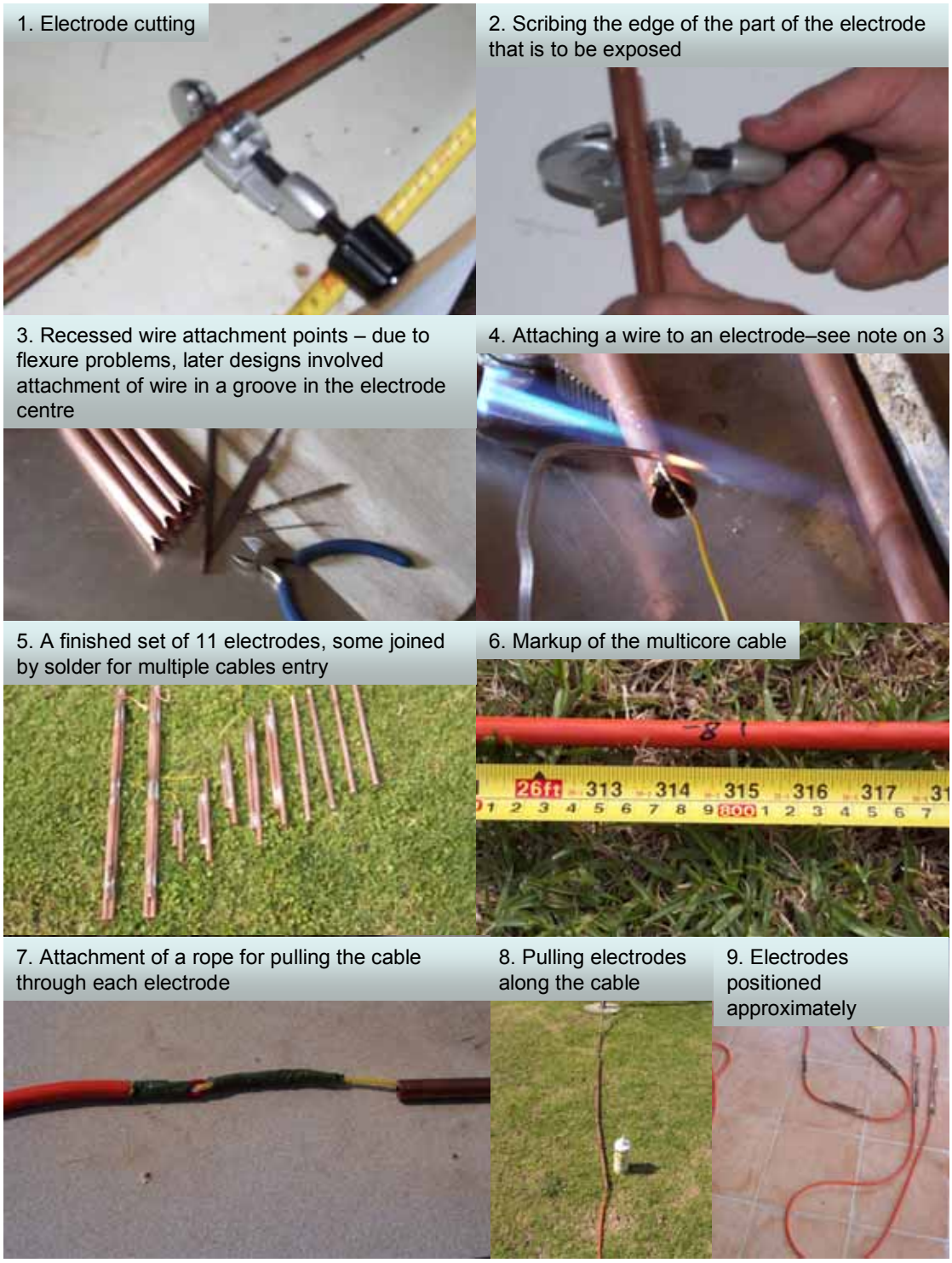

Figure A1-1 Towed geo-electric array construction – part 1.

Figure A1-2 Towed geo-electric array construction, part 2.

A1.3 Extra strength

Extra strong cables can be purchased from harsh environment cable manufacturers. They have thick sheaths with Kevlar in their core and cost around $30 per metre. Some others have a Kevlar braid in their sheath however this braid is not very effective for arresting strain. Cables can also contain waterblock compound that prevents water from trickling or condensing within the cable. Geo-electric array design using such cables works the same way as with the standard cheap 15A cable but costs many times more. 500 kg breaking strain can easily be attained by such cables but this does not ensure that takeout wires at electrodes will not get severed off if an electrode becomes caught and pulls the sheath of the cable along its core. The cheaper cable alternative is likely to be more efficient for many applications as many geo-electric arrays made from such cable can be made for the same price as one made of extra strong cable. Also, the thick conductors in the cheap cable are less likely to be severed off at electrodes, when electrodes get caught, than the thin conductors in the expensive cables.

A1.4 Varying length and configuration

At different sites, different exploration depths and depth resolutions must be provided. Navigational limitations and the necessity to operate practically where the arrays need to be lifted over numerous obstacles mean that array length needs to be limited to different lengths at different sites. It has been found that it is practical to make the last electrode of floating arrays detachable but no more. In other situations, a completely different array should be used. By removing the last electrode from an array however, about one third of the array length is removed. Connectors need to be stress bearing (100 - 500 kg), streamlined within the small diameter of the array, robust and completely watertight. Such a combination of properties does not appear to exist in commercially available connectors. Downhole logging tool connectors could work but they are expensive, heavy and time consuming and trouble prone to connect and disconnect and require regular maintenance for abrasion resistance. Keeping such connectors afloat in a streamlined cable would require very long rigid floats.

By inventing an array design that is cheap to manufacture, the problem of providing arrays of varying lengths has been overcome by making multiple arrays rather than arrays with disconnectable electrodes.

A1.5 Visibility and drag

If an array has constantly diminishing cross section area it will have least drag and the arrays described here have this. The end of the array however is not visible from the boat due to its length. Fluorescent floats added to the array cause drag thus making navigation difficult. They also catch on obstacles and therefore must be tethered in a weak manner so that they do not break the array when caught. Fortunately, the only rivers where floats are required in order to prevent other waterway users from colliding with the array are large and free of obstacles. Spring wire marker flags that folded back when they collided with obstacles were added to some arrays but caused significant drag and are not recommended.

A1.6 Geo-electric array designs that were rejected

Early geo-electric array design attempts were rejected after experimentation. First, in the earliest prototype (Allen, 1991) individual floats were used, tied on by string and these caught every obstacle they came into contact with. Wire with thin sheathing which contained many hidden faults that were only evident once the array was added to water was used. The importance of thick sheathing became evident.

Three arrays were constructed with wires running within tubing which was filled with air (or sand and Neatsford oil for a submerged array) in an attempt to keep the wire dry and thus prevent problems resulting from voltage leakage from connectors and nicks in wire insulation (see Figure A1-3). This was a success but construction time was about 4 weeks per array – wires being difficult to feed through such tubing and connect with electrodes. The electrodes were of the same large diameter as the tubing which meant that they had lots of surface area and low contact resistance, which was good. Since then, the contact resistance and current injection problems have been remedied by inventing mathematics that can cope with linear current electrodes. The necessary contact resistance of the potential electrodes was found to be met by small diameter electrodes in water/mud. The arrays with wires within tubing have been predominantly rejected because they are hard to

construct and repair – at each electrode, tubing must be terminated by hose clamps. To access wires which break, the tubing must be slid back but this is not easy as it does not crumple up easily within the space between adjacent electrodes where it is anchored. Kevlar rope was added inside the arrays to give them 750kg breaking strain and thus eliminate wire breakage. During a test where a strengthened array was towed at power using a 140 hp motor wires still broke as a result of binding against the rope. As a result of wire flexing, it is believed that the wires broke where the rope slid along the wire at a point then bound tight at two different points and broke wires. Anchoring the rope at the electrodes in such confined space proved to be difficult. The Kevlar rope is expensive and the whole idea turned out to be a very expensive mistake. This style of design is routinely used in large seismic streamers but obviously cannot be simply scaled down for use in small diameter streamers. Numerous surveys were conducted with such cables successfully.

Figure A1-3 An old rejected design of geo-electric array in which all wires and a strain bearing cable are inside the float tube.

The first submersible array design was made very heavy and towing force required was excessive. In order to reduce towing forces, and consequently, cable wear and tear, submersible arrays should be made to be very lightweight, particularly at their far extremity. They should also be constructed at a density just greater than that of water so they almost have neutral buoyancy.

One array was made with numerous electrodes and connectors along its length so that its length and configuration could be adjusted. This proved to be a bad idea as the weight and complexity brought additional problems, particularly when trying to diagnose wire breakages. It is more sensible to make multiple arrays with connectors only for adding/removing the most distant electrodes.

A1.7 Noise considerations

Tests of electrodes submerged in water were conducted using a Terraohm RIP924 24 bit geo-electric receiver by Allen and Dahlin (2005). The electrodes used were stainless steel and stacking interval was 2 seconds. When the electrodes were stationary in the water, noise was around 50 uV per 2 second sample. When the electrodes were pulled at 1-2km per hour, noise increase to 2mV.

Bronze, copper and stainless steel electrodes were used by the author but in field conditions, no difference in noise could be detected. Due to the high cost of rental of transmitters and receivers, few noise tests could be conducted for this PhD. Lead electrodes are commonly used for borehole IP logging due to their inertness. Similar electrodes could easily be made on towed geo-electric arrays described above by melting solder (principally lead with some tin and silver) over copper electrodes. Non polarizing electrodes have been used on land based surveys for many years. They consist of copper electrodes in copper sulphate solution in porous pots. Fixing of this type of electrode onto a towed array would result in a protrusion in the cable that would catch on obstacles and would require considerable engineering. Iris instruments www.IrisInstruments.com and Advanced Geosciences Institute www.AGI.com have experimented with graphite electrodes but the author could not find any publication on the performance of such electrodes.

As noise testing requires use of transmitters and receivers for periods of time and funding for rental of such equipment could only be arranged for field surveying, the electrode noise issue could not be adequately addressed. A flume tank is recommended for such testing because field conditions are very difficult to control.

APPENDIX 2 - TOWING DEVICES, LOGISTICS AND SURVEY PRODUCTIVITY

Chapter 7 summarized a range of towing devices and the logistics and productivity of operating them. In this appendix, details of those devices will be given along with logistics for operating in particular environments and at different speeds.

A2.1 Towing devices – details

Detailed notes about more viable towing devices and their applications are given here.

A2.1.1 Boats with outboard motors – river and lake surveys

A 14 foot boat with a 30hp 4 stroke engine, canopy and tilt trailer was used for most of the large river surveys and proved to be very appropriate (see Figure A2.1). The space, shade and power were very much appreciated as was the fuel economy of the 4 stroke motor for the many 60km long surveys conducted around Mildura. In contrast, a smaller 2 stroke outboard jet propelled boat once used proved to require too much fuel (80 litres per day) and was very unpleasant to operate for such long periods of time. Use of a co-ordinated land vehicle (even a taxi at some more populated locations) is highly recommended as it removed the need to return upstream slowly by boat which, at some sites meant that 60 km rather than 25km of river could be surveyed in one day.

On rivers with numerous fallen trees across them, a flat vee 12 foot boat proved to be appropriate. It could be rushed at fallen trees, pushing a bow wave of water over them. Backing of the power upon reaching the fallen tree then meant that the boat rose up on the bow wave and scraped over the fallen tree. At the last moment, the motor needed to be raised to avoid impact. Use of a flat bottom punt at such locations would reduce draught but result in serious problems (sinking) when the punt tilted on or got pushed up against logs by river currents.

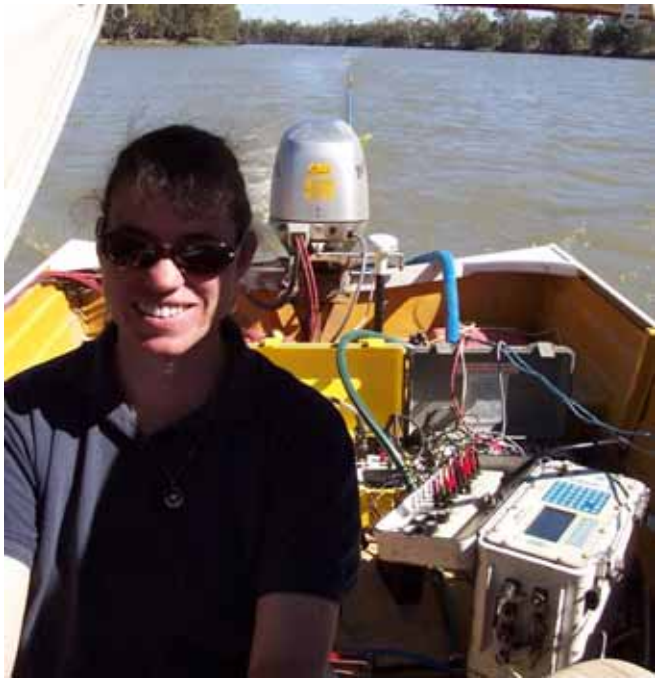

Figure A2-1 A 144m array being towed by a 14' boat with 40hp 4 stroke motor on the Murray River near Mildura.

A2.1.2 Boom extending from a 4wd – canals with maintained bank access

The boom towed geo-electric array capably functioned at about 7 km per hour and negotiated isolated obstacles at this speed simply by towing the device out of the canal and along the ground and then back into the canal. Weed in canals presented no problems at all to the boom towed array. Fences were negotiated by raising the boom, feeding in the array and proceeding to a gate. An improved boom design could permit survey out to 6 metres with the ability to straddle large shrubs and fold when raised to avoid exceeding legal on road vehicle dimensions. The submerged array, typically towed by the boom for survey of canals for seepage investigations had a lifespan of reliable operation that has not finished but is estimated to be of 200-1000km. As such arrays can be constructed in 3 days, this survey combination seems to be about as good as can be offered.

The original boom design is presented in Figure A2-2 below. FigureA2-2 and A2-6 are photos of the boom in ideal conditions while Figure A2-4 shows its application in challenging circumstances. Figure A2-5 is a photo of the boom partially raised in preparation for high speed travel away from canals. The raised boom can be driven stably at at least 80 km per hour. A Landrover was chosen as the 4wd because of its excellent

articulation and lack of stabilizer bars. Such suspension results in smooth travel along non-graded canal banks. Without such suspension, the boom would bounce up and drop down repeatedly during survey. The boom is easily dismantled and tied on the roof rack for long distance travel. It is made of fiberglass encased bamboo with PVC fittings at its extremity. Near the vehicle, it is made of steel. The long reach of the boom gives it a lot of vehicle tilting leverage so it must be kept very light, especially since the 4wd must travel at times along uneven precarious slumped canal banks.

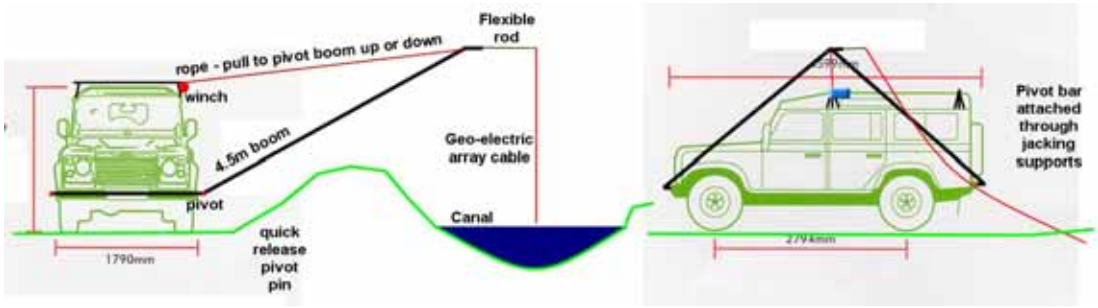

Figure A2-2 Design of a 4.5m boom for towing electrode arrays along canals.

Figure A2-3 The boom towing an array along a weed filled irrigation canal.

Figure A2-4 The 4.5m boom towing an array along a drain. Note that the boom reach has been exhausted and that a 6 metre boom would be more appropriate at this location.

Figure A2-5 The boom partially raised in preparation for high speed travel. The blue tube towed a pressure sensor which, on this survey was not incorporated into the array due to short term rental.

The array could be towed through canals and furrows with just mud at their base such as in Figure A2-6. Intermittent contact problems resulted but these could be accommodated using software filters.

Figure A2-6 Using a boom towed array, farm canals, furrows and rice bays with less than 20mm of water in the bottom of them could be surveyed as shown. Data from such canals had to be filtered with a low current filter due to the current electrodes coming out of the intermittent water at some locations.

Just before completing this thesis, a 6 metre long boom operated by an electric winch and with a joint in the middle of it was constructed. The joint enabled the boom to be raised over shrubs and small trees on canal banks without stopping survey. This device, pictured in Figure A2-7, was made of aluminium encased dowel, PVC pipe and joiners and joint reinforcement made of resin encased string and glass fibres.

A problem with towing arrays with booms is that grass on canal banks clogs vehicle radiators. Regular and extensive radiator cleaning adds survey cost.

Figure A2-7 A recent enhanced boom design with a 6 metre reach and electric winch control. Articulation allows for raising over shrubs and folding for on road travel.

A2.1.3 Canoes/Dingies, various propulsion devices and 4wd mounted cranes – canals and rivers with weed and/or numerous obstructions and discontinuous bank access

Canoe/dingy towed EC-arrays, either floating or submerged, require assistance from a 4wd mounted long reach crane in order to be productive except on the larger less obstructed canals because there are simply too many obstacles on the canals. There is also much weed in the canals that would foul an outboard motor propeller so the canoe/boat would need to be alternatively propelled in order to be practical. Suitable propulsion devices have been investigated but sufficient funding was never applied in this thesis to create a viable full size device. Devices investigated were lightweight paddle wheel or air propeller propelled devices. Figure A2-8, below, shows a prototype small scale air propeller propelled canoe that could pass easily over weed filled shallow rapids. The engine was not sufficient for towing an array at speed and an upsizing is planned and designed. The submerged array, which is the main array used on canals, requires

significant towing power. A paddlewheel propelled device has been used by water weed harvesters (see photo on Coleambally Irrigation wall).

Long floating arrays are useful for imaging to a depth of 40m for groundwater studies and siting of bores but the cost to productivity ratio of pulling in long arrays in order to negotiate obstacles does not warrant their use solely for canal seepage studies where a 20-36m submersible array is most efficient.

Figure A2-8 A prototype small scale air-propeller propelled canoe capable of negotiating weeds without fouling shown here crossing rapid filled shallow rapids in the Macquarie River. This prototype is being scaled up and refined to produce a useful survey device.

Although problems with watercraft on canals are numerous, most of this thesis was conducted with a canoe or small boats in weed filled canals with a 3.3 hp 2 stroke motor and a paddle. A 4wd mounted crane could not be afforded so the canoe was physically lifted over numerous obstacles after removing heavier objects from it. It was found that it could easily be rolled across roads by dropping PVC pipes under the front of it. The canoe was chosen due to its ability to fit in very narrow canals and due to its light weight necessary for man handling of it over obstacles. After crossing canal regulators, the canoe would be put into the water and survey would continue while an assistant pulled the array over the regulator with assistance of the outboard motor. This procedure saved considerable time and reduced the size of gaps in data at regulators.

Outriggers were added to the canoe regularly (see Figure 7-1c) and greatly stabilized the canoe without adding much weight. Without them, it was very difficult to get out of the canoe in deep water.

The following photos (Figures A2-9, A2-10, A2-11 and A2-12) demonstrate the types of problems experienced when using boats and canoes in canals.

Figure A2-9 Passing through a patch of weed that totally clogged a medium sized irrigation canal.

Figure A2-10 Pulling a canoe along an acid sulfate and acid loving weed filled swamp drain in a skewed manner using an outrigger and ropes to keep it away from a canal bank while straddling an electric fence. The canoe is towing a functioning 144m array. The outboard motor would not function in this weed. This looks hard but is actually fairly easy and fast. It is easy to see how an alternate motorized propulsion device could improve productivity in situations like this.

Figure A2-11 Passing under a typical bridge while towing a geo-electric array.

Figure A2-12 Passing under a typical fence canal crossing with a boat.

A2.1.4 Argo – marshes and swamps

The Canadian-made Argo (see Figure A2-13) amphibious vehicle is probably an ideal vehicle for large swamp surveys as it can move across boggy land as well as water. For higher speed travel, an outboard motor can be attached to the rear. For most waterborne surveys it is not appropriate because it has limited capacity to drive up steep slopes out of waterways.

Figure A2-13 An Argo amphibious vehicle appropriate for survey in marshes. Note the problem of driving the Argo up steep banks out of waterways.

A2.1.5 Radio controlled devices – highly obstructed canal studies

Some brands of geo-electric array electronics are very light and compact. For canal seepage surveys, often only shallow sub-canal investigation is required so towing forces are minimal. The author figured that efficient crossing of weed filled parts of canals, and of canal obstacles, the main factors affecting canal survey productivity, would be much easier if a lightweight radio-controlled air propeller driven watercraft could be used instead of a heavier manned watercraft. Attempts at design were made with the assistance of some experimentation. Results are presented in Figures A2-14 and A2-15.

The radio controlled device now appears to be inappropriate because submerged arrays proved to be most successful for identifying canal seepage and submerged arrays require considerable towing force which in turn requires a heavier towing device which may as well have a pilot rather than radio controls. The radio control device, once refined and miniaturized, could however be very useful for carrying other sensors on water bodies, particularly on dangerous tailings dams. On canals it has a major drawback because it has no way of propelling itself in reverse off obstacles. Lack of a sensible solution to this drawback discouraged further development of the radio-controlled airboat.

Figure A2-14 Experimentation leading towards production of a radio controlled platform for geo-electric surveying in weed filled canals. Note the 18'' propeller attached to the grass trimmer used for initial experimentation.

Figure A2-15 A close-up of a experimentation leading towards a radio controlled platform designed for geo-electric surveying.

A2.1.6 PACES and ripping tine towed arrays – soil stratification studies

The possibility of conducting towed geo-electric arrays across land exists but is immensely challenging. Devices for EC imaging across land are discussed in detail in the chapter on terrestrial EC imaging included in this thesis.

A2.2 Survey logistics for particular jobs

A2.2.1 Open waterways

Open waterways such as large canals, dams and lakes can have large waves propagated in them. Such waves can often only be crossed head on and have made some surveys very difficult and frightening in small watercraft.

A2.2.2 Long river surveys with limited access

On long river surveys with limited bank access, such as the Border Rivers surveys, productivity was almost entirely determined, and compounded, by a combination of communication difficulties with the land vehicle, difficult boat launching site access and fallen trees that blocked the river at places. Continuous survey was only possible at all on the Border Rivers due to raised water level conditions resulting from flooding. After attempting continuous survey for one day, only isolated site up-and-back type surveying was conducted.

Although many fallen trees were negotiated, the 144m long array only tangled once. When up-and-back style surveying was conducted, the array length was reduced to 80m as letting out 144m of cable numerous times in a day is time consuming.

Figures A2-16, A2-17 and A2-18 reveal some of the difficulties encountered when surveying on the Border Rivers which are typical of many inland Australian waterways.

Figure A2-16 Every 100m or so along sections of the Border Rivers, fallen trees complicate navigation. The boat and array had to be weaved in and out through interfingering branches at sufficient speed to prevent current from pulling the boat sideways into branches and sufficient speed to get the boat to launch and slide over shallowly submerged branches.

Figure A2-17 More ‘snags’ typical of the Border Rivers.

Figure A2-18 More ‘snags’ typical of upper floodplain stretches of Murray Darling Basin rivers.

A2.2.3 Dams

Dams often need to be surveyed to determine where most seepage losses are occurring from them. Submerged arrays towed in a grid pattern across dams give a 3D picture of the hydro-stratigraphy beneath the dam. A canoe propelled by an outboard motor or other device travels the grid plus some perpendicular lines and a perimeter line while towing a pressure sensor and a submerged geo-electric array. A typical ring tank can be surveyed with lines spaced 20m apart in a matter of hours. There is just one unique factor about surveying dams – the course that must be followed is not readily identifiable. Either one has to set up high visibility markers every 40m along opposite banks before commencing or they have to obtain a GPS routing device and optionally, a track-bar. Most base level GPS have some routing capability which is sufficient but more expensive agricultural GPS routing devices designed for tractors are much more appropriate.

A2.2.4 Canals and drains

Canal and drain surveys typically need to be conducted very cheaply due to meager budgets offered for seepage and salinization site identification. The key to efficient surveying of them is in rapid obstacle negotiation. To compete, it seems that it is appropriate to be set up to use diverse towing devices to quickly negotiate all the obstacles most appropriately. For productivity, it is important to have a two-man crew even when using a 4wd mounted boom that can easily be operated by one person. The second person deals with all the obstructions as, or preferably before, they are encountered.

A2.3 Speed versus data quality

Surveys are typically conducted at between 6 and 10 kilometres per hour. Above about 11 kilometres per hour, watercraft break into a more turbulent and inefficient manner of flow which makes further increase in speed difficult. The increase in electrical noise with respect to speed is thought to be a result of electro-kinetic double layer breakdown in the polarized water around the electrodes but at high speeds it is also because the electrodes skip off the top of bow waves. Understanding of the noise will only be achieved through further research.

APPENDIX 3 - SAFETY, LEGAL AND ENVIRONMENTAL CONCERNS

Various legal, safety and environmental concerns must be addressed by geo-electric surveyors of waterways. Identified concerns have been addressed as follows:

A3.1 High voltage hazards

The geo-electric transmitters can output significant voltages and currents. The Syscal Pro is designed to output up to 1000V while some Zonge battery powered transmitters are designed to output up to 400V. In this thesis, 400V was used initially with the dipole dipole arrays however, once the AXB arrays were put into use, voltages between 12 and 120 volts were used, partly because of the greater efficiency of the AXB arrays, and partly due to lack of available high power transmitters. These voltages, and the resultant injected currents range from insignificant, as a safety concern, to seriously dangerous and lethal. The AXB array keeps the transmitter electrodes as close as possible to the boat which means that safety monitoring is somewhat easier.

The Australian Code of Electrofishing Practice (1997 – included on the thesis DVD) details precautions for use of high voltages in waterways. With discretion, these same precautions can be transferred to waterborne geo-electric surveying. Major points that can be gained from this document are:

Operators of equipment need to be experienced and aware of the dangers they are dealing with. ‘Direct effects of electric shock may include heart failure, respiratory interference and/or electrical burns. There may also be indirect injuries through a worker recoiling violently and striking an object.’

Grounded high voltages are a risk to personnel – if exposed electrodes (grounded) and insulated wiring and components are tampered with incorrectly then they may all cause electrocution. Electrocution usually will not occur from contact as grounding usually provides a preferential path for current flow.

High voltages stun fish. Moderate voltages cause them to convulse. Voltages in excess of 1000V are not permitted. Voltages should be kept as low as is practical

to reduce effects on fish. DC current tends to cause fewer injuries to fish and people.

'The utmost care possible should be taken to avoid shocking platypus, birds and other native aquatic animals.'

'The utmost care must be taken to prevent the transfer of biological materials between waterways.'

Operators need to be aware of dangers to other water users and stop transmitting if a danger is imminent. 'Danger, High Voltage' signs should be attached to each side of the boat. (Note that in the case of geo-electric surveys, such signs are next to useless due to the length of the array).

Geo-electric arrays are often operated while being lifted by hand over canal regulators. Should dangerous voltages be used, then assistants must be trained to avoid touching the transmitter electrodes. As a compound precaution, the operator can turn off the transmitter until the transmitter electrodes have been lifted over the regulator. When electrodes touch grounded fences or other metallic grounded objects such as regulators, current goes direct to ground and there is not a risk to personnel however personnel need to make sure that the metal object is well grounded before going near it if a transmitter electrode is going to contact it.

Although not recommended, hypothetically, when approaching high voltage electrodes in the water, there will come a point where one can feel the current, if it has not killed you first. As current dissipates with the inverse square of distance from the electrode, no electric shock is likely until one is very close (typically much closer than 0.5m). Nevertheless, caution is necessary particularly as the water flow may move the electrodes. It is appropriate to stay at least 3 metres away from transmitting electrodes.

Always observe wear and tear of high voltage wiring and of the survey vessel. Regular checking of insulation each day as well as after negotiating damaging obstacles is important. Should insulation or connectors be damaged, then fix them or at least carefully observe the hazard and decide whether there is a safe way to continue or not.

Never fail to observe what is happening near the high voltage electrodes.

Never move around the boat without observing the risk of disturbing high voltage equipment.

The transmitter must be isolated by a method such as operating it off a completely separate battery or generator so that any grounded equipment is not at a high potential with respect to the surrounding charged water. Otherwise one may receive a shock or be electrocuted by activity such as touching a grounded metal framed instrument in the boat and metal parts of the outboard motor simultaneously.

A3.2 Marine traffic hazards

Boat operators should hold a relevant boating license and be fully aware of rules for trawling. No license is legally required when surveying is done with low speed watercraft capable of less than 8 knots however it would be ludicrous to survey on popular waterways without learning the rules in the license exam. Because most other waterway users do not seem to know or recall the rules, clear, simple, conservative and observant navigation must be executed in populated waters. House boat operators are not required to know rules even though they drive enormous craft and therefore must be treated with caution. Water skiers and jet ski riders tend to arrive so fast that they fail to observe the long towed array so it is best to avoid surveying when they are operating.

Fluorescent buoys or flags placed along the array improve its visibility and should be used in populated waterways.

A3.3 General boating precautions

Never fail to observe risk of navigation hazards – the array will generally follow the path of the boat but it can be drawn or blown onto partially submerged trees – requiring doubling back on rare occasions. Invisible submerged obstacles exist (rocks, fallen trees and star pickets on pump inlets) so the operator must be traveling in a manner and at a speed at which they can negotiate those obstacles.

Numerous further precautions and recommended preparatory measures are listed in the NSW Recreational Boating Handbook.

A3.4 The array towed by a raise-able boom attached to a 4wd and transport regulations

A letter from the NSW Roads and Traffic Authority stating regulation height and width and other details for the raised 4wd mounted boom is included in the safety directory on the thesis DVD. As long as it fits regulation dimensions, it may travel, raised, on public roads without any special permit even though it is somewhat unusual.

A3.5 The array towed by a raise-able boom attached to a 4wd and risk of collapsing canal sides

When travelling along canal banks towing an array with the boom, the canal bank may slump into the canal under the weight of the 4wd. If the boom was heavy, it would tend to force the vehicle to lean over into the direction of the canal making risk worse. Canal attendants are aware of the danger, which they face every day, and recommend reservation about surveying after or during rain. The driver must be ready to steer off the canal wall in an instant.

Long grass on canal walls is common and hides slumps. In such conditions it is common that the driver has to drive so slowly, in order to feel their way along, that survey becomes impractical. Some canal banks are severely undercut by lapping water. These banks look firm but are not. Drivers must take precautions to accommodate such risks.

Driving on and off some banks is awkward due to their slope. A great deal of back and fill is necessary to adequately align a vehicle for bank dismounting or after bank mounting if the bank is narrower than the vehicle length.

A3.6 Negotiating canal regulation structures while surveying from watercraft

If travelling downstream, particularly with a floating array, operators need to pull up short of regulators so that the array is not pulled down through the regulator possibly pulling the boat through with it.

A3.7 Navigation of inland rivers

Operators should become familiar with all flowing water hazards and devise a plan for avoiding them – this plan must take into account the timing required to execute required actions within flowing water. Surveys in a downstream direction should be avoided if water is fast flowing and unpredictable navigation hazards will need to be negotiated. This is because the electrode array including the high voltage current electrodes near the boat will collapse up against the boat – there may not be sufficient time left to turn off the electrodes. Strong currents additionally can capsize a boat if they push it up against an obstacle. The array is likely to get crumpled against the obstacle as well and then a person may need to climb along or swim to the obstacle in order to pull the array off it. This procedure can involve serious hidden dangers and in some cases a decision to abandon surveying and execute a slow cautious, perhaps partial, equipment recovery may be made for safety reasons. Many obstacles can only be crossed with the assistance of current so there is risk of prevented return in the case of problems if surveying downstream.

Many surveys can only be conducted downstream. There are some rivers/flows that are best surveyed only with an amphibious vehicle (eg. Argo) or not at all.

A3.8 Access restrictions on inland rivers

Public access to inland rivers is not very good. Some locations where many tens of kilometres of river without access exist. Where access does exist, it may be in the form of bush with no tracks of any sort. Full remote area precautions are required in such areas. A rescue, even from just delayed progress resulting in finishing a day at an unpredicted location, will require communication of location so good communication equipment is critical. On most inland rivers, only satellite phones and HF radios will work. Both the land vehicle and the boat should have a satellite phone or HF radio as the nearest site that the land vehicle can make contact on normal phones or UHF radio may be 50 or more kilometres away along bush tracks in many instances. Experience in the use of a satellite phone just in the boat and not in the land vehicle has shown that delays in pickup of 8 hours can easily occur. As part of a safety management plan, an external party needs to be informed of planned movements in case the land vehicle and therefore the boat both need to be rescued.

APPENDIX 4 - ARCHIVING OF MULTI-DEPTH EC DATA COLLECTED ALONG IRREGULAR TRACKS

A4.1 Introduction

Composition of a format suitable for layered multi-depth data collected along irregular tracks has been one of the most important and fundamental parts of this thesis. One of the reasons for creating the software, HydroGeoImager, along with this thesis was to design and evaluate such a format that facilitates rapid viewing of huge volumes of data in 3D ribbon images. HydroGeoImager data formats are designed for archiving layered multi-depth electrical conductivity, induced polarization, hydraulic conductivity and other data sourced from a wide variety of instruments that collect data along irregular tracks. Although most support is provided for geo-electric array systems, EM data such as can be produced by instruments made by Geonics and Zonge is supported. Throughout this chapter, numerous data formats and programs will be mentioned. Documentation of those 3rd party formats is available as referenced in the software and data formats section at the end of the reference section of this thesis. All data collected in this thesis has been stored in the universally known and facilitated dBase IV format and accompanied by INI files of machine and human readable documentation. Final data is archived in dBase datasets of channels and depths, an INI file documenting each dataset, an INI file of inversion parameters and an INI file of equipment configuration parameters. It is debatable whether simple INI files or more flexible XML files, which are now becoming popular, should have been used for archiving of parameters, however, conversion of INI files to XML files is simple and unlikely to cause problems in the future. dBase format has been chosen principally because it is easily extended to form ESRI shapefiles which are used almost universally by agencies and companies working on environmental GIS data in Australia. Shapefile specifications are available from www.ESRI.com. Furthermore, dBase files can be edited or even generated in MS Excel or Access as well as almost all database packages. They offer both a simple format, that can be manipulated by most non-GIS experts, and relational database efficiency and flexibility. When extended to become shapefiles, they become GIS compatible. dBase file specifications are very old and lack many features that more modern database file formats have, however the author believes

that the backward compatibility they offer with products such as ESRI ArcView makes up for the lack of features.

A4.2 Archive searching and EC ribbon viewing

When large volumes of data must be processed, good archiving practices are essential. If data is split into datasets of segments of manageable length and point shapefiles are added to each dBase dataset, then ArcView or competing shapefile compatible GIS systems can be used to locate segments and view them in maps along with other features of relevance. HydroGeoImager can be run alongside ArcView for rapid 3D viewing of EC Ribbons of files identified in ArcView.

A4.3 Management of confidential datasets

Should a database of multi-depth EC data be set up including confidential datasets, then ESRI products can readily facilitate limited access arrangements so that the public can view the bounding rectangles of all surveys and interrogate metadata on each bounding rectangle. If clients wish to access the data they can then ask permission using contact details stored in the metadata.

A4.4 File naming conventions

Files for each field dataset are named using the file naming convention of FILECORE + DATATYPE + . + FILETYPE. An example set of files is (Day1.INI, Day1GPS.DBF, Day1Volt.DBF, Day1Ohmm.DBF and Day1Chargeability.DBF) Segmenting and/or concatenations of some files may be conducted resulting in new filecore names.

A4.5 Instrument dump formats

Equipment providers dump data in formats that they decide. Typically they are regularly modified and usually are in straight ASCII or proprietary binary formats. The formats are constrained by the limitations of the various instruments and therefore are often not appropriate for general use. Such formats cannot be thoroughly understood by most generic software. ASCII file parsers do not typically cope with file modifications well. ASCII files cannot be indexed on multiple columns and can only be accessed

sequentially. Such formats are thus not suitable for optimized generalized processing. Conversion to the more flexible dBase and INI file format is therefore appropriate.

A4.6 Data storage formats

dBase and shapefile formats have been chosen for storing data records and accompanying INI files have been chosen for unique variable storage. Conversion to files compatible with a future extension of the exploration and mining markup language - XMML (Cox, 2004) would be straight forward using these INI files. These file formats are publicly available and extremely widely utilized. Creation of dBase files is widely facilitated. As ESRI shapefiles are an elaboration of dBase files, conversion to ESRI shapefiles is simple. Even once the conversion is made, the dBase part of the shapefile is still available to programs that cannot read shapefiles. The conversion is readily made in ESRI ArcView software or using freeware components.

To use Arcview to convert the dBase files to Shapefiles it is possible to use the following two options :

1. Recommended - In ArcCatalog, dBase files are automatically displayed, right click on a dBase file and select “Export - create Feature Class from XY Table”. Select the X, Y and (optionally Z) columns as Easting, Northing and WaterDep and then select to convert the table to either a shapefile or a geodatabase feature class. For data storage, the shapefile is recommended as the format is more widely readable and the format documentation is freely available.

2. In ArcMap, use the AddXYData option then export a shapefile.

For more elaborate file conversion and processing, a freeware DLL (http://gdal.velocet.ca/projects/shapelib/shapelib.html) and purchasable ESRI COM components are also available as documented on the ESRI website. The freeware DLL is available to anyone that is not able to purchase ESRI software.

Steema Software are facilitating imaging of dBase and Shapefile data. Their software components offer a much cheaper but less integratable imaging solution than do ESRIs. Sensible presentation solutions may involve a use of both products.

Shapefiles can also be viewed in a variety of ways by the free ESRI software – ArcExplorer as well as most GIS packages. dBase files may be input and output from Microsoft Excel and Access and manipulated within almost all database systems.

A4.7 Types of files included in the format specifications

A4.7.1 Raw GPS and Sonar data

This may be streamed into geo-electric data collection instruments or stored in a file with time stamps. NMEA0183 format is most common, however programs such as Fugawi may be used to make other formats. NMEA needs to be converted to UTM co-ordinates using Redfearn's formula.

A4.7.2 Standard GPS/WaterDepth Field Data Format

A dBase file with a time column, UTM coordinate columns, water depth and/or elevation columns and data quality and validity columns forms the basis of this file. In cases where GPS and sonar are streamed with geoelectric data by field equipment, then this file may not be necessary. A shapefile may be created incorporating the dBase file.

A4.7.3 Raw data dumps and streams

Field equipment may store and dump data to computers or may stream it in real time. Instrument format data should be stored by the data providers and converted to Standard field data format as follows.

A4.7.4 Standard Geo-electric or EM Field Data Format

One dBase file is made for each raw data dump file or streaming session. If GPS and sonar data are incorporated in the data, then they are inserted at the same time. Otherwise, they are inserted from separate files by using time as a common field and interpolation. One record exists for each sounding. Data is stored as voltages as many possible algorithms for conversion to EC exist and post-processing may invoke any algorithm. EC data is stored in a separate file of a very similar format but with depth columns.

A4.7.5 Standard EC data file

Again this is a dBase file which may be elaborated to form a shapefile. It has one record per sounding and additional columns for depths of each of the EC measurements. An accompanying entry in the dataset INI file indicates to presentation packages whether the EC data is for a smoothed layer or stepped layer model. It also holds all the documentation for the voltage to EC transformation applied. These files are the standard form in which data would be distributed to interpreters. In this format, data from different instruments and processed using different algorithms can be compared and presented together.

A4.7.6 Pallete Files

Multidepth EC data may exist over an enormous dynamic range while variations at a particular site or depth may be very small. For this reason a palette file format exists with correlations between EC and colours. One correlation is included for application to all depths and a set of correlations is included for application to each depth – this set facilitates the prevention of washout of detail in cases where extreme vertical contrast in EC is combined with minor horizontal contrast in EC.

A4.7.7 Imaging files

Imaging of the data as 3D ribbons requires specialized files that are quick to create so documentation of such files is not included as a public standard. Output images and videos are in imaging package formats that are well known such as BMP and JPG so they do not need to be documented. Georeferenced BMP images of orthographically projected ribbons may be added to 2D GIS packages. 3D ribbons may be distributed as 3D Polygon shapefiles for use in ESRI ArcScene however HydroGeoImager is proposed to contain a routine for generating such files so that data in this format does not need to be stored. Data stored in such formats lacks documentation and is unnecessarily voluminous so the format is not appropriate for archiving.

A4.8 Standard Voltage, EC, IP or Resistivity data dBase file format column IDs and formats

Tables A4-2 and A4-3 present the voltage and resistivity data file fields and their formats.

Table A4-1 Voltage/IP dBase format

Field	*Field Type*	*Size.Decimals*
Time	Floating Point	12.7
Distance	Floating Point	12.3
Omit	Logical	
Easting	Floating Point	12.3
Northing	Floating Point	12.3
Lat	Floating Point	15.10
Long	Floating Point	15.10
Chn	Numeric	3
Current	Floating Point	12.5
WaterDepth	Floating Point	12.3
V##	Floating Point	15.7
.		
.		
IP## (optional)	Floating Point	15.7
.		
.		
Error## (optional)	Floating Point	15.7
.		
.		

Table A4-2 Resistivity, and Chargeability dBase file formats.

Field	*Field Type*	*Size.Decimals*
Time	Floating Point	12.7
Distance	Floating Point	12.3
Omit	Logical	
Easting	Floating Point	12.3
Northing	Floating Point	12.3
Lat	Floating Point	15.10
Long	Floating Point	15.10
Chn	Numeric	3
Current	Floating Point	12.5
WaterDepth	Floating Point	12.3
Error	Floating Point	10.2
Chn##	Floating Point	10.2
.		
.		
Depth##	Floating Point	8.3
.		
.		
Error## (optional)	Floating Point	10.2
.		
.		

Indexes :- are not required however HydroGeoImager often adds the following

byDistance
byTime
byEasting (when required)
byNorthing (when required)

Note:- All depths are to be positive (increasing downwards)

The filename, as well as the ini file should indicate what quantity type the file holds (eg Ohmm or Chargeability or Volt). The filename should include the quantity type as a suffix just before the .dbf in the filename (eg. *Ohmm.dbf, *Chargeability.dbf, *Volt.dbf, *.GPS.dbf).

A4.9 Standard GPS/Depth dBase file format column IDs and formats

Table A4-3 GPS dBase file format

Field	***Field Format***	***Size.Precision***
Time	Floating Point	12.7
Distance	Floating Point	12.3
Easting	Floating Point	12.3
Northing	Floating Point	12.3
WaterDep	Floating Point	12.3
Omit	Logical	
Lat	Floating Point	15.10
Long	Floating Point	15.10
FixQual	Numeric	3
SVs	Numeric	3
HDOP	Floating Point	5.3
Altitude	Floating Point	12.3

Indexes are not required but HydroGeoImager often adds the following

byTime
byDistance
byEasting (when required)
byNorthing (when required)
byLat (when required)
byLong (when required)

A4.10 Standard Time/WaterDepth file format column IDs and formats

Table A4-4 Time/Water Depth dBase file format

Field	*Field Format*	*Size.Precision*
Time	Floating Point	12.7
WaterDep	Floating Point	12.3

Indexes are not required but HydroGeoImager often adds the following.

ByTime

A4.11 HydroGeoImager_IniFiles

Inverse, Forward and Configuration INI files contain parameters for their respective menus in HydroGeoImager. The defaults are Inverse.Ini, Forward.Ini and Config.Ini which reside in the application directory. Each dataset is accompanied by a dataset INI file and there is also a workspace INI file.

A4.11.1 IniName Inifile

IniName.Ini which resides in the application directory contains the current workspace Ini filename.

A4.11.2 Workspace IniFile

Workspace Inifiles (default is ECRibbon.Ini in the application directory) can accompany sets of datasets in a particular survey. They may contain all menu parameters except Inversion, Forward and Config menu entries.

The default workspace Ini file is ECRibbon.Ini but this can (and should) be changed so that each job directory contains a workspace Inifile especially formulated for that job.

A4.11.3 Dataset IniFile

This is named *Filecore*.Ini where *filecore* is the core for the filenames that are specified for the dataset by the processor. It contains important information about its dataset and should be kept together with all of its dataset files. Among other things, it contains names of configuration, workspace and inversion inifiles.

A data INI file accompanies each dataset. As the dataset is processed, parameters are added to it as each menu is used. It stores the names of other INI files last used with it and when it is loaded, it changes the active workspace, forward, inverse and config ini files to those specified by it. If however a new dataset is loaded, current inifiles will remain. It records important information particular to the dataset that is also recorded in the other INI files but will not override configuration and inverse INI files. It will override workspace INI files.

The data inifile will automatically be stored with data. It is left as a responsibility of the user to copy and store appropriate inifiles of the other types with their data. If users continually change directories and jobs without copying inifiles to each job directory, then they will be forever changing menu items in order to reprocess their datasets. Although many parameters stored in various INI files are stored to the data inifile, they are not always retrieved to menus from that inifile.

A4.11.4 Configuration IniFile

The Configuration inifile contains all information about a particular equipment configuration. Its name is user supplied and should identify the equipment the inifile documents. A range of standard configuration inifiles exist in the application directory. As dataset inifiles refer to configuration inifiles for documentation, they should never be changed. It is sensible to store a copy of them with datasets – a copy facility is provided in the main form for this purpose. If this is not done, a later user could accidentally lose them when transferring data to another location. The software provides many warning messages to persuade the processor to rigorously copy these inifiles.

A4.11.5 Forward Modelling IniFile

This inifile is not normally needed for routine processing. It stores menu parameters for the forward modelling component of the application.

A4.11.6 Inversion IniFile

This file stores menu parameters for the inversion component of the application.

A4.12 INI File Examples

A4.12.1 Filecore INI Files

All data are stored in common format. dBase files with the wildcard *Ohmm.DBF are datasets for imaging. They are accompanied with *.INI files. Filenames of Workspace, Configuration and Inversion inifiles are included in the Filecore inifile. Paths are included in these filenames. If the paths are different from the path of the filecore inifile, yet the files exist in the directory of the filecore inifile then the user is asked if the paths should be changed otherwise the user is asked if the files should be copied to the directory containing the filecore inifile. This assists greatly in making the datasets transportable from one location to another without loss of information.

An example transcript of an Inifile for a dataset is as follows:

```
[IniFiles]
Workspace=D:\03\Mildura\Workspace.Ini
ConfigIni=D:\03\Mildura\144m1m7ExpConfig.Ini
InverseIni=D:\03\Mildura\Inverse.INI

[Offsets]
ZongeStnCoordsMergedUsingElectrode=F2x

[Files]
VoltFileSourceType=ZongeDatStnFilePair
VoltageDataSource=D:\03\Mildura\Mar03\MalleeNorth.DAT
DirectoryAtCreation=D:\03\Mildura\Mar03\
VoltdBase=MCNthVolt.DBF
maxNumChan=7
InvertedOhmmFile=MCNthOhmm.DBF

[Units]
Voltages=Volts
Current=Amps
Distances=Metres
VoltagesCurrentNormalized=0
MCNthOhmm.DBF=Ohm.m
MetresOrFeet=Metres
VoltagesNotCurrentNormalized=Volts
RawIPdata=mRadians
Depths represent layer=bottoms

[Annotation]
Project=Mildura,Buronga and Mallee Cliffs EC Monitoring Trials
DataProvider=David Allen - National Centre For Groundwater Management
Client=DIPNR
JobNum=NCGM2004/4
Site=Mallee Cliffs North Bank
SurveyEquipment=Zonge GDP32 with 160V Tx
SurveyDate=12/03/2003

[VoltageFilters]
MinCurrent=0.02
MinVoltage=0.0005
MinDistInc=0.4
ExcessiveMeanderFilterApplied=1
%DevFromStraightGeomFactAllowed=4
MonopolesExceedingEndOfGPSTrackCropped=1

[SmoothFile_D:\03\Mildura\Mar03\MCNthPreSmoothVolt.dbf]
SourceFile=D:\03\Mildura\Mar03\MCNthVolt.dbf
```

```
NumberOfFilterPasses=3
NumberOfPointsInFilter=17

[InitModel]
UserEstimatedRiverWaterResistivity=100

[SegmentRange]
SourceFile=D:\03\Mildura\Mar03\MCNthOhmm.DBF
StartDistance=10219
EndDistance=20113
```

A4.12.2 Array Configuration File

For all data completed with a particular geo-electric array or other device, there is a geo-electric array configuration INI file (eg. 144m1m7Config.INI). The configuration file format is set up to facilitate use of linear electrodes and curved arrays so many of the entries are superfluous for the average survey as will be self evident from observation of the example file. Transcript of the file is as follows:

```
[Array]
RxBipoles=7
MaxMonopoles=4
TxElectrodeLength=0.5
PortionSizer=0.3
AConfigType=ExponentialBipole

[Offset]
Behind=24
Right=0

[Submerged]
SubDepth=0
GeomFact1=0
GeomFact2=0
GeomFact3=0
GeomFact4=0
GeomFact5=0
GeomFact6=0
GeomFact7=0

[numMonopoles]
numMonopoles1=4
numMonopoles2=4
numMonopoles3=4
numMonopoles4=4
numMonopoles5=4
numMonopoles6=4
numMonopoles7=4

[GeomFact]
GeomFact1=12.6490441052431
GeomFact2=25.7039398930074
GeomFact3=53.8558740615393
GeomFact4=120.637157897848
GeomFact5=301.59289474462
GeomFact6=861.693984984629
GeomFact7=2783.93441302726

[EffDepth]
EffDepth1=0.516416490077972
EffDepth2=1.01859164237976
EffDepth3=1.9588451385498
EffDepth4=3.65594887733459
EffDepth5=6.65273380279541
EffDepth6=12.1618642807007
EffDepth7=22.7509822845459
```

```
[MonopoleSeparations]
CP1_1=1
CP1_2=2
CP1_3=17
CP1_4=18
Cut short to save paper….
….
 [ExponentialBipole]
CurrElecSeparation=16
FirstPotentDist=-1
TwoToPowerOfnIncr=1
RadiusOfCurvature=100
```

A4.12.3 Inversion Configuration File

An inversion configuration file (eg. Inverse.INI) exists. Many of the entries are for options not typically used such as fixed initial models. Other entries such as those in [FIXED], [INVCONST] and [INPUTFILTER] are very relevant. Transcript of Inverse.INI is as follows:

```
[Data]
RField1=63.7828049006884
RField2=82.3489974322225
RField3=86.034758813309
RField4=41.7404566326554
RField5=8.8517514607546
RField6=1.76539555173726
RField7=8.61279689779208
DataSource=0
DataFileName=D:\Program Files\ECRibbon\SampleBlueEelData.Sur
[InitModel]
Method=2
FileName=D:\Program Files\ECRibbon\SampleInitModel.Mdl
Sonar=1
MaxLayers=6
RiverWaterResistivity=100
nLayer=3
Param1=1
Param2=2
Param3=3
Param4=4
Param5=5
VarOrFix1=0
VarOrFix2=0
VarOrFix3=0
VarOrFix4=0
VarOrFix5=0
LayersPerEffDepth=1
[Fixed]
AllThick=0
[InvConst]
RMSCut=5
EDecr=1.5
EIncr=10
NIncr=25
NIter=15
FilterNumber=1
Norm=1
WtOrigThick=0.1
WtVertSmooth=0.1
SubNoiseInversion=1
AddSubNoiseLayers=1
[InputFilter]
RejectPlusSubsequent=0.000020
RejectOnlySubsequent=0.001800
MinAppRes=0.100000
DummyMask=-999.989990
IgnoreSign=0
```

```
ApplyWeight=1
WeightLimit=0.014000
Noise=0.002500
WeightAtNoise=0.100000
[Output]
SaveDBase=1
SaveFinal=0
ProgressMonitor=0
ShowDeriv=0
FinalModelFilename=D:\Program Files\ECRibbon\SampleFinalModel.IPM
Method=2
```

A4.13 EC Ribbons, EM31, EM38 and airborne electromagnetic EC data.

The various ground and airborne ECdataset types are currently considered by many in the political and agricultural sectors as individual data types that are not mixable. ECRibbon file format allows mixing of all this information in a common form. Delivery of EC data currently suffers from a lack of combination.

The HydroGeoImager file format that ties down EC distribution with respect to depth along transects is a useful medium for combined common archiving of all types of EC data (Geo-electric, FDEM such as EM31 and EM38, and airborne EC data).

HydroGeoImager presentation developed here for geo-electric array data also is useful for ground and airborne multi-depth electromagnetic EC data presentation. Using the approach developed, EC ribbons representing data from the various techniques can all be integrated into a single image. Furthermore, new opportunities for the use of airborne data open up. In the past, airborne datasets collected for salinity mapping have been plotted predominantly as depth or time slices. Because the surveys have had to be conducted using line spacings that greatly exceed the spatial variability of most of the features being identified, the depth or time slices miss much of the detail. The data is however of sufficient value that it warrants viewing in EC ribbons plotted over airphoto and topography imagery. Small features, glazed over by depth slices, can be identified by their geometry in the images and interrelation with features of the DEMs and airphotos. Vertical variation information is not clearly evident in sets of depth slices and often only is evident in EC ribbons. The EC ribbons of data collected on the ground are useful as pilot datasets for airborne surveys and for filling in detail in areas of high interest identified by airborne data. The presentation technique allows for common archiving and presentation of the data in uniform format.

EM31, EM38 and other FDEM data normally collected at a single depth can also be stored in the same format using the effective depth of the instrument involved.

Airborne data must be collected in bulk to be cost effective. Both before and after such bulk surveys, ground based surveys can be used to collect small amounts of data of more focused specialized interest to be integrated into the airborne dataset.

APPENDIX 5 - COMPUTER CODE, WITH EXPLANATORY NOTES, FOR GEO-ELECTRIC ARRAY PROCESSING.

The fundamental mathematical code of the executable software (see DVD) accompanying this thesis has been included here. Complete code is not supplied for reasons including that it contains 3rd party code that cost a lot of money and cannot be freely distributed. User interface code is not included as it includes the commercial 3rd party code, is voluminous and would remove emphasis from the fundamental code but all the fundamental code is present in this appendix and can be implemented by others. The scope of and effort put into the full software package goes much further than the PhD requirements and refinement is continuing. The code in this appendix can, however, be utilized as is by anyone who adds an interface, as described below. The program units included here are not dependant on any graphical components. Dependence on a few units that pass variables such as inversion parameters exist and will prevent the code from running as is. It is clear, however, what these variables are from the descriptions below. Inclusion of those units would have resulted in loss of emphasis on the core mathematical code of this thesis. It is the author's intent to provide this code and executable freely to those who may wish to understand it and improve on it, use it for forward modelling or geo-electric array design analysis or do small research projects with it.

A5.1 FwdInv – explanatory notes

Forward modelling and inversion of individual soundings has been facilitated in the Delphi7 unit FwdInv.Pas. Other units with user interfaces control flow of data to and from routines in this unit.

For array configuration information, FwdInv.Pas relies on another fundamental unit – ConfigCore.Pas which totally separates array configuration considerations from the FwdInv.Pas code and allows for complete generalization of array configuration possibilities.

In order to understand how FwdInv.Pas works, it is first necessary to become familiar with the variable types used. FwdInv.Pas relies on the following variable types:

```
  TModel=Record
    NParam:Integer;
    NLayer:Integer;
    Param :Array[1..32] of Single;
  end;
```

TModel contains a complete list of parameters needed to define a 1D layered horizontal model. It is only used in forward modelling. For inversion, it is passed into TVariableParam.

NParam is the total number of parameters in the model and equals NLayer*2-1.

NLayer is the number of layers in the model. For submerged arrays, it includes the water layer above the array.

Param is an array of parameters. The first NLayer-1 variables are layer thicknesses, the rest (up to NParam) are layer resistivities. The array is fixed currently but may be made dynamic or enlarged upon request.

```
  TVariableParam=Record
    nVParam:Integer;
    VIndex:Array[1..32]   of   Integer;   {Param   index   of
variable in TModel.Param}
    VarOrFix:Array[1..32]   of   Boolean;   {Variable   False,
Fixed True mapped to TModel.Param}
    VParam :Array[1..32] of Single;
    Deriv        :Array[1..30,1..33]        of        Single;
{1..maxNumBipoles,1..maxNParam+1}
    nData :integer; {=TConfig.numBipoles for DCResistivity
inversion}
  end;
```

TVariableParam is the record that the inversion routine works with. In order to speed up and stabilize inversion, fixed forward model parameters are not passed into the inversion routine. Unlike TModel, TVariableParam contains a derivative matrix with derivatives of datapoints with respect to each variable parameter. In order to facilitate this arrangement,

various indexes are included in the record that allow for transition between TModel and TVariableParam.

nVParam is the number of variable parameters in the model.

VIndex is an array with one entry for each variable parameter that holds the index of the variable parameter in the corresponding TModel.Param array. It is used to feed variable parameters back into TModel records.

VarOrFix is an array with one entry for each parameter in the corresponding TModel record. Each entry is false if the parameter is variable or true if it is fixed. It is used to feed TModel parameters into TVariableParam records.

VParam is an array of all the variable parameters being inverted.

Deriv is a 2D matrix[1..nData,1..nVParam+1] containing derivatives of datapoints with respect to each variable parameter. The last column is a duplication of VParam. The duplication allows for more efficient passing of parameters. The fixed size of this array may be made dynamic or enlarged upon request.

nData is the number of datapoints in a sounding and is carried by TVariableParam records because it is one of the dimensions of Deriv.

```
TResponse=Record
  Voltages:Array[1..30] of Single;
  AppReses:Array[1..30] of Single;
  AppResDeriv:Array[1..30,1..32] of Single;
end;
```

TResponse is a record of the data parameters in a sounding.

Voltages is an array of the voltages of all the datapoints in the sounding.

AppReses is an array of the Apparent Resistivities of all the datapoints in the sounding.

AppResDeriv is an array like TVariableParam.Deriv but with Apparent Resistivity derivatives rather than voltage derivatives but is not appended with a column containing `TVariableParam.VParam`.

Descriptions of global variables used in FwdInv are as follows:

```
Model:TModel;
```

The model under consideration.

```
VPar:TVariableParam;
```

The variable parameter record under consideration

```
Response:TResponse;
```

The response under consideration

```
DerivEps :Array[1..34,1..32] of Double;
{Maxnumparam+2,Maxnumparam}
```

DerivEps is a matrix like TVariableParam.Deriv but is damped by the Marquardt damping variable epsilon.

nUsual:Integer;

```
Eps,SumOfSquares,RMS:Double;
```

Eps (Epsilon) is the Marquardt damping parameter that is used to prevent singularity problems with very non-linear inversion problems.

SumOfSquares (phi) is the weighted sum of squares (or if L1 inversion is chosen, the weighted absolute deviation) of the difference between field data and model data.

RMS is the weighted root mean square of differences between model and field data.

```
Iter:Integer;
```

Iter is the number of iterations in the inversion.

```
RModel :Array[1..25] of Double; {MaxBipoles}
```

RModel is an array of model datapoint resistivities.

```
RField :Array[1..25] of Double; {MaxBipoles}
```

RField is an array of field datapoint resistivities.

```
IPField:Array[1..25] of Double; {MaxBipoles}
```

IPField is an array of field datapoint resistivities.

```
  Weight :Array[1..25] of Single; {MaxBipoles}
```

Weight is an array of weights for the datapoints. The weights depend on signal to noise ratios and are used in SumOfSquares and RMS calculations so that inversion is not unduly affected by low signal to noise ratio data.

```
  SumWeight:Single;
```

SumWeight is a normalization variable used with the Weight array.

The forward modelling and inversion code is made up of the following routines:

```
Function MonopoleTAndDeriv(const Model:TModel;
                           var LogX:Double;
                           var CalcDeriv:Boolean;
                           var TDeriv:Array of Double
                           ):Double;
```

This function calculates the transform function and, optionally, its derivative. The derivative is calculated only if CalcDeriv is set to true. In practice, it is only used with CalcDeriv set to true because it is much more efficient to use function MonopoleT if derivatives are not required.

```
Function MonopoleT(const Model:TModel;
                   var LogX:Double):Double;
```

This function calculates the transform function.

```
Procedure ForwardModel(CalcDeriv:Boolean;
                       Const Model:TModel;
                       const
ArrayConfig:TArrayConfiguration;
                       var Response:TResponse;
                       const Fltr:TFilter);
```

This model calculates a forward model.

```
Procedure Invert(Var VPar:TVariableParam;
                 Var Response:TResponse;
                 Var Model:TModel;
                 Const InvConst:TInversionParam;
                 Const ShowDeriv:Boolean);
                 //Invert also uses general FwdInv scope
variables
```

Invert inverts one sounding.

```
Procedure Orfac(Var VPar:TVariableParam);
```

Orfac conducts orthogonal factorization for Invert.

```
Procedure EpsFac(Var VPar:TVariableParam; var EPS:Double);
                //EpsFac also uses general FwdInv scope
variables
```

EpsFac conducts orthogonal factorization damped using epsilon for procedure Invert.

```
Procedure BakSub(Var VPar:TVariableParam);
                //BakSub also uses general FwdInv scope
variables
```

BakSub conducts backward substitution for procedure Invert.

```
Procedure   VParamToParam(const   CalcDeriv:Boolean;   var
Model:TModel;const         VPar:TVariableParam;         var
Response:TResponse);
```

VParamToParam is an interface for passing parameters from Invert back to ForwardModel.

```
Procedure   ParamToVParam(const   CalcDeriv:Boolean;   const
Model:TModel;var         VPar:TVariableParam;         const
Response:TResponse);
```

ParamToVParam is an interface for passing parameters to Invert from an initial model and from ForwardModel.

```
Procedure TieUp(Const ShowDeriv:Boolean);
```

TieUp is used by Invert to present the final model.

```
Procedure OutputProgress(const Last:Boolean);
```

OutputProgress is called on each iteration of Invert in order to update any selected user interfaces.

Invert uses the unit InvParam.Pas which stores inversion control variables.

The record InvConst has a type as follows:

```
  TInversionParam = record
    RMSCut:Single;
    Edecr:Single;
    EIncr:Single;
    NIncr:Integer;
    NIter:Integer;
    FilterNumber:Integer;
    Norm:Integer;  //L1  (Least  Absolute  Deviation)=1;  L2
(Least Squares)=2
    WtOrigThick:Double;
    WtVertSmooth:Double;
  end;
```

RMSCut

Inversion ceases to iterate once RMS is less than or equal to RMSCut

Edecr

Eps (Epsilon) is decreased by division of Eps by Edecr each time SumOfSquares is reduced in order to hasten convergence.

EIncr

Eps (Epsilon) increased by multiplication of Eps by EIncr each time SumOfSquares is increased (divergence).

NIncr

This is the maximum number of increments of Epsilon permitted before the inversion routine gives up. It is necessary for preventing perpetual looping of troublesome inversions.

NIter

This is the maximum number of iterations that the inversion routine can make before abandoning troublesome inversions.

FilterNumber

FilterNumber is an index in a list of filters given as follows:

```
  Case FilterNumber of
    0:ChosenFilter:=J0Filter3;
    1:ChosenFilter:=J0Filter6;
    2:ChosenFilter:=J0Filter12;
```

```
  end;
```

More filters will probably be added in future.

`Norm`

L1 (Least Absolute Deviation)=1; L2 (Least Squares)=2

`WtOrigThick`

If Model thicknesses are not fixed then this variable is the weighting given to the L1 or L2 norm of original model thicknesses by the inversion routine. Otherwise it equals zero and indicates that inversion will not take original model thicknesses into consideration.

`WtVertSmooth`

If this variable is not zero, then inversion resistivities will be smoothed and this variable will represent the weight given to model smoothness by the inversion routine.

The inversion control variables are initialized as follows but can be adjusted by the operator.

```
With InvConst do begin
    RMSCut:= 3;
    Edecr := 10;
    EIncr := 1.5;
    NIncr := 10;
    NIter := 10;
    FilterNumber := 1;
    Norm:=1;
    WtOrigThick:=0;
    WtVertSmooth:=0;
End;
```

The Digital Convolution Filter records used in the Inversion of type as follows:

```
type
  TFilter = record
    Decade: Integer;
    Shift: Double;
    Length: Integer;
    Upper: Integer;
    Filter: array[1..167] of Double;
  end;
```

Decade is the number of points per decade in the filter.

Shift is the shift applied in order to get crossovers to fall onto the sampled points.

Length is the number of points in the filter.

Upper is the number of points in the filter with ordinates greater than zero.

Filter is an array of filter coefficients. The size is fixed so that one type can be used for all filters and excess entries are filled with zeros.

FwdInv.Pas

```
unit FwdInv;

interface

uses sysutils,math,filters,configCore,InvParam,InversionProgress,UnitDerivDisplay;

type
  TModel=Record
    NParam:Integer;
    NLayer:Integer;
    Param :Array[1..32] of Single;
    RMS:Single; //Model Fitting error;
  end;
  TVariableParam=Record
    nVParam:Integer;
    VIndex:Array[1..32] of Integer; {Param index of variable in TModel.Param}
    VarOrFix:Array[1..32] of Boolean; {Variable False, Fixed True mapped to TModel.Param}
    VParam :Array[1..32] of Single;
    Deriv :Array[1..30,1..33] of Single; {1..maxNumBipoles,1..maxNParam+1}
    nData :integer; {=TConfig.numBipoles for DCResistivity inversion}
  end;
  TResponse=Record
    Voltages:Array[1..30] of Single;
    AppReses:Array[1..30] of Single;

    AppResDeriv:Array[1..30,1..32] of Single;
  end;
  TInputFilter = record
    //Total Rejection
    RejectPlusSubsequent:Single;
    RejectOnlySubsequent:Single;
    //Miscellaneous
    minAppRes:Single;
    DummyMask:Single;
    IgnoreSign:Boolean;
    //Weight
    ApplyWeight:Boolean;
    WeightLimit:Single;
    Noise:Single;
    WeightAtNoise:Single;
  end;

var
  Model:TModel;
  VPar:TVariableParam;
  Response:TResponse;
  InputFilter:TInputFilter;
  // The following variables are used in various inversion subroutines so are declared with general scope
  DerivEps :Array[1..34,1..32] of Double; {Maxnumparam+2,Maxnumparam}
  DeltaR :Array[1..25] of Double; {MaxBipoles}
  ModelMinusField:Array[1..25] of Double; {MaxBipoles}
  DeltaRNew:Array[1..25] of Double; {MaxBipoles}
  DeltaP :Array[1..32] of Double; {Maxnumparam}
  nUsual:Integer;
  Eps,SumOfSquares:Double;
```

```
  Iter:Integer;
  RModel :Array[1..25] of Double; {MaxBipoles}
  RField :Array[1..25] of Double; {MaxBipoles}
  IPField:Array[1..25] of Double; {MaxBipoles}
  Weight :Array[1..25] of Single; {MaxBipoles}
  SumWeight:Single;
  NoiseDivCurrent:Double; //Used only by SubNoiseInversion
  RiverWaterResistivity:Double; //This is used only with submerged inversion
Function MonopoleTAndDeriv(const Model:TModel;
                     var LogX:Double;
                     var CalcDeriv:Boolean;
                     var TDeriv:Array of Double
                     ):Double;
Function MonopoleT(const Model:TModel;
                var LogX:Double):Double;
Procedure ForwardModel(CalcDeriv:Boolean;
                   Const Model:TModel;
                   const ArrayConfig:TArrayConfiguration;
                   var Response:TResponse;
                   const Fltr:TFilter);
Procedure Invert(Var VPar:TVariableParam;
              Var Response:TResponse;
              Var Model:TModel;
              Const OrigModel:TModel;
              Const InvConst:TInversionParam;
              Const ShowDeriv:Boolean;
              Const ShowProgressMonitor:Boolean);
              //Invert also uses general FwdInv scope variables
Procedure Orfac(Var VPar:TVariableParam);
Procedure EpsFac(Var VPar:TVariableParam; var EPS:Double);
              //EpsFac also uses general FwdInv scope variables
Procedure BakSub(Var VPar:TVariableParam);
              //BakSub also uses general FwdInv scope variables
Procedure VParamToParam(const CalcDeriv:Boolean; var Model:TModel;const VPar:TVariableParam; var Response:TResponse);
Procedure ParamToVParam(const CalcDeriv:Boolean; const Model:TModel;var VPar:TVariableParam; const Response:TResponse);
Procedure TieUp(Const ShowDeriv:Boolean; Const ShowProgressMonitor:Boolean);
Procedure OutputProgress(const Last:Boolean);

implementation

// Take forward or initial model parameters and feed into inversion parameters
Procedure ParamToVParam(const CalcDeriv:Boolean;
                    const Model:TModel;
                    var VPar:TVariableParam;
                    const Response:TResponse);
var
  i,j,k:integer;
begin with Model,VPar,Response do begin
  k:=0;
  For i:= 1 to NParam do begin
    If not VarOrFix[i] then begin
      inc(k);
      VParam[k]:=Param[i];
      If CalcDeriv then For j:= 1 to nData do Deriv[j,k]:=AppResDeriv[j,i];
    end;
  end;
  For j:= 1 to nData do Deriv[j,nVParam+1]:=AppReses[j];
end {with}; end;

// Take inversion parameters and feed into forward or final model parameters
Procedure VParamToParam(const CalcDeriv:Boolean;
                    var Model:TModel;
                    const VPar:TVariableParam;
                    var Response:TResponse);
var
  i,j:integer;
begin with Model,VPar,Response do begin
  For i:= 1 to nVParam do begin
      Param[Vindex[i]]:=VParam[i];
      If CalcDeriv then
      For j:= 1 to nData do AppResDeriv[j,VIndex[i]]:=Deriv[j,i];
  end;
  For j:= 1 to nData do AppReses[j]:=Deriv[j,nVParam+1];
end {with}; end;
```

```
{C ************************************************
C            ForwardModel    MERRICK (Modified by ALLEN, 2005)
C            ------------
C    Calculate APPARENT RESISTIVITIES and derivatives.
C ************************************************}
procedure ForwardModel(CalcDeriv:Boolean;
                  const Model:TModel;
                  const ArrayConfig:TArrayConfiguration;
                  var Response:TResponse;
                  const Fltr:TFilter);

var
 i,j,k,l,pair:integer;
 prop:Array[1..30] of single;

 {Model}
 R:Array[1..30] of Double;  {30 is num of CurPot portions allowed}
 T:Array[1..30] of Double;
 TDeriv:Array[0..31] of Double; {zero cell never used - just prevents shifting on passing}
 TDerivative:Array[1..30,1..31] of Double; //[pair,model parameter]
 TonR:Array[1..167] of Double;
 TDerivativeOnR:Array[1..167,1..31] of Double;
 VoltagDeriv:Array[1..31] of Double;
 Left,LnStep,LogX:Double;

 {Response}
 Offset,Voltag,AppRes,GeomFactOn2Pi:Double;
begin with model,ArrayConfig,Response do begin

 {!!!!!Unnessessary initialization for debugging clarification}
 For i:= 0 to 31 do TDeriv[i]:=99;
 For i:= 1 to 30 do for j:= 1 to 31 do TDerivative[i,j]:=99;
 For i:= 1 to 167 do TonR[i]:=99;
 For i:= 1 to 167 do for j:= 1 to 31 do TDerivativeOnR[i,j]:=99;
 For i:= 1 to 31 do VoltagDeriv[i]:=99;

 {Forward Model to Compute Apparent Resistivities}

 LNSTEP:=ln(10.0)/Fltr.Decade; {Step at which filter is incremented}
 LEFT:=Fltr.Upper*LNSTEP + Fltr.Shift; {Displacement of the filter to the left of the origin}

 {Step through Electrode Distances}
 For i:=1 to NumBipoles do begin
  GeomFactOn2Pi:=GeomFact[i]/(2*Pi);
  For j:= 1 to numCurPot[i] do begin
   R[j]:=CP[i,j];
   Prop[j]:=CPProp[i,j];
  end;

  {Generate Transform Array for each Electrode Distance}
  For j:=1 to Fltr.Length do begin
   Offset:=(j-1)*LnStep - Left;
   For pair:=1 to numCurPot[i] do begin

    {The following If statements and k loop just avoids recalculating identical transforms}
    If pair<>1 then begin
     For k:=1 to pair-1 do begin
      If R[pair]=R[k] then begin
       T[pair]:=T[k];
       For l:= 1 to NParam do TDerivative[pair,l]:=TDerivative[k,l];
       break;
      end;
      If k=(pair-1) then begin
       {Calculate Monopole Transform and possibly derivatives}
       LogX:=Ln(R[pair])+Offset;
       If CalcDeriv then begin
        T[pair]:=MonopoleTAndDeriv(Model,LogX,CalcDeriv,TDeriv);
        For l:= 1 to NParam do TDerivative[pair,l]:=TDeriv[l];
       end else T[pair]:=MonopoleT(Model,LogX);
      end;
     end;
    end else begin
     {Calculate Monopole Transform and possibly derivatives}
     LogX:=Ln(R[pair])+Offset;
```

```
        If CalcDeriv then begin
          T[pair]:=MonopoleTAndDeriv(Model,LogX,CalcDeriv,TDeriv);
          For l:= 1 to NParam do TDerivative[pair,l]:=TDeriv[l];
        end else T[pair]:=MonopoleT(Model,LogX);
      end;
    End; {pair}

    {initialize}
    TonR[j]:=0;
    For k:= 1 to NParam do TDerivativeOnR[j,k]:=0;

    {Combine monopole Transform Functions to T/inter-electrode-distances}
    For pair:= 1 to numCurPot[i] do begin
      TonR[j]:=TonR[j]+  T[pair]*Prop[pair]/R[pair];
      If CalcDeriv then For k := 1 to NParam do
        TDerivativeOnR[j,k] := TDerivativeOnR[j,k] + TDerivative[pair,k]*Prop[pair]/R[pair];
    end;
  End; {j}

  {************************************************
          Convolution Sum
  CONVOLUTION of RESISTIVITY TRANSFORMS (normalized
  by electrode spacings) and DERIVATIVES with
   an INVERSE FILTER to give MODEL APPARENT
   RESISTIVITIES.
  ************************************************}
  VOLTAG:=0.;
  For k:=1 to NParam do VoltagDeriv[k]:=0;

  For J:=1 to Fltr.Length do
    VOLTAG:=VOLTAG+Fltr.Filter[J]*TonR[Fltr.Length-J+1];
  If CalcDeriv then For K:=1 to NParam do begin
    For J:= 1 to Fltr.Length do
      VOLTAGDeriv[k]:=VOLTAGDeriv[k]+Fltr.Filter[J]*TDerivativeOnR[Fltr.Length-J+1,k];
    {As pos and neg electrodes are not known, we need to check and correct signs here}
    If GeomFactOn2Pi<0 then VoltagDeriv[k]:=-1*VoltagDeriv[k];
  end;

  {Compute Apparent Resistivity for each Array Position}
  APPRES:=Abs(GeomFactOn2pi*VOLTAG);
  If AppRes<0.000001 then AppRes:=0.000001; {Prevent crashes in chaotic model mismatches}

  {Store results in (i := 1 to numBipoles) arrays for external use}
  Voltages[i]:=Voltag/(2*pi); //divide by 2pi to get voltages normalized to a current of 1 amp
  AppReses[i]:=Appres;
  If CalcDeriv then For k := 1 to NParam do begin
    AppResDeriv[i,k]:=VoltagDeriv[k]*GeomFactOn2Pi;
    If Abs(AppResDeriv[i,k])<0.000001 then If AppResDeriv[i,k]>0 then AppResDeriv[i,k]:=0.000001 else AppResDeriv[i,k]:=-
0.000001;
  end;

 end;{i:Next Array Position}

end {with model};end;

Function MonopoleT(const Model:TModel;
             var LogX:Double):Double;
var
 Lambda,Exp2LH,TanHLH,Arg,RAbove:Extended;
 j:Integer;
begin with model do begin
 {C**********************************************************************
 C    Calculate Monopole Resistivity transform function by recursion
 C**********************************************************************}

 LAMBDA:=1/Exp(LogX);
 Result:=PARAM[NPARAM];
 For j:= 2 to NLayer do begin
   EXP2LH:=0;
   ARG:=2*LAMBDA*PARAM[NLAYER+1-j];
   IF (ARG<=50.0) then EXP2LH:=Exp(-ARG);  {If <=50 then exp2lh becomes insignificant}
   TANHLH:=(1-EXP2LH)/(1+EXP2LH);
   RABOVE:=PARAM[NPARAM+1-j];
   Result:=(Result+RABOVE*TANHLH)/(1+Result*TANHLH/RABOVE);
 end;
```

```
end {with}; end;


Function MonopoleTAndDeriv(const Model:TModel;
                    var LogX:Double;
                    var CalcDeriv:Boolean;
                    var TDeriv:Array of Double
                    ):Double;
{*****************************************************
     CALCULATE MONOPOLE RESISTIVITY TRANSFORMS
         and DERIVATIVES by RECURSION.
    Input: Model, LogX
    Result := Monopole Resistivity Transform Function
    Other Output := TDeriv[0..NParam] Note [0] never used - just avoids displacement when parameter passing
 *****************************************************}
var
  Lambda,ARG,RABOVE:Double;
  TPart : Array[1..15] of Double;
  C,D,AA,Exp2LH,TanHLH:Double;
  j,k,J1,Npar1J,NLay1,NPar1,NLay1J,KNLay1:Integer;
begin with model do begin
{  MemoProgress.Lines.Append(' TDeriv');}
  NLAY1 := NLAYER + 1;
  NPAR1 := NPARAM + 1;
  LAMBDA := 1.0/Exp(LogX);
  TPART[1] := PARAM[NPARAM];
  IF CalcDeriv then TDeriv[NPARAM] := 1.0;
  For J := 2 to NLAYER do begin
    NLAY1J := NLAY1-J;
    ARG    := 2*LAMBDA*PARAM[NLAY1J];
    EXP2LH := 0.0;
    IF (ARG <= 50) then EXP2LH := EXP(-ARG);
    TANHLH := (1.0-EXP2LH)/(1.0+EXP2LH);
    NPar1J := NPar1-J;
    RABOVE := PARAM[NPAR1J];
    J1 := J-1;
    TPART[J] := (TPART[J1] + RABOVE*TANHLH)/(1. + TPART[J1]*TANHLH/RABOVE);
    IF CalcDeriv then begin
      C := TPART[J1]/RABOVE;
      D := sqr(1 + TanHLH*C);
      TDeriv[NPAR1J] := TanHLH*(1 + sqr(C) + 2*TanHLH*C)/D;
      TDeriv[NLAY1J] := ((4*LAMBDA*RABOVE*Exp2LH/sqr(1+Exp2LH))*(1-sqr(C)))/D;
      AA := (1 - Sqr(TanHLH))/D;
      For K := NLAYER+2-J to NLAYER do begin
        IF (K < NLAYER) then TDeriv[K] := TDeriv[K] * AA;
        KNLAY1 := K+NLAYER-1;
        TDeriv[KNLAY1] := TDeriv[KNLAY1] * AA;
      end; {k}
    end; {If CalcDeriv}
  end; {j}
  Result := TPART[NLAYER];
end {with}; end; {MonopoleTAndDeriv}

Procedure Invert(Var VPar:TVariableParam;
              Var Response:TResponse;
              Var Model:TModel;
              Const OrigModel:TModel;
              Const InvConst:TInversionParam;
              Const ShowDeriv:Boolean;
              Const ShowProgressMonitor:Boolean);
{C-------------------------------------------------------------
C       COMMENCE INVERSION PROCESS. COMPUTE APPARENT
C       RESISTIVITIES FOR FIRST MODEL AT EACH ITERATION.
C-------------------------------------------------------------}
var
  Converge:Boolean; {Becomes false if Iter >= NIter}
  RMSD, RMS1,RMS2,RMS3,RMS4 :Double;
  OldMod:Array[1..32] of Double;
  OldRes: Array[1..25] of Double;
  ChosenFilter:TFilter;
  Incr,i,j,k:Integer;
  CalcDeriv:Boolean;
  SumOfSquaresNew:Double;
  Stretch,Roughness:Double;
begin with model,VPar,Response,InvConst do begin
```

```
{Initialize}
CalcDeriv:=False;
ParamToVParam(CalcDeriv,Model,VPar,Response);
RMS3  :=5000;
RMS2  :=5000;
ITER := 0;
Case FilterNumber of
  0:ChosenFilter:=J0Filter3;
  1:ChosenFilter:=J0Filter6;
  2:ChosenFilter:=J0Filter12;
end;
Repeat
  INCR := 0;
  CalcDeriv := True;
  VParamToParam(CalcDeriv,Model,VPar,Response);
  ForwardModel(CalcDeriv,Model,AConfigParticular,Response,ChosenFilter);
  ParamToVParam(CalcDeriv,Model,VPar,Response);

  {C-------------------------------------------------------
  C      NORMALISE DERIVATIVES FOR LOG SCALE
  C-------------------------------------------------------}

  For i:=1 to nData do begin
    RMODEL[I] := DERIV[I,nVParam+1];
    If SubNoiseInversion and (RField[i]<=NoiseDivCurrent*AConfigParticular.GeomFact[i]) then begin
      If RModel[i]<=NoiseDivCurrent*AConfigParticular.GeomFact[i] then begin
        Deltar[i]:=0;
        ModelMinusField[i]:=0;
      end else begin
        Deltar[i]:=ln(RModel[i]/(NoiseDivCurrent*AConfigParticular.GeomFact[i]));
        ModelMinusField[i]:=RModel[i]-NoiseDivCurrent*AConfigParticular.GeomFact[i];
      end;
    end else begin
      If (RField[i]/RModel[i])<0.00001 then Deltar[i]:=ln(0.00001)
        else DELTAR[I] := Ln(RFIELD[I]/RMODEL[I]);
      ModelMinusField[i]:=RModel[i]-RField[i];
    end;
    For J := 1 to nVParam do
      DERIV[I,J] := DERIV[I,J]/RMODEL[I];
  end;
  IF (ITER=0) then begin
    //Compute Roughness for initial model
    //     notes:any fixed resistivities are included in smoothing for logical reason
    //          :included is an L1 algorithm which weighs the bulk of the data more than
    //           occasional high contrast data.
    //          :logarithms are not used so high contrast data is weighted even less than in normal L1 algorithm.
    Roughness:=0;
    If WtVertSmooth>0 then
      If norm=1 then begin
        For i:= nLayer+1 to nParam do
          Roughness:=Roughness+2*abs(Param[i]-Param[i-1])/(Param[i]+Param[i-1]);
        Roughness:=SumWeight*wtVertSmooth*Roughness/(nLayer-1);
      end else begin
        For i:= nLayer+1 to nParam do
          Roughness:=Roughness+sqr(2*(Param[i]-Param[i-1])/(Param[i]+Param[i-1]));
        Roughness:=SumWeight*wtVertSmooth*Roughness/(nLayer-1);
      end;
    //Compute Layer thickness stretch for the initial model
    Stretch:=0; //Because initial model thickesses equal OrigModel thicknesses.

    {C-------------------------------------------------------
    C      COMPUTE SUM OF SQUARES FOR INITIAL MODEL.
    C-------------------------------------------------------}

    SumOfSquares := 0;
    If norm=1 then For i:=1 to nData do //Least absolute deviation
      SumOfSquares := SumOfSquares + abs(DeltaR[i])*Weight[i]
    else For i:=1 to nData do          //Least squares
      SumOfSquares := SumOfSquares + Sqr(DeltaR[i])*Weight[i];

    SumOfSquares := SumOfSquares + Roughness + Stretch;

    {C-------------------------------------------------------
    C      COMPUTE PERCENT RMS ERROR FOR INITIAL MODEL.
    C-------------------------------------------------------}
```

```
 RMS := 0.;
 For i:= 1 to nData do begin
  OLDRES[I] := RMODEL[I];
  //RMS := RMS + sqr(1-RMODEL[I]/RFIELD[I])*Weight[i]; Merricks RMS rejected
  //New RMS formula added that is normalized to the average of model and field data
  //does not blow out when field data is much smaller than model data
  //but is computationally slower
  If norm=1 then
   RMS := RMS + abs(2*(ModelMinusField[i])/(RModel[i]+RField[i]))*Weight[i]
  else  RMS:=RMS+sqr(2*(ModelMinusField[i])/(RModel[i]+RField[i])*Weight[i]);
 end;
 If Norm=1 then begin
  RMS := 100. * RMS/SumWeight;
 end else begin
  RMS := 100. * SQRT(RMS/SumWeight);
 end;

 {C-------------------------------------------------------
 C      COMPUTE INITIAL EPSILON (MARQUARDT PARAMETER)
 C-------------------------------------------------------}

 EPS := 0;
 For i:=1 to nData do for j:=1 to nVParam do begin
  EPS := EPS + Sqr(DERIV[I,J]);
 end;
 EPS := SQRT(EPS/(nData*nVParam));
 VParamToParam(CalcDeriv,Model,VPar,Response);
 IF (RMS<=RMSCUT) then begin TieUp(ShowDeriv,ShowProgressMonitor); exit; end;
 If ShowProgressMonitor then OutputProgress(False);
end;

{C-------------------------------------------------------
C      ORTHOGONAL FACTORISATION AND BACK SUBSTITUTION
C-------------------------------------------------------}

ORFAC(VPar);
Repeat
 Converge := True;
 EPSFAC(VPar,EPS);
 BAKSUB(VPar);

 {C-------------------------------------------------------
 C      PARAMETERS OF NEW MODEL
 C-------------------------------------------------------}

 For i := 1 to nVParam do begin
  OLDMOD[I] := VPARAM[I];
  VPARAM[I]  := VPARAM[I] + DELTAP[I];
  IF (VPARAM[I]<=0.0) then VPARAM[I] := 0.0001;
 end;
 CalcDeriv := False;

 {C-------------------------------------------------
 C      COMPUTE APPARENT RESISTIVITIES FOR NEW MODEL
 C-------------------------------------------------}

 VParamToParam(CalcDeriv,Model,VPar,Response);
 ForwardModel(CalcDeriv,Model,AConfigParticular,Response,ChosenFilter);
 ParamToVParam(CalcDeriv,Model,VPar,Response);

 //Compute new Roughness
 //     notes:any fixed resistivities are included in smoothing for logical reason
 //          :included is an L1 algorithm which weighs the bulk of the data more than
 //           occasional high contrast data.
 //          :logarithms are not used so high contrast data is weighted even less than in normal L1 algorithm.
 Roughness:=0;
 If WtVertSmooth>0 then
  If norm=1 then begin
   For i:= nLayer +1 to NParam do
    Roughness:=Roughness+2*abs(Param[i]-Param[i-1])/(Param[i]+Param[i-1]);
   Roughness:=SumWeight*wtVertSmooth*Roughness/(nLayer-1);
  end else begin
   For i:= nLayer+1 to NParam do
    Roughness:=Roughness+2*sqr(Param[i]-Param[i-1])/(Param[i]+Param[i-1]);
```

```
    Roughness:=SumWeight*wtVertSmooth*Roughness/(nLayer-1);
   end;

  //Compute new Layer thickness stretch
  Stretch:=0;
  If WtOrigThick>0 then
   If norm=1 then begin
    //Do not ever want L1 norm for stretch - adjust by taking Sqrt of result before blending with other constriants
    For i:= 1 to NLayer-1 do
     Stretch:=Stretch+{abs}sqr(Param[i]-OrigModel.Param[i])/OrigModel.Param[i];
    Stretch:=SumWeight*wtOrigThick*Sqrt(Stretch/(nLayer-1));
   end else begin
    For i:= 1 to Model.NLayer-1 do
     Stretch:=Stretch+sqr((Param[i]-OrigModel.Param[i])/OrigModel.Param[i]);
    Stretch:=SumWeight*wtVertSmooth*Stretch/(nLayer-1);
   end;

  {C-----------------------------------------------------
  C      COMPUTE NEW SUM OF SQUARES
  C-----------------------------------------------------}

  For i := 1 to nData do begin
   RMODEL[I] := DERIV[I,nVParam+1];
   IF (RMODEL[I] <= 0.0001) then RMODEL[I] := 0.0001;
   If SubNoiseInversion and (RField[i]<=NoiseDivCurrent*AConfigParticular.GeomFact[i]) then begin
    If RModel[i]<=NoiseDivCurrent*AConfigParticular.GeomFact[i] then begin
     DeltaRNew[i]:=0;
    end else begin
     DeltaRNew[i]:=ln(RField[i]/(NoiseDivCurrent*AConfigParticular.GeomFact[i]));
    end;
   end else begin
    If (RField[i]/RModel[i])<0.00001 then DeltarNew[i]:=ln(0.00001)
     else DELTARNew[I] := Ln(RFIELD[I]/RMODEL[I]);
   end;
  end;

  SumOfSquaresNEW := 0;
  If norm=1 then For i := 1 to nData do begin //Least absolute deviation
   SumOfSquaresNEW := SumOfSquaresNEW + Abs(DeltaRNew[i])*Weight[i];
  end else For i := 1 to nData do begin      //Least Squares
   SumOfSquaresNEW := SumOfSquaresNEW + Sqr(DeltaRNew[i])*Weight[i];
  end;
  SumOfSquaresNew := SumOfSquaresNew + Roughness + Stretch;


  If SumOfSquaresNew < SumOfSquares then break;
  {C-----------------------------------------------------
  C      INCREASE EPSILON
  C-----------------------------------------------------}

  For i := 1 to nVParam do
   VPARAM[I] :=  OLDMOD[I];
  EPS := EPS * EINCR;
  INCR := INCR + 1;
  If Incr>=NIncr then begin
   Converge:=False;
   If ShowProgressMonitor then FormInvProg.MemoProgress.Lines.append(IntToStr(Incr)+
    ' Increases in Epsilon. Trial Model Will Not Converge');
   For i := 1 to nData do RModel[i] := OldRes[i];
   break;
  end;
 Until False; {SumOfSquaresNew < SumOfSquares;} {always found true due to break statement above}
 If Converge = False then break; {A way of breaking out of 2 loops}
 SumOfSquares := SumOfSquaresNew;

 {C-----------------------------------------------------
 C      COMPUTE PERCENT RMS ERROR
 C-----------------------------------------------------}

 RMS := 0.;

 //Old RMS procedure of Merrick
 //For i:= 1 to nData do
 //  RMS := RMS + Sqr(1-RMODEL[I]/RFIELD[I])*Weight[i];
 //RMS := 100. * SQRT(RMS/SumWeight);
```

```
  For i:= 1 to nData do begin
   If SubNoiseInversion and (RField[i]<=NoiseDivCurrent*AConfigParticular.GeomFact[i]) then begin
    If RModel[i]<=NoiseDivCurrent*AConfigParticular.GeomFact[i] then begin
     ModelMinusField[i]:=0;
    end else begin
     ModelMinusField[i]:=RModel[i]-NoiseDivCurrent*AConfigParticular.GeomFact[i];
    end;
   end else begin
    ModelMinusField[i]:=RModel[i]-RField[i];
   end;
  end;

  If Norm=1 then
   For i:= 1 to nData do
    RMS:=RMS+abs(2*(ModelMinusField[i])/(RModel[i]+RField[i]))*Weight[i]
  else
   For i:= 1 to nData do
    RMS:=RMS+sqr(2*(ModelMinusField[i])/(RModel[i]+RField[i])*Weight[i]);
  If Norm=1 then RMS := 100. * RMS/SumWeight
  else RMS := 100. * SQRT(RMS/SumWeight);

  Inc(ITER);
  IF (RMS <= RMSCUT) then Break;
  RMS1 := RMS;
  RMSD := RMS3 - RMS1;
  IF (RMSD <= 0.05) then Break;
  RMS3 := RMS2;
  RMS2 := RMS1;
  IF (ITER >= NITER) then begin
   If ShowProgressMonitor then FormInvProg.MemoProgress.Lines.append(IntToStr(Iter)+' Iterations. Limit Set at '+IntToStr(NIter));
   Break;
  end;
  VParamToParam(CalcDeriv,Model,VPar,Response);
  If ShowProgressMonitor then OutputProgress(False);


  {C-----------------------------------------------------
  C      COMPUTE NEW EPSILON FOR NEXT ITERATION.
  C-----------------------------------------------------}

  IF INCR=0 then  EPS := EPS/EDECR;
  For I:=1 to nData do OLDRES[I] := RMODEL[I];
 until false; {Iter>=NIter;} {Always true due to previous break statement}

 {_____________________________________________________________
 |       End of main loop
 _____________________________________________________________}
 TieUp(ShowDeriv,ShowProgressMonitor);
end {with model}; end;  {End of Inversion}

procedure Orfac(Var VPar:TVariableParam);
{C ***************************************************
C             ORFAC.FOR             MERRICK, 1981
C             ---------
C    ORTHOGONAL FACTORISATION.
C ***************************************************}
var
 i,i1,j,k:integer;
 S1,S3,S4:Double;
begin with VPar do begin
 //FormInvProg.MemoProgress.Lines.Append(' ORFAC');
 NUSUAL := nVParam;
 IF (nData = nVParam) then NUSUAL := nVParam-1;
 For I := 1 to NUSUAL do begin
  S3 := 0;
  For J :=I to nData do S3 := S3 + Sqr(Deriv[J,I]);
  IF (S3 = 0)  then continue;
  S3 := SQRT(S3);
  IF (Deriv[I,I]> 0) then S3 := -S3;
  S4 := 1./SQRT(2.*S3*(S3-Deriv[I,I]));
  I1:=I+1;
  For J := I+1 to nData do Deriv[J,I] := -S4*Deriv[J,I];
  Deriv[nData+1,I] := S4*(S3-Deriv[I,I]);
  Deriv[I,I] := S3;
  IF (I = nVParam) then continue;
```

```
   For J := I+1 to nVParam do begin
    S1 := Deriv[I,J] * Deriv[nData+1,I];
    For K := I1 to nData do S1 := S1 + Deriv[K,J]*Deriv[K,I];
    S1 := -2.*S1;
    Deriv[I,J] := Deriv[I,J] + S1*Deriv[nData+1,I];
    For K := I1 to nData do Deriv[K,J] := Deriv[K,J] + S1*Deriv[K,I];
   end; {j}
  end; {i}
end {with}; end;

procedure EPSFAC(var VPar:TVariableParam; var EPS:Double);
{C ****************************************************
C            EPSFAC.FOR            MERRICK, 1981
C            ----------
C   ORTHOGONAL FACTORISATION WITH EPSILON APPENDAGE.
C ****************************************************}
var
  i,j,k,i1:integer;
  S1,S3,S4:Double;
  //General scope variable also used : DerivEps :Array[1..34,1..32] of Double; {Maxnumparam+2,Maxnumparam}
begin with VPar do begin
  I1:=0; {Unnecessary initialization}
  {MemoProgress.Lines.Append(' EPSFAC');}
  For I:=1 to nVParam do begin
   IF (I <> nVParam) then begin
    I1 := I+1;
    For J := I1 to nVParam do DerivEps[I,J] := 0;
   end;
   DerivEps[I,I] := EPS;
   S3 := Sqr(Deriv[I,I]);
   For J:=1 to I do S3 := S3 + Sqr(DerivEps[J,I]);
   S3 := SQRT(S3);
   IF (Deriv[I,I] > 0) then  S3 := -S3;
   S4 := 1./SQRT(2.*S3*(S3-Deriv[I,I]));
   DerivEps[nVParam+2,I] := S4*(S3-Deriv[I,I]);
   For J :=1 to I do DerivEps[J,I] := -S4*DerivEps[J,I];
   DerivEps[I+1,I] := S3;
   IF (I = nVParam) then continue;
   For J := I1 to nVParam do begin
    S1 := Deriv[I,J]*DerivEps[nVParam+2,I];
    For K:=1 to I do S1 := S1 + DerivEps[K,J]*DerivEps[K,I];
    S1 := -2.*S1;
    For K:=1 to I do DerivEps[K,J] := DerivEps[K,J] + S1*DerivEps[K,I];
    DerivEps[J+1,I] := Deriv[I,J] + S1*DerivEps[nVParam+2,I];
   end; {j}
  end; {i}
end {with}; end;


procedure BakSub(Var VPar:TVariableParam);
{C ****************************************************
C            BAKSUB.FOR            MERRICK, 1981
C            ----------
C   SOLUTION BY BACK SUBSTITUTION.
C ****************************************************}
var
  C:Array[1..44] of Double;
  i,j,k,i1,j1,mi,mj:integer;
  S1:Double;
  //General scope variable also used : DerivEps :Array[1..34,1..32] of Double; {Maxnumparam+2,Maxnumparam}
begin with VPar do begin
  {C-------------------------------------------------------------
  C      CALCULATE VECTORS C1, C2.
  C-------------------------------------------------------------}
  {MemoProgress.Lines.Append(' BAKSUB');}
  For I :=1 to nData do C[I] := DeltaR[I];
  For I :=1 to NUSUAL do begin
   S1 := C[I] * Deriv[nData+1,I];
   I1 := I+1;
   For J:=I1 to nData do S1 := S1 + C[J] * Deriv[J,I];
   S1 := -2.*S1;
   C[I] := C[I] + S1 * Deriv[nData+1,I];
   For J:=I1 to nData do C[J] := C[J] + S1 * Deriv[J,I];
  end;
```

```
 {C-------------------------------------------------------
 C      CALCULATE VECTORS C3, C2, C4.
 C-------------------------------------------------------}

 For I:=1 to nVParam do begin MI:=nData+I; C[MI]:=0; end;
 For I:=1 to nVParam do begin
  S1 := DerivEps[nVParam+2,I] * C[I];
  For J:=1 to I do begin MJ := nData+J; S1 := S1 + C[MJ] * DerivEps[J,I]; end;
  S1 := -2.*S1;
  C[I] := C[I] + S1 * DerivEps[nVParam+2,I];
  For J:=1 to I do Begin MJ := nData+J; C[MJ]:=C[MJ]+S1*DerivEps[J,I]; end;
 end; {i}

 {C-------------------------------------------------------
 C      CALCULATE PARAMETER CORRECTION VECTOR, DELTA-P.
 C-------------------------------------------------------}

 For I:=1 to nVParam do DeltaP[I] := 0;
 DeltaP[nVParam] := C[nVParam]/DerivEps[nVParam+1,nVParam];
 DeltaP[nVParam-1] := (C[nVParam-1] - DerivEps[nVParam+1,nVParam-1] * DeltaP[nVParam]) / DerivEps[nVParam,nVParam-1];
 For I:=3 to nVParam do begin
  J := nVParam-I+1;
  S1 := 0;
  J1 := J+1;
  For K:=J1 to nVParam do S1 := S1 + DerivEps[K+1,J] * DeltaP[K];
  DeltaP[J] := (C[J] - S1) / DerivEps[J+1,J];
 end; {i}
end {with}; end;

procedure TieUp(Const ShowDeriv:Boolean; Const ShowProgressMonitor:Boolean);
 {C-------------------------------------------------------
 C      PRINT THE FINAL MODEL  (& LAST ITERATION)
 C-------------------------------------------------------}
var
 i,j:integer;
begin
 If ShowProgressMonitor then OutputProgress(True);
 If ShowDeriv then begin
  With Model,VPar,Response,FormDeriv.StringGridDeriv do begin
   RowCount:=nData+1;
   ColCount:=NParam+2;
   For i:= 1 to NLayer -1 do Cells[i,0]:=Format('Thick %2.0d',[i]);
   For i:= NLayer to NParam do Cells[i,0]:=Format('Res %2.0d',[i-NLayer+1]);
   Cells[NParam+1,0]:='AppR';
   Cells[0,0]:='Config';
   For j:= 1 to nData do Cells[0,j]:=Format('%2.0d',[j]);
   For i:= 1 to NParam do For j:= 1 to nData do
    Cells[i,j]:=Format('%5.3g',[AppResDeriv[j,i]]);
   For j:= 1 to nData do
    Cells[nParam+1,j]:=Format('%5.3g',[AppReses[j]]);
  end;
  FormDeriv.Show;
 end;
end;

procedure OutputProgress(const Last:Boolean);
{C ******************************************************
C       OutputProgress adapted from MERRICK, 1981
C       --------------
C   RESISTIVITY INVERSION ITERATION MONITOR AND
C    MODEL OUTPUT.
C ******************************************************}
var
 Thick,Depth,Res,Transv,LongCN,SumT,SumL,Error:Double;
 NLayM1,i,j,inLayM:integer;
 Mark1,Mark2:Char;
begin
 with InvConst,Model,VPar,Response,FormInvProg.MemoProgress.Lines do begin
  //Append(' OUTPUT');
  SUMT := 0;
  SUML := 0;
  NLAYM1 := NLAYER - 1;

  {C-------------------------------------------------
  C      ITERATION MONITOR
```

```
  C-------------------------------------------------------}

  Append('Iteration '+IntToStr(Iter));
  Append(Format(' Epsilon = %11.3e   Sum-of-Squares = %11.3e  %10.2fPercent RMS'
   ,[EPS,SumOfSquares,RMS]));
  Append(' LAYER NO.      THICKNESS    RESISTIVITY     THICK*RES   THICK/RES');
  For i:= 1 to NLayM1 do begin
   THICK  := PARAM[I];
   INLAYM := I+NLAYM1;
   RES    := PARAM[INLAYM];
   TRANSV := THICK * RES;
   LONGCN := THICK / RES;
   SUMT   := SUMT + TRANSV;
   SUML   := SUML + LONGCN;
   Append(Format('%6d       %10.3f   %10.3f    %12.3f%12.4f'
    ,[I, THICK, RES, TRANSV, LONGCN]));
  End; {i}
  Append(Format('%6d                  %10.3f    %12.3f%12.4f',
   [NLAYER, PARAM[NPARAM], SUMT, SUML]));
  IF not LAST then exit;

  {C-------------------------------------------------------
  C      FINAL MODEL
  C-------------------------------------------------------}

  Append(' POINT      DISTANCE      RA(FIELD)      RA(MODEL)     PERCENT ERROR');
  For I :=1 to nDATA do begin
   ERROR := 200. * (RFIELD[I]-RMODEL[I])/(RFIELD[I]+RMODEL[I]);
   Append(Format('%4d      %10.3f      %10.3f      %10.3f      %10.3f',
    [I, AConfigParticular.EffDepth[I], RFIELD[I], RMODEL[I], ERROR]));
  end;
  Append('');
  Append('');
  Append(Format('     PERCENT RMS ERROR =%6.2f                 (CUTOFF SET AT%6.2f )'
   ,[RMS, RMSCUT]));
  Append('     INTERPRETED MODEL...                    : FIXED PARAMETER');
  DEPTH := 0.;
  THICK := 0.;
  For I := 1 to NLAYER do begin
   J := I + NLAYM1;
   DEPTH := DEPTH + THICK;
   Append(Format('          ----------------------------------------%8.2f',[Depth]));
   MARK1 := ' ';
   MARK2 := ' ';
   IF (NParam <> NVParam) then begin
      IF VarOrFix[J] then MARK1 := '*';
      IF (I < NLAYER) and VarOrFix[I] then MARK2 := '*';
    end;
    Append('                          '+MARK1+'                '+MARK2);
    Append(Format('              RES =%9.2f',[PARAM[J]]));
    IF (I = NLAYER) then break;
    THICK := PARAM[I];
    Append(Format('                                THICK =%7.2f',[THICK]));
  end; {i}
  Append('');
  Append('');
  Append('         LAYER          T=THICK*RES        S=THICK/RES');
  For i :=1 to NLAYM1 do begin
   INLAYM := I+NLAYM1;
   TRANSV := PARAM[I] * PARAM[INLAYM];
   LONGCN := PARAM[I] / PARAM[INLAYM];
   Append(Format('          %2d          ,%12.3f        %10.4f',
   [I, TRANSV, LONGCN]));
  end; {i}
  Append('');
  Append(Format('         Total        %12.3f        %10.4f'
   ,[SUMT, SUML]));
 end;
end;

initialization
 RiverWaterResistivity:=100; //This is used only with submerged inversion
 //Initialization will always be overwritten if run from Inversion.pas.
end.
```

A5.2 Horizontal Smoothing

Continuously acquired data usually is more useable if smoothed horizontally. Significant reduction in random noise levels can be achieved by smoothing before inversion. In cases where surface inhomogeneities exist or other 3D structure is problematical, horizontal smoothing has an effect similar to lateral constraint of inversion. Auken (2004) and others have applied lateral constraint to 1D layered inversion which is theoretically superior to smoothing of data but has much the same effect. Smoothing can be conducted before or after inversion but is most practical before inversion as errors in unsmoothed data are generally greatly amplified by the inversion process. Smoothing increases the effectiveness of differencing of datasets where errors have greater significance and facilitates resolution of deeper layers by reducing random noise levels.

Horizontal smoothing can be applied using orthogonal polynomial weighting functions by simply convolving the data sequence with a set of polynomial terms, then dividing by the sum of the terms. That is :

$$[SmoothedDataset] = [Dataset] * [PolynomialTerms] / \sum PolynomialTerms$$

If the smoothed dataset is made to be the input dataset rather than a completely separate dataset, then smoothing still takes place but has a slightly asymmetrical response to outliers. The procedure is further explained in Davis (1986) pp268-273. The degree of smoothing may be increased by using larger sets of terms. It may be further increased by running the algorithm multiple times. Most geo-electric array and TEM data collected at intervals of a few seconds as part of this work has been smoothed with 17 point filters 6 times. Further smoothing could result in blurring of features larger than the minimum dimensions of interest so should be avoided.

Datasets have records with variable numbers of channels due to noise cutoffs, dataset ends, or other faults so smoothing operations must detect and avoid smoothing channels of records with corresponding channels missing in records covered by the smoothing filter being applied. It is sensible to apply the smoothing before clipping data at noise level. Failure to do so will result in some failure of smoothing of later channels.

Smoothing has been implemented in HydroGeoImager.EXE as follows. A Voltage or Chn/Depth dBase dataset of format described in the Appendices is referenced by a TTable component – 'TableSmooth' and backed up. An index is created using the 'DISTANCE' column then the procedure – 'SmoothHoriz' is run on the Table as many times as is requested. Documentation of the smoothing is added to the corresponding INI file. The Delphi7 code for procedure 'SmoothHoriz' documents the Quadratic/Cubic polynomial terms taken from Davis (1986) and is as follows :

```
procedure SmoothHoriz(VoltOrChnDepth:Boolean; FilterNum:Integer);
type TSmoothFilter = array[0..18] of integer;
const
 W:Array[0..4] of TSmoothFilter =(
 (5, -3,12,17,12,-3, 35,0,0,0,0,0,0,0,0,0,0,0),
 (7, -2,3,6,7,6,3,-2, 21,0,0,0,0,0,0,0,0,0,0),
 (9, -21,14,39,54,59,54,39,14,-21, 231,0,0,0,0,0,0,0,0),
 (13, -11,0,9,16,21,24,25,24,21,16,9,0,-11,143,0,0,0,0),
 (17, -21,-6,7,18,27,34,39,42,43,42,39,34,27,18,7,-6,-21, 323));

var
  i,j,Chn,ChnIndex,Chn01Index,NumDepths:integer;
  SumR: Array[0..49] of Double; //only 50 channels are facilitated
  DummyR:Array[0..49] of Boolean;
  tmp:string;
begin
  With FormSmooth.TableSmooth do begin
    Active:=False;
    Indexname:='byDistance';
    Active:=True;
    FieldDefs.Update;
    If VoltOrChnDepth then Chn01Index:=FieldDefs.IndexOf('CHN01')
      else Chn01Index:=FieldDefs.IndexOf('V01');
    ChnIndex:=FieldDefs.IndexOf('CHN');
    //Determine numDepths here to allow routine to be more general.
    NumDepths:=1;
    Repeat
      If VoltOrChnDepth then begin
        tmp:=Format('CHN%2.2d',[NumDepths+1]);
        If FieldDefs.IndexOf(tmp)<>-1 then
          Inc(NumDepths);
      end else begin
        tmp:=Format('V%2.2d',[NumDepths+1]);
        If FieldDefs.IndexOf(tmp)<>-1 then
          Inc(NumDepths);
      end;
    until FieldDefs.IndexOf(tmp)=-1;
    First;
    MoveBy(W[FilterNum,0]+1); //This starting point has been chosen to avoid filtering past EOF.
    While not EOF do begin
      For j:=0 to NumDepths-1 do begin SumR[j]:=0; DummyR[j]:=False; end;
      MoveBy(-1*W[Filternum,0]-1);
      For i:= 1 to W[Filternum,0] do begin
        next;
        Chn:=Fields[ChnIndex].AsInteger;
        For j:=0 to NumDepths-1 do
          If (Fields[Chn01Index+j]<>nil) and (Chn<=j+1) then
            SumR[j]:=SumR[j]+W[Filternum,i]*Fields[Chn01Index+j].AsFloat
          else DummyR[j]:=True;
      end;
      MoveBy(-1*(W[Filternum,0]-1)div(2));
      Edit;
      For j:=0 to NumDepths-1 do
        If DummyR[j]=False then
          Fields[Chn01Index+j].AsFloat:=SumR[j]/W[Filternum,W[FilterNum,0]+1];
      Post;
```

```
    MoveBy((W[FilterNum,0]+1)div(2));
    Next;
   end;
   Active:=False;
  end;
end;
```

A5.3 ConfigCore

Config core contains the code central to describing and analyzing geo-electric arrays.

The code is as follows:

```
unit ConfigCore;

interface

uses
  Windows, Messages, SysUtils, Classes, IniFiles, IniFile, Math, Dialogs;

type
  //Array Configuration Record Format
  TArrayConfiguration = Record
    numBipoles:integer;
    MaxCP:integer; {maximum numCurPot in the sounding = 4 usually}
    {25       = number of array configs allowed in one sounding}
    numCurPot :Array[1..25] of integer;
    EffDepth  :Array[1..25] of single;
    {30       = num of electrode combos allowed}
    CP        :Array[1..25,1..30] of Double; {CP = an interelectrode dist - curr to potential}
    CPProp    :Array[1..25,1..30] of Double; {Proportion of current for each Rcp x sign used in Geom.Factor}
           {RcpProp is for permitting significant finite length current electrodes to be processed}
    GeomFact  :Array[1..25] of Double;
    SubmergedGeomFact :Array[1..25] of Double;
    SubDepth :Double;
    MidpointX:Array[1..25] of Double; //plotting x positions relative to Tx1
  end;
  //Array Configuration Record Format extension for 2D work
  TArrayConfigExt = Record
    //Signed fractional monopole electrode pairs needed for 2D inversion
    //MonopoleTx[n,1] and MonopoleTy[n,1] should always be 0 (ie the origin).
    MonopoleTx,MonopoleTy,MonopoleRx,MonopoleRy:Array[1..25,1..30] of Double;
    //Straight 4 electrodes - ignores fractionation of linear electrodes.
    //Used in programs that do not allow for linear electrodes.
    Elecx,Elecy:Array[1..25,1..4] of Double; //Transmit1,Transmit2,Pot1,Pot2
    TxElectrodeLength:Double;
    MidpointY:Array[1..25] of Double; //plotting y positions relative to Ty1
    AConfigType:String;
    PortionSizer:Double;
  end;


var
  ConfigIni :TMemIniFile;
  OffsetBehind,OffsetRight:Double;
  AConfig:TArrayConfiguration; //Fixed basic configuration
  AConfigExt:TArrayConfigExt;  //Fixed basic configuration Ext
  AConfigParticular:TArrayConfiguration; //Particular configuration for indiv
  AConfigParticularExt:TArrayConfigExt; // -idual records (meandering, truncated etc)
  i,j,k:integer;

  //ExponentialBipole
  CurrElecSeparation:Double;
  FirstPotentDist:Double;
  TwoToPowerOfnIncr:Double;
  RadiusOfCurvature:Double;
  //LinearBipoleBipole
  //Schlumberger
```

```
  SamplePerDecade:Double;
  SchlumbL:Array[1..25] of Double;
  Schlumblittlel:Array[1..25] of Double;
  //Wenner
  //AarhusPACES
  //GeneralPhiTheta
  PhiThetaInfo:Array[1..6,1..25] of String;
  //GeneralXY

  function Sgn(x:Double):integer;
  procedure CalcGeomFact(Var ArrayConfig:TArrayConfiguration);
  procedure CalcSubmergedGeomFact(var ArrayConfig:TArrayConfiguration);
  procedure ReadConfigIni;
  procedure NDICEffDepth;
  procedure CalcMidpoints;

implementation

function Sgn(x:Double):integer;
begin
  If x>=0 then Result:=1 else Result:=-1;
end;

procedure CalcGeomFact(var ArrayConfig:TArrayConfiguration);
var
  i,j:integer;
begin with ArrayConfig do begin
  {Calculate Geometric Factors}
  For i:= 1 to numBipoles do begin
    GeomFact[i]:=0;
    For j:= 1 to numCurPot[i] do
      If CP[i,j]<0.0000001 then
        MessageDlg('Cannot calculate geometric factor for separations<0.0000001',mtWarning,[mbOK],0)
      else GeomFact[i]:=GeomFact[i]+CPProp[i,j]/CP[i,j];
    GeomFact[i]:=2*Pi/Abs(GeomFact[i]);
  end;
end {with}; end;

procedure CalcSubmergedGeomFact(var ArrayConfig:TArrayConfiguration);
var
  i,j:integer;
begin with ArrayConfig do begin
  {Calculate Geometric Factors}
  For i:= 1 to numBipoles do begin
    SubmergedGeomFact[i]:=0;
    For j:= 1 to numCurPot[i] do
      If CP[i,j]<0.0000001 then
        MessageDlg('Cannot calculate geometric factor for separations<0.0000001',mtWarning,[mbOK],0)
      else SubmergedGeomFact[i]:=SubmergedGeomFact[i]+CPProp[i,j]/CP[i,j]
        +CPProp[i,j]/hypot(CP[i,j],SubDepth*2);
    SubmergedGeomFact[i]:=4*Pi/Abs(SubmergedGeomFact[i]);
  end;
end {with}; end;

procedure NDICEffDepth;
var
  NDIC,z,dz:Array[0..5000] of extended;
  CumNDIC,uppersum,lowersum,sqrz:extended;
  i,j,k:integer;
const
  log10DepthIncr:Single = 0.001;
begin with AConfig do begin
  {Calculate NDIC curves, cumulative NDIC curves and effective depths}
  For j:= 0 to 5000 do  z[j]:=power(10,-2.00+log10DepthIncr*j);
  For j:= 1 to 4999 do dz[j]:=(z[j]-z[j-1])/2 + (z[j+1]-z[j])/2;
  For i:= 1 to numBipoles do begin
    j:=0; CumNDIC:=0;
    Repeat
      inc(j);
      sqrz:=sqr(z[j]);
      uppersum:=0; lowersum:=0;
      for k:= 1 to numCurPot[i] do begin
        uppersum:=uppersum + CPProp[i,k]/power(sqr(CP[i,k]) + 4*sqrz,1.5);
        lowersum:=lowersum + CPProp[i,k]/CP[i,k];
      end;
```

```
      if lowersum<>0 then NDIC[j]:=dz[j]*4*z[j]*uppersum/lowersum else NDIC[j]:=0;
      CumNDIC:=CumNDIC+NDIC[j];
    until (j=4999) or (CumNDIC>=0.5);
    EffDepth[i] := z[j];
  end;
end {with}; end;

procedure CalcMidpoints;
var
  i,j:Integer;
  PortionWeight,SumWeights:Double;
begin with Aconfig,AConfigExt do begin
  //Calculate Midpoints
  For i:= 1 to numBipoles do begin
    MidpointX[i]:=0;
    MidpointY[i]:=0;
    SumWeights:=0;
    For j:= 1 to AConfig.numCurPot[i] do begin
      PortionWeight:=Abs(CPProp[i,j]/CP[i,j]);
      SumWeights:=SumWeights+PortionWeight;
      MidpointX[i]:=MidpointX[i]+PortionWeight*(MonoPoleTx[i,j]+MonoPoleRx[i,j])/2.0;
      MidpointY[i]:=MidpointY[i]+PortionWeight*(MonoPoleTy[i,j]+MonoPoleRy[i,j])/2.0;
    end;
    MidpointX[i]:=MidpointX[i]/SumWeights;
    MidpointY[i]:=MidpointY[i]/SumWeights;
  end;
end; {with} end;

Procedure ReadConfigIni;
var
  i,j:integer;
begin
  {Read defaults in from Ini file}
  ConfigIni := TMemIniFile.Create(IniFile.ConfigIniName);

  With ConfigIni, AConfig, AConfigExt do begin
    {numBipoles}
    numBipoles:=ReadInteger('Array', 'RxBipoles', 8);

    {Offset}
    OffsetBehind:=ReadFloat('Offset','Behind',0);
    OffsetRight:=ReadFloat('Offset','Right',0);

    {Main Config Form variables}
    MaxCP:=ReadInteger('Array','MaxMonopoles',4);
    For i:= 1 to numBipoles do begin
      numCurPot[i]:=ReadInteger('numMonopoles', 'numMonopoles'+Trim(IntToStr(i)),4);
      //Geometric factors and effective depths calculated again rather than read from config inifile
      If numCurPot[i]>MaxCP then MaxCP:=numCurPot[i];//error corrector trap
      For j:= 1 to numCurPot[i] do begin
        Case j of
          1:begin
            CP[i,j]:=ReadFloat('MonopoleSeparations', 'CP'+Trim(IntToStr(i))+'_'+Trim(IntToStr(j)),1);
            CPProp[i,j]:=ReadFloat('SignedMonopoleFractions', 'CPProp'+Trim(IntToStr(i))+'_'+Trim(IntToStr(j)),1);
          end;
          2:begin
            CP[i,j]:=ReadFloat('MonopoleSeparations', 'CP'+Trim(IntToStr(i))+'_'+Trim(IntToStr(j)),16+Power(2,(i-2)));
            CPProp[i,j]:=ReadFloat('SignedMonopoleFractions', 'CPProp'+Trim(IntToStr(i))+'_'+Trim(IntToStr(j)),1);
          end;
          3:begin
            CP[i,j]:=ReadFloat('MonopoleSeparations', 'CP'+Trim(IntToStr(i))+'_'+Trim(IntToStr(j)),16+Power(2,(i-1)));
            CPProp[i,j]:=ReadFloat('SignedMonopoleFractions', 'CPProp'+Trim(IntToStr(i))+'_'+Trim(IntToStr(j)),-1);
          end;
          4:begin
            CP[i,j]:=ReadFloat('MonopoleSeparations', 'CP'+Trim(IntToStr(i))+'_'+Trim(IntToStr(j)),Power(2,(i-2)));
            CPProp[i,j]:=ReadFloat('SignedMonopoleFractions', 'CPProp'+Trim(IntToStr(i))+'_'+Trim(IntToStr(j)),-1);
          end;
          else begin
            CP[i,j]:=ReadFloat('MonopoleSeparations', 'CP'+Trim(IntToStr(i))+'_'+Trim(IntToStr(j)),Power(2,(i-1)));
            CPProp[i,j]:=ReadFloat('SignedMonopoleFractions', 'CPProp'+Trim(IntToStr(i))+'_'+Trim(IntToStr(j)),1);
          end;
        end;
      end;
      For j:=1 to AConfig.numCurPot[i] do begin
        MonopoleTx[i,j]:=ReadFloat('MonoPoleCoordsTx','Tx'+Trim(IntToStr(i))+'_'+Trim(IntToStr(j)),0);
```

```
      MonopoleTy[i,j]:=ReadFloat('MonoPoleCoordsTy','Ty'+Trim(IntToStr(i))+'_'+Trim(IntToStr(j)),0);
      MonopoleRx[i,j]:=ReadFloat('MonoPoleCoordsRx','Rx'+Trim(IntToStr(i))+'_'+Trim(IntToStr(j)),j);
      MonopoleRy[i,j]:=ReadFloat('MonoPoleCoordsRy','Ry'+Trim(IntToStr(i))+'_'+Trim(IntToStr(j)),0);
    end;
    For j:= 1 to 4 do //Transmit1,Transmit2,Pot1,Pot2
      Elecx[i,j]:=ReadFloat('ArrayCoordsx', 'Elecx'+Trim(InttoStr(i))+'_'+Trim(IntToStr(j)),j);
    For j:= 1 to 4 do
      Elecy[i,j]:=ReadFloat('ArrayCoordsy', 'Elecy'+Trim(InttoStr(i))+'_'+Trim(IntToStr(j)),0);
    MidpointX[i]:=ReadFloat('MidpointX','MidpointX'+Trim(IntToStr(i)),0);
    MidpointY[i]:=ReadFloat('MidpointY','MidpointY'+Trim(IntToStr(i)),0);
  end {i ... numBipoles};
  AConfigExt.TxElectrodeLength:=ReadFloat('Array','TxElectrodeLength',0);
  PortionSizer:=ReadFloat('Array','PortionSizer',0.45);

  AConfigType:=ReadString('Array', 'AConfigType', 'GeneralXY');

  If AConfigType='ExponentialBipole' then begin
    CurrElecSeparation:=ReadFloat('ExponentialBiole','CurrElecSeparation',16);
    FirstPotentDist:=ReadFloat('ExponentialBiole','FirstPotentDist',-1);
    TwoToPowerOfnIncr:=ReadFloat('ExponentialBiole','TwoToPowerOfnIncr',1);
    RadiusOfCurvature:=ReadFloat('ExponentialBiole','RadiusOfCurvature',100);
  end;

  If AConfigType='LinearBipoleBipole' then begin

  end;

  {Schlumberger}
  If AConfigType='Schlumberger' then begin
    SamplePerDecade:=ReadFloat('Schlumberger', 'SamplePerDecade', 6);
    For i:= 1 to numBipoles do begin
      SchlumbL[i]:=ReadFloat('Schlumberger', 'L'+Trim(IntToStr(i)), power(10,(i-1)/6));{L}
      Schlumblittlel[i]:=ReadFloat('Schlumberger', 'little'+Trim(IntToStr(i)), power(10,(i-1)/6-1));{l}
    end;
  end;

  If AConfigType='Wenner' then begin

  end;

  If AConfigType='AarhusPACES' then begin

  end;

  {General Phi Theta}
  If AConfigType='GeneralPhiTheta' then begin
    For i:= 1 to AConfig.numBipoles do begin
      PhiThetaInfo[1,i]:=ReadString('GeneralPhiTheta', 'TxWidth'+Trim(IntToStr(i)), '16');
      PhiThetaInfo[2,i]:=ReadString('GeneralPhiTheta', 'Width'+Trim(IntToStr(i)), FloatToStr(Power(2,(i-2))));
      PhiThetaInfo[3,i]:=ReadString('GeneralPhiTheta', 'MidpointSep'+Trim(IntToStr(i)), FloatToStr(Power(2,(i-2))*1.5+8));
      PhiThetaInfo[4,i]:=ReadString('GeneralPhiTheta', 'Theta'+Trim(IntToStr(i)), '0');
      PhiThetaInfo[5,i]:=ReadString('GeneralPhiTheta', 'Phi'+Trim(IntToStr(i)), '180');
      PhiThetaInfo[6,i]:=ReadString('GeneralPhiTheta', 'EffDepth'+Trim(IntToStr(i)), FloatToStr(Power(2,(i-2))));
    end;
  end;

  {General XY}
  If AConfigType='GeneralXY' then begin

  end;

  CalcGeomFact(AConfig);
  NDICEffDepth;

 end; {with Configini etc}
 ConfigIni.Free;
end;

end.
```

APPENDIX 6 - AUGERED SOIL SAMPLES AND ANALYSIS

Results of auger sample testing are given in the table on the next page. Figure A6-1 is a photo of some of the samples. Locations of the samples are given in the borehole data base included on the DVD. Approximate location of the auger samples is evident from their graphical representation on the relevant case study images. Boona and Bundure samples numbers have been prefixed by 999 in the borehole database.

Figure A6-1 Auger samples (Boona and Bundure Canal test sites).

Coleambally and Whitton Soil Samples - Nov 2003 and Feb 2004														MGA94	
Site	Av. Depth	From	To	1:5 mix	Coherence	Feel	Ribbon Ler	Colour	TextureGp	TextConvF	ECe uS/cm	Notes	Height to Lvl Gnd	Wetness	ECe Ohmm	Easting	Northing
Stott1	**0.20**	0.10	0.30	0.07	firm	gritty plastic	<10	Grey	Clayey Sand	10.00	**700**	DrainWater 450EC	1.5m		142.86	426230	6176700
Stott1	**0.45**	0.30	0.60	0.08	strong	gritty plastic	<5	GreyBrown	Clayey Sand	10.00	**800**				125.00		
Stott1	**0.75**	0.60	0.90	0.13	firm	gritty	<5	Brown minorGy	Clayey Sand	10.00	**1300**				76.92		
Stott1	**1.05**	0.90	1.20	0.14	firm	gritty	<5	Brown minorGy	Clayey Sand	10.00	**1400**				71.43		
Stott2	**0.20**	0.10	0.30	0.41	strong	plastic greas	25.00	Grey minor Brown	Light Clay	8.60	**3526**	DrainWater 400EC	1.5m		28.36	427000	6176485
Stott2	**0.45**	0.30	0.60	0.32	strong	plastic greas	55.00	Grey minor Brown	Light Clay	8.60	**2752**				36.34		
Stott2	**0.75**	0.60	0.90	0.39	strong	plastic greas	55.00	Grey	Light Clay	8.60	**3354**				29.82		
Stott3	**0.20**	0.10	0.30	0.10	nil	gritty	0.00	Grey	Sand traceClay	15.00	**1500**	DrainWater 450EC	1.5m		66.67	428980	6177445
Stott3	**0.45**	0.30	0.60	0.05	nil	gritty	0.00	Green Tan	Sand traceClay	15.00	**750**				133.33		
Stott3	**0.75**	0.60	0.90	0.05	nil	gritty	0.00	Green Tan	Sand traceClay	15.00	**750**				133.33		
Stott3	**1.05**	0.90	1.20	0.06	mixed	gritty plastic	<10	Tan	Sand & Clayey bits	12.00	**720**				138.89		
Stott3	**1.35**	1.20	1.50	0.11	strong	plastic	too hard	Grey Brown	Heavy Clay	7.00	**770**				129.87		
Stott3	**1.65**	1.50	1.80	0.30	strong	plastic	too hard	Blotchey Grey Brown	Heavy Clay	7.00	**2100**				47.62		
Stott3	**1.95**	1.80	2.10	0.31	strong	plastic	too hard	Grey	Heavy Clay	7.00	**2170**				46.08		
Stott4	**0.20**	0.10	0.30	0.05	firm	gritty	too hard	Grey	Heavy Clayey Sand	11.00	**550**	DrainWater 450EC	1.5m		181.82	428175	6176305
Stott4	**0.45**	0.30	0.60	0.03	firm	gritty	too hard	Grey	Heavy Clayey Sand	11.00	**330**				303.03		
Stott4	**0.75**	0.60	0.90	0.05	firm	gritty	too hard	Grey	Heavy Clayey Sand	11.00	**550**				181.82		
Stott5	**0.20**	0.10	0.30	0.09	firm	plastic	too hard	Grey Brown	Light Clay	8.60	**774**	Beside irrigation canal	0m		129.20	427450	6175000
Stott5	**0.45**	0.30	0.60	0.98	firm	plastic	too hard	Grey Brown	Light Clay	8.60	**8428**	on road			11.87		
Stott5	**0.75**	0.60	0.90	1.51	firm	plastic	too hard	Grey Brown	Light Clay	8.60	**12986**	High salinity from			7.70		
Stott5	**1.05**	0.90	1.20	1.03	firm	plastic	too hard	Grey Brown	Light Clay	8.60	**8858**	evapotranspiration			11.29		
Stott6	**0.30**	0.10	0.50	0.23	strong	plastic	too hard	Dark Grey	Heavy Clay	7.00	**1610**	In Drain	1.5m		62.11	424800	6175740
Stott6	**0.70**	0.50	0.90	0.26	strong	plastic	too hard	Dark Grey	Heavy Clay	7.00	**1820**				54.95		
Stott7	**0.25**	0.20	0.30	0.07	firm	gritty plastic	too hard	Brown	Sandy Clay	8.60	**602**	In Paddock	0m		166.11	428180	6178170
Stott7	**0.35**	0.30	0.40	0.08	firm	gritty plastic	too hard	Brown	Sandy Clay	8.60	**688**	Fallow			145.35		
Stott7	**0.55**	0.40	0.70	0.14	firm	gritty plastic	too hard	Brown	Sandy Clay	8.60	**1204**				83.06		
Stott7	**0.80**	0.70	0.90	0.15	firm	gritty plastic	too hard	Brown	Sandy Clay	8.60	**1247**				80.19		
Stott7	**1.60**	1.30	1.90	0.21	firm	gritty plastic	too hard	Brown	Sandy Clay	8.60	**1806**				55.37		
Stott7	**2.20**	1.90	2.50	0.17	firm	gritty plastic	too hard	Brown	Sandy Clay	8.60	**1462**				68.40		
Stott7	**3.20**	2.90	3.50	0.12	firm	gritty plastic	too hard	Brown	Sandy Clay	8.60	**1032**				96.90		
Stott7	**3.75**	3.50	4.00	0.07	firm	gritty plastic	too hard	Brown	Sandy Clay	8.60	**602**				166.11		
Stott7	**4.50**	4.00	5.00	0.09	firm	gritty plastic	too hard	Brown	Sandy Clay	8.60	**774**				129.20		
Stott7	**5.50**	5.00	6.00	0.09	firm	gritty plastic	too hard	Brown	Sandy Clay	8.60	**774**				129.20		
Boona1	**0.15**	0.00	0.30	0.21	firm	sandy	8.00	Tan	Loamy Sand	15	**3150**			Loose	31.75	394550	6143560
Boona1	**0.45**	0.30	0.60	0.60	strong	smooth gritty	35.00	Tan Brown	Clay Loam	8.6	**5160**			Hard	19.38		
Boona1	**0.8**	0.60	1.00	0.45	strong	smooth	30.00	Grey Brown	Clay Loam	8.6	**3870**	Gypsum Nodules		Friable	25.84		
Boona1	**1.25**	1.00	1.50	0.13	strong	gritty plastic	40.00	Grey	Clay Sand	8.6	**1118**	Gypsiferous		Slightly M	89.45		
Boona1	**1.75**	1.50	2.00	0.06	strong	gritty smooth	25.00	DkGrey	Clay Loam	8.6	**516**			Moist	193.80		
Boona2	**0.2**	0.10	0.30	0.21	strong	slightly gritty	40.00	Tan Brown	Clay Loam	8.6	**1806**			Hard Dry	55.37	394670	6143570
Boona2	**0.4**	0.30	0.50	0.52	strong	slightly gritty	25.00	Brown	Loam	9.5	**4940**			Dry	20.24		
Boona2	**0.75**	0.50	1.00	0.69	strong	smooth plast	40.00	Grey Brown	Light Clay, nearly loam	8.6	**5934**	Gypsiferous,most at top		Dry	16.85		
Boona2	**1.25**	1.00	1.50	0.68	strong	smooth plast	40.00	Grey	Clay Loam	8.6	**5848**			Dry	17.10		
Boona2	**1.7**	1.5	1.90	0.58	strong	smooth plast	30.00	Grey	Clay Loam	8.6	**4988**			Dry	20.05		
Boona2	**1.95**	1.9	2.00	0.50	strong	plastic	65.00	Grey	Light Clay	8.6	**4300**			Dry	23.26		
Boona3	**0.15**	0.00	0.30	0.12	slight	sandy	5.00	Grey Brown	Sand	17	**2040**			Dry	49.02	394800	6143570
Boona3	**0.5**	0.30	0.70	0.41	strong	plastic	45.00	Grey Brown	Clay Loam	8.6	**3526**			Dry	28.36		
Boona3	**1.1**	0.7	1.50	0.19	strong	plastic	30.00	Grey	Clay Loam	8.6	**1634**	Gypsum Nodules		Dry	61.20		
Boona3	**1.6**	1.5	1.70	0.06	strong	plastic	65.00	White Gypsum with blotches	Light Clay	8.6	**473**	Gypsum Nodules		Moist	211.42		
Boona3	**1.85**	1.7	2.00	0.02	strong	plastic	50.00	Brown Grey	Light Clay	8.6	**172**	Blotchy		Moist	581.40		
Boona3	**2.25**	2	2.50	0.02	firm	smooth	25.00	Brown Grey	Loam	9.5	**190**	Blotchy Micaceous		Wet	526.32		
Boona3	**2.65**	2.5	2.80	0.00	slight	sandy	10.00	Grey	Sand	17	**34**	Micaceous		Sloppy	2941.18		
Boona3	**2.9**	2.8	3.00	0.00	nil	sandy	5.00	Grey	Sand	17	**34**			Liquid	2941.18		
Boona4	**0.1**	0	0.20	0.14	slight	sandy	5.00	Grey Tan	Sand	17	**2380**			Loose Dry	42.02	395020	6143570
Boona4	**0.35**	0.2	0.50	1.14	strong	slightly gritty	80.00	Grey	Medium Clay with minor sand	7.8	**8892**			Hard Dry	11.25		
Boona4	**0.75**	0.5	1.00	0.98	strong	nodules and	nodules br	White Gypsum	Gypsum nodules and Light clay	11	**10780**	Gypsum nodules		Soft Dry	9.28		
Boona4	**1.25**	1	1.50	0.95	strong	nodules and	30.00	Tan	Clay Loam	8.6	**8170**	minor gypsum crystals		Dry	12.24		
Boona4	**1.75**	1.5	2.00	1.07	strong	plastic sandy	60.00	Blotchey Grey Brown	Light Clay	8.6	**9202**			Dry	10.87		
Bund1	**0.25**	0	0.50	0.14	strong	plastic	85.00	Tan	Light to Medium Clay	7.8	**1092**			Dry	91.58	412720	6132620
Bund1	**0.7**	0.5	0.90	1.16	firm	smooth plast	40.00	Grey Tan	Clay Loam	8.6	**9976**			Slightly M	10.02		
Bund1	**1.2**	0.9	1.50	0.62	firm	smooth	30.00	Brown Tan	Loam to Clay Loam	9	**5580**			Slightly M	17.92		
Bund1	**1.75**	1.5	2.00	0.46	firm	smooth	25.00	Grey Tan Mottled	Sandy Loam to Loam	11	**5060**	Micaceous		Slightly M	19.76		
Bund1	**2.4**	2	2.80	0.54	firm	smooth plast	50.00	Grey Tan Mottled	Loam	9.5	**5130**			Moist	19.49		
Bund1	**2.9**	2.8	3.00	0.69	strong	stiff plastic	85.00	Grey & Black	Medium Clay	7	**4830**	Bituminous bits		Very Moist	20.70		
Bund2	**0.1**	0	0.20	0.09	firm	smooth	10.00	Tan	Sandy Loam	13.8	**1242**	Excavation overspill		Dry	80.52	412720	6132550
Bund2	**0.35**	0.2	0.50	0.46	strong	stiff plastic	85.00	DkBrown Tan	Medium Clay	7	**3220**			Dry	31.06		
Bund2	**0.7**	0.5	0.90	0.64	strong	smooth plast	50.00	Tan	Light Clay	8.6	**5504**	Minor gypsum crunchy		Moist	18.17		
Bund2	**1.2**	0.9	1.50	0.33	strong	plastic	50.00	DkGrey	Light Clay	8.6	**2838**			Moist	35.24		
Bund2	**1.65**	1.5	1.80	0.23	strong	plastic	50.00	DkGrey	Light Clay	8.6	**1978**	Minor gypsum & bituminous bits		Moist	50.56		
Bund2	**1.9**	1.8	2.00	0.04	strong	plastic	85.00	Black	Medium Clay	7	**280**	smelly organic clay mix		Wet	357.14		

APPENDIX 7 - COMPLEMENTARY INVESTIGATION TECHNIQUES

EC images of aquifers beneath watercourses are generally only useful once they are interpreted in the context of other information. Appraisal of certain topical and/or promising investigation techniques has been conducted here for this purpose. Some of the techniques are important for saline inflow to watercourses studies, others for seepage investigations and some for groundwater recharge and recovery projects. The Case studies section of this thesis gives examples of use of most of these techniques. Other techniques are included simply because the author was asked, by many, about the use of them in conjunction with EC imaging. At the end of this appendix, other geo-electrical techniques used on watercourses are discussed.

Techniques that will be discussed are as follows:

Assessment of local knowledge, geomorphological, geological, biological and cultural observations,

River salt load difference surveys,

Drilling and graphical co-presentation of EC ribbons and drill logs,

Yabby Pump Sampling of sediment cores from watercourse beds,

Auger sampling and soil mapping,

Sediment testing and engineering analysis,

Chlorofluorocarbon measurements and variation of seepage rates over time,

Absolute seepage rate determination

Electro-magnetic devices such as the Geonics-EM31

Induced polarization

Self potential

Guelph Permeameter.

A7.1 Assessment of local knowledge, geomorphological, geological, biological and cultural observation.

Assessment of local knowledge, and simple geomorphological, geological, biological and cultural observation is most important for interpreting EC imagery. Procurement of such information usually is the most productive aid for interpretation. It determines what factors are relevant at a particular site and what other techniques may produce useful complementary data. Background information combined with EC imagery often reveals clues about palaeo-environments which have created sedimentary environments that are fundamental in controlling groundwater flow and salinity concentration. Extensiveness, connectivity and depth of point bar and channel sands, for instance, determine whether groundwater flow is restricted to small isolated reservoirs or is connected to a larger continuum of permeable strata. Knowledge of local water tables (perched or otherwise) is critical to assessment of the effect of sediment saturation on EC ribbon data.

A7.2 River salt load difference surveys

River salt load difference surveys are critical for quantitative interpretation of EC imagery collected for isolation or monitoring of saline inflow into waterways.

River salt load increase (or decrease) can be measured in tonnes per kilometre per day using flow meters, river cross section area and very accurate water EC meters. Flow of water down the river is measured over time while stationary EC meters measure the change in salinity of water coming down the river. At the same time, salinity along the river is measured using an EC meter in a boat. The stationary EC meter data and flow data are used to correct EC data collected in the boat for differences in salinity of water coming down the river so that resulting EC data only reflects saline inflow into the river from groundwater. The difference in EC with respect to river chainage is then converted into tonnes of salt load increase per kilometre per day using an EC to salinity conversion factor and the flux of water down the river.

This technique provides quantitative information essential to saline inflow studies. It is of limited spatial accuracy however because EC is only measured at the surface. Saline inflow typically generates salinity concentrations at the bottom of rivers which mix gradually with the whole mass of river water as the concentrations move downstream. In

meandering rivers, the concentrations typically are moved helically along the river, reappearing at the surface at several sites downstream of the sources.

When assessed with EC images of aquifers beneath rivers, salt load increase data can show exact inflow locations. The EC images additionally show sites where high risk of saline inflow exists – ie. locations where saline groundwater is not quite in contact with the river bottom. Combined monitoring of both types of data over time can result in accurate indication of the effectiveness of groundwater management practices on saline inflow mitigation.

A7.3 Drilling and graphical co-presentation of EC ribbons and drill logs.

Databases of drill logs are available in most locations. Drill logs can be converted to files that can be plotted graphically, using a list of colour codes, in 3D along with EC ribbon images. The codes used by the author along with sample logs are presented in Figure A7-1.

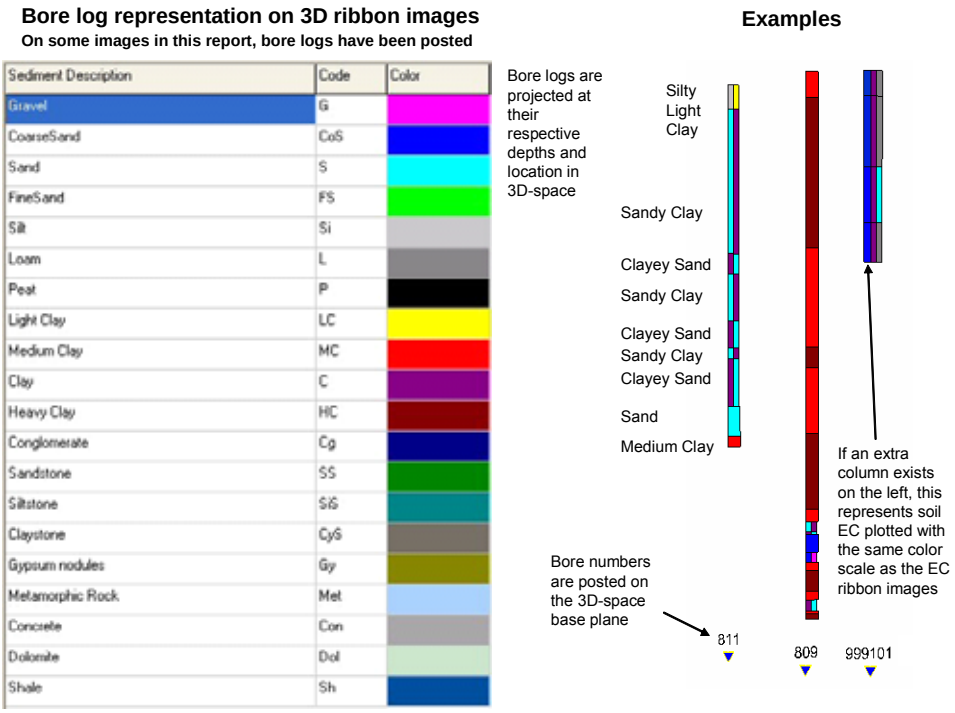

Figure A7-1 Colour codes and examples of graphical presentation of bore logs and bore log EC that can be placed in 3D interfaces along with EC ribbons.

A7.4 Yabby Pump Sampling of sediment cores from watercourse beds.

A good indication of sediment type under a canal can be obtained by jumping in and sampling with a yabby pump. Alternatively, the pump can sample from a boat in deeper water if an extension tube is added. Should the soil be permeable, the pump will easily slide into the sediment and extract a long core of sediment. Should it be impermeable, it will generally not penetrate the sediment very far (see Figure A7-2). The core obtained can be examined and tested for exchangeable sodium percentage. The thickness of the 'silt' layer at the base of the canal will be evident as will the depth to which the 'silt' has impregnated the underlying sediment. Structure in clays will be evident as granular texture on occasions because the sediment core has not been disturbed. Yabby pump sampling is a very low cost way of getting important qualitative information on seepage.

Figure A7-2 Yabby pump samples of both soft permeable waterlogged clay core (grey) and hard impermeable clay core (red). Note the different penetration depths attained.

A7.5 Auger sampling

Auger sampling adjacent to canals or in drains was conducted at some sites as a 'poor man's' alternative to drilling. The method gave the author access to soil samples for testing of soil EC at various depths. A great deal of effort was required to auger to 3m and, since the EC images extend to 20m, sufficient depth to adequately ground truth the

images could not be attained. Because geology is not uniform transverse to canals but varies in 3D, auger samples did not directly intersect anomalous targets found in canals.

As presented in Chapters 16 and 17 case studies, auger sampling was conducted on the Dallas Clay Pan, Boona Canal near salinas and Bundure Canal at a distinctive low EC anomaly site (see Figure A7-3).

Figure A7-3 A three metre auger sampler, and bits for various soil types. (Bundure canal inferred seepage site).

A7.6 Sediment testing and engineering analysis

Sediment from yabby pump, auger or drill hole samples can be tested for texture, $EC_{1:5}$, dispersion, and exchangeable sodium percentage. These properties all play an important

part in controlling groundwater flow. Hulme (2002) discusses the dependence of seepage rate on such variables. All auger samples collected as part of this thesis were subject to texture and $EC_{1:5}$ analysis. Table A7-1 shows how sediment texture controls permeability. Hulme (2002) gives further information on this correlation and its significant limitations.

Sediment Type	Hydraulic Conductivity (m/s)
Gravel	log10K>-2
Clean sand	-2>log10K>-5
Silt	-5>log10K>-8
Fissured clay	-4>log10K>-8
Intact clay	log10K<-8

Table A7-1 An indication of the effect of sediment type on hydraulic conductivity (exact source lost, see Fetter 1988).

Clays are sometimes relatively permeable. It depends on their sodicity and composition. Fresh canal water seeping into sodic montmorillonite rich clay results in swelling and sealing of the clay. More calcium rich clay will however permit water to continue to seep through the clay. Exchangeable sodium percentage of soils has been found to be a good indicator of soil permeability (Shaw 2002) and needs to be considered when assessing the seepage potential of clayey sediments.

Electrical conductivity in clays will reflect the salinity of water present in the clay. In permeable clay, more fresh water that has seeped from surface water above will be present and EC will be less than in low permeability clay. For this reason, EC is a useful tool for identifying localized sites where variation in clay properties has controlled seepage.

A7.7 Chlorofluorocarbon measurements and variation of seepage rates over time

Seepage from canals generally diminishes over time as a result of:

build up of stable groundwater mounds underneath canals,

'siltation' of canals.

Seepage variation over time may also vary as a result of shallow groundwater pumping or other drainage works or as a result of the fresh groundwater seeping through clays altering exchangeable sodium percentage of the clay and therefore its structure and permeability.

Leany (1998) presented chlorofluorocarbon (CFC) groundwater dating results (Figure A7-4) that suggest that most shallow groundwater under the Murrumbidgee Irrigation Area seeped out of canals or infiltrated from crops when the irrigation area was first filled. Only 1 sample had an age that suggested that it left the ground surface in recent years (see Figure A7-4).

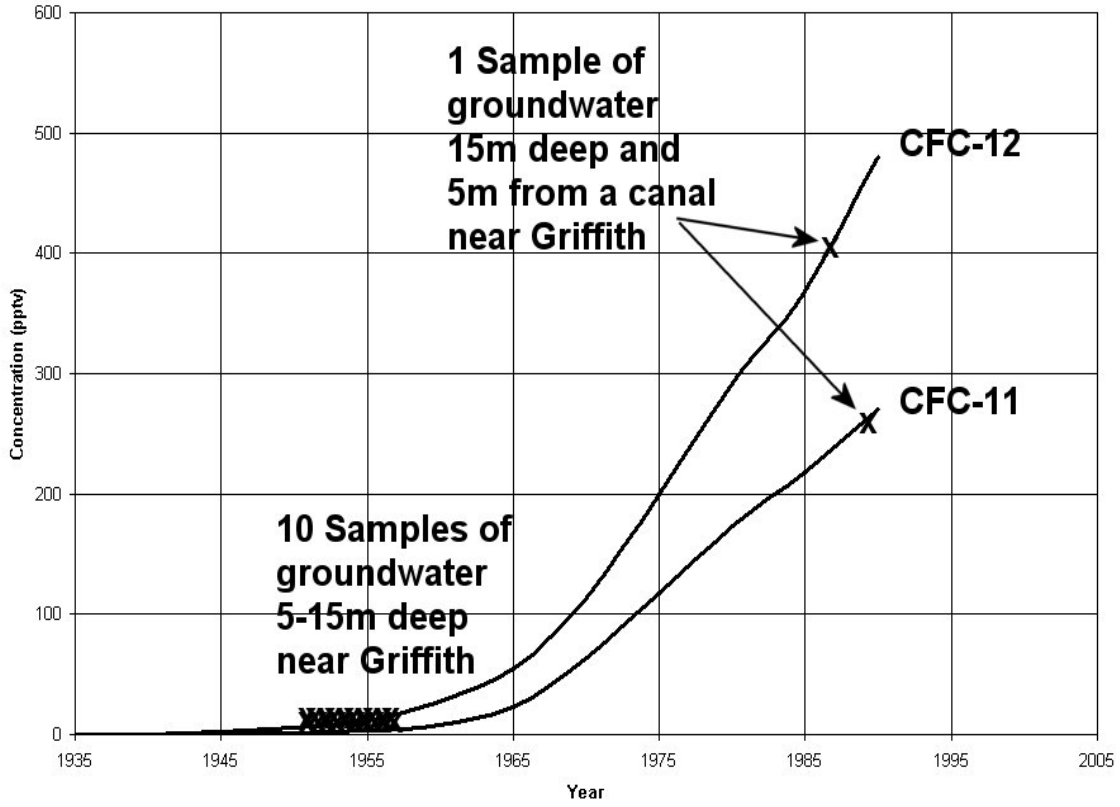

Figure A7-4 Determining the date that groundwater samples entered the ground using CFC concentrations (from Leany, 1998)

After discussion with Leany, his data has been reproduced and published here because it was never formally published and because it is possibly the best data available for demonstrating how most water under irrigation canals seeped out when the canals were initially filled.

A7.8 Absolute seepage rate measurement

Seepage rates in most Murray Darling Basin Canals are beyond reliable detection limits of point source equipment except at anomalous sites. The author believes that any significant seepage in the canals is likely to be via the canal walls where less silt has settled and where point source instruments are difficult to operate reliably. The following methods of determining absolute seepage rates were investigated as possible methods of relating EC results to actual seepage rates:

Idaho seepage meters,

Bladder type seepage meters,

Pondage tests,

Inflow-outflow tests,

Pondage tests with continuously sampling water depth sensors for elimination of day time evaporation loss error, and

Vertical pipe infiltrometers.

The very comprehensive ANCID seepage investigation report (www.ANCID.org.au) is recommended for those interested in these and other seepage investigation techniques. This chapter, however, reports new designs that aim to rectify limitations evident in the technology detailed in the report.

A7.8.1 Idaho seepage meters

Idaho seepage meters measure the rate of flow of water out of a bell inserted into the bottom of a canal (see Figure A7-5). The top of the bell can be unscrewed using a handle that extends 1.5m. This allows trapped biogenic gasses to be released from the entire bell prior to commencement of measurements. Measurement is made by equilibrating level of water in an attached tube with the level of water in the canal, then raising the tube 5 cm to make it easier to read, and measuring the drop of water level in the tube over time. An inverted manometer is attached to the bell by another tube for the purpose of maintaining equal head with the canal. Limitations of the equipment include sealing problems between the bell and the canal caused by roots, bioturbation or faulty seals. Biogenic gas build-up and lack of sensitivity limit the detectability limit of the instrument. Readings are time consuming and can only practically be made in up to 1.4m of water and on flat or slightly inclined substrates. Venturi effects make the Idaho meter inaccurate in water flowing faster than 0.6m/s.

The readings are considered to be unreliable if less than 3mm/day. These problems are documented in detail in Byrnes (1979) and Stewart (1994).

It would appear that Idaho meter readings could correlate EC imagery with absolute seepage rates. In practice this is not clearly so because different parts of a canal cross

section seep, typically, at drastically different rates. A blanket of silt on the bed may almost stop seepage yet a small section somewhere up the steep banks may seep drastically. Near the top of the banks, seepage is minimal because pressure from the canal is minimal.

Figure A7-5 An Idaho seepage meter.

A7.8.2 Bladder type seepage meters

An alternative type of seepage meter (Figure A7-6) can be cheaply mass produced and left at numerous locations over extended periods of time in order to measure very low seepage rates. A bell is inserted in the base of a canal and attached to a plastic bag via a hose with a tap and connector in it. The bag is partially filled with water and weighted before and after the test on an electronic scale.

The author found that problems with entrapped biogenic gases tend to prevent accurate measurement of seepage in typical Murray Darling Basin canals using this type of device, even after a breather tube was added to it. Design improvement involving reshaping of the bell to prevent gas entrapment may make the device more reliable.

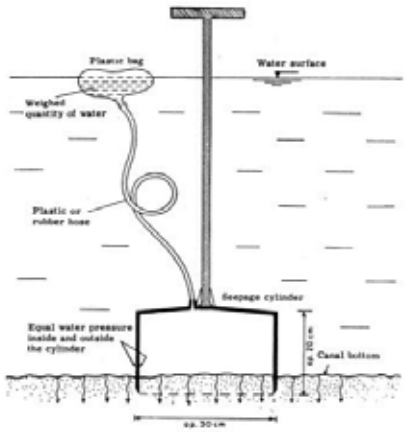

Diagram from ANCID web site

Figure A7-6 Bladder type seepage meters.

A7.8.3 Pondage tests

Pondage tests are recommended by ANCID (www.ANCID.org.au) as the best standard for measuring seepage. Readers are referred to their website for comprehensive instructions on pondage test methodology). Pondage tests are expensive and disruptive to canal operations as earth banks must be placed across the canal and left there for up to two months.

Even pondage tests lack accuracy in warm and windy weather due to limitations on measurement of evaporation which must be subtracted from losses. Evaporation is strongly dependant on wind and water interaction. This is not duplicated in evaporation pans.

A7.8.4 Determination of seepage rates using Inflow – Outflow Measurement

Inflow – Outflow measurement is an elaboration of the pondage test method of determining seepage that does not require that the canals be ponded to conduct the test. In addition to having all the sources of errors of pondage tests, the inflow-outflow method must consider error in determining flow in and out of the canal. This error is almost invariably too high to allow for measurement of seepage. Consider the following example which demonstrates the problem:

10 km of channel 10m wide seeps at 1mm per day and has a flow of 100Ml/day.

The surface area of the canal bed under higher pressure (channel sides excluded) = $10000 \times 10 m^2$

Seepage loss per day = $1 \times 10^{-3} \times 10\,000 \times 10 \times 10^{-3} = 0.1$ Megalitres per day

%Change in flow = $100 \times 0.1/100 = 0.1\%$

If this % change in flow is compared with the accuracy of devices typically used to measure flow then it is easy to see that inflow-outflow testing of seepage rarely is feasible.

%Accuracy of a Dethridge wheel (a device that typically measures outflow from canals) = approx 10%

%Accuracy of a Rubicon Flume Gate (a highly accurate device installed on some canals for measuring flow) = approx 2%

A7.8.5 Pondage tests with day time evaporation loss error eliminated

With high accuracy continuously sampling water depth sensors it is possible to separate day and night time losses from a pond. On some nights, wind effect will be negligible and evaporation will be negligible and stable. On such nights, seepage losses can be measured with some accuracy. Craig (2004) has been using this method to determine losses from cotton water storages (Figure A7-7).

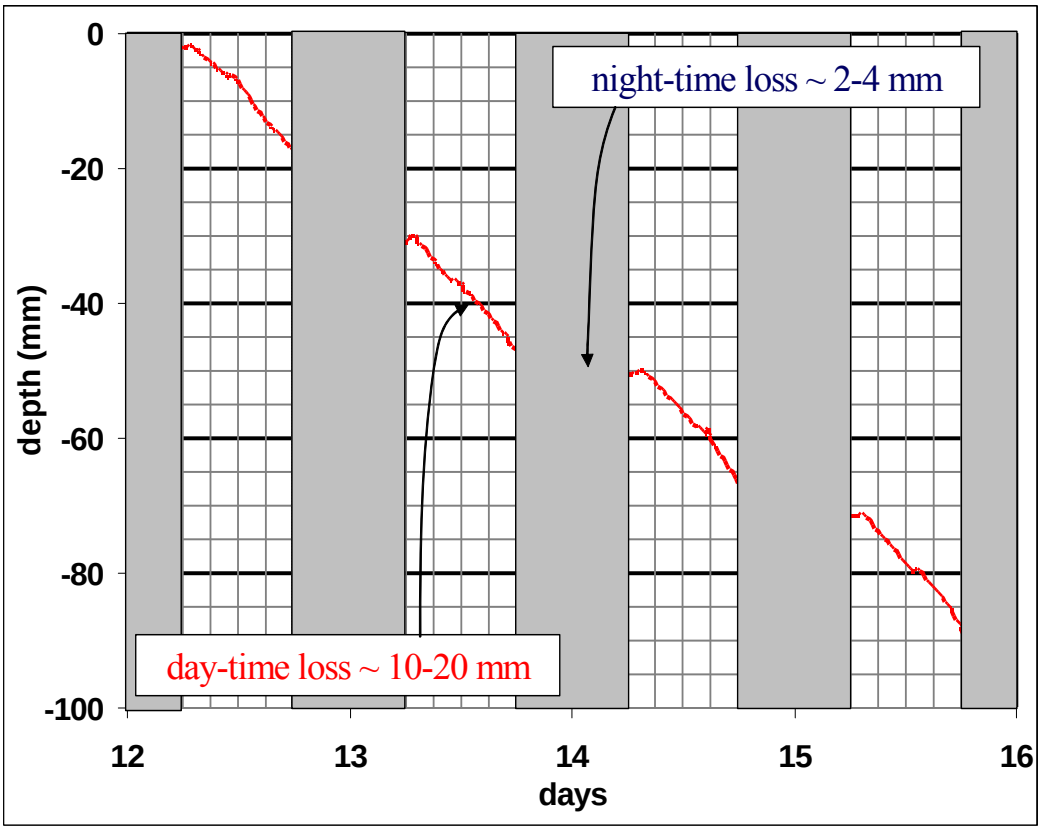

Figure A7-7 Separation of seepage losses from evaporation losses using continuous water level monitoring of ponded water and assuming that night time evaporation losses are stable on still nights. On such nights, evaporation losses will correlate with evaporation pan losses and therefore will be separable from seepage losses (from Craig, 2004).

A7.8.6 Vertical pipe infiltrometer.

In areas where seepage rates generally are very low, Idaho seepage meters and similar flexible reservoir seepage meters cannot give reliable seepage measurements – being affected by biogenic gas that rises from the canal bottom and clings as air bubbles to tubing and reservoir surfaces. Numerous seals and airpockets can all cause havoc when trying to measure small seepage rates. For these reasons, and because most canals are too deep to easily work such meters in, vertical pipe infiltrometers were developed by Sustainable Soils Management Pty. Ltd., Kevin Kelly of Coleambally Irrigation Cooperative Limited and the author.

The vertical pipe infiltrometer, also dubbed ‘Seepage Penetrating Observation Tube’ or SPOT is simply a pipe in which water level drop is measured. It operates on the same

principle as a double ring infiltrometer and, therefore, must be driven into canal beds far enough to eliminate the effect of minor canal level fluctuations on the level of water within it. Large canal level variations will render them temporarily useless so canal level must be controlled during tests.

Vertical pipe infiltrometers are prepared as follows using 150mm stormwater grade pvc pipes driven into the canal bed and sides. Evaporation controls are similar short lengths of pipe attached to the sides of other pipes but capped on the bottoms so they will have no seepage loss. All the pipes are driven into the canal bed using a 20kg lump of wood until stable from a boat anchored to the shores by a length of rope straddling the canal. The pipes are cut about 500mm above the current water surface, to prevent waves overtopping them, and a small hole is drilled near the top. A wire is suspended from the drilled hole and the bottom of it turned over to form a hook gauge at the water level. The wire is taped to the inside and outside of the infiltrometer to prevent it from moving. The pipes are not capped – that way evaporation losses are similar to the canal and less water level difference develops. Time of emplacement is logged. The seepage meters are monitored by measuring the water volume needed to maintain water level at that of the hook gauges by topping up the water level or lowering it using a syringe with 4mm tubing attached to it or a measuring jug. Vertical pipe infiltrometer installation shown in Figure A7-8.

Figure A7-8 Installation of a vertical pipe infiltrometer or SPOT.

A7.9 Frequency domain electro-magnetic devices such as the Geonics-EM31

The Geonics EM31 frequency domain electromagnetic receiver can detect ECa of soil relatively rapidly without the need for direct ground contact. Joseph Harding used the EM31 in 2002 to survey 139 km of canals in the Coleambally Irrigation Area using the pontoon shown in Figure A7-9 (Harding, 2002). He made his watercraft largely out of non-metallic materials in order to avoid distorting the survey results. He states that others have used quad bikes, four wheeled drives, hovercraft and aluminium boats to conduct EM31 surveys of canals, generally when they are dry, but that the results were severely affected by metallic parts of those vehicles. The worst vehicle is no doubt the aluminium boat. Such surveys have been conducted by Heslop (2002) and Akbar (2002).

The EM31 measures bulk ECa across a depth distribution that peaks at about 1.5m deep and is largely diminished by a depth of 6m (see Figure A7-10). The EM31 is, therefore, capable of detecting EC below canals for the purpose of identifying seepage sites but is affected greatly by its distance from the canal bed and banks and by water EC. With the instrument 800mm from the canal surface as shown in the photo of Joseph Harding, it may be 3m above the canal bed which means that most of the signal received is dependant on EC of the variable portions of air and water above the bed. The bulk EC measured will be a composite measurement of the air, water, canal banks and a small sample of the canal bed sediment. The significance of these sources of systematic error can be observed in the contrast in results of survey by Joseph Harding of Coleambally Channels 9 and 9b (see case studies chapter on canals – Chapter 16). Subsequent surveys of these canals using a submerged geo-electric array did not show this contrast. Should the EM31 be placed on the canal bed, then it will be much more reliable and consistent. A correction could be made mathematically for the canal water if present. The EM31, with a bulky control box at its centre is a difficult instrument for submerging (if it is to function!). The new DualEM range of instruments are much better for this application as they are easy to encase and are remotely controlled. Geo-electric arrays are much simpler, lighter and cheaper to submerge and can image deeper than an encased FDEM device of similar weight. The main advantage that FDEM has is that it has a smaller, more concentrated footprint.

Geo-electric arrays have none of the problems mentioned here and additionally can measure EC at multiple depths below a canal thus separating out response from clay lining, siltation and undisturbed sediment.

Figure A7-9 EM-31 surveying of an irrigation canal using a lightweight non-metallic water craft. (from Harding, 2002).

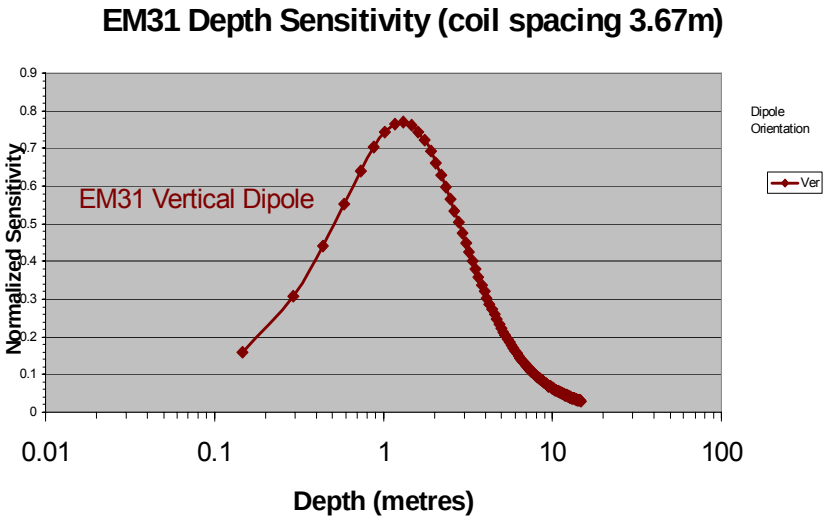

Figure A7-10 Depth sensitivity of the EM-31 in vertical dipole orientation. (see McNiell - Geonics TN6).

In order to avoid confusion, note that the exploration depth limit quoted by Geonics (www.geonics.com) for their FDEM equipment uses a normalized sensitivity level of 0.3

(equivalent to 70% of area under an NDIC curve) while exploration depths of geo-electric arrays are usually quoted as effective depths equal to a normalized sensitivity level of 0.5.

A7.10 Induced Polarization surveying along canals

Induced polarization (IP) occurs when electric current flowing through a medium is suddenly cut off and particle/fluid boundaries act capacitively, continuing to dissipate some current over time in the reverse direction to the primary current. Clay particle boundaries are the primary cause of such activity and Brandes and Acworth (2003) discovered that IP response peaks in soil with a 5 to 10 % clay percentage. IP data was collected in all fieldwork conducted in this thesis using the Zonge GDP32. The Syscal Pro would not collect IP data in continuous mode. Very good signal levels and very low cable crosstalk are needed to collect useable IP data. The AXB array produced good signal levels and so useable IP data was generated. It has been interpreted in the Mildura dataset – see case studies but generally was ignored. This is because the volume of data collected was immense and the time the author could allocate to processing such data was limited. Effective display may be attempted in the future in which IP data is somehow added to the 3D EC images (ie. beneath the EC data or superimposed on it as texture). The IP data was supplied to Andrea Viezzoli of Monash University for analysis and he submitted his analysis of a subset of the data for publication (see Viezzoli and Cull, 2005 which is included on the DVD accompanying this thesis).

A7.11 Self potential surveying along canals

Self potential is the voltage between two electrodes placed in contact with a medium. It is typically microvolts or millivolts in size when measured over tens of metres. Part of the self potential response is formed by the process of electrokinesis in which flowing fluids passing through a solid matrix carry charged particles. In theory, seepage from canals can be directly measured using electrokinesis. As two well spaced electrodes pass along a canal, voltages will build up between them as a result of electrokinesis caused by water seeping out of the canal. In practice, electrochemical reactions at the electrodes, streaming potentials resulting from the electrodes flowing through the water and electrochemical processes occurring between ground of different composition add to self potential measurements resulting in data of questionable value. Corwin and Butler (1989),

Sjostrom and Hotchkiss (1996) and Song *et al.* (2005) have successfully used self potential to delineate seepage.

A7.12 Guelph Permeameter

The Guelph Permeameter measures field saturated hydraulic conductivity along with other properties in-situ from a 3 cm diameter hole 15 to 75 cm below the ground surface. Measurement time ranges from ½ to 2 hours. At sites where soil inhomogeneities exist such as expansive clay desiccation cracks, unreliable results are obtained by the device. Due to desiccation cracks choice of sites where the device can be reliably used in the Murray Darling Basin are very limited. It is however probably the best device for measuring unsaturated zone permeability which is a major factor affecting canal seepage rates. A Guelph permeameter is displayed in Figure A7-11 in operation with an Idaho seepage meter operating in the canal behind it. Details on the Guelph Permeameter are available from Soil Moisture Equipment Corporation (1986).

Figure A7-11 A Guelph Permeameter with an Idaho seepage meter in operation in the background.

APPENDIX 8 - PROCESSING SEQUENCE

Extending on from Chapter 9, the various towed waterborne survey processing steps listed in Figure A8-1 are explained in this Appendix.

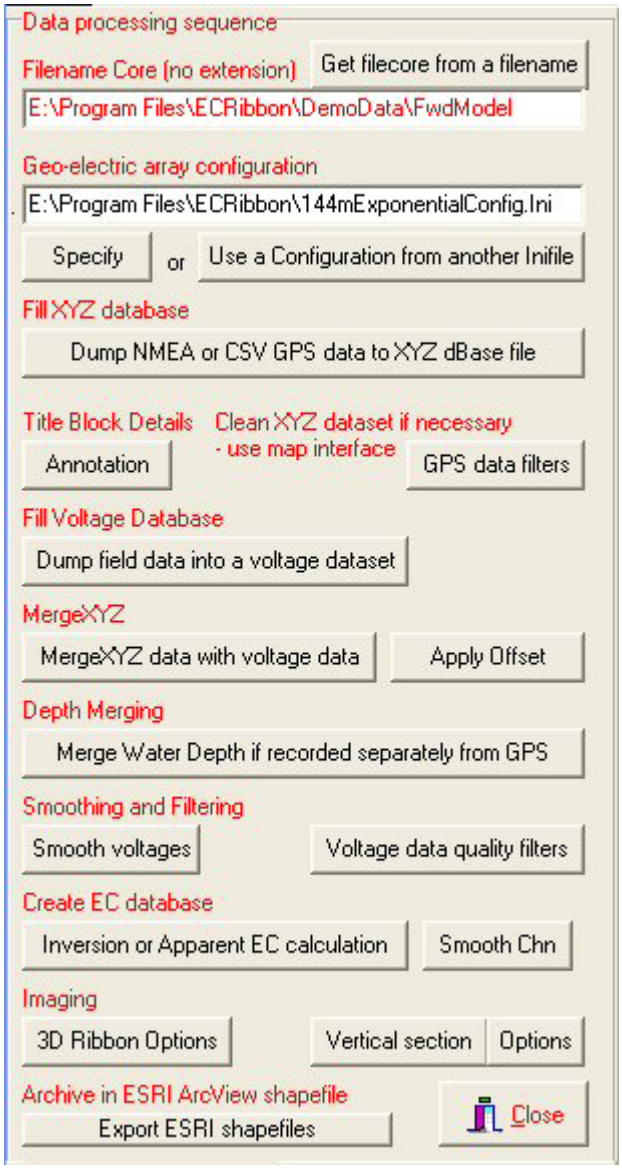

Figure A8.1 The data processing sequence menu, designed to act as a checklist, from the software produced along with this thesis.

A8.1 Selection of a filename core

Every dataset is made of numerous files. A filename core is chosen to group these together.

A8.2Selection of sensor parameters

The geo-electric, or transient electromagnetic equipment parameters must be specified and documented. This is done by generating or selecting a configuration parameter file.

A8.3Annotation

Annotation is added to the field dataset at an early stage and then carried through the processing stream so that all files and presentation products can be thoroughly identified. Default annotation is carried over from previously processed files so that minimal changes need to be typed in.

A8.4 Locating EC and water depth data

A8.4.1 A summary of the tasks required to locate data

Geo-electric array data may be stored with or without location data or timestamps however one or the other is essential for continuous geo-electric surveys. GPS and Water Depth data stored separately must have some common field so that they can be merged. Time is preferred as a common field as merging data using X,Y co-ordinates is a relatively complex procedure.

Additional to merging, survey track resampling is generally required. Often large gaps occur in GPS data where data quality is inadequate. This is especially common in deeply incised rivers or canals or rivers lined with trees. These gaps need filling by interpolation. In the worst cases, some points may need to be added manually by comparison of the survey track with published maps before interpolation can be reliable.

Resampling is essential before 2D inversion is attempted. All data points must be separated by a multiple of the finite grid node spacing used in the inversion.

Even though GPS derived locations and sonar derived water depth are routinely collected into the same NMEA file, it is sensible to separate them, interpolate them separately, and

then remerge them. This is because gaps in each of these types of data are independent of each other. Much quality data would be lost if they were not interpolated separately.

A8.4.2 Co-ordinate transformation

NMEA files and the Syscal Pro files only store XY data as latitude and longitude. Geo-electric array data must be geo-referenced in metres so Redfearn's formula has had to have been used to convert Latitude and Longitude to Eastings and Northings. Code for the formula was translated from an MS Excel spreadsheet obtainable from the Geoscience Australia website (http://www.ga.gov.au/nmd/geodesy/datums/calcs.jsp#coords).

A8.4.3 Integrated software solution

Software has been developed to cope with all these merging tasks. It has been a very time consuming task given that almost every survey used a different combination of equipment. Now that these tasks have been addressed, geo-electric surveying can move into production mode as massive delays caused by these tasks have been eliminated.

A8.4.4 GPS and Sonar data filtering, quality monitoring and editing

GPS data is typically collected at between 0.6 second and 10 second intervals. Long sections of data with poor signal are regularly collected on watercourses because steep high banks and trees obstruct satellite signal so signal quality must be recorded and bad data must be devalidated by an appropriate filter. NMEA data strings record horizontal dilution of precision and number of satellites along with an indicator of presence or absence of differential corrections. These parameters are good for filtering of data but are not adequate for detection of problems with satellites such as position near the horizon resulting in severe ionospheric effects. Graphical display such as in Figure A8-2 may show the data prior to filtering. Figure A8-2 shows the result of automated filtering of the particularly bad GPS data blowout evident in Figure A8-2. The surveyor knows, or can find on maps, the actual course he took and identify any remaining parts of the GPS data that are faulty. Faulty segments, such as the one remaining in the centre of Figure A8-3, typically are very obvious. With an interactive graphical display, manual point deletion and point addition followed by interpolation through the resultant data gaps can patch up remaining faults in GPS datasets.

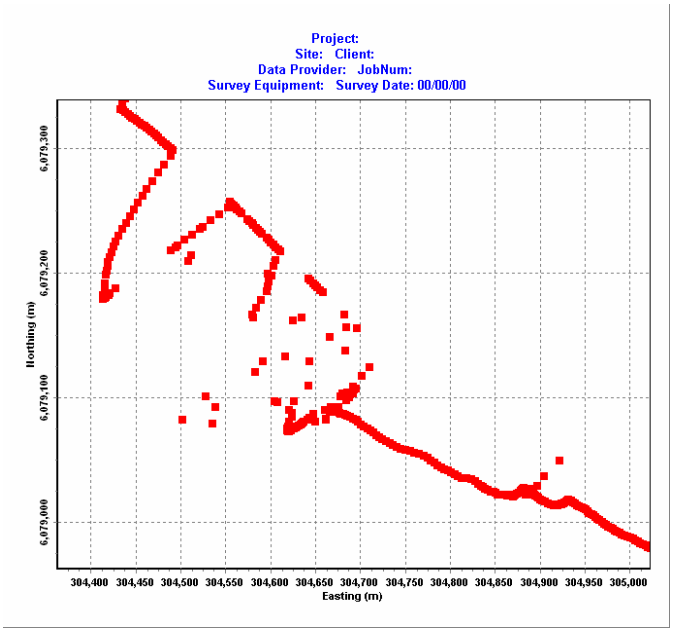

Figure A8.2 A GPS data 'blowout' recorded on a canal survey. Note that the actual canal position is evident as an approximately straight line diagonally crossing the grid display.

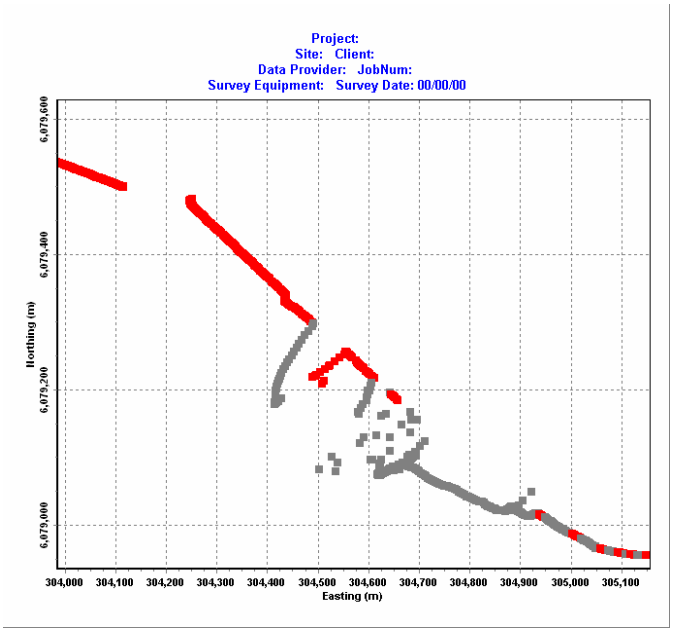

Figure A8.3 The GPS data blowout of Figure A8.2 after very conservative automated GPS data quality filtering. Note the undetected part of the blowout in the screen centre that needed manual removal by point-and-click point deletion.

Sonar is typically provided with GPS data but bad sonar data is not co-incident with bad GPS data, so filtering and interpolation must happen separately. This can be achieved with a file format in which every record must have a valid time. Geo-electric arrays are long and trail behind the GPS receiver. At the start of a run, the GPS may not have followed the path of the array and data there too may need replacing with a digitized point and extrapolation.

A8.5 Dumping and conversion of voltage and/or EC/depth datasets

The data from the geo-electric or electromagnetic systems needed to be dumped using the equipment manufacturers procedures and then converted to the standard voltage data relational database format described in the previous chapter. Some equipment manufacturers have incorporated much of the processing procedure described here into their own processing software however this has only occurred simultaneously with execution of this work and so was not available to the author of this thesis. Numerous conversion routines were written due to changes in equipment providers formats and equipment during the progress of this thesis. Conversion routines were written for Zonge streamed data, Zonge internally stored data (both geo-electric and TEM), Iris instruments binary dump format, Iris Instruments converted ASCII format and general columnar and comma separated variable data format with header rows. A routine was also provided for the interpolation of times for Syscal-Pro data that did not include co-ordinates but was located simply by recording start and end times (or start times and recording interval time) of files exactly.

At this point, voltage data files do not generally contain merged co-ordinates and water depths. The exception was with some Syscal-Pro data which was missing time data and co-ordinate transformation of XY data instead.

A8.6 Merging data – a ‘can of worms’

The filtered GPS and waterdepth data were then merged with the voltage data (geo-electric array or TEM) using a common index. Time is a very practical index to use for merging but with some equipment, use of eastings, northings and sequence as merge indexes were necessary – a somewhat involved merge procedure.

Collection of the data in this thesis involved the use of Zonge and Iris Instrument geo-electric receivers, various GPS receivers, some including sonar and some without, pressure sensors that logged water depth against time and sonar units that logged independently from GPS either on a time base or XY base. The Zonge receiver timestamps its data while the Iris Instruments Syscal Pro currently records but does not dump its timestamps. It did however record latitude and longitude on one survey, but not another due to firmware changes, but requires permanent connection to an external computer to record sonar derived depth. Numerous spurious GPS co-ords were recorded internally by the Syscal Pro and had to be manually removed before any merging could take place. A pressure sensor used along with the Syscal Pro only logged against time so its data could only be merged with the Syscal Pro data indirectly via GPS data stored externally with timestamps.

Data was merged after routines were written to merge by time, or by latitude and longitude or easting and northing by nearest neighbour search on interpolated data or by latitude and longitude or easting and northing on sequential nearest neighbour search.

The filtered water depth data, separated out so that deleted and interpolated GPS data or sonar data would not result in both datasets being interpolated, was merged using the same types of routines.

A8.7 Selection of sounding reference coordinates

EC soundings collected with a bipole array represent EC focussed approximately around the midpoint of the inner electrodes of each configuration in the array. These midpoints do not necessarily all co-incide. When the exponential bipole-bipole array is used, the configurations that sample more shallowly approximate a pole-pole array with the inner electrodes so close together that, for referencing purposes, the midpoint is approximated by the inner current electrode which is at the same location for all configurations in the array. For configurations in the array that sample deeper, position referencing does not need to be as accurate because the lateral resolution at such depths is much poorer (ie. the footprint at those depths is much larger). Therefore the same inner current electrode can be used for the position reference of the whole sounding. A slightly more accurate approach would be to plot the sounding as a sloping line in the vertical plane under the array and then resample to create vertical soundings but the author considers such an

approach to be practically unviable due to the complexity of it and due to the new sources of ambiguity that complexity brings with it. Offsets to the midpoints of the signal contribution distributions of the individual configurations in the geo-electric array have not been applied but they are stored in the array configuration file.

The sounding position reference in a towed array is not typically directly measured, but needs to be calculated using offsets from the GPS antenna.

A8.8 Calculating Offset between GPS antenna and Sounding reference coordinates.

In towed array surveying, the GPS antenna is normally situated on the towing vehicle. EC sounding reference locations are somewhere along the towed geo-electric array. To get co-ordinates of the sounding reference locations, an offset needs to be applied to the GPS co-ordinates. In the case of an array towed behind a boat, a simple offset back along the survey track is made. If the survey platform is a vehicle with a boom extending sideways, a sideward offset also needs to be applied BEFORE the backwards offset. It needs to be applied before the backwards offset because the sidewards offset coordinates will be separated by different distances than the GPS antenna coordinates when the vehicle turns corners. In order to calculate this offset, the smoothed orientation of the array at each point is used. Spatially based smoothing is needed to avoid GPS noise and random orientations occurring when the vehicle is stationary. An additional offset is needed with some GPS data loggers because the time stamp for each record occurs a small time after the position is actually acquired.

Although all this offsetting may seem simple in principle, the following rather complicated algorithm is required in order to take account of numerous details.

A8.8.1 Offset application algorithm

A schematic (Figure A8-4) has been prepared to convey variables used and the principles involved with data offsetting.

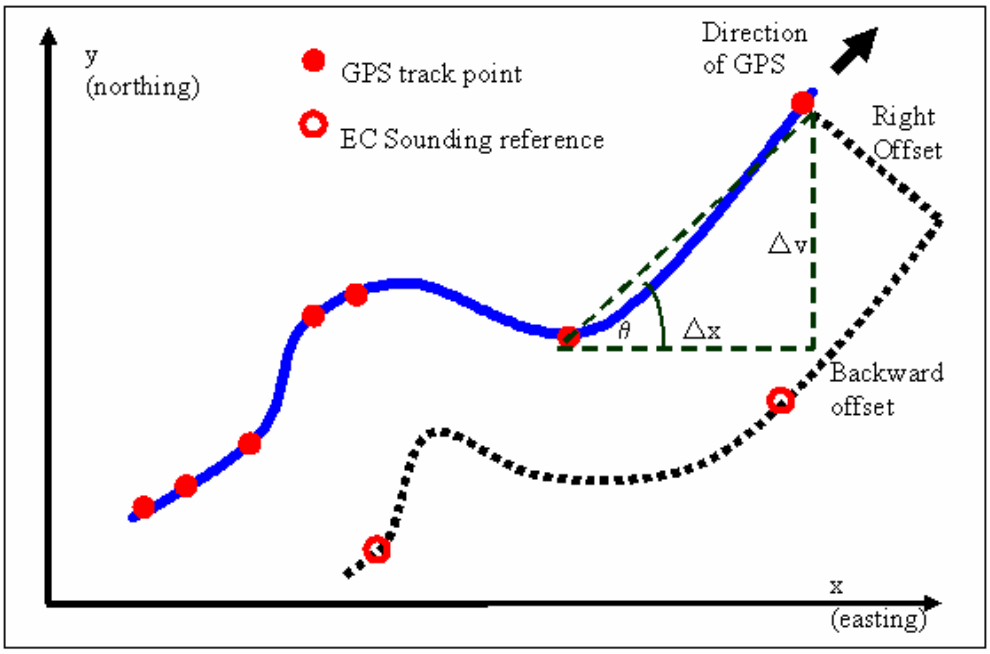

Figure A8.4 A diagram showing application of offset between GPS antenna co-ordinates and sounding reference points without the assumption of equal data point spacing.

A8.8.1.1 Fast co-ordinate transformation during offsetting

If latitude and longitude are stored in the datafile, local conversion factors for converting Eastings differences to Longitude differences and for converting Northings differences to Latitude differences are calculated using the co-ordinates of the first and last points of the GPS track. This is faster than re-applying Redfearn's formula.

A8.8.1.2 Sidewards Offset

Using the first point of the track and another point a suitable distance along the track to allow for what may be considered as orientation noise, orientation of the start of the track is calculated (see formula below) and stored for later use.

Starting at the last coordinate pair in a file, so as not to overwrite coordinates needed for calculating offsets of other points, each set of sideways offset co-ordinates is calculated as follows:

Array Orientation at a point offset backwards (θ) and Sideward_and_Backward_offset coordinates *(OffsetX,OffsetY)* are then calculated as follows using Backward_Offset coordinates *(x,y)*:

$$\theta = \tan^{-1}\left(\frac{\Delta North}{\Delta East}\right), \Delta East \neq 0$$

$$\theta = \frac{\pi}{2} or \frac{-\pi}{2}, \Delta East = 0$$

$$OffsetX = X + OffsetR \times Sin(\theta)$$

$$OffsetY = Y - OffsetR \times Cos(\theta)$$

where:

$\triangle North$ and $\triangle East$ = the differences between the x and y coordinates on either side of the backwards_offset point that are at least a specified minimum distance apart. The minimum separation is necessary as the GPS data is of limited accuracy and when the survey vehicle moves slowly or stops, orientation of the track at point to point scale becomes erratic or even random. If the start of the survey track is encountered, then the orientation of the points at the start of the survey track calculated previously is used for calculations.

θ = corrected to the correct quadrant by observing the signs of $\triangle North$ and $\triangle East$.

OffsetR = the Sideward offset in metres (positive to the right of the direction of motion of the survey platform).

OffsetX and OffsetY = the final fully offset co-ordinates.

Offset Latitude and Longitude co-ordinates are calculated using the new and old eastings and northings and the conversion factors calculated previously.

Once the sidewards offset is applied to the point, the previous point is selected and the process repeated until all points are sidewards offset.

A8.8.1.3 Backwards Offset

Now the backward offset can be applied.

The first point in the file is reselected.

By projecting backward from the first point a distance in excess of the backward offset in the direction specified by -1 x orientation, a pair of extrapolated x and y co-ordinates are calculated and stored for later use.

Starting again at the last coordinate pair in a file, so as not to overwrite coordinates needed for calculating offsets of other points, each set of backwards and sideways offset co-ordinates is calculated as follows:

Backward_Offset(x,y) is determined by incrementing backwards along the GPS antenna track a distance equal to the *Backward_Offset*. Interpolation is required to get the exact position from the GPS data which is recorded at finite intervals. If the start of the survey track is encountered then the extrapolation conducted previously is used in order to create an artificial extension of the survey track.

Offset Latitude and Longitude co-ordinates are calculated using the new and old eastings and northings and the conversion factors calculated previously.

At this stage, one point is calculated, the previous point is then observed and the whole process is repeated. Once all points have been offset, distances between the points need to be recalculated again due to the change in the discretization of the curved array path. What at first seems like a simple exercise actually turns out to be very involved because of end effects, GPS data noise and discretization of the GPS track.

A8.8.1.4 Documentation of offsets applied

The offsets applied are recorded with the data so that accidental re-application or omission of application can be prevented by software warning prompts.

A8.8.2 Navigation skills and accuracy of the offsetting algorithm

The offset calculated using the above algorithm assumes that the array follows in its track rather than pulling sideways as it goes around corners. When sonar is used, the same assumption applies. This assumption has proved, by observation of arrays passing close to obstacles to be reasonably valid when the array is streamlined and has minimal drag. Non turbulent drag increases with the square of velocity with respect to the water (which also

is moving) so greater sidewards pull is noted if the array is towed too fast around corners. At very slow speed, a 156m array was towed through a 2 m gap 30m before turning a right angle bend without touching the sides of the gap. In windy conditions, the array can easily be blown sideways, particularly if the watercraft is moving downstream at about the same rate as the water flow. To minimize the effect of wind, it is better to travel faster and/or upstream rather than downsteam (increasing the ratio of the velocity of the array with respect to the water, to the velocity of the wind with respect to the direction of movement of the array). Watercurrents move the array, however the array is usually towed parallel to the current flow lines so these currents do not usually cause errors in array positioning. There is one exception where a boat travelling downstream stops, such as when it bottoms out and the array then tries to overtake the boat. In this situation, everything needs to be turned off (in a hurry). For this reason, any river or canal with significant navigation hazards should not be surveyed in the downstream direction. Submerged arrays do not suffer the effects of water currents and wind but do have navigation problems of their own (encountering submerged debris).

An additional assumption made is that position is logged frequently enough to accurately sample the array path. By taking the sampling interval into consideration when deciding how fast and sharply to negotiate corners, errors caused by deficient sampling can be avoided. This is especially pertinent when poor GPS signal is encountered resulting in a break in sampling over which linear interpolation needs to occur. As stopping the boat will result in the array drifting out of control, GPS outages normally need to be dealt with by very slow travel and linear interpolation.

As the cost of placing GPS receivers and loggers along the array is high, practical surveys will need to be conducted assuming that the navigator can minimize array positioning errors as explained here.

A8.8.3 Offsetting water depth measurements

Water Depth is generally measured with a pressure sensor or sonar transducer. Two options for water depth measurements offsetting are considered:

- The case where the depth sensor is near the GPS antenna - When a boat is used in deep water the sonar transducer can typically be placed approximately at the

same location as the GPS antenna so that the coordinate offsets applied for the GPS antenna should not be applied for water depth. This means that as backwards offset is being applied, the distance of each water depth should be retained so that water depth measurements can be re-attached to the offset sounding records without any offset being applied to the water depth measurements.

- The Case where the depth sensor is near the sounding reference point - In shallow water, a pressure sensor is used. It is best placed in the streamer at approximately the sounding reference position so that water depth offset is applied as the sounding offset is applied.

A8.9 Voltage data filtering

Voltage data is filtered, removing channels of data that are below noise level or with current below acceptable limits or with other defects. The geometry of the array in each sounding is assessed for excessive curvature by calculation of difference between straight array and actual meandering array geometric factors and in some cases data is rejected due to array curvature. An option to reject data containing electrodes with locations that could not be determined without extrapolation off the start of recorded survey tracks is included in the processing software and used on occasions where extrapolation is not known to be valid. Data that would create excessively large or small apparent resistivities is rejected. Data that are recorded using excessively low currents is rejected. This last filter is particularly useful, and remarkably helpful, when combined with high frequency data collection across land or muddy or vegetated shallow water where intermittent electrode contact occurs (see Figure 17-10 where survey was conducted through rice fields).

A8.10 Voltage data smoothing

Voltage data was frequently smoothed horizontally using the algorithm and code listed in Appendix 5. Smoothing of towed array data is similar to stacking with statically collected data. It reduces random noise levels in the data at the expense of horizontal resolution. Appropriate degrees of smoothing were determined by the operator using a trial and error

approach involving trying a degree of smoothing, plotting the data, observing the lateral resolution and then trying another degree of smoothing etc.

A8.11 Conversion of voltages to EC and depths

Geo-electric arrays and TEM produce a set of voltages at each location. These need to be converted into distributions of EC with respect to depth. They can be converted to apparent EC distributions using formulae that assume they are collected over a homogeneous half space. Leaving data as apparent EC is however not going to allow the full potential of the data to be assessed. True EC distributions can be approached using inversion. Inversion attempts to determine the distribution of EC throughout the water and ground under the electrodes that would most accurately reproduce the observed measurements. Data normally is first transformed using apparent resistivity formulae and then later inverted. This allows the operator to identify some artefacts in the inverted data and adjust the inversion procedure to remove them.

The procedure of geo-electric array data inversion has been explained in Chapter 6. A summary of the transient electromagnetic data inversion procedure, as conducted in this work, will be given here.

A8.11.1 Transient Electromagnetic data inversion

The methodology of transient electromagnetic data inversion is introduced in Nabighian (1987). In this work voltages are converted to 1D smoothed layer models using a program by Scott McInnes (Zonge Engineering and Research Organization) – STEMInv by Zonge Australia.

Raw voltage data are first corrected for current and run through pre-processing that removes early channels of data exhibiting behaviour not understood by STEMInv and late channel data with unacceptable signal to noise levels. Also, any data after and including pairs of points exhibiting positive gradients is removed.

STEMInv inversion assumes that 1D horizontal layer stratigraphy dominates the area where the TEM signal has passed. Modelling is done with many thin fixed thickness layers and a smoothness constraint. The result is a smoothed representation of the real

layers in the ground with distortion and loss of detail near the surface due to mathematical formula breakdown in early times after turnoff.

A8.12 Vertical profile viewing

During, and optionally after, inversion, data is displayed progressively on a vertical image along with a root mean square fitting error. For small sample datasets, it is also practical to display and store an inversion progress monitor and other data. These facilities, along with the fast speed of the inversion code, permit trial and error modification of the inversion procedure to be executed.

A8.13 3D ribbon image viewing

At this stage, 3D ribbon imaging is also possible. The ribbons are viewed at this stage to see if anomalies in the inverted data relate sensibly with features at their respective geographic locations. Presentation is discussed much more in the next chapter.

A8.14 File segment selection

Inverted data files are usually not arranged so that data that is to be viewed is all in one file and nothing else is in that file. Segments of various files often need selecting and concatenating together to form final files containing only the data required for presentations. File segmenting and concatenation routines were written and utilized. The segmenting routine can be operated in a point-and-click manner using the graphical interface. Rigorous data documentation transfer and integration and file naming procedures were incorporated into these two processes.

Note that the graphical user interface does allow operators to zoom in on features but permanent segmentation of data files is often considered appropriate for creating logical final data sets. This is particularly so in cases such as where survey up one river bank and down the other is conducted in single files.

At this point, processing of most datasets is complete. The next step – presentation – is explained in Chapter 10.

APPENDIX 9 - TERRESTRIAL TOWED GEOPHYSICS CASE STUDIES.

A9.1 Ploughed geo-electric array tests – Coleambally

Ploughed geo-electric array tests were conducted on a property NW of Coleambally. An AXB array with 2m transmitter electrode separation and receiver electrodes at 0.5, 1, 2 and 4 metres from the second transmitter electrode was used. A traverse across a sandy paddock, and one across a clayey paddock were attempted, irrigating the ploughed array from a 200 litre drum during progress. Meaningful results were only obtained when the earth was pressed down on the array behind the plough. As this could only be done with the driver's feet (no assistant), driving and stomping could not be done simultaneaously. Reliable readings were therefore only collected over very small intervals which have been grouped into two soundings as given in Table A9-1. Error (that is variation) in these soundings (after ground was pressed down) was negligible. The system would function if the array was ripped deeper than 150mm into the ground. Watering seemed unnecessary as sufficient moisture was in the ground at that depth to make suitable electrical contact. A press-wheel will need to be added to the device to make it useable. The trial was abandoned after a few hours due to the rental cost of the Syscal-Pro. No cable or electrode wear and tear was evident.

Site	***Current***	***Effective Depth 0.3m***	***Effective Depth 0.7m***	***Effective Depth 1.3m***
Sandy	100mA	22 Ohm.m	4 Ohm.m	4.2 Ohm.m
Clayey	140mA	3.5 Ohm.m	3.4 Ohm.m	6.1 Ohm.m

Table A9-1 Two soundings conducted with a ploughed array.

A9.2 Towed transient EM - Whitton Clay Pan – MIA

Right at the end of this thesis survey program, an initial attempt at towed TEM was made. This dataset and the next (Benerembah) were the result. Considering that these datasets

were collected entirely in strong wind using only 200 µm thick builders plastic sheet to tow the loop, the author is extremely pleased with the results. This data, collected on the Whitton Clay Pan, is of the same site as the geo-electric data collected on the Whitton Clay Pan. Indeed, the reader may notice gaps in this image where the canals surveyed using geo-electric arrays pass.

Figure A9-1 presents the 8 x 8 m towed TEM data as EC ribbons. One can see that the image is cluttered and, therefore, difficult to interpret thoroughly. For this reason, Figure A9-2, Figure A9-3 and Figure A9-4 present the same data as depth slices using the colour scale of Figure A9-5.

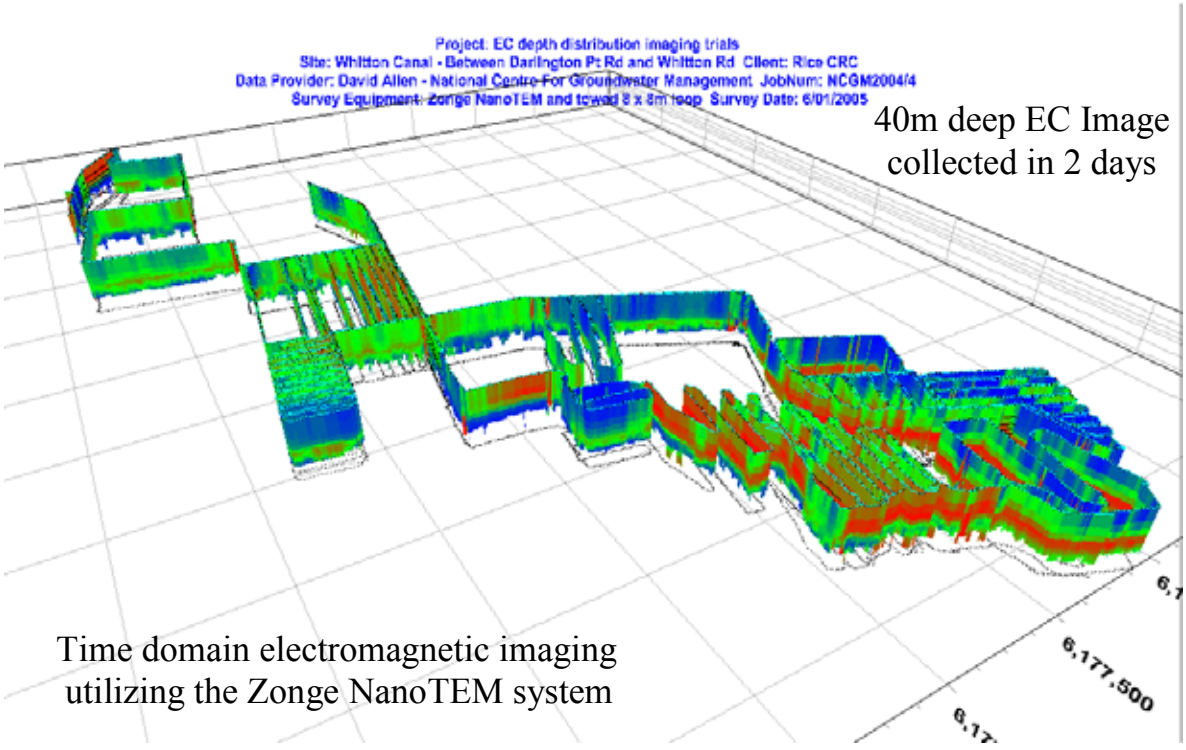

Figure A9.1 Towed Zonge NanoTEM data collected on the Dallas Clay Pan – looking from the southeast. Depth ranges from 1 metre to between 15 and 40 metres depending on EC distribution. Inversion was conducted by Zonge using StemInv (MacInnes, 2005).

Figure A9.2 Towed NanoTEM EC slice at a depth of 8 metres – Dallas Clay Pan. Red represents high EC, Blue represents low. Note strong correlation with the floating AXB array data presented in Figure 17-7 of the Chapter 17 'Networks of farm canals and drains'.

Figure A9-2 and Figure A9-3 present a set of depth slices along with three corresponding depth slices for 20m AXB array data collected in canals interspersed throughout the site. By comparing the two types of data one can observe that they are not very similar. One reason for this is the effects of the canals and furrows on salinity leaching and concentration, however this only explains small differences. The main reason is the breakdown of TEM analytical and numerical approaches and assumptions used at early times which correspond to shallow depths. Additional reasons are lack of instrument ability to accurately detect very early time data and unductive ringing that occurs between the transmitter and receiver coil. One can see that by a depth of 4 metres, in data as conductive as observed at this site, that the TEM data is beginning to become reliable and similar to the geo-electric data. TEM data at depths less than 4 metres is obviously spurious, insensitive to EC and appears erroneously resistive. From 4 metres down to 20 metres, the data appears to be reliable. The decrease in EC below 15 metres is

unexplained. Investigation of borehole records in the region (www.nratlas.nsw.gov.au) did not provide explanation due to the sparseness of the boreholes. Plausible explanation include concentration of salts above the water table.

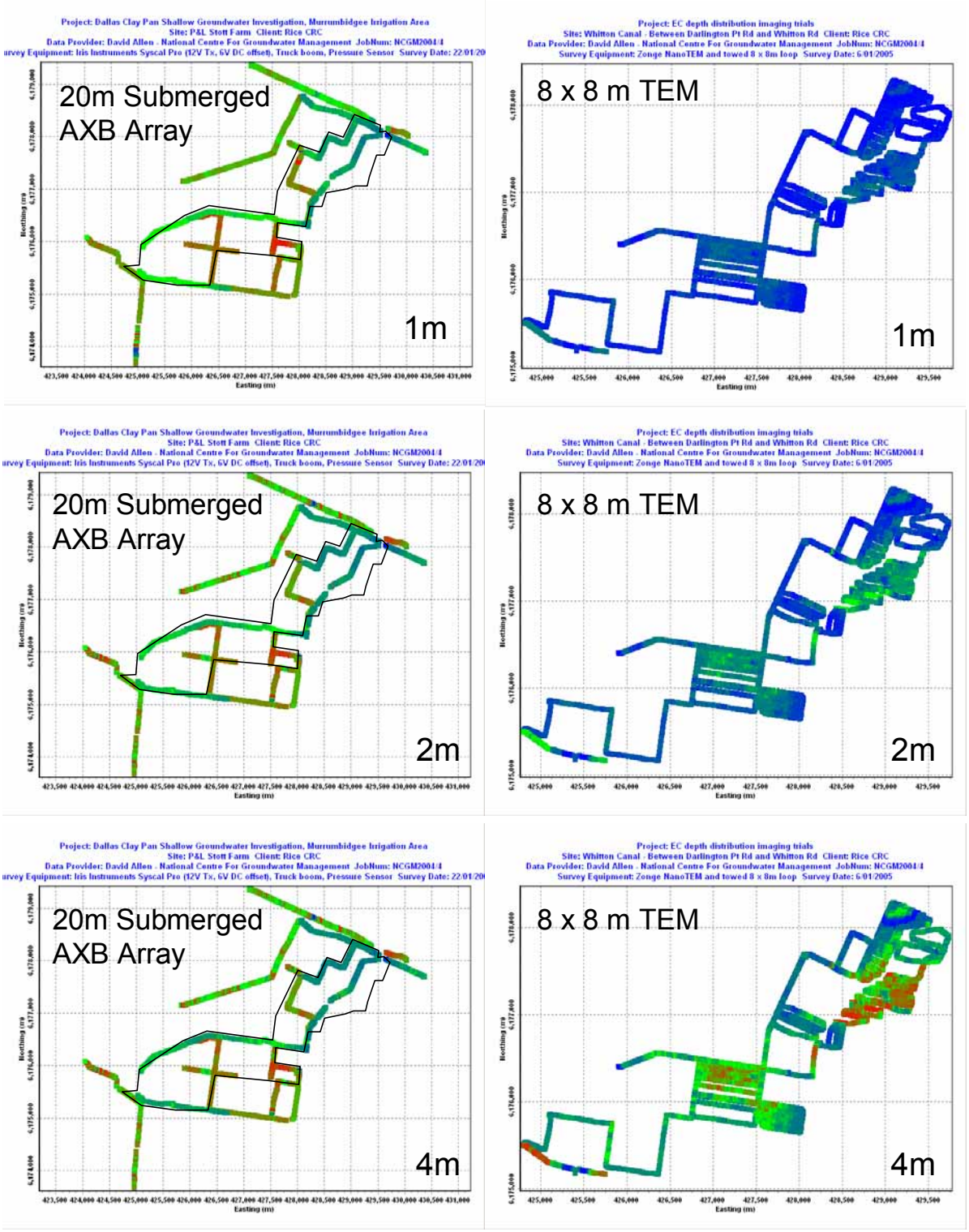

Figure A9.3 Geo-electric and TEM depth slices of farms on the Dallas Clay Pan. A black line on the geo-electric data is the outline of the TEM data.

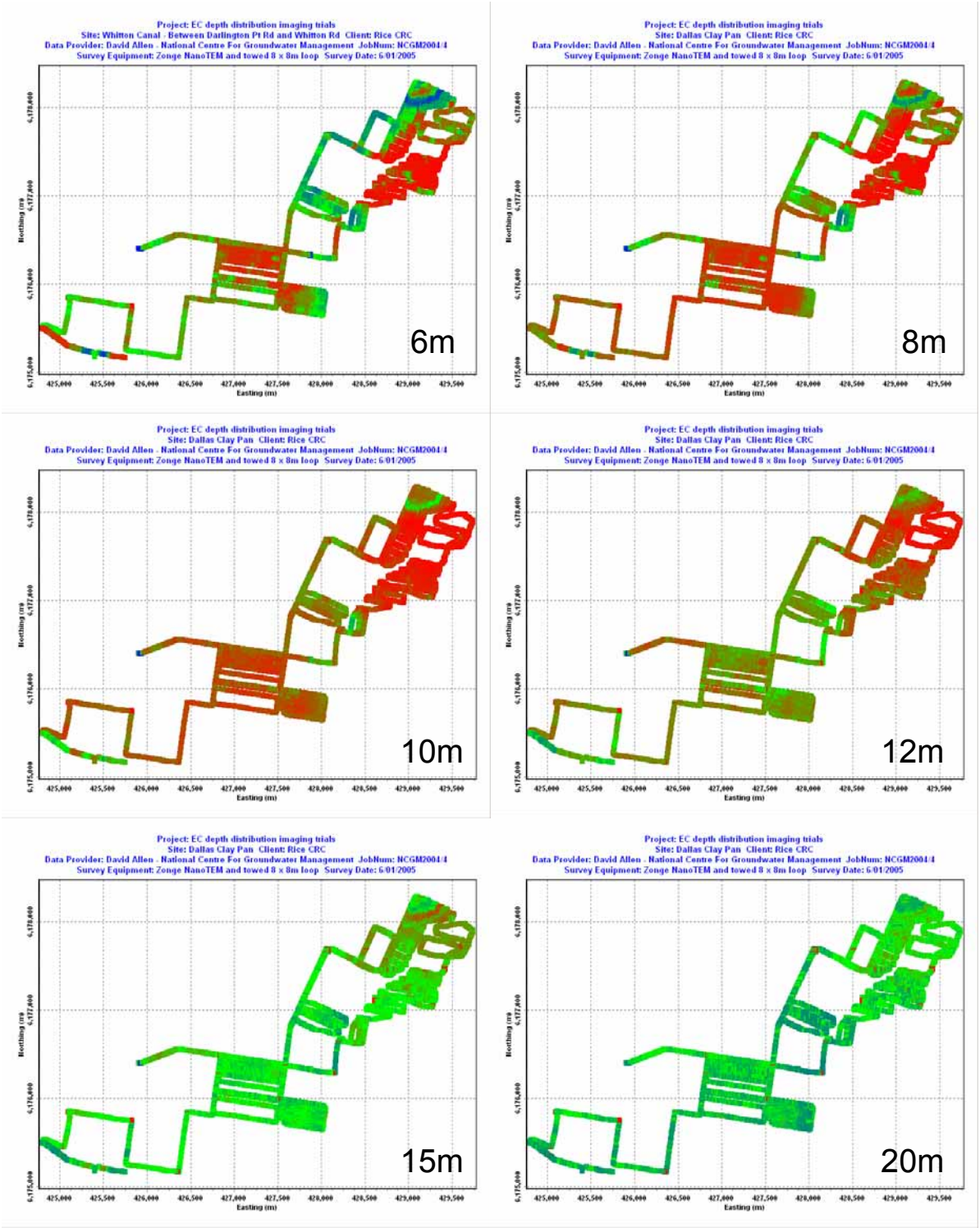

Figure A9.4 TEM depth slices of farms on the Dallas Clay Pan.

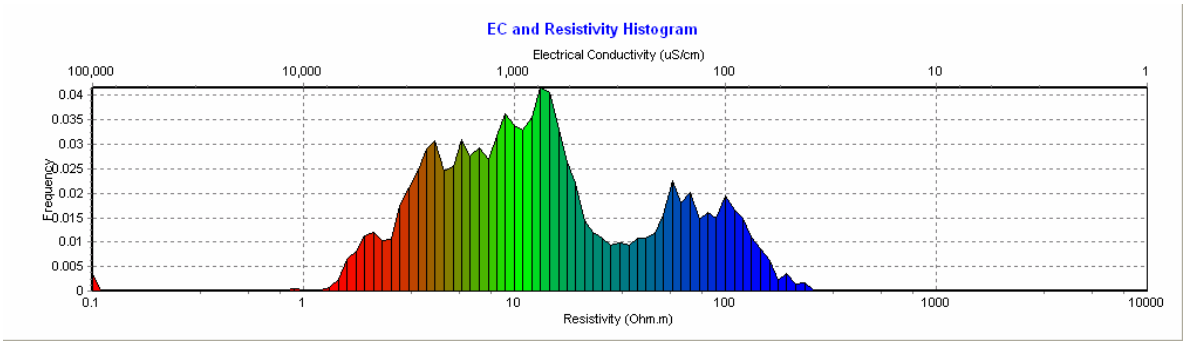

Figure A9.5 The colour scale for the data of Figures A9-1 to A9-4.

A9.3 Towed transient EM - Benerembah – MIA

A transect of towed TEM was recorded on Barber Road from Benerembah Railway siding heading north. This site is about 30 kilometres southwest of Griffith on the edge of the Murrumbidgee Irrigation Area. It was chosen because Pels (1964) extensively drilled numerous prior braided stream channels along the transect. His interpretation of those results is presented in Figure A9.6. A digital copy of this figure is included on the thesis DVD because it needs to be magnified greatly before it becomes fully legible. In 1964, Pels was able to identify the position of the prior streams using remnant vegetation and charred earth from the camp fires of aborigines that we may assume camped on the streams when they still held water (perhaps as billabongs). Barber Road receives very little traffic so survey along the actual road was practical. A fence on each side of the road reserve was considered as a source of possible current channeling and this possibility was tested by driving the loop as close as 0.3m from the fence in order to look for interference in the data. The survey results are presented in Figure A9.7. The Prior streams detected by Pels are evident as well as some he did not detect. A shallow, low EC anomaly representing the sand dune that Pels detected on the north of his section also is evident. When comparing the sections, realize that Pels has left gaps of tens of chains in his section and that the geophysical section extends further north than Pels section. Murrumbidgee Irrigation supplied shallow bore details for a bore south of, a bore in the centre of, and a bore north of the geophysical data but could not find Pels original records. Details of the bores are presented in Table A9-2. All the bores missed the prior streams and indicate the high background salinity present in the region. If a bore is sunk in one of the deeper prior stream channels it appears as if good quality water can be obtained.

Table A9-2 Details of three shallow bores along the Benerembah traverse.

Easting	Northing	WT (m) Mar05	EC uS/cm
392400	6197800	2	1660
391500	6190900	7	9140
391100	6188200	11	11100

Tests conducted by driving near the wire fence seem to have produced the broad low EC anomaly that appears below 12 metres deep in the centre left of the Figure A9-7 (Distances 3000 to 5000 m). The loop was driven within 2 metres of the fence all along this anomalous part of the transect in order to determine how much fences can corrupt such TEM data. Figure A9-8 presents a subset of the data and is designed to show the clarity of the data at a more respectable scale for viewing prior stream channel anomalies.

Figure A9-9 is a photo of excavation of the north most stringer sand evident in Figure A9-7. The shallow water table is evident.

This has been a very preliminary attempt at terrestrial towed TEM designed just to prove its potential and much improvement in quality, both of data and presentation can be expected to be made once more effort is applied to it.

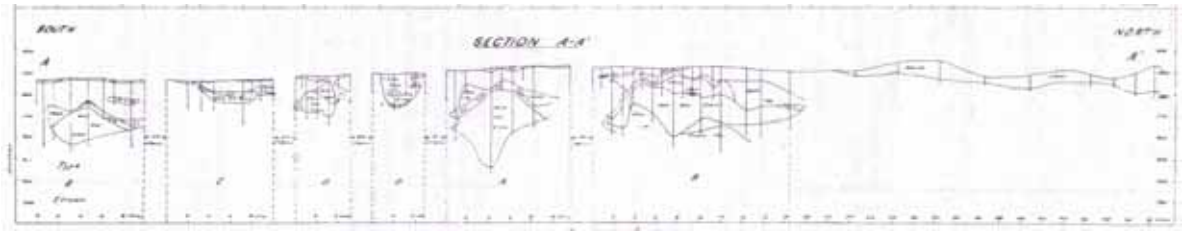

Figure A9.6 Pel's (1964) documentation of extensive drilling of prior braided streams along Barber Road.

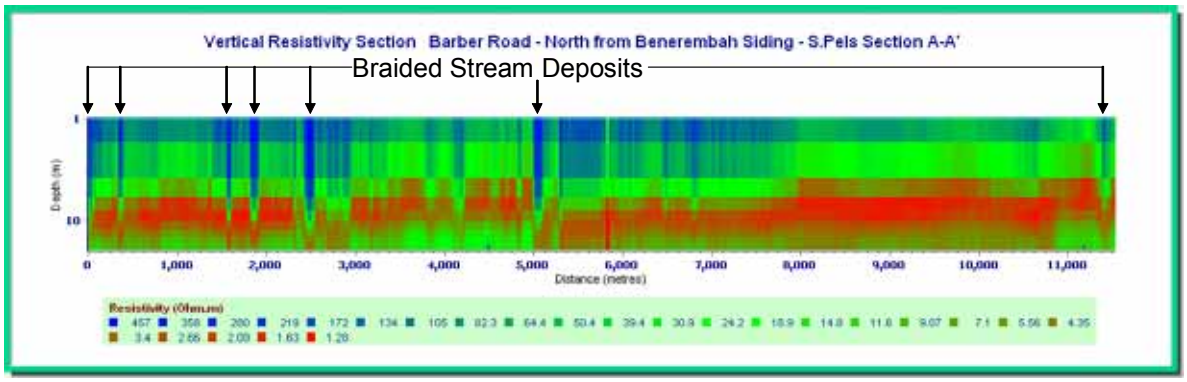

Figure A9.7 Towed Zonge NanoTEM data collected along Barber Road north from Benerembah railway siding along a drilling transect by Pels (1964) that identified numerous prior stream deposits. Inverted by Zonge using StemInv (MacInnes, 2005).

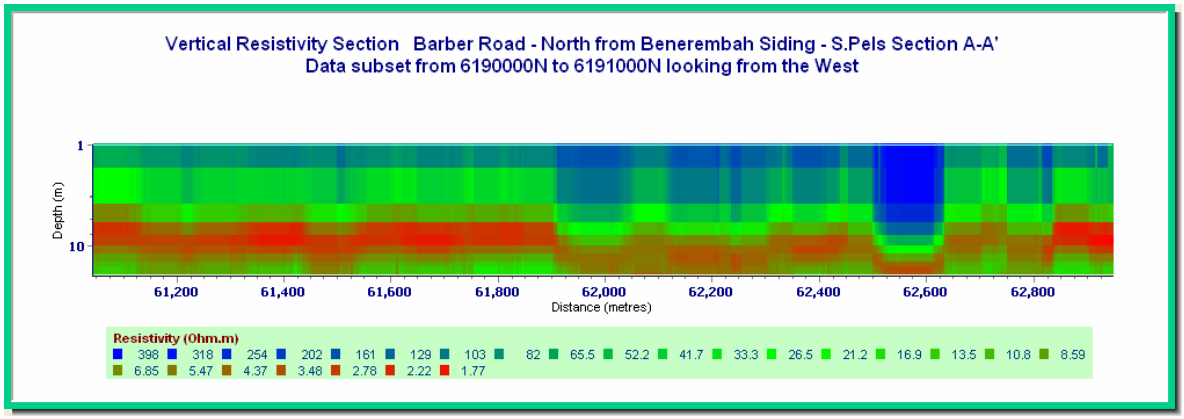

Figure A9.8 A close-up of some of the braided stream anomalies on the Barber Road TEM transect.

Figure A9.9 Excavation of the north most prior channel evident in Figure A9-7.

A9.3 Concluding remarks on terrestrial towed TEM

Towed terrestrial TEM is a useful tool for cost effective imaging of aquifers beneath farmland and open plains. It is not presently useful for imaging the top 4 metres. It may not be as easy to conduct as FDEM surveys using equipment such as the Geonics EM31 but can image much deeper and distinguish features at different depths from each other. It is potentially of great use for managing aquifer recharge and waterlogging. Because the technique has received very little use in towed mode there is a lot of potential for improved equipment performance compared to what is presented here. Airborne TEM systems have been developed comprehensively and the technology in those systems can readily be transferred to towed systems. Towed TEM survey is likely to develop a niche market complementing and extending the effectiveness of towed FDEM survey and airborne TEM and FDEM survey.

Attach DVD envelope here